Increasing the knowledge on the drivers of climate change during the Holocene and its consequences is fundamental to understand the processes that determine the global climate system. Accordingly, this research is focused to determine the natural evolution of the present interglacial period and to evaluate the anthropogenic contribution to it. To get insight into these objectives the present study compares the Holocene records with those of previous interglacial periods. Obviously, these warm intervals represent potential past analogues of the current interglacial not influenced by human activities. The comparison focuses in particular on the timing and duration of the interglacials and subsequent glacials, on the: i) nature of the climate response in the marine and terrestrial environments and ii) the presence of stability or instability conditions.

Teresa Rodrigues

High-resolution Climate Study of the Past (570,000 to 300,000 years) and Present Interglacial in the Iberian Margin: a biomarkers view

2009

Universitat Politècnica de Catalunya

High-resolution Climate Study of the Past (570,000 to 300,000 years) and Present Interglacial in the Iberian Margin: a biomarkers view

Teresa Rodrigues

Ph.D. Thesis

High-resolution Climate Study of the Past (570,000 to 300,000 years) and Present Interglacial in the Iberian Margin: a biomarkers view

Teresa Rodrigues

Ph. D. thesis
2009

High-Resolution Climate Study of the Past (570,000 to 300,000 years) and Present Interglacial in the Iberian Margin: a biomarkers view

Teresa Rodrigues

Ph. D. thesis

FCT Fundação para a Ciência e a Tecnologia
Ministério da Ciência e do Ensino Superior

CSIC

Department of Environmental Chemistry
Institute of Environmental Assessment and Water Research IDÆA
Spanish National Research Council (CSIC)
Jordi Girona, 18 08034-Barcelona

INGMAR

LNEG

Unidade de Geologia Marinha
Laboratório Nacional de Energia e Geologia, I.P.
Estrada da Portela, Bairro do Zambujal – Alfragide
Apartado 7586 - 2720-866 Amadora

UNIVERSITAT POLITÈCNICA DE CATALUNYA

Doctoral studies in Marine Sciences & Environmental Technology

Thesis supervisors: Professor Joan O. Grimalt
Professor Fatima Abrantes

Para ti, Xavier

INDEX

Chapter 2

Shallow marine sediment cores record climate variability and earthquake activity off Lisbon (Portugal) for the last 2,000 years.

Chapter 3

Holocene Interdependences of changes in sea surface temperature, productivity and fluvial inputs in the Iberian continental shelf (Tagus Mud patch)

Chapter 4

The last glacial-interglacial transition (LGIT) in the western mid-latitudes of the North Atlantic: abrupt sea surface temperature change and sea level implications

Chapter 5

Millennial-scale climate variability off Portugal during Marine Isotope Stages 15-9 (570 to 300 ka): Evidence from marine and terrestrial biomarker records

Chapter 6

APPENDICES

Main Publications of relevance to the Thesis

APPENDIX 1

Climate change and coastal hydrographic response along the Atlantic Iberian margin (Tagus Prodelta and Muros Ría) during the last two millennia.

APPENDIX 2

Variability of the North Atlantic Current during the last 2000 years based on shelf bottom water and sea surface temperatures along an open ocean/ shallow marine transect in western Europe.

APPENDIX 3

Proxy Calibration to instrumental dataset: Implications for Paleoceanographic reconstructions

APPENDIX 4

Variations in mid-latitude North Atlantic surface water properties during the mid-Brunhes: Does Marine Isotope Stage 11 stand out?

ABSTRACT

Increasing the knowledge on the drivers of climate change during the Holocene and its consequences is fundamental to understand the processes that determine the global climate system. Accordingly, this research is focused to determine the natural evolution of the present interglacial period and to evaluate the anthropogenic contribution to it. To get insight into these objectives the present study compares the Holocene records with those of previous interglacial periods. Obviously, these warm intervals represent potential past analogues of the current interglacial not influenced by human activities. The comparison focuses in particular on the timing and duration of the interglacials and subsequent glacials, on the: i) nature of the climate response in the marine and terrestrial environments and ii) the presence of stability or instability conditions.

High-resolution paleoclimate oscillations off the western Iberian margin during the Marine Isotopic Stages (MIS) 1 (covering the last 13,5 ka) and MIS 15 to 9 (between 580 and 300 ka) have been reconstructed. These are based on multiproxy analyses of several sediment archives retrieved from the Tagus mud patch and from the Estremadura spur. The multi-proxy analysis includes alkenone-based sea surface temperature reconstructions ($U^{k'}_{37}$-SST), terrigenous biomarkers: *n*-alkanes and *n*-alcohols (which reflect the evolution of the terrestrial vascular plants), concentrations of total alkenones and percentages of total organic carbon (which provide information on the marine productivity) and percent abundance of tetra-unsaturated alkenone (which records freshwater inputs).

According to the results, the last two centuries were marked by large variations of SST possibly reflecting the increasing occurrence of extreme conditions. The last 2 ka shows SST variability of 2ºC on a century scale that allows the identification of the Medieval Warm Period (MWP, 550–1300 AD), the Little Ice Age (LIA, 1300–1900 AD) and the discontinuity associated to the well known 1755 AD Lisbon earthquake. The biomarker data observed in this study shows drier continental conditions and increased coastal upwelling during the MWP which was associated with the positive phase of the North Atlantic Oscillation (NAO). During the LIA that is related to the negative NAO phase, the same proxies indicate increased river influx and river induced marine

productivity. The beginning of the Holocene was marked by an abrupt increase in SST until optimum climate conditions at the beginning of this period. After this episode there is a general trend of SST decrease and superimposed to it rapid cooling events have been identified. These climate patterns have also been previously recorded in other sites such as the NE Atlantic and Mediterranean areas.

The glacial-interglacial transition in the Tagus area is marked by a sharp SST increase contemporaneous with a strong sea level rise synchronously with the well-known mwp-1B and consequent retreat of the coastline in the Tagus mud patch which probably precluded the input of terrigenous material to the inner-shelf.

The new results for the period from 580 to 300 ka show a general trend of warm and relative stable interglacial periods and high-frequency variability during the glacial inceptions and glacials. Periods of interglacial warmth were longer prior to MIS 9 with MIS 13 showing relative stable conditions for about 54 ka, the longest period during the last 580 ka. Cross-correlation of SST and the orbital cycles shows a change of predominant periodicity from obliquity to eccentricity around 430 ka, the time of the mid-Brunhes event. The Sub-orbital scale SST variability marks the colder periods (glacial inceptions and glacials). The most pronounced of these events are related to Heinrich-type events. In our record we have identified 8 Heinrich-type events. The general pattern recorded during the deglaciations are similar to the younger climatic cycles. The composed Iberian SST records over the last 6^{th} climate cycles show that SST of the MIS 11.3 is analogous to the present interglacial, the Holocene.

This work provides an important contribution to further research on the mechanisms involved in rapid climate variability.

RESUMO

Aumentar o conhecimento sobre os mecanismos forçadores de clima e suas consequências para as condições climáticas no Atlântico Norte é fundamental para melhor compreender o sistema climático. Os principais objectivos deste trabalho são determinar a evolução natural do presente período interglacial (Holocénico) e avaliar a contribuição antropogénica para as alterações climáticas observadas. Detectar e compreender a frequência, duração e amplitude, assim como os mecanismos responsáveis pela variabilidade climática natural em períodos com condições análogas ao Holocénico, mas que não são influenciadas pelas actividades humanas é o método mais fiável. Assim, foi reconstruído com resolução elevada o registo das oscilações paleoclimaticas ocorridas na margem ocidental Ibérica durante os eventos isotópicos marinhos (MIS) 1 (que abrange os últimos 13,5 ky) e MIS 15 - 9. (entre 570 e 300 ky), com base na análise de duas sequências sedimentares. Uma recolhida na zona de deposição preferencial de sedimentos transportados pelo Rio Tejo, na zona interna da plataforma que contem os últimos 13,5 ky, e uma outra do esporão da Estremadura que cobre os últimos 570 ky. Esta análise incluiu a utilização de vários proxies; a reconstrução da temperatura das águas superfíciais do oceano é feita a partir de alquenonas (Uk'37-SST), a quantificação de biomarcadores terrígenos: n-alcanos e n-álcoois, é usada como indicador da evolução das plantas vasculares superiores, a concentração total de alquenonas e a percentagem de carbono orgânico total dão informações sobre a produtividade marinha, a abundância em percentagem da alquenonas tetra-insaturadas indica a presença de água doce.

Os dois últimos séculos foram marcados por uma grande amplitude na variação da temperatura o que possivelmente reflecte o aumento da ocorrência de condições extremas resultantes do impacto sobre o clima global do aumento rápido dos gases de estufa. Nos últimos 2 ky a SST mostra uma variabilidade de 2 ºC e permite a identificação do Período Medieval Quente (MWP, 550-1300 AD) e da Pequena Idade do Gelo (LIA, 1300-1900 AD). Os dados apontam para condições continentais de seca e aumento do upwelling costeiro durante o MWP mas um aumento do caudal rio o que induz produtividade marinha durante LIA. Estas condições podem ser explicadas com base na circulação atmosférica actual do Atlântico norte, a oscilação do Atlântico norte (NAO), se considerarmos o MWP

como um período dominado por fases essencialmente positivas de NAO e a LIA com a predominância de NAO em fase negativa. O início do Holocénico é marcado por um aumento acentuado de SST que define o óptimo climático, a que se segue uma tendência de descisda continuada, com um gradiente de cerca de 4 ºC até ao Presente. Superimposta nesta tendência geral de diminuição da SST, observam-se episódios de arrefecimento rápido também registrados em outros locais do NE Atlântico e do Mediterrâneo.

A comparação do registo Holocénico com o dos períodos interglaciares do Pleistocénico recente (580-300 ky) indicam que aqueles duraram mais tempo do que o actual e terminaram abruptamente e sempre associados a variaões milenares nas condições climáticas. Além disso, os períodos mais recentes mostram um maior gradiente de temperatura entre os extremos quentes e frios, glaciar vs interglaciar. Por outro lado, a elevada estabilidade climática que caracteriza os interglaciares contrasta com a elevada variabilidade detectada durante os glaciares. As transições, especialmente as Terminações IV e V estão marcadas por aumento rápido de SST com padrões semelhantes ao observado durante a transição do último glacial/interglacial.

Este trabalho oferece uma contribuição importante para aprofundar a investigação dos mecanismos envolvidos nas alterações climáticas.

Acknowledgements

This work would not have been possible without the contribution of many people and entities, whom I wish to express my most sincere gratitude, in particular:

To my supervisors:

À Professora Fátima Abrantes, pela oportunidade de fazer parte do grupo do DGM e desenvolver o meu gosto pela investigação no mundo da paleoceanografia. Pela confiança em mim deposita, por acreditar que eu seria capaz. Pela sua imprescindível ajuda, entusiasmo e amizade, por todos os momentos que me dispensou, por partilhar comigo a sua generosidade e afecto ao longo destes 10 anos.

Al Professor Joan O. Grimalt que m'acceptés en el seu grup. Per donar-me totes les facilitats i l'oportunitat d'aprendre la metodologia d' anàlisi de biomarcadores. Per les discussions i support general. Molts gràcies.

Special thanks to Dr. Antje Voelker, she gave me full personal and scientific support, through numerous fruitful discussions, reviews and helpful suggestions and permanent availability and friendship, which greatly improved this work.

À Doutora Susana Lebreiro por ter compartilhado comigo a sua experiência, profissional e pessoal, pela sua amizade e apoio em todos os momentos, pelo exemplo de força e vontade de fazer mais e melhor e encarar a vida sempre com um sorriso!

Ao meu "Coach" Filipa Naughton pelo imprescindível apoio neste ultimo ano, pelos "brainstorm" que muito me ajudaram, pelas muitas correcções e sugestões, pelo teu entusiasmo e amizade e por me fazeres acreditar que vale a pena…

Ao Dr. Hipólito e Dr. Gaspar pelo seu apoio e por partilharem a sua experiência de Vida.

Al grupo de Salamanca en especial a la Elena Colmenero y al Profesor José-Abel Flores, por su amistad y disponibilidad en colaborar en este trabajo y por sus imprescindible ayuda en la identificación de los cocolitos.

Ao laboratório “321” vale al 306 también e a todo el personal del Departamento de Química Ambiental CID (actual IDÆA) – CSIC Barcelona, por la forma como me han recibido, por el apoyo paciencia en enseñarme el “mundo de las alkenonas”, pelos muchos momentos de alegría y humor que pasamos y pela amistad que hicieron muy agradables los días que pasé en Barcelona. En especial a Belén Martrat e a Jordi Lopez por el apoyo amistad e importante comentarios e sugestiones Molts gràcies.
A los que ya no están en el CSIC pero que me acuerdo mucho de los buenos ratos que vivimos allí. Y claro a las amistades que quedaron mas allá, A las nuevas mamas Montse y Cons por su cariño e apoyo aunque de legos… A ti Bea y claro a Carles por acogerme en su casa e compartir conmigo vuestra amistad y los buenos momentos de vuestras vidas (bueno a ver vamos el día 25 de Julio).

O meu especial agradecimento com carinho e apreço a todo o pessoal do Departamento (actual Unidade) Geologia Marinha, pelo acolhimento e amizade que sempre demonstraram. Ao pessoal do laboratório, em especial à D. Apolónia e à Cremilde pela preocupação e amizade ao longo destes anos, aos que já não estão lá, Ana Margarida e a Zé, mas que não esqueço os bons momentos que passamos. À Margarida Henriques pela sua amizade, apoio, paciência e ajuda. E em geral aos colegas do grupo da Paleo.

Quero agradecer a Susana Costas a sua axuda na elaboración da portada da tese. A Isabelle pelos “arranjos” de ultima hora.

Por ultimo mas não menos importante, à minha família, em especial aos meus Queridos Pais pelo carinho paciência, apoio e incentivo que sempre me transmitiram. À “menina Tia” pela compreensão apoio ajuda e incondicional disponibilidade em todos os momentos.

A todos os amigos que me têm apoiado, pelo seu afecto e amizade, o meu bem haja!!

Dedico, também, esta tese à memória das minhas *avós* pelos princípios e experiência de vida que partilharam comigo.

A ti Rafa, por estares sempre perto apesar da distância, pelo apoio e motivação para continuar a lutar. Por fim, mas para o mais importante, dedico esta tese a ti Xavier, pela magnifica experiência de vida que me deste de ser MÃE, pela alegria e felicidade nos momentos que passamos juntos e pelos miminhos que tu me dás.

This study could not have been completed without financial support received from FCT - Fundação para a Ciência e Tecnologia through PhD (SFRH/BP/13749/2003) fellowships, the PORTO (PDCT/MAR/58282/2004) and SEDPORT projects (PDCTM/40017/2003), and European Science Foundation, who support participation in scientific conferences, EU projects and HOLSMEER (EVK2-CT-2000-00060), the Spanish Ministry of Science and Technology (REN2003-08642-C02-01), Consolider-Ingenio 2100 Project CE-CSD2007-0067. Coring of MD03-2699 was made possible through a European Access to Research Infrastructure grant.

PREFACE

This dissertation is presented in manuscript format as outlined by the Universitat Politècnica de Catalunya. It consists of six chapters which as a group provide a high resolution record of climate variability during the present interglacial (Holocene) and during the late Pleistocene (570 to 300 ka) in the western Iberian Margin.

The first chapter reports an overview of the state of the art and fundamental concepts of the use of biomarkers for paleoclimatology studies. The used material and methodology used are presented in this chapter.

The second chapter describes a high resolution record of sea surface temperatures (SST), riverine discharges and biological productivity for the last 2,000 years obtained in a sedimentary sequence recovered from the Tagus deposition centre off Lisbon (Portugal). This work was done within the framework of the HOLSMEER EU project "Late Holocene shallow marine environments of Europe". and has been published in *Quaternary Science Reviews* 24, 2477-2494 (2005).

The third chapter describes Holocene Interdependences of changes in sea surface temperature, productivity and fluvial inputs in the Iberian Continental shelf (Tagus mud patch). This work extends the previous study back to 11.5 ka and has been performed in the framework of the SEDPORT, EUROMARGIN project (Sedimentation Processes on the Portuguese Margin: the role of the continental climate, ocean circulation, sea-level and neotectonics). It has been published in *Geochemistry, Geophysics, Geosystems* 10, doi:10.1029/2008GC002367 (2009)

The fourth chapter describes the last glacial-interglacial transition (LGIT) of the western mid-latitudes of the North Atlantic. It compares the abrupt sea surface temperature and sea level changes during this period. To achieve these goals, we proposed an high resolution study of the shallow core used for the chapter 3 study which covering the last 13.5 ka, gives a better insight of the last glacial-interglacial transition (LGIT) over Western Iberia. The high resolution study of the previous shallow core covering the last 13.5 ka retrieved from the Tagus mud patch was compared to the the deep-sea core studied in the framework of the PORTO project (FCT). These results are under revision in *Quaternary Science Reviews*.

The fifth chapter will soon be submitted, soon to *Paleoceanography* and reports the first multi-proxy record covering the period between 570 and 300 ka in the western Iberian margin for a deep sea core collected in the Estremadura spur.

The sixth chapter presents general conclusions and some remarks that proposes a new approach for future work.

The appendices encompass other publications of relevance for the topic of this thesis for which I have contributed.

Appendix 1 was published in the HOLSMEER special issue (*The Holocene* nº 16,7, 2006) and reports the climate change and coastal hydrographic response along the Atlantic Iberian margin (Tagus Prodelta and Muros Ría) during the last two millennia.

Appendix 2 was published in the same HOLSMEER special issue and describes the variability of the North Atlantic Current during the last 2000 years. The results are based on measurements of shelf bottom water and sea surface temperatures along an open ocean / shallow marine transect in western Europe.

Appendix 3 present a paper published in *Geochemistry, Geophysics, Geosystems* and reports the first attempt to calibrate sediment proxy data for both continental climate and oceanic productivity to the existing 100 years instrumental time-series of data for sea surface temperature (SST), precipitation river runoff and upwelling strength.

Appendix 4 was published in *Climate of the Past* Discussions, 5 (2009) and reports the findings on a study of variations in mid-latitude North Atlantic surface water properties during the mid-Brunhes: Does Marine Isotope Stage 11 stands out? New planktonic stable isotope and ice-rafted debris records from three core sites in the mid-latitude North Atlantic are combined with records of eastern and central North Atlantic to reconstruct hydrographic conditions during the middle Pleistocene spanning Marine Isotope Stages (MIS) 9–14 (300–540 ka). This work was performed within the framework of the PORTO FCT project.

Chapter 1

General Introduction

1. INTRODUCTION

The climatic conditions of our planet have changed along history. The more recent climatic oscillations have influenced Human life in drastic ways. Many geological records prove these climate changes. Some of them evidence the occurrence of glaciers in regions that are now temperate.

The climate changes documented for the last 250 years have been influenced by increasing greenhouse gas emissions (CO_2; CH_4; N_2O) [*Alley et al.*, 2007]. Fossil fuel combustion and cutting of tropical forests have modified the balance between absorbed solar radiation on land and sea and absorbed the radiations in the atmosphere. The cause-effect present day relations between human activity and global warming, now accepted by the majority of the scientific community, seems to be in agreement with a 60% contribution due to the human activity while the remaining 40% represent natural climatic variation [*Alley et al.*, 2007].

Carbon dioxide, resulting primarily from the burning of fossil fuels and land-use change, is the most important anthropogenic greenhouse gas. The global atmospheric concentration of carbon dioxide has increased from a pre-industrial value of about 280 ppm to 387 ppm in 2009 while the amount of methane, primarily due to agriculture, has increased from a pre-industrial value of about 715 ppb to 1790 ppb in the early 1990s, and to 1790 ppb in 2009 (data from the NOAA annual greenhouse gas index). The global atmospheric nitrous oxide concentration increased from a pre-industrial value of about 270 ppb to 322 ppb in 2009. The atmospheric concentration of methane and carbon dioxide in 2009 exceeded by far the natural range of the last 650,000 years as showed from ice core records [*Alley et al.*, 2007]. The atmospheric CO_2 concentration of the last 400,000 years is show in Figure 1.1. This greenhouse gas followed the glacial-interglacial pattern of this period. Glacial periods are characterized by lower concentrations in the order of 190 ppm, and interglacial periods by high concentrations about 280 ppm. As shown in the figure the CO_2 rise due to the present human activity has brought atmospheric concentration well above this natural range of variation.

Understanding what will be the long term effects of this greenhouse gas increase requires a considerable understanding of climate conditions in the past, as well as of the forcing factors behind the variability.

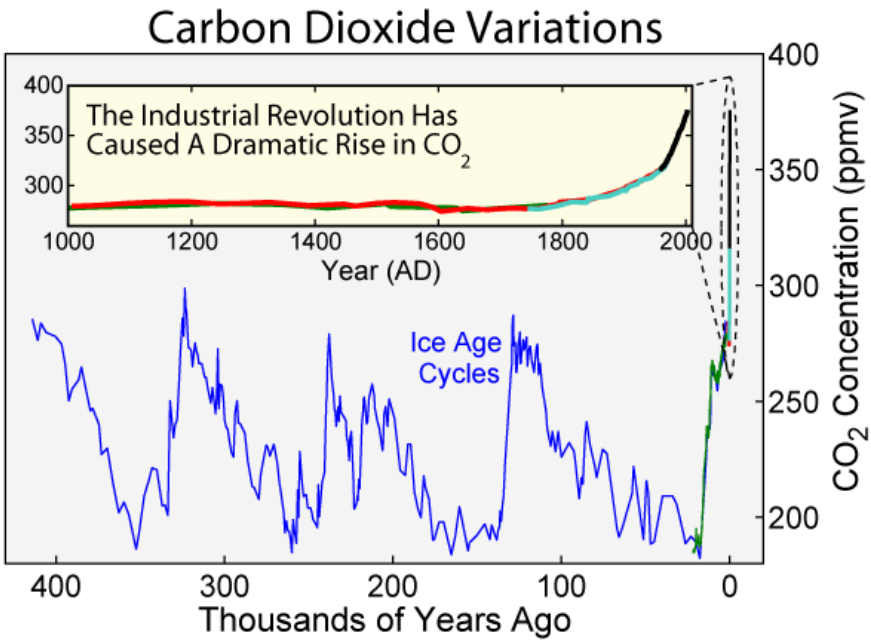

Figure 1.1. Variations of atmospheric carbon dioxide concentration during the last 400 thousand years The largest changes in CO_2 concentration are related to glacial/interglacial cycles. Since the Industrial Revolution, about 1900, the burning of fossil fuels has caused a dramatic increase of CO_2 in the atmosphere, reaching unprecedented levels in the last 400 thousand years (from www.transitiontownshaftesbury.org.uk).

The internal climate variability is a global phenomena resulting from the interaction between, atmosphere, ocean, biosphere (fauna and flora), lithosphere (bottom of the oceans and continents) and cryosphere (Earth's surface where water is in solid form). The atmosphere is the most variable of all and the one responding more quickly to any external influence. The oceans have a very important role in maintaining the balance of climatic conditions, especially with regard to exchanges of heat and moisture with the atmosphere. Their large extension, about 70% of the earth surface, determines their main role in the energy dynamics of the planet. Accordingly, marine sediments constitute potential key archives of past climate conditions and consequently understanding of the climate system.

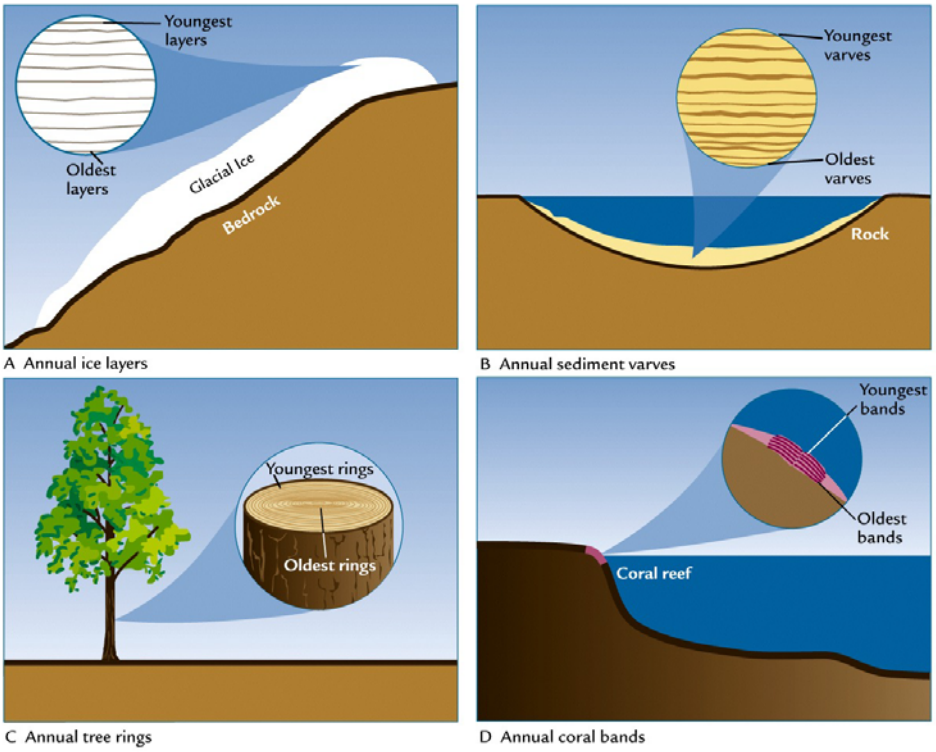

Figure 1.2.Indicator of climate archives, A-ice core, B-marine sediments, C- tree rings, D-corals [*Ruddiman*, 2001].

Increasing the knowledge on the earth's past climate natural variability depends on the study of indirect indicators recorded in climate archives such as: ice cores, marine sediments, corals, lake sediments, speleotems, tree rings, etc (Fig.1.2). Depending on the selected archive, the paleoclimatic results will be more regional or global, and they will be able to cover a shorter or longer time interval (years to millions of years), with higher or lower temporal resolution (from years to thousands of years).

Marine sediments are composed of material of marine and terrestrial origin, that generally accumulate in the bottom ocean. They may provide palaeoclimatic records for a time period that covers the last 165 million years. The biogenic material of marine origin (Figure 1.3), contained in these marine sediments allows water masses characterization in terms of sea surface temperature (SST), salinity and nutrients and the reconstruction of oceanic circulation. The terrestrial material included in the marine sediments provides substantial information on the continental conditions such as: a) changes in humidity and aridity, b) wind directions and intensities, c) river outflow and the discharge of material transported by icebergs.

The material recovered from the seafloor (as that from lakes) provides documentation of environmental changes in the region where the sediments have been deposited. This information has to be extracted through the use of "proxies" that, in the paleoenviromental reconstruction context are measurable descriptors linked to "non-fossilisible" variables such as temperature, salinity, global ice volume, nutrient content, oxygen content, CO_2 concentration, wind speed, productivity, and so forth. Each proxy follows their own physical, biological and chemical rules that allow the transformation the proxy value into the target parameter. Usually this process is performed by using a transformation algorithm that has been established through proxy calibration. The quality of a proxy is given by the confidence limits of the calibration equation in many different environments [*Wefer et al.*, 1999].

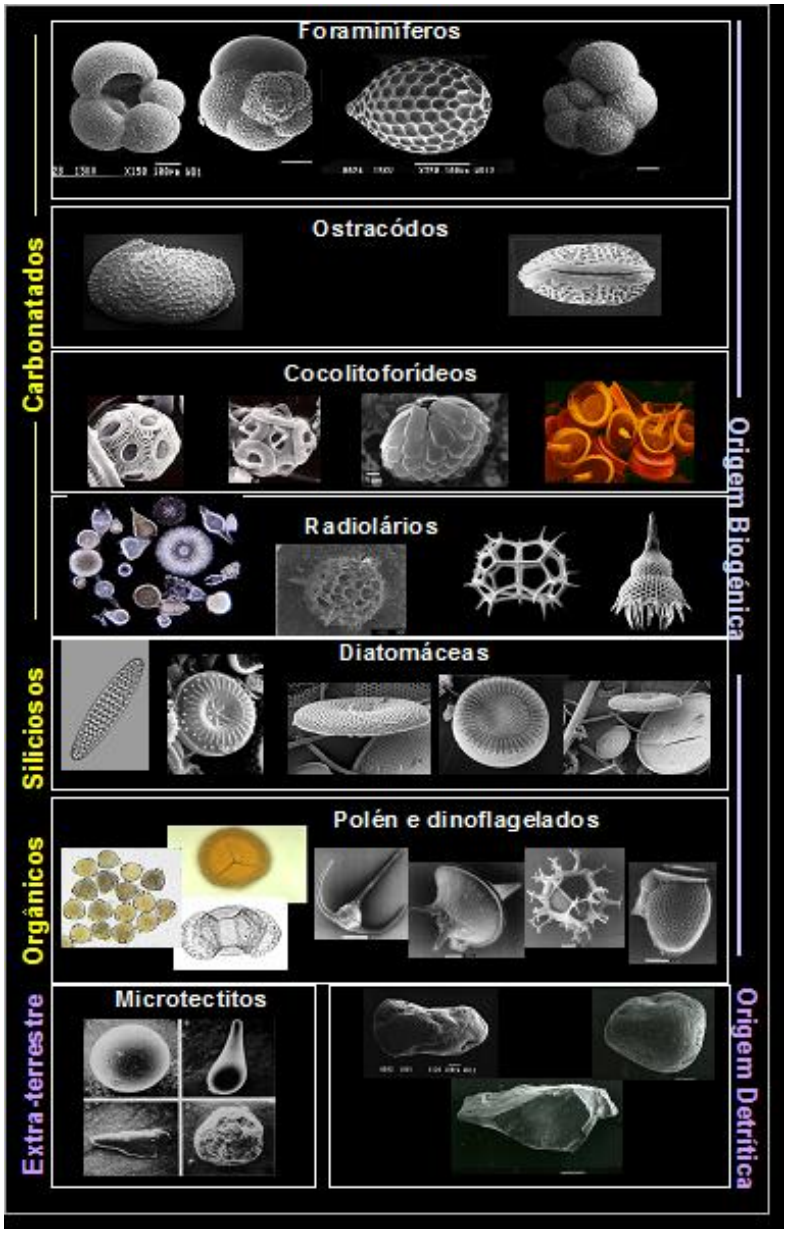

Figure 1.3. Images of various microorganisms, found within the biogenic constituents of marine sediments used as paleoclimatic proxies (adapted from de Abreu, 2002 personal communication).

1.1 Climate Oscillations over the Late Quaternary

1.1.1 Orbital Climate Variability

The climate conditions of the earth depend on external mechanisms, such as the earth's position relatively to the sun, and the internal mechanisms, e.g. thermohaline circulation, ice sheet mechanisms, volcanic eruption, greenhouse gas concentrations, albedo, etc…. These processes, together with the anthropogenic impact on global climate highlight the need of paleoceanography for understanding the frequency, time rate and amplitude of variability of the climate system. Increasing the knowledge of the natural past climate change and its causes, in particular for the periods during which conditions were similar to the present ones is mandatory for understanding the process that determine the present and future climate conditions.

During the last million years, the climate changed between glacial and interglacial periods, in response to changes in the earth's position relatively to the sun [*Imbrie et al.*, 1992; *Milankovitch*, 1920]. These orbital changes can be expressed as a combination of astronomical parameters such as eccentricity, obliquity and precession of the equinoxes, which modified the amount of energy received from the sun and their planetary distribution both seasonally and latitudinally. [*Berger*, 1978] (Figure 1.1.1).

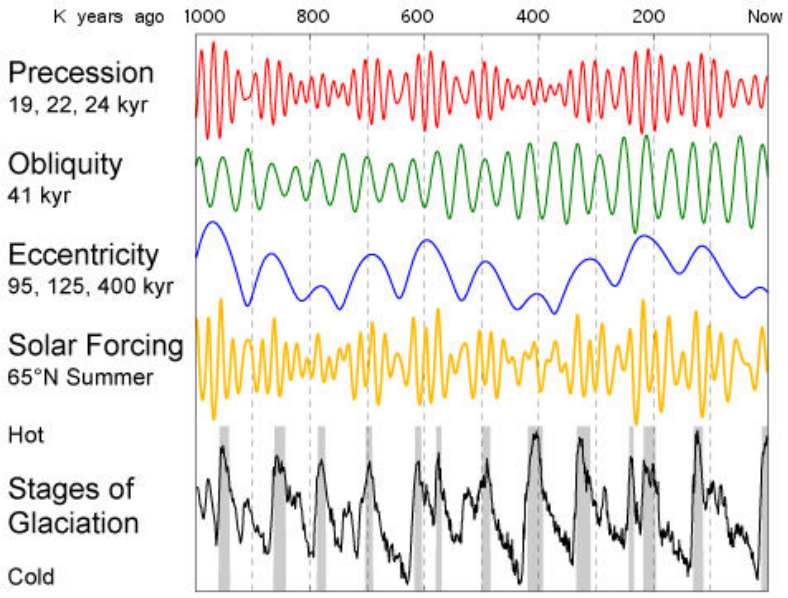

Figure 1.1.1. Milankovitch cycles describing the precession, eccentricity and translation orbit axis movements of the Earth. These movements have influenced climate change in 100 ka periods and determined the frequency of Quaternary glaciations [*Berger*, 1978].

Eccentricity is a term used to describe the shape of Earth's orbit around the sun. This shape ranges from an almost exact circle (eccentricity = 0.0006) to a slightly elongated shape (eccentricity = 0.0535). The time frame for the cycle is approximately 98 ka [*Berger and Loutre*, 1992]. This variation involves a change in the amount of solar energy from perihelion, closest distance from sun, (around January 3) to aphelion, farthest distance from sun, (around July 4) (Fig. 1.1.2). Currently the Earth's eccentricity is 0.016 and there is about a 6.4% increase in insolation from July to January [*Berger*, 2001].

The tilt of the Earth's axis with respect to the orbital plane is called obliquity, the orbital cycle that primarily determines the differences in seasonal energy (Fig. 1.1.2). Obliquity varies between 22° and 25° in a cycle of 41 ka [*Berger and Loutre*, 1992]. Higher obliquity involves higher seasonal contrast, e.g. very cold winters and very hot summers in both hemispheres at high latitudes. Temperate summers and wet and cold winters promote the ice cap growth at the polar regions and evolution to glacial conditions.

Precession is the change in the orientation of the Earth's rotational axis (Fig. 1.1.2). The precession cycle takes about 19 - 23 ka and is caused by two factors: a wobble of the Earth's axis and a turning of the elliptical orbit of the Earth itself. While obliquity affects the tilt of the Earth's axis precession affects the direction of the Earth's axis. This effect leads to increases in the seasonal contrast in one hemisphere and decreases in the other. Currently, the Earth is closest to the sun in the northern hemisphere winter (perihelion 3 January) and farthest in the northern hemisphere summer (aphelion 4 July), which makes the winters and summers of the northern hemisphere less severe [*Ruddiman*, 2001].

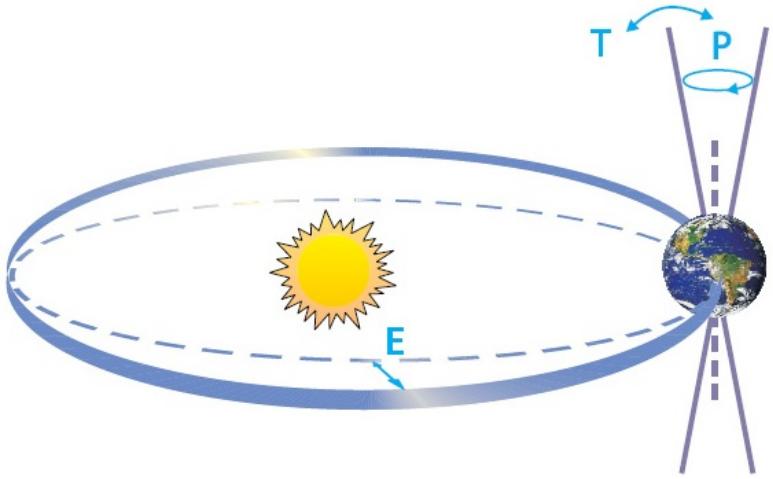

Figure1.1.2. Schematic representation of the Earth's orbital changes (Millankovitch, Serbian engineer and mathematician Milutin Milankovic who proposed the theory Cycles) that drive the ice age cycles. "T" denotes changes in the tilt (or Obliquity) of the Earth's axis; "E" denotes changes in the eccentricity of the orbit (due to variations in the minor axis of the ellipse, and "P" denotes precession, that is, the changes in the direction of the axis tilt at a given point of the orbit. Source: [*Rahmstorf*, 2006]

The orbital variability described by Millankovitch led to the regular glacial-interglacial pattern of the Quaternary. This pattern has even been observed along longer periods such as the last 5Ma (Figure 1.1.3). This benthic $\delta^{18}O$ record shows 41 and 100 ka periodicities that are also found in other marine records around the world. The record of the Figure 1.1.3 [*Lisiecki and Raymo*, 2005] also shows a general cooling along this 5 Ma period.

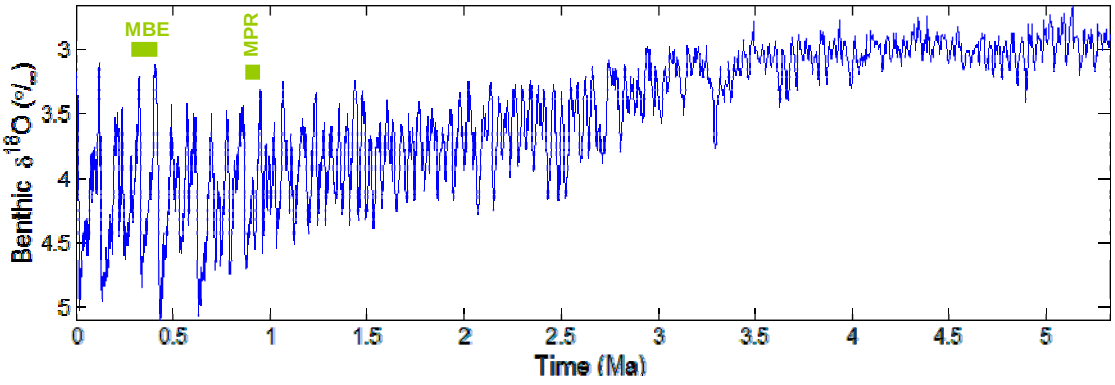

Figure 1.1.3. The LR04 stack spans 5.3 Ma. It is based on an average of 57 globally distributed benthic $\delta^{18}O$ records (which measure global ice volume and deep ocean temperature) [*Lisiecki and Raymo*, 2005]. MBE reflects the period recognized by the mid-Brunhes event, and the MPR the Mid Pleistocene Revolution.

In the Early Quaternary, the dominant cyclicity was 41 ka, but between 1.2 and 0.6 Ma, a period known as the Mid Pleistocene Revolution, there is a transition from 41 ka to 100 ka climate cycles [*Imbrie et al.*, 1993] (Figure 1.1.4). After the mid-Brunhes event around 430 ka, the 100 ka eccentricity cycle becomes the dominant glacial-interglacial cycle and the amplitude of glacial and interglacial states is larger because of the increase in glacial ice volume [*Loutre and Berger*, 2003].

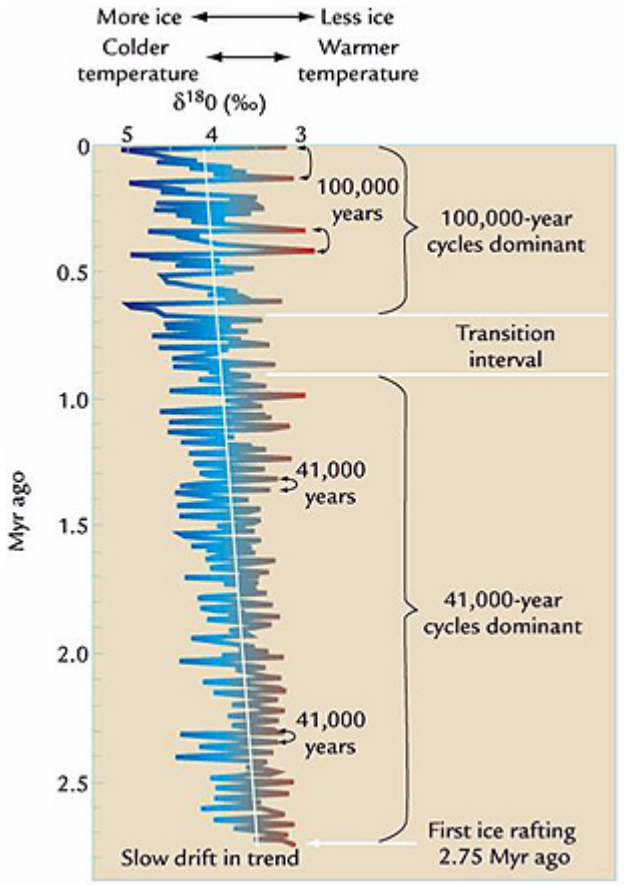

Figure 1.1.4. Orbitaly induced 100,000 and 41,000 years climatic oscillations, [*Ruddiman*, 2001]

Changes between glacial and interglacial cycles were firstly detected by Shackleton (1967) through $\delta^{18}O$ measurements of the fossil skeletons of the marine benthic fauna preserved in marine sediments. [*Shackleton*, 1967].

This work clearly showed that the climate varied from glacial (heavy $\delta^{18}O$ values) to interglacial (light $\delta^{18}O$ values) conditions. The $\delta^{18}O$ sequences were later used with stratigraphic propose and numbered marine isotope stages (MIS) [*McManus et al.*, 1999; *Shackleton*, 1967].

1.1.2 Suborbital climate variability

Superimposed on the glacial-interglacial oscillations, several short-lived abrupt climatic changes have been detected during the last glacial period (70 to 15 ka) in the Greenland ice cores, the so called D-O events (Figure 1.1.5) [*Dansgaard et al.*, 1993; *Grootes et al.*, 1993; *Grootes and Stuvier*, 1997; *Johnsen et al.*, 1992]. These abrupt transitions were also observed in marine sediments of the northern hemisphere. Although the most pronounced millennial-scale fluctuations have been registered in the North Atlantic region [*Chapman et al.*, 2000; *Maslin et al.*, 1995], there is growing evidence that these climate oscillations occurred also on a global scale [*Blunier et al.*, 1998; *deMenocal et al.*, 2000; *Huls and Zahn*, 2000; *Lowell et al.*, 1995; *Schulz et al.*, 1998; *Voelker et al.*, 2006; *Voelker*, 2002].

This sub-orbital climate variability, exhibit a periodicity of 1500 years [*Bond et al.*, 1993; *Bond et al.*, 1997; *Mayewski et al.*, 1997; *Schulz and Timmermann*, 2004] and is characterized by an alternation between episodes of rapid warming (Greenland interestadial - GIS) and gradual cooling (Greenland stadials - GS) [*Dansgaard et al.*, 1993]. The amplitude of temperature changes associated with these DO oscillations has reached 16°C in Greenland [*Severinghaus and Brook*, 1999].

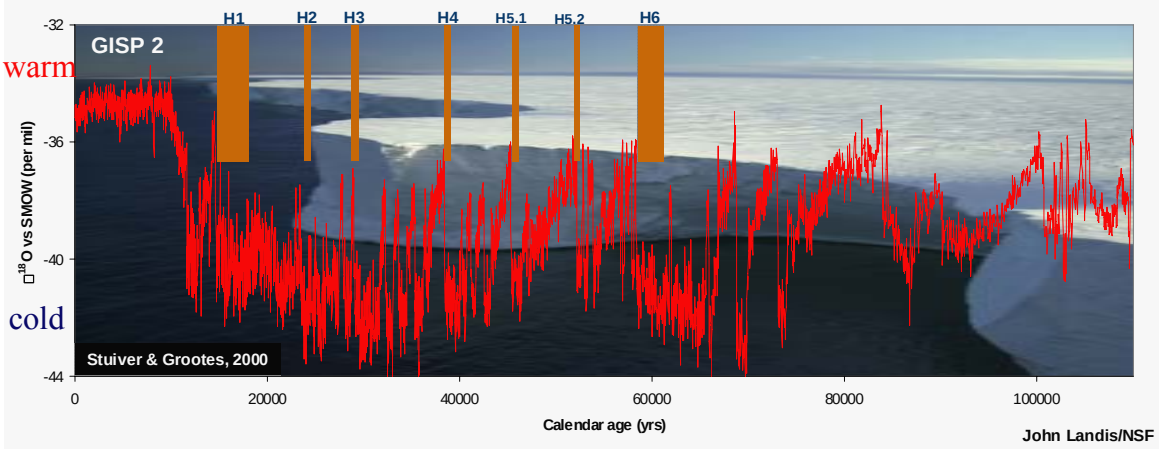

Figure 1.1.5. Millenial-scale Climate Oscillations: Dangaard-Oeshger Cycles of warm interstadials/cold stadials. Ice core $\delta^{18}O$ temperature records are clearly dominated by Orbital frequencies. Some stadials coincide with Heinrich (H) events, major ice rafting events that indicate that icebergs from the ice sheets of North America, Greeland and Scandinavia traveled across the North Atlantic (adapted from deAbreu personal communication).

Extreme cold episodes within the Dansgaard-Oescheger events are associated with the release of great discharges of icebergs into the North Atlantic [*Heinrich*, 1988] which constitute the well known Heinrich events [*Bond et al.*, 1993; *Bond and Lotti*, 1995; *Broecker*, 1994]. These cyclic events occurred approximately every 5-10 ka at intervals of 1-2 ka in the last glacial period [*Elliot et al.*, 1998] and are associated with major palaeoceanographic changes in the north Atlantic [*Bond et al.*, 1993; *Ruddiman*, 1977]. Heinrich layers have been recognized in oceanic sediments by the presence of high relative abundance of terrigenous detritus in the coarse sediment fraction [*Heinrich*, 1988], magnetic susceptibility increases [*Grousset et al.*, 1993], SST decreases [*Bond et al.*, 1993; *Bond and Lotti*, 1995; *Cortijo et al.*, 1997], reduction in planktonic foraminiferal numbers [*Bond et al.*, 1992; *Broecker*, 1994], increase in polar planktonic foraminifera *Neogloboquadrina pachyderma* sin percentages [*Bond et al.*, 1992; *McManus et al.*, 1999], lightening in the $\delta^{18}O$ of the surface water masses in the north Atlantic [*Cortijo et al.*, 1997] and decreases of SSS [*Chapman et al.*, 2000].

Heinrich layers have firstly been detected in several north Atlantic deep sea-cores from the IRD belt (Rudiman's Belt, between 40 and 50° N) (Figure 1.1.6), but are also recorded further north (>50° N) [*Bauch et al.*, 2001; *Elliot et al.*, 1998] and south in the southwestern Iberian margin (37° N) [*Abrantes et al.*, 2001; *Abreu et al.*, 2003b; *Baas et al.*, 1997; *Bard et al.*, 2000; *Lebreiro et al.*, 1997]. However, outside the IRD belt the quantity of coarse detritus decreases and there is an increase in the number of contributing sources [*Hemming et al.*, 1998]. Heinrich like events associated with massive Iceberg discharges have also been observed during other ancient glacial periods in the north Atlantic [*Abreu et al.*, 2003b; *McManus et al.*, 1999].

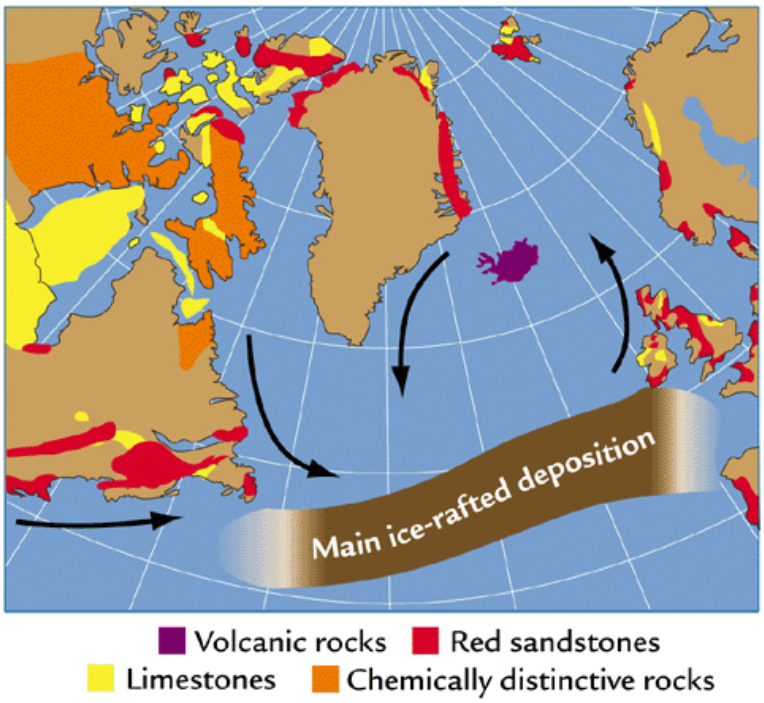

Figure 1.1.6. Heinrich events represent the melting of debris-charged icebergs that originated from sources along the eastern margin of the Laurentide Ice-Sheet [*Bond et al.*, 1992; *Broecker*, 1994], Greenland and Iceland [*Elliot et al.*, 1998], Scandinavian and British ice-sheets [*Grousset et al.*, 1993]. From [*Ruddiman*, 2001].

According to [*MacAyeal*, 1993] northern ice sheets grow until they get unstable and/or partially collapse originating the flux of icebergs on to the North Atlantic [*Broecker*, 1994]. Such process may also result in the input of large amounts of fresh water into the north Atlantic surface waters leading to a salinity decrease [*Labeyrie et al.*, 1987]. An occurrence that would also reduce northward advection of relatively warm upper ocean water (Figure 1.1.7) [*Cortijo et al.*, 1997]. This mechanism may further cool the north Atlantic region [*Bond et al.*, 1993; *Cortijo et al.*, 1997] and reduce or even prevent NADW formation [*Keigwin and Lehman*, 1994; *Maslin et al.*, 1995]. On the contrary, the end of a Heinrich event is marked by an increase of the NADW production and abrupt warming of the north Atlantic region [*Bond et al.*, 1993; *Paillard and Labeyriet*, 1994; *Vidal et al.*, 1997].

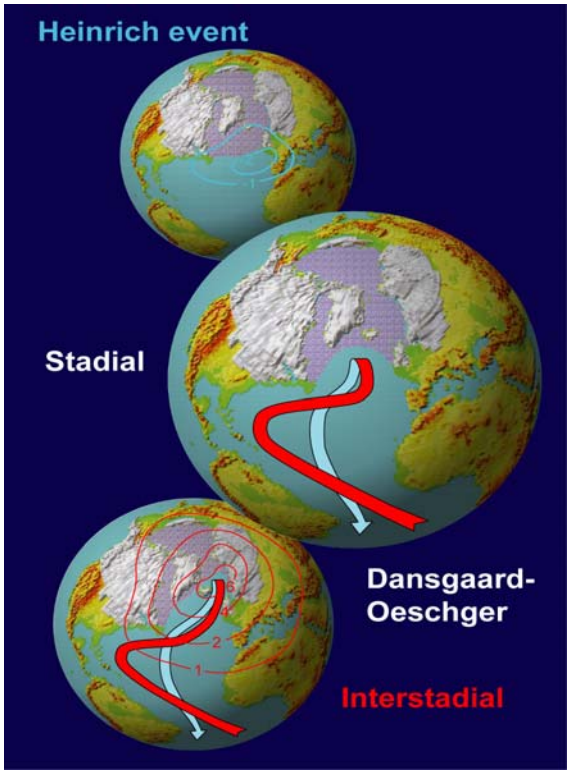

Figure 1.1.7. Thermohaline circulation during D-O and Heinrich [*Ganopolski and Rahmstorf*, 2001]. During Heinrich events deep water formation in the North Atlantic ceased / was highly reduced (top scheme)
During stadial phases, which are not Heinrich events, the main convection area for glacial deep water formation shifted southwards – south of the Iceland - Faeroe ridge. (middle scheme)
During interstadials, deep water convection occurred in the Nordic Seas - similar to present (bottom scheme).

The changes in the thermohaline ocean circulation in the North Atlantic are considered to be one of the key mechanisms which might amplify an initial climatic signal (e.g. [*Broecker*, 1994; *Paillard and Labeyriet*, 1994; *Rahmstorf*, 1996]). Once the equilibrium between surface water temperature and salinity of a stable climatic mode is distorted, changes in the Atlantic thermohaline circulation may be produced and these may cause further climatic changes [*Ganopolski and Rahmstorf*, 2001; *Maslin et al.*, 1995; *Seidov and Maslin*, 1999].

The thermohaline circulation is triggered by the SST and salinity gradients of surface water between low and high latitudes. It generates a transporting band of heat (conveyor belt) that includes the formation of deep water masses at high latitudes. Changes in the intensity of solar radiation have often led to variation in thermohaline circulation (THC) as recorded in ocean sediments. This model has been illustrated by [*Broecker and Denton*, 1989] (Figure 1.1.8).

The ocean circulation changes and the thermohaline circulation on orbital time scales, i.e. for the glacial-interglacial cycles, have still many aspects to be clarified. Reconstructions of the rate of deep water formation and Meridional Overturning Circulation during glacial times are still tentative. The latitude of deep water formation

is more important for climate than the overturning rate. Data and some numerical models indicate a southward shift of the main deep water formation sites from the Nordic Seas to a location south of Iceland in the glacial periods, which implies a reduced ocean heat transport into high latitudes and an expansion of sea ice. Models also suggest that these factors could have amplified glacial cooling. During deglaciation, melting ice sheets surrounding the North Atlantic have apparently lead to episodic influx of meltwater into the ocean. The effect of this meltwater on the thermohaline circulation could explain the oscillations and abrupt cold reversals observed in Greenland ice cores during this time, including the Younger Dryas and the 8.2k cold events. This contrasts with the much smoother history of deglaciation found in Antarctic ice cores [*Rahmstorf*, 2006].

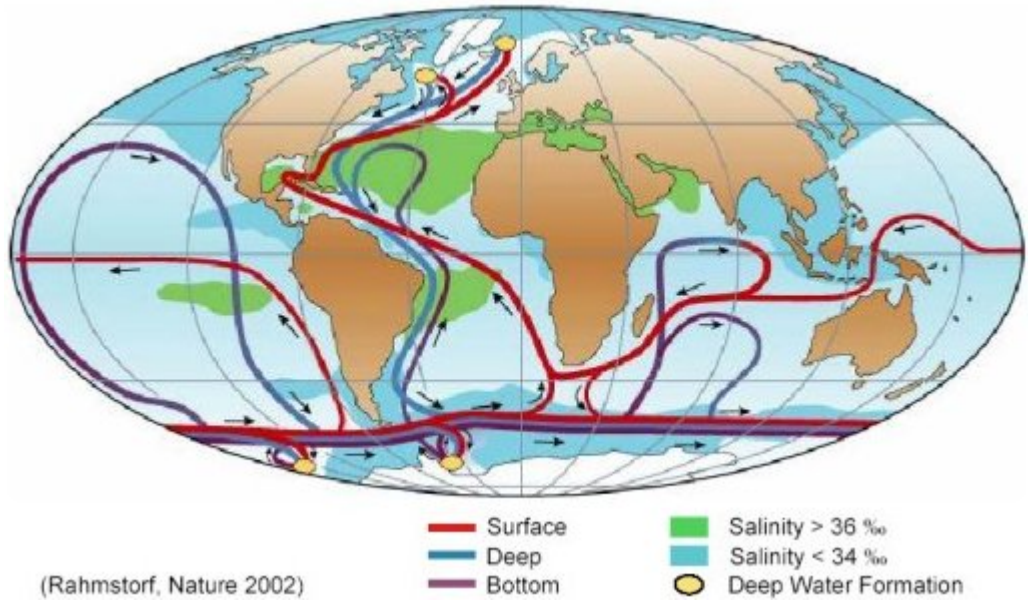

Figure 1.1.8. Schematic representation of the thermohaline circulation. The surface water mass is represented in red, deep currents in light blue and deep waters in dark blue, areas of deep water formation are marked in orange.

The Paleoarchives retrieved in the Antarctic region were crucial to confirm what was known as the bipolar seesaw between the northern and the southern hemispheres.

One of the pressing questions was where the centers of activity responsible for the abrupt climate changes observed in the north Atlantic were located. A simple mechanical analogue suggests that the system might react like a seesaw to perturbations

occurring in the north [*Stocker*, 1998] (e.g. meltwater from the continental ice sheets); consequently, the magnitude of climate warming events is considerable in the north Atlantic, whereas events in the southern hemisphere are inversely weak in magnitude and show a cooling trend; this situation could also be the reverse i.e. cooling events in the north occur simultaneously to a warming in the south. Results from Greenland and West Antartic paleotemperature for the last 90 000 years show the in general, Antarctic temperatures increased gradually while Greenland temperatures were decreasing or constant, and the termination of Antarctic warming was apparently coincident with the onset of rapid warming in Greenland [*Blunier and Brook*, 2001].

1.2. Main Objectives and Motivation

The Holocene is the most recent climate period of the Earth history, the one we live in today. It started about 11,5 ka ago, after the last glacial period. For a long time paleoceanographic studies considered that the Holocene interglacial had been also a period of remarkably stable climate. However, an apparent long-term cooling trend driven by northern high latitude summer insolation was observed in studies published in 2002 onward [*Andersen et al.*, 2003; *Marchal et al.*, 2002; *Moros et al.*, 2004]. This general cooling trend generally started during or after the Holocene thermal maximum (HTM), a period that is observed at the beginning of the Holocene in marine sites and Greenland ice cores [*Andrews and Giraudeau*, 2002; *Duplessy et al.*, 2001; *Kaufman et al.*, 2004; *Knudsen et al.*, 2004; *Marchal et al.*, 2002; *Vernal et al.*, 2005] but at different time periods depending on the studies sites [*Kaufman et al.*, 2004], on a later time period [*Bauch et al.*, 2001; *Dahl-Jensen et al.*, 1998; *Johnsen et al.*, 2001; *Kaplan and Wolfe*, 2006; *Kaufman et al.*, 2004; *Keigwin et al.*, 2005; *Levac et al.*, 2001; *Solignac et al.*, 2004].

Besides this long-term cooling pattern, several sub-orbital millennial scale climatic oscillations have been observed (e.g. [*Bond et al.*, 1997; *Mayewski et al.*, 2004]. The global impact, amplitude, periodicities and causes triggering these short-lived climate oscillations have been discussed in the last decade (e.g.[*Bianchi and McCave*, 1999; *Bond et al.*, 2001; *Keigwin et al.*, 2005; *Mayewski et al.*, 2004]. The most extreme short-lived Holocene cold episode, first noted in the Greenland Ice cores [*O'Brien et al.*, 1995] and known as the “8.2 event” [*Alley et al.*, 1997], is related with

changes in surface and deep waters of the North Atlantic Ocean, and on the climate of Europe, the Americas, Africa and Asia [*Alley and Ágústsdóttir*, 2005]. In contrast, the millennial scale climate changes after the "8.2 event" (Mid- and Late-Holocene) have not left a global record and there is no consensus on the amplitude and frequency of these oscillations. For example, following the last stages of the Laurentide ice sheet decay, at around 8 ka, climate oscillations became relatively modest [*Keigwin and Boyle*, 2000] since freshwater input into the North Atlantic region was probably negligible [*Mayewski et al.*, 2004]. Nevertheless, although the amplitude of natural climate fluctuations was somehow weaker after the "8.2 event", they were strong enough to affect human societies, as historically documented for the Little Ice Age (LIA) and the Medieval Warm Period (MWP).

Recent studies on previous climatic cycles showed that millennial-scale variability is an inherent pattern of the Late Pleistocene climates affecting glacial periods [*Bond et al.*, 1993; *Bond and Lotti*, 1995; *Dansgaard et al.*, 1993; *Grootes et al.*, 1993] but also intervals of reduced ice volume, such as the current or the last interglacial period [*Bond et al.*, 1997; *Delmotte et al.*, 2004; *EPICA*, 2004; *Martrat et al.*, 2004; *Martrat et al.*, 2007; *McManus et al.*, 1999; *Oppo et al.*, 1998].

The last glacial period is characterized by strong millennial-scale climate variability. This variability has also been observed during MIS 1, which includes the Last Glacial-Interglacial Transition (LGIT 15 500 - 11 500 cal years BP) and the Holocene (last 11 500 cal years BP) [*Lowe et al.*, 2008]. This transition phase, LGIT, is characterized by a maximum of summer insolation and a strong reduction of the ice volume in the high latitudes. Although the orbital conditions were favoring the last interglacial inception, the LGIT was punctuated by a series of abrupt climatic oscillations. Extreme cold episodes such as the Younger Dryas have been recorded in most of the northern hemisphere marine sedimentary archives. This episode is attributed to the catastrophic drainage of the proglacial Lake Agassiz [*Teller et al.*, 2002].

Forecasting the future climatic evolution of the current interglacial period is a great challenge. Therefore it is necessary to determine the evolution of past interglacials and evaluate the response of the different components of the Earth's climatic system [*Desprat et al.*, 2007]. For a long period, paleoceanographic studies have considered that MIS 11 (400,000 yr ago) is a better analogue of our current status than any other

more recent interglacial due to the similar orbital situation. Accordingly, recent studies have shown similarities between the Holocene and MIS11 records [*Abreu et al.*, 2003a; *EPICA*, 2004; *Loutre and Berger*, 2003; *McManus et al.*, 2003; *Ruddiman*, 2005]. However, MIS 11 stands out as unique since it, exhibits warm interglacial climatic conditions for an interval of at least 30 ka, a duration twice as long as the most recent interglacial stages [*Loutre and Berger*, 2003; *McManus et al.*, 2003]. Sea level, ocean temperature, salinity and ice isotopic composition were similar to those of the Holocene [*McManus et al.*, 2003]. However, comparison of MIS 1 and MIS 11 will change depending on the astronomical analogy used for comparison (Figure 1.2.1). Synchronization of the two intervals using the precessional variations in insolation at 65º N. Show that the present should correspond to 398 ka [*Loutre*, 2003; *Loutre and Berger*, 2003] but aligning terminations I and V in the δD of Epica Dome C record suggests that today should correspond to ~407 ka [*EPICA*, 2004]. This alignment was done using synchronization with the obliquity and was justified because obliquity changes triggered deglaciation during intervals of weak precessional signal (e.g. MIS 11 and MIS 1) [*Masson-Delmotte et al.*, 2006].

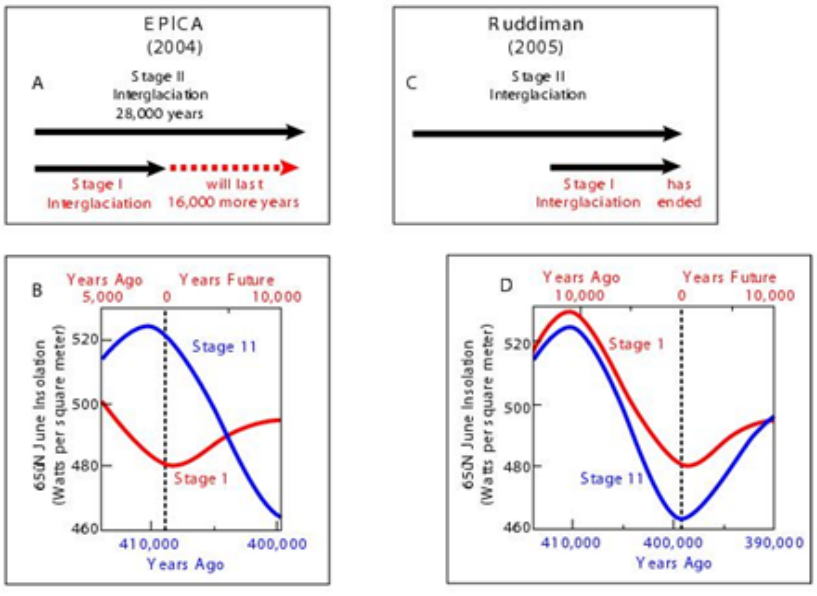

Figure 1.2.1. Diagram illustrating the different approaches used to compare the MIS 1 (Holocene) to the MIS 11(www.realclimate.org/Rudd_fig.jpg).

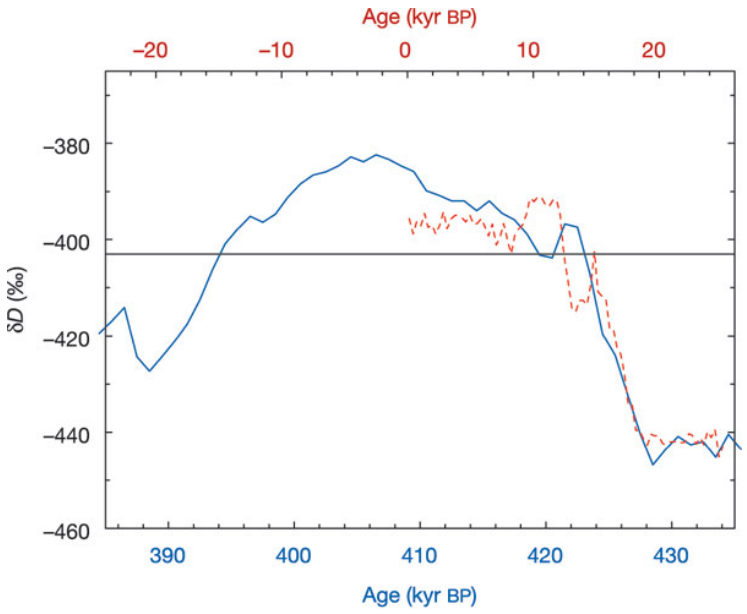

Figure1.2.2. Comparison of Termination V plus MIS 11 with Termination I plus Holocene. δ*D* data for MIS 11 (1-kyr averages) are shown as a solid blue line using the lower *x* axis; data for the Holocene are shown as a dashed red line using the upper *x* axis [*EPICA*, 2004].

The precessional alignment suggests that the Holocene is near its end while the obliquity alignment suggests that it will take 12 ka more to run its course, in the absence of anthropogenic interferences [*Tzedakis*, 2009]. A better understanding of climatic variations during MIS 11 (430 to 360 ka), is needed for a global understanding of climate change during interglacials as well as to foresee future climate change. Furthermore, this period is also important to understand the transition periods (Terminations) such as glacial to interglacial transitions.

Having in mind these antecedents, the present Ph.D thesis is aimed to contribute to a better response to the following question:

1) Which was the ocean-land interaction due to climate variability in the last 2000 years in the Tagus area?

2) How did climate change during the present interglacial in the western Iberian Margin?

3) How the marine and continental environments respond to the rapidly Sea level changes in shallow environmental conditions in the Iberian margin during the LGIT?

4) Did short-lived climate fluctuations persist invariably between 600 and 300 ka? Were they more common during the glacial or interglacial periods?

5) Was the amplitude of these climate oscillations similar to those of the last glacial period?

6) Were sea surface Temperatures (SST) and hydrographic conditions similar during the present Interglacial and MIS 11 in the western Iberian Margin?

The few available long and quantitative SST records already obtained in the North Atlantic [*McManus et al.*, 1999; *Oppo et al.*, 1998] need to be reassessed regarding both the glacial-interglacial variability and the millennial-scale variability. As established by previous researchers, interglacial climate similarities in the North Atlantic during the last five glacial-interglacial cycles [*Ruddiman et al.*, 1989] seem to be peculiar since in other regions interglacial conditions differ considerably between each other [*Bauch and Weinelt*, 1997; *Lyle et al.*, 1992]. In addition, these records are of insufficient resolution to trace short-term climate fluctuations. Evidence of millennial-scale climate variability in the North Atlantic for periods older than 400,000 years is scarce and only represented by few fragmentary data [*McManus et al.*, 1999; *Oppo et al.*, 1998]. Accordingly, the present study aims to reconstruct the climate variability at high resolution recorded from the present and past interglacials in marine sedimentary cores of the western Iberian Margin. SST, productivity and signals of continental influence were generated for the Holocene (last 11.5 ka) and LGIT, and late Pleistocene (580-300 ka), mainly from biomarkers. In particular we:

I) characterize the sediments from the Portuguese Continental Shelf in areas of preferential deposition, by measuring the concentrations of *n*-alkanes, *n*-alkan-1-ols and *n*-alkenones at high resolution and compare the results to the variability recorded in other key areas of the Ocean, to available continental records and also to the Arctic and Antarctic ice cores;

II) use the alkenone unsaturation index ($U^{k'}_{37}$) as a tool to estimate the sea surface temperature (SST) and to explore the potential of this methodology in coastal sediments;

III) reconstruct the terrigenous inputs from the longest river of the Iberian Peninsula, the Tagus River, from the concentrations of *n*-alkanes and *n*-alkan-1-ols;

IV) obtain high-resolution continuous records to unravel the Paleoceanographic and paleoclimatic conditions of the Holocene and the late Pleistocene;

V) quantify the magnitude of climate change in surface waters and evaluate the intensity and speed at which the Tagus River region responded to global climatic oscillations;

VI) sort out the interdependences between climate-dependent surface water changes from those, associated with productivity and/or the ecosystems evolution.

2. MATERIAL

In order to achieve answer to the previously mentioned questions the following cores, have been studied: I) tubes of 2 box core (PO287-26B and PO287-28B), 1 gravity core (PO287-26G) and 2 piston cores (D13902 and D13882) retrieved in the shallow Tagus mud patch. II) 1 box core (PO287-44B) and 1 piston core (MD03-2699) retrieved in the Estremadura spur (Table 2.1 and Figure 2.1).

The PO287 cores were collected during the paleoceanographic cruise on board RV Poseidon in the spring of 2002 [*Monteiro et al.*, 2002]. The piston-cores were collected in 2000 on board RV Discovery during the oceanographic cruise 249 [*Lebreiro*, 2000]. The long piston-core MD03-2699 was collected in July 2003 during the oceanographic cruise Picabia on board RV Marion Dufresne [*Voelker*, 2003].

Table 2.1. Description of the cored sites

Core Ref	Longitude (W)	Latitude (N)	Water depth (m)	Core lenth (m)	Ship	Cruise	Sampler
D13902	9º 20'13'	38º 33'24'	90	6	Discovery	249	Piston corer
D13882	9º 27' 25'	38º 38'07'	88	13,61	Discovery	249	Piston corer
PO287-26 G / 1B	9º 21' 8'	38º 33'5'	96	0,31	Poseidon	PALEO I	Box corer
PO287- 28B	9º30,9'	38º037,5'	105	0,23	Poseidon	PALEO I	Box corer
PO 287- 44B	10º 39,6'	39º02,6'	1866	0,25	Poseidon	PALEO I	Box cores
MD03 - 2699	10º39.63'	39º02.20'	1895	26,56	Marion Duffrene	Picabia	Calypso Corer

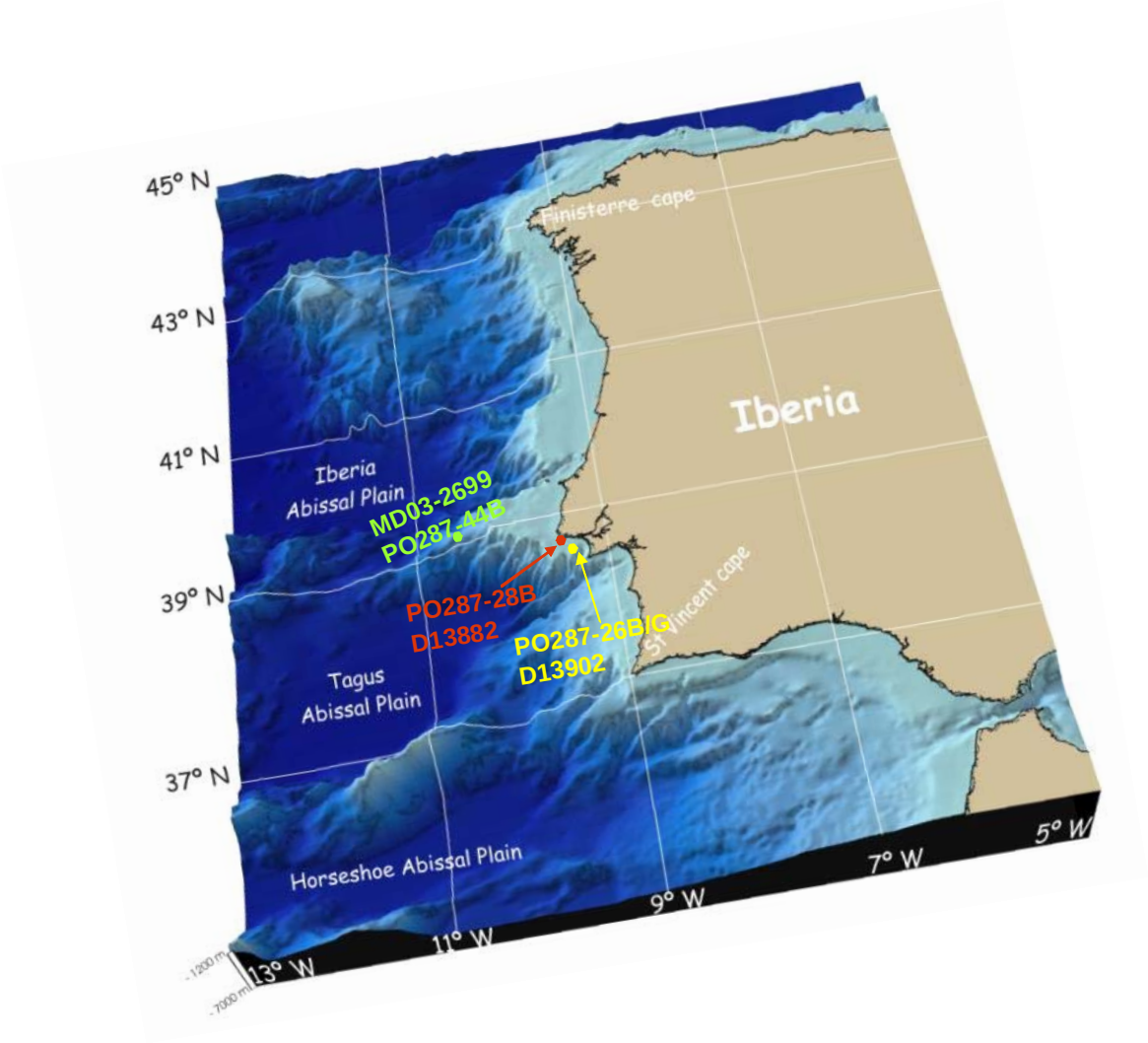

Figure 2.1 Map of southwest Portugal with the location of the sedimentary records used in this study.

The shallow cores allowed a high resolution record of the last 13,5 ka. The deep and long core has permitted the study of the last 580 ka. A complete sedimentary sequence covering the last 2000 years and a resolution of 18 yr have been obtained with the boxcore PO287-26B, the gravity core PO287-26G, and the piston cores D13902 (Table 2.2). This record was extended to the entire Holocene using the piston core D13882 which allowed a resolution that varies between 6.5 and 65 years (Table 2.2). The last deglaciation and the glacial Interglacial transition was studied using core D13882 (6.5 yr resolution) and the deep sea core MD03-2699 (213 yr average resolution) (Table 2.2).

Al the study cores contain hemipelagic silty clays as exemplified by the picture of the long piston core MD03-2699 sediments (Figure 2.2).

Table 2.2. The Resolution of the cores selected for study:

Core ID	Depth interval (cm)	Sedimentation Rate (cm/yr)	Resolution (yr/cm)	Sampling Interval (cm)	Resolution (yr/cm)
D13882	10 - 770	0.09	11	5	55
	770 - 880	0.15	6.5	1	6.5
	880 - 960	0.15	6.5	5	32
	960 - 1351	0.15	6.5	10	65
D13902	0 -583	0.11	9	2	18
PO287-26G	0 -149	0.14	7	2	14
PO287-26B	0 - 31	0.47	2	0.5	1
PO287-28B	0 - 23	0.57	1.75	0.5	0.9
PO287-44B	0 - 27	0.005	190	0.5	95
MD03-2699	0 - 296	0.0142	70	2	140
	1130 - 1260	0.0046	217	2	434
	1260-1280	0.0027	366	1	366
	1280 - 1800	0.0056	179	2	358
	1800 - 1950	0.0059	168	1	168
	1950 – 2654	0.0075	133	2	266

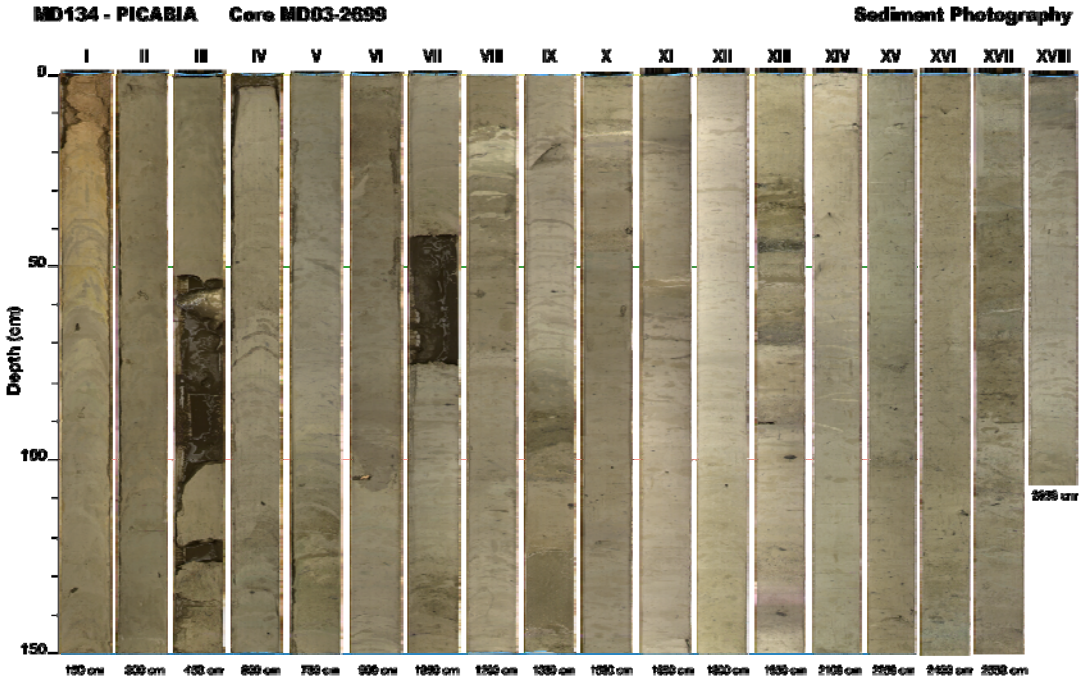

Figure 2.2. Core section photos of MD03-2699.

2.1. Environmental setting

Portugal is located at the southwestern tip of Europe, on the Atlantic margin of the Iberian Peninsula. Its climate is strongly influenced by the climatic and oceanographic processes of the coastal ocean.

In terms of atmospheric circulation the North Atlantic Oscillation (NAO) is, nowadays, the dominant mode of atmospheric circulation over the entire Northern Hemisphere (NH) known to control the climate of the Iberian Peninsula [*Jones et al.*, 2001; *Trigo et al.*, 2002]. Two NAO modes are defined by an Index calculated as the atmospheric pressure difference between Stykkidhólmur (Iceland) and Lisbon (Portugal) [*Hurrell*, 1995]. In NAO positive phases, the strong north-south atmospheric pressure gradient and the clockwise flow around the Azores high-pressure center generate strong coastal upwelling conditions the Portuguese Margin. Negative NAO phases are marked by a weak subtropical high and a weak Icelandic low. The reduced pressure gradient results in more frequent and stronger winter storms crossing on a more west-east pathway that bring moist air to Southern Europe and the Mediterranean and cold air to northern Europe.

According to [*Wooster et al.*, 1976] and [*Fiúza et al.*, 1982] the western Portuguese coast is characterized by seasonal (May- Sept) coastal upwelling. A process associated with the North Atlantic anticyclonic gyre, whose position depends on the location of the Azores anticyclone, and conditioned by the northern wind cycles. The patterns of coastal upwelling offshore Portugal are, however, not only determined by wind strength and direction, the morphology of the coast and the bathymetric features of the shelf and upper part of the continental slope are also very important [*Fiúza*, 1983]. The upwelled water reaches the surface quite close to the coast and can extend offshore reaching 30-50 km from the coast in calm conditions. In periods of strong northern winds the area of upwelling influence can reach 100-200 km [*Fiúza*, 1983]. Upwelled water temperature varies from 13ºC in March to 22ºC in August [*Oliveira et al.*, 1996]. This seasonal upwelling generates high primary production, major phytoplankton blooms and the predominance of diatoms [*Abrantes and Moita*, 1999; *Moita*, 2001] so that the species associated with these waters are good indicators of the upwelling conditions.

During winter the prevailing winds are from South being associated with a center of low pressure located west of the Iberian Peninsula [*Fiúza*, 1983]. The current on the surface is relatively warm, heading out to North along the west coast of Portugal and the coasts of northwestern Spain. This current is called Portugal Countercurrent, it is visible on satellite images and occupying the first 200 to 300 meters in the water column [*Fiúza et al.*, 1998; *Sousa and Bricaud*, 1992].

In terms of water column it can be divided in 3 vertical layers: upper, intermediate and deep. The top layer includes waters to a depth of 500m. The first 100 to 200 m encompasses a superficial layer where all kind of interactions between the ocean and atmosphere occur (solar radiation, evaporation, the wind surface area, precipitation and discharge of rivers). Below the surface layer there is a "Central Water" originated by convection during the winter: 1) The East North Atlantic Central Water with subtropical characteristics (ENACWst) that is formed along the Azores front, 2) The Eastern North Atlantic Central Water with sub polar characteristics (ENACWsp) which originates in the northern Iberian Peninsula, and that constitutes the upwelling source water [*Fiúza et al.*, 1998; *Rios et al.*, 1992] .

The intermediate layer extends from 500 to 1500 m. In the Portuguese coastal ocean, this layer is located just below the ENACW and filled by the Mediterranean Water (MW). The evaporation of water in the Mediterranean area facilitates the entry of Atlantic waters, less salty and dense, through the Gibraltar Straits, boosting the outflow of a saltier and denser Mediterranean water in-depth as a high speed stream (Mediterranean Outflow Water, MOW). The Mediterranean water loses much of its high density and salinity through mixing with the Atlantic waters in the Gulf of Cadiz. This intermediate Mediterranean water flows to the north, reaching the Norwegian Sea and the coast of Canada. Along the Iberian Continental Margin it is a contour current, formed by a narrow strip of about 100 km wide, centered at two main levels of movement: the first between 600 and 900 m, a second between 1100 and the 1200 m depth, and there is also existence of a third branch centered around the depth of 400 m [*Ambar*, 1982; *Haynes and Barton*, 1990]. The deeper layer, below 1500 m, is mainly occupied by oxygen-rich deep-water masses originating from North Atlantic Deep Water (NADW) (Figure 2.1.1). The influence of this water in deeper zones, below is counter-balanced by Antarctic Bottom Water (AABW) that appears to became dominant in most time of the glacial periods [*Martrat et al.*, 2007].

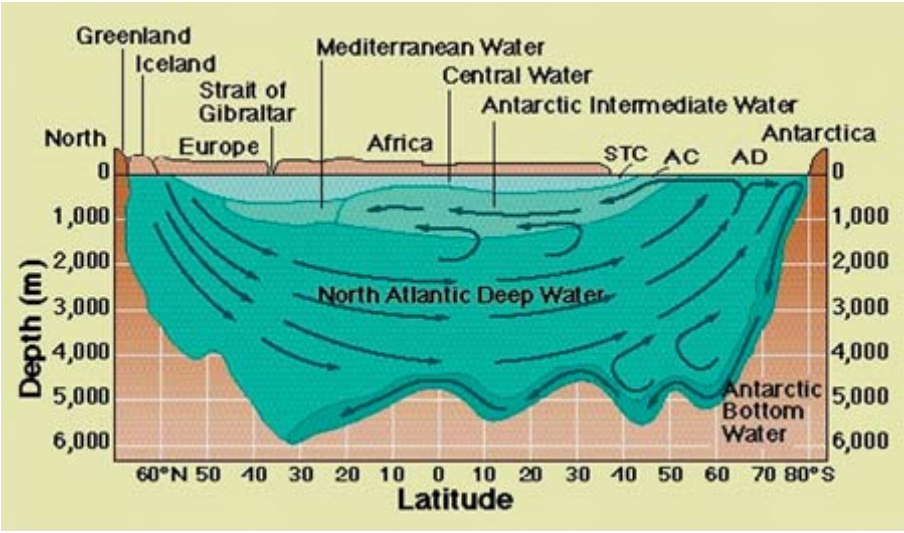

Figure 2.1.1 Scheme of the Atlantic Ocean Circulation. The North Atlantic deep water, the intermediate AAIW (Antarctic Atlantic Intermediate Water) and the Antarctic Bottom Water (AABW). The arrows indicate the direction of the movement of the water masses. Subtropical convergence (STC), Antarctic Convergence (AC) and the Antarctic divergence (AD).(from http://geology.uprm.edu/Morelock/GEOLOCN_/dpseabiogenic.htm)

The study area is located in the Portuguese continental shelf near the most western part of Europe, immediately to the north of the Lisbon and Setubal submarine canyon (Figure 2.1.2). It is a region heavily influenced by the specific characteristics of the basin and the Tagus River outflow which directly connected to NAO (North Atlantic Oscillation) conditions. The sedimentary sequences collected in the Tagus Prodelta, given the high accumulation rates, afford high resolution studies on the effect of global climate variations on the local circulation and the river Tagus regime and their consequences.

Rivers have a very important role in the transference of dissolved and particulate matter from the continents to the ocean. Generally, the export of material by the rivers occurs mainly in suspension with specific dynamics for each river system, which depends on physical, chemical, biological and geological factors.

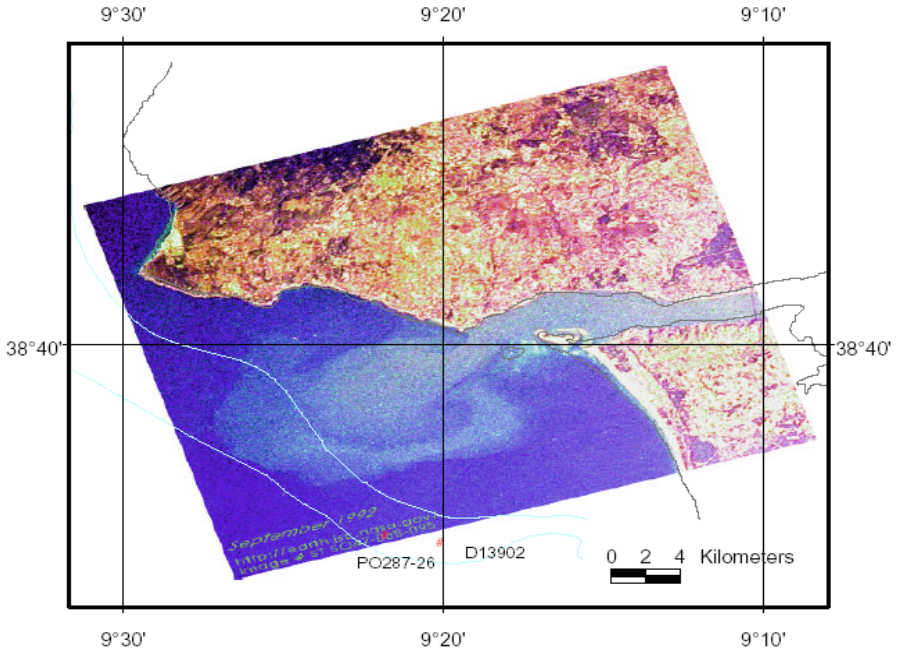

Figure 2.1.2 Plume of suspended sediments brought out by the Tagus River. This plume covers the area of thin and organic rich sediments showing the existence of a zone of preferential deposition for these materials. (Adapted from [*Abrantes et al.*, 2005]).

The specific characteristics of each river basin, such as climate, vegetation, geomorphology and rock and soil mineralogical composition, are determinant for the quantity and composition of the material carried by a river. Thus the areas of sediment accumulation contain well defined records of the changes of these factors through time [*Milliman and Syvitski*, 1992].

In recent years, the river natural regime has been altered by construction of large dams and increased water consumption, both in Spain and Portugal, which have resulted into a significant decrease in river flow [*Benito et al.*, 2003].

The estuary receives an average annual flow of around 300 to 400 $m^3s\text{-}^1$, but it can vary between 100 and 1000 m^3s^{-1} depending on the river regulation in Spain. At times, strong precipitation flooding can occur, such as in February 1979 when the largest flood of the century was recorded. During floods, the average flow values were in the order of 12 000m^3s^{-1}, surpassing the annual average value by two orders of magnitude [*Vale*, 1981].

The Portuguese continental shelf between Cape Raso and Cape Espichel occupies an area of about 1600 km^2 and is conditioned by the morphological accidents, including the submarine canyons in Lisbon and Setubal, which involve widths of about

30 km [*Jouanneau et al.*, 1998] increasing in width southwards, from 22 km in front of the Cape Raso to 34 km in front of Cape Espichel [*Monteiro and Moita*, 1971].

Three distinct areas along the Portuguese continental shelf have been recognized [*Fiúza*, 1983], one of them is located between Cabo da Roca and Cabo Espichel and is described as an area of quick transition, where the temperature and salinity change from less than 15ºC and 35.70 in winter to over 19°C and 36.00 in summer. The sediment coverage is marked by bands of sand at 50 and 200 m These sands have a similar composition to that of the coastal sediments, which, according to the same authors, is due to the reduced contribution of the river in sandy material due to the retention of the sand fraction upstream of the estuary [*Monteiro and Moita*, 1971]. The area in light blue in Figure 2.1.2 represents an area of fine sediments accumulation (silt + clay > 80%) and high organic carbon contents (1.4 w%), and defines the zone of preferential deposition of suspended sediments from the Tagus River [*Gaspar and Monteiro*, 1977; *Lima*, 1971].

3. BIOMARKERS: TYPE AND USE

Molecular biomarkers are used in the present study to contribute to the reconstruction of climatic variations. A biomarker is a lipid that contains useful environmental information that, after calibration can be used for the reconstruction of climate features in past geologic times. A biomarker has to have a specific biosynthetic precursor. However, to be useful it has to be resistant to alteration within various sedimentary regimes. The most successful biomarkers used to date are the molecular alkenones of 37 carbon atoms (C_{37}) that are widely accepted by the paleocenographic / paleoclimatic international community as a SST indicators [*Chaler et al.*, 2000; *Conte and Eglinton*, 1993; *Grimalt et al.*, 2000; *Jasper and Gagosian*, 1989; *Mix et al.*, 2000; *Müller*, 1999; *Prahl et al.*, 2000; *Sicre et al.*, 2002].

In the first paleoceanographic studies, information for the reconstruction of the past climatic and oceanographic conditions was only available from the planktonic and benthic microfossil assemblages (foraminifera, coccolitophores, diatoms and radiolaria). That is microorganisms that have a hard shell / skeleton of $CaCO_3$ or opal. The preservation of these tests in the sediments was constituting a useful source of information on the existing environmental conditions at the time of these existence of the organisms. However, marine sediments also contain organic compounds synthesized by these and other non-shelled organisms. New methodologies to investigate these organic materials and other, generally lipids, as possible molecular marker of environmental conditions were developed in the 90s. [*Brassell*, 1993; *Eglinton et al.*, 1992; *Marlowe et al.*, 1984a; *Poynter and Egliton*, 1990; *Rosell-Melé et al.*, 1994; *Villanueva*, 1996]. Given the resistance of biomarkers to dissolution, their abundance in the sediments can also be used as indication of the production of the precursor organisms (Figure 3.1). However, other control factors need to be considered, such as the efficiency of transport mechanisms, and preservation conditions in the deposition environment. In the present study the following biomarkers have been identified and quantified.

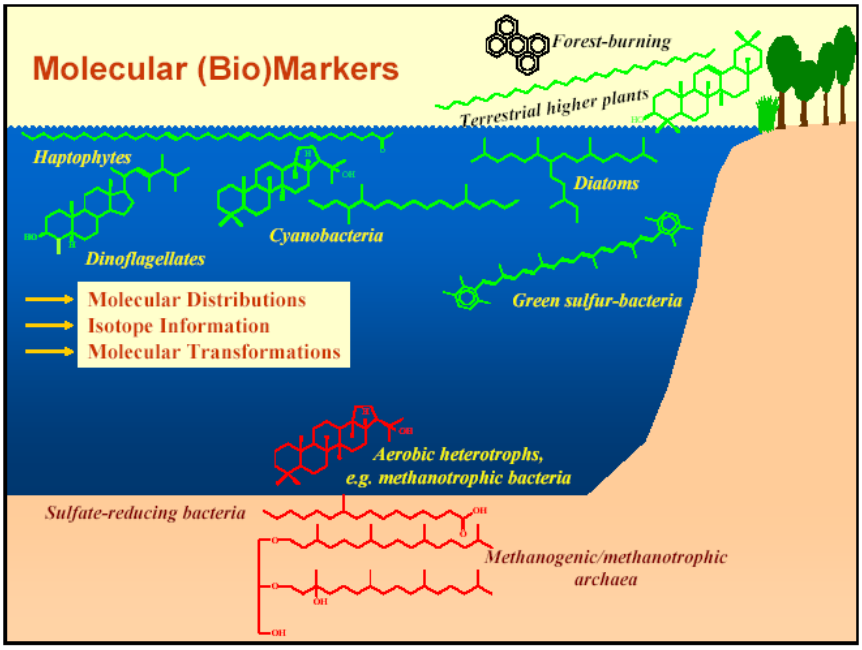

Figure 3.1. Common biomerkers in marine sediments, illustration from Marine Organic Geochemistry [*Eglinton*, 2005].

3.1. Alkenones

The Haptophyte algae are a class of unicellular autotrophic marine organism. At present, these algae constitute one of the most important phytoplankton group in the oceans. The most abundant are the coccolithophores which are photosynthetic organisms and consequently their habitat is restricted to the photic zone. In this class, the cocolitophore *Emiliania huxleyi* is the dominant species since 73 ka. This is a cosmopolitan eurythermal species with a wide oceanographic distribution [*Conte et al.*, 1998; *McIntyre and Bé*, 1967; *McIntyre et al.*, 1970; *Okada and Honjo*, 1973; *Okada and McIntyre*, 1979], with a high tolerance to temperature (1 to 31ºC) and salinity (10 to 45). Thus, it can be found from sub-polar to equatorial regions, occasionally developing dense blooms [*McIntyre et al.*, 1970; *Winter et al.*, 1994] (Figure 3.1.1).

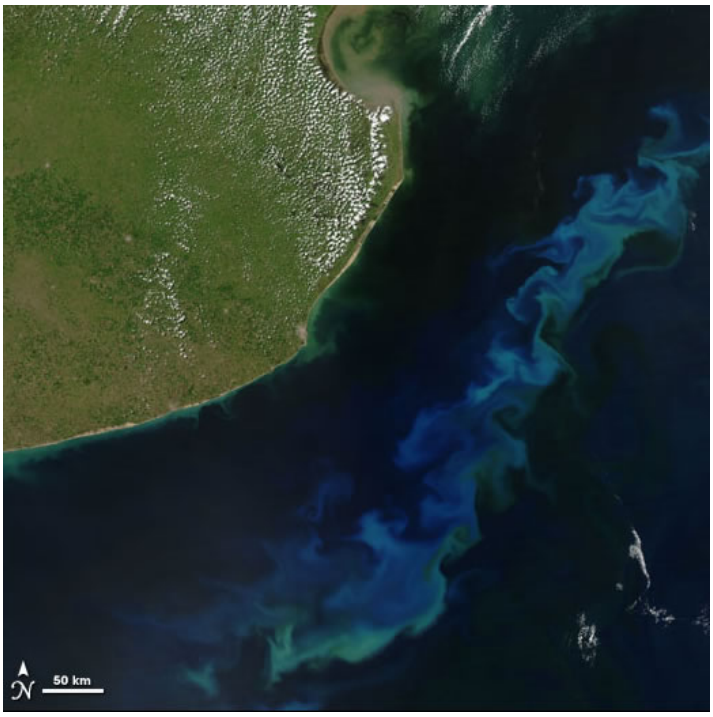

Figure 3.1.1. Marine phytoplankton bloom observed from a NASA satellite. This image shows a blue green swirl in this from the coast of Argentina. These colors are created by light reflection from chlorophyll and other pigments contained within billions of tiny plants (phytoplankton) growing in the surface waters. This bloom is sustained by nutrients brought to the ocean by freshwater rivers carrying nutrients into the ocean.

This species is important in the carbon cycle, since they fix dissolved CO_2 to synthesize carbonate plates (coccoliths) and they also synthesize a the C_{37} alkenones that are preserved in the marine sediments [*Volkman et al.*, 1980].

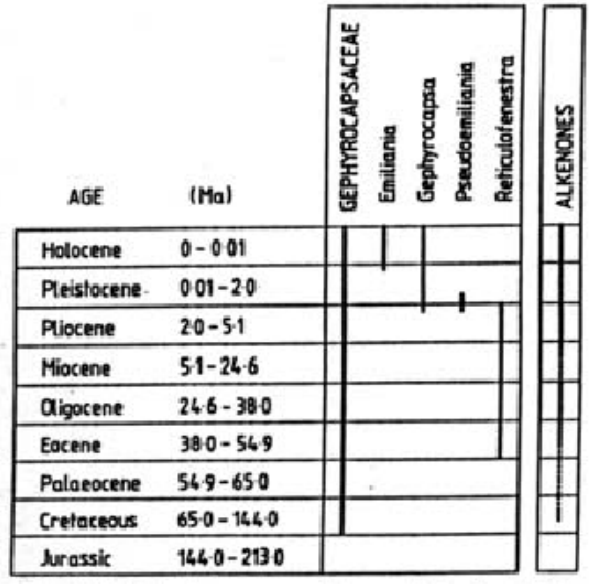

Figure 3.1.2. Temporal distribution of different species of the *Gephyrocapsaceae* family, [*Farrimond et al.*, 1986]

Alkenones have been found in most oceans, including Antarctic seas, as well as lakes and salt marshes [*Brassell*, 1993; *Li et al.*, 1996; *Volkman et al.*, 1988; *Zink et al.*, 2001] They are found since the cretaceous 144 MA ago (Figure 3.1.2). Besides E. *huxleyi* alkenones are also synthesized by other algae of the family *Gephyrocapsaceae* but limited to the class Haptophytea [*Marlowe et al.*, 1984b; *Marlowe et al.*, 1990; *Volkman et al.*, 1995].

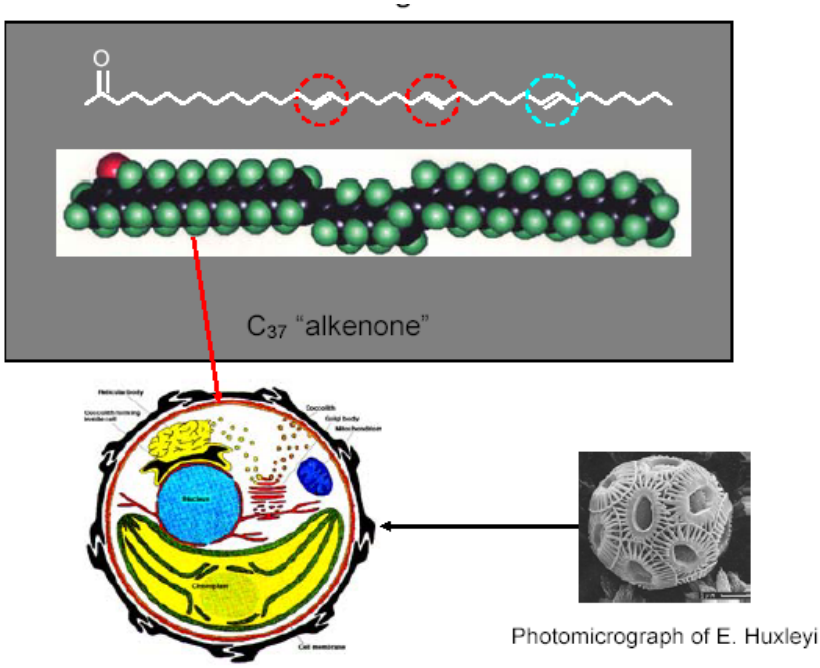

Figure 3.1.3. Photomicrograph of *E. Huxley*, and scheme of a cell and a chain of a tri unsaturated alkenone. From [*Eglinton*, 2005]

Alkenones are linear methyl-etylketones with 37 to 42 carbon atoms, containing two, three or four unsaturations (Figure 3.1.3). In the sediments, the most abundant alkenones are those with 37 and 38 carbon atoms (Figure 3.1.4).

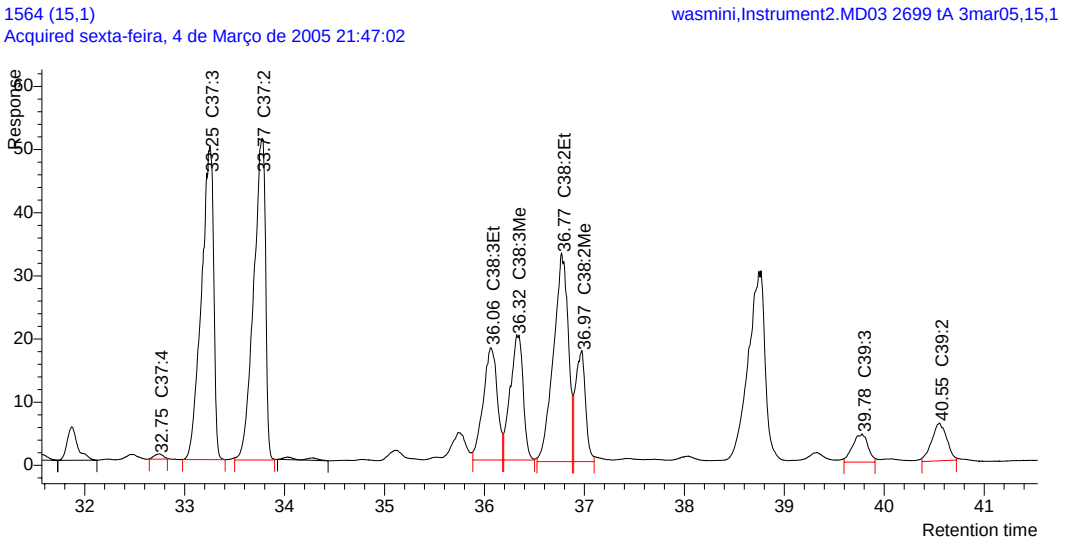

Figure 3.1.4. Distribution of alkenones in a sample at 1564 cm depth in the core MD03 2699.

The alkenones most abundant found in the sediments are those presented in table 3.1.1 among these the C_{37} alkenones are those used for paleoclimatic applications.

Table 3.1.1. Identification and chemical structures of the ketones with 37, 38 and 39 carbon atoms with two, three or four unsaturations (di $C_{n:2}$; tri $C_{n:3}$ and tetra $C_{n:4}$ alkenones).

Name and Structure of the compound	Short name	molecular Ion
heptatriaconta-8E,15E,22E,29E-tetraen-2-one 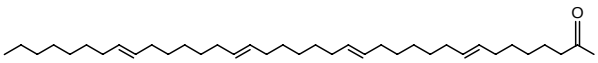	$C_{37:4}$Me	526
heptatriaconta-8E,15E,22E-trien-2-one 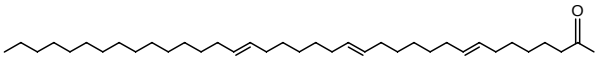	$C_{37:3}$Me	528
heptatriaconta-15E,22E-dien-2-one 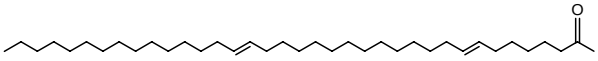	$C_{37:2}$Me	530
octatriaconta-9E,16E,23E,30E-tetraen-3-one 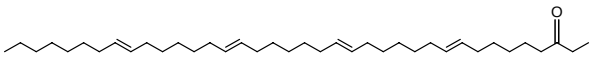	$C_{38:4}$Et	540
octatriaconta-9E,16E,23E-trien-3-one 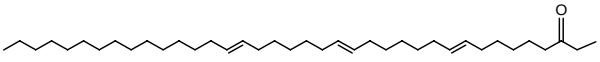	$C_{38:3}$Et	542
octatriaconta-8E,15E,22E-trien-2-one 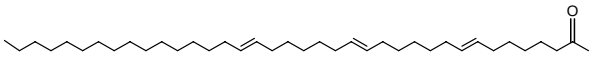	$C_{38:3}$Me	542
octatriaconta-16E,23E-dien-3-one 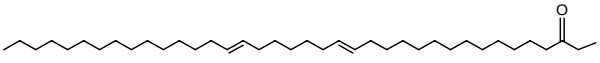	$C_{38:2}$Et	544
octatriaconta-15E,22E-dien-2-one 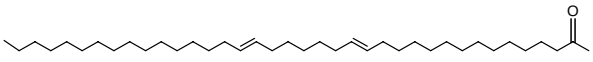	$C_{38:2}$Me	544
nonatriaconta-8E,15E,22E-trien-2-one 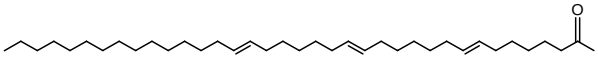	$C_{39:3}$Me	556
nonatriaconta-15E,22E-dien-2-one 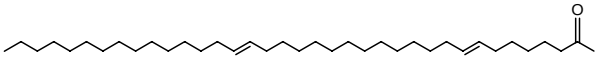	$C_{39:2}$Me	558

The chemical configuration of the alkenones has given to them a good resistance to depositional degradation. In addition, no selective degradations between tri and diunsaturated alkenones has been observed [*Rechka and Maxwell*, 1988; *Volkman et al.*, 1980].

The relative composition of the alkenones synthesized by the Haptophyte algae is strongly related to the temperature of the environment in which they were synthesized. In cold conditions, these organisms generate higher relative amounts of the more unsaturated forms ($C_{37:3}$ and $C_{37:4}$), while in temperate environments the unsaturation degree decreases and it prevails the di-unsaturated compound ($C_{37:2}$).

Laboratory experiments with *E. huxleyi*, cultures proved this relationship and allowed the definition of an unsaturation index U^{k}_{37} [*Brassell et al.*, 1986].

$$U_{37}^{K} = \frac{[C_{37:2}] - [C_{37:4}]}{[C_{37:2}] + [C_{37:3}] + [C_{37:4}]}$$

where $C_{37:2}$, $C_{37:3}$ and $C_{37:4}$ are the concentrations of the alkenone with 37 carbon atoms and 2, 3 and 4 unsaturations, respectively. [*Prahl and Wakeham*, 1987] proposed a simplified index $U^{k'}_{37}$ in which the tetra-unsaturated alkenone, was eliminated given its generally very low concentrations.

$$U_{37}^{K'} = \frac{[C_{37:2}]}{[C_{37:2}] + [C_{37:3}]}$$

The linear relationship between the unsaturation index and the water temperature of the cultures was:

$$U_{37}^{K'} = 0{,}040 \times T - 0{,}110 \qquad r = 0.989$$

Where T is temperature.

This calibration was valid for temperatures between 8 and 25ºC [*Prahl and Wakeham*, 1987; *Prahl et al.*, 1988].

Subsequent studies, with particulate matter, led to minor modifications of this initial calibration equation [*Brassell*, 1993; *Sikes and Volkman*, 1993]. Besides regional calibrations were also performed in different study areas [*Conte et al.*, 1992; *Conte and Eglinton*, 1993; *Ternois et al.*, 2001].

Other calibrations have been performed using measurements of superficial sediments and instrumental sea surface temperature (SST - Sea Surface Temperature) compiled from oceanic databases. These calibrations have been performed in the: North Atlantic Ocean [*Conte et al.*, 1992; *Rosell-Melé et al.*, 1995], North Pacific [*Herbert et al.*, 1995; *Prahl and Wakeham*, 1987], the South China sea [*Pelejero et al.*, 1997] and Indian Ocean [*Sonzogni et al.*, 1997]. In all case similar calibration have been obtained.

In 1998 *Müller et al.* analyzed the different existing calibrations, and proposed a global calibration for all the oceans between the 60ºN and the 60ºS and from 0 to 29ºC (Figure 3.1.5),

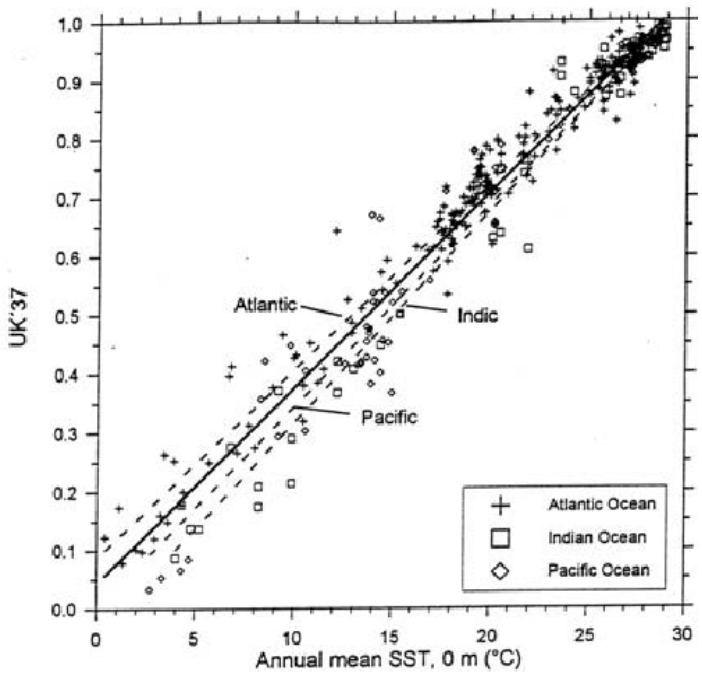

Figure 3.1.5. Calibration using $U^{k'}_{37}$ in core tops and instrumental SST proposed by [*Müller et al.*, 1998].

The resulting equation was:

$$U_{37}^{K'} = 0{,}033 \times SST - 0{,}044 \qquad R = 0{,}958$$

This linear relationship between the unsaturation index and SST is the one adopted in the present work.

The alkenones are one of the better preserved lipid compounds in the sediments, due to this long chain of carbon atoms, low water solubility and the configuration of the double bounds [*Grimalt et al.*, 2000; *Teece et al.*, 1998; *Volkman et al.*, 1983].

The main advantages in using this index for SST determinations are follows:

i) The index is not affected by post depositional organic matter transformation, even if the concentration of total alkenones are decreased as consequence of these processes the $U^{K'}_{37}$ index remains unalterated because both $C_{37:2}$ and $C_{37:3}$ are degraded equally [*Prahl and Muehlhausen*, 1989].
ii) The index remains unaffected even under different $CaCO_3$ dissolution conditions [*Sikes et al.*, 1991]. The $U^{K'}_{37}$ method allows SST determination of sediments located below the lysocline
iii) SST estimates are independent of environmental variation, such as nutrient concentrations, the heatstroke, water oxygenation and salinity [*Pelejero et al.*, 1997].
iv) The $C_{37:2}$ and $C_{37:3}$ alkenones are major constituents of the neutral lipid portion of marine sediments which possibilities the determination of $U^{K'}_{37}$ ratios when small amounts of sediments are available or even in sediments with low organic mater content.

3.2. Alkanes and alkohols

The n-alkanes and n-alcohols are long linear chain lipid molecules that mostly originate from the cuticles of the vascular plants [*Eglinton and Hamilton*, 1967] (Figure 3.2.1). The cuticle is a wax layer, impermeable and mechanically resistant, that covers the epidermis cells of the leaves providing protection against dissection and bacterial attacks. The resistance to degradation of cuticular wax *n*-alkanes and *n*-alcohols allow their detection in sediments of all the oceans. They are air transported in

association with aerosols in oceanic sediments [*Gagosian et al.*, 1987; *Poynter et al.*, 1989].

In areas close to the coast line the transport of these compounds is mainly due to river discharge or to the erosion of the continental shelf, and can also be affected by sea level changes [*Pelejero et al.*, 1999; *Prahl et al.*, 1994].

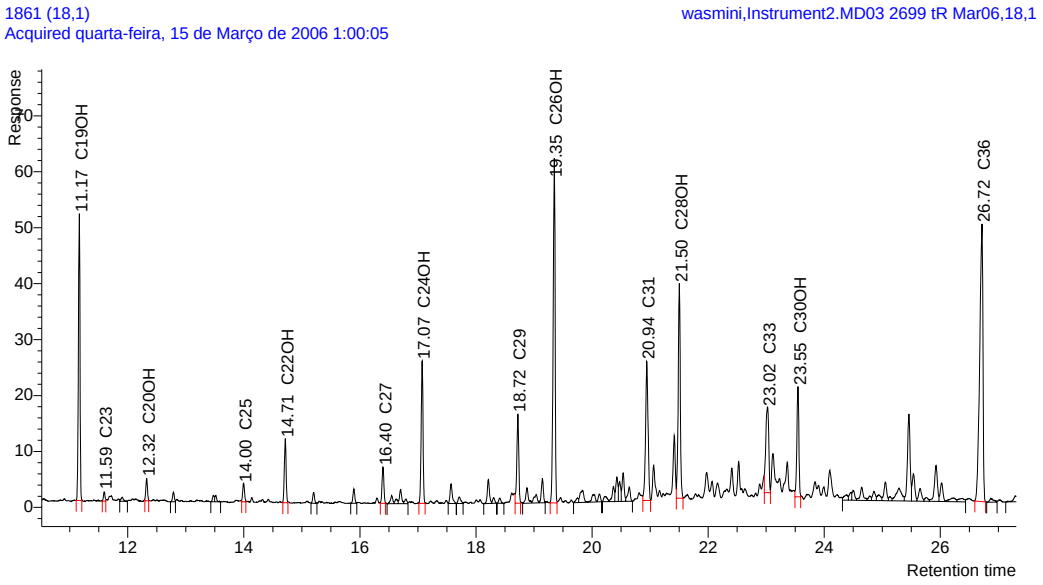

Figure 3.2.1. Example of the distribution of *n*-alkanes and *n*-alcohols in core MD03 2699 retrieved at 1861cm water depth.

3.2.1. Alkanes

The marine sedimentary mixtures of these compounds have linear distributions of straight-chain homologues usually in the range of C_{13} to C_{40}. Alkanes synthesized by higher plants exhibit homologues series of linear chain C_{21} to C_{33} alkanes with odd carbon number preferences particularly among the C_{27}, C_{29} and C_{31} homologues [*Brassell*, 1993].

Table 3.2.1. Common n-alkanes found in marine sediments

Coumpound name	**Empirical formula**	molecular Ion
Heneicosane	$C_{21}H_{44}$	296
Docosane	$C_{22}H_{46}$	310
Tricosane	$C_{23}H_{48}$	324
Tetracosane	$C_{24}H_{50}$	338
Pentacosane	$C_{25}H_{52}$	352
Hexacosane	$C_{26}H_{54}$	366
Heptacosane	$C_{27}H_{56}$	380
Octacosane	$C_{28}H_{58}$	394
Nonacosane	$C_{29}H_{60}$	408
Triacontane	$C_{30}H_{62}$	422
Hentriacontane	$C_{31}H_{64}$	436
Dotriacontane	$C_{32}H_{66}$	450
Tritriacontane	$C_{33}H_{68}$	464
Tetratriacontane	$C_{34}H_{70}$	478
Hexatriacontane	$C_{36}H_{74}$	506
Tetracontane	$C_{40}H_{82}$	562

Several ratios among these *n*-alkanes homologues are useful to get insight into the origins of the *n*-alkane distributions

Average chain length:

$$ACL = \frac{27[C_{27}] + 29[C_{29}] + 31[C_{31}]}{[C_{27}] + [C_{29}] + [C_{31}]}$$

The higher values are associated with vegetation from warm regions while the lower values are associated with plants from cold regions [*Poynter and Egliton*, 1990]

Hydrocarbon Vegetation Index:

$$HVI = \frac{[C_{27}]+[C_{29}]}{[C_{31}]}$$

Grass and herbaceous plants in which n-hentriacontane is more abundant have an HVI Index < 1. Vegetation patterns mainly associated with trees, are dominated by *n*-heptacosane and *n*-nonacosane and the HIV is >1 [*Cranwell*, 1973; *Maffei*, 1996; *Maffei et al.*, 2004]. HVI index together with other geochemical records (e.g. elemental carbon, $\delta^{13}C$) can help to trace vegetation changes both spatially and temporally [*Tareq et al.*, 2005].

3.2.2. Alcohols

Unlike the *n*-alkanes, the *n*-alcohols show a distribution with prevalence of even carbon number chain lengths. The most abundant are $C_{22}OH$, $C_{24}OH$, $C_{26}OH$ and $C_{28}OH$. Like the *n*-alkanes these compounds are found in marine sediments as consequence of transport of plant waxes from the continental to the marine environment by eolian, fluvial or ice mobilizations [*Cacho*, 2000; *Calvo*, 2001; *Gagosian et al.*, 1987; *Madureira et al.*, 1997; *Pelejero et al.*, 1999; *Poynter et al.*, 1989; *Prahl and Muehlhausen*, 1989; *Prahl et al.*, 1994; *Villanueva et al.*, 1997].

The relationship between alcohols and alkanes can reflect the intensity of organic mater of degradation. The *n*-alcohols are more unstable and degrade before than the *n*-alkanes [*Madureira et al.*, 1995; *Poynter et al.*, 1989]. In Quaternary sediments in which diagenisis are still at early stages an alcohol preservation index can be defined. This index may be related to the degree of renewal of deep waters since it may carry more oxygen for organic matter degradation.

Thus, the API may ultimately reflect the intensity of deep bottom waters [*Cacho et al.*, 1999; *Matrat et al.*, 2007].

Alcohol preservation Index: $$API = \frac{\sum(C_{24}OH+C_{26}OH+C_{28}OH)}{\sum(C_{24}OH+C_{26}OH+C_{28}OH)+\sum(C_{27}AK+C_{29}AK+C_{31}AK)}$$

Table 3.2.2. Identification of the linear alcohols

Compound name	Empirical Formula	Molecular Ion (M-15)
octadecanol	$C_{18}H_{37}OH$	327
nonadecanol	$C_{19}H_{39}$ OH	341
eicosanol	$C_{20}H_{41}$ OH	355
heneicosanol	$C_{21}H_{43}$ OH	369
docosanol	$C_{22}H_{45}$ OH	383
tricosanol	$C_{23}H_{47}$ OH	397
tetracosanol	$C_{24}H_{49}$ OH	411
pentacosanol	$C_{25}H_{51}$ OH	425
hexacosanol	$C_{26}H_{53}$ OH	439
heptacosanol	$C_{27}H_{55}$ OH	453
octacosanol	$C_{28}H_{57}$ OH	467
nonacosanol	$C_{29}H_{59}$ OH	481
triacontanol	$C_{30}H_{61}$ OH	495
heneitriacontanol	$C_{31}H_{61}$ OH	509
dotriacontanol	$C_{32}H_{65}$ OH	523
tetratriacontanol	$C_{34}H_{69}$ OH	551

4. METHODOLOGY

4.1. Samples extraction and purification

The analytical procedure used for determination and purification of the alkenones, *n*-alkanes and *n*-alkohols is the one applied at the Department of Environmental Chemistry of the Institute of Environmental Assessment and Water Research. This methodology was developed and optimized elsewhere [*Villanueva*, 1996; *Villanueva and Grimalt*, 1997; *Villanueva et al.*, 1997].

The used methodology can be described by the following steps:

1- Freeze dry and sample homogenization:

Samples were rapped in aluminum foil and freeze-died for 24 h. This method allows efficient evaporation of the interstitial waters and avoid heating of the sediment. Sample homogenization was then performed manually. Approximately 2g of sediment were weighed.

2- Standard addition

A solution of *n*-tetracontane, *n*-hexatriacontane and *n*-nonadecanol-1-ol (10 or 20 μl) was added to the sediments with a microseryinge as internal standard.

3- Extraction

Sediment extraction was done with Dichloromethane (CH_2Cl_2) and vortex stirring and ultrasounds for 15 minutes. This solvent affords 90% recuperation of alkenones and *n*-alkanes and *n*-alcohol [*Villanueva and Grimalt*, 1997]. Samples were then centrifuged for 5 min and supernatant solvent was transferred to another tube were it was evaporated with a gentle nitrogen current at 37ºC temperature. This extraction procedure was repeated 3 times for a better recuperation of the compounds. All the extracts were collected together.

4- Clean-up

Extracts purification was performed using 3 ml of 6% potassium hydroxide dissolved in methanol and 100μl of toluene. The mixture was left to react during 12 hours at room temperature.

The neutral lipid compounds were recovered by liquid-liquid extraction using n-hexane as solvent. This extraction after agitating the mixture with the solvent in vortex and ultrasounds is carried out three times to secure good recuperation. Traces of KOH

were removed by addition of small quantity of Mili-Q water and agitation. Then the hexanic phase was extracted again and concentrated under gentle current of nitrogen. Additional clean up was performed with the box core samples by fractionation through column chromatography columns of 30 cm length and 0.5 cm internal diameter were used. They were packed with 2 g of silica (activated during 12 h at 120ºC) suspended in dichloromethane / n-hexane CH_2Cl_2/hexa (4:1) by three successive volumes of 200-300 µl of the same solvents mixture of solvents. Alkenones and the alkanes were eluted with 10 ml of the above mentioned solvent mixture 10 ml of diclorometane/metanol (9:1). The recovered fractions were evaporated under a gentle nitrogen flow.

5- Derivatization

The evaporated fractions were transported to small conical vials with three volumes of 300 µl of dichloromethane / hexane (8/2). The extracts were evaporated in a Speed-Vac, and derivatized by addition of 60 µl of BSTFA (bistrimetil sillil trifluoroacetamid) diluted in 50% with toluene.

4.1.1. Gas Chromatography with Flame Ionization Detection (GC-FID)

The extracts were analyzed using Varian gas chromatograph GC-3400 equipped with a septum programmed temperature injector (SPI) and a flame ionization detector (Figure 4.2.1). A capillary column CPSIL-5CB capillary column (50 m length, 0.32 mm internal diameter and 0.12 µm stationary phase thickness) used for compound separation. Hydrogen was used as carrier gas. Samples were injected in on-column mode.

The temperature programs were as follows:

Injector: From 90ºC to 310ºC at 200ºC/min and a final holding time of 58 min.

Oven : From 90ºC holding time (min) to 170ºC at 20ºC/min and to 280ºC at 6ºC/min with a holding time of 25 min and then to 315ºC with a final holding time of 12 min.

Detector: Constant Temperature of 320ºC

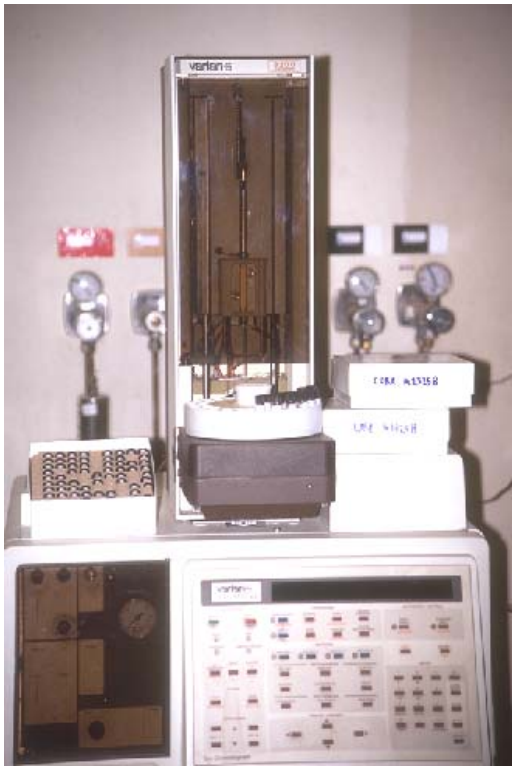

Figure 4.2.1. Varian 3400 –Gás Chromatograph equipped with automatic injector. Department of Environmental Chemistry Institute of Environmental Assessment and Water Research (IDÆA-CSIC).

Figure 4.2.2. Varian 3800 –Gas Chromatograph equipped with an automatic injector, Laboratory of Biogeochemistry of the Marine Geology Unit on LNEG.

Alkenone quantification was performed by comparison of the peak areas with those of n-hexatriacontane peak, using the formula:

$$[Biomar\,\mathrm{ker}]ng/g = \left(\frac{biomar\,\mathrm{ker}\,area}{C_{36}area}\right)\times\left(\frac{ngC_{36}}{dryweight(g)}\right)$$

At UGM-LNEG, a Varian gas chromatograph CP-3800 GC with an Auto Sampler CP-8400 with a standard 100 sample carousel for 2 mL vials, is used and now in full operation (Figure 4.2.2).

% recoveries were calculated as a check of the performance of the analytical method. The following formula was used for the calculations:

$$\%\,\mathrm{Recovers} = 100\times\left[\left(\frac{Am\times Qp}{Ap}\right)/Qm\right]$$

Am- area of the standard in the sample
Ap- area of the standard in the solution
Qp- concentration of the standard in solution
Qm- concentration of the standard in the sample

4.1.2. Gas Chromatography – Mass Spectrometry (GC-MS)

A quadruple mass spectrometer (Thermo Trace GCMS, Thermo Instruments, and UK) was used for compound identification. The GC coupled to this detector was operated with Helium as the carrier gas at a flow of 1 ml/min. The ion source and transfer lines were maintained at 200ºC. Injection was in splitless mode at 280ºC. The capillary column and then oven temperature program were the same as those described for the GC-FID analyses.

4.2. Other methodologies used

4.2.1. Grain size analyses

Samples were introduced in weighed aluminum capsules, of known volume (between 5 to 8 cm^3). They were dried in a stove at 40ºC during 48 hours. This slow drying allowed to withdraw the water without damaging the clay particles. After determining sample dry weight sodium hexametafosfate (calgon 0.033M) was added for particle dispersion sediment particles. Each sample was agitated occasionally during 48h until complete separation.

Organic matter was removed by oxidation with Basic Hydrogen Peroxide (peroxide H_2O_2 130 vol., with some drops of ammonia). This procedure was repeated four times, with increasing volumes of H_2O_2 (25, 50, 50 and 75 ml). Sample were stirred during this process to increase reaction efficiency.

When the reaction was completed samples were put in a water-bath at 60ºC in order to eliminate the H_2 residual, such as exemplified by the chemical reaction:

$$C_x(H_2O)_y + H_2O_2 \Rightarrow CO_2 + H_2O + \uparrow H_2$$

Samples were subsequently washed to remove peroxide traces. The samples washing was performed in a vacuum system with filters composed of porous of diatomite cylinders, and activated coal in their interior. Sediments were washed by 6 successive extractions of 800 ml of distilled water.

Grain separation was done by wet sieving with a 2 mm inox mesh. The 2 mm fraction was subsequently analyzed in a Coulter count analyzer (LS238).

This Coulter may measure particles size between 0.04 and 2000 μm in diameter. This model is equipped with an optical Laser diffraction system and another hemp of polarized light in the horizontal and vertical planes. This system of polarized light is known as P.I.D.S (Polarisation Intensity Differential of Scattered light) and it allows the detection of very small particles, up to 0.04 μm. The characterization method is based on particle shape, and assumes spherical forms. Factor shape was calculated using the ratio of the smallest to the largest diameter:

$$\text{Factor Shape} = (\varnothing <) / (\varnothing >)$$

Grain size data allows the determination of sediment grain composition. That is, the relative proportion of clay (fraction < 4 μm), silt (4 μm < fraction < 63 μm), sand (> 63 μm fraction < 2 mm) and gravel (> 2 mm) present in each sample.

4.2.3. Elemental analyses

Samples elemental composition (C, H, N and S) was determined with a LECO-CHNS-932 analyzer. The instrument uses two methods of detection (manual User CHNS-932 Leco Instrumental, S.A) infrared absorption of for the determination of C, H, S and thermal conductivity for N determination. The gases used for analyses were CO_2, H_2O, N_2 and SOx. They are carried through the system by the helium. The oxidation tubes which are filled with copper removes the excess oxygen and completes the conversion of SOx into SO_2 which measurements are obtained from comparison of the signals obtained in reference and a sample chambers.

Total organic carbon (TOC) was determined by quantification of total carbon. After that, a sample aliquot was heated to 500ºC to burn the organic material in an oven and further analyzed with the elemental analyzer for the specific determination inorganic carbon. TOC contents were calculated by difference between total and inorganic carbon.

5- REFERENCES

Abrantes, F., and M. T. Moita (1999), Water column and recent sediment data on diatoms and coccolithophorids, off Portugal, confirm sediment record of upwelling events, *Oceanologica Acta*, *22*, 319-333.

Abrantes, F., N. Loncaric, J. Moreno, M. Mil-Homens, and U. Pflauman (2001), Paleoceanographic Conditions along the Portuguese Margin during the last 30 Ka: Multiple Proxy Study, *Comunicações Instituto Geológico e Mineiro*, *88*, 161-184.

Abrantes, F., S. Lebreiro, T. Rodrigues, I. Gil, H. Bartels-Jonsdottir, P. Oliveira, C. Kissel, and J. G. O. (2005), Shallow-marine sediment cores record climate variability and earthquake activity off Lisbon (Portugal) for the last 2000 years, *Quaternary Science Reviews*, *24*, 2477-2494.

Abreu, L. d., J. Schonfeld, M. Vautravers, N. J. Shackleton, and F. Abrantes (2003a), High-frequency ocean variations off the Western Iberian Margin during an extreme interglacials: is early MIS 11 equivalent to the Holocene?, paper presented at AGU-EGS-EUG, Joint assembly AGU-EGS_EUG, Nice.

Abreu, L. d., N. J. Shackleton, J. Schonfeld, M. Hall, and M. Chapman (2003b), Millennial-scale oceanic climate variability off the Western Iberian margin during the last two glacial periods, *Marine Geology*, *3297*, 1-20.

Alley, R., Terje Berntsen, Nathaniel L. Bindoff, Zhenlin Chen, Amnat Chidthaisong, Pierre Friedlingstein, Jonathan Gregory, Gabriele Hegerl, Martin Heimann, Bruce Hewitson, Brian Hoskins, Fortunat Joos, Jean Jouzel, Vladimir Kattsov, Ulrike Lohmann, Martin Manning, Taroh Matsuno, Mario Molina, Neville Nicholls, Jonathan Overpeck, Dahe Qin, Graciela Raga, Venkatachalam, Ramaswamy, Jiawen Ren, Matilde Rusticucci, Susan Solomon, Richard Somerville, Thomas F. Stocker, Peter Stott, R. J., Stouffer, Penny Whetton, Richard A. Wood, and D. Wratt (2007), Climate Change 2007: The Physical Science Basis, *Intergovernmental panel on climate Change*.

Alley, R. B., P. A. Mayewski, T. Sowers, M. Stuiver, K. C. Taylor, and P. U. Clark (1997), Holocene Climatic instability: A prominent, widespread event 8200yr ago, *Geology*, *25*, 483-486.

Alley, R. B., and A. M. Ágústsdóttir (2005), the 8k event: cause and consequences of a major Holocene abruot climate change, *Quaternarty Science Reviews*, *24*, 1123-1149.

Ambar, I. J. (1982), Mediterranean influence off Portugal. Actual problems of Oceanography in Portugal, *JNICT /NMSP*, 74-97.

Andersen, A., N. Koç, A. Jennings, and J. T. Andrews (2003), Nonuniform response of the major surface currents in the Nordic Seas to Insolation forcing: Implications for the Holocene climate variability, *Palaeogeography*, *19*(DOI:10.1029/2002PA000873).

Andrews, J. T., and J. Giraudeau (2002), Multi-proxy records showing Holocene oceanographic variability: the inner N. Iceland Shelf (Húnaflói), *Quaternarty Science Reviews*, *22*, 175-193.

Baas, J. H., J. Nienert, F. Abrantes, and M. A. Prins (1997), late Quaternary sedimentation on teh portugueses continental margin: climate-related processes and products, *Paleo*, *130*, 1-23.

Bard, E., F. Rostek, J.-L. Turon, and S. Gendreau (2000), Hydrological Impact of Heinrich Events in the Subtropical Northeast Atlantic, *Science*, *289*, 1321-1324.

Bauch, H. A., and M. S. Weinelt (1997), Surface water changes in the norwegian sea during last deglacial and holocene times, *Quaternary Science Reviews*, *16*(10), 1115-1124.

Bauch, H. A., H. Erlenkeuser, R. F. Spielhagen, U. Struck, J. Matthiessen, J. Thiede, and J. Heinemeier (2001), A multi-proxy reconstrution of the evolution of deep and surface waters in the subartic Nordic seas over the last 30,000yr, *Quaternarty Science Reviews*, *20*, 659-678.
Benito, G., A. Sopena, Y. Sánchez-Moya, M. J. Machado, and A. P.-. González (2003), Paleoflood record of the Tagus River (Central Spain) during the LAte Pleistocene and Holocene, *Quaternary Science Reviews*, *22*, 1737-1756.
Berger, A., and M. F. Loutre (1992), Astronomical solutions for paleoclimate studies over the last
3 million years, *Earth and Planetary Science Letters 111*, 369-382.
Berger, A. (2001), Where astronomy meets geology: from Ice Ages to global warming, edited, Retrieved November 24.
Berger, A. L. (1978), Long-Term Variations of Daily Insolation and Quaternary Climatic Changes
Journal of the Atmospheric Sciences, *35*(12), 2362-2367.
Bianchi, G. G., and I. N. McCave (1999), Holocene periodicity in North Atlantic climate and deep-ocean flow south of Iceland, *Nature*, *397*, 515-517.
Blunier, T., J. Chappelaz, J. Schwander, A. Daellenbach, B. Stauffer, T. F. Stocker, D. Raynaud, J. Jouzel, H. B. Clausen, C. U. Hammer, and S. J. Johnsen (1998), Asynchrony of Antarctic and Greenland climate change during the last glacial
period, *Nature*, *394*, 739-743.
Blunier, T., and E. J. Brook (2001), Timing of Millennial-Scale Climate Change in Antarctica and Greenland During the Last Glacial Period, *Science*, *291*.
Bond, G., H. Heinrich, W. Broecker, L. Labeyrie, J. McManus, J. Andrews, S. Huon, R. Jantschik, S. Clasen, C. Simet, K. Tedesco, M. klas, G. Bonani, and S. Ivy (1992), Evidence for massive discharges of icebergs into the North Atlantic Ocean during the last glacial period, *Nature*, *360*, 245-250.
Bond, G., W. Broecker, S. Johnsen, J. McManus, L. Labeyrie, J. Jouzel, and G. Bonani (1993), Correlations between climate records frm North atlantic sediments and Greenland Ice, *Nature*, *365*, 143.
Bond, G., W. Showers, M. Cheseby, R. Lotti, P. Almasi, P. deMenocal, P. Priore, H. Cullen, I. Hajdas, and G. Bonani (1997), A Pervasive Millennial-Scale Cycle in North Atlantic Holocene and Glacial Climates, *Science*, *278*, 1257-1266.
Bond, G., B. Kromer, J. Beer, R. Muscheler, M. N. Evans, W. Showers, S. Holffmann, R. Lotti-Bond, I. hajdas, and G. Bonani (2001), Persistent Solar Influence on North Atlantic Climate During the Holocene, *Science*, *294*, 2130-2136.
Bond, G. C., and R. Lotti (1995), Iceberg Discharges into the North Atlantic on Millennial Time Scales During the Last Glaciation, *Science*, *267*, 1005-1010.
Brassell, S. C., G. Eglinton, I. T. Marlowe, U. Pflaumann, and M. Sarnthein (1986), Molecular statigraphy: a new tool for climatic assessment, *Nature*, *320*, 129-133.
Brassell, S. C. (1993), Aplication of biomarkers for delineating marine paleoclimate flutuations during the Pleistocene. , in *Organic Geochemistry: principles and applications*, edited by M. S. A. Engel M. H., pp. 699-738, Plenum, New York.
Broecker, W. S., and G. H. Denton (1989), The role of ocean-atmosphere reorganizations in glacial cycles, *Geochimica et Cosmochimica Acta*, *53*, 2465-2501.
Broecker, W. S. (1994), Massive iceberg discharges as triggers for global climate change, *Nature*, *372*, 421-424.
Cacho, I. L. (2000), Respuesta del Mediterráneo Occidental a los cambios climáticos rápidos de los últimos 50.000 anos. Análisis de biomarcadores moleculares., 147 pp, University of Barcelona, Barcelona.

Calvo, E. (2001), Reconstrucció de les condicions climàtiques de l`Atlàntic Nord durant els Darrers dos cicles glacial-interglacial mitjançant els Biomarcadors Moleculars, 197 pp, Politècnica de Barcelona (UPC), Barcelona.

Chaler, R., J. Grimalt, C. Pelejero, and E. Calvo (2000), Sensitivity Effects in U^{k37} Paleotemperature Estimate by Chemical Ionization Mass Spectrometry, *Analytical Chemistry*, *24*(72), 5892-5897.

Chapman, M. R., N. J. Shackleton, and J. C. Duplessy (2000), Sea surface temperature variability during the last glacial-interglacial cycle: assessing the magnitude and pattern of climate change in the North Atlantic, *Palaeogeography, Palaeoclimatology, Palaeoecology*, *157*, 1 -25.

Conte, M. H., G. Eglinton, and L. A. S. Madureira (1992), Long-chain alkenones and alkyl alkenoates as palaeotemperture indicators in their production, flux and ealy sedimentary diagenesis in the Eastern North Atlantic, *Oganic Geochemistry*, *19*(1-3), 287-298.

Conte, M. H., and G. Eglinton (1993), Alkenone and alkenoate distributions within the euphotic zone of the eastern North Atlantic: Correlation with production temperature, *Deep-Sea Research*, *40*(10), 1935-1961.

Conte, M. H., A. Thompson, D. Lesley, and R. P. Harris (1998), Genetic and physiological influences on the alkenone/alkenoate versus growth temperature relationship in *Emiliania huxleyi* and *Gephyrocapsa oceanica.*, *Geochimica et Cosmochimica Acta*, *62*, 51-68.

Cortijo, E., L. Labeyrie, L. Vidal, M. Vautravers, M. Chapman, J. C. Duplessy, M. Elliot, M. Arnold, J. L. Turon, and G. Auffret (1997), Changes in sea surface hydrology associated with Heinrich event 4 in the North Atlantic Ocean between 40°N and 60°N, *Earth and Planetary Science Letters*, *146*, 29-45.

Cranwell, P. A. (1973), Chain-length distribution of n-alkanes from lake sediments in relation to post-glacial environmental change *Freshwater Biology*, *3*, 259-265.

Dahl-Jensen, D., K. Mosegaard, N. Gundestrup, G. D. Clow, S. J. Johnsen, A. W. Hansen, and N. Balling (1998), Past temperatures directly from the Greenland Ice Sheet, *Science*, *282*, 268-271.

Dansgaard, W., S. J. Johnsen, H. B. Clausen, D. Dahl-Jensen, N. S. Gundestrup, C. U. Hammer, C. S. Hvidberg, J. P. Steffensen, A. E. Sveinbjornsdottir, J. Jouzel, and G. Bond (1993), Evidence for general instability of past climate from a 250-kyr ice-core record, *Nature*, *364*(6434), 218-220.

Delmotte, M., J. Chappellaz, E. BrooK, P. Yiou, J. M. Barnola, C. Goujon, D. Raynaud, and V. I. Lipenkov (2004), Atmospheric methane during the last four glacial-interglacial cycles: Rapid changes and their link with Antarctic temperature, *Journal of Geophysical Research*, *109*.

deMenocal, P., J. Ortiz, T. Guiderson, J. Adkins, M. Sarnthein, L. Baker, and M. Yarusinsky (2000), Abrut onset and termination of the African Humid Period rapid Climate responses to gradual insolation forcing, *Quaternary Science Reviews*, *19*, 347-361.

Desprat, S., M. F. Sánchez Goñi, F. Naughton, J.-L. Turon, J. Duprat, B. Malaizé, E. Cortijo, and J.-P. Peypouquet (2007), Climate variability of the last five isotopic interglacials: direct land-sea.ice correlation from the multiproxy analysis of north western Iberian margin deep-sea cores., in *The climate of the past interglacials*, edited by F. Sirocko, et al., Elsevier.

Duplessy, J.-C., E. Ivanova, I. Murdmaa, M. Paterne, and L. Labeyrie (2001), Holocene paleoceanography of the northern Barents Sea and variations of the nortward heat transport by the Atlantic Ocean, *BOREAS*, *30*.

Eglinton, G., and R. J. Hamilton (1967), Leaf epicuticular waxes, *Science*, *156*, 1322-1335.
Eglinton, G., S. A. Bradshaw, A. Rosell, M. Sarnthein, U. Pflaumann, and R. Tiedemann (1992), Molecular record of secular sea surface temperature changes on 100-year timescales for glacial terminations I, II and IV
Nature, *356*.
Eglinton, G. (2005), Molecular Markers as tools, edited.
Elliot, M., L. Labeyrie, G. Bond, E. Cortijo, J.-L. Turon, N. Tisnerat, and J.-C. Duplessy (1998), Millenial-scale iceberg discharges in the Irminger Basin during the last glacial period: Relationship with the Heinrich events and environmental settings, *Paleoceanography*, *13*(433-446).
EPICA, c. m. (2004), Eight glacial cycles from an Antartic ice core, *Nature*, *429*.
Farrimond, P., G. Eglinton, and S. C. Brassell´ (1986), Alkenones in cretaceous black shales, Blake-Bahama basin, western North Atlantic, *Organic Geochemestry*, *10*, 897-903.
Fiúza, A., M. E. Macedo, and M. R. Guerreiro (1982), Climatological space and time variation of the Portuguese coastal upwelling, *Oceanol. Acta*, *5*, 31-40.
Fiúza, A., M. Hamann, I. Ambar, G. D. d. Rio, N. Gonzalez, and J. M. Cabanas (1998), Water masses and their circulation off Western Iberian during May 1993, *deep-Sea Research I*, *45*, 1127-1160.
Fiúza, A. F. G. (1983), Upwelling patterns off Portugal, edited, pp. 85-98.
Gagosian, R. B., E. T. Peltzer, and J. T. Merrill (1987), Long-range transport of terrestrially derived lipids in aerosols from the south Pacific, *Nature*, *325*, 800-803.
Ganopolski, A., and S. Rahmstorf (2001), Rapid changes of glacial climate simulated in a coupled climate model *Nature 409*, 153-158.
Gaspar, L. C., and J. H. Monteiro (1977), Matéria Orgânica nos sedimentos da plataforma continental portuguesa entre os cabos Espichel e Raso, *Comunicações dos Serviços Geológicos de Portugal*, *T. 62*, 69-83.
Grimalt, J. O., J. Rullkotter, M.-A. Sicre, R. Summons, J. Farrington, H. R. Harvey, M. Goñi, and K. Sawada (2000), Modification of the C_{37} alkenone and alkenoate composition in the water column and sediment: Possible implications for sea surface temperature estimates in paleocenography, *Geochemistry Geophysics Geosystems*, *1*(1525-2027), 2000GC000053.
Grootes, P. M., M. Stuiver, J. W. C. White, S. Johnsen, and J. Jouzel (1993), Comparison of oxigen isotopes records from the GISP2 and GRIP Greeland ice cores, *Nature*, *366*, 552-554.
Grootes, P. M., and M. Stuvier (1997), Oxygen 18/16 variability in Greenland snow and ice with 10− 3 to 105 year time resolution,, *Journal of Geophysical Research*, 102
Grousset, F. E., L. Labeyrie, J. A. Sinko, M. Cremer, G. Bond, J. Duprat, E. Cortijo, and S. Huon (1993), Patterns of ice-rafted detritus in the glacial North Atlantic (40-55°N), *Paleoceanography*, *8*, 175-192.
Haynes, R., and E. D. Barton (1990), A poleward flow along the Atlantic coast of the Iberian Peninsula, *Journal of Geophysical Research*, *95*, 11425-11441.
Heinrich, H. (1988), Origin and consequences of cyclic ice rafting in the northeast Atlantic Ocean during the past 130,000 years, *Quaternary Research*, *142-152*, 29.
Hemming, S. R., W. S. Broecker, W. D. Sharp, G. C. Bond, R. H. Gwiazda, J. F. McManus, M. Klas, and I. Hajdas (1998), Provenance of Heinrich layers in core V28-82, northeastern Atlantic: 40Ar/39Ar ages of ice-rafted hornblende, Pb isotopes in feldspar grains, and Nd-Sr-Pb isotopes in the fine sediment fraction, *Earth and Planetary Science Letters*, *164*, 317-333.

Herbert, T. D., M. Yasuda, and C. Burnett (1995), Glacial-Interglacial sea -surface temperature record inferred from alkenone unsaturation indices, site 893, Santa Barbara Basin, *Proceedings of the Ocean Drilling Program. Scientific Results*, *146*, 257-264.
Huls, M., and R. Zahn (2000), Millennial-scale sea surface temperature variability in the western tropical North Atlantic from planktonic foraminiferal census Counts:, *Paleoceanography*, *15*, 659-678.
Hurrell, J. W. (1995), Decadal Trends in the North Atlantic Oscilation: regional Temperatures and Precepitation, *Science*, *269*.
Imbrie, J., E. A. Boyle, S. C. Clemens, A. Duffty, W. R. Howard, G. Kukla, J. Kutzbach, D. G. Martinson, A. McIntyre, A. C. Mix, B. Molfino, J. J. Morley, L. C. Peterson, N. G. Pisias, W. L. Prell, M. E. Raymo, N. J. Shackleton, and J. R. Toggweiler (1992), On the Struture and origin of Major Glaciation Cycles
1. Linear response to Milankovitch Forcing, *Paleoceanography*, *7*(6), 701-738.
Imbrie, J., E. A. Boyle, S. C. Clemens, A. Duffty, W. R. Howard, G. Kukla, J. Kutzbach, D. G. Martinson, A. McIntyre, A. C. Mix, B. Molfino, J. J. Morley, L. C. Peterson, N. G. Pisias, W. L. Prell, M. E. Raymo, N. J. Shackleton, and J. R. Toggweiler (1993), On the Struture and origin of Major Glaciation Cycles
2- The 100,000 Year Cycle, *Paleoceanography*, *8*(6), 699-735.
Jasper, J. P., and R. B. Gagosian (1989), Alkenones Molecular Stratigraphy in an Oceanic Enviroment Affected by Glacial Freshwater Events, *Paleoceanography*, *4*(6), 603-614.
Johnsen, S., H. B. Clausen, W. Dansgaard, K. Fuhizer, N. Gundestrup, C. V. Hammer, P. Iversen, J.Jouzel, B. Stauffer, and J. P. Steffesen (1992), Irregular glacial interstadials recorded in a new Greenland ice core, *Nature*, *359*, 311-313.
Johnsen, S. J., D. Dahl-Jensen, N. S. Gundestrup, J. P. Steffensen, H. B. Clausen, H. Miller, V. Masson-Delmotte, A. E. Sveinbjornsdottir, and J. W. C. White (2001), Oxygen isotope and palaeotemperature records from six Greenland ice-core stations: Camp Century, Dye-3, GRIP, GISP, Renland and NorthGRIP, *Journal of Quaternary Science*, *16*, 299-307.
Jones, P. D., T. J. Osborn, K. R. Briffa, C. K. Folland, E. B. Horton, L. V. Alexander, D. E. Parker, and N. A. Rayner (2001), Adjusting for sampling density in grid box land and ocean surface temperature time series, *Journal of Geophysical Research*, *106*, 3371-3380.
Jouanneau, J. M., C. Garcia, A. Oliveira, A. Rodrigues, J. A. Dias, and O. Weber (1998), Dispersal and deposition of suspend sediment on the shelf off the Tagus and sado estuaries S. W. Portugal, *Progress in Oceanography*, *42*.
Kaplan, M. R., and A. P. Wolfe (2006), Spatial and temporal variability of Holocene temperature in the North atlantic region, *Quaternary Research*, *65*, 223-231.
Kaufman, D. S., T. A. Ager, N. J. Anderson, P. M. Anderson, J. T. Andrews, P. J. Bartlein, L. B. Brubaker, L. L. Coats, L. C. Cwynar, M. L. Duvall, A. S. Dyke, M. E. Edwards, W. R. Eisner, K. Gajewski, A. Geirsdóttir, F. S. Hu, A. E. Jennings, M. R. Kaplan, M. W. Kerwin, A. V. Lozhkin, G. M. MacDonald, G. H. Miller, C. J. Mock, W. W. Oswald, B. L. Otto-Bliesner, D. F. Porinchu, K. Ruhland, J. P. Smol, E. J. Steig, and B. B. Wolfe (2004), Holocene thermal maximum in the western Arctic (0-180ºW), *Quaternarty Science Reviews*, *23*, 529-560.
Keigwin, L. D., and S. J. Lehman (1994), Deep Circulation Change Linked to HEINRICH Event 1 and Younger Dryas in a Middepth North Atlantic Core, *Paleoceanography*, *9*.
Keigwin, L. D., and E. A. Boyle (2000), Detecting Holocene Changes in thermohaline circulation, *PNAS*, *97*(4), 1345.

Keigwin, L. D., J. P. Sachs, Y. Rosenthal, and E. A. Boyle (2005), The 8200 year B. P. event in the slope water system, western subpolar North Atlantic core, *Paleoceanography*, *20*, PA2003, doi:2010.1029/2004PA001074.
Knudsen, K. L., H. Jiang, E. Jansen, J. Eiriksson, J. Heinemeier, and M. S. Seidenkrantz (2004), Environmental changes off North Iceland during the deglaciation and the Holocene: foraminifera, diatoms and stable isotopes, *Marine Micropaleontology*, *50*, 273-305.
Labeyrie, L., J. C. Duplessy, and P. L. Blanc (1987), Variations in mode of formation and temperature of oceanic deep water over the past 125,000 yrs, *Nature*, *327*, 477-482.
Lebreiro, S. (2000), Oceanographic cruise onboard the British RV Discovery 249-Gulf of Cadiz and Portuguese Continental Shelf off Lisbon, Dep. Geologia Marinha, IGM.
Lebreiro, S. M., J. C. Moreno, F. F. Abrantes, and U. Pflaumanm (1997), Produtivity and paleoceanographic implications on the Tore Seamount (Iberian Margin) during the last 225Kyr: Foraminiferal evidence, *Paleoceonagraphy*, *12*(5), 718-727.
Levac, E., A. d. Vernal, and W. Jr.Blake (2001), Sea surface conditions in northernmost Baffin bay during the Holocene. palynologicalevodence, *Journal of Quaternary Science*, *16*, 353-363.
Li, J., R. P. Philip, F. Pu, and J. Allen (1996), Long-chain alkenones in Qinghai Lake sediments, *Geochimica et Cosmochimica Acta*, *60*(2), 235-241.
Lima, L. M. C. S. (1971), Distribuição dos Minerais argilosos na Plataforma Continental entre os Cabos Espichel e Raso, *1º Congresso Hispano-Luso Americano de Geologia Economia*, 253-271.
Lisiecki, L. E., and M. E. Raymo (2005), A Pliocene-Pleistocene stack of 57 globally distributed benthic d18O records, *Palaeogeography*, *20*(PA1003).
Loutre, M. F. (2003), Clues from MIS 11 to predict the future climate a modelling point of view, *Earth and Planetary Science Letters*, *212*, 213-224.
Loutre, M. F., and A. Berger (2003), Marine Isotope Stage 11 as an analogue for the present interglacial, *Global and planetary change*, *762*, 1-9.
Lowe, J. J., S. O. Rasmussen, S. Bjorck, W. Z. Hoek, J. P. Steffensen, M. J. C. Walker, Z. C. YU, and t. I. group (2008), Synchronisation of palaeoenvironmental events in the North Atlantic region during the last Termination: a revised protocol recommended by the INTIMATE group, *Quaternarty Science Reviews*, *27*, 6-17.
Lowell, T. V., C. J. Eusser, B. G. Andersen, P. I. Moreno, A. Hauser, L. E. Heusser, C. Schluchter, D. R. Marchant, and G. H. Denton (1995), Interhemispheric correlation of late Pleistocene glacial events, *Science*, *269*, 1541-1549.
Lyle, M. W., F. G. Prahl, and M. A. Sparrow (1992), Upwelling and productivity changes inferred from a temperature record in the central equatorial Pacific, *Nature*, *355*, 812-815.
MacAyeal, D. R. (1993), Binge/purge oscillations of the Laurentide Ice Sheet as a cause of the North Atlantic's Heinrich events, *Paleoceanography*, *8*, 775-784.
Madureira, L. A. s., M. H. Conte, and G. Eglinton (1995), Early Diagenesis of lipid biomarker compounds in North Atlantic sediments, *Paleoceanography*, *10*(3), 627-642.
Madureira, L. A. S., S. A. v. Kreveld, G. Eglinton, M. H. Conte, G. Ganssen, J. E. v. Hinte, and J. J. Ottens (1997), Late quaternary high-resolution biomarker and other sedimentary climate proxies in a northeast Atlantic core, *Paleoceanography*, *12*(2), 255-269.
Maffei, M. (1996), Chemataxonomic significance of wax alkanes in the gramineae, *Biochemical Systematics and Ecology*, *24*(1), 53-64.
Maffei, M., S. Badino, and S. Bossi (2004), Chemataxonomic significanceof the leaf wax n-alkanes in the Pinales (Coniferals), *Journal of Biological Research*, *1*, 3-19.

Marchal, O., I. Cacho, T. F. Stocker, J. O. Grimalt, E. Calvo, and B. Martrat (2002), Apparent long-term cooling of the sea surface in the northeast Atlantic and Mediterranean during the Holocene, *Quaternary Science Reviews*, *21*, 455-483.
Marlowe, I. T., S. C. Brassell, G. Eglinton, and J. C. Green (1984a), Long chain unsatured Ketones and esters in living algae and marine sediments, *Org. Geochemistry*, *6*, 135-141.
Marlowe, I. T., J. C. Green, A. C. Neal, S. C. Brassell, G. Eglinton, and P. A. Course (1984b), Long chain (n-C37-C39) Alkenones in the Prymnesiophyceae. Distribution of Alkenones and other Lipids and their Taxonomic Significance, *British Phycological J.*, *19*, 203-216.
Marlowe, I. T., S. C. Brassell, G. Eglinton, and J. C. Green (1990), Long-chain alkenones and alkyl alkenoates and fossil cocolith record of marine sediments, *Chemical Geology*, *88*, 349-375.
Martrat, B., J. O. Grimalt, C. Lopez-Martinez, Isabel Cacho, F. Sierro, J. A. Flores, R. Zahn, M. Canals, J. H. Curtis, and D. A. Hodell (2004), Abrupt Temperature Changes in the Western Mediterranean over the Past 250,000 Years, *Science*, *306*, 1762-1765.
Martrat, B., J. O. Grimalt, N. J. Shackleton, L. d. Abreu, M. A. Hutterli, and T. F. Stocker (2007), Four Climate Cycls of Recurring Deep and Surface Water Destabilizations on the Iberian Margin, *Science 317*(1139994), 502-507.
Maslin, M. A., N. J. Shackleton, and U. Pfaumann (1995), Surface water temperature,salinity, and density changes in the northeast Atlantic during the last 45,000 years:
Heinrich events, deep water formation, and climatic rebounds, *Paleoceanography*, *10: 527-544*.
Masson-Delmotte, V., G. Dreyfus, P. Braconnot, S. Johnsen, J. Jouzel, M. Kageyama, A. Landais, M.-F. Loutre, J. Nouet, F. Parrenin, D. Raynaud, B. Stenni, and E. Tuenter (2006), Past temperature reconstructions from deep ice cores: relevance for
future climate change, *Climate of The Past*, *2*, 145-165.
Mayewski, P. A., L. D. Meeker, M. S. Twickler, S. Whitlow, Q. Yang, W. B. Lyons, and M. Prentice (1997), Major features and forcing of high-latitude northern hemisphere atmospheric circulation using a 110,000-year-long glaciochemical series, *Journal of Geophysical Research*, *102*, 26345-26366.
Mayewski, P. A., E. E. Rohling, J. C. Stager, W. Karlen, K. A. Maasch, L. D. Meeker, E. A. Meyerson, F. Gasse, S. v. Kreveld, K. Holmbren, J. Lee-Thorp, G. Rosqvist, F. Rack, M. Staubwasser, R. R. Schneider, and E. J. Steig (2004), Holocene climate variability, *Quaternary Research*, *62*, 243-255.
McIntyre, A., and W. H. Bé (1967), Modern coccolithophoridae of the Atlantic Ocean-I. Placoliths and cyrtolith, *Deep-Sea Research*, *14*, 561-597.
McIntyre, A., A. W. Bé, and M. B. Roche (1970), Modern Pacific coccolithophorida: a paleontological thermometer, *Transactions of the New York Academy of science*, *32*, 720-731.
McManus, J., D. Oppo, J. Cullen, and S. Healey (2003), Marine Isotope Stage 11 (MIS 11): Analog for Holocene and Future Climate?
McManus, J. F., D. W. Oppo, and J. L. Cullen (1999), A 0.5- Million-Year Record of Millennial-Scale Climate Variability in the North Atlantic, *Science*, *283*, 971-975.
Milankovitch, M. M. (1920), Théorie mathématique des phénomènes thermique produits par la radiation solaire, Gauthier-Villars, Paris.
Milliman, J. D., and J. P. M. Syvitski (1992), *Geomorphic/Tectonic control of Sediment Discharge to the Ocean: The importance of Small Mountainous Rivers*, 525-544 pp., University of Chicago, Chicago.

Mix, A. C., E. Bard, G. Eglinton, L. D. Keigwin, A. C. Ravelo, and Y. Rosenthal (2000), Alkenones and multiproxy strategies in paleoceanogrphic studies, *Geochemistry Geophysics Geosystems*, *1*, 2000GC000056.
Moita, M. T. (2001), Estrutura variabilidade e dinâmica do fitoplânton na Costa de Portugal Continental, 272 pp, Facudade de Ciências de Lisboa, Lisboa.
Monteiro, J. H., and I. M. C. Moita (1971), Morfologia e sedimentos da plataforma continental e vertente continental superior ao largo da Península de Setúbal, paper presented at Congresso de Geologia.
Monteiro, J. H., A. Voelker, A. Ferreira, M. Mil-Homens, S. Nave, V. Magalhães, E. Salgueiro, S. Vaqueiro, S. Muiños, and P. Freitas (2002), Report of the cruise PALEO I (PO287) on FS Poseidon (April 22-May3, 2002), Tecnical Repo, IGM, Alfragide, Portugal.
Moros, M., K.-C. Emeis, B. Risebrobakken, I. Snowball, A. Kuipers, J. McManus, and E. Jansen (2004), Sea surface temperatures and ice rafting in the Holocene North Atlantic: climate influences on northern Europe and Greenland *Quaternarty Science Reviews*, *23*, 2113-2126.
Müller, P., G. Kirst, G. Ruhland, I. v. Storch, and A. Rosell-Melé (1998), Calibration of the alkenone index Uk'37 based on core-tops the eastern South Atlantic and global ocean (60ºN-60ºS), *Geochimica et Cosmochimica Acta*, *62*, 1757-1772.
Müller, P. J. (1999), Temperature Determinations with alkenones.
O'Brien, S. R., P.A. Mayewski, L. D. Meeker, D. A. Meese, M. S. Twickler, and S. I. Whitlow (1995), Complexity of Holocene Climate as Reconstructed from a Greeland Ice Core, *Science*, *270*, 1962-1964.
Okada, H., and S. Honjo (1973), The distribution of oceanic coccolithophorids in the Pacific., *Deep-Sea Research*, *20*, 355-374.
Okada, H., and A. McIntyre (1979), Seasonal distribution of moderm coccolithophores in the Western North Atlantic Ocean, *Marine Biology*, *54*, 319-328.
Oliveira, P. B., M. Amraoui, A. F. G. Fiúza, M. Grosjean, and H. Wanner (1996), Sea Surface Temperature Atlas of the Northeast atlantic Derived from NOAA Advanced Very High Resolution Radiometer data., Technical report 42, 1-44 pp, Lisbon.
Oppo, D. W., J. F. McManus, and J. L. Cullen (1998), Abrupt Climate Events 500,000 to 340,000 years agoÇ: Evidence from Subpolar North Atlantic Sediments, *Science*, *279*.
Paillard, D., and L. Labeyriet (1994), Role of the thermohaline circulation in the abrupt warming after Heinrich events, *Nature*, *372*(6502), 162-164.
Pelejero, C., J. O. Grimait, and I. Cacho (1997), Aplicaciones de los Biomarcadores moleculares en estudios paleoclimáticos: las alquenonas y el Índice U^{K37}, *Thalassas*, *13*, 49-58.
Pelejero, C., M. Kienast, L. wang, and J. O. Grimalt (1999), The flooding of Sundaland during the last deglaciation: Imprints in hemipelagic sediments from the southern south China sea, *Earth and Planetary Science Letters*, *171*, 661-671.
Poynter, J., and G. Egliton (1990), Molecular composition of three sediments from Hole 717C: the Bengal Fan, *Proceedings of the Ocean Drilling Program, scientific results*, *116*, 155-161.
Poynter, J. G., P. Farrimond, N. Robinson, and G. Eglinton (1989), Aeolian-derived higer plant lipids in the marine sedimentary record: links with paleocliamte, in *Paleoclimatology and paleometerology: modern and past patterns of global atmosphweric transport*, edited by M. Leinen and M. Sarnthein, pp. 435-462, Kluwer Academic Publishers, Dordrecht.

Prahl, F., and S. G. Wakeham (1987), Calibration of unsaturation patterns in long-chain ketones compositions for palaeotemperature assessment, *Nature*, *330*, 367-369.
Prahl, F., and L. A. Muehlhausen (1989), Lipid Biomarkers as Geochemical Tools for Paleoceanographic Study, *Productivity of the Ocean: Present and past*, 271-289.
Prahl, F., T. Herbert, S. C. Brassel, N. Ohkouchi, M. Pagani, D. Repeta, A. Rossell-Melé, and E. Sikes (2000), Status of alkenones paleothermometer calibration: Report from Working Group 3, *Geochemistry Geophysics Geosystems*, *1*, 2000GC000058.
Prahl, F. G., L. A. Muehlhausen, and D. L. Zahnle (1988), Futher evaluationof long chain alkenones as indicator of paleoceanographic conditions, *Geochimica et Cosmochimica Acta*, *52*, 2303-2310.
Prahl, F. G., J. R. Ertel, M. A. Goni, M. A. Sparrow, and B. Eversmeyer (1994), Terrestrial organic carbon contribution to sediments on the Washington margin, *Geochimica et Cosmochimica Acta*, *58*(14), 3035-3048.
Rahmstorf, S. (1996), On the freshwater forcing and transport of the Atlantic thermohaline circulation, *Climate Dynamics*, *12*, 799-811.
Rahmstorf, S. (2006), Thermohaline Ocean Circulation, in *Encyclopedia of Quaternary Sciences*, edited by S. A. Elias, Elsevier, Amsterdam.
Rechka, J. A., and J. R. Maxwell (1988), Unsusual long chain ketones of algal origin, *Tetrahedron Letters*, *29*(21), 2599-2600.
Rios, A., F. Pérez, and F. Fraga (1992), Water masses in the upper and middle north Atlantic Ocean east of the Azores., *Deep-Sea Res.*, *39*, 645-658.
Rosell-Melé, A., J. Carter, and G. Eglinton (1994), Distributions of long-chain alkenones and alkyl alkenoates in marine surface sediments from the North East Atlantic, *Organic Geochemistry*, *22*(3-5), 501-509.
Rosell-Melé, A., G. Eglinton, U. Pflaumann, and M. Sarnthein (1995), Atlantic core - top calibration of the UK37 index as a sea-surface paleotemperature indicator, *Geochimica et Cosmochimica Acta*, *59*(15), 3099-3107.
Ruddiman, W. F. (1977), Late Quaternary deposition of ice-rafted sand in the subpolar North Atlantic (lat. 40' to 65ON), *Geological Society of America Bulletin*, *88*, 1813-1821.
Ruddiman, W. F., M. E. Raymo, D. G. Martinson, B. M. Clement, and J. Backman (1989), Pleistocene evolution: northern hemisphere ice sheets and North Atlantic Ocean, *Paleoceanography*, *4*(4), 353-412.
Ruddiman, W. F. (2001), *Earth's Climate: Past and Future*, New York.
Ruddiman, W. F. (2005), Cold climate during Stage 11 anlog to recent Millennia, *Quaternary Science Reviews*, *24*, 1111-1121.
Schulz, H., U. von Rad, and H. Erlenkeuser (1998), Correlation between Arabian Sea and Greenland climate oscillations of the past 110,000 years, *Nature*, *393*, 54-57.
Schulz, M., Paul, A. , and A. Timmermann (2004), Glacial-interglacial contrast in climate
variability at centennial-to-millennial timescales: observations and conceptual model, *Quaternary Science Reviews*, *23*, 2219-2230.
Seidov, D., and M. Maslin (1999), North Atlantic deep water circulation collapse during Heinrich events, *Geology*, *27*(1), 23-26.
Severinghaus, J. P., and E. J. Brook (1999), Abrupt Climate Change at the End of the Last Glacial Period Inferred from Trapped Air in Polar Ice, *Science*, *286*, 930-934.
Shackleton, N. J. (1967), Oxygen Isotope analysis and pleitocene temperature reassessed., *Nature*, *215*, 15-17.

Sicre, M.-A., E. Bard, U. Ezat, and F. Rostek (2002), Alkenone distributions in the North Atlantic and nordicsea surface waters, *Geochemistry Geophysics Geosystems*, *3*(2), 10.1029/2001GC000159.
Sikes, A. E. L., and J. K. Volkman (1993), Calibration of alkenone unsaturation ratios U^{k37} for paleotemperature estimation in cold polar waters, *Geochimica et Cosmochimica*, *57*, 1883-1889.
Sikes, E. L., J. W. Farrington, and L. D. Keigwin (1991), Use of alkenone unsaturation ratio Uk37 to determinepast sea surface temperatures:core-top SST calibrations and methodology considerations., *Earth and Planetary Science Letters*, *104*, 36-47.
Solignac, S., A. d. Vernal, and C. Hillaire-Marcel (2004), Holocene sea surface conditions in the North Atlantic- contrasted trends and regimes in the western and eastern sectors(Labrador Sea vs. Iceland basin), *Quaternarty Science Reviews*, *23*, 319-334.
Sonzogni, C., E. Bard, F. Rostek, D. D. Cerege, A. Rosell-Mele, and G. Eglinton (1997), Alkenones in recent surface sediments from the subtropical and tropical Indian Ocean, *Organic Geochemistry Unit*.
Sousa, F. M., and A. Bricaud (1992), Satellite-Derived Phytoplankton Pigment Strutures in the Portuguese Upwelling Area, *Journal of Geophysical Research*, *97*(C7), 11,343-311,356.
Stocker, T. F. (1998), The seesaw effect, *Science*, *282*, 61-62.
Tareq, S. M., E. Tanoue, H. Tsuji, N. Tanaka, and K. Ohta (2005), Hydrocarbon and elemental carbon signatures in a tropical wetland: Biogeochemical evidence of forest fire vegetation changes, *Chemosphere*, *59*, 1655-1665.
Teece, M. A., J. M. Getliff, J. W. Leftley, R. J. Parkes, and J. R. Maxwell (1998), Microbial degradation of the marine prymnesiophyte *Emiliania huxleyi* under oxic and anoxic conditions as a model for early diagenesis: long chain alkadienes, alkenones and alkenoates., *Organic Geochemistry*, *29*(4), 863-880.
Teller, J. T., D. W. Leverington, and J. D. Mann (2002), Freshwater outbursts to the ocean from glacial Lake Agassiz and their role in climate change during the last deglaciation, *Quaternary Science Reviews*, *21*, 879-887.
Ternois, Y., K. Kawamura, L. Keigwin, N. Ohkouchi, and T. Nakatsuka (2001), A Biomarker approch for assessing marine and terrigenous inputs to the sediments of Sea of Okhotsk for the last 27,000 years, *Geochimica et Cosmochimica acta*, *65*(5), 791-802.
Trigo, R. M., T. J. Osborn, and J. Corte-Real (2002), The North Atlantic Oscilation influence on Europe: Climate impacts and associated physical mechanisms, *Climate Research*, *20*, 9-17.
Tzedakis, P. C. (2009), The MIS 11 - MIS 1 analogy, southern European vegetation, atmospheric methane and the "early anthropogenic hypothesis", *Climate of The Past Discussions*, *5*, 1337-1365.
Vale, C. (1981), Entrada de matéria em suspensão no estuário do Tejo durante as chuvas de Fevereiro de 1979, *Recursos Hídricos*, *2*, 37-45.
Vernal, A. d., C. Hillaire-Marcel, and D. A. Darby (2005), Variability of sea cover in the Chukchi Sea (western Arctic Ocean) during the Holocene *Palaeogeography*, *20*(DOI:10.1029/2005PA001157).
Vidal, L., L. Labeyrie, E. Cortijo, M. Arnold, J. C. Duplessy, E. Michel, S. Becqué, and T. C. E. van Weering (1997), Evidence for changes in the North Atlantic Deep Water linked to meltwater surges during the Heinrich events, *Earth and Planetary Science Letters*, *146*, 13-27.

Villanueva, J. (1996), Estudi de les variaciones climàtiques i oceanogràfiques a l`atlantic Nord Durant els últims 300.000 anys mitjançant l`análisi de marcadores moleculars., 186 pp, Ramon Llull, Barcelona.
Villanueva, J., and J. O. Grimalt (1997), Gas Chromatographic Tuning of the UK37 Paleothermometer, *Analytical Chemistry*, *69*(16), 3329-3332.
Villanueva, J., C. Pelejero, and J. O. Grimalt (1997), Clean-up procedures for the unbiased estimation of C_{37} alkenone sea surface temperatures and terrigenous *n*-alkane in paleoceanography, *Journal of Chromatography 757*, 145-151.
Voelker, A. (2003), Cruise report for thePortuguese sites during the MD134 - PICABIA cruise on board "Marion Dufresne", INETI-Departamento de Geologia Marinha, Alfragide-Portugal.
Voelker, A. H. L., S. M. Lebreiro, J. Schonfeld, I. Cacho, H. Erlenkeuser, and F. Abrantes (2006), Mediterranean outflow strengthening during northern hemisphere coolings: A salt source for the glacial Atlantic?, *Earth and Planetary Science Letters*, *245*, 39-55.
Voelker, A. H. L. a. w. p. (2002), Global distribution of centennialscale records of centennial-scale records for Marine Isotope Stage (MIS) 3: a database, *Quaternary Science Reviews*, *21*, 1185-1212.
Volkman, J. K., G. Eglinton, E. D. S. Corner, and T. E. V. Forsberg (1980), Long-chain Alkenes and Alkenones in the Marine Coccolithpphorid Emiiania Huxleyi, *Phytochemistry*, *19*, 2619-2622.
Volkman, J. K., J. W. Farrington, R. B. Gagosian, and S. G. Wakeham (1983), Lipid composition of coastal marine sediments from the Peru upwelling region, in *Advances in Organic Geochemistry*, edited by M. E. A. Bjoroy, pp. 228-240, Wiley, Chichester.
Volkman, J. K., H. R. Burton, D. A. Everitt, and I. D. Allen (1988), Pigment and lipid compositions of algal and baterial communities in Ace Lake, Vestfold Hills Antarctica, *Hydrobiologia*, *165*, 41-57.
Volkman, J. K., S. M.Barrett, S. I. Blackburn, and E. L. Sikes (1995), Alkenones in Gephyrocpsa oceanica: Implications for studies of paleoclimate, *Geochimica et Cosmochimica Acta*, *59*(3), 513-520.
Wefer, W. H. Berger, J. Bijma, and G. Fischer (1999), Clues to Ocean History a Brief Overview of Proxies in *Use of Proxies in Paleoceanography*, 1-68.
Winter, A., R. W. Jordan, and P. H. Roth (1994), Biogeography of living coccolithophores in ocean waters, in *Coccolithophores*, edited by A. Winter and W. G. Siesser, pp. 161-177, University Press, Cambrige.
Wooster, W., A. Bakun, and D. Mclain (1976), The seasonal upwelling cycle along the eastern boundary of the North Atlantic, *Jounal of Marine Research*, *34*, 131-141.
Zink, K., D. Leythaeuser, M. Melkonian, and L. Schwark (2001), Temperature dependency of long-chain alkenone distributions in recent to fossil limnic sediments and in lake waters *Geochimica et Cosmochimica Acta*, *65*(2), 253-265.

Chapter 2

SHALLOW MARINE SEDIMENT CORES RECORD CLIMATE VARIABILITY AND EARTHQUAKE ACTIVITY OFF LISBON (PORTUGAL) FOR THE LAST 2,000 YEARS.

Abrantes, F[1*]; Lebreiro, S[1]; **Rodrigues, T[1]**; Gil, I[1]; Bartels-Jónsdóttir, H[1]; Oliveira, P[2].; Kissel, C[3]; Grimalt, J. O.[4]

[1] – Instituto Geológico e Mineiro, Departamento de Geologia Marinha, Estrada da Portela - Zambujal. Apartado 7586, 2721-866 Alfragide, Portugal

[2] – Instituto Nacional de Investigação Agrária e das Pescas (INIAP), Av. Brasilia, 1449-006 Lisboa, Portugal

[3] – Laboratoire des Sciences du Climat et de l'Environnement, Unité de recherche mixte CEA/CNRS, Campus du CNRS, Avenue de la Terrasse, Bat 12, 91198 Gif-sur-Yvette Cedex, France

[4] – Department of Environmental Chemistry, Institute of Chemical and Environmental Research (CSIC), Jordi Girona, 18, 08034-Barcelona, Spain

Published in *QUATERNARY SCIENCE REVIEWS* **24** (2005) 2477–2494

ABSTRACT

Sea Surface Temperature (SST), river discharge and biological productivity have been reconstructed from a multi-proxy study of a high-temporal-resolution sedimentary sequence recovered from the Tagus deposition center off Lisbon (Portugal) for the last 2,000 years. SST shows 2ºC variability on a century scale that allows the identification of the Medieval Warm Period (MWP) and the Little Ice Age (LIA).

High Iron (Fe) and fine-sediment deposition accompanied by high n-alkane concentrations and presence of freshwater diatoms during the LIA (1300–1900 AD) suggest augmented river discharge, whereas higher total alkenone concentrations point to increased river-induced productivity. During the MWP (550–1300 AD) larger mean-grain size and low values of magnetic susceptibility, Fe, n-alkanes, and n-alcohols are interpreted to reflect decreased runoff. At the same time, increased benthic and planktonic foraminifera abundances and presence of upwelling related diatoms point to increased oceanic productivity. On the basis of the excellent match found between the negative phases of the North Atlantic Oscillation (NAO) index and the intensified Tagus River discharge observed for the last century, it is hypothesized that the increased influx of terrigenous material during the LIA reflects a negative NAO-like state or the occurrence of frequent extreme NAO minima. During the milder few centuries of the MWP, stronger coastal upwelling conditions are attributed to a persistent positive NAO-like state or the frequent occurrence of extreme NAO maxima.

The peak in magnetic susceptibility, centred at 90 cm, is interpreted as the result of the well-known 1755 AD Lisbon earthquake. The Lisbon earthquake and accompanying tsunami are estimated to have caused the loss of 39 cm of sediment (355 years of record - most of the LIA) and the instantaneous deposition of a 19 cm sediment bed.

1. INTRODUCTION

Climatic conditions have oscillated over the past 100,000 years, with an average period of about 1,500 years (Bond *et al.*, 1997). The large millennial-scale abrupt events of the last glacial are clearly recorded on the Portuguese Margin (Shackleton, 2000; deAbreu, 2000; Voelker *et al.,* 2002). The Holocene is also marked by repeating but less severe climate shifts, the most recent of which are the Medieval Warm Period (MWP) and subsequent Little Ice Age (LIA) (Bond *et al.*, 1997, 2001).

Primary forcing factors of climate change on millennial and centennial time scales are yet poorly understood. Broecker (2001) hypothesized that recent millennial-scale climatic oscillations are caused by changes in the North Atlantic thermohaline circulation. Variations in solar activity (Stuiver and Braziunas, 1989) have also been suggested as the driver for the North Atlantic cycles (Bond *et al.*, 2001). In addition, the North Atlantic Oscillation (NAO) index which describes the steepness of a north-south atmospheric pressure gradient across the North Atlantic Ocean (Hurrell, 1995), has also been pointed as a useful analog for interpreting longer-term climatic conditions observed for the last 2,000 years (Keigwin, 1996; Keigwin and Pickart, 1999).

Today, the NAO is believed to dictate climate variability across most of the Northern Hemisphere, especially during wintertime. Defined as the atmospheric sea level pressure difference between Iceland and Lisbon-Portugal, it is in a positive phase when the meridional pressure gradient over the North Atlantic is large, due to the enhancement of both pressure centers (the Icelandic low and the Azores high), and in a negative phase when both centers are weakened (Hurrell, 1995). Swings from a positive to a negative phase produce changes in mean wind speed and direction over the Atlantic, seasonal mean heat and moisture transport across the ocean, the path and number of storms, and may also induce significant variations in ocean temperature, and heat content, current patterns, and sea ice cover in the Arctic (Hurrel, et al., 2003). Its largest amplitude anomalies occur near Iceland and across the Iberian Peninsula. Over Iberia, atmospheric storminess and increased precipitation coincide with NAO negative conditions. The strong north-south atmospheric pressure gradient and strong clockwise flow around the Azores high-pressure center during NAO positive conditions enhances coastal upwelling conditions. Further insight on the impact of NAO on precipitation over Europe through the analysis of a 40-yr-long global coverage of consistent

precipitation-related data was reported by Trigo *et al*., (2002). Results show that cloud cover as well as precipitation rate anomaly fields (mm/d) for winter months with low NAO index (< -1.0) have high values in the area of the Tagus Basin.

The Tagus is the longest river of the Iberian Peninsula and extreme flood events lead to a major discharge of suspended and bed-load sediments (Vale, 1981). Clayey-silty sediment is transported to the Tagus deposition center on the continental shelf (Monteiro and Moita, 1971). The sediment is characterized by high concentration of organic matter (Gaspar and Monteiro, 1977; Cabeçadas and Borgueira, 1997). Additionally, the Tagus deposition center is influenced by seasonal (May to September) coastal upwelling, mainly by the Cape Roca upwelling filament (Fiúza, 1983, 1984; Sousa and Bricaud, 1992; Sousa, 1995; Abrantes and Moita, 2000; Moita, 2001).

Our objective is to reconstruct a detailed record of river influx and coastal upwelling variability over the last 2,000 years, through a multi-proxy study of a sedimentary sequence recovered from the Tagus River prodelta deposition centre, off Lisbon (Portugal).

The study of a site directly under the influence of the Azores High Pressure center, does not only enlarge the data network needed to validate climate models on time scales of many decades to centuries, but it also offers new insights into the view of modern NAO conditions as a good modern analog for the decadal to century-scale climate variability.

2. MATERIAL AND METHODS

The material used in this study was obtained from core D13902 collected at 38º33.24’ N, 9º20.13’ W and 90 m water depth. The core was taken during the British Research Vessel (RV) Discovery cruise 249 in August-September 2000 using the British long-piston coring system. Box-core PO287-26B and gravity core PO287-26G (38º33.49’ N, 9º21.84’ W, 96 m water depth) were recovered in May 2002 during the PALEO1 campaign aboard the German RV Poseidon (Fig. 1). The two top liners of core D13902 (189 cm) were half-filled and disturbed, as such, this material was discarded and a zero depth assigned to the initial 189 cm liner level.

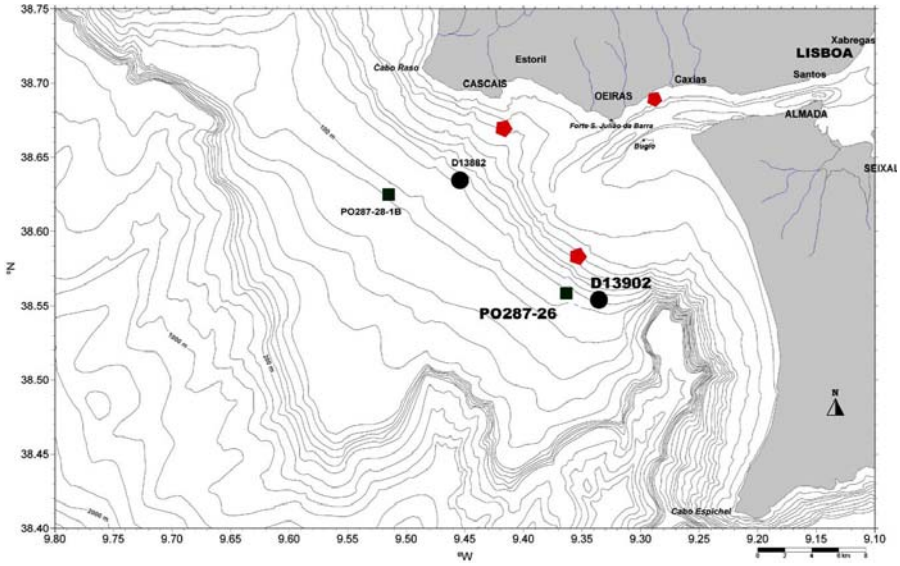

Figure 1. Detailed bathymetric map of the Tagus Estuary mouth and prodelta with location of the sedimentary sequences used in this work. Bathymetric contour interval is 10 m. Circles correspond to cores recovered on RV Discovery using the long piston coring system of Southampton Oceanographic Center. Squares indicate positions of the gravity and box-cores retrieved aboard RV Poseidon. Pentagons indicate position of pré 1950 shells dated by AMS ^{14}C.

Magnetic susceptibility (MS) of core D13902 and cores PO287-26 (B and G) were measured on a multi-parameter logging system at the Southampton Oceanography Center and at Bremen University respectively. Iron (Fe) concentrations in counts per second (cps) were determined at 1 cm intervals in cores PO287-26 and at 2 cm intervals in core D13902 by X-ray fluorescence core scanning for non-destructive semi-quantitative analysis of major elements at Bremen University (Jansen *et al.*, 1998).

Paleomagnetic analyses were performed at the Laboratoire des Sciences du Climat et de l'Environnement (LSCE/ CNRS) in Gif-sur-Yvette. Continuous analyses were made using u-channels (2x2x150 cm). The low-field susceptibility was measured using a 45 mm diameter Bardington coil, which yields 4 cm resolution. The remanent magnetizations were measured using 2G 755-R cryogenic magnetometers within a shielded room at LSCE (Weeks *et al.*, 1993). The spatial resolution is similar to the low-field susceptibility resolution (about 4 cm). Anhysteretic Remanent Magnetization (ARM) was imparted along the axis of the u-channel at a translation speed of 1 cm/sec using a 100 mT AF in a bias 50μT DC field (Kissel *et al.*, 1999).

Sediments were sliced at 1 cm intervals in 3 sub cores of the box-core (Table 1) and the gravity and piston cores. Grain size, total carbon, $CaCO_3$, and diatom analysis were performed on all samples from D13902 and PO287-26B. Alkenones, n-alkanes, n-alcohols, and foraminifera were analyzed every cm in the box-core, every 2 cm in PO287-26G, and at 5 to 20 cm intervals in the piston core.

Table 1. Sub-cores of box-core PO287-26B used for the different analysis

Subcore 1	Subcore 2	Subcore 3	Subcore 4
MST	Grain-size	Diatoms	Alkenones
XRF	$CaCo_3$		*n*-Alkanes
	Corg		*n*-Alcohols
	Foraminifera		
	Isotopes		
	AMS ^{14}C		
	^{210}Pb		

Grain size analysis was performed on 5-8 cc of sediment with a Coulter LS230 laser instrument. Prior to grain-size analysis, organic matter was removed using peroxide (H_2O_2) and dispersed with sodium hexametaphosphate (0.033M).

Total carbon content was determined using a CHNS-932 LECO elemental analyzer. Three replicates of dried and homogenized sediment (2 mg) were analysed per level. The same set of samples was later subjected to combustion for 8 hours through a predefined stepwise increase in temperature up to 400^{o}C to remove organic carbon and re-analyzed for inorganic carbon. The organic carbon content (Corg) was determined by difference between total carbon and inorganic carbon concentration. Data are presented in weight percent (wt%). The relative precision of repeated measurements of both samples and standards was 0.03 wt%.

Oxygen stable isotopic compositions were determined on the planktonic foraminifera *Globigerina bulloides* and the benthic species *Uvigerina* sp. 221 on a Finnigan MAT 251 mass spectrometer at Bremen University. The $^{18}O/^{16}O$ ratio is reported in per mil (‰) relative to the Vienna Peedee Belemnite (VPDB) standard**.** Analytical standard deviation is ± 0.07‰.

Alkenones, higher plant n-alkanes, and n-alcohols were determined on 2 g of homogenized sediment using a Varian 3400 gas chromatograph equipped with a septum programmable injector at the Department of Environmental Chemistry, Institute of Chemical and Environmental Research (CSIC), Barcelona, following the methods described in Villanueva, (1996), Villanueva and Grimalt, (1997a) and Villanueva *et al*., (1997b). For SST reconstruction, the $U^{k'}_{37}$ calibration proposed by Müller *et al.* (1998) was used due to its global character. Analytical precision was 0.5°C.

Benthic foraminifera quantification and assemblage determinations are based on census counts of splits (≈ 300 individuals) of the 125 μm fraction, whereas planktonic foraminifera quantification is based on census counts of splits (≈ 300 individuals) of the 149 μm fraction. Benthic foraminifera were classified according to Loeblich and Tappan (1988).

Siliceous microfossil quantification and diatom assemblages determinations followed the methods of Abrantes (1988).

3. CHRONOLOGY

3.1. Reservoir Effect Correction

The site of study is under the influence of the Tagus River, whose waters cross limestone-rich areas. The site is also under the influence of coastal upwelling. Both processes may lead to large reservoir ages (Little, 1993; Goodfriend and Flessa, 1997).

In order to better constrain the reservoir correction for the Iberian site, we measured apparent radiocarbon ages on 3 live-collected, pre-bomb mollusk shells from the region (Portuguese King D. Carlos collection housed at the *Aquário Vasco da Gama* in Lisbon) (Table 2). Analyses were performed at the Aarhus University AMS Laboratory and results indicate that the 400 yr global average is a good reservoir correction value.

Table 2. Results of AMS C-14 dating of Tagus region shells collected alive before 1950. King D. Carlos of Portugal Collection / Vasco da Gama Aquarium.

Sample Type	Collection Site	Collection Date	Lat. (°N)	Long. (°W)	Water Depth (m)	^{14}C Ages (BP)
Bivalve (*Chamelia gallina*)	Portugal, Trafaria	16 Sept. 1896	38° 34.4'	9° 21.5'	55	420±38
Bivalve (*Mactra solida*)	Portugal, Cascais	26 Aug. 1896	38° 40.0'	9° 25.0'	35	477±33
Bivalve (*Mactra corallina*)	Portugal, Dafundo	19 Nov. 1938			10	556±39

3.2. Age Model

An age-depth model has been constructed by combining ^{210}Pb dates of the box-core PO278-26B and piston-core D13902 (Table 3) and accelerator mass spectrometry (AMS) ^{14}C dates from the two cores (Table 4).

Table 3 - Results of 210 Pb activity for the Tagus prodelta box and piston cores (PO287-26B and D13902).

Core ID	Spliced Depth (cm)	210Pb(tot) (mBq/g)
PO287-26 (0-1 cm)	0,5	296
PO287-26 (2-3 cm)	2,9	299
PO287-26 (4-5 cm)	5,3	283
PO287-26 (6-7 cm)	7,6	271
PO287-26 (9-10 cm)	11,1	221
PO287-26 (11-12 cm	13,5	217
PO287-26 (11-12 cm	13,5	224
PO287-26 (14-15 cm	17,0	151
PO287-26 (14-15 cm	17,0	158
PO287-26 (16-17 cm	19,3	216
PO287-26 (16-17 cm	19,3	211
PO287-26 (19-20 cm	22,8	216
PO287-26 (19-20 cm	22,8	217
PO287-26 (24-25 cm	28,7	131
PO287-26 (29-30 cm	34,5	116
PO287-26 (34-35 cm	40,4	74
D13902 (27-28 cm)	75,4	47
D13902 (62-63 cm)	110,9	47

Table 4. Results of AMS dating of the Tagus prodelta box-, gravity and piston cores (PO287-26B, PO287-26G and D13902). Ages were reservoir corrected by 400 yr, considering the results presented in Table 1. Levels in *italic* correspond to ages not considered for the age model.

Sample ID	Spliced Depth (cm)	Sample Type	14C Age (BP)	Reservoir Corr 14C Age (BP)	Calendar Age BP	Age AD
PO287-26B (32-33 cm)	51.0-52.0	Mollusk shell	440 ± 25	40 ± 25	51 ± 25	1899
D13902 (27-28 cm)	75.4-76.4	Mollusk shell	492 ± 39	92 ± 39	111 ± 39	1839
D13902 (31-32 cm)	*79.4-80.4*	*Mollusk shell*	*2100 ± 80*	*1700 ± 80*	*1700 ± 80*	-
D13902 (37-38 cm)	*85.4-86.4*	*Mollusk shell*	*8955 ± 70*	*8555 ± 70*	*8555 ± 70*	-
D13902 (46-47 cm)	*94.4-95.4*	*Mollusk shell*	*7075 ± 50*	*6675 ± 50*	*6675 ± 50*	-
D13902 (62-63 cm)	110.4-111.4	Mollusk shell	1160 ± 45	760 ± 45	691 ± 45	1259
D13902 (62-63 cm)	110.4-111.4	Turritela	1185 ±40	785 ±40	704 ± 45	1246
D13902 (96-97 cm)	144.4-145.4	Mollusk shell	1370 ±45	970 ± 45	863 ±40	1087
D13902 (124-125 cm)	172.4-173.4	Shell Frag.	1880 ± 80	1480 ± 160	1394 ± 45	556
D13902 (151-152 cm)	199.4-200.4	Mollusk shell	2007 ± 37	1607 ± 37	1487 ± 160	463
D13902 (199-200 cm)	247.4-248.4	Mollusk shell	2340 ± 55	1940 ± 55	1885 ± 37	65
PO287-26G (86-87 cm)	101.6 - 102.6	Mollusk shell	545±25	145±25	1394 ± 45	1801

^{210}Pb analysis was performed on 18 samples (16 box-core and 2 piston-core samples), enabling the assessment of recent mass accumulation rates. The down-core total ^{210}Pb activity profile is shown in Fig. 2. The ^{210}Pb background (^{226}Ra supported ^{210}Pb) of these two core sediments was assumed to be 47 Bq/kg, since this was the value measured in a 760±45 yr BP dated sample (62-63 cm of the D13902 core). The activity profile (Fig. 2) shows an upper interval (≈ 12 cm) of slow exponential downward decline in ^{210}Pb activity, followed by a more rapid decline in the middle (12 to 60 cm), and a lower interval with constant activity. The steep slope observed for the upper interval of the activity profile is attributed to biological mixing (Appleby and Oldfield, 1992). The two higher activity values, found at 19 and 23 cm, are associated with relatively lower values in dry bulk density and at the level of a burrow visible on the box-core picture, and were therefore excluded from the model. The accumulation rate (ω) has been calculated using a constant sedimentation model, with no correction for mixing. Compaction was corrected through the dry bulk density values. The model that best fits the data indicates a mass accumulation rate of 0.55 g/cm^{2}yr and a sedimentation rate in the order of 0.51 cm/yr (Fig. 2).

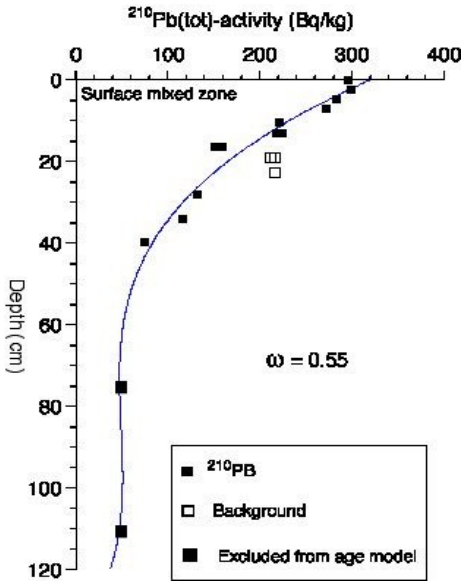

Figure 2. 210Pb activity (Bq/kg) profile obtained for box-core PO287-26 and top of core D13902.

AMS ^{14}C analysis was performed on 13 samples (Table 4). In the box-core, at 32-33 cm, the AMS ^{14}C age obtained is 40±25 yr BP, however, if the box-core depth is corrected for compaction during sub sampling (using the difference in length between the original core and the sub core), the decompacted depth for this sample is 51.5 cm. Assuming that the top sample corresponds to 2001, the estimated sedimentation rate is 0.47 cm/yr.

If this sedimentation rate is considered constant down to the next dated level in core D13902, AMS ^{14}C dated as 92±39 yr BP, then one can estimate that piston core D13902 failed to recover the uppermost 48 cm of the seafloor at this location, a result also given by a simple correlation of the MST and U^{k}_{37} data of both cores, and used to splice the piston with the box-core PO287-26B in order to develop a continuous record throughout the late Holocene (Fig. 3).

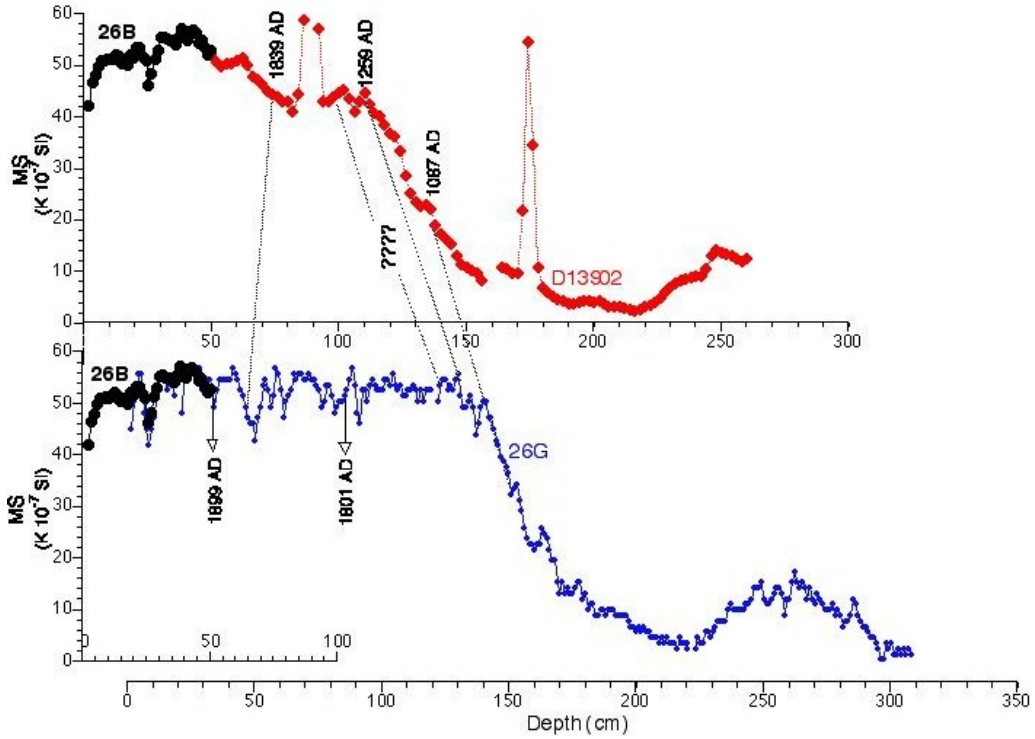

Figure 3. Correlation between cores PO287-26B and D13902, and PO287-26B and PO287-26G based on the MS (10^{-7}SI) record and AMS 14C dates.

The sequence of 3 AMS dates, between 95 to 76 cm which deviate considerably from the remaining 9 dates are not included in the age-depth model for core D13902 (Fig. 4) as they are probably related to redeposition, and their possible sedimentological significance will be discussed in section 4.1.

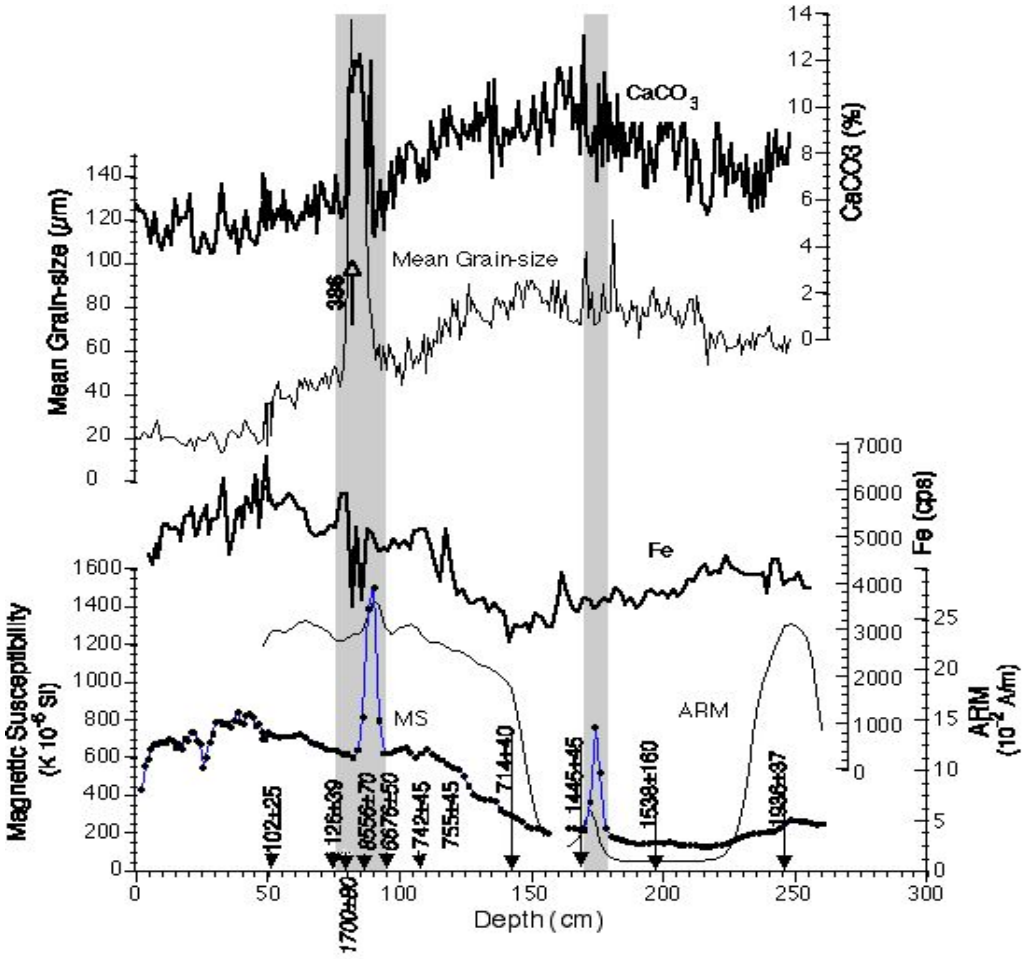

Figure 4. Magnetic susceptibility, ARM, Fe, grain-size mean, CaCO3 percent abundance, and, radiocarbon chronology versus PO287-26 and D13902 composite depth. Ages as calendar yr BP (2001); MS (10^{-6} SI—full dots) and mean grain-size (mm—open diamonds). Gray bands mark the intervals of high magnetic susceptibility.

Gravity core PO287-26G was dated by AMS ^{14}C at 86 cm (Table 4), correlated to the other two cores as shown in Fig.3, and used to fill the gap detected in the record of core D13902.

AMS ^{14}C ages are corrected for a marine reservoir effect of 400 years, as determined for the area (section 3.1) and converted to calendar ages and *Anno Domini* (AD) with the Calib 4.2 program (Stuiver *et al*, 1998).

To avoid major changes in the sedimentation rate resulting from the traditional linear interpolation between ^{14}C dated levels, we have chosen to interpolate linearly between all accepted dated points (Fig. 5) and an estimated sedimentation rate of 0.11 cm/yr is found. However, a major change in sedimentation rate is obvious below and above the interval with anomalous older ages, implying a major hiatus and/or change in sedimentation regime at this level.

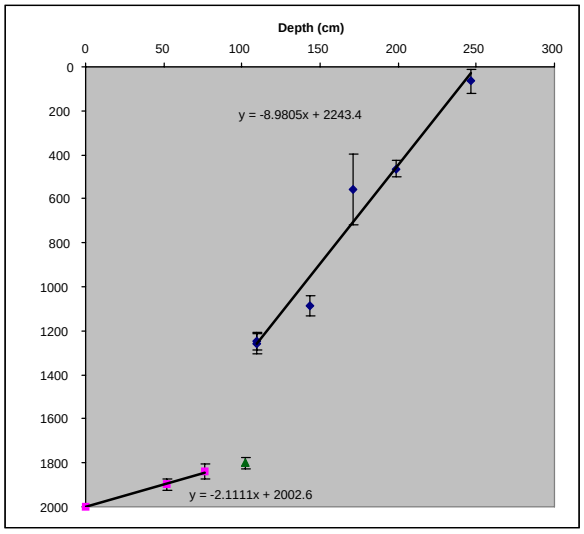

Figure 5. Age versus depth model for cores PO287-26 and top of core D13902 based on AMS 14C ages listed in Table 4. Squares correspond to the box-core PO287-26B and top of core D 13902; diamonds represent ages determined for core D13902, triangle represents the age obtained for core PO287-26G, and circles represent the estimated depth for PO287-26G of D13902 dated levels (as in Fig. 3)

Consistent with the accepted sedimentations rates (0.47 cm/yr for box-core, top 75 cm of piston core D13902, and top 100 cm of gravity core 26G, and 0.11cm/yr for the rest of the piston core and 0.14 cm/yr for the gravity cores (Fig. 5)), a sampling spacing of 1cm provides a mean temporal resolution of 1.5 yr between 1759 and 2001 AD and 8.4 yr between 1600 and 0 AD.

4. RESULTS AND DISCUSSION

4.1. Earthquake Activity

MS, ARM, mean grain size, and $CaCO_3$ content along the spliced sequence (box-core PO287-26B and piston-core D13902) are shown in Fig. 4. Extremely high magnetic susceptibility values are coincident with an ARM increase centered at 90 cm, and are followed around 85 cm by contemporary maxima in mean grain size (up to 386 μm) and in $CaCO_3$ concentration. A smaller maximum in MS and ARM, but no clear increase in mean grain size or in $CaCO_3$, is centered at 174 cm.

The sequence of 3 levels (Table 4) giving ages much older than expected, when all the other dated samples are considered, was found within the 95 to 76 cm interval. Such interval coincides with the first abnormally high peaks in magnetic susceptibility and grain size referred above, which points to a major event / process that caused reworking of older sequences during a short period of time.

Taking into account the above described age model, this sequence is embedded between 1259±45 and 1839±39 AD. This time encompasses 1755, the date of the major earthquake and tsunami felt in the Iberian Peninsula, noted in historical records as the Lisbon earthquake. The earthquake, which had a devastating effect in the Lisbon area, was a multiple event, composed of three shocks (Vilanova *et al.*, 2003) and had an estimated magnitude M of 8.7 (Baptista *et al.*, 1988a) and modified Mercalli (MM) intensity X (Wood and Newmann, 1931 in Vilanova et al, 2003). According to historical records, the earthquake was felt as far north as Sweden and Finland, while the tsunami waves have reached the Caribbean Sea (Baptista *et al.*, 1988b). Eyewitness accounts of the event were compiled and analyzed by Sousa, (1928). In this work one can read "*…waves approached Lisbon with an angle from SE to NE, submerging the downtown area of the city and depositing boats on the top of the old town" (Sousa, 1928);* or yet *" the sea retreated in such a way that for moments the beach was extended to the Torre de S. Juliao"* (close to an old fortress located about 15 km from Lisbon on the estuary N margin, Fig. 1).

Although different epicenters have been proposed by different authors, a SE position relative to the SW Portuguese coast is accepted (Machado, 1966; Zitelini *et al*., 2001; Terrinha *et al*., 2003; Vilanova *et al*., 2003), corroborating the SE direction of water transport indicated by the above translated eyewitness report. A southward origin

is also indicated by the on land deposits found mainly in the southern part of Portugal (Andrade, 2002). However, Vilanova *et al*., (2003) defend that the stress changes resulting from the offshore main shock induced the rupture of Lower Tagus Valley Fault (LTVF in Fig. 1 of Vilanova *et al*, (2003)) a few minutes after the main shock.

This would have resulted in a sequence of high-energy tsunami waves, a tsunami-like wave in the Tagus followed by the arrival of the offshore generated tsunami, which have most likely caused enormous alteration on both the bed of the Estuary and the shallow shelf area of our cores (90 m water depth). Nevertheless, it is also likely that an instantaneous lag deposit was formed by the deposition of part of the material transported by those high-energy waves on their way out. According to J. Dingler (1981) a sedimentary sequence resulting from artificially generated mass flows result in a deposit similar to the one found in this core (Fig. 4), that is, a level of fine magnetic grain size below a much coarser and carbonate rich layer deposited above.

According to the above referred information and the model of Vilanova *et al*., (2003), the western area of the Tagus prodelta is likely to have received more sediment from the tsunami-like wave generated in the Estuary, while a stronger impact by the offshore-generated tsunami wave is likely to have occurred southeastwards of the Tagus estuary mouth. Several cores collected in the area (Fig. 1) were correlated through their magnetic susceptibility records and a few dates (Fig. 6). The records reveal that a general increase in magnetic susceptibility is noticeable at all sites, but the strong magnetic susceptibility peak found in D13902 was not observed in any of the other sites. Spatial comprehensive studies of shallow marine tsunami deposits, such as the one generated on a shallow marine embayment NW of Java by the Krakatau eruption, have revealed major variability in both the composition and thickness of the tsunamite with lack of a record on the north open sea facing part of the bay (van der Bergh *et al*., 2003).

The non-occurrence of a major mark on the sites located to the west of the Tagus river mouth, an area certainly more sheltered from the south coming waves is understandable, but the lack of an equally important mark in PO287-26 is suspicious. Visual examination of the archive halves of both cores does not reveal major perturbations. The MS measurements for D13902 were repeated on U-channels sampled from the central part of the archive core for magnetic measurements to verify for possible liner contamination with downcore sediments through pistonage. Those analyses confirmed the occurrence of a major magnetic susceptibility peak and the

AMR data validates the existence of an exceptionally high concentration of magnetic minerals in fine-grained sediment with no equivalent record found at the bottom of the core. The relative position of the two southern sites may be the explanation. A closer examination of the local bathymetry shows that site PO287-26 has been recovered at a minor canyon, that may have worked as a washout pathway of material towards the deeper Tagus Abyssal Plain, where a major turbidite records the event (Thomson and Weaver, 1994).

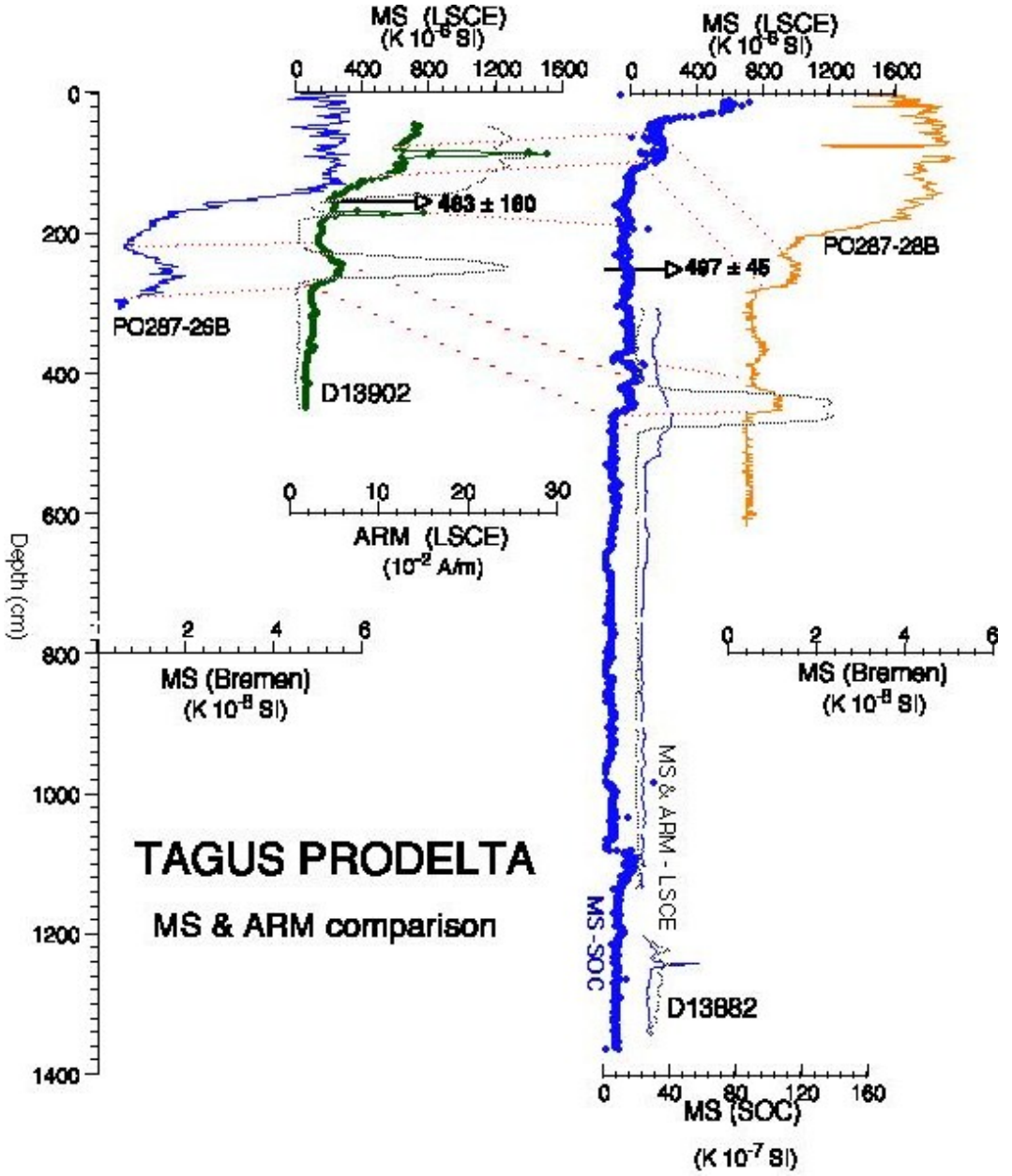

Figure 6. Magnetic susceptibility and ARM comparison for four cores collected on the Tagus Prodelta and depicted on Fig. 1. (Research Institutions where measurements were preformed: LSCE—Laboratoire des Sciences du Climat et de l'Environnement; SOC—Southampton Ocenographic Center; Bremen—University of Bremen.)

With this hypothesis in mind, the 19 cm of older sediments found in D13902 between 95 and 76 cm are likely to correspond to an instantaneous deposit of reworked material transported by the high-energy waves constituting a "tsunami" record. The last dated level below the "tsunamite" (110.9 cm) has an age of 1259 AD. If we assume that the sedimentation rate was maintained at 0.11cm/yr, the estimated age for the last level below the event (95.4 cm) is 1400 AD. Based on the age difference between this level and the year of the tsunami (1755), 355 years of record, about 39 cm of sediment, have been eroded. Even though no clear change in sedimentation pattern is perceived on the MS record of core PO287-26G, from the correlation of the two cores (Figs. 3, 5), either a major change in SR is implied between 86.5 and 130 cm, or there is a loss of ≈ 22 cm sediment (≈160 years of record).

If, on the other hand, one considers a change in sedimentation regime and accepts a drastic decrease in sedimentation rate between 1259 and 1839 AD (Fig. 5), the estimated age limits of the older D13902 sediment sequence become 1515 and 1832 AD, with 1755 AD at 80 cm.

The smaller magnetic susceptibility and ARM maxima centered at 174 cm has an estimated age of 716 AD. In spite of the large number of earthquakes registered in the historical records [Matias/Terrinha, personal communication], no earthquake occurrence is noted between 382 AD and 944 AD. A lack of data that may reflect no occurrence of earthquakes or no registration of those occurrences during this period. As such, this increased magnetic susceptibility and ARM may be a record of another, yet, not historically registered, important earthquake event.

4.2. Climate

Considering the position of this core relative to the major hydrographic processes that presently characterize the Portuguese margin, we intend to reconstruct both the river input/continental climate variability and productivity/upwelling intensity oscillations throughout the last 2,000 years.

4.2.1. Temperature

The SST - $U^{k'}_{37}$ record shows changes between 14ºC and 18ºC (Fig. 7). From 0 to 200 AD, SST values are around 18ºC. Between 200 and 500 AD there is a decrease to ≈ 17°C followed by a new rise to 18ºC at 630 AD. After this date, although variable, SST shows an overall decreasing trend to 17°C at 1080 AD. A period of relatively stable temperatures (17°C) between 1060 and 1200 AD is followed by a minimum at 1365 AD and a new rapid and sharp decrease of 2°C to temperatures ≈ 15°C by 1600 AD. Temperatures that are maintained from 1759 to 1880 AD, with a short duration minima centered at 1860 AD. Since 1900 AD, SST in the Tagus deposition center shows rapid and high amplitude oscillations between 14°C and 17°C at a decadal scale (mean 15.5°C, Stdev 0.82°C) and the top sample of the box-core sequence gives a temperature estimate of 15°C.

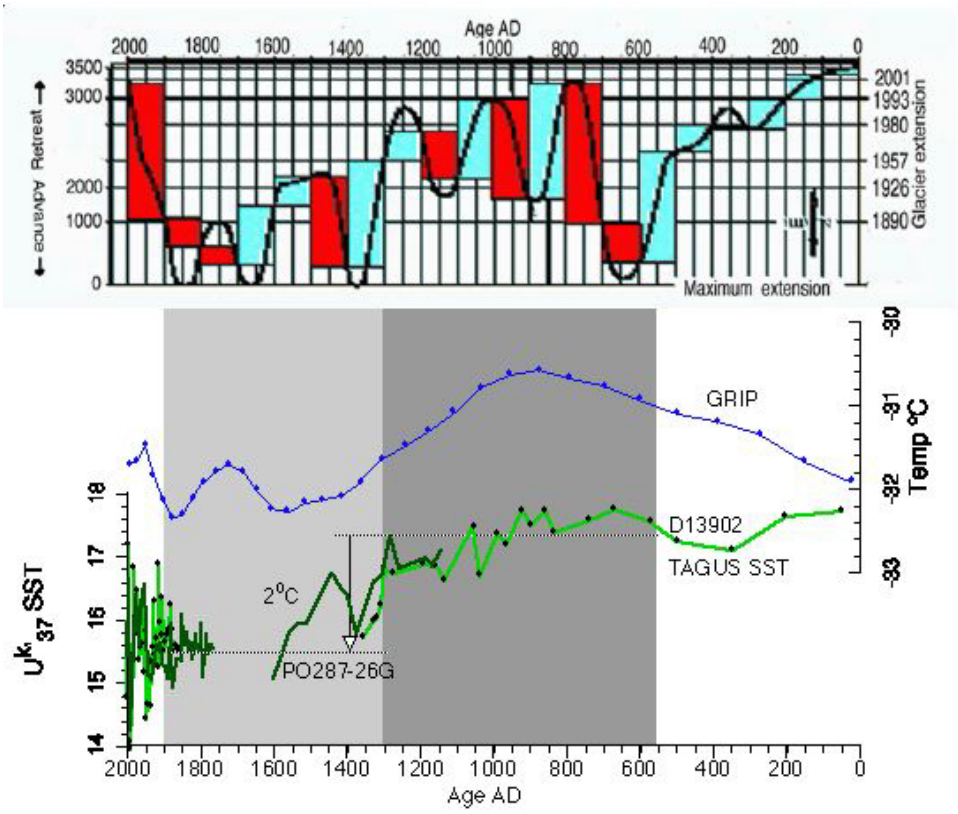

Figure 7. Uk037 derived SST anomaly along the Tagus site compared with GRIP borehole and Alpine glaciers advance. SST record with symbols— D13902 and PO287-26B spliced sequence; Line without symbols—PO287-26G. Light Gray Band—LIA; Dark Gray Band—MWP.

Instant *in situ* temperatures reported by Moita (2001) between summer of 1985 and winter of 1986 vary between 16°C and 14°C respectively (Table 5). Furthermore, satellite derived average SST, calculated from monthly mean values and a time series of data comprising years 1987 to 1999, indicate 15.5ºC for winter, and 19.5ºC for summer temperature (Table 5).

Table 5 - SST and Phytoplankton data for the Tagus prodelta

	Summer	Winter	Spring	Fall
SST (°C)				
In situ (Instantaneous)*	16,0	14,0	14,5	-
Satellite mean (1987-1999)	19,5	15,5	17,5	17,5
Total Phytoplankton (# cells/L)*	20.000	1.000	10.000	-
% Coccolithophores*	25-50	50-75	>80	-

* - Data from Moita (2001)

Alkenones are produced by coccolithophores. The work of Moita (2001) has shown that in the Tagus pro-delta coccolithophores dominate the plankton for most of the year, being outcompeated by diatoms only during the upwelling season. Given that upwelling is more likely to occur between May and September (Fiuza, 1983; 1984), we expect SST - $U^{k'}_{37}$ will mainly reflect winter to early spring temperatures. The SST - $U^{k'}_{37}$ temperature calculated from the box-core levels corresponding to this same time interval is 15ºC, in good agreement with the satellite-derived values, considering the errors of each method.

The SST - U^{k}_{37} off Lisbon (Fig. 7) shows a general decreasing trend for the last 2,000 years, marked by the first sharp decline at 1300 AD, but reaching minimum temperatures at ≈ 1600 AD. Although interrupted, between 1759 and 1900 AD, temperatures were still ≈ 15ºC with a short minima at 1860 AD. A wide range of climate proxies measured throughout the globe indicate that temperatures were colder than present during the LIA from 1300 to 1900 AD (deMenocal *et al*., 2000a; Dunbar and Cole, 1999; Esper *et al.*, 2002; Grudd *et al.*, 2002; Gupta *et al*., 2003; Keigwin, 1996; Keigwin and Pickart, 1999; McDermott *et al.,* 2001; Stuiver and Braziunas, 1989). This cold period was preceded by warmer temperatures in the medieval times. Although less clearly defined and dated in a lower number of sites, the MWP is considered to have occurred between 800 and 1300 AD (Cronin *et al*., 2003, Dahl-~

Jensen *et al*., 1998, deMenocal *et al*., 2000; Jones *et al*, 2001). In our record, temperatures for this period show a mean value 1.5 to 2^{o}C higher than the mean temperature observed between 1300 and 1900 AD. A record that shows good agreement with both the trend and the magnitude of change observed in the Greenland boreholes (Fig. 7) (Dahl-Jensen *et al*., 1998). However, SST starts to raise around 550 AD, again in good agreement with the GRIP record, but about 100 years earlier than the Alpine Glacier receding (Holzhauser 1997, Haeberli and Holzhauser, 2003). In addition, most sedimentological parameters indicate that the 550 – 1300 AD interval had climatic and oceanographic characteristics clearly different from the ones recorded before and after it, and it is by this reason considered to represent the warmer period of the last 2000 years at the Tagus site.

Within the last 100 years the mean SST value registered in the Tagus record equals the mean value for the 1300-1900 AD interval. However, the existing record shows rather stable SSTs between 1759-1900 AD, while for the last 100 years rapid variability of broadening amplitude towards the Present is observed.

4.2.2. River input / Continental Climate

Satellite derived estimations of the suspended load in the Tagus river plume for a time series between May 1992 and January 1993 (Williams, 1994) indicate that the load of suspended particles, although higher in winter, is important throughout the year. As shown in Fig. 8 from an image of the space shuttle taken in September 1992, sites PO287-26 and D13902 fall within the area of influence of river discharge. In addition, short but strong rainfall events may lead to floods such as the one observed in February of 1979, causing river flows (12000 m^3/s) 10^6 times higher than the month average (0.9 m^3/s) and 30 times higher than the mean annual flow (400m^3/s). During these flood events the suspended load reaches 300 mg/l while the regular values are around 20mg/l (Vale, 1981). Having these observations in consideration, the increase in deposition of fine continental derived material at sites PO287-26 and D13902 can be related with rainfall increases.

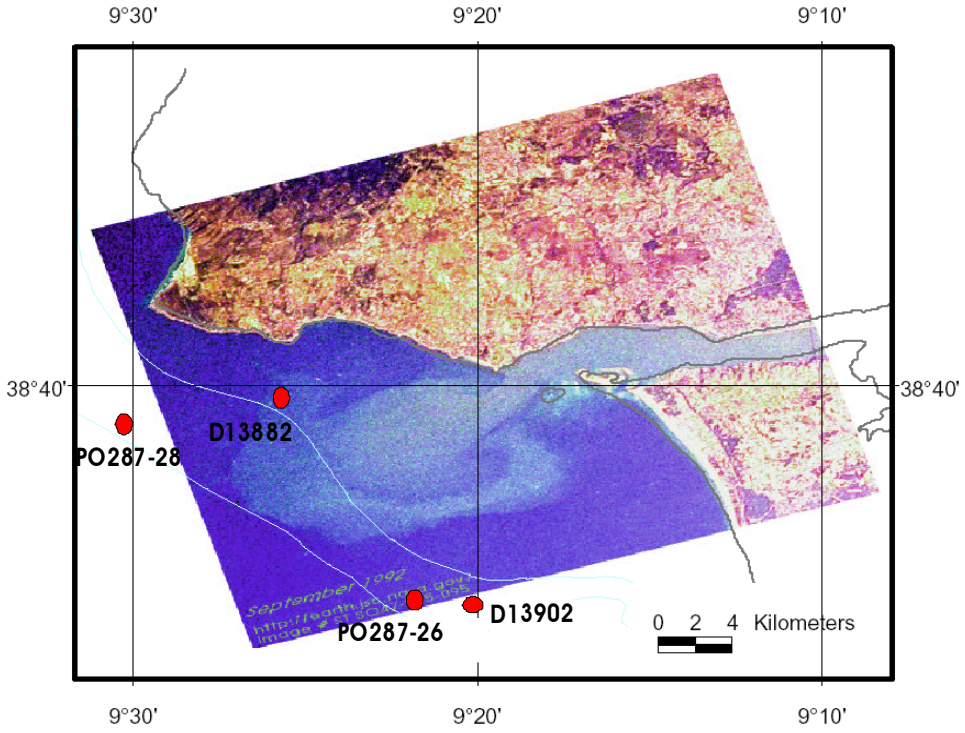

Figure 8. Space shuttle image of the Tagus River plume (September 1992). http://earth.jsc.nasa.gov/image#SO47-085-095.

At our site the sediments are mainly constituted of terrigenous material with low $CaCO_3$ contents between 4 and 14% (Fig. 9). In terms of grain size, this sequence can be divided in three sections: 0-550 AD, 550-1300 AD and 1300 AD-Present, encompassing essentially mud (sediment fraction < 63µm - 50-60%), sand (47%), and mud again (70-80%). This suggests increased river input before 550 AD and after 1300 AD.

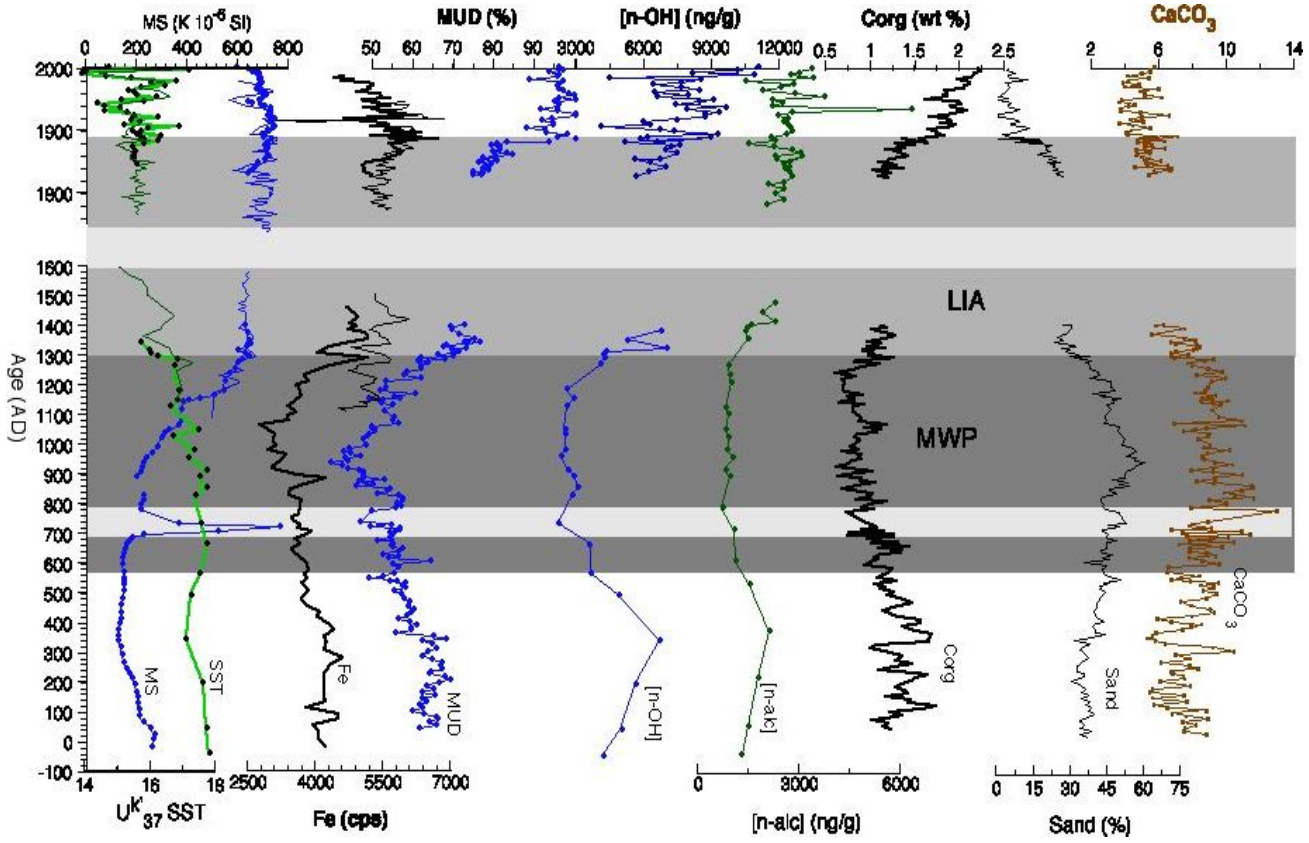

Figure 9. Continental climate proxies along cores PO287-26 and D13902. MS—magnetic susceptibility (10^{-6} SI units); Uk37 derived SST, Fe content as determined by XRF in cps units; Mud—Percent abundance of the sediment fraction o63 mm; [n-OH]—alcohols concentration; [n-alc]—alkanes concentration; Corg—Organic Carbon content; Percent abundance of Sand; grain-size mean (mm). For MS, SST and Fe thick line represents the data for the D13902 and PO287-26-B spliced sequence, and the thin line the data for core PO287-26G. Medium Gray Band—LIA; Dark Gray Band— MWP; Light Gray bands—Intervals of high MS.

From the other parameters measured along these cores, MS, Fe, n-alkanes, and n-alcohols are well-accepted indicators of terrigenous input (Farrington *et al.*, 1988; Fischer and Wefer, 1999; Lamy *et al.*, 1998; Ortiz and Rack, 1999; Poynter *et al.*, 1989).

MS shows extremely high values at the 76 – 95 cm and 170 - 174 cm intervals, which most certainly correspond to reworked material (Fig. 4, section 4.1). If these maxima are excluded, MS shows values between 100 and 700 K 10^{-6} SI units, with highest values above 1300 AD, and a broad minimum between 200 and 1200 AD (Fig. 9). Similarly, increases in Fe content (cps) clearly follow the mud distribution along the

core, being essentially associated with the finer material. The same is observed for the organic carbon (Corg) content, with percentage abundances varying between 0.5% and 1.5% and a tendency to increase in association to mud content, while higher $CaCO_3$ abundances are found concurrently with the coarser sediments between 550 and 1300 AD (Figs. 4, 9).

The lipid composition of this sedimentary sequence is dominated by compounds of terrigenous origin, such as the C_{23}-C_{33} n-alkanes and C_{20}-C_{30} n-alcohols, with higher concentrations for the later. The strong correlation of both lipid groups to the previously discussed indicators of alocthonous input and the presence of fresh water diatoms (Figs. 9, 10), confirm an increase in sedimentation of continental derived material mainly during the LIA. Within the last century all parameters show decadal cyclicity, but a decreasing tendency is observable in the Fe concentration and mean grain-size (Figs. 4, 9) also accompanied by a decrease in Mass Accumulation Rate (MAR – Fig. 10). The decrease may be due to the retention of sediments that resulted from the construction of 52 dams along both the Spanish and Portuguese sides of the Tagus. In particular between 1940 and 1960 when rapid construction of a large number of dams increasedthe areal surface and water volume retained by about 5 times (www.snirh.inag.pt; www.chtajo.es).

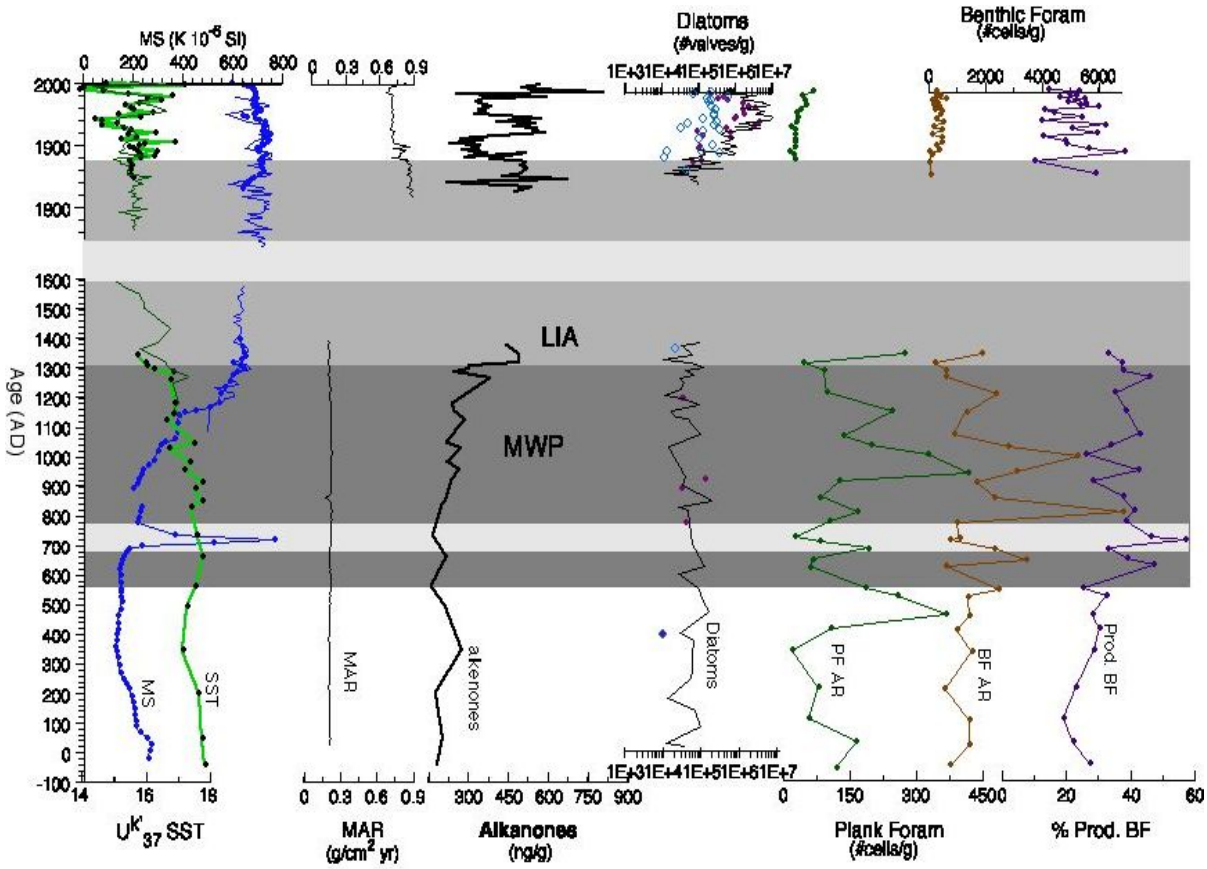

Figure 10. Productivity proxies along cores PO287-26 and D13902. MS—magnetic susceptibility (data in cgs units 10^{-6}); Uk37 derived SST anomaly to the mean; MAR—Mass Accumulation Rate as g/cm2 yr; Alkenones abundance (ng/g); Diatom abundance as #valves/g of dry sediment, freshwater diatoms, K—upwelling related diatoms; Planktonic Foraminifera Abundance in #shells/g; Benthic Foraminifera Abundance as #shells/g; % Prod. PF—Percent abundance of the high carbon flux benthic foraminiferal species. Medium Gray Band—LIA; Dark Gray Band—MWP; Light Gray bands—Intervals of high magnetic susceptibility.

4.2.3 Sea Water Salinity

The oxygen stable isotopic composition ($\delta^{18}O$) of the planktonic foraminifera *Globigerina bulloides* and the benthic species *Uvigerina* sp. 221 along the composite sequences are shown in Fig. 11. The results show parallel trends for both records, with an almost constant offset between 0 and 1300 AD. $\delta^{18}O$ oscillates around 0.5‰ and 1.75‰ for *G. bulloides* and *Uvigerina* respectively. In the last 100 years, the *G. bulloides* record shows a more pronounced variability exhibiting an overall decrease in $\delta^{18}O$ towards -0.1‰ for the most recent samples.

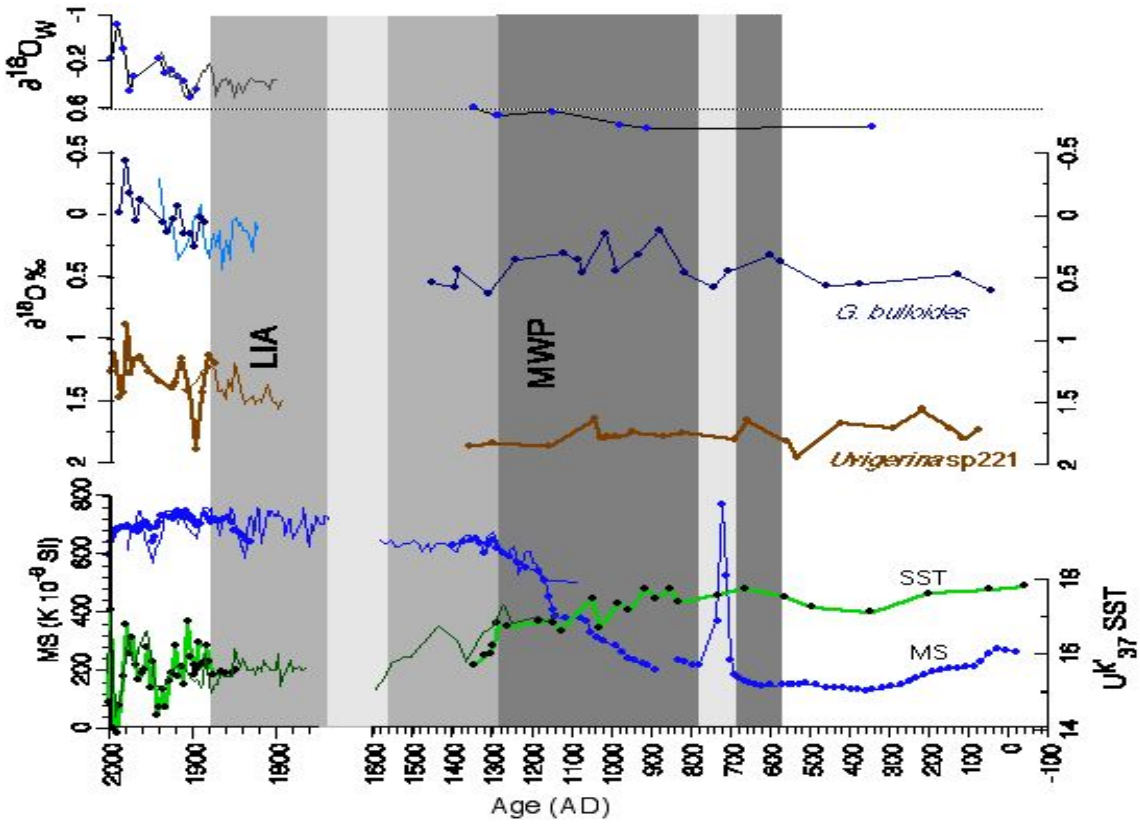

Figure 11. Isotopic record for $\delta^{18}O$ on G. bulloides and Uvigerina sp. 221 and $\delta^{18}Ow$ anomaly along cores PO287-26B and D13902. Medium Gray Band—LIA; Dark Gray Band—MWP; Light Gray bands—Intervals of high magnetic susceptibility.

Comparison of the variations in terrigenous inputs with past salinities should provide information on the magnitude of the river flow. Salinity in the river plume is generally bellow 35 p.s.u. during Winter and most of Spring (Moita, 2001). $\delta^{18}O$ of

foraminifera is mainly determined by $\delta^{18}O$ of ambient seawater and temperature. During the time interval in focus no major global ice volume related $\delta^{18}O$ variations have occurred, thus, at this location, most of the *G. bulloides* $\delta^{18}O$ signal must reflect regional temperature and salinity conditions, while the *Uvigerina* values are likely to record the bottom water (90 m water depth) and oceanic conditions. Lighter $\delta^{18}O$ values of *G. bulloides* do appear to be associated with increases in MST and Fe, consistently with increased precipitation and river runoff (Fig. 9). As $\delta^{18}O$ is linearly related to salinity, paleosalinities (SSS) can be reconstructed if independent measures of SST are available (Duplessy *et al*., 1991; Rostek *et al*., 1993). In the present study, $\delta^{18}O$ of *G. bulloides* and SST - $U^{k'}_{37}$ are used. Both proxies reflect surface temperatures within the photic zone (Bentaleb *et al*., 1999). Thus, given the shallow depth of the site, no correction for temperature was applied to the *G. bulloides* $\delta^{18}O$ values.

The paleotemperature equation of Shackleton (1974) was used for the reconstruction of $\delta^{18}O$ of ambient seawater:

$$T = 16.9 - 4.38\ (\delta^{18}O_{carb} - \delta^{18}O_w) + 0.1\ (\delta^{18}O_{carb} - \delta^{18}O_w)$$

where T is paleotemperature (^oC), $\delta^{18}O_w = \delta^{18}O$ of ambient seawater (per mil versus SMOW), and $\delta^{18}O_{carb} = \delta^{18}O$ of carbonate (*G. bulloides*) (per mil versus PDB).

The lack of a local $\delta^{18}O$ / salinity relationship, prevents the calculation of SSS values, but in the absence of major ice cap changes within the last 2,000 years, the anomaly is assumed to be related to changes in salinity driven by river flux.

Calculations can only be done for the levels with foraminifera and alkenone measurements, but the general tendency to lighter $\delta^{18}O$ of ambient waters observed after 1300 AD can certainly reflect fresher waters (Figs. 9, 11). Besides, a relation between decreased salinity and lower temperatures is clear above 1900 AD.

4.2.4 The North Atlantic Oscillation and the Tagus regime

The MWP as defined from the alkenone derived temperature (Fig. 7), corresponds to the carbonate maxima positioned between the LIA $CaCO_3$ minima and the earlier $CaCO_3$ minima between 200 and 550 AD. This carbonate increase is accompanied by an increase in mean grain size and minima in continental input indicators.

The relevance of the NAO to the wintertime temperatures, wind speed and direction, and, precipitation across much of the Northern Hemisphere in general, and over the Atlantic / European sector in particular, has been well documented through a number of different studies (Hurrel, 1995, 1996; Rogers, 1997, Osborn *et al*., 1999; Ulbrich *et al*., 1999; Qian *et al.*, 2000). Furthermore, the work of Trigo *et al*., (2002) indicates a high correlation between precipitation rate during winter months and low NAO index for the area of the Tagus Basin. A comparison of Hurrel's NAO index (difference between normalized winter sea-level atmospheric pressures between Lisbon, Portugal, and Stykkisholmur, Iceland – Hurrel, 1995) to the Tagus river mean winter (December-March) discharge between 1900 and 2000 AD is presented in Fig. 12 and reveals a good negative correlation to NAO. Both these results support the influence of the NAO on river regime, and are consistent with, though not proof of, a possible long-term association as well. As so, a NAO-like mechanism or the NAO itself, which tended to remain in a low index phase during LIA, and in a high phase during the MWP, could account for the findings off Lisbon. Further indications of a primarily negative NAO during LIA have been found from the study of sedimentary sequences off Norway (Koç *et al.*, 2003) and off Newfoundland (Keigwin and Pickart, 1999), as well as from dendrochronologic summer temperature reconstruction (Grudd *et al.*, 2002). An essentially NAO negative like phase before 1800 AD is also supported by Luterbarcher et al., (2002) NAO reconstruction (1400 AD to Present).

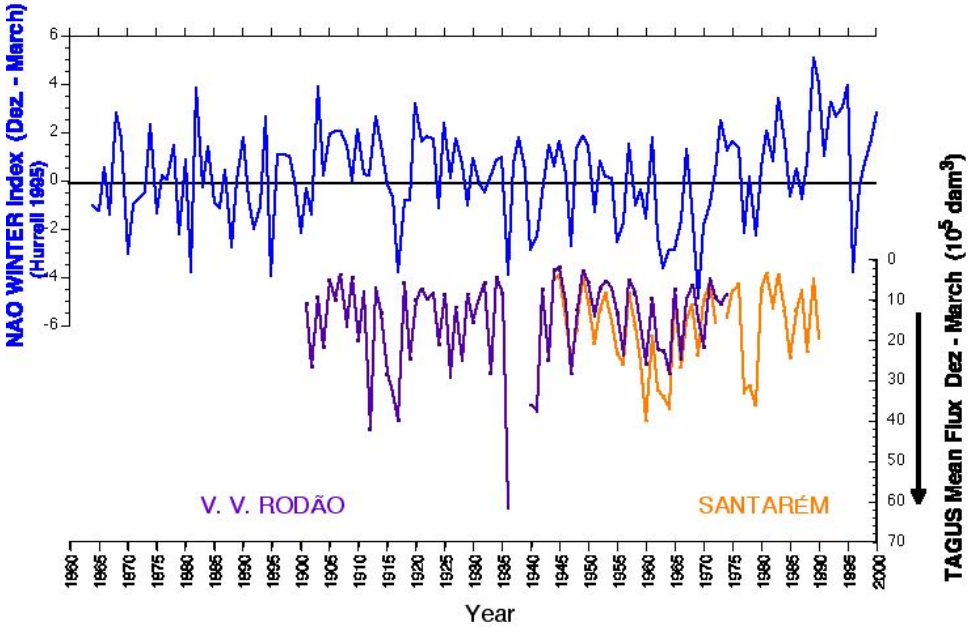

Figure 12. Comparison of the NAO Index of Hurrell (1995) to the Tagus mean flux during the winter months (December–March) as measured at Vila Velha de Rodão and Santarem between 1900 and 2003.

4.3 Coastal Productivity

Increased primary productivity is generated by the input of new nutrients into the euphotic zone (Dugdale and Goering, 1967; Margalef, 1985). Both coastal upwelling and river runoff can bring new nutrients into coastal regions. However, the water column conditions generated by these processes are different, involving strong mixing and stratification respectively. While strong mixing caused by upwelling favors the dominance of diatoms, stratification leads to a coccolithophore dominated community (Margalef, 1978; Moita, 2001).

Foraminifera, in the second level of the food chain, react to the increase in primary producers. Increases in planktonic foraminifera fluxes as a response to upwelling pulses have been observed in sediment trap experiments (Sautter and Thunell, 1991; Curry and Ostermann, 1992; Ortiz and Mix, 1992; Thunnel and Sautter, 1992; Sautter and Sancetta, 1992; Wefer and Fisher, 1993; Abrantes *et al*., 2002). In addition, increased abundances of benthic foraminifera have been reported as consequence of increases in particle rain to the sea floor (Lutze and Coulbourn, 1984; Altenbach and Sarnthein, 1989; Loubere, 1991; Herguera, 1992; Rathburn and Corliss, 1994).

At our site, diatoms are present in small numbers, one order of magnitude lower than observed in the surface sediments along the rest of the Portuguese coast (Abrantes, 1988) (Fig. 10). Although the evident dissolution indicated by the rapid and important decrease in diatom abundance at about 1940 AD (≈ 30 cm within the sediment), the occurrence of low values both in large grain-size sediments and during periods of increased sedimentation of fine continental derived particles, when a sealing effect could lead to better preservation (Broecker and Peng, 1982), points to initial production as its main control. In terms of assemblages, benthic forms are dominant, but upwelling related species (F) are present between 550 and 1300 AD (MWP) and in the last 100 years, while freshwater forms (A) are only present before 500 and after 1300 AD (Fig10).

As for the total alkenones, considered to represent coccolithophore production (Shubert *et al*., 1998; Schulte *et al*., 1999; Villanueva *et al.,* 1998; 2001), concentrations are also lower than those found in cores from the open Atlantic (Bard *et al*., 2000; Villanueva *et al*., 1998; 2001). In this case, alkenone concentration increases from 200 ng/g (0 to 1300 AD) to cyclicity between 300 and 600 ng/g after 1300 AD, mimicing increments in continental input indicators, such as Fe and n-alkanes or n-alcohols (Fig. 9). Based on the work of Cabeçadas *et al*., (2003), winter NO_3 concentrations at the Tagus estuary mouth are about 15 µmol/l decreasing to 4 µmol/l at 1.5 nautical miles further offshore. The significance of the Tagus River as a source of PO_4^{3-} into the coastal water column has also been calculated by quantification of the sediment P and N pool sizes (Cabeçadas and Burgueira, 1997). River-induced coccolithophore production is then likely to have occurred during the LIA (1300 to 1900 AD).

At this shallow site, planktonic foraminifera have abundances (100-450 shells/g) one order of magnitude lower than benthic foraminifera (500-6000 shells/g) and most of the observed forms are juvenile. However, the downcore trend is similar for both groups. Higher abundances and amplitude variation are observed between 500 and 1300 AD, while lower abundances and less variability are observed before 500 AD and at the top of the sequence.

Within the benthic foraminifera species found in these cores, *Bolivina dilatata (Bolivina spathulata* in Levy *et al.,* 1995*), Bolivina striatula,* and *Hyalinea balthica* have been related to productivity in the overlying waters (Levy *et al*., 1993; Jónsdóttir *et al*., 2003). Besides, the works of Lutze, (1984), Altenbach, (1988), Altenbach and

Sarnthein, (1989) and Schmiedl, (1995) have shown that the *Uvigerina* group responds to high carbon fluxes. The percent contribution of all these species to the benthic assemblage (Fig. 10) varies between 20 and 60%, with clear cyclicity and higher average values between 550 and 1300 AD.

Increased abundances of foraminifera, both benthic and planktonic, and the presence of upwelling related diatoms during the MWP (Fig. 10), point to the MWP as an interval of stronger upwelling conditions. These results are in good agreement with the results of Diz *et al.,* (2003) for a northern Iberian site (Ria de Muros), but in apparent contradiction with the published data for NW Africa by deMenocal *et al*. (2000b). This author hypothesized an enhanced eastern boundary current delivery of cold subpolar waters or an increase in regional upwelling as a possible explanation for the lower temperatures observed off the NW African coast during the LIA. Iberia and the NW African coasts are influenced by the same eastern boundary current, the Portuguese-Canary current. Nevertheless, significant differences exist between the two sites: (1) at modern times, upwelling favorable conditions occur year round off NW Africa, but only for about 5 months off Portugal; (2) the Tagus site is right under the influence of the river plume and can only feel the Cape Roca filament productivity if and when upwelling conditions are strong. Considering the results of Salgueiro *et al.*, (2003) who did planktonic foraminifera sensus counts and foraminifera derived SST on four box-cores located along a profile on the SW Portuguese margin, no major changes in upwelling conditions are observed between the LIA and the MWP, despite the SST variations. This may indicate that even though the eastern boundary system is likely to have been maintained, the Portuguese/Canary Current System transported colder subpolar waters. The decrease in SSTs by 2ºC (Tagus) and 4ºC off NW Africa (deMenocal et al., 2000) is consistent with other data from the Bermuda Rise (Keigwin, 1996) and may indeed reflect the advection of anomalous temperatures by the Gulf Stream/North Atlantic Current system considered by Visbeck et al., (2003) as the reason for Hemispheric SST variability on multidecadal time scales.

As for the MWP, one could argue that less river input of alochthonous material to the Tagus site, could lead to an apparent increase in the productivity indicators, just by a lower dilution effect. However, MAR does not vary throughout the MWP, but the sediment terrigenous content decreases during this period, as indicated by grain-size and all other river input indicators. As such, a real increase in carbonate biogenic particles

production and sedimentation, certainly caused by more persistent and/or intense coastal upwelling conditions, takes place (Figs. 9, 10).

Instrumental data indicates that during positive NAO index, precipitation is reduced and the stronger north Atlantic pressure gradient generates winds favorable to the occurrence of coastal upwelling as well as a strengthening of the North Atlantic current system. Nykjaer and Van Camp (1994) and Oliveira (2000), have calculated the interannual variability of SST, upwelling Index, and Ekman Upwelling Index for the years 1981-1989 and found that the largest anomalies (i.e., more intense upwelling than average occurred in 1982, 1985 and 1988) are in good agreement with positive NAO index (Fig. 10). As for the LIA, modern NAO conditions might also be used as an analogue to explain the Tagus MWP record (drier continental conditions and increased coastal upwelling) if more consistent or extreme positive NAO conditions were maintained during the few centuries that preceded the LIA.

5. CONCLUSIONS

Proxy evidence illustrates the high sensitivity of the Tagus river regime to the climatic variability of the last two millennia and reveals a record of a major earthquake felt in the region, as recorded by a large peak in MS centred at 90 cm. The well known 1755 AD Lisbon earthquake and tsunami, is estimated to have caused the erosion of 160 to 355 years of sedimentary record (most of the LIA) and the instantaneous deposition at site D13902 of a 19 cm sediment bed consisting of a lower layer of silt sized heavy mineral particles, followed by a coarser layer composed of reworked shell fragments.
Within dating uncertainties (± 50 years) and even though the spliced sequence lacks ≈160 years of record, the SST - $U^{k'}_{37}$ for the latest Holocene (2,000 years) off Lisbon, can be correlated to the GRIP borehole temperature, allowing the identification of a warm period (MWP) that spans from 550 to 1300 AD, as well as the LIA.

The marine geological data presented here point to dryer continental conditions and increased coastal upwelling conditions during MWP, and indicate increased river influx and river induced marine productivity during LIA. Because negative NAO is correlated with precipitation anomaly fields in the Tagus basin, the LIA increased influx of terrigenous material into the studied site is hypothesized to reflect NAO-like variability with more persistent negative state or frequent extreme NAO minima during

the LIA. During the milder few centuries of the MWP coastal upwelling favorable conditions are attributed to more persistently positive state or frequent extreme NAO maxima.

ACKNOWLEDGEMENTS

We thank the captain and crew of RV Discovery and RV Poseidon for their help in collecting the samples. A. Inês, C. Monteiro, M.J. Custódio, A. Silva and C. Trindade of the Institute of Geology and Mining are acknowledged for analytical assistance. The EU PALEOSTUDIES project supported the XRF measurements. Monika Siegel is acknowledged by her help with the isotope measurements, and J. Heinnemeier and W. Boer by the AMS ^{14}C dating and ^{210}Pb measurements respectively. We also thank the Aquário Vasco da Gama for allowing the use of the D. Carlos collection. Thanks are also due to A. Voelker and two anonimous reviewers for the careful review of the initial manuscript. Financial support was provided by the EU projects HOLSMEER (EVK2-CT-2000-00060) and PACLIVA (EVK2-CT2002-00143). Funding for T. Rodrigues was provided by the Fundação para a Ciência e Tecnologia, through the INGMAR project.

6. REFERENCES

Abrantes, F. 1988. Diatom assemblages as upwelling indicators in surface sediments in Portugal. Marine Geology 85, 15-39.

Abrantes, F., Meggers, H., Nave, S., Bollman, J., Palma, S., Sprengel, C., Hendericks, J., Spies, A., Salgueiro, E., Moita, T., and Neuer, S., 2002. Fluxes of micro-organisms along a productivity gradient in the Canary Islands region (29º N): implications for paleoreconstructions. Deep-Sea Research II 49, 3599-3629.

Abrantes, F., and Moita, T., 1999. Water Column and Recent Sediment Data on Diatoms and Coccolithophorids, off Portugal, Confirm Sediment Record as a Memory of Upwelling Events. Oceanologica Acta 22, 319-336.

Altenbach, A. V., 1988. Deep sea benthic foraminifera and flux rates of organic carbon. Review Paléobiologie (vol spéc.) 2, 719-720.

Altenbach, A. V., and Sarnthein, M., 1989. Productivity Record in Benthic Foraminifera. In: W. H. Berger, V. S. Smetacek, and G. Wefer, (Eds.), Productivity of the Ocean: Present and Past. Dahlem Workshop - Life Sciences research Reports. John Wiley & Sons, Berlin, pp. 255-270.

Andrade, C., 2002. Assinaturas Geológicas de Inundação Tsunamigénica no Litoral do Algarve. In: 3º Encontro de Professores de Geociências do Algarve.

Appleby, P. G., and Oldfield, F., 1992. Applications of lead-210 to sedimentation studies. Clarendon Press, Oxford.

Baptista, M., Miranda, P., and Mendes Victor, L., 1988a. Constraints on the source of the 1755 Lisbon tsunami inferred from numerical modelling of historical data. Journal of Geodynamics 25, 159-174.

Baptista, M. A., S.Heitor, Miranda, J. M., Miranda, P., and Victor, L. M., 1988b. The 1755 Lisbon tsunami; evaluation of the tsunami parameters. Journal of Geodynamics 25, 143-157.

Bard, E., Rostek, F., Turon, J.-L., and Gendreau, S., 2000. Hydrological Impact of Heinrich Events in the Subtropical Northeast Atlantic. Science 289, 1321-1324.

Bond, G., Kromer, B., Beer, J., Muscheler, R., Evans, M., Showers, W., Hoffmann, S., Lotti-Bond, R., Hajdas, I., and Bonani, G., 2001. Persistent Solar Influence on North Atlantic Climate During the Holocene. Science 294, 2130-2136.

Bond, G., Showers, W., Cheseby, M., Lotti, R., Almasi, P., and deMenocal, P., 1997. A pervasive millenial-scale cycle in North Atlantic Holocene and Glacial climates. Science 278, 1257-1266.

Broecker, W. S., 2001. Was the Medieval Warm Period Global? Science 291, 1497-1499.

Broecker, W. S., and Peng, T. H., 1982. Tracers in the sea. Eldigio Press, New York.

Cabeçadas, G., and Brogueira, M. J., 1997. Sediments in a Portuguese coastal area - pool sizes of mobile and immobile forms of nirogen and phosphorus. Mar. Freshwater Research 48, 559-563.

Cabeçadas, G., Rogueira, M. J., Nogueira, M., Cabeçadas, L., Cavaco, H., and Nogueira, P., 2003. Coastal phytoplankton productivity associated with different stability and Nutrient patterns. EGS-AGU-EUG Joint meeting. AGU, Nice, France. pp. EAE-A-09277.

Cronin, T. M., Dwyer, G. S., Kamiya, T., Schwede, S., and Willard, D. A., 2003. Medieval Warm Period, Little Ice Age and 20th century temperature variability from Chesapeake Bay. Global and Planetary Change 36, 17-29.

Curry, W. B., and Ostermann, D. R., 1992. Foraminiferal production and monsoonal upwelling in the Arabian sea: evidence from sediment traps. In: C. P. Summerhayes, W. L. Prell, and K. C. Emeis (Eds.), Evolution of upwelling systems since the early Miocene. Geological Society Special Publication Nº64, London. pp. 93 - 106.

Dahl-Jensen, D., Mosegaard, K., Gundestrup, N., Clow, G. D., Johnsen, S., Hansen, A. W., and Balling, N., 1998. Past Temperatures Directly from the Greenland Ice Sheet. Science 282, 268-271.

de Abreu, L., 2000. High Resolution Paleoceanography off Portugal During the Last Two Glacial Cycles. Unpublished Dissertation thesis, University of Cambridge.

deMenocal, P., Ortiz, J., Guilderson, T., Adkins, J., Sarnthein, M., Baker, L., and Yarusinsky, M., 2000a. Abrupt onset and termination of the African Humid Period: rapid climate responses to gradual insolation forcing. Quaternary Science Reviews 19, 347-361.

deMenocal, P., Ortiz, J., Guilderson, T., and Sarnthein, M., 2000b. Coherent High- and Low-Latitude Climate Variability During the Holocene Warm Period. Science 288, 2198-2202.

Dingler, J. and Anima, R., 1981. Field study of subaqueous avalanching. AAPG Bulletin 65-5, 918-919.

Diz, P., Francés, G., Pena, L., Nombela, M. A., and Alejo, I., 2003. Benthic Foraminifera response to Holocene Environmental Changes in the Ría de Muros (NW Spain). EGU-AGU-EUG General Assembly. AGU, Nice.

Dugdale, R., and Goering, J., 1976. Uptake of new and regenerated forms of nitrogen in primary productivity. Limnology and Oceanography 12, 196-206.

Dunbar, R., and Cole, J., 1999. Annual Records of Tropical Systems (ARTS), Recommendations for Research. PAGES Workshop Report. pp. 72

Duplessy, J.-C., Laberyie, J., Juillet-Leclerc, A., Maitre, F., Duprat, J., and Sarnthein, M., 1984. Surface salinity reconstruction of the North Atlantic Ocean during the Last Glacial Maximum. Oceanologica Acta 14, 311 –324.

Esper, J., Cook, E. R., and Schweingruber, F. H., 2002. Low-Frequency Signals in Long Tre-Ring Chronologies for Reconstructing Past Temperature. Science 295, 2250-2253.

Farrington , H.W., Davis, A. C., Sulanowski, J., McCaffrey, M.A., McCarthy, M., Clifford, C.H., Dickinson, P. and Volkman, J.K., 1988. Biogeochemistry of lipids in surface sediments of the Peru upwelling area at 15ºS. Organics Geochemistry 13(4-6), 607-617.

Fischer, G., and Wefer, G., 1999. Use of Proxies in Paleoceanography. Springer-Verlag, Berlin.

Fiuza, A., 1983. Upwelling patterns off Portugal. In: Suess, E., and Thiede, J. (Eds.), Coastal Upwelling its sediment record. Plenum, New York. pp. 85-98.

Fiuza, A., 1984. Hidrologia e Dinamica das Aguas Costeiras de Portugal. Unpublished Dissertation Thesis, University of Lisbon.

Gaspar, L., and Monteiro, H., 1977. Matéria Orgânica nos sedimentos da plataforma continental portuguesa entre os cabos Espichel e Raso. Comunicações dos Serviços Geológicos de Portugal LXII, 69-83.

Goodfriend, G., and Flessa, K., 1997. Radiocarbon Reservoir Ages in the Gulf of California: Roles of Upwelling and Flow from the Colorado River. Radiocarbon 39, 137-148.

Grudd, H., Briffa, K. R., Karlen, W., Bartholin, T., Jones, P. D., and Kromer, B., 2002. A 7400-year tree-ring chronology in northern Swedish Lapland: natural climatic variability expressed on annual to millenial timescales. The Holocene 12, 657-666.

Gupta, A., Anderson, D., and Overpeck, J., 2003. Abrupt changes in the Asian southwest monsoon during the Holocene and their links to the North Atlantic Ocean. Nature 421, 354-357.

Haeberli, W., and Holzhauser, H., 2003. Alpine Glacier Mass Changes During the Past Two Millenia. PAGES News 11, 13-15.

Herguera, J. C., 1992. Deep-sea benthic foraminifera and biogenic opal: Glacial to postglacial productivity changes in the western equatorial Pacific. Marine Micropaleontology 19, 79-98.

Holzhauser, H., 1997. Fluctuations of the Grosser Aletsch Glacier and the Gorner Glacier during the last 3200 years: new results. Palaeoclimate Research 24, 35-58.

Hurrell, J., 1995. Decadal trends in the North Atlantic Oscillation - regional temperatures and precipitation. Science 269, 679.

Hurrell, J., 1996. Influence of varitions in extratropical wintertime teleconnections on Northern Hemisphere temperature. Geophysical Research Letters 23, 665-668.

Hurrell, J., Kushnir, Y., Ottersen, G., and Visbeck, M. 2003. An overview of the North Atlantic Oscillation. In: Hurrel, J., Kushnir, Y., Ottersen, G., and Visbeck, M. (Eds.), The North Atlantic Oscillation: Climatic Significance and Environmental Impact. AGU, Washington, pp.1-35.

Jones, P. D., Osborn, T. J., and Briffa, K. R., 2001. The Evolution of Climate Over the Last Millenium. Science 292, 662-667.

Jónsdóttir, H. B. B., Knudsen, K. L., Abrantes, F., and Heinnemeier, J., E., 2003. Late Holocene climate variability on the Western Iberian Margin: benthic foraminiferal perspective. Newsletter of Micropalaeontology 68, 26.

Keigwin, L., 1996. The Little Ice Age and Medieval Warm Period in the Sargasso Sea. Science 274, 1504-1507.

Keigwin, L., and Pickart, R., 1999. Slope Water Current over the Laurentian Fan on Interannual to Millenial Time Scales. Science 286, 520-523.

Kissel, C., Laj, C., Labeyrie, L., Dokken, T., Voelker, A., and Blamart, D., 1999. Magnetic signature of rapid climatic variations in North Atlantic sediments. In: Abrantes, F. and Mix, A. (Eds.), Reconstructing Ocean History: a Window into the Future, Plenum Publishing, London. pp. 419-437.

Koç, N., Andersen, C., Andrews, J., and Jennings, A., 2003. Decadal-scale Holocene Climate Variability in Nordic Seas. EGS-AGU-EUG Joint meeting. AGU, Nice, France. pp. EAE03-A-14116.

Lamy, F., Hebbeln, D., and Wefer, G., 1998. Late Quaternary precessional cycles of terrigenous sediment input off the Norte Chico, Chile (27.5^{o}S) and paleoclimatic implications. Palaeogeography Palaeoclimatology Palaeoecology 141, 233-251.

Levy, A., Mathieu, R., Poignant, A., Rosset-Moulinier, M., Ubaldo, M. d. L., and Ambroise, D., 1993. Recent foraminifera from the continental margin of Portugal. Micropaleont. 39, 75-87.

Little, E. 1993. Radiocarbon age calibration at archeological sites of coastal Massachusetts and vicinity. Journal of Archeological Science 20, 457-471.

Loeblich, A. R., and Tappan, H., 1988. Foraminiferal genera and their classification. Van Nostrand Reinhold Company, New York. pp. 1 - 212.

Loubere, P., 1991. Deep-sea benthic foraminiferal assemblage response to a surface ocean productivity gradient: a test. Paleoceanography 6, 193-204.

Luterbacher, J., Schmutz, C., Gyalistras, D., Xoplaki, E., Wanner, H., 2002. Extending North Atlantic Oscillation reconstructions back to 1500. Atmospheric Science Letters 2, 114-124.

Lutze, G.-F., and Coulbourn, W. T., 1984. Recent benthic foraminifera from the continental margin of Northwest Africa: community structure and distribution. Marine Micropaleontology 8, 361-401.

Mann, M. E., Bradley, R. and Hughes, M., 1998. Global-scale temperature patterns and climate forcing over the past six centuries. Nature 392, 779-787.

Margalef, R., 1985. Primary production in upwelling areas. Energy, global ecology and resources. In: Bas, C., Margalef, R., and Rubies, P. (Eds.), Simposio International Sobre las areas de Afloramiento mas

importantes del oeste Africano (Cabo Blanco Y Buenguela). Instituto de Investigaciones Pesqueras, Barcelona. pp. 225-232.

McDermott, F., Mattey, D., and Hawkesworth, C., 2001. Centennial-Scale Holocene Climate Variability Revealed by a High-Resolution Speleothem ∂^{18}O Record from SW Ireland. Science 294, 1328-1331.

Moita, T., 2001. Estrutura, Variabilidade e Dinâmica do Fitoplâncton na Costa de Portugal Continental. Unpublished Article Compilation Thesis, University of Lisbon.

Monteiro, H., and Moita, I., 1971. Morfologia e sedimentos da plataforma continental e vertente continental superior ao largo da Peninsula de Setúbal. Congresso de Geologia. pp. 301-330.

Müller, P. J., Kirst, G., Ruhland, G., von Storch, I., and Rosell-Meré, A., 1998. Calibration of the alkenone paleotemperature index $U^{K'}_{37}$ based on core-pops from the eastern South Atlantic and the global ocean (60ºN-60ºS). Geochimica et Cosmochimica Acta 62, 1757-1772.

Nykjaer, L., and Van Camp, L., 1994. Seasonal and interannual variability of coastal upwelling along northwest Africa and Portugal from 1981 to 1991. Journal of Geophysical Research 99, 14,197-14,207.

Oliveira, P., 2000. Aplicação de Dados de Satélite ao Estudo da Variabilidade da Temperatura da Superfície do Mar no Atlântico Nordeste Subtropical. Unpublished Dissertation Thesis, University of Lisbon.

Ortiz, J., and Mix, A., 1992. The spatial distribution and seasonal succession of planktonic foraminifera in the California Current off Oregon, September 1987-September 1988. In: Summerhayes, C., Prell, W., and Emeis, K. (Eds.), Upwelling Systems: Evolution Since the Early Miocene. Geological Society Special Publications, London. pp. 197-214.

Osborn, T. J., Briffa, K. R., Tett, S. F., Jones, P. D., and Trigo, R. M., 1999. Evaluation of the North Atlantic Oscillation as simulated by a climate model. Climate Dynamics 15, 685-702.

Pisias, N., Prell, Prahl, F., Delaney, M., Lea, D., Jasper, J., Popp, B., Rau, G., Murray, R., McCorkle, D., Rea, D., and Derry, L., 1995. Marine aspects of Earth System History (MESH). Proxy Development Workshop. Corvallis, Oregon.

Poynter, J.G, Farrimond, P., Robinson, N. and Eglinton, G., 1989. Aeolian-derived higher plant lipids in the marine sedimentary record: Links with paleoclimate. In : Leinen, M., Sarnthein, M. (Eds), Paleoclimatology and Paleometerology: Modern and past patterns of global atmospheric transport. Kluwer Academic Publishers, Dordrecht. pp. 435-462.

Qian, B., Corte-Real, J., and Xu, H., 2000. Is the North Atlantic Oscillation the most important atmospheric pattern for precipitation in Europe? Journal of Geophysical Research 105, 11901-11910.

Rathburn, A., and Corliss, B., 1994. The ecology of living (stained) deep-sea benthic foraminifera from the Sulu Sea. Paleoceanography 9, 87-150.

Rogers, J. C., 1997. North Atlantic storm track variability and its association to the North Atlantic Oscillation and climate variability of northern Europe. Journal of Climatology 10, 1635-1647.

Rostek, F., Ruhland, G., Bassinot, F. C., Mueller, P. J., Labeyrie, L. D., Lancelot, Y., and Bard, E., 1993. Reconstructing sea surface temperature and salinity using δ^{18}O and alkenone records. Nature 364, 319–321.

Salgueiro, E., Abrantes, F., Loncaric, N., Lebreiro, S., Moreno, J., Pflaumann, U., Oliveira, P., and Meggers, H., 2003. Productivity changes off Portugal: foraminiferal evidence for the last 1500 years. EGS-AGU-EUG Joint meeting. AGU, Nice, France. pp. EAE03-00488.

Sautter, L. R., and Sancetta, C., 1992. Seasonal associations of phytoplankton and planktic foraminifera in an upwelling region and their contribution to the seafloor. Marine Micropaleontology 18, 263-278.

Sautter, L. R., and Thunell, R. C., 1991. Planktonic foraminiferal response to upwelling and seasonal hydrographic conditions: sediment trap results from San Pedro Basin, Southern California bight. Journal of Foraminiferal Research 21, 347 - 363.

Schmiedl, G., 1995. Late Quaternary benthic foraminiferal assemblages from the eastern South Atlantic Ocean: Reconstruction of deep water circulation and productivity changes. Berichte zur Polarforschung 160, 207 pp.

Schubert, C. J., Villanueva, J., Calvert, S. E., Cowie, G. L., von rad, U., Schulz, H., and Berber, U., 1998. Stable phytoplankton community in the Arabia Sea over the last 200,000 years. Nature 394, 563-566.

Schulte, S., Rostek, F., Bard, E., Rullkötter, J., and Marchal, O., 1999. Variations of oxygen-minimum and primary productivity recorded in sediments of the Arabian Sea. Earth and Planetary Science Letters 173, 205-221.

Shackleton, N., 1974. Attainment of isotopic equilibrium between ocean water and the benthonic foraminifera genus *Uvigerina*: Isotopic changes in the ocean during the last glacial. Colloq. Int. CNRS 219, 203– 209.

Shackleton, N., Hall, M., and Vincent, E., 2000. Phase relationships between millenial-scale events 64,000-24,000 years ago. Paleoceanography 15, 565-569.

Sousa, F., and Bricaud, A., 1992. Satellite-derived phytoplankton pigment structures in the Portugueseupwelling area. Journal of Geophysical Research 97, 11343-11356.

Sousa, F. M., 1995. Processos de Mesoescala ao largo da Costa Portuguesa utilizando dados de Satélite e Observações in Situ. Unpublished Dissertation Thesis. University of Lisbon.

Sousa, F. P. de, 1928. Distritos de Lisboa. Serviços Geológicos de Portugal, Lisboa.

Stuiver, M., and Braziunas, T., 1989. Atmospheric ^{14}C and century-scale solar oscillations. Nature 338, 405-408.

Terrinha, P., Pinheiro, L. M., Henriet, J.-P., Matias, L., Ivanov, M. K., Monteiro, J. H., Akhmetzhanov, A., Volkonskaya, A., Cunha, T., Shaskin, P., and Rovere, M., 2003. Tsunamigenic-seismogenic structures, neotectonics, sedimentary processes and slope instability on the southwest Portuguese Margin. Marine Geology 195, 55-73.

Thomson, J., and Weaver, P. P. E., 1994. An AMS radiocarbon method to determine the emplacement time of recent deep-sea turbidites. Sedimentary Geology 89, 1-7.

Thunnel, R., and Sautter, L. R., 1992. Planktonic foraminiferal faunal and stable isotopic indicators of upwelling: results from sediment trap study in the Califoria Current. In: Summerhayes, C., Prell, W., and Emeis, K. (Eds.), Upwelling Systems: Evolution Since the Early Miocene. Geological Society Special Publications, London. pp.. 77-92.

Trigo, R. M., Osborn, T. J., and Corte-Real, J., 2002. The North Atlantic Oscillation influence on Europe: climate impacts and associated physical mechanisms. Climate Research 20, 9-17.

Ulbrich, U., Christoph, M., Pinto, J. G., and Corte-Real, J., 1999. Dependence of winter precipitation over Portugal on NAO and baroclinic wave activity. International Journal of Climatology 19, 379-390.

Vale, C., 1981. Entrada de matéria em suspensão no estuário do Tejo durante as chuvas de Fevereiro de 1979. Recursos Hídricos 2, 37-45.

van der Bergh, G. D., Boer, W., Haas, H., van Weering, T., and van Wijhe, R., 2003. Shallow marine tsunami deposits in Telik Banten (NW Java, Indonesia), generated by the 1883 Krakatau eruption. Marine Geology 197, 13-34.

Vilanova, S., Nunes, C., and Fonseca, J., 2003. Lisbon 1755: A case of Triggered Onshore Rupture? Bulletin of the Seismological Society of America 93, 2056-2068.

Villanueva, J., 1996. Estudi de les variaciones climàtiques i oceanogràfiques a l`Atlantic Nord Durant els últims 300.000 anys mitjançant l`análisi de marcadores moleculars. Disseration Thesis. Universitat de Barcelona.

Villanueva, J., and Grimalt, J. O., 1997. Gas Chromatographic Tuning of the $U^{K'}_{37}$ Paleothermometer. Analytical Chemistry 69, 3329-3332.

Villanueva, J., Pelejero, C., and Grimalt, J. O., 1997. Clean-up procedures for the unbiased estimation of C37 alkenone sea surface temperatures and terrigenous n-alkane in paleoceanography. Journal of Chromatography A757, 145-151.

Visbeck, M., Chassignet, E., Curry, R., Delworth, T., Dickson, R. and Krahmann, G., 2003. The Ocean's response to North Atlantic Oscillation Variability. In: Hurrel, J., Kushnir, Y., Ottersen, G., and Visbeck, M. (Eds.), The North Atlantic Oscillation: Climatic Significance and Environmental Impact. AGU, Washington. pp.113-145.

Voelker, A., Lebreiro, S., Schonfeld, J., Abrantes, F., and Erlenkeuser, H., 2002. Dansgaard-Oeschger Cyclicity in the Eastern Gulf of Cadiz: Synchroneity between surface and deep water response and Greenland temperature? AGU Fall meeting. AGU, S. Francisco. pp. 47 (OS21A-0183).

Weeks, R., Laj, C., Endignoux, L., Fuller, M., Roberts, A., Manganne, R., Blanchard, E., and Goree, W., 1993. Improvements in long-core measurement techniques: applications in paleomagnetism and paleoceanography. Geophysical Journal International 114, 651-662.

Wefer, G., and Fisher, G., 1993. Seasonal Patterns of Vertical Flux in Equatorial and Coastal Upwelling Areas of the Eastern Atlantic. Deep-Sea Research 40, 1615-1645.

Williams, D., 1994. Satellite study of the Tagus sediment plume. Institute of Geology and Mining, Marine Geology Department Report 21/94, Lisbon.

Zitellini, N., 2001. Source of 1755 Lisbon earthquake and tsunami investigated. EOS Trans. 82.

Chapter 3

HOLOCENE INTERDEPENDENCES OF CHANGES IN SEA SURFACE TEMPERATURE, PRODUCTIVITY AND FLUVIAL INPUTS IN THE IBERIAN CONTINENTAL SHELF (TAGUS MUD PATCH)

Teresa Rodrigues[1,2], Joan O. Grimalt[2], Fátima G. Abrantes[1], Jose A. Flores[3], and Susana M. Lebreiro[1,4]

[1]Department of Marine Geology, INETI, Estrada da Portela-Zambujal, Apartado 7568, 2721-866 Amadora, Portugal

[2]Institute of Environmental Assessment and Water Research (IDÆA-C.S.I.C.), Jordi Girona, 18, 08034-Barcelona, Catalonia, Spain

[3]Department of Geology, Faculty of Sciences, University of Salamanca, 37008-Salamanca, Spain

[4]Present address: Spanish Geological and Mining Institute, Dept. of Geosciences Research and Prediction - Global Change, c/ Ríos Rosas, 23, 28003-Madrid, Spain

Published in *GEOCHEMISTRY, GEOPHYSICS, GEOSYSTEMS* (G^3), 2009

ABSTRACT

Sea surface temperature (SST), marine productivity and fluvial input have been reconstructed for the last 11.5 cal ky BP using a high-resolution study of C_{37} alkenones, coccolitophores, iron content and higher plant *n*-alkanes and *n*-alkan-1-ols in sedimentary sequences from the inner shelf off the Tagus River Estuary, in the Portuguese Margin. The SST record is marked by a continuous decrease from 19ºC, at 10.5 and 7 ka, to 15ºC at Present. This trend is interrupted by a fall from 18ºC during the Roman and Medieval Warm Periods to 16ºC in the Little Ice Age. River input was very low in the early Holocene but increased in the last 3 cal ky BP in association with an intensification of agriculture and deforestation and possibly the onset of the North Atlantic Oscilation / Atlantic Multidecadal Oscillation modes of variability. River influence must have reinforced the marine cooling trend relatively to the lower amplitude in similar latitude sites of the eastern Atlantic. The total concentration of alkenones reflects river-induced productivity, being low in the early Holocene but increasing as river input became more important.

Rapid cooling, of 1-2ºC occurring in 250 years, is observed at 11.1, 10.6, 8.2, 6.9 and 5.4 cal ky BP. The estimated age of these events matches the ages of equivalent episodes common in the NE Atlantic-Mediterranean region. This synchronicity reveals a common widespread climate feature, which considering the twentieth century analog between colder SSTs and negative North Atlantic Oscillation (NAO), is likely to reflect periods of strong negative NAO.

1. INTRODUCTION

Until recently the present interglacial, the Holocene, has been considered as a period of stable climate [*McManus et al.*, 1999]. However, high-resolution studies of paleo-proxies in marine sediments [*Bianchi and McCave*, 1999; *Cacho et al.*, 2001; *Frigola et al.*, 2007] and ice cores [*O'Brien et al.*, 1995], as well as dust records [*Jackson et al.*, 2005], have revealed the occurrence of suborbital millennial-scale climate variability during the last 11 cal ky BP of the Holocene [*Bianchi and McCave*, 1999; *Bond et al.*, 1997; *Bond et al.*, 2001; *Cacho et al.*, 2001; *Dokken and Jansen*, 1999; *Frigola et al.*, 2007; *Lorenz et al.*, 2006; *Sarnthein et al.*, 2003]. Since the early studies of the Holocene in the North Atlantic Ocean, the occurrence of a 1,500-year cycle has been attributed to solar activity [*Bond et al.*, 2001], to ocean current intensity variation [*Bianchi and McCave*, 1999], or yet to atmospheric processes linked to the North Atlantic Oscillation [*Giraudeau et al.*, 2000]. During this period, Sea Surface Temperature (SST) reconstructed by the alkenone method shows long-term cooling in the northeast Atlantic (36ºN to 75ºN) and in the Mediterranean Sea, involving drops of 1.2-2.9ºC between the Holocene Optimum and the Present [*Marchal et al.*, 2002]. This temperature decrease is consistent with other climate proxy records and with model simulations based on Milankovitch forcing [*Lorenz et al.*, 2006; *Marchal et al.*, 2002]. At 10.2 cal ky BP, a SST fall of 1-1.5ºC marks the Preboreal oscillation in the North Atlantic, which in turn corresponds to a southward advance of the polar front by about 500 km [*Ruddiman and McIntyre*, 1981]. The most extreme cold episode of this present interglacial was the 8.2 cal ky BP "event" detected in North Atlantic marine deep sea sediments by several climate proxy data. This '8.2 event' is often attributed to a meltwater outflow from the Hudson Basin (Canada) deglaciation into the North Atlantic Ocean and the consequent slowdown of the North Atlantic Deep Water formation [*Alley et al.*, 1997; *Alley and Ágústsdóttir*, 2005; *Barber et al.*, 1999; *Clark et al.*, 2002; *Mayewski et al.*, 2004]. The introduction of large amounts of freshwater into the North Atlantic triggers an important decrease of SST that occurs earlier and lasts longer than the isotopic signal recorded in the Greenland ice cores [*Alley et al.*, 1997; *Clark et al.*, 2001; *Kleiven et al.*, 2008], as shown by long climate cooling anomalies of multi-centennial scale between ~ 8.9 and 8 cal ky BP [*Ellison et al.*, 2006; *Naughton et al.*, 2007a; *Naughton et al.*, 2007b; *Rohling and Palike*, 2005].

Climate changes identified during the late Holocene have been less severe like the Roman Period (RP, AD 0-400 [*Lamb*, 1985]), the Medieval Warm Period (MWP, AD 800-1300 [*Hughes and Diaz*, 1994]) and the subsequent Little Ice Age (LIA, AD 1350-1900 [*Bradley and Jones*, 1993]). All the above referred studies and many other available in the literature provide an oceanic perspective of such climate changes since they were performed in cores retrieved from open sea sites. The continental response, although also reconstructed from marine sediment cores [*Naughton et al.*, 2007a; *Naughton et al.*, 2007b; *Roucoux et al.*, 2006; *Sanchez-Goñi et al.*, 2002], has been mainly studied in other palaeo-archives such as ice cores [*O'Brien et al.*, 1995], lake sediments [*Cranwell*, 1973], speleothems [*Baldini et al.*, 2008], tree-rings [*Briffa et al.*, 2002]. Marine and continental approaches give complementary information, but the dependence of the respective climate reconstructions from different paleo-archives restricts the possibilities of an integrated understanding of the overall changes. The use of the same archive in interface areas between the ocean and the continent has a strong potential for providing a better combined picture of the climate processes than those emerging from separate studies. In this perspective, climate reconstructions have also been done from continental shelf sediments. Besides variations in SST or salinity (SSS), these environments also record major variations in discharge of continental materials that affect the areas under fluvial influence [*Amorosi et al.*, 2005; *Müller and Stein*, 2000; *Rivera et al.*, 2006; *Stein et al.*, 2004; *Tanabe et al.*, 2006; *Xiao et al.*, 2006] and experience significant coastline variations [*Lambeck and Chappell*, 2001; *Siddall et al.*, 2003; *Siddall et al.*, 2004; *Siddall et al.*, 2006; *Yokoyama et al.*, 2000].

Studies of marine cores close to continental land masses have been performed in sites such as the Arabian Sea (ODP Site 723A, [*Gupta et al.*, 2003]), western tropical Atlantic (GeoB3129-3911, [*Weldeab et al.*, 2006]), eastern tropical Atlantic (GeoB 6518, [*Schefuß et al.*, 2005; *Weijers et al.*, 2007]), Gulf of Guinea (MD03-2707, [*Weldeab et al.*, 2007]), eastern equatorial Pacific Ocean (EEP, [*Leduc et al.*, 2007]), Timor Sea (MD01-2378, [*Xu et al.*, 2006]) and Cap Blanc (ODP Site 658C, [*deMenocal et al.*, 2000b]). Those sites are located at water depths of 807, 830, 962, 1295, 1619, 1738 and 2263 m, respectively, which is obviously deeper than the continental shelf. On the other hand, there is a large number of studies concerning the variability of sediment supply in different coastal areas, like the Laptev Sea [*Müller and Stein*, 2000; *Rivera et al.*, 2006], the Amazon Basin [*Maslin and Burns,* 2000], the Yangtze River [*Liu et al.*,

2004; *Xiao et al.*, 2006], the Kara Sea [*Stein et al.*, 2004], the Mahakam Delta [*Storms et al.*, 2005], the Po River [*Amorosi et al.*, 2005] or the Red River delta system [*Tanabe et al.*, 2006], but they lack the information from the climate proxies performed in open sea sites.

Until now, few previous studies have considered both climate change and river contribution to the continental shelf during the late Holocene (e.g. the Tagus mud patch, water depths 88-96 m [*Abrantes et al.*, 2005; *Lebreiro et al.*, 2006]; the Muros Ria, water depths 33-38 m, [*Diz et al.*, 2002; *Lebreiro et al.*, 2006]).

The Tagus River crosses the Iberian Peninsula and discharges a major load of suspended organic-rich sediments into the continental shelf off Lisbon forming the Tagus mud patch [*Cabeçadas and Brogueira*, 1997; *Gaspar and Monteiro*, 1977; *Monteiro and Moita*, 1971; *Vale*, 1981]. Variations in river contribution and seasonal changes in coastal hydrology are described for the Cape Roca upwelling filament area for the last 2 ky [*Abrantes and Moita*, 1999; *Abrantes et al.*, 2005; *Fiúza*, 1983; *Moita*, 2001]. Going further, the present work extends the initial evaluation of *Abrantes et al.* [2005] back to 11.5 ky. Biomarkers have been analyzed at high-resolution using the $U^{K'}_{37}$ index to determine SST. Primary productivity is estimated from the alkenone concentration and coccolithophore's assemblages and TOC, while river input is reconstructed from the concentration of Fe and higher plant *n*-alkanes and *n*-alkan-1-ols. The combined study of the these proxies contributes to understand the Holocene climate evolution in eastern Atlantic coastal areas providing unambiguously time-related information on changes occurring in the marine and continental environment and their interaction.

2. MATERIAL AND METHODS

The study area is located in the western Portuguese continental shelf, between Cape Raso and Cape Espichel (Fig. 1), in a region strongly influenced by the Tagus River. The Tagus is the longest river in the Iberian Peninsula. Periodic flood events lead to major discharge of suspended and bed-load sediments [*Vale*, 1981]. The sediments transported in suspension are preferentially deposited at the inner and middle shelf, and

are characterized by organic-rich silty-clays (> 80%) [*Gaspar and Monteiro*, 1977; *Monteiro and Moita*, 1971].

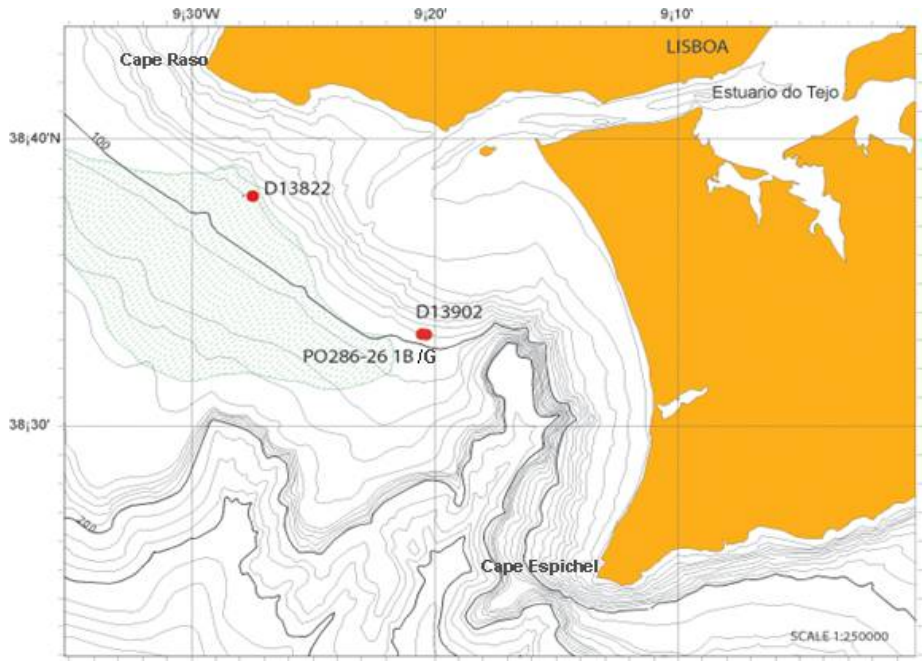

Figure 1. Area of study indicating the position of the sedimentary sequences used in this work.

Two sedimentary sequences are studied in this paper: a composite of box-core PO287-26B, gravity core PO287-26G and piston cores D13902; and the piston core D13882 (Table 1 and Fig. 1). The box-core and the gravity core were retrieved in May 2002 during the PALEO 1 campaign on board the RV POSEIDON [*Monteiro et al.*, 2002]. The piston cores were collected during the Discovery cruise 249 in August-September 2000 using the National Oceanography Centre long-piston coring system (Table 1). The first 189 cm of core D13902 were disturbed and half-filled. As age determinations confirmed this disturbance, the zero depth of the core was moved downward to the 189 cm liner level [*Abrantes et al.*, 2005].

Table 1. Location, water depth and length of the studied cores

Core ID	Core type	Water depth (m)	Core length (m)	Latitude (N)	Longitude (W)
PO287-26-B	box	96	0.32	38º33.49’	9º21.84’
PO287-26-G	gravity	96	3.05	38º33.49’	9º21.84’
D13902	piston	90	6.00	38°33.24’	9°20.13’
D13882	piston	88	13.61	38°38.07’	9°27.25’

Iron (Fe) concentrations in counts per 30 seconds (cts) were determined at 1 cm intervals in cores PO287-26 and D13882 and at 2cm intervals in core D13902 by X-ray fluorescence core scanning for non-destructive semi-quantitative analysis of major elements [*Jansen et al.*, 1998] at Bremen University.

For biomarkers analyses and TOC measurements, sediments were sampled every 1 cm in the box core, every 2-5 cm in cores D13902 and PO 287-26G, and every 5 cm in piston core D13882.

Haphtophyte-synthesized C_{37} alkenones and higher-plant biomarkers, such as C_{23}-C_{33} *n*-alkanes and *n*-alkan-1-ols C_{20}-C_{30}, were analyzed following the methods described in [*Villanueva et al.*, 1997]. Briefly, sediment samples (2 g) were freeze-dried and extracted by sonication with dichloromethane and then hydrolysed with 6% potassium hydroxide in methanol. After derivatization with bis(trimethylsilyl)trifluoroacetamide, the extracts were analyzed with a Varian gas chromatograph Model 3400 equipped with a septum programmable injector and a flame ionization detector. The concentrations of each compound were determined using nonadecan-1-ol, hexatriacontane and tetracontane as internal standards.

Selected samples were analyzed by gas chromatography coupled to mass spectrometry (GC-MS) for compound verification and identification of possible coelutions. The GC-MS used was a Fisons MD800 (THERMO Instruments, Manchester, UK). The carrier gas was helium (flow 2.1 mL/min). Injection and transfer

line temperatures were 300ºC. The quadrupole mass spectrometer was operated in EI mode (70 eV), scanning between *m/z* 50-650 in 1 sec. The ion source temperature was 200ºC.

SST determinations were based on the alkenone unsaturation index, $U^{K'}_{37}$, which was calibrated to the temperature equation of [*Müller et al.*, 1998]. Replicate injections and sample dilution tests allowed assessing measurement errors to less than 0.5ºC [*Grimalt et al.*, 2001].

Total organic and inorganic carbon were determined on aliquots (2 mg) of dry and homogenized sediment subsamples of the same levels used for biomarker determination. Total carbon was analyzed in the ground sediment with a CHNS-932 Leco elemental analyzer. Aliquots of those same samples were burnt at 400ºC in an oven and further analyzed for determination of the inorganic carbon weight %. Organic carbon (OC) weight % was calculated by difference between the two measurements. The relative precision of repeated measurements of both samples and standards was 0.03 wt%.

Smear slides for coccolithophore identification were prepared as described in [*Flores and Sierro*, 1997]. A light polarizing microscope (1250x) was used for observation and counting.

3. CHRONOLOGY

The age models are based on 18 accelerator mass spectrometry (AMS) ^{14}C dates of *Turritela* and other mollusk shells and 16 ^{210}Pb measurements in the top part of the sequence. These ^{14}C dated samples were chosen from core D13882 (six), core D13902 (eight) and core PO287-26G (three) and one in the bottom of box-core PO287-26B (Table 2). All samples were collected at levels with no evidence of reworking, that is, the shells selected were the ones found in their living position, well integrated in the sediment level and in good degree of preservation. When available, complete bivalve mollusks still articulated were selected.

Table 2. Results of AMS dating of the Tagus mud patch, box, gravity and piston cores (PO287-26B, PO287-26G, D13902, D13882).

Lab Code	Sample ID	§Spliced Corrected Depth (cm)	Sample Type	14C Age (BP)	Calendar Age BP	Error	Age AD
*AAR-8368.2	PO287-26B	51	Mollusk shell	440	51	25	1899
*OS-42380	PO287-26G	21	Mollusk shell	55	>1950		
*OS-42381	PO287-26G	86	Mollusk shell	545	186	25	1764
*KIA 23661	PO287-26G	125	Mollusk shell	905	855	25	1095
*AAR-7825	D13902 (27-28)	75.4	Mollusk shell	492	111	39	1839
*AAR-7207	D13902 (62-63)	110.4	Mollusk shell	1160	691	45	1259
*AAR-7208	D13902 (62-63)	110.4	Turritela	1185	704	40	1246
*AAR-7209	D13902 (96-97)	144.4	Mollusk shell	1370	863	45	1087
*OS-37307	D13902 (124-125)	172.4	Foraminifera	1880	1394	160	556
*AAR-7828	D13902 (151-152)	199.4	Mollusk shell	2007	1487	37	463
*AAR-7210	D13902 (199-200)	247.4	Mollusk shell	2340	1885	55	65
OS-37710	D13902 (342-343)	390.4	Mollusk shell	5860	6270	40	
OS- 37706	D13882	257	Turritela	1960	1511	45	
KIA 27301	D13882	464	Turritela	2920	2710	35	
KIA 29730	D13882	522	Mollusk shell	3690	3596	30	
KIA 27303	D13882	632	Turritela	6120	6542	55	
KIA 29729	D13882	699	Mollusk shell	8215	8753	45	
KIA 29728	D13882	738	Mollusk shell	9735	10614	55	

* Data published in [*Abrantes et al.*, 2005]
§ Spliced for core D13902

The age model for the last 2 cal ky BP of cores D13902 and PO287-26B/G is reported in [*Abrantes et al.*, 2005]. The top part of core D13882 was correlated to D13902 via the Fe and MS records. Furthemore, six AMS-^{14}C dates from core D13882 and one from D13902 (Table 2, Fig.2), using the MARINE04 calibration data and CALIB 5.0 program, were used for the rest of the sequence [*Hughen et al.*, 2004; *Stuiver and Reimer*, 1993; *Stuiver et al.*, 1998]. As such, all ages listed through the rest of the text correspond to calendar ky (ky =1000 year) BP but will be referred as ky for simplification.

The age model of box core PO287-26B, elaborated from the ^{210}Pb measurements and using the values determined in two levels collected from D13902 as background level, result in a sedimentation rate of 0.47 cm yr^{-1} and a temporal resolution of 2 yr per centimeter. The same resolution was found in the upper 75 cm of piston core D13902 and the top 100 cm of gravity core PO287-26G.

In cores D13902 and PO287-26G sedimentation rates were 0.11 and 0.14 cmyr^{-1}, allowing resolutions of 9 and 7 yr, respectively [*Abrantes et al.*, 2005]. In core D13902, the section between 95 cm and 76 cm showed an instantaneous deposit of reworked material as consequence of the Lisbon earthquake and its associated tsunami [*Abrantes et al.*, 2005]. Considering the last dated level below this event and the year of this earthquake (AD 1755) it was assumed that 355 yr of record were eroded. The same event was found in core PO287-26G where approximately 160 years of the core were lost. For core D13882, sedimentation rates vary between 0.02 cmyr^{-1} and 0.2 cmyr^{-1} allowing a temporal resolution between 4 and 48 years respectively.

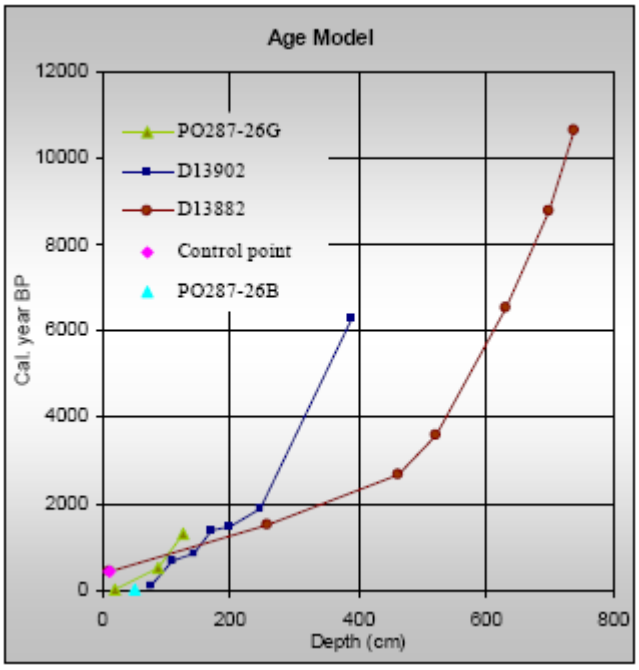

Figure 2. Age models between 0 and 10 500 cal AD for cores D13882, D13902 and PO287 26G and B based on accelerator mass spectrometry ^{14}C dating of marine carbonates. The top age for the core D13882 was defined based in a correlation with top parte of D13902. The age model for the last 2000year BP (core D13902 and PO287 26G /B) was published in [*Abrantes et al.*, 2005].

4. RESULTS

4.1. Sea Surface Temperature

The $U^{k'}_{37}$-SST record of the composite Holocene sediment sequences (Fig. 3a) fluctuates between 19ºC and 14ºC, showing maximum values between 11 – 6 ky and a minimum at the beginning of the 1990's. Furthermore, it exhibits a 4ºC-decreasing trend between 10 ky and the Present but is interrupted between 2 and 0.6 ky by the RP and the MWP. At the end of the MWP, there is an additional 2ºC cooling, to an average temperature of 15.5ºC, marking the beginning of the LIA. The last 130 years exhibit a strong variability with marked minima at AD 1930-1940 and AD 1990, 14.5ºC and 14ºC respectively, and maxima of about 17ºC at AD 1905, AD 1950-1970 and AD 1995. These changes involve SST drops and increases of 3ºC in periods of 10 years or less (Fig. 3a).

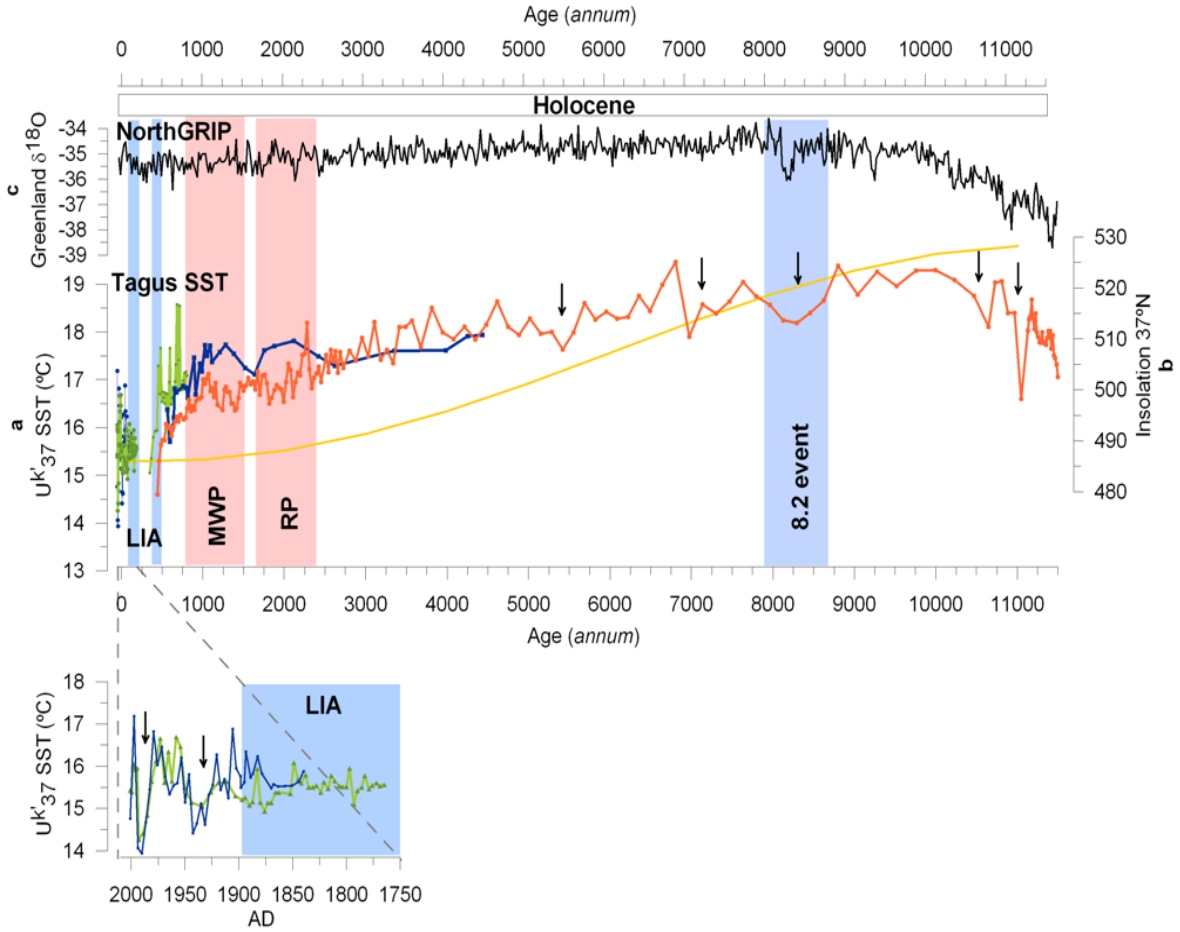

Figure 3. (a) $U^{k'}_{37}$-SST profile along the Tagus Mud patch sequences for the last 11 ky; (b) 21 June Insolation curve at 37ºN. (c) Greenland $\delta^{18}O$ record from NGRIP [*Johnsen et al.*, 2001; *NGRIP Members*, 2004; *Rasmussen et al.*, 2006]. The vertical arrows show cooling events in the Holocene. Note that in the x- scale there is a change in time amplitude before and after year 2000 BP. RP: Roman Period, MWP: Medieval Warm Pperiod, LIA: Little Ice Age.

4.2. Paleoproductivity

Total alkenones have been used as paleoproductivity indicators in open ocean sites [*Schubert et al.*, 1998; *Schulte et al.*, 1999; *Villanueva et al.*, 1998; *Villanueva et al.*, 2001]. In coastal areas, rivers input both particles and nutrients. While the particles will dilute the flux of sediments relative to the alkenone carrying organisms, the nutrients may enhance algal productivity. Off the Tagus, coccolithophores are dominant most of the year [*Moita*, 2001], governing the phytoplankton composition during winter and early spring when influence of nutrients from the river is high. Only during the upwelling season (May to September) are these algae outcompeted by diatoms [*Abrantes and Moita*, 1999]. On this basis alkenones may not be good markers for upwelling related productivity.

In our sediments, the concentration of total alkenones is low (200 ng/g or less than 20ng/cm^{2}y) during the early Holocene, starting to rise at 5.5 ky and becoming more pronounced (up to 800 ng/g; or 300 ng/cm^{2}y Fig. 4b,c) after 3 ky. This same trend is observed for the total organic carbon (TOC) that ranges between 0.3 and 2% (Fig. 4e). The strong similarity between these two proxies in D13882 supports a response to high amounts of river-transported nutrients to the coastal area, in particular during the last 3 ky.

Examination of the distribution of coccolithophores reveals *Gephyrocapsa* (*G.*) as the most abundant genus, with dominance of the small sized *Gephyrocapsa* (<3 μm) followed by *G. oceanica* and *G. muellerae* (Fig. 4D). While the group of small *Gephyrocapsa* and *G. oceanica* is known to live in nutrient rich environments [*Brand*, 1994; *Wells and Okada*, 1997; *Winter et al.*, 1994], *G. muellerae* is characteristic of cold waters [*Flores and Sierro*, 1997].

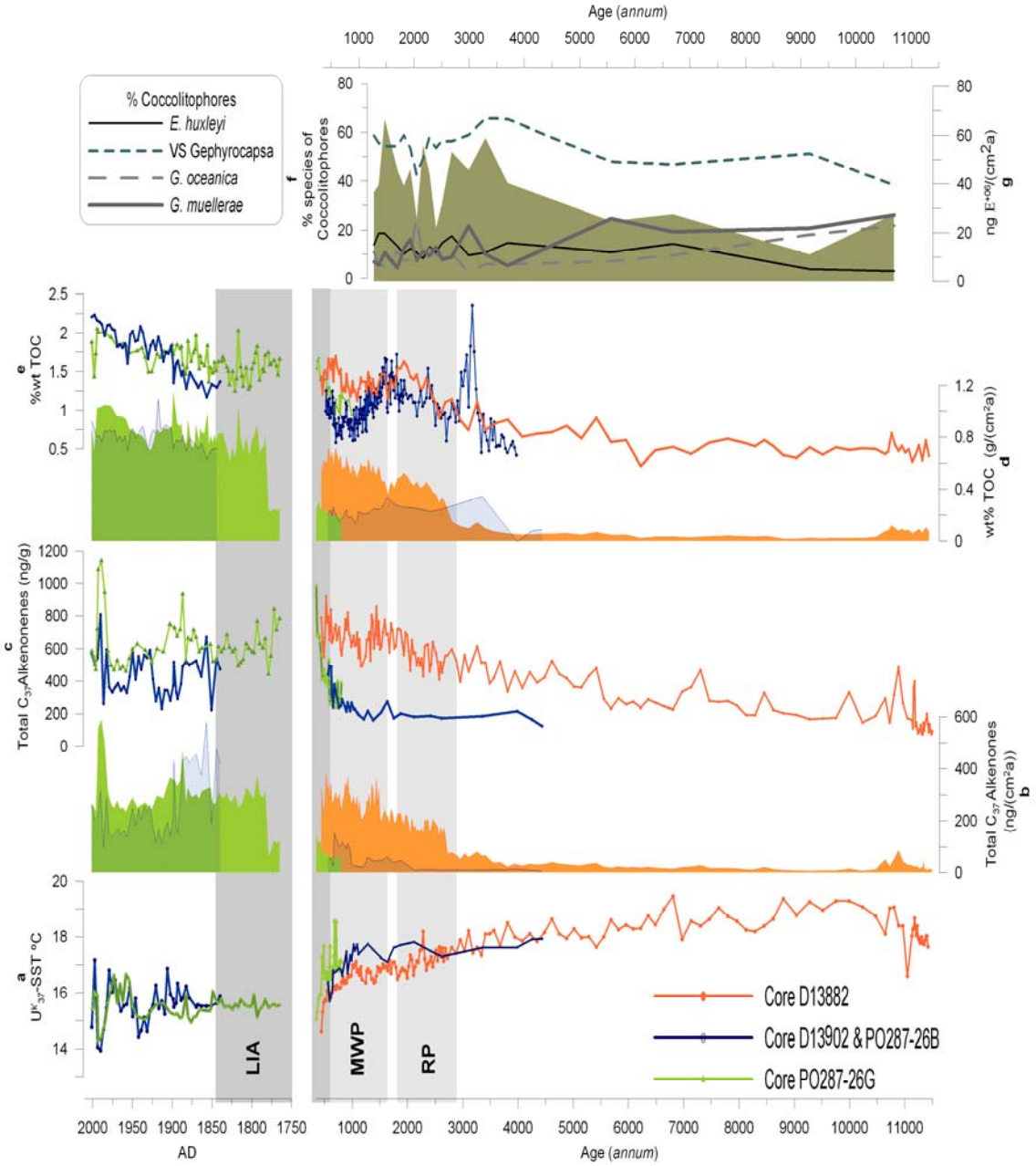

Figure 4. Productivity proxies along the sedimentary sequences. (a) SST-$U^{k'}_{37}$; (b) Flux of total C_{37} alkenones; (c) Concentration of C_{37} alkenones (ng/g); (d) Flux of Total Organic Carbon; (e) Total Organic Carbon (%wt); (f) % of coccolitophore species (g) flux of total cocolithophores (ng/cm^2 y). RP, MWP and LIA as in Fig. 3.

4.3. River contribution

The influence of the Tagus River discharge in the studied area is easily observed in the satellite and space shuttle images [*Abrantes et al.*, 2005]. C_{23}-C_{33} *n*-alkanes and C_{20}-C_{30} *n*-alkan-1-ols originate from higher plants [*Eglinton and Hamilton*, 1967] and their concentrations in the continental shelf can be used as an indicator for fluvial terrigenous input [*Grimalt et al.*, 1990]. In addition, changes in the concentration of lipid compounds give information on the type of continental vegetation close to the study area. The alkanes index (C_{29}/C_{31}) has been defined based on the existing relationship between the two main *n*-alkanes compounds following the suggestions made by previous studies [*Cranwell*, 1973; *Poynter and Egliton*, 1990; *Tareq et al.*, 2005]. This index allows us to know about the kind of vegetation that dominates in the river's hydrographic basin, in the adjacent continent. An index <1 reflects higher abundance of the alkane with 31 carbon atoms and indicates the dominance of grass and herbaceous plants. An index >1 results from a larger amount of alkanes with 29 carbon atoms, and so, the dominance of trees and shrubs in the adjacent continent.

These Tagus sequences show a clear prevalence of C_{29} during the early Holocene (Fig. 5g). The concentrations of *n*-alkane-1-ols (Fig. 5c) are currently higher (up to 11,000 ng/g) than those of *n*-alkanes (up to 4,000 ng/g, Fig. 5e). However, both terrigenous proxies exhibit a similar trend, pointing to a common origin. The concentrations of these biomarkers are also parallel to the Fe content as measured by XRF (Fig. 5f). This metal is a good marker for terrigenous input and therefore for river contribution. These three markers together validate clear trend towards higher terrigenous input in the last 3 ky, coincident with the onset of Neoglaciation [*Andersson et al.*, 2003; *Bauch and Weinelt*, 1997].

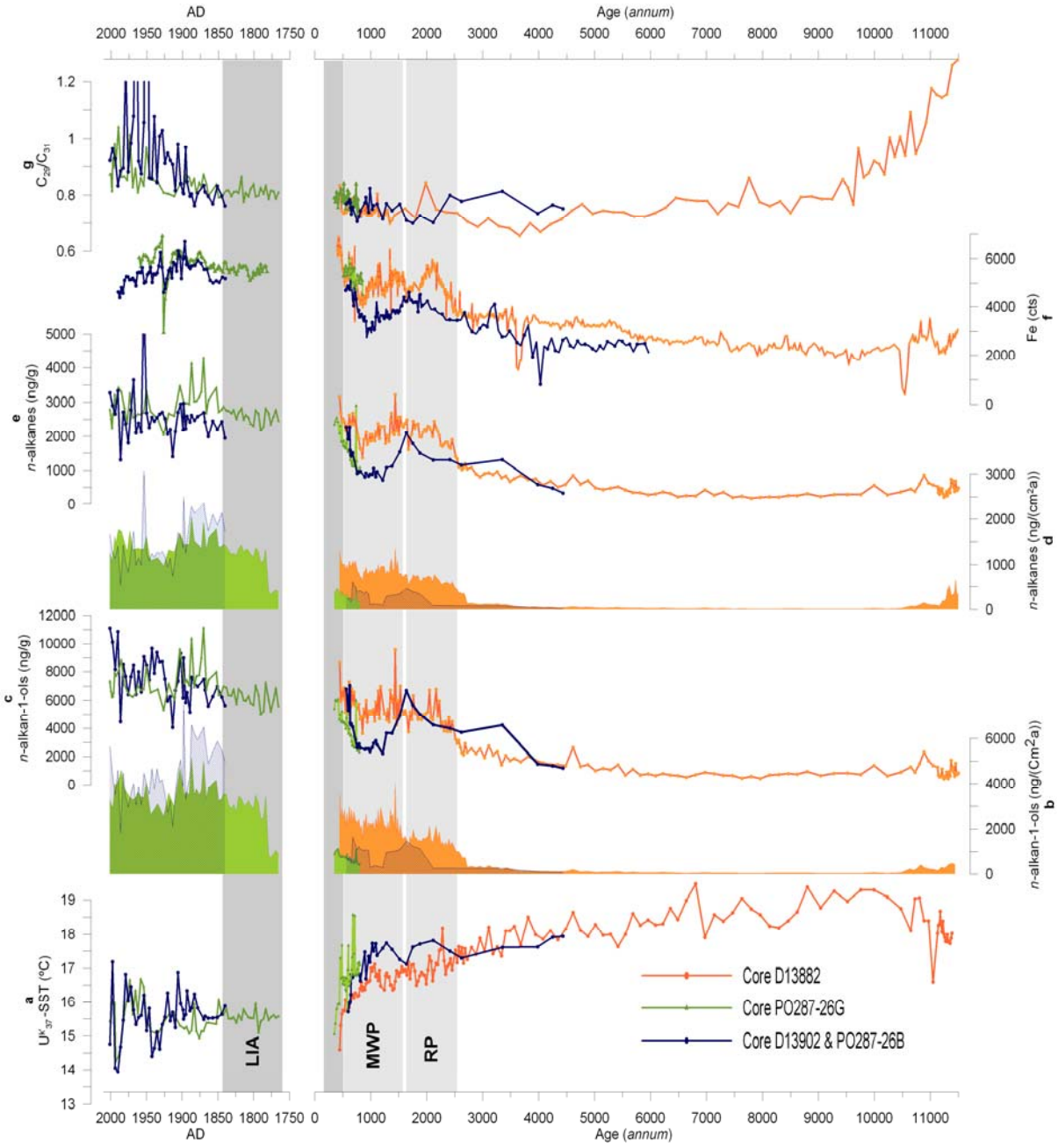

Figure 5. Terrigenous inputs along the sedimentary sequences. (a) SST-$U^{k'}_{37}$.; (b) Flux of *n*-alkan-1-ols (ng/cm^{2}y); (c) Concentrations of *n*-alkan-1-ols (ng/g); (d) Flux of *n*-alkanes (ng/cm^{2}y); (e) Concentrations of *n*-alkanes (ng/g); (f) Fe content determined by XRF (cts units); (g) Ratio between C_{29} and C_{31} *n*-alkanes;. RP, MWP, and LIA as in Fig. 3.

5. DISCUSSION

5.1. Climate variability and river evolution during the Holocene

The continuous SST decreasing trend observed between 10.5-7 ky and the Present (Fig. 3a) follows the summer insolation at 37ºN (Fig. 3b). Similar trends have also been detected in $U^{k'}_{37}$-SST records from extratropical sites of the Atlantic Ocean (between -0.69 and + 4.41ºC; [*Marchal et al.*, 2002]), contrary to the warming progress observed in the Pacific Ocean (between -0.31 and +1.08ºC; [*Kim et al.*, 2004]) and in tropical areas (between +0.19 and +1.05ºC; [*Lorenz et al.*, 2006]). This divergent SST evolution in the Atlantic and the Pacific is attributed to a dipole pattern generated by the interaction between the positive Pacific North American Oscillation (PNA) and the negative North Atlantic Oscillation (NAO) phases by [*Kim et al.*, 2004], while [*Lorenz et al.*, 2006] attribute the divergent Holocene climate trend between northern and tropical locations to seasonally opposing insolation changes.

The strong cooling of 4ºC observed in the Tagus record is of similar intensity to that found at high latitudes, such as the North Atlantic [*Marchal et al.*, 2002], but differs from the cooling trends of lower intensity observed in other similar latitudes sites [*Cacho et al.*, 2001; *Marchal et al.*, 2002]. This strong SST decrease may reflect higher sensitivity to seasonal changes by continental influence, e.g. an additional cooling effect due to the fact that in the cold seasons, river waters are cooler than seawater. An influence reflected by a clear contrast between river and sea surface temperature, recognized in satellite images (Fig. 6 (Oliveira et al., 2007 personal communication)). As such, the river output of colder waters resulted in a relatively stronger Holocene SST cooling gradient in this area. A gradient that is also noticeable in the terrigenous markers which show a continuous increase toward the Late Holocene (Figures 5b-f).

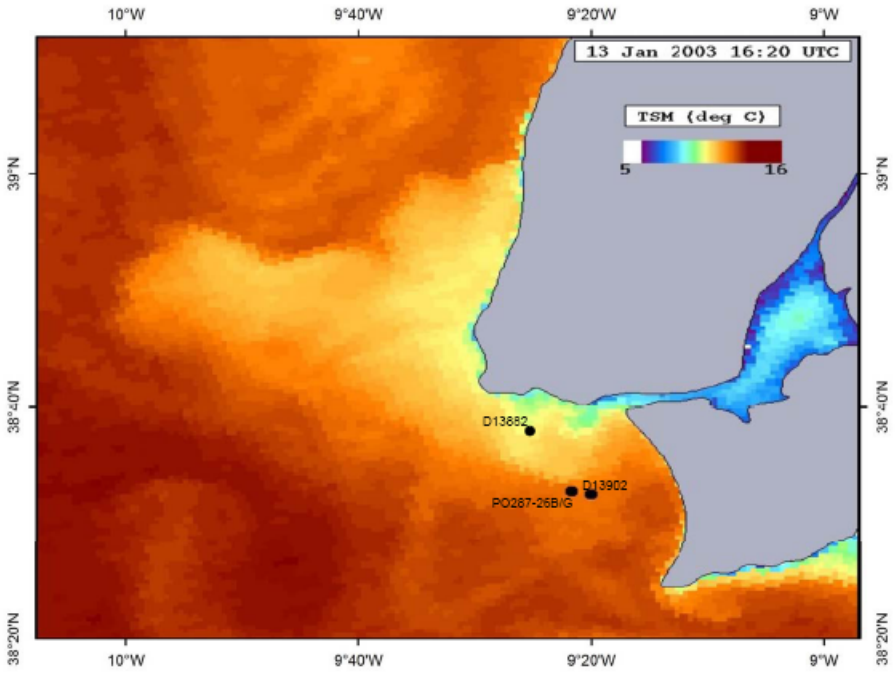

Figure 6: Satellite images of the river water Sea Surface Temperature on Tagus mud patch. Projection data: Geographic Coordinate System, Datum: WGS 1984, [*Oliveira et al.*, 2007].

The period between 10 and 8 ky, reflects the highest sea surface temperatures of the Holocene in the western Iberian margin, and is also marked by the maximum extent of forested area, with the predominance of pine forests along the Portuguese coast [*Queiroz*, 1999], oak in high altitudes, like in the Serra da Estrela mountains [*VanderKnaap and VanLeeuwen*, 1985] and by oak and pine in the mid- and low-altitude sites of the north-western Iberian Peninsula [*Naughton et al.*, 2007a; *Naughton et al.*, 2007b]. This suggests that both the Iberian margin and the adjacent landmasses have experienced the highest sea and atmospheric temperature values at the beginning of the Holocene. The C_{29}/C_{31} ratio shows a remarkable coincidence with the percent abundance of semi-desert plants [*Naughton et al.*, 2007a; *Turon et al.*, 2003]. In the Early Holocene, the C_{29} is dominant and the alkane index is higher than 1 indicating forest cover with high soil stability and consequently, lower drainage. From 9 to 6 ky the concentration of terrigenous markers and Fe content is continuously low, accompanying the SST decrease, and in good agreement with the gradual contraction of the forest defended by [*Naughton et al.*, 2007a; *Turon et al.*, 2003].

In terms of sea-level, at ^{14}C 10 ky the regional curve of [*Dias et al.*, 2000] indicates a sea-level 60 m below its Present level, resulting in a water depth of 40 m at the study area. On the lower Tagus valley, river sediments of that age correspond to channel deposits [*Vis et al.*, 2008], and is only after 9 ky that the retention of sediments inside the estuary becomes important. A retention that caused a major decrease in the amount of terrigenous material transported to the deep sea through the Lisbon canyon (Abrantes et al., 2006 personal communication), and possibly also to the shelf, although not reflected in the sedimentation rate (SR) (Fig. 2).

Between 6 and 3 ky, changes in the vegetation patterns on land are associated with deforestation. Soils became unstable and contribute more to river input. Concentrations of n-alkanes and n-alkan-1-ols start to rise progressively at 6 ky to a rapid increase around 3 ky, apparently coincident with the onset of the Atlantic Mutidecadal Oscilation (AMO) mode of variability [*Lorenz et al.*, 2006]. High concentrations are maintained up to the Present. Compared to the Holocene Climatic Optimum, during the two last warm periods, the Roman and the Medieval Warm Periods, the terrigenous biomarkers show prominent concentrations along with higher Fe contents. These enrichments are not coincident with SST drops. In fact, between 3 and 1.5 ky, pollen records from the southern Tagus River basin confirm an increase in agriculture activity and suggest deforestation and possibly higher soil erosion [*Mateus*, 1992; *Queiroz*, 1999]. Therefore, a higher concentration of terrigenous biomarkers during these warm periods seems a more direct response to an increase in soil use at times of amerioration than to river flow enhancement and climate cooling or high sea level stands.

5.2. Short-term variability

Short cooling episodes of 1-2ºC punctuate the general SST cooling trend at 11.1, 10.6, 8.2, 6.9 and 5.4 ky (Fig. 3a). Within dating errors these episodes exhibit a very good match with the millennial-scale variation observed during the Holocene both in high and low-latitude sites like in the North Atlantic (11.1, 10.3, 8.2 and 5.9 ky [*Bond et al.*, 1997]), the Alboran Sea (11.0, 10.3, 8.2 and 5.4 ky [*Cacho et al.*, 1999]), the Thyrrenian Sea (11.6, 9.9, 5.9 ky [*Cacho et al.*, 2002]), the Gulf of Cadiz (10 and 8.0 ky

[*Cacho et al.*, 2000]), and in subtropical west Africa ODP Site 658C (10.2, 8.0, 6.0, 4.6, 3.0, 1.9 ka [*deMenocal et al.*, 2000b]). These cooling episodes are therefore not just a local effect and must represent a recurrent climatic instability in the northeast Atlantic-Mediterranean region at least, which considering the twentieth century positive relationship between colder SSTs and NAO negative modes as an analog, are likely to reflect periods of strong negative NAO.

In the Tagus mud patch the longest and better marked of these cooling episodes is the 8.2 ky cooling that lasted about 700 years. This event was the most intense cooling recorded in the GISP 2 [*Alley et al.*, 1997] and NGRIP Holocene records (Fig. 3d *[Johnsen et al., 2001; North Greeland Ice Core project member, 2004; Rasmussen et al., 2006]*). Several studies show similar amplitude of duration for this event. In northwestern France the maximum expansion in *Corylus* woodlands (between *cc*. 8.74 and 8.06 ky) was associated with a high seasonality episode [*Naughton et al.*, 2007a], and occurs synchronously with a succession of events that starts with the last stages of the Laurentide Ice sheet decay and the catastrophic final drainage episodes of the 'glacial lakes Agassiz-Ojibway'into the Hudson Bay at around 8.470 ky [*Clarke et al.*, 2004] (error range of 8.160–8.740 ky; [*Barber et al.*, 1999]), followed by the consequent 8.2 ky event [*Clarke et al.*, 2004; *Teller et al.*, 2002]. The introduction of large amounts of freshwater into the North Atlantic triggers the decrease in sea surface temperatures, and earlier start than the 8.2 ky isotopic event of the Greenland ice cores, lasting several centuries, between ~8.9 and 8 ky [*Ellison et al.*, 2006]. This multicentennial SST cooling detected in the high-resolution North Atlantic deep-sea core MD99-2251 is roughly contemporaneous of the climate cooling defined by [*Rohling and Palike*, 2005], and has also been observed between ~8.6 and 8 ky in other regions of the North Atlantic, such as the Laurentian Fan and the north of Iceland [*Keigwin et al.*, 2005; *Knudsen et al.*, 2004].

In the last 1.5 ky the Tagus mud patch SST record shows higher amplitude of decadal to sub-decadal variation (Fig. 3A). The warm phase between 1.3 and 0.75 ky (SST~17ºC) is coincident with the MWP [*Cronin et al.*, 2003; *Dahl-Jensen et al.*, 1998; *deMenocal et al.*, 2000a; *Jones et al.*, 2001; *Jones and Mann*, 2004]. The available sedimentary record for the beginning of the LIA [*deMenocal et al.*, 2000a; *Jones et al.*, 2001; *Jones and Mann*, 2004; *Keigwin*, 1996], (0.18 to 0.08 ky - Fig. 3), exhibits a rapid decrease to SST values 2ºC lower than those of the MWP. However, when looked in

detail while both the RP and the MWP are marked by an increase in SST at site D13902 accompanied by a decrease in Fe, site D13882 shows a slight decreasing tendency in SST. According to *Abrantes et al.* [2005], the RP and MWP were times of low river input but high marine production associated with strong coastal upwelling; this process is responsible for the SST decrease SST at site D13882. During cold periods, at our location, there is a general correspondence between the SST decrease (Fig. 3a) and increase of river input (Figs. 5b-f) as reflected by higher concentrations of biomarkers of terrestrial origin and Fe. However, there are episodes of higher concentrations of terrigenous biomarkers that do not parallel the SST drops. These probably reflect changes in vegetation sources like those recorded in the C_{29}/C_{31} ratio (Fig. 5g).

Two rapid cooling periods are observed in the twentieth century, one between AD 1925-1950 involving a 2ºC decrease, and another one, exhibiting a 3ºC drop, extending from AD 1980 to AD 1990 (Fig. 3a). These SST changes, namely the 3ºC increase from 14 to 17ºC, occurred within 3 years and is observed at AD 1994 in the instrumental record (Abrantes et al., 2006 personal communication). They follow variations from extreme positive to extreme negative values of the NAO index [*Houghton et al.*, 2001; *Jones and Mann*, 2004]. Although their larger amplitude of variation relatively to older events might be valid, amplification may also result from the less severe smoothing effect generated by the compaction and bioturbation that generally occurs down core.

The C_{37} alkenone productivity record shows concomitant changes with SST but in the opposite direction (Fig. 4d) indicating higher alkenone production during cold episodes when higher amounts of continental material reflect increased river flow and nutrient incorporation into the marine environment (Fig. 5c and e). These oscillations are likely to reflect NAO cyclicity [*Jones et al.*, 2001; *Trigo et al.*, 2002], since during negative phases the weak north-south pressure gradient induces storminess and precipitation in Southern Europe, leading to high precipitation anomaly fields in the Tagus Basin area during the winter months [*Trigo and DaCamara*, 2000]. Assuming that this mechanism has been operative during most of, or the entire Holocene [*Lorenz et al.*, 2006], it can be hypothesized that higher precipitation during negative NAO mode involved higher nutrients transport and therefore higher river-induced productivity at lower SST conditions.

6. CONCLUSIONS

This high-resolution study of sedimentary sequences covering the last 11.5 ky provides the first integrated picture of the marine and continental climate changes at the inner –middle Portuguese continental shelf site under the influence of the Tagus River. The obtained proxy data reveals climatic events comparable with existing open sea and inland sites, and help to clarify the land-sea interaction during the Holocene.

The general decrease trend in Holocene SST, from 19ºC at 11-7.0 ky to 15ºC at Present, follows the general summer insolation trend and is in agreement with observations in other mid latitude marine sites. However, the Tagus mud patch sequences exhibits higher amplitude of variation, involving a 4ºC decrease, likely to reflect a continental climate-dependent influence besides the marine variability at the site. Furthermore, the higher amounts of terrigenous markers at lower SST suggest a land effect by means of colder river outflow.

The occurrence of rapid cooling periods of 1-2ºC within 250 years at 11.1, 10.6, 8.2, 6.9 and 5.4 ky, within the general Holocene SST decreasing trend, match the ages of similar events recorded in the NE Atlantic - Mediterranean area showing that they correspond to a common widespread climate feature. Higher amplitude SST variation observed during the last 1.5 ky, relatively to the preceding Holocene times, exhibit the warm Roman Period and MWP followed by a 2ºC decrease during the LIA.

Decadal to sub-decadal cold episodes are also recorded in the twentieth century, e.g. a 2ºC decrease at AD 1925-1950 and a 3ºC drop at AD 1980-1990. These proxy-defined episodes are coincident with low instrumental values measured during NAO negative phases and suggest that the known climate sensitivity of the Tagus marine area to this index is superbly recorded in the sediments deposited during the 150 years of instrumental record.

River influence is observed to increase towards recent times, when comparing the early with the later Holocene, including the RP and MWP, and might reveal that AMO variability has operated since 5-3 ky. This change goes together with the climate cooling observed in the SST records but may also reflect deforestation by agricultural activities. Higher river influence results in an increase in the amount of nutrients brought from the continent to the sea, and consequently higher river-induced marine productivity.

Acknowledgements

Financial support was received from FCT - Fundação para a Ciência e Tecnologia (SFRH/BD/13749/2003), EU projects SEDPORT (PDCTM/40017/2003) and HOLSMEER (EVK2-CT-2000-00060), the Spanish Ministry of Science and Technology (REN2003-08642-C02-01), Consolider-Ingenio 2100 Project CE-CSD2007-0067 and INETInovação. XRF measurements were made at University of Bremen through funding from the PaleoStudies programme. We are grateful to C. Monteiro (INETI) for TOC measurements, R. Mas (IDAEA) for laboratory assistance and Belén Martrat for useful comments.

7. REFERENCES

Abrantes, F., and M. T. Moita (1999), Water column and recent sediment data on diatoms and coccolithophorids, off Portugal, confirm sediment record of upwelling events, *Oceanologica Acta*, *22*, 319-333.

Abrantes, F., S. Lebreiro, T. Rodrigues, I. Gil, H. Bartels-Jonsdottir, P. Oliveira, C. Kissel, and J. G. O. (2005), Shallow-marine sediment cores record climate variability and earthquake activity off Lisbon (Portugal) for the last 2000 years, *Quaternary Science Reviews*, *24*, 2477-2494.

Alley, R. B., P. A. Mayewski, T. Sowers, M. Stuiver, K. C. Taylor, and P. U. Clark (1997), Holocene Climatic instability: A prominent, widespread event 8200yr ago, *Geology*, *25*, 483-486.

Alley, R. B., and A. M. Ágústsdóttir (2005), the 8k event: cause and consequences of a major Holocene abruot climate change, *Quaternarty Science Reviews*, *24*, 1123-1149.

Amorosi, A., M. C. Centineo, M. L. Colalongo, and F. Fiorini (2005), Millennial-scale depositional cycles from the Holocene of the Po Plain, Italy, *Marine Geology*, *222-223*, 7-18.

Andersson, C., B. Risebrobakken, E. Jansen, and S. O. Dahl (2003), Late Holocene surface ocean conditions of the Norwegian Sea (Vøring Plateau), *PALEOCEANOGRAPHY*, *18*(2), 1044.

Baldini, L. M., F. McDermott, A. M.Foley, and J. U. L. Baldini (2008), Spatial variability in the European winter precipitation /δ/^18 O-NAO relationship: Implications for reconstructing NAO-mode climate variability in the Holocene, *Geophysical Reserch Letters 35*(doi:10.1029/2007GL032027).

Barber, D. C., A. Dyke, C. Hillaire-Marcel, A. E. Jennings, J. T. Andrews, M. W. Kerwin, G. Bilodeau, R. McNeely, J. Southon, M. D. Morehead, and J.-M. Gagnon (1999), Forcing of the cold event of 8,200 years ago catactrophic drainage of Laurentide lakes, *Nature*, *400*, 344-348.

Bauch, H. A., and M. S. Weinelt (1997), Surface water changes in the norwegian sea during last deglacial and holocene times, *Quaternary Science Reviews*, *16*(10), 1115-1124.

Bianchi, G. G., and I. N. McCave (1999), Holocene periodicity in North Atlantic climate and deep-ocean flow south of Iceland, *Nature*, *397*, 515-517.

Bond, G., W. Showers, M. Cheseby, R. Lotti, P. Almasi, P. deMenocal, P. Priore, H. Cullen, I. Hajdas, and G. Bonani (1997), A Pervasive Millennial-Scale Cycle in North Atlantic Holocene and Glacial Climates, *Science*, *278*, 1257-1266.

Bond, G., B. Kromer, J. Beer, R. Muscheler, M. N. Evans, W. Showers, S. Holffmann, R. Lotti-Bond, I. hajdas, and G. Bonani (2001), Persistent Solar Influence on North Atlantic Climate During the Holocene, *Science*, *294*, 2130-2136.

Bradley, R. S., and P. D. Jones (1993), Little Ice Age Summer temperature variations: their nature and relevance to recent global warming trends, *The Holocene*, *3*, 367-376.

Brand, L. E. (1994), Physiological ecology of marine coccolithophores. , in *Coccolithophores*, edited by A. Winter y W.G. Siesser, pp. 39-49, Cambridge University Press, Cambridge.

Briffa, K. R., T. J. Osborn, F. H. Schweingruber, P. D. Jones, S. G. Shiyatov, and E. A. Vaganov (2002), Tree-ring width and density data around the Northern Hemisphere: Part 1, local and regional climate signals, *The Holocene*, *12*, 737-757.
Cabeçadas, G., and M. J. Brogueira (1997), Sediments in a Portuguese coastal area-pool sizes of mibile and immobile forms of nitrogen and phosphorus., *Marine and Freshwater Research*, *48*, 559-563.
Cacho, I., J. O. Grimalt, C. Pelejero, M. Canals, F. J. Sierro, J. A. Flores, and N. Shackleton (1999), Dansgaard-Oeschger and Heinrich event imprints in Alboran Sea Paleotemperatures, *Paleoceanography*, *14*, 698-705.
Cacho, I., J. O. Grimalt, F. Sierro, N. J. Shackleton, and M. Canals (2000), Evidence for enhanced Mediterranean thermohaline circulation during rapid climatic coolings, *Earth and Planetary Science Letters*, *183*, 417-429.
Cacho, I., J. O. Grimalt, M. Canals, L. Sbaffi, N. J. Shackleton, J. Schönfeld, and R. Zahn (2001), Variability of the Western Mediterranean Sea Surface Temperature during the last 25,000 years and its connection with the Northern hemisphere climatic changes, *Paleoceanography*, *16*, 40-52.
Cacho, I., J. O. Grimalt, and M. Canals (2002), Response of the Western Mediterranean Sea to rapid climatic variability during the last 50,000 years: a molecular biomarker approach, *Journal of Marine Systems*, *33-34*, 253-272.
Clark, P. U., S. J. Marshall, G. K. C. Clarke, S. W. Hostetler, J. M. Licciardi, and J. T. Teller (2001), Freshwater forcing of abrupt cliamte change during the last glaciation, *Science*, *293*, 283-287.
Clark, P. U., J. X. Mitrovica, G. A. Milne, and M. E. Tamisiea (2002), Sea-Level Fingerprinting as a Direct Test for the Source of Global Meltwater Pulse 1A, *Science*, *295*, 2438-2441.
Clarke, G. K. C., D. W. Leverington, J. Teller, and A. S. Dyke (2004), Paleohydraulics of the last outburst flood glacial Lake Agassiz and the 8200 BP cold event, *Quaternary Science Reviews*, *23*, 389-407.
Cranwell, P. A. (1973), Chain-length distribution of n-alkanes from lake sediments in relation to post-glacial environmental change *Freshwater Biology*, *3*, 259-265.
Cronin, T. M., G. S. Dwyer, T.Kamiya, S. Schwede, and D. A. Willard (2003), Medieval warm period, Little Ice Age and 20th century temperatures variability from chesapeake Bay, *Global and planetary change*, *36*, 17-29.
Dahl-Jensen, D., K. Mosegaard, N. Gundestrup, G. D. Clow, S. J. Johnsen, A. W. Hansen, and N. Balling (1998), Past temperatures directly from the Greenland Ice Sheet, *Science*, *282*, 268-271.
deMenocal, P., J. Ortiz, T. Guiderson, J. Adkins, M. Sarnthein, L. Baker, and M. Yarusinsky (2000a), Abrut onset and termination of the African Humid Period rapid Climate responses to gradual insolation forcing, *Quaternary Science Reviews*, *19*, 347-361.
deMenocal, P., J. Ortiz, T. Guiderson, and M. Sarnthein (2000b), Coherent High-and Low-Latitude climate variability during the Holocene Warm Period, *Science*, *288*, 2198.
Dias, J. M. A., T. Boski, A. Rodrigues, and F. Magalhães (2000), Coast line evolution in Portugal since the last Glacial Maximum until present - a synthesis, *Marine Geology*, *170*, 177-186.
Diz, P., G. Francés, C. Pelejero, J.O.Grimalt, and F. Vilas (2002), The last 3000 years in the Ría the Vigo (NW Iberian Margin): climatic and hidrographic signals, *The Holocene*, *12*, 459-468.
Dokken, T. M., and E. Jansen (1999), Rapid changes in the mechanism of ocean convection during the last glacial period, *Nature*, *401*, 458-461.
Eglinton, G., and R. J. Hamilton (1967), Leaf epicuticular waxes, *Science*, *156*, 1322-1335.
Ellison, C. R. W., M. R. Chapman, and I. R. Hall (2006), Surface and deep Ocean Interaction During the cold Climate Event 8200 Years Ago, *Science*, *312*, 1929-1932.
Fiúza, A. F. G. (1983), Upwelling patterns off Portugal, edited, pp. 85-98.
Flores, J. A., and F. J. Sierro (1997), Revised technique for calculation of calcareous nanofossil accumulation rates, *Micropaleontology*, *43*, 321-324.
Frigola, J., A. Moreno, I. Cacho, M. Canals, F. J. Sierro, J. A. Flores, J. O. Grimalt, D. A. Hodell, and J. H. Curtis (2007), Holocene climate variability in the western Mediterranean region from a deeepwater record, *Paleoceanography*, *22*(doi:10.1029/2006PA001307), PA2209.
Gaspar, L. C., and J. H. Monteiro (1977), Matéria Orgânica nos sedimentos da plataforma continental portuguesa entre os cabos Espichel e Raso, *Comunicações dos Serviços Geológicos de Portugal*, *T. 62*, 69-83.
Giraudeau, J., C. Michel, S. Manthé, L. Labeyrie, and G. Bond (2000), Coccolith evidence for instabilities in surface circulation south of Iceland during Holocene times, *Earth and Planetary Science Letters*, *179*, 257-268.
Grimalt, J. O., P. Fernández, J. Bayona, and J. Albaigés (1990), Assessment of Fecal Sterols and Ketones as Indicators of Urban Sewage Input to Coastal Waters, *Environ. Sci. Technology*, *24*, 357-363.

Grimalt, J. O., E. Calvo, and C. Pelejero (2001), Sea Surface pleotemperature errors in Uk'37 estimation due to alkenone measurements near the limit of detection, *Paleoceanography*, *16*, 226-232.
Gupta, A. K., D. M. Anderson, and J. T. Overpeck (2003), Abrupt changes in the Asian southwest monsoon during the Holocene and their links to the North Atlantic Ocean, *Nature*, *421*, 354-357.
Houghton, J. T., Y. Dring, D. J. Griggs, M. Noguer, P. J. Van der Linden, and D. M. Xiaosu (2001), Climate Change 2001. The scientific basis edited by IPCC, p. 944, University Press, Cambridge.
Hughen, K. A., M. G. L. Baillie, E. Bard, A. Bayliss, J. W. Beck, C. J. H. Bertrand, P. G. Blackwell, C. E. Buck, G. S. Burr, K. B. Cutler, P. E. Damon, R. L. Edwards, R. G. Fairbanks, M. Friedrich, T. P. Guilderson, B. Kromer, F. G. McCormac, S. W. Manning, C. Bronk Ramsey, P. J. Reimer, R. W. Reimer, S. Remmele, J. R. Southon, M. Stuiver, S. Talamo, F. W. Taylor, J. van der Plicht, and Weyhenmeyer (2004), Marine04 Marine radiocarbon age calibration, 26 - 0 ka BP, *Radiocarbon*, *46*, 1059-1086.
Hughes, M. K., and H. F. Diaz (1994), Was there a "Medieval Warm Period" and if so, where and when?, *Climate Change*, *26*, 109-142.
Jackson, M. G., N. Oskarson, R. G. Trønnes, J. F. McManus, D. Oppo, K. Gröveld, S. R. Hart, and J. P. Sachs (2005), Holocene loess deposition in Iceland: Evidence for millennial scale atmosphere-ocean coupling in the North-Atlantic, *Geology*, *33*, 509-512.
Jansen, J. H. F., S. J. VanderGaast, B. Koster, and A. J. Vaars (1998), Cortex, a shipboard XRF-scanner for element analyses in split sediment cores, *Marine Geology*, *151*, 143-153.
Johnsen, S. J., D. Dahl-Jensen, N. S. Gundestrup, J. P. Steffensen, H. B. Clausen, H. Miller, V. Masson-Delmotte, A. E. Sveinbjornsdottir, and J. W. C. White (2001), Oxygen isotope and palaeotemperature records from six Greenland ice-core stations: Camp Century, Dye-3, GRIP, GISP, Renland and NorthGRIP, *Journal of Quaternary Science*, *16*, 299-307.
Jones, P. D., T. J. Osborn, and K. R. Briffa (2001), The Evolution of Climate Over the Last Millennium, *Science*, *292*, 662-667.
Jones, P. D., and M. E. Mann (2004), Climate over past Millennia, *Reviews of Geophysics*, *42*, 1-42.
Keigwin, L. (1996), The Little Ice Age and Medieval Warm Period in the Sargasso Sea, *Science*, *274*, 1503-1508.
Keigwin, L. D., J. P. Sachs, Y. Rosenthal, and E. A. Boyle (2005), The 8200 year B. P. event in the slope water system, western subpolar North Atlantic core, *Paleoceanography*, *20*, PA2003, doi:2010.1029/2004PA001074.
Kim, J.-H., N. Rimbu, S. J. Lorenz, G. Lohmann, S.-I. Nam, S. Schouten, C. Ruhlemann, and R. R. Schneider (2004), North Pacific and North Atlantic sea surface temperature variability during the Holocene, *Quaternary Science Research*, *23*, 2141-2154.
Kleiven, H. F., Catherine Kissel, Carlo Laj, Ulysses S. Ninnemann, Thomas O. Richter, and Elsa Cortijo (2008), Reduced North Atlantic Deep Water Coeval with the Glacial Lake Agassiz Freshwater Outburst, *Science*, *319*, 60 - 64, doi: 10.1126/science.1148924.
Knudsen, K. L., H. Jiang, E. Jansen, J. Eiriksson, J. Heinemeier, and M. S. Seidenkrantz (2004), Environmental changes off North Iceland during the deglaciation and the Holocene: foraminifera, diatoms and stable isotopes, *Marine Micropaleontology*, *50*, 273-305.
Lamb, H. H. (1985), *Climate history and the future*, 835 pp., Princeton University press.
Lambeck, K., and J. Chappell (2001), Sea Level Change Through the Last Glacial Cycle, *Science*, *292*, 679-686.
Lebreiro, S. M., G. Francés, F. F. G. Abrantes, P. Diz, H. B. Bartels-Jónsdóttir, Z. N. Stroynowski, I. M. Gil, L. D. Pena, T. Rodrigues, P. D. Jones, M. A. Nombela, I. Alejo, K. R. Briffa, I. Harris, and J. O. Grimalt (2006), Climate change and coastal hydrographic response along the Atlantic Iberian margin (Tagus Prodelta and Muros Ría) during the last two millennia, *The Holocene*, *16*, 1003-2006.
Leduc, G., L. Vidal, K. Tachikawa, F. Rostek, C. Sonzogni, L. Beaufort, and E. Bard (2007), Moisture transport across Central America as a positive feedback on abrupt climatic changes, *Nature*, *445*, 908-911.
Liu, J. P., J. D. Milliman, S. Gao, and P. Cheng (2004), Holocene development of the Yellow River´s subaqueous delta North Yellow Sea, *Marine Geology*, *209*, 45-67.
Lorenz, S. J., J.-H. Kim, N. Rimbu, and R. R. Schneider (2006), Orbitally driven insolation forcing on Holocene climate trends: Evidence from alkenone data and climate modeling, *Paleoceanography*, *21*, PA1002, doi:1010.1029/2005PA001152.
Marchal, O., I. Cacho, T. F. Stocker, J. O. Grimalt, E. Calvo, and B. Martrat (2002), Apparent long-term cooling of the sea surface in the northeast Atlantic and Mediterranean during the Holocene, *Quaternary Science Reviews*, *21*, 455-483.
Mateus, J. E. R. R. (1992), Holocene and Present-Day Ecosystems of the Carvalhal Region, Southwest Portugal, 184 pp, Rijksuniversity, Utrecht.

Mayewski, P. A., E. E. Rohling, J. C. Stager, W. Karlen, K. A. Maasch, L. D. Meeker, E. A. Meyerson, F. Gasse, S. v. Kreveld, K. Holmbren, J. Lee-Thorp, G. Rosqvist, F. Rack, M. Staubwasser, R. R. Schneider, and E. J. Steig (2004), Holocene climate variability, *Quaternary Research*, *62*, 243-255.
McManus, J. F., D. W. Oppo, and J. L. Cullen (1999), A 0.5- Million-Year Record of Millennial-Scale Climate Variability in the North Atlantic, *Science*, *283*, 971-975.
Moita, M. T. (2001), Estrutura variabilidade e dinâmica do fitoplânton na Costa de Portugal Continental, 272 pp, Facudade de Ciências de Lisboa, Lisboa.
Monteiro, J. H., and I. M. C. Moita (1971), Morfologia e sedimentos da plataforma continental e vertente continental superior ao largo da Península de Setúbal, paper presented at Congresso de Geologia.
Monteiro, J. H., A. Voelker, A. Ferreira, M. Mil-Homens, S. Nave, V. Magalhães, E. Salgueiro, S. Vaqueiro, S. Muiños, and P. Freitas (2002), Report of the cruise PALEO I (PO287) on FS Poseidon (April 22-May3, 2002), Tecnical Repo, IGM, Alfragide, Portugal.
Müller, C., and R. Stein (2000), Variability of fluvial sediment supply to the Laptev Sea continental margin during Late Weichselian to Holocene times: implications from clay-mineral records *International Journal of Earth Sciences 89*, 592-604.
Müller, P., G. Kirst, G. Ruhland, I. v. Storch, and A. Rosell-Melé (1998), Calibration of the alkenone index Uk'37 based on core-tops the eastern South Atlantic and global ocean (60ºN-60ºS), *Geochimica et Cosmochimica Acta*, *62*, 1757-1772.
Naughton, F., J.-F. Bourillet, m. f. S. Goñi, J.-L. Turon, and J.-M. Jouanneau (2007a), Long-term and Millennial-scale climate variability in northwestern France during the last 8850 years, *The Holocene*, *17*, 939-953.
Naughton, F., M. F. Sánchez Goñi, S. Desprat, J.-L. Turon, J. Duprat, B. Malaizé, C. Joly, E. Cortijo, D. T., and M. C. Freitas (2007b), Present-day and past (last 25 000 years) marine pollen signal off western Iberia, *Marine Micropalentology 62*, 91-114.
North Greeland Ice Core project member (2004), High resolution record of Northern Hemisphere climate extending into the last interglacial period, *Nature*, *431*, 147-151.
O'Brien, S. R., P.A. Mayewski, L. D. Meeker, D. A. Meese, M. S. Twickler, and S. I. Whitlow (1995), Complexity of Holocene Climate as Reconstructed from a Greeland Ice Core, *Science*, *270*, 1962-1964.
Oliveira, P., P. Relvas, and M. Santos (2007), Surface Circulation on the western margin, The Portuguese Coastal Current associated Upwelling & the Portuguese Counter Current, paper presented at Circum-Iberia Paleoceanography and Paleoclimate – What do we know and what do we still need to study/ verify?, Iberian margin Workshop, Peniche, Janeiro 2008.
Poynter, J., and G. Egliton (1990), Molecular composition of three sediments from Hole 717C: the Bengal Fan, *Proceedings of the Ocean Drilling Program, scientific results*, *116*, 155-161.
Queiroz, P. F. (1999), Ecologia Histórica Da Paisagem do Nordeste Alentejano, 300 pp, Universidade de Lisboa, Lisboa.
Rasmussen, S. O., K. K. Andersen, A. M. Svensson, J. P. Steffensen, B. M. Vinther, H. B. Clausen, M. L. Siggaard-Andersen, S. J. Johnsen, L. B. Larsen, D. Dahl-Jensen, M. Bogler, R. Rothlisberger, H. Fischer, K. Goto-Azuma, M. E. Hansson, and U. Ruth (2006), A new Greenland ice core chronrlogy for the last glacial termination, *Journal of Geophysical Research*, *111*, doi:10.1029/2005JD006079.
Rivera, J., E. B. Karabanov, D. F. Williams, V. Buchinskyi, and M. Kuzmin (2006), Lena River discharge events in sediments of Laptev Sea, Russian Arctic, *Estuarine, Coastal and Shelf Science*, *66*, 185-196.
Rohling, E., and H. Palike (2005), Centemial-scale climate cooling with a sudden cold event around 8,200 years ago, *Nature*, *434*, 975-979.
Roucoux, K. H., P. C. Tzedakis, L. Abreu, and N. Shacketon (2006), Climate and vegetation changes 180000 to 345000 years ago recorded in a deep-sea core off Portugal, *Earth and Planetary Science Letters*, *249*, 307-325.
Ruddiman, W. F., and A. McIntyre (1981), The Mode and Mechanism of the Last Deglaciation: Oceanic Evidence, *Quaternary Research*, *16*, 125-134.
Sanchez-Goñi, M. F., I. Cacho, J. L. Turon, J. Guiot, F. J. Sierro, J.-P. Peypouquet, J. O. Grimalt, and N. J. Shackleton (2002), Synchroneity between marine and terrestrial responses to millennial scale climatic variability during the last glacial period in the Mediterranean region, *Climate Dynamics*, *19*, 95-105.
Sarnthein, M., S. Van Kreveld, H. Erlenkeuser, P. M. Grootes, M. Kucera, U. Pflaumann, and M. Schulz (2003), Centennial-to-millennial-scale periodicities of Holocene climate and sediment injections off the western Barents shelf, 75Â°N, *Boreas*, *32*(3), 447 - 461.
Schefuβ, E., S. Schouten, and R. Schneider (2005), Climatic controls on central African hydrology during the past 20,000 years, *Nature*, *437*, 1003-1006.
Schubert, S. J., J. Villanueva, S. E. Calvert, G. L. Cowie, U. V. Rad, H. Schulz, and U. Berber (1998), Stable phytoplankton community in the Arabia Sea over the last 200,000 years, *Nature*, *394*, 563-566.

Schulte, S., F. Rostek, E. Bard, J. Rullkotter, and O. Marchal (1999), Variations of oxygen-minimum and primary productivity record in sediments of the Arabian Sea, *Earth and Planetary Science Letters*, *173*, 205-221.
Siddall, M., E. J. Rohling, A. Almogi-Labin, C. Hemleben, D. Meischner, I. Schmeizer, and D. A. Smeed (2003), Sea-level flutuations during the last glacial cycle, *Nature*, *423*, 853-858.
Siddall, M., D. A. Smeed, C. Hemleben, E.J.Rohling, I.Schmelzer, and W. R. Peltier (2004), Understanding the Red Sea response to sea level, *Earth and Planetary Science Letters*, *225*, 421–434.
Siddall, M., E. Bard, E. J. Rohling, and C. Hemleben (2006), Sea-level reversal during Termination II, *Geology*, *34*, 817-820.
Stein, R., Dittfsmers K, Fahl K, Kraus M, Matthiessen J, Niessen F, Pirrung M, Polyakova Ye, Schoster F, Steinke T, and F. DK (2004), Arctic (palaeo) river discharge and environmental change: evidence from Holocene Kara Sea sedimentary records. , *Quaternary Science Reviews*, *23*, 1485-1511.
Storms, J. E. A., R. M. Hoogendoorn, R. A. C. Dam, A. J. F. Hoitink, and S. B. Kroonenberg (2005), Late-Holocene evolution of the Mahakam delta, East Kalimantan, Indonesia, *Sedimentary Geology*, *180*, 149-166.
Stuiver, M., and P. J. Reimer (1993), Extended 14C data base and revused CALIB radiocarbon calibration program, *Radiocarbon*, *35*, 215-230.
Stuiver, M., P. J. Reimer, E. Bard, W. J. Beck, G. S. Burr, A. Hughen, B. Kromer, F. G. M. Cormac, J. V. d. Plicht, and M. Spurk (1998), INTCAL98 radiocarbon age calibration, 24000 cal BP, *Radiocarbon*, *40*, 1041-1083.
Tanabe, S., Y. Saito, Q. Lan Vu, T. J. J. Hanebuth, Q. Lan Ngo, and A. Kitamura (2006), Holocene evolution of the Song Hong (Red River) delta system, northern Vietnam, *Sedimentary Geology*, *187*, 29-61.
Tareq, S. M., E. Tanoue, H. Tsuji, N. Tanaka, and K. Ohta (2005), Hydrocarbon and elemental carbon signatures in a tropical wetland: Biogeochemical evidence of forest fire vegetation changes, *Chemosphere*, *59*, 1655-1665.
Teller, J. T., D. W. Leverington, and J. D. Mann (2002), Freshwater outbursts to the ocean from glacial Lake Agassiz and their role in climate change during the last deglaciation, *Quaternary Science Reviews*, *21*, 879-887.
Trigo, R., and C. C. DaCamara (2000), Circulation Weather Types and Influence on the Precipitation Regime in Portugal, *International Journal of Climatology*, *20*, 1559-1581.
Trigo, R. M., T. J. Osborn, and J. Corte-Real (2002), The North Atlantic Oscilation influence on Europe: Climate impacts and associated physical mechanisms, *Climate Research*, *20*, 9-17.
Turon, J. L., A.-M. Lézine, and M. Denèfle (2003), Land-sea correlations for the last glaciation inferred from a pollen and dinocyst record from the Portuguese Margin, *Quaternary Research*, *59*, 88-96.
Vale, C. (1981), Entrada de matéria em suspensão no estuário do Tejo durante as chuvas de Fevereiro de 1979, *Recursos Hídricos*, *2*, 37-45.
VanderKnaap, W. O., and J. F. N. VanLeeuwen (1985), Holocene vegetation succession and degradation as response to climatic change and human activity in the Serra da Estrela, *Review of Paleobotany and Palynology 60*, 25-129.
Villanueva, J., C. Pelejero, and J. O. Grimalt (1997), Clean-up procedures for the unbiased estimation of C_{37} alkenone sea surface temperatures and terrigenous *n*-alkane in paleoceanography, *Journal of Chromatography 757*, 145-151.
Villanueva, J., J. O. Grimalt, L. D. Labeyrie, E. Cortijo, L. Vidal, and J. Louis-Turon (1998), Precessional forcing of productivity in the North Atlantic Ocean, *Paleoceanography*, *13*, 561-571.
Villanueva, J., E. Calvo, C.Pelejero, J. O. Grimalt, A. Boelaert, and L. Labeyrie (2001), A latitudinal productivity band in the central North Atlantic over the last 270 Kyr: An alkenone perspective, *Paleoceanography*, *16*, 1-10.
Vis, G.-J., C. Kasse, and J. Vandenberghe (2008), Late Pleistocene and Holocene palaeogeography of the Lower Tagus Valley (Portugal): effects of relative sea level, valley morphology and sediment supply, *Quaternary Science Reviews*, *27*, 1682-1709.
Weijers, J. W. H., E. Schefuβ, S. Schouten, and J. S. S. Damsté (2007), Coupled Thermal and Hydrological Evolution of Tropical Africa over the last Deglaciation, *Science*, *315*, 1701-1704.
Weldeab, S., R. R. Schneider, and M. Kölling (2006), Deglacial sea surface temperature and salinity increase in the western tropical Atlantic in synchrony with high latitude climate instabilities, *Earth and Planetary Science Letters*, *241*, 699-706.
Weldeab, S., D. W. Lea, R. R. Schneider, and N. Andersen (2007), 155,000 Years of West African Monsoon and Ocean Thermal Evolution, *Science*, *316*, 1303-1307.

Wells, P., and H. Okada (1997), Response of nannoplankton to major changes in sea-surface temperature and movements of hydrological fronts over Site DSDP 594 (south Chatham Rise, southeast New Zealand) during the last 130ky, *Marine Micropaleontology*, *32*, 341-363.
Winter, A., R. W. Jordan, and P. H. Roth (1994), Biogeography of living coccolithophores in ocean waters, in *Coccolithophores*, edited by A. Winter and W. G. Siesser, pp. 161-177, University Press, Cambrige.
Xiao, S., A. Li, J. P. Liu, M. Chen, Q. Xie, F. Jiang, T. Li, R. Xiang, and Z. Chen (2006), Coherence between solar activity and the East Asian winter monsoon variability in the past 8000 years from Yangtze River-derived mud in the East China Sea, *Palaeogeography, Palaeoclimatology, Palaeoecology*, *237*, 293-304.
Xu, J., W. Kuhnt, A. Holbourn, N. Andersen, and G. Bartoli (2006), Changes in the vertical profile of the Indonesian Throughflow during Termination II: Evidence from the Timor Sea, *Paleoceanography*, *21*, PA4204.
Yokoyama, Y., P. DeDeckker, K. Lambeck, P. Johnston, and L. K. Fifield (2000), Timing of the Last Glacial Maximum from observed sea-level minima, *Nature*, *406*, 713-716.

Chapter 4

THE LAST GLACIAL-INTERGLACIAL TRANSITION (LGIT) IN THE WESTERN MID-LATITUDES OF THE NORTH ATLANTIC: ABRUPT SEA SURFACE TEMPERATURE CHANGE AND SEA LEVEL IMPLICATIONS

Teresa Rodrigues[1,2], Joan O. Grimalt[2], Fatima Abrantes[1], Filipa Naughton[1], José-Abel Flores[3]

[1]Department of Marine Geology, INETI, Estrada da Portela-Zambujal, Apartado 7568, 2721-866 Amadora, Portugal

[2]Institute of Chemical and Environmental Research (C.S.I.C.), Jordi Girona, 18, 08034-Barcelona, Catalonia, Spain

[3]Department of Geology, Faculty of Sciences, University of Salamanca, 37008-Salamanca, Spain

Submitted to *QUATERNARY SCIENCE REVIEWS*

ABSTRACT

High resolution reconstructions of sea surface temperature ($U^{k'}_{37}$-SST) coccolithophores associations and continental input (total organic carbon, higher plant *n*-alkanes and *n*-alkan-1-ols) from a shallow core (D13882) from the Tagus mud patch are compared with SST records from deep sea core MD03- 2699 and other available western Iberian Margin records. Results reveal millennial scale climate variability over the last deglaciation, in particular during last glacial and interglacial transition (LGIT). In the Iberian margin the Heinrich event 1 (H1) and the Younger Dryas (YD) represent two extreme episodes of cold sea surface condition separated by a marine warm phase that coincides with the Bolling-Allerod event (B-A) in the neighboring continent.

Following the YD event, an abrupt sea surface warming marks the beginning of the Holocene in this region. However, SST changes recorded in core D13882 are abruptly when compared with core MD03- 2699 and other available palaeoclimate sequences from this region. While the SST values from most deep sea cores reflect the latitudinal gradient detected on the Iberian Peninsula atmospheric temperature proxies during H1 and B-A, the shallow core (D13882) shows colder SSTs during both events. This is most certainly related with the supplementary input of cold freshwater coming from the continent, to the Tagus mud pach record. A hypothesis supported by the high content of terrigenous biomarkers and of total organic carbon as well as by the tetra alkenone dominance observed at this site.

Furthermore, the comparison of all western Iberia SST records suggest that the SST increase that characterizes the B-A event in this region has started 1,000 yr before the meltwater pulse 1A (mwp-1A) and reaches its maximum values during or slightly after this substantial sea level rise episode. In contrast, during the YD/Holocene transition, the sharp SST increase in the Tagus mud patch is synchronous with the meltwater pulse 1B (mwp-1B). The decrease of continental input in the Tagus mud patch confirms a sea level rise in the region. Thus, the synchronism between the maximum warming in the mid-latitudes off the western Iberian margin, the adjacent landmasses and Greenland indicates that mwp-1B and the associated sea level rise probably initiated in the Northern Hemisphere rather than in the South.

1. INTRODUCTION

The increase of high-latitude summer insolation that followed the Last Glacial Maximum (LGM), favoured the northern hemisphere ice sheets retreat and triggered a 120-130 m increase of the global sea level [*Fairbanks*, 1990; *Fairbanks et al.*, 2005; *Peltier and Fairbanks*, 2006; *Stanford et al.*, 2006]. Superimposed on this orbitally induced long-term warming trend, abrupt widespread millennial-scale climate variability have punctuated the last deglaciation in Greenland [*Alley et al.*, 1993; *Dansgaard et al.*, 1993; *Johnsen et al.*, 2001], in the North Atlantic [*Andrews et al.*, 1995; *Andrews*, 1999; *Bond et al.*, 1993; *Boyle and Keigwin*, 1987; *Duplessy et al.*, 1992; *Hughen et al.*, 1996; *Keigwin and Lehman*, 1994; *McManus et al.*, 2004; *Peterson et al.*, 2000; *Ruddiman and McIntyre*, 1981; *Rühlemann et al.*, 1999] in North America and Europe [*Iversen*, 1954; *Mangerud et al.*, 1974; *Naughton et al.*, 2007a; *Peteet et al.*, 1993]. Within this millennial scale climate variability, extreme cold episodes such as Heinrich event 1 (H1) and Younger Dryas (YD) have been detected in most of the northern hemisphere archives. H1 is likely the result of abrupt and massive icebergs discharges into the north Atlantic region [*Bond et al.*, 1993] while the YD is related to catastrophic drainage episodes of the proglacial Lake Agassiz [*Teller et al.*, 2002].

Although resulting from different processes, climate simulations suggest that the input of freshwater in the North Atlantic region disturbed the general pattern of thermohaline circulation and triggered a substantial atmosphere and oceanic cooling in both cases [*Fawcett et al.*, 1997; *Ganopolski and Rahmstorf*, 2001; *Knutti et al.*, 2004; *Paillard and Labeyriet*, 1994; *Seidov and Maslin*, 1999; *Stouffer et al.*, 2006].

Northern hemisphere archives detect a warm period that reflects the Bölling-Alleröd (B-A) episode and is squeezed in between the H1 and YD cold events [*Bond et al.*, 1993; *Dansgaard et al.*, 1993; *Hughen et al.*, 1996; *Iversen*, 1954; *Johnsen et al.*, 2001; *Keigwin and Lehman*, 1994; *Mangerud et al.*, 1974; *McManus et al.*, 2004; *Naughton et al.*, 2007a; *Peteet et al.*, 1993; *Teller et al.*, 2002]. Another warm episode occurred after the YD and marks the onset of the present-day interglacial, the Holocene.

This millennial-scale climate variability that characterises the last deglaciation had also a great impact on the northern hemisphere ice sheet dynamics [*Dyke*, 2004; *McCabe and Clark*, 1998; *McCabe et al.*, 2005; *McCabe et al.*, 2007; *Millera et al.*, 2005] and sea level changes [*Bard et al.*, 1990; *Bard et al.*, 1996; *Fairbanks* 1989;

Lambeck and Chappell, 2001]. Thus, the last deglaciation is marked by episodes of sudden sea level rise, called meltwater pulses (mwp), 2A, 1B and 1A [*Bard et al.*, 1996; *Fairbanks*, 1990; *Fairbanks et al.*, 2005; *Yokoyama et al.*, 2000]. However, controversy surrounds the precise timing, sources and global impact of this last deglaciation meltwater pulse episodes.

This paper presents the first highest resolution multi-proxy study ($U^{k'}_{37}$ and cocolitophore associations, total of organic carbon and higher plant *n*-alkanes and *n*-alkan-1-ols) of a shallow core D13882 retrieved in the Tagus mud patch, that allows to further explore the sea level and the climatic variability implications on south-western Iberian margin during the last glacial-interglacial transition. Furthermore, the fact that our site is located in the continental shelf provides an integrated picture of the marine and continental conditions, and its comparison to core MD03-2699 and other available deep-sea records from western Iberian margin allows for a latitudinal and cross-shelf evaluation.

2. MATERIAL AND METHODS

Cores D13882 and MD03-2699 were retrieved from 88 m and 1865 m water depth from the western Iberian margin (38º38.07´N, 9º27.25'W and 39º02.20'N, 10°39.63'W, respectively) using the National Oceanography Centre long-piston coring system and the giant CALYPSO corer during the Discovery 249 and PICABIA oceanographic cruises on board of R/V Discovery and Marion Dufresne (Fig. 1; Table 1).

Table 1. Location, water depth and length of the shallow and deep sea cores from western Iberian margin.

Core ID	Core type	Water depth (m)	Core length (m)	Latitude (N)	Longitude (W)
D13882	piston	88	13.61	38°38.07'	9°27.25'
MD03-2699	piston	1865	26.5	39º02.20'	10°39.63'

Core D13882 is 12 m long and covers the last 13.1 ka providing the highest resolution palaeoclimatic record of the western Iberian margin for the Last Glacial-Interglacial Transition (LGIT). In contrast, core MD03-2699, is 26.5 m long and covers the last 570 ka (from Marine Isotopic Stages (MIS 1 to 15). In this paper, we will focus this study in the first 3 m of core MD03-2699.

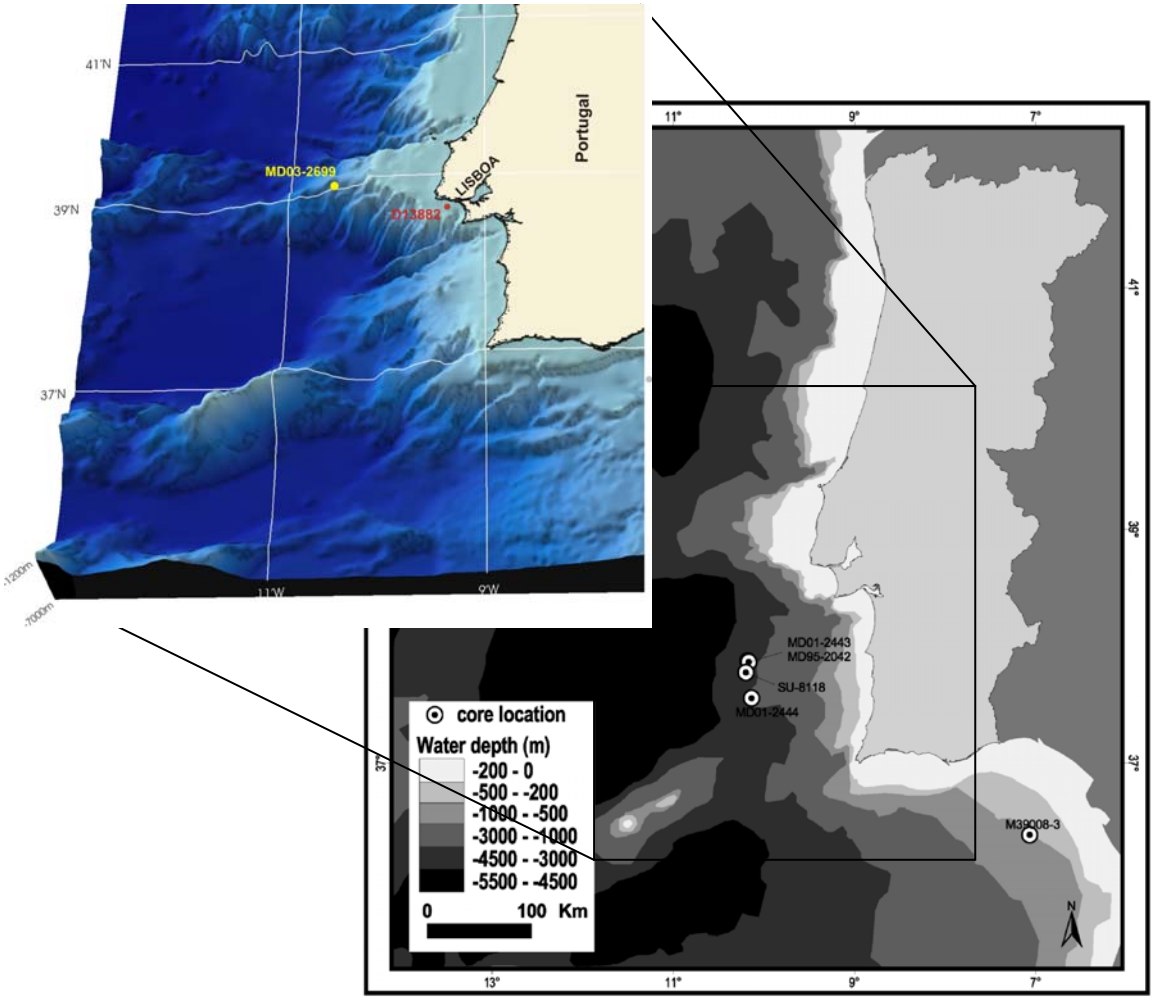

Figure 1. Area of study indicating the position of western Iberian margin cores D13882 and MD03-2699 (this study) and other discussed in this manuscript.

102 and 103 samples from cores D13882 and MD03-2699, respectively, were used to quantify haphtophyte-synthesized C_{37} alkenones and terrigenous biomarkers, such as C_{23}-C_{33} *n*-alkanes and *n*-alkan-1-ols C_{20}-C_{30}, following the methods described in [*Villanueva and Grimalt*, 1997]. Samples (2g) were freeze-dried and extracted by

sonication with dichloromethane and then hydrolysed with 6% potassium hydroxide in methanol. After derivatization with bis(trimethylsilyl)trifluoroacetamide, they were analyzed with a Varian gas chromatograph Model 3800 equipped with a septum programmable injector and a flame ionization detector. The concentrations of each compound were determined using *n*-nonadecan-1-ol, *n*-hexatriacontane and *n*-tetracontane as internal standards. Sea surface temperatures were estimated from the relative composition of C_{37} unsaturated alkenones using the $U^{k'}_{37}$ index and the core top calibration equation described in [*Müller et al.*, 1998].

Total organic carbon (TOC) was determined using a CHNS-932 Leco elemental analyzer on aliquots (2 mg) of dry and homogenized sediments. Organic Carbon content was calculated using the loss of ignition procedure (heat up to 400ºC during 3 hours). For coccolithophore analysis smear slides were prepared using the methodology described in [*Flores and Sierro*, 1997] and identified and counted with the use of a light polarizing microscope (1250x).

3. CHRONOLOGY

The age model of core D13882 has been constructed based on four accelerator mass spectrometer (AMS) ^{14}C dates obtained on turritella, and bivalve shells (Table 2). AMS ^{14}C dates were calibrated using CALIB Rev 5.0 program and the "global" marine calibration dataset (marine 04.14c) [*Hughen et al.*, 2006; *Hughen et al.*, 2004; *Stuiver and Reimer*, 1993]. Calibrated thousand years before present will be referred as ka (kila anum (ka), in the figures appear in anum) and were determined using the 95.4% (2 sigma) confidence intervals and the relative areas under the probability curve as suggested by [*Stuiver et al.*, 2005]. Our sampling interval is 1cm which gives a temporal resolution of 2.5 yr (Fig. 2A).

Table 2. Radiocarbon ages of cores D13882 and MD03-2699.

Lab Code	Sample ID	Depth (cm)	Material	14C Age (BP)	Calendar Age BP	Error
OS- 37707	D13882	798-799	Turritela	10450	11578	75
KIA 27307	D13882	820-821	Bivalve	10490	11627	70
OS- 37708	D13882	975-976	Shell F>2mm	11100	12749	50
OS- 37709	D13882	1140-1141	Bivalve	11500	13011	70
KIA 30539	MD03-2699	3-4	G. ruber white & pink; G. inflata	2025	1189.5	25
KIA 30540	MD03-2699	25-26	G. inflata	3650	3078	30
KIA 30541	MD03-2699	61-62	G. inflata	5810	5785.5	35
KIA 31227	MD03-2699	99-100	G. inflata	10165	11168.5	45
KIA 30542	MD03-2699	113-114	G. inflata	13770	15336	60
KIA 30543	MD03-2699	145-146	G. inflata	25270	29720	+210/-200
KIA 31228	MD03-2699	164-165	G. inflata	23320	27770	160
KIA 35296	MD03-2699	210-211	G. inflata	24930	29530	+230/-220
KIA 35297	MD03-2699	278-279	G. inflata	>44910		

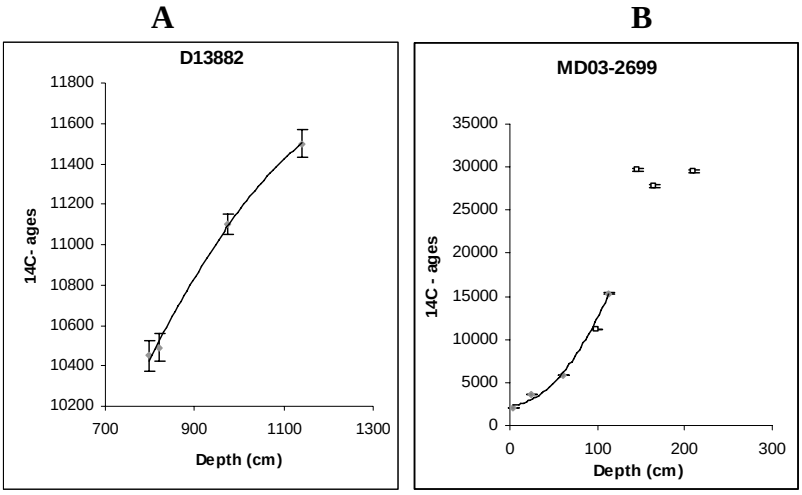

Figure 2. Chronostratigraphy of cores D13882 (A) and MD03-2699 (B). Grey diamonds with error bars represent the radiocarbon ages. Three ages have been rejected (see explanation in the text). A second-order polynomial adjustment performed in each core is represented by the continuous dark line.

To reconstruct the age model of core MD03-2699, we used AMS ^{14}C dating and a sea surface temperature (SST) correlation between this core and core MD01-2443 [*Martrat et al.*, 2007] (correlation coefficient of 0,97%) (Fig 2) [*Paillard et al.*, 1996]. Eight AMS ^{14}C dates were obtained on monospecific foraminifers' samples (*Globigerina inflata*) and one on a multiespecies (Table 2). However, only four dates were included in the age model since the other five seem contaminated with old material (Fig 2B). For the bottom part we correlated our SST record with SST record of south-western Iberian margin [*Bard*, 2001; *Martrat et al.*, 2007] (Fig. 3).

Indeed, the contamination of levels below 100 cm depth with old material could be the consequence of increasing slope instability derived from changes in the sea level during the last deglaciation (Lebreiro et al.,in press).

Sedimentation rates are in the order of 14 cm/ka allowing an average resolution with 2 cm sampling interval of 140 year.

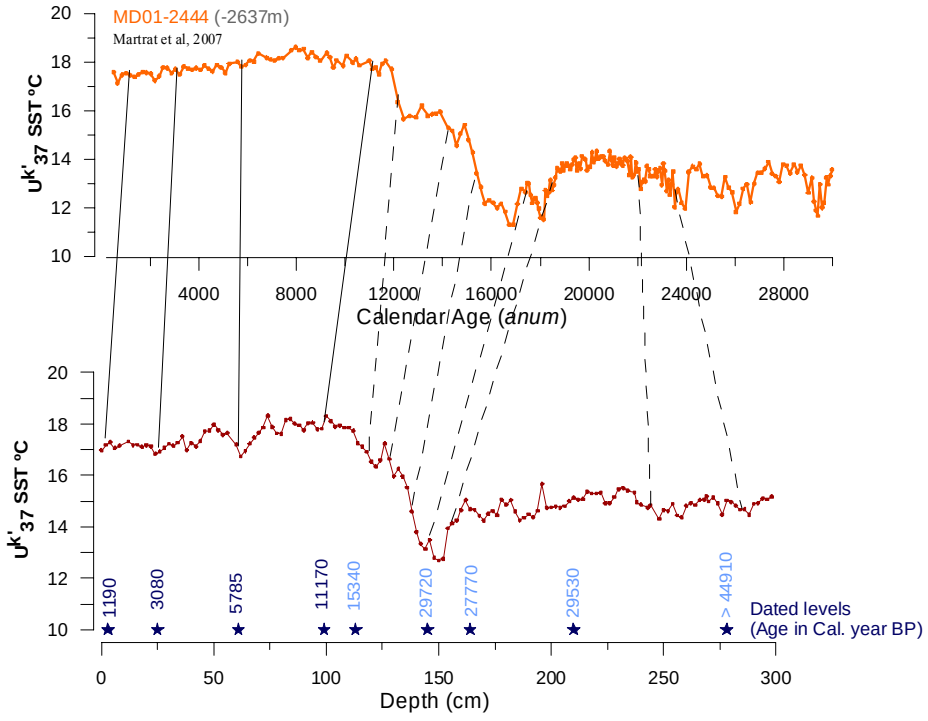

Figure 3. Correlation of the $U^{k'}_{37}$-SST values in cores MD03 2699 (this study) and MD01-2444 [*Martrat et al.*, 2007].

4. RESULTS

4.1 Sea Surface Temperature

In this study SST is reconstructed in two cores, the MD03-2699 located at 1865 m water depth allowing a SST reconstruction for the last 21 ka, and a shallow core D13882 collected at 88m water depth that permits a reconstruction of the last 13.5 ka. Core MD03-2699 shows SST changes between 13ºC to 18ºC, the coldest temperature is recorded at around 18 ka and the maximum at the beginning of the Holocene and warmer conditions (11.2 ka). During the last deglaciation our records show a gradual SST increase from 13º at 16.95 ka to 17ºC at 13.5 ka. After that, this SST increase was interrupted by a drop of 1ºC at around 12.6 ka. Arround 12 ka the SST increases again to 18.3ºC in 800 years. During the Holocene SST remains shows a slight and gradual decrease trend towards the Present. However, short cooling episodes of 1 – 1.5ºC punctuate the general cooling trend at around 8.2, 6.2, 4.3 ka.

Core D13882 SST record for the last 11.5 ka is published in [*Rodrigues et al.*, 2009], for this study only the data for the period between 13.5 and 11.5 ka is considered. The record reveals a cold period that is actualy composed by two cold phases framed by a relatively warmer period (11ºC). The first plateau with SSTs of 8ºC occurs from 12.5 to 12 ka, while the second phase, with 1ºC warmer temperatures, goes up to 11.6 ka. The final transition to the present interglacial is marked by a 7ºC (from 10ºC to 17ºC) rapid increase, 40 years, from 11.6 to 11.56 ka.

4.2 Other Proxies analyzed in core D13882

For the shallow core D13882 we have also quantify the marine and terigenous biomarker signal for the study period. The terrigenous biomarkers (*n*-alkanes and *n*-alcohols) show a decrease trend with the maximum values around 2000ng/g at 13.5 ka and lower values around 300 ng/g after 11.2 ka. The ratio C_{29}/C_{31} used to identify the vegetation type in the source, shows higher and stable values until 11.5 ka , indicating a dominance of the C_{29} alkane. After the 11.5 ka the ratio shows a decreasing trend to values close to 1.

The organic content of the sediments was quantified by TOC measurements and shows higher values close to 0.8 %wt, on average, until 11.5 ka, followed by a decrease to values around 0.4 %wt. Total alkennones concentration shows lower values before 11.5 ka and a slight increase in the Holocene (< 11.5 ka). Within the alkenones concentration we highlight the presence of the tetra-alkenone only during the period between 13.5 and 11.5 ka, a trend also observed for the cocolitophore specie *G. mullerae* wich has its highest percent abundance during this period.

5. DISCUSSION

5.1 Climate variability in the western Iberian margin

Since the last 21 ka, the Iberian margin experienced the most extreme cold sea surface conditions during H1 as demonstrated by alkenone based SST estimates for cores MD03-2699, SU81-18 [*Bard et al.*, 2000], MD95-2042 [*Pailler and Bard*, 2002], MD01-2444 [*Martrat et al.*, 2007] and M39-008 [*Cacho et al.*, 2001] (Fig. 4). Although the SST values recorded for H1 are quite similar (11° to 13°C) in most of the western Iberian margin cores (Fig. 4), the southermost one (core M39-008) is marked by 1ºC warmer SSTs (> 14°C), suggesting a latitudinal gradient along the Iberian margin during Heinrich event 1 similarity to the gradual pattern of air temperatures detected in a southern-north transect in the neighbour continent. [*Naughton et al.*, 2007b]. Thus, the temperate and pine forest contraction, reflecting extreme cold temperatures, was more pronounced in the north rather than in the south Iberian Peninsula, during the Oldest Dryas (terrestrial equivalent of H1 event) [*Naughton et al.*, 2007b]. The sharp increase in SST around 15 ka marks the beginning of the warm Bølling-Allerød interstadial (B-A) in the western Iberian margin but maximum SSTs are reached around 14 ka (Fig. 4).

This warm event is marked by alkenone based SST estimates of about 15° to 17°C in cores: MD03-2699, SU81-18 [*Bard et al.*, 2000], MD95-2042 [*Pailler and Bard*, 2002], and MD012444 [*Martrat et al.*, 2007] (Fig. 4). Again, SST values are highest (about 18° to 19°C) in core M39-008 [*Cacho et al.*, 2001] located in the southernmost area of the Iberian margin. This climate improvement that characterizes the B-A interstadial, is well expressed in marine and terrestrial pollen sequences from Iberian margin and adjacent landmasses [*Allen et al.*, 1996; *Naughton et al.*, 2007b;

Peñalba et al., 1997; *Turon et al.*, 2003]. The expansion of temperate and humid forest suggests increasing temperatures and precipitation in the southern part of the Iberian Peninsula, [*Allen et al.*, 1996; *Naughton et al.*, 2007b; *Peñalba et al.*, 1997; *Turon et al.*, 2003].

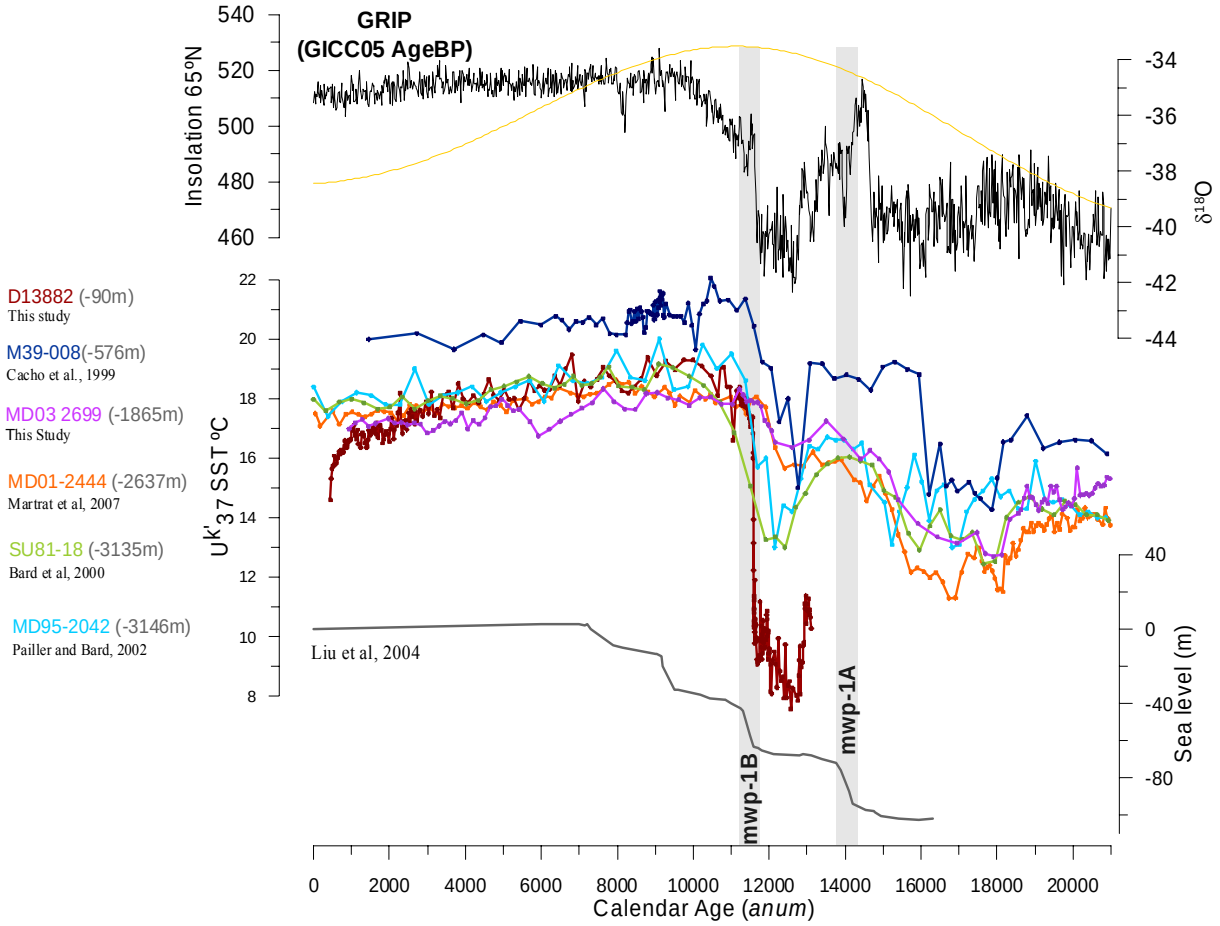

Figure 4. Alkenone–based SST values of the last 21 ka obtained in the Iberian margin cores: D13882 and MD03 2699 (this study); M39-008 [*Cacho et al.*, 1999]; MD01-2444 [*Martrat et al.*, 2007]; SU81-18 [*Bard et al.*, 2000]; MD95 2042 [*Pailler and Bard*, 2002]. $\delta^{18}O$ record of Greenland ice core GRIP (GICC05 age scale). High resolution Sea level curve [*Liu et al.*, 2004].Insolation curve at 65ºN [*Berger*, 1978]

The SST record of core D13882 does not cover the entire B-A but only the final stages of this event (Fig. 4). These final stage is marked by SST values around 11ºC, that is, 3ºC to 5°C lower than those recorded in all the other western Iberian margin sites (Fig. 4). This core is located closer to the continent, and in the area of influence of

the Tagus River (Fig. 1). Indeed, although the total organic carbon (TOC) curve parallels the total alkenones record of core D13882 in most of the sequence (Fig.4), the high TOC content (1% W) contrasts with low total alkenone concentrations (less than 100 ng/g) during the B-A event. This suggests that the TOC increase is likely the result of higher terrigenous input as in fact indicated by the *n*-alkanes and *n*-alkan-1-ols increase in concentrations (about 2500 ng/g and 5000 ng/g, respectively; Fig. 5) supporting the hypothesis of higher terrestrial input during the B-A event. The tetra-unsaturate alkenone ($C_{37:4}$) recorded has its high values during extreme cold events such as Heinrich events. In the north Atlantic their presence is attributed to an increase of cold water input from iceberg melting [*Bard et al.*, 1987; *Rosell-Melé et al.*, 1998; *Rosell-Melé*, 2004; *Schulz et al.*, 2000], the dominance of $C_{37:4}$ during the B-A in core D13882 suggests that substantial amounts of cold freshwater were reaching the study area. However, this freshwater input cannot be explained by ice melting processes but rather than by increasing fluvial input during the B-A event.

Following these warm conditions, cold conditions return to most of Iberian margin as recorded in deep cores that reveal the YD event at around 12,9 ka (Fig. 4). Temperate forest decline, reflecting atmospheric cooling, was less extreme during the YD than during H1 event but occurred both in the north- and southwestern Iberian Peninsula [*Allen et al.*, 1996; *Naughton et al.*, 2007b; *Peñalba et al.*, 1997; *Turon et al.*, 2003] Besides, the expansion of semi-desert plants' associations in the Iberian Peninsula vegetation cover during the YD event, indicates also lower humidity conditions relatively to the previous B-A warm phase [*Allen et al.*, 1996; *Turon et al.*, 2003]. SST was colder in the shallow (about 8°C at 90 m depth; core D13882: Fig. 4) and deepest sea cores (about 12 to 13°C at depths > 3000 m; SU8118 [*Bard et al.*, 2000], MD95-2042 [*Pailler and Bard*, 2002]) than in mid-water depth cores (Fig. 4). It is believed that the catastrophic episode of Lake Agassiz freshwater discharges into the North Atlantic lead to a substantial cooling of the North Atlantic and Europe, resulting in a significant reduction in the Meridional Overturning Circulation (MOC) [*Eltgroth et al.*, 2006; *McManus et al.*, 2004]. However, this mechanism alone cannot explain the observed SST differences between the shallow, deep and mid-depth cores. As for the B-A event, the shallow core was probably also affected by colder freshwater input by the Tagus river during the YD event. The percentages of $C_{37:4}$ are higher than those recorded in offshore cores such as in core SU8118 [*Bard et al.*, 2000], where the occurrence of $C_{37:4}$

above 5% is taken as reflecting low-salinity water [*Bard et al.*, 1987; *Rosell-Melé et al.*, 1998; *Schulz et al.*, 2000] and has been used for the reconstruction of the North Atlantic polar front position during the H1 [*Bard et al.*, 2000]. Furthermore *G. mullerae* abundances are synchronous with high percentages of $C_{37:4}$ (Fig. 5), which comes as a confirmation that the area was under the influence of cold freshwater masses also during the YD (Fig. 5) [*Flores et al.*, 1999; *Flores and Sierro*, 1997; *Wells and Okada*, 1997].

The high resolution alkenone based SST estimates of core D13882 further show a complex pattern within the YD event, composed by two cold phases framing one relatively warm period (Figs. 3 and 4). A 3ºC cooling episode detected at around 12.9 ka is followed by a continuous increase in temperatures up to 11ºC at 11.9 ka and by a second phase cooling (about 2°C) after 11.8 ka. A similar complex pattern has been detected in the temperature record of Greenland [*Alley*, 2000; *Lowe et al.*, 2008], in the $\delta^{18}O$ contained in ostracods shells from lake Ammersee [*VonGrafenstein et al.*, 1999], and in the Alboran sea surface temperatures [*Cacho et al.*, 2001]. Concomitantly marine pollen records from western Iberian reveal changes in the deciduous forest cover in the neighbor continent [*Naughton et al.*, 2007b; *Turon et al.*, 2003].

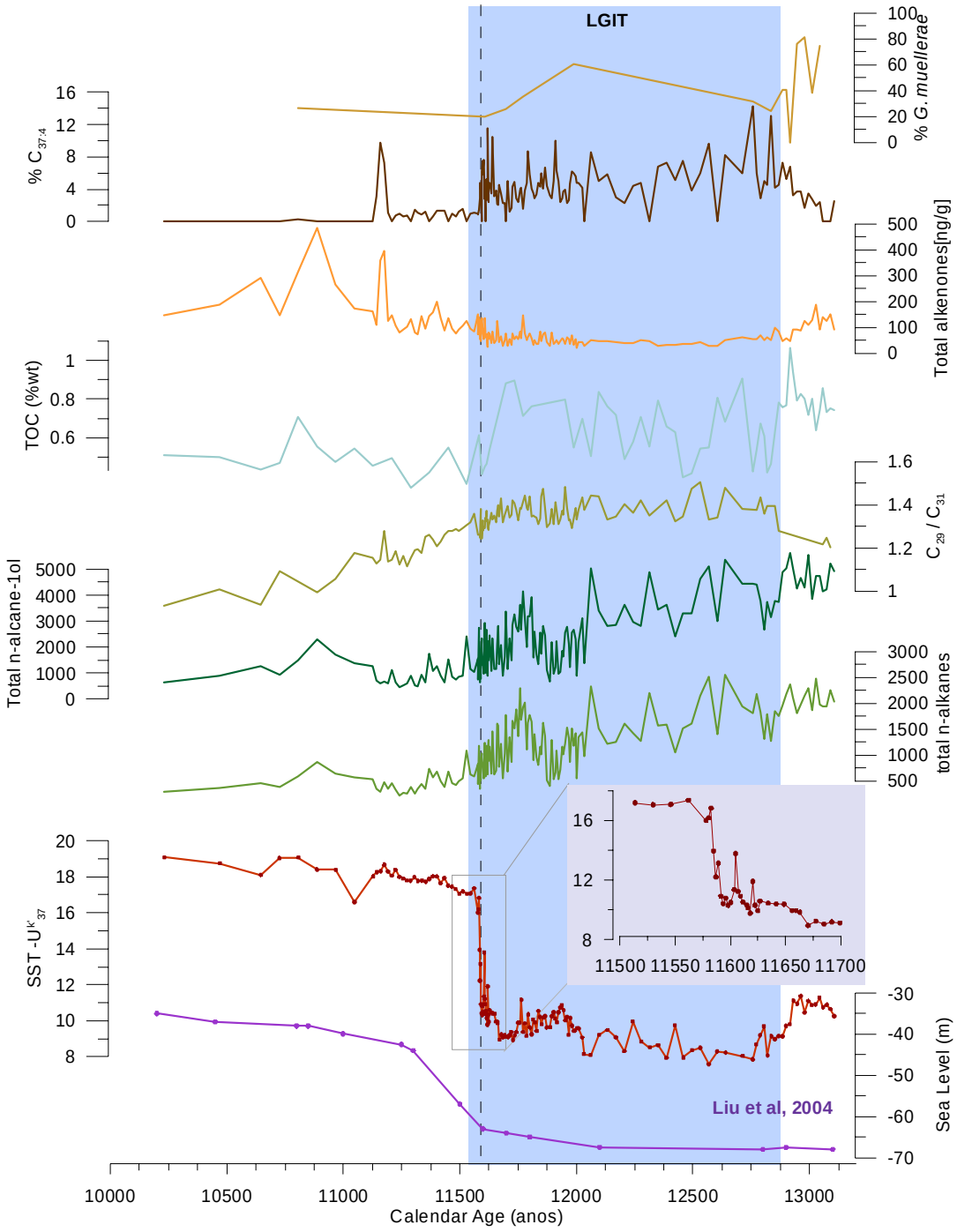

Figure 5. Last Glacial-Interglacial transition in the shallow core D13882. From the top to the bottom: % of *G. mullerae*; % of Tetyra-unsaturated Alkenone ($C_{37:4}$); Total Alkenone concentration (ng/g); Total organic carbon content (%wt); Alkanes ratio of C_{29}/C_{31}; total n-alkanes concentration (ng/g); Alkenone –based $U^{k'}_{37}$-SST including a zoom (200 years) of the glacial- Interglacial transition; High resolution sea level curve [*Liu et al.*, 2004].

The comparison of western Iberian margin SST records (cores D13882 and MD03-2699) with the $\delta^{18}O$ NGRIP record from Greenland [*Johnsen et al.*, 2001; *North Greeland Ice Core project member*, 2004; *Rasmussen et al.*, 2006] demonstrates that the timing of the YD event is similar at both areas, occurring between 12.8 ka and 11.6 ka (about 1200 year long) (Fig. 4). These age limits are coincident with those obtained from $^{230}Th/^{234}U$ measurements in the Barbados corals [*Fairbanks*, 1990] and in varved sediments from European lakes [*Goslar et al.*, 2000]. The timing of the YD in northwestern Scotland is also synchronous with that of NGRIP as showed by the presence of the Verdi ash layer in both records [*Kroon et al.*, 1997], as well as the YD episode recorded in Cariaco basin [*Hughen et al.*, 1998].

The transition zone between the YD and the Holocene is marked by a steep increase of SST in most Iberian margin records (cores: D13882, SU81-18, MD95-2042 and M39-008; Fig. 4) [*Bard et al.*, 2000; *Cacho et al.*, 2001; *Pailler and Bard*, 2002] at 11.6 ka which is synchronous with the expansion of temperate trees in the neighbour continent [*Naughton et al.*, 2007b; *Turon et al.*, 2003] In addition, this sharp SST increase is contemporaneous with a strong sea level rise the consequent retreat of the coastline in the Tagus mud patch as revealed by the western Portugal shore line evolution [*Dias et al.*, 2000]. A sea level rise likely to favour sedimentation within the estuary and preclude the input of terrigenous material into the Iberian shelf. This is in fact the case at the Tagus mud patch region where TOC decrease from 1W% to less than 0.5W% and the higher plant proxies concentration also decrease markedly (*n*-alkanes: 2000 ng/g to 500 ng/g and *n*-alkane-1-ols: 5000 ng/g to 1000 ng/g) during the YD-Holocene transition (Fig. 5). Furthermore, the decreases of $C_{37:4}$ and G. *mullerae* percentages in core D13882 also testify to the decrease of continental cold freshwater input into this area (Fig. 5).

5.2 Is there evidence of the meltwater pulses in the Iberian Margin?

In recent years, many studies have been carried out to understand the timing, sources and global impact of the mwp episodes during the last deglaciation [*Clark et al.*, 1996; *Clark et al.*, 2002; *McManus et al.*, 2004; *Peltier*, 2005; *Weaver*, 2003] [*Bassett et al.*, 2005; *Liu and Millinan*, 2004; *Roche et al.*, 2007; *Stanford et al.*, 2006; *Tarasov and*

Peltier, 2005]. Based in AMS ^{14}C [*Fairbanks* 1989] and U-Th [*Bard et al.*, 1990; *Bard et al.*, 1996] dating of the Barbados and Tahiti coral records, two major mwp have been identified after the well-known Heinrich 1 event, the mwp-1A and mwp-1B. These events occurred at around 14.5 - 13.8 ka (mwp -1A) and 11.5 – 11.1 ka (mwp -1B) reflecting a sea level rise of about 20 and 15 m, respectively [*Liu and Millinan*, 2004]. Studies from the South China Sea suggest that the mwp-1A was synchronous with the warm Bølling episode, which has contributed for massive meltwater discharges and consequent weakening of deep-water formation in the North Atlantic region [*Kienast et al.*, 2003; *Pelejero et al.*, 1999]. In addition, it has been proposed that the abrupt resumption of the MOC at the beginning of B-A event together with the increase of high latitude summer insolation accelerated the Laurentide Ice sheet melting and triggered the mwp-1A [*McManus et al.*, 2004; *Peltier*, 2005]. These hypotheses have been corroborated by [*Flower et al.*, 2004] based on $\delta^{18}O$ records of the Gulf of Mexico, which suggest that the SST warming precede the Laurentide Ice Sheet decay and consequent input of freshwater into the ocean. This mechanism should induce the subsequent reduction or a shutdown of the conveyor belt [*Roche et al.*, 2007]. However, the mwp-1A occurred more than 1000 years before the next significant change in the MOC which arises during the Younger Dryas cold interval [*Clark et al.*, 2002]. This implies that the mwp occurring during the B-A event was primarily originated from Antarctica reducing its impact on the Atlantic MOC [*Clark et al.*, 2002]. Other studies suggest that the mwp-1A did not occur during the fast warming phase of the Bølling but rather through the Older Dryas cooling event [*Stanford et al.*, 2006].

The Iberian margin cores show that the rise in sea surface temperatures, which characterizes the B-A event, started 1000 yr before the mwp-1A and attain its maximum values during or slightly after this substantial sea level rise episode (Fig. 4). A result in accordance with the findings of [*Clark et al.*, 2002], where the mwp-1A occurred more than 1000 years before the next significant change in the MOC which arises during the Younger Dryas cold interval, leading the authors to consider that this mwp event was primarily originated from Antarctica what reduced its impact on the Atlantic MOC. Although we cannot infer about the origin / source of this meltwater pulse, the fact is that the western Iberian margin sea surface temperatures show a gradual increase synchronously with the increase of the high latitude summer insolation and attain its maximum values after the Older Dryas event.

In which respects the YD/Holocene transition, it is marked by a gradual increase of SST in the lowermost resolution records (MD03-2699, SU81-18, MD95-2042, MD012444 and M39-008) and by an abrupt SST increase in the higher resolution D13882 record (Fig. 4). This SST abrupt increase is contemporaneous with a substantial warming over Greenland [*Johnsen et al.*, 2001] and with a maximum in high-latitude summer insolation [*Berger*, 1978]. Additionally, this SST increase is contemporaneous with an important decrease of continental input into the Tagus mud pacth, as revealed by D13882 terrigenous biomarkers record, suggestive of an abrupt sea level rise favoring the deposition of continental material in the estuaries rather than in the ocean. Thus, the abrupt SST increase of 7ºC in 40 years together with the decrease of continental input in the Tagus mud patch occurs synchronously with the well known mwp-1B (Fig. 5). This event, occurred between 11.5 and 11.2 ka and is marked elsewhere by a sea level rise of about 13m (Figs. 3 and 4) [*Liu et al.,* 2004]. Besides the substantial sea level rise, the expansion of temperate and humid trees in the adjacent landmasses [*Naughton et al.*, 2007b] would have also precluded the land-sea transport of continental material.

All these evidences show that the timing of the maximum marine and terrestrial warming at the mid-latitudes of western Iberia, together with maxima temperatures over Greenland is synchronous with that of the mwp-1B. This suggest that this drastic melting episode (mwp-1B) must have been initiated in the Northern Hemisphere rather that in the South.

6. CONCLUSIONS

The comparison between marine climatic indicators ($U^{k'}_{37}$-SST), coccolithophore associations and proxies of terrestrial input (total organic carbon and higher plant *n*-alkanes and *n*-alkan-1-ols) of a core D13882 retrieved from the inner-shelf Tagus mud patch provides the highest resolution record of the last deglaciation and in particular of the last glacial-interglacial transition (LGIT) for western Iberia. Sea surface temperatures downcore have been compared with those obtained for deep-sea core MD03-2699 and other deep-sea records from the western Iberian margin.

The SST records of the deeper cores demonstrate Heinrich event 1 (H1) as the extreme cold event (11º to 13º C) of the last 21 ka. During this period the SST is less cold in the southernmost site, suggesting a latitudinal gradient along the Iberian margin.

The beginning of the Bølling-Allerød interstadial is marked by a sharp SST increase to 15° - 17°C, around 15 ka. This SST increase has started 1000 yr before the mwp -1A and attain its maximum values during or slightly after this substantial sea level rise episode.

The shallow core D13882 only covers the last part of this warm interstadial (B-A) and shows lower temperatures (11ºC) when compared to the deeper cores. This site reflects the dominance of tetra-unsaturated alkenone, and, a higher concentration of terrigenous biomarkers and TOC provide evidence of the arrival of cold freshwater to the area. This freshwater input although possibly associated with the melting of ice sheets is most certainly reflecting the strong input of freshwater by the Tagus River.

Returning cold conditions mark the Younger Dryas event at around 12.9 ka. During the YD, as for B/A, SSTs were lower, by about 4-5ºC, in the Tagus mud patch than in the open sea sites, indicating the continuity of the cold freshwater input by the River. The high-resolution alkenone based SST estimates of core D13882 further show that the YD event is composed by two cold phases surrounding a relatively warm one. That is, a 3ºC cooling episode detected at around 12.9 ka is followed by a continuous temperature increase up to 11ºC at 12.0 ka and followed by a second cooling phase (about 2°C) after 11.8 ka.

The glacial-interglacial transition is marked by a sharp SST increase from 10ºC to 17ºC in the shallow core, contemporaneous with a strong sea level rise and consequent retreat of the coastline in the Tagus mud patch which probably precluded the input of terrigenous material to the inner-shelf.

The abrupt SST increase of 7ºC in 40 yr together with the decrease of continental input to the Tagus mud patch occurs contemporaneously with the well-known mwp-1B. The synchronous timing between the drastic melting episode 1B and the abrupt marine and terrestrial warming at the mid-latitude of western Iberia, together with warm temperatures over Greenland, suggest that this melting water episode and consequent sea level rise were initiated in the Northern Hemisphere.

Acknowledgements

Support from FCT- Fundação para a Ciência e Tecnologia (SFRH/BD/13749/2003), the Spanish Ministry of Science and Technology (REN2003-08642-C02-01), the Consolider-Ingenio 2100 Project CE-CSD2007-0067 and INETI are acknowledged. The AMS ^{14}C dating was supported by EU project SEDPORT (PDCTM/40017/2003). We are grateful to C. Monteiro for TOC measurements and R. Mas for laboratory assistance, and C. Trindade and C.N. Prahbul for picking the AMS samples.

7. REFERENCES

Allen, J. R. M., B. Huntley, and W. A. Watts (1996), The vegetation and climate of nortwest Iberia over the last 14000 yr, *Journal of Quaternary Science*, *11*, 125-147.

Alley, R. B., D. A. Meese, C. A. Shuman, A. J. Gow, M. Ram, E. D. Waddington, P. A. Mayewski, and G. A. Zielinski (1993), Abrupt increase in Greenland snow accumulation at the end of the Younger Dryas event, *Nature*, *362*.

Alley, R. B. (2000), The Younger Dryas cold interval as viewed from central Greenland, *Quaternary Research*, *19*, 213-226.

Andrews, J. T., A. E. Jennings, M. Kerwin, M. Kirby, W. Manley, G. H. Miller, G. Bond, and B. MacLean (1995), A Heinrich-like event, H-0 (DC-0): Source(s) for detrital Carbonate in the North Atlantic during the Younger Dryas chronozone, *Paleoceanography*, *10*.

Andrews, J. T., L. Keigwin, F. Hall and Anne E. Jennings (1999), Abrupt deglaciation events and Holocene palaeoceanography from high-resolution cores, Cartwright Saddle, Labrador Shelf, Canada, *Journal of Quaternary Science*, *14*(5), 383-397.

Bard, E., M. Arnold, P. Maurice, J. Duprat, J. Moyes, and J.-C. Duplessy (1987), Retreat velocity of the North Atlantic polar front during the last deglaciation determined by 14 C accelator mass spectrometry, *Nature*, *328*, 791-794.

Bard, E., B. Hamelin, and R. G. Fairbanks (1990), U-Th ages obtained by mass spectrometry in corals from Barbados, *Nature*, *346*, 456-458.

Bard, E., C. Jouannic, B. Hamelin, P. Pirazzoli, M. Arnold, G. Fraure, P. Sumosusastro, and Syaefudin (1996), Pleistocene sea levels and tectonic uplift based on dating of corals from Sumba Island, Indonesia, *Geophysical Research letters*, *23*(12), 1473-1476.

Bard, E., F. Rostek, J.-L. Turon, and S. Gendreau (2000), Hydrological Impact of Heinrich Events in the Subtropical Northeast Atlantic, *Science*, *289*, 1321-1324.

Bard, E. (2001), Comparison of alkenone estimate with other paleotemperature proxies, *Geochemistry Geophysics Geosystems*, *2*, 2000GC000050.

Bassett, S. E., G. A. Milne, J. X. Mitrovica, and P. U. Clark (2005), Ice Sheet and Solid Earth Influences on Far-Field Sea-Level Histories, *Science*, *309*(5736), 925-928.

Berger, A. L. (1978), Long-Term Variations of Daily Insolation and Quaternary Climatic Changes *Journal of the Atmospheric Sciences*, *35*(12), 2362-2367.

Bond, G., W. Broecker, S. Johnsen, J. McManus, L. Labeyrie, J. Jouzel, and G. Bonani (1993), Correlations between climate records frm North atlantic sediments and Greenland Ice, *Nature*, *365*, 143.

Boyle, E. A., and L. Keigwin (1987), North Atlantic thermohaline circulation during the past 20,000 years linked to high-latitude surface temperature, *Nature*, *330*, 35-40.

Cacho, I., J. O. Grimalt, C. Pelejero, M. Canals, F. J. Sierro, J. A. Flores, and N. Shackleton (1999), Dansgaard-Oeschger and Heinrich event imprints in Alboran Sea Paleotemperatures, *Paleoceanography*, *14*, 698-705.

Cacho, I., J. O. Grimalt, M. Canals, L. Sbaffi, N. J. Shackleton, J. Schönfeld, and R. Zahn (2001), Variability of the Western Mediterranean Sea Surface Temperature during the last 25,000 years and its connection with the Northern hemisphere climatic changes, *Paleoceanography*, *16*, 40-52.

Clark, P. U., R. B. Alley, L. D. Keigwin, J. M. Licciardi, S. J. Johnsen, and H. Wang (1996), Origin of the First Global Meltwater Pulse Following the Last Glacial Maximum, *Paleoceanography*, *11*.

Clark, P. U., J. X. Mitrovica, G. A. Milne, and M. E. Tamisiea (2002), Sea-Level Fingerprinting as a Direct Test for the Source of Global Meltwater Pulse 1A, *Science*, *295*, 2438-2441.
Dansgaard, W., S. J. Johnsen, H. B. Clausen, D. Dahl-Jensen, N. S. Gundestrup, C. U. Hammer, C. S. Hvidberg, J. P. Steffensen, A. E. Sveinbjornsdottir, J. Jouzel, and G. Bond (1993), Evidence for general instability of past climate from a 250-kyr ice-core record, *Nature*, *364*(6434), 218-220.
Dias, J. M. A., T. Boski, A. Rodrigues, and F. Magalhães (2000), Coast line evolution in Portugal since the last Glacial Maximum until present - a synthesis, *Marine Geology*, *170*, 177-186.
Duplessy, J. C., L. Labeyrie, M. Arnold, M. Paterne, J. Duprat, and T. C. E. V. Weering (1992), Changes in surface salinity of the North Atlantic Ocean during the last deglaciation, *Nature*, *385*, 485-488.
Dyke, A. S. (2004), *An outline of North American deglaciation with emphasis on central and northern Canada, in Quaternary Glaciations-Extent and Chronology, Part II*, 373– 424 pp., Elsevier, New York.
Eltgroth, S. F., J. F. Adkins, L. F. Robinson, J. Southon, and M. Kashgarian (2006), A deep-sea coral record of North Atlantic radiocarbon through the Younger Dryas: Evidence for intermediate water/deepwater reorganization, *Paleoceanography*, *21*.
Fairbanks , R. G. (1989), A 17,000 year glacio-eustatic sea level record: influence of glacial melting rates on the Younger Dryas event and deep ocean circulation, *Nature*, *342*, 637-642.
Fairbanks, R. G. (1990), The age and origin of the "Younger Dryas Climate event" in Greeland ice cores, *Paleoceanography*, *5*, 937-948.
Fairbanks, R. G., R. A. Mortlock, T.-C. Chiu, L. Cao, A. Kaplan, T. P. Guilderson, T. W. Fairbanks, A. L. Bloom, P. M. Grootes, and M.-J. Nadeau (2005), Radiocarbon calibration curve spanning 0 to 50,000 years BP based on paired 230Th/234U/238U and 14C dates on pristine corals, *Quaternarty Science Reviews*, *24*(doi:10.1016/J.quascirev.2005.04.007), 1781-1796.
Fawcett, P. J., A. M. Agustsdottir, R. B. Alley, and C. A. Shuman (1997), The Younger Dryas termination and North Atlantic deepwater formation: insights from climate model simulations and Greenland ice core data. , *Paleoceanography*, *12* 23-28.
Flores, J.-A., R. Gersonde, and F. Sierro (1999), Pleistocene fluctuationsin the Agulhas Current Retroflection based on the the calcareous plankton record, *Marine Micropaleontology*, *37*, 1-22.
Flores, J. A., and F. J. Sierro (1997), Revised technique for calculation of calcareous nanofossil accumulation rates, *Micropaleontology*, *43*, 321-324.
Flower, B., D. Hastings, H. Hill, and T. M. Quinn (2004), Phasing of deglacial warming and Laurentide ice sheet meltwater in the Gulf of Mexico, *Geology*, *32*(7), 597-600.
Ganopolski, A., and S. Rahmstorf (2001), Rapid changes of glacial climate simulated in a coupled climate model *Nature 409*, 153-158.
Goslar, T., M. Arnold, N. Tisnerat-Laborde, J. Czernik, and K. Wieckowski (2000), Variations of Younger Dryas atmospheric radiocarbon explicable without ocean circulation changes, *Nature*, *403*, 877-880.
Hughen, K., J. Southon, S. Lehman, C. Bertrand, and J. Turnbull (2006), Marine-derived 14C calibration and activity record for the past 50,000 years updated from the Cariaco Basin, *Quaternary Science Reviews*, *25*(23-24), 3216-3227.
Hughen, K. A., J. T. Overpeck, L. C. Peterson, and S. Trumbore (1996), Rapid climate changes in the tropical Atlantic region during the last deglaciation, *Nature*, *380*(6569), 51-54.
Hughen, K. A., J. T. Overpeck, S. J. Lehman, M. Kashgarian, J. Southon, L. C. Peterson, R. B. Alley, and D. E. Sigman (1998), Deglacial Changes in ocean circulation from an extended radiocarbon calibration, *Nature*, *391*, 65-68.
Hughen, K. A., M. G. L. Baillie, E. Bard, A. Bayliss, J. W. Beck, C. J. H. Bertrand, P. G. Blackwell, C. E. Buck, G. S. Burr, K. B. Cutler, P. E. Damon, R. L. Edwards, R. G. Fairbanks, M. Friedrich, T. P. Guilderson, B. Kromer, F. G. McCormac, S. W. Manning, C. Bronk Ramsey, P. J. Reimer, R. W. Reimer, S. Remmele, J. R. Southon, M. Stuiver, S. Talamo, F. W. Taylor, J. van der Plicht, and Weyhenmeyer (2004), Marine04 Marine radiocarbon age calibration, 26 - 0 ka BP, *Radiocarbon*, *46*, 1059-1086.
Iversen, J. (1954), The Late Glacial flora of Denmark and its relations to climate and soil, *Danmarks Geol. Unders*, *80*, 87–119.
Johnsen, S. J., D. Dahl-Jensen, N. S. Gundestrup, J. P. Steffensen, H. B. Clausen, H. Miller, V. Masson-Delmotte, A. E. Sveinbjornsdottir, and J. W. C. White (2001), Oxygen isotope and palaeotemperature records from six Greenland ice-core stations: Camp Century, Dye-3, GRIP, GISP, Renland and NorthGRIP, *Journal of Quaternary Science*, *16*, 299-307.
Keigwin, L. D., and S. J. Lehman (1994), Deep Circulation Change Linked to HEINRICH Event 1 and Younger Dryas in a Middepth North Atlantic Core, *Paleoceanography*, *9*.
Kienast, M., T. J. J. Hanebuth, C. Pelejero, and S. Steinke (2003), Synchroneity of meltwater pulse 1a and the Bolling warming: New evidence from Nordic Seas and North Atlantic, *Geology*, *31*, 67-70.

Knutti, R., J. Fluckiger, T. F. Stocker, and A. Tirmmermann (2004), Strong hemispheric coupling of glacial climate through freshwater discharge and ocean circulation, *Nature*, *430*, 851-856.
Kroon, D. W. E. N., W. E. N. Austin, M. R. Chapman, and G. M. Ganssen (1997), Deglaciation surface circulation changes in the northeastern Atlantic: temperature and salinity records off NW Scotland on a century scale, *Palaeogeography*, *12*, 757-762.
Lambeck, K., and J. Chappell (2001), Sea Level Change Through the Last Glacial Cycle, *Science*, *292*, 679-686.
Liu, J. P., J. D. Milliman, S. Gao, and P. Cheng (2004), Holocene development of the Yellow River´s subaqueous delta North Yellow Sea, *Marine Geology*, *209*, 45-67.
Liu, J. P., and J. D. Millinan (2004), Reconsidering Melt-water Pulses 1A and 1B: Global Impacts of Rapid Sea-level Rise, *Journal of Ocean University of China*, *3*(2), 183-190.
Lowe, J. J., S. O. Rasmussen, S. Bjorck, W. Z. Hoek, J. P. Steffensen, M. J. C. Walker, Z. C. YU, and t. I. group (2008), Synchronisation of palaeoenvironmental events in the North Atlantic region during the last Termination: a revised protocol recommended by the INTIMATE group, *Quaternarty Science Reviews*, *27*, 6-17.
Mangerud, J., S. V. Andersen, B. E. Berglund, and J. J. Donner (1974), Quaternary stratigraphy of Norden, a propossal for terminology and classification, *Boreas*, *3*, 109-128.
Martrat, B., J. O. Grimalt, N. J. Shackleton, L. d. Abreu, M. A. Hutterli, and T. F. Stocker (2007), Four Climate Cycls of Recurring Deep and Surface Water Destabilizations on the Iberian Margin, *Science 317*(1139994), 502-507.
McCabe, A. M., and P. U. Clark (1998), Ice-sheet variability around the North Atlantic Ocean during the last deglaciation, *Nature*, *392*(6674), 373-377.
McCabe, A. M., P. U. Clark, and J. Clark (2005), AMS 14C dating of deglacial events in the Irish Sea Basin and other sectors of the British-Irish ice sheet, *Quaternary Science Reviews*, *24*(14-15), 1673-1690.
McCabe, A. M., P. U. Clark, J. Clark, and P. Dunlop (2007), Radiocarbon constraints on readvances of the British-Irish Ice Sheet in the northern Irish Sea Basin during the last deglaciation, *Quaternary Science Reviews*, *26*(9-10), 1204-1211.
McManus, J., R. Francois, J.-M. Gherardi, L. D. Keigwin, and S.Brown-Leger (2004), Collapse and rapid resumption of Atlantic meridinal circulationlinked to deglacial climate changes, *Nature*, *428*.
Millera, G. H., A. P. Wolfeb, J. P. Brinera, P. E. Sauerc, and A. Nesje (2005), Holocene glaciation and climate evolution of Baffin Island, Arctic Canada, *Quaternary Science Reviews*, *24*(14-15), 1703-1721.
Müller, P., G. Kirst, G. Ruhland, I. v. Storch, and A. Rosell-Melé (1998), Calibration of the alkenone index Uk'37 based on core-tops the eastern South Atlantic and global ocean (60ºN-60ºS), *Geochimica et Cosmochimica Acta*, *62*, 1757-1772.
Naughton, F., J.-F. Bourillet, m. f. S. Goñi, J.-L. Turon, and J.-M. Jouanneau (2007a), Long-term and Millennial-scale climate variability in northwestern France during the last 8850 years, *The Holocene*, *17*, 939-953.
Naughton, F., M. F. Sánchez Goñi, S. Desprat, J.-L. Turon, J. Duprat, B. Malaizé, C. Joly, E. Cortijo, D. T., and M. C. Freitas (2007b), Present-day and past (last 25 000 years) marine pollen signal off western Iberia, *Marine Micropalentology 62*, 91-114.
North Greeland Ice Core project member (2004), High resolution record of Northern Hemisphere climate extending into the last interglacial period, *Nature*, *431*, 147-151.
Paillard, D., and L. Labeyriet (1994), Role of the thermohaline circulation in the abrupt warming after Heinrich events, *Nature*, *372*(6502), 162-164.
Paillard, D., L. Labeyrie, and P. Yiou (1996), Macintosh program performs time-series analysis, *Eos Trans, AGU*, *77*, 379.
Pailler, D., and E. Bard (2002), High frequency paleoceanographic changes during the past 140 000 yr recorded by the organic matter insedimentaf the Iberin Margin, *Paleoceanigrphy, paleoclimatology, Palaeoecology*, *2799*, 1-22.
Pelejero, C., M. Kienast, L. wang, and J. O. Grimalt (1999), The flooding of Sundaland during the last deglaciation: Imprints in hemipelagic sediments from the southern south China sea, *Earth and Planetary Science Letters*, *171*, 661-671.
Peltier, W. R. (2005), On the hemispheric origins of meltwater pulse 1a, *Quaternary Science Reviews*, *24*(14-15), 1655-1671.
Peltier, W. R., and R. G. Fairbanks (2006), Global glacial ice volume and Last Glacial Maximum duration from an extended Barbados sea level record, *Quaternarty Science Reviews*, *25*(doi:10.1016/j.quascirev.2006.04.010), 3322-3337.
Peñalba, C., M. Arnold, J. Guiot, J. C. Duplessy, and J.-L. Beaulieu (1997), Termination of the last glaciation in the Iberian Peninsula inferred from the pollen sequence of Quintanar de la Sierra, *Quaternary Research*, *48*, 205-214.

Peteet, D. M., R. A. Daniels, L. E. Heusser, J. S. Vogel, J. R. Southon, and D. E. Nelson (1993), Late-glacial pollen, macrofossils and fish remains in Northeastern, USA: The Younger Dryas oscillation, *Quaternary Science Reviews*, *12*(doi:10.1016/0277-3791(93)90002-4), 597-612.
Peterson, L. C., G. H. Haug, K. A. Hughen, and U. Rohl (2000), Rapid Changes in the Hydrologic Cycle of the Tropical Atlantic During the Last Glacial, *Science*, *290*(5498), 1947-1951.
Rasmussen, S. O., K. K. Andersen, A. M. Svensson, J. P. Steffensen, B. M. Vinther, H. B. Clausen, M. L. Siggaard-Andersen, S. J. Johnsen, L. B. Larsen, D. Dahl-Jensen, M. Bogler, R. Rothlisberger, H. Fischer, K. Goto-Azuma, M. E. Hansson, and U. Ruth (2006), A new Greenland ice core chronrlogy for the last glacial termination, *Journal of Geophysical Research*, *111*, doi:10.1029/2005JD006079.
Roche, D. M., H. Renssen, S. L. Weber, and H. Goosse (2007), Could meltwater pulses have been sneaked unnoticed into deep ocean during the last glacial?, *Geophysical Reserch Letters*, *34*, L24708.
Rodrigues, T., J. O. Grimalt, F. Abrantes, J. A. Flores, and S. Lebreiro (2009), Holocene interdependences of changes in sea surface temperature, productivity, and fluvial inputs in the Iberian continental shelf (Tagus mud patch), *Geochemistry Geophysics Geosystems*, *10*.
Rosell-Melé, A., M. Weinelt, M. Sarnthein, N. Koç, and E. Jansen (1998), Variability of the Arctic front during the last climatic cycle: application of a novel molecular proxy, *Terra Nova*, *10*(86-89).
Rosell-Melé, A. (2004), Sea surface temperature in the oceans at the LGM estimated from the alkenone-Uk'37index: comparison with GCMs, *Geophysical Research letters*, *31*, 1-4.
Ruddiman, W. F., and A. McIntyre (1981), The Mode and Mechanism of the Last Deglaciation: Oceanic Evidence, *Quaternary Research*, *16*, 125-134.
Rühlemann, C., S. Mulitza, P. J. Muller, G. Wefer, and R. Zahn (1999), Warming of the tropical Atlantic Ocean and slowdown of thermohaline circulation during the last deglaciation, *Nature*, *402*(6761), 511-514.
Schulz, H.-M., A. Schoner, and K.-C. Emeis (2000), Long-chain alkenone patterns in the Baltic Sea - an ocean-fresh water transition, *Geochimica et Cosmochimica Acta*, *64*, 469-477.
Seidov, D., and M. Maslin (1999), North Atlantic deep water circulation collapse during Heinrich events, *Geology*, *27*(1), 23-26.
Stanford, J. D., E. J. Rohling, S. E. Hunter, A. P. Roberts, S. O. Rasmussen, E. Bard, J. Mcmanus, and R. G. Fairbanks (2006), Timing of meltwater pulse 1a and climate responses to meltwater injections, *Palaeogeography*, *21*(PA4103).
Stouffer, R. J., D. Seidov, and B. J. Haupt (2006), Climate Response to External Sources of Freshwater: North atlantic versus the Southern Ocean, *Journal of Climate*, *20*, 436-448.
Stuiver, M., and P. J. Reimer (1993), Extended 14C data base and revused CALIB radiocarbon calibration program, *Radiocarbon*, *35*, 215-230.
Stuiver, M., P. J. Reimer, and R. W. Reimer (2005), CALIB 5.0 (WWW program and documentation), edited.
Tarasov, L., and W. R. Peltier (2005), Arctic freshwater forcing of the Younger Dryas cold reversal, *Nature*, *435*(7042), 662-665.
Teller, J. T., D. W. Leverington, and J. D. Mann (2002), Freshwater outbursts to the ocean from glacial Lake Agassiz and their role in climate change during the last deglaciation, *Quaternary Science Reviews*, *21*, 879-887.
Turon, J. L., A.-M. Lézine, and M. Denèfle (2003), Land-sea correlations for the last glaciation inferred from a pollen and dinocyst record from the Portuguese Margin, *Quaternary Research*, *59*, 88-96.
Villanueva, J., and J. O. Grimalt (1997), Gas Chromatographic Tuning of the UK37 Paleothermometer, *Analytical Chemistry*, *69*(16), 3329-3332.
VonGrafenstein, U. H. Erlernkeuserb, and P. Trimbornc (1999), Oxygen and carbon isotopes in modern fresh-water ostracod valves: assessing vital offsets and autecological effects of interest for paleoclimate studies., *Palaeogeography, Palaeoclimatology, Palaeocology*, *148 (1-3)*, 133-152.
Weaver, P. P. E. (2003), RRS Discovery Cruise 249, 19 Aug-10 Sep 2000. History of sedimentation in the Gulf of Cadiz: investigations with the SOC giant piston corer., 19 pp, Southampton Oceanography Centre, Southampton, UK.
Wells, P., and H. Okada (1997), Response of nannoplankton to major changes in sea-surface temperature and movements of hydrological fronts over Site DSDP 594 (south Chatham Rise, southeast New Zealand) during the last 130ky, *Marine Micropaleontology*, *32*, 341-363.
Yokoyama, Y., P. DeDeckker, K. Lambeck, P. Johnston, and L. K. Fifield (2000), Timing of the Last Glacial Maximum from observed sea-level minima, *Nature*, *406*, 713-716.

Chapter 5

CLIMATE CHANGES OFF PORTUGAL DURING MARINE ISOTOPE STAGES 15-9 (580 TO 300 KA): SUBORBITAL GLACIAL VARIABILITY AND INTERGLACIAL STABILITY

Teresa Rodrigues[1,2], A. H. L. Voelker[1,3], Joan O. Grimalt[2], Fatima Abrantes[1]

[1]Unit of Marine Geology, LNEG, Estrada da Portela-Zambujal, Apartado 7568, 2721-866 Amadora, Portugal
[2]Institute of Environmental Assessment and Water Research (IDÆA-CSIC), Jordi Girona, 18, 08034-Barcelona, Catalonia, Spain
[3] CIMAR Associated Laboratory, Porto, Portugal

Will be submitted to **PALEOCEANOGRAPHY**

ABSTRACT

The present study of sea surface water conditions based on Calypso-core MD03-2699 sediments from the Estremadura Spur north off Lisbon provide insights into orbital and suborbital-scale climate variability between MIS 15 and MIS 9 (580 to 300 ka). The results extend the existing biomarker record in the Iberian Margin back in time to the 6th climatic cycle (580 ka). They show a general trend of warm and relative stable interglacial periods in contrast to high-frequency variability during the glacial inceptions and glacials. They also show a change in the orbital dependence of sea surface temperature (SST) from predominance of obliquity to predominance of eccentricity at around 430 ka, the mid-Brunhes event. This change is consistent with the observations in Antarctica ice temperatures. However, despite of this eccentricity dominance, the warming of termination IV closely matches obliquity.

Several short-lived climatic oscillations have been identified: 5 during the interval from MIS 15.1 to MIS 14, and 8 stadial-type oscillations from MIS 13.1 to MIS 12 and MIS 11.3 to MIS 10. Some of these event were extremely cold and are similar to the Heinrich events of MIS 3 found in the north Atlantic. They can be identified by the strong SST decreases, the occurrence of ice-rafted detritus (IRD) and high % of the tetra-unsaturated alkenone $C_{37:4}$ In this study they are named as Ht1 in MIS10.2; Ht2, Ht3 during MIS 11.24 and 11.23; Ht4 at the onset of termination V; Ht5 (MIS 12.2); Ht6 and Ht7 during the glacial inception of MIS 12 and Ht8 during the glacial inceptions of MIS 14. The general pattern recorded during the deglaciations are similar to the previous climatic cycles, i.e. two coolings separated by a small warming that are associated to the southward and northward migration of the polar front.

The composed Iberian SST record for the last 580 ka shows that SST of the MIS 11.3 are analogous with the present interglacial, the Holocene.

1. INTRODUCTION

The Earth's climate gradually cooled during the past 5 Ma [*Lisiecki and Raymo*, 2005]. Within this long-term climate trend several orbital-induced climate oscillations, with periodicities of 20 ka, 41 ka and 100 ka have been observed in numerous deep sea cores distributed throughout the planet [*Lisiecki and Raymo*, 2005]. A transition from prevailing symmetrical low-amplitude and high-frequency ice volume variations (41-kyr) to prevailing asymmetrical high-amplitude and low-frequency ice volume variations (100-kyr) is attributed to the period between 1.2 and 0.6 Ma, a climate transition that is called as the Mid-Pleistocene Revolution (MPR) [*Imbrie, et al.*, 1993]. This change was concurrent with a variation in the mean state of the global climate system, involving an evolution towards lower atmospheric temperatures and higher global ice volume [*Shackleton, et al.*, 1990]. After the mid-Brunhes event (around 430 ka) the global climate became mainly controlled by the 100-kyr cyclicity [*Loutre and Berger*, 2003] and started to be characterized by relatively short warm episodes during interglacials and longer cold phases during glacial periods [*Jouzel, et al.*, 2007; *Shackleton, et al.*, 2000].

The Mid-Brunhes interval between MIS 11 and MIS 9 is considered to be an unusual long warm period within the last 1.0 Ma [*Droxler and Farrell*, 2000]. This period displays long-lasting and perhaps intense warmth and is generally characterized by the highest sea level stands, unusual far poleward penetration of warm waters and the increase of carbonate accumulation on the sea floor. These characteristics give to MIS 11 a unique climate condition exhibiting warm interglacial climatic conditions for an interval of at least 30 ka, a duration twice as long as the most recent interglacial stages [*Desprat, et al.*, 2005; *Loutre*, 2003; *Loutre and Berger*, 2003; *McManus, et al.*, 2003]. The beginning of MIS 11 is characterized by the highest amplitude deglacial warming of the past 5 Ma and is associated with higher sea levels than present, maybe +2, +7 or +20 m above mean level, as consequence of melting of the Greenland and West Antarctic ice sheets [*Droxler and Farrell*, 2000]. The orbital conditions of interglacial MIS 11 were similar to those experienced during the Holocene. Both interglacials occurred in times that eccentricity was at its minimum, so that the amplitude of the precessional cycle was damped. Accordingly,

MIS 11 has often been considered a better analogue for our current climate conditions than any other of the more recent interglacials [*Abreu, et al.*, 2005; *Bowen*, 2009; *Droxler and Farrell*, 2000; *Loutre*, 2003; *Loutre and Berger*, 2003]. Both the Holocene and MIS 11 are characterized by small amounts of continental ice [*Loutre and Berger*, 2003]**.**

However, the parallelism of the climate evolution between MIS 11 and Holocene is not straightforward. Thus, extrapolation of the past conditions to present leads to different perspectives on the length of the current interglacial depending on which parameter is used for chronological alignment [*Tzedakis*, 2009]. Synchronization according to precession shows that the present-day should be analogue to MIS 11 at 398 ka [*Loutre and Berger*, 2003]. In contrast, synchronization based on obliquity, i.e. terminations I and V, shows that present-day would correspond to 407 ka of MIS 11 [*EPICA*, 2004; *Masson-Delmotte, et al.*, 2006].

High resolution climate records are needed for the understanding of the climate processes that occurred in the past. Recent studies on the EPICA Dome C (EDC) ice core have described the history of the Antarctic temperature and the atmospheric gas concentrations during the past 900 ka [*Jouzel, et al.*, 2007; *Loulergue, et al.*, 2008; *Luethi, et al.*, 2008] which is contemporaneous with that revealed by the marine benthic oxygen isotopic records [*Jouzel, et al.*, 2007; *Shackleton, et al.*, 2000]. In this respect, the CO_2 record during the glacial-interglacial cycles exhibits remarkable differences prior to and after Marine Isotope Stage (MIS) 11 [*Luethi, et al.*, 2008; *Siegenthaler, et al.*, 2005] with lower CO_2 levels during the earlier warm phases. However, records of sea surface temperatures –SST- from different world areas are needed for the description of the rates of climate change and trigger mechanisms that occurred as consequence of the orbital changes during these periods.

Marine sediment studies have shown that the western Iberian margin is a strategic area for the description of the climate evolution of the planet because it reflects the influences of the processes that occurred both in the Arctic and Antarctica [*Shackleton et al.*, 2000]. In this area, climate variability of the last four climate cycles has been described [*Abreu, et al.*, 2003; *EPICA*, 2004; *Martrat, et al.*, 2004; 2007; *Roucoux, et al.*, 2006; *Tzedakis, et al.*, 2003]. However, high-resolution marine data prior to MIS 11 is lacking which makes difficult to understand the North Atlantic's response to Mid-Pleistocene

climate variability. In this paper we present the first high resolution biomarker-based climate reconstruction in the Iberian margin extending behind MIS 11. The study is based on the analyses performed in core MD03-2699 that is located in the area of the present descending branch of the north Atlantic's subtropical gyre (Fig. 1).

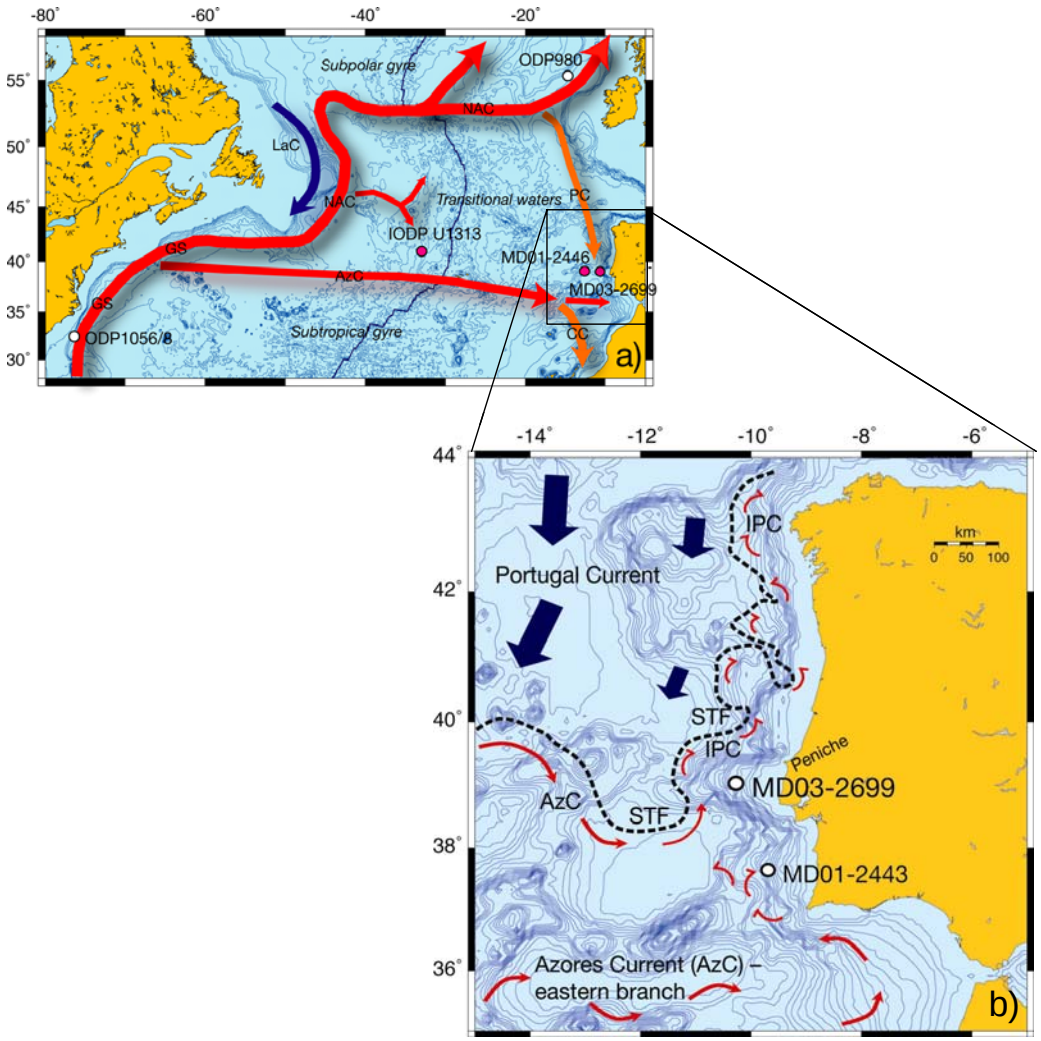

Figure 1: (a) Core locations considered in this study and major surface water currents in the North Atlantic, MD03-2699 (this study); MD01-2443/4 [*Martrat et al.*, 2007]; MD01-2446 [*Voelker et al.*, 2009]; ODP 980 [*McManus et al.*, 1999]; IODP U1313 [*Stein et al.*, 2009]; ODP 1056 [*Billups et al.*, 2004]. GS = Gulf Stream; NAC = North Atlantic Current; AzC = Azores Current; CC = Canary Current; PC = Portugal Current; LaC = Labrador Current. (b) Close-up of the Iberian margin circulation after *Peliz et al.* [2005] IPC = Iberian Poleward Current. STF = Subtropical front (adapted from *Voelker et al.* [2009]).

The time-scale studied in this core provides information on the impact, amplitude, periodicities and triggering mechanisms of climate variability that occurred before and after the Mid-Brunhes event. The proxies analyzed afford information on the past oceanographic conditions such as SST, productivity (determined from coccolithophore abundances, total organic carbon –TOC- and alkenone concentrations) and terrestrial inputs arriving to this coastal site (odd carbon numbered C_{27}-C_{31} n-alkanes and even carbon numbered C_{22}-C_{30} alkan-1-ols) and intensities of the deep water currents (n-hexacosan-1-ol index).

2. MODERN HYDROLOGIC CONDITIONS

The MD03-2699 deep-sea core was recovered from the south-western Iberian margin (39º02.20'N, 10°39.63'W; Estremadura site) at about 100 km offshore and 1895 m water depth (Fig. 1). This region is at present dominated by the surface Portugal Current System (PCS), the descending branch of the North Atlantic's subtropical gyre [*Fiúza*, 1983; *Peliz, et al.*, 2005] which is composed of a slow equatorward current in the open sea and a fast, seasonally reversing, coastal current [*Ambar*, 1994]. The Portugal Current (PC) advects slowly southward, freshly ventilated surface and subsurface waters. During winter, waters from this eastern branch of the subtropical Azores current recirculate northward along the western Iberian margin as the Iberian Poleward Current (IPC) [*Peliz, et al.*, 2005]. Coastal upwelling of sub-surface cold and nutrient-rich waters occurs between May and September as a response to the strong northerlies [*Fiúza et al.*, 1982]. In these conditions, upwelling filaments are observed off Peniche and Cape Roca [*Fiúza et al.*, 1982].

3. MATERIAL AND METHODS

Core MD03-2699 was obtained using a giant CALYPSO corer during the PICABIA oceanographic cruise on board the R/V Marion Dufresne (Fig. 1). This sedimentary record is mainly composed of hemipelagic clay and its retrieved length of 26.56 m cover from MIS 15 to 1. In this study, we will focus on the core section covering MIS 1 and 580-300 ka (MIS 15-9) involving sedimentary rates between 75 cm kyr^{-1} to 46 cm kyr^{-1}.

MD03-2699 core was sub-sampled for biomarker analyses with a spacing of 1 to 2 cm allowing average time resolutions between 266 and 733 years. Alkenones were used to reconstruct SST ($U^{k'}_{37}$ index), productivity and the abundance of the $C_{37:4}$ alkenone was an indicator of the advection of (sub)polar water masses [*Bard, et al.*, 2000; *Rosell-Melé, et al.*, 1998]. The analytical procedure for determining the organic biomarkers is described in detail elsewhere [*Villanueva, et al.,* 1997] and was performed in the laboratory of IDÆA-CSIC, Barcelona. Sediment samples were freeze-dried and the organic compounds were extracted by sonication using dichloromethane. The extracts were digested with 6% potassium hydroxide in methanol to eliminate interferences from wax esters, proteins and other hydrolysable compounds. The neutral lipids were extracted with hexane, evaporated to near dryness under a N_2 stream and finally derivatised with bis(trimethylsilyl)trifluoroacetamide. They were then analyzed with a Varian Gas chromatograph Model 3400 equipped with a septum programmable injector and a flame ionization detector. Selected samples were examined by gas chromatography (GC) coupled to mass spectrometry for confirmation of the GC peak assignments.

A small number of biomarker samples (30) were replicated in the Biogeochemistry lab of the Department of Marine Geology (DGM) of LNEG (formerly INETI), after a rigorous calibration of the new Varian Gas chromatograph Model 3800. This instrument was equipped with a septum programmable injector and a flame ionization detector. Comparison of the results showed deviations lower than 0.5ºC which is within method error [*Grimalt, et al.*, 2001]. Transformation of $U^{k'}_{37}$ indices into SST was performed using a general core-top calibration that provides estimations of annual SSTs [*Müller, et al.*, 1998].

TOC was determined on aliquots (2 mg) of dried and homogenized sediment samples collected at the same levels as those used for biomarker determination. TOC was analyzed in ground sediment with the CHNS-932 Leco elemental analyzer of DGM-LNEG by difference between total and inorganic carbon. The relative precision of repeated measurements of both samples and standards was 0.03 wt%.

Ice-rafted debris was measured by counting. Data was represented as number of particles > 315 μm per gram [*Voelker et al.,* 2009].

4. CHRONOSTRATIGRAPHY

The age model was reconstructed from the correlation of the benthic $\delta^{18}O$ records of cores MD03-2699 and ODP Site 980 from (Feni drift, 55.5 ºN; [*Flower, et al.*, 2000; *McManus, et al.*, 1999; *Oppo, et al.*, 1998]) as previously proposed by *Voelker et al.* [2009]. This ODP Site 980 record was placed on the LR04 chronology [*Lisiecki and Raymo*, 2005] before comparison with MD03-2699.

Age correlation was difficult in some periods such as MIS 13.3, 13.2 and MIS 12 inception because of deviations between the benthic $\delta^{18}O$ records of MD03-2699 and ODP Site 980. Two well known nannofossil events were used to constrain the age model during these intervals. One involved the last occurrence of the nannofossil *Pseudoemiliana lacunosa* which has been recorded in the early MIS 12 in several deep sea cores [*Amore, et al.*, in prep.] and was observed at 1895 cm in core MD03-2699. This depth was therefore assigned to 453.6 ka taking as reference the LR04 stack [*Raffi, et al.*, 2006]. The other concerned the onset of the *G. caribbeanica* bloom at the beginning of MIS 14 [*Bauman and Freitag*, 2004; *Flores, et al.*, 2003] which was used to assign the MIS 15/MIS 14 transition in core MD03-2699.

Both the age model and the resulting sedimentation rates are consistent with a correspondence of the benthic $\delta^{18}O$ record at the basement of MD03-2699 with MIS 15.1. However, in the absence of any isotope signal for MIS 15.2 in this core, this assignment is tentative.

The age model for the last 23.37 ka (upper 3 m core) was based on AMS ^{14}C dates [*Rodrigues, et al.*, submitted] and correlation of the SST records from cores MD03-2699 and MD01-2444 [*Martrat, et al.*, 2007]. Sedimentation rates were in the order of 0.01 cm yr^{-1} allowing an average resolution of 168 year for the 2 cm sampling interval. SST of this record is only presented here for comparison between the Holocene and MIS 11.3.

5. RESULTS

5.1. Sea Surface Temperature variability

The alkenone-derived SST record in core MD03-2699 varied between 8 and 20°C in the 580 and 300 ka period (Fig. 2). The warmest temperature values occurred during the interglacial maximum at MIS 9.3 and the coldest at the end of MIS 12 (termination V). This SST record follows, in general, the interglacial profile of the LR04 benthic stack showing increases that parallel the $\delta^{18}O$ decreases. The correlation between SST and $\delta^{18}O$ is much weaker in the glacial periods when the former often exhibit much warmer values than expected according to the changes observed in the benthic record. In any case, the coldest SST values occurred during pleni-glacial and glacial inception periods (Fig. 2). Sharp SST increases of about 9 and 8ºC mark both terminations V and IV, respectively. In contrast termination VI is characterized by a small SST change of 2ºC.

5.1.1. Interglacial temperatures

Comparison of the mean SST values of the warmest periods of interglacials MIS 13, 11 and 9 shows a general warming trend involving 16.5ºC in MIS 13, 17.5ºC in MIS 11 and 19.5ºC in MIS 9 (Fig. 2). This trend towards higher temperatures is opposite to the duration of the interglacial periods. The previous periods of peak interglacial warmth were longer than MIS 9.3 that lasted 21.2 ka (338.5 to 317.2 ka). Thus, MIS 11.3 lasted 34.6 ka (427.9 to 393.3 ka) and MIS 13.1-2 lasted 34.7 ka (514.7 to 480.06 ka). In fact, according to the SST record of MD03-2699 the whole MIS 13 was a long, relatively stable period of 61 ka

(539.3 to 478.4 ka) with average SST values around 16.5ºC. These diverse time spans defined by the periods of SST warmth are roughly consistent with the intervals of low $\delta^{18}O$ benthic values that characterized the interglacials.

However, in the last two interglacial periods studied in MD03-2699 SST tend to exhibit rapid warm values at the onset of the isotope changes while the $\delta^{18}O$ benthic stack tend to arrive to the lowest isotope values some ka after the system is already in interglacial conditions. Thus, in MIS 9.3 SST increased abruptly from 13ºC at 339.7 ka to 19.2ºC (close to the maximum value for the interglacial) at 336.3 ka whereas the benthic $\delta^{18}O$ stack changed from 4.8‰ at 339 ka to 3.6‰ (close to maximum for the interglacial) at 331 ka (Fig. 2). A similar case is observed at the onset of MIS 11 in which SST changed from 8ºC to 17.7ºC in 4.2 ka (430 ka – 425.8 ka) whereas the $\delta^{18}O$ benthic stack changed from 5.3‰ to 3.5‰ in 19 ka (429 ka - 419 ka). In contrast, in MIS 13 the onset is represented by an SST change from 14ºC to 16.2ºC in 5.1 ka (536.5 ka – 531.4 ka) and the $\delta^{18}O$ benthic stack changed from 4.9‰ to 4.28‰ in 5 ka (536 ka – 531 ka) showing much higher synchrony between the two records.

MIS13 exhibited a general warming trend from 14.7ºC at 536.7 ka to 16.6ºC at 483.2 ka that was punctuated by maxima of 17.6ºC at 506.4 ka and 17.8ºC at 490.8 ka.

5.1.2. Abrupt variability

Millennial scale variability is often represented in the SST record in the form of high amplitude changes. These are more frequent in the glacial periods, e.g. MIS 14, MIS 12 and MIS 10, in which cooling-warming events of 4-7ºC are observed.

The base of MD03-2699 is characterised by a transition between MIS 15.1 to MIS 14 that is marked by an abrupt SST cooling episode (from 16ºC to 12.45ºC in 3.4 ka; 567.1 ka - 563.6 ka) that is similar to others observed during younger glacial inceptions. After this extreme cooling, SST increased until 16.7ºC in 2 ka and then dropped to 13.8ºC between 560.2 ka to 553 ka. At 548.9 ka SST increased again from 14ºC to 15ºC in 2 ka and then declined to 14ºC at the glacial maximum of MIS 14.

The deglacial SST rise to 16.6ºC (531.1 ka) at the beginning of MIS 13.3 started at 539.7 ka and was shortly followed by an abrupt SST drop of 0.9ºC at 528.5 ka before recovering to warm values. The overall glacial/interglacial transition involved an increase of 3.5ºC. Then, the transition to MIS 12 was recorded as an initial SST drop from 16.6ºC at 483.2 ka to 13.7ºC at 477.7 followed by an abrupt drop to 10.1ºC at 474.5 ka (in a time interval of 3 ka) and recover to warm values, 15.0ºC, at 470.6 ka (time interval 3.9 ka).

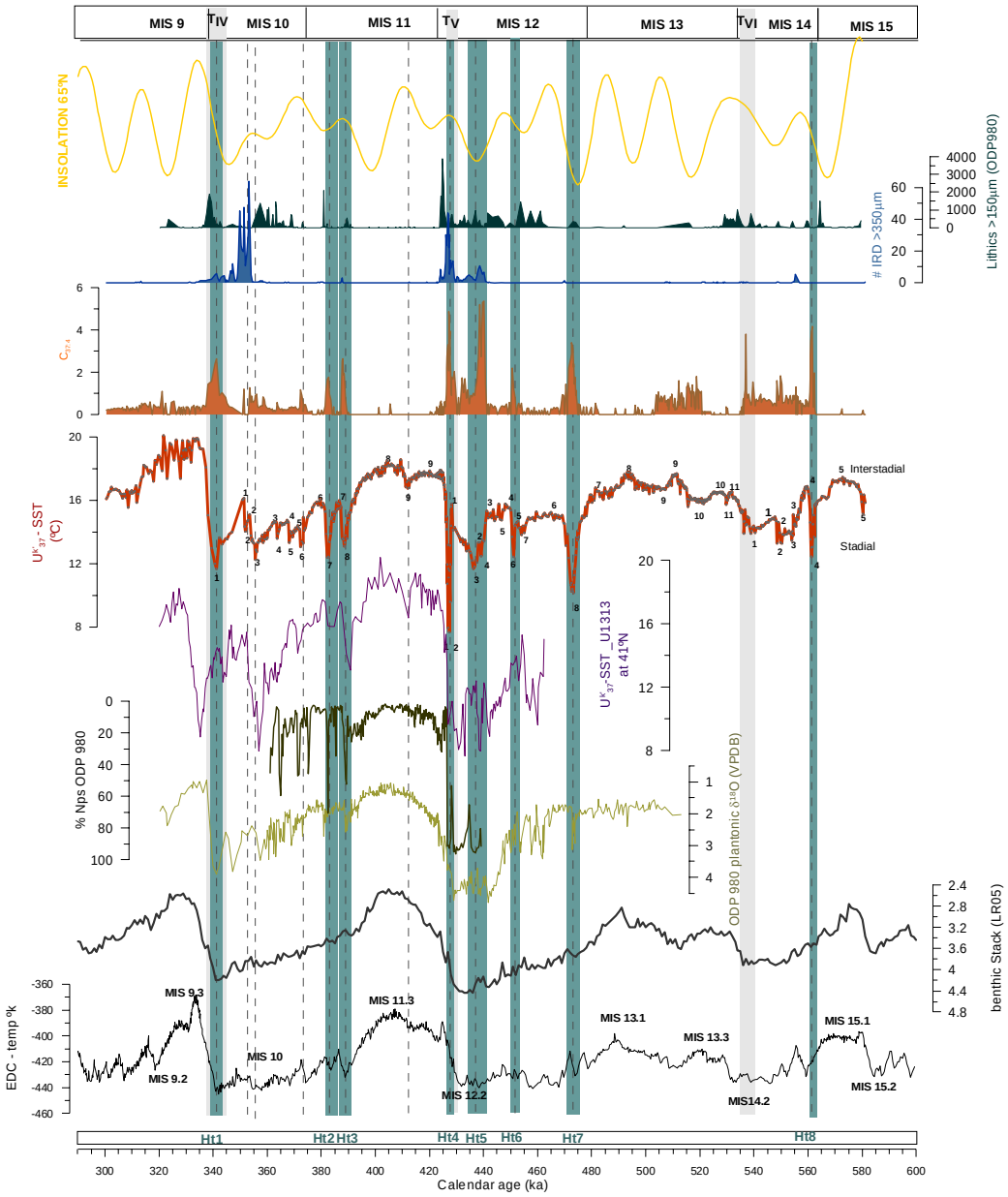

Figure 2: Comparison of SST, $C_{37:4}$ and lithics content in MD03-2699 with other temperature records from the north Atlantic. Temperature (ºK) of the ice core EPICA dome C [*Jouzel, et al.*, 2007]. Benthic $\delta^{18}O$ LR04 stack [*Lisiecki and Raymo*, 2005]. Alkenone–based SST values of core IODP U1313 were reported by Stein, et al. [2009]. Percentage of polar planktic foraminifera (*N. pachyderma* s.) were described by ODP 980 [*Oppo, et al.*, 1998]. ODP 980 planktonic $\delta^{18}O$ (VPDB) was compiled by *McManus, et al.* [1999]. $\%C_{37:4}$ MD03 2699 have been generated in the present study. Ice-rafted detritus (IRD) of core MS03-2699 is reported in *Voelker et al.* [2009]. Ice-rafted detritus (IRD) of core ODP 980 is described in *McManus et al.* [1999]. Daily Insolation at 37ºN during the summer solstice was calculated by *Berger* [1978]. The dash lines mark the abrupt SST decreases; the grey bars mark the terminations and the blue bands the Heinrich-type ice-rafting events.

The first warming phase of MIS 12 (470.6 ka – 450 ka) was characterised by SST values of about 15ºC and was interrupted by a cooling episode of 12.4ºC at 459 ka that lasted 2.3 ka. Then, there was a gradual SST decay to MIS 12 glacial maximum, 11.7ºC at 444.2 ka. SST did not stay cold during the whole glacial maximum period but began to rise at 444.7 ka until 435.8 ka when it reached 15.8ºC. Then, it dropped abruptly to 7.7ºC (the coldest values recorded in the studied section of the core) at 432.1 ka (in a time interval of 3.7 ka). Subsequently, it increased to 11.6ºC at 431.6 ka and it dropped back to 7.9ºC at 430 ka. The glacial to interglacial termination involved an increase from this last SST to 17.4ºC (at 426.4 ka; MIS 11.3) in 3.6 ka.

The period between 427.3 ka to 394.2 ka includes interglacial MIS 11.3, a long warm period with SST between 17.5-18.5ºC. In close-up, this interglacial was actually subdivided into three intervals: a first SST plateau (427.3 – 413.3 ka) with mean SST values of 17.5ºC and a second period of uniform SST (from 411.1 to 394.2 ka) with average values of 18°C that were separated by a rapid cold episode at 412.4 ka where SST dropped down to 16.8ºC. MIS 11 is also characterized by a SST drop from16.5ºC at 394.2 ka to 13.3ºC at 390 ka followed by a rapid increase back to 16.0ºC at 387.7 ka. This warm period, MIS 11.2, lasted 2.3 ka and involved a moderate cooling to 1ºC until 385.4 ka (15ºC). This episode ended in a strong SST drop of 12.4ºC at 383 ka (in a time interval of 2.4 ka) followed by a strong increase back to 15.7ºC at 381.1 ka (in a time interval of 1.9 ka). This warm period, MIS 11.1, lasted 8.4 ka and involved a moderate cooling to 14.9ºC. The period ended with a SST drop to 13ºC at 371.7 ka followed by a subsequent rise to 14.2ºC at 371.4 ka.

The initial MIS 10 is characterized by a period of 12.3 ka with SST around 14ºC with variations of about 0.3-1ºC (373 ka – 356 ka; Fig.2). Then, there is a SST increase up to 16.1ºC at 352.5 ka and a drop to 11.7ºC to glacial maximum at 341.6 ka. The transition to MIS 9 involved a SST increase to 19.23ºC at 336.3 ka (in a time period of 5.3 ka).

MIS 9.3 is the warmest period observed in the studied interval of MD03-2699 core. This interglacial lasted about 16 ka and is characterised by SST values of about 19ºC. The last 12 ka (332 to 320 ka) were marked by rapid SST oscillations of 2ºC. MIS 9.2 is marked by a drop from 18.5ºC to 17ºC between 318.3 ka and 315.7 ka and then a uniform period of

16.2ºC along 10 ka. During this MIS, SST shows, in general, a decreasing trend to 16ºC at the end of MIS 9, with the major drop of 2ºC between 318.3 ka and 315.7 ka.

5.2. Advection of subpolar water masses and ice rafted detritus

$\%C_{37:4}$ show maximum values during the coldest SST events (Fig. 2). That is, terminations IV, V and VI and the abrupt coolings. The highest $\%C_{37:4}$ values are found during MIS 12 which is the coldest glacial period of the studied series. Episodes of high $\%C_{37:4}$ are also observed in MIS 14 and in the two cooling events of MIS 11. In the warm periods of the interglacial MIS the concentrations of $C_{37:4}$ were negligible except in a long section of MIS 13 (517 ka – 498.6 ka) in which this alkenone was found in relative proportions of 0.3-1%. According to these results, the coldest SST occurred simultaneously to arrival of subpolar waters to the site of core MD03-2699. This strong correspondence between SST minima and arrival of subpolar waters has also been observed in more recent MIS of the Iberian Margin [*Martrat et al.*, 2007] and the Alboran Sea [*Cacho et al.*, 1999; *Martrat et al.*, 2007].

The counts of IRD > 350 μm are high in MIS 12, mostly at termination V, where they are roughly in agreement with the events of abundant $\%C_{37:4}$ (Fig. 2). They are also high in MIS 10 but in this case they do not parallel $\%C_{37:4}$ increases. Several episodes of high $\%C_{37:4}$ do not have concurrent IRD increments.

One of the events of highest IRD > 350 μm counts occurred at termination V and was concurrent with the strong SST drop and increase observed in this episode as well as the increase in $\%C_{37:4}$ (Fig. 3). All these features are consistent with a strong pulse of subpolar waters arriving to MD03-2699 site at this termination. In contrast, Terminations IV and VI did not record IRD increases. As mentioned above, Termination VI only involved a moderate SST rise because MIS 15 was already in rather mild conditions. Termination IV is recorded by strong SST together with a significant change in $\%C_{37:4}$ (Fig. 3) which again indicates arrival and retrieval of subpolar waters in this episode.

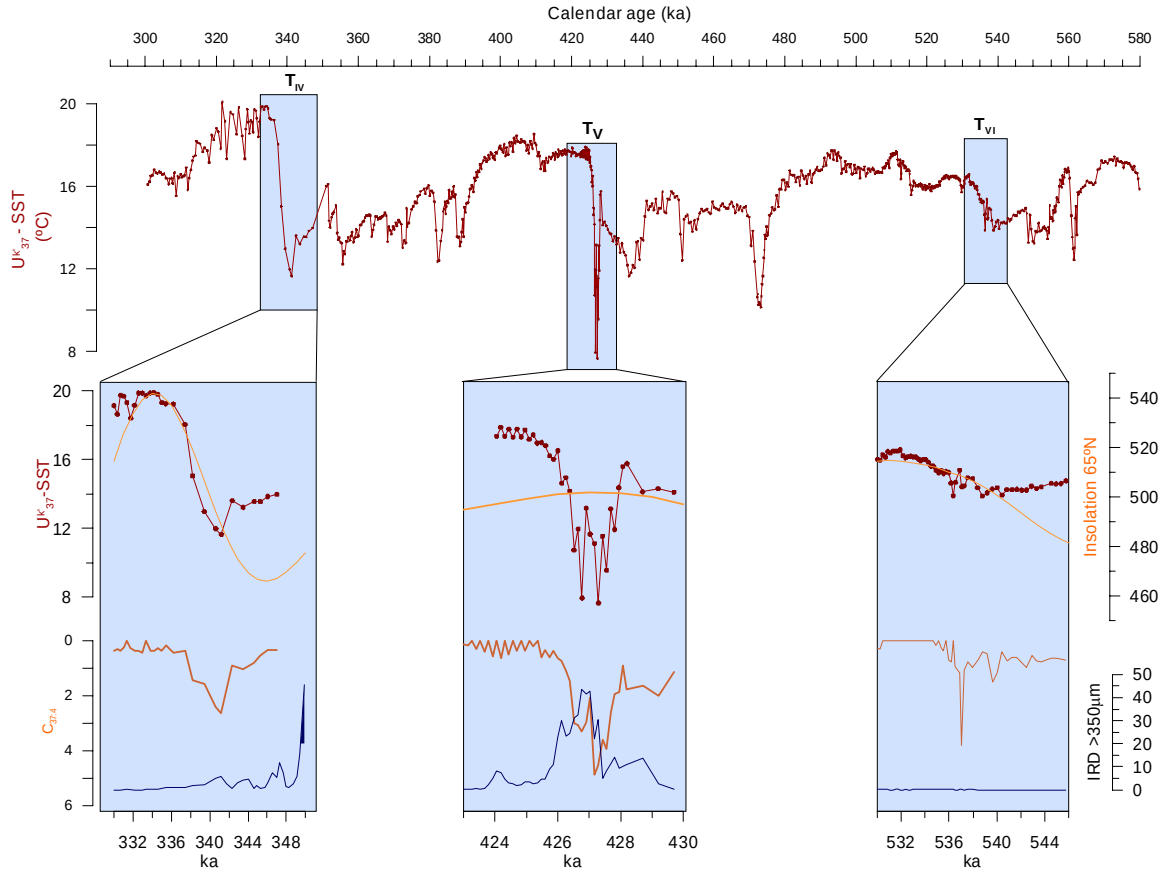

Figure 3: Close-ups of SST terminations IV, V and VI in core MD03 2699 showing $U^{k'}_{37}$-SST, $\%C_{37:4}$ (reverse scale) and abundance of ice-rafted detritus (IRD).

5.3. Variations in concentrations of terrigenous and marine biomarkers and organic carbon

In the MD03-2699 record the two high-resolution terrigenous biomarker records (Fig.4) reveal the same variability between *n*-alkanes and *n*-akane-1-ols, with a coefficient of correlation about 0.77. These proxies exhibit highest concentrations in MIS 10 but they are also in high abundances in the initial periods of MIS 13, 11 and 9. Concentrations of total C_{37} alkenones and TOC also exhibit a general good agreement. These two proxies are often used as markers of marine productivity. C_{37} alkenones exhibit a stronger variability that is also well correlated with the changes of terrigenous biomarkers. TOC exhibits less variability than C_{37} alkenones with a higher background that probably reflects inespecific organic matter residues. The coefficients of correlation between total C_{37} alkenones and *n*-

alkane-1-ols and n-alkanes are 0.79 and 0.66, respectively. In general, the higher concentrations of organic biomarkers (close to 2500 ng/g for C_{37} alkenones and for *n*-akane-1-ols and 1200 ng/g for *n*-alkanes) are recorded in MIS 10 and during the first warm episodes that followed the terminations (Fig. 4).

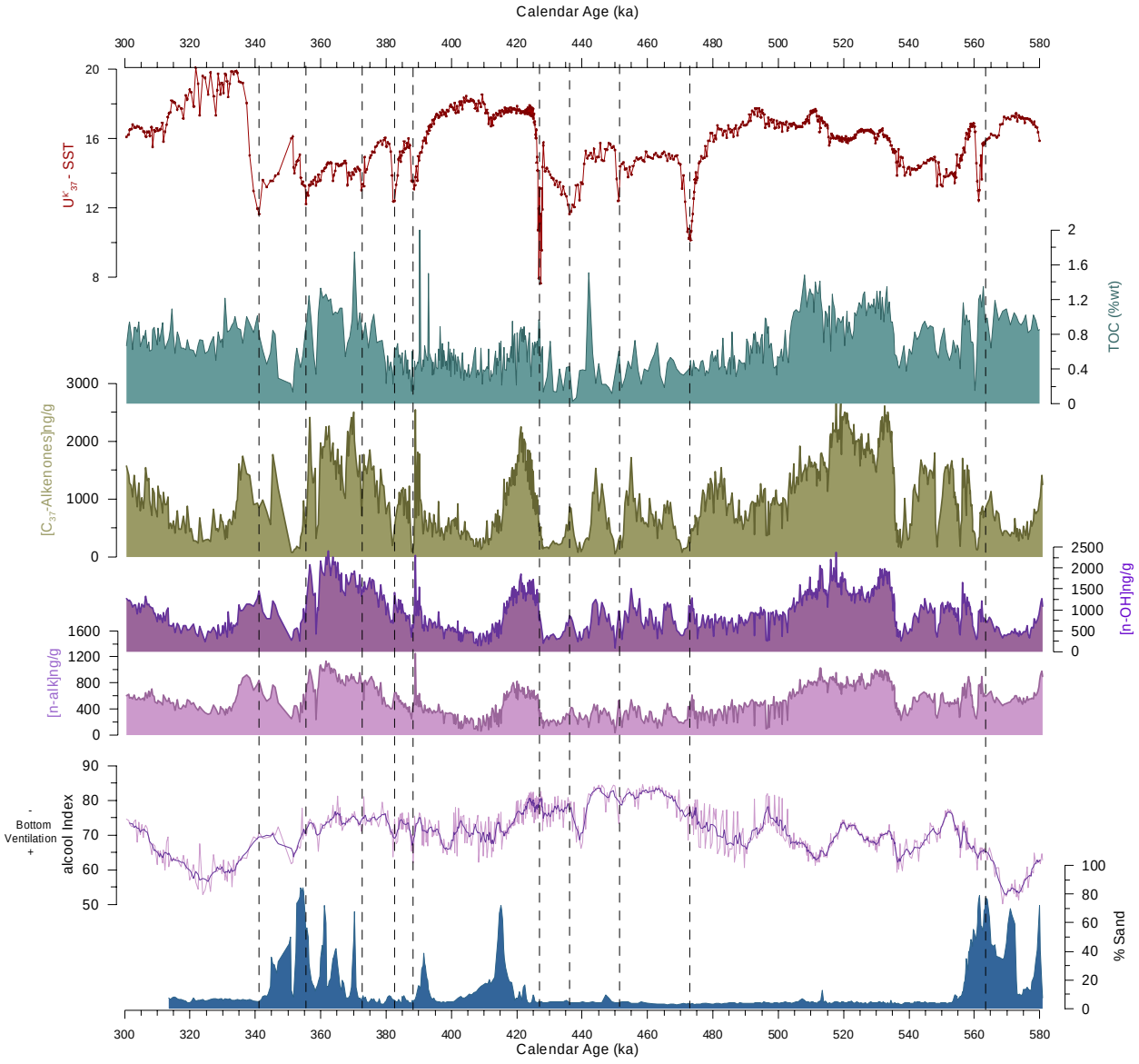

Figure 4: Biomarker concentration and grain size analyse of the core MD03-2699. From the bottom to the top: % sand; alcohol Index; Concentration of total *n*-alkanes; concentration of total *n*-alkane-1ol (ng/g) ; total alkenone concentration (ng/g); % Wt of total organic carbon and Alkenone-based SST.

In general, there is no correspondence between changes in these proxies and the variability of the n-hexacosan-1-ol index (Fig. 4) indicating that the observed variations in the markers of terrigenous and marine inputs are not related to changes in bottom preservation conditions. The periods of longest high values of both terrigenous and marine productivity proxies ocurred at MIS 13 and 10, encompassing interglacial and glacial stages, respectively.

Abrupt variability is also recorded in the profiles of C37 alkenones, n-alkan-1-ols and n-alkanes. SST drops are generally coincident with rapid concentration decreases of these proxies.

6. DISCUSSION

6.1. Rapid Climate Changes and Surface Water Mass variability

Compilation of a general SST record using the Iberian Margin data from cores MD01-2443 [*Martrat et al.*, 2007] and MD03-2699 (this study) shows a good agreement between the two records (Fig. 5). The temperature profile of the Holocene matches the same values in both records and in the common section between 300 ka and 420 ka. SST from these two records exhibit a good agreement in both the general profile and the abrupt variability that shows about the same episodes (but higher intensity in MD01-2443).

The spliced SST-$U^{k'}_{37}$ profile confirms previous observations [*Martrat et al.*, 2004; 2007] showing that each climatic cycle was different during the last 570 ka. Glacial MIS 14 had temperatures around 14ºC and was warmer than any of the later glacials (Fig. 2). This difference is consistent with evidences for lesser glacial conditions in other studied areas such as the southeast Atlantic Ocean [*Chen et al.*, 2002], the North Atlantic (ODP site 982 [*Wright and Flower*, 2002]), the eastern equatorial Pacific (ODP site 849 [*Mix et al.*, 1995]), the subtropical North Atlantic (ODP site 1058 [*Billups et al.*, 2006] and offshore northwest Africa (ODP site 658 [*Eglinton et al.*, 1992]). In turn, the glacial ice temperatures observed in EPICA during this period were also milder than those recorded in the more recent glacials (Fig. 2). Overall, the agreement of these MD03-2699 results with the ice

core data and the SST measurements from other marine sites identifies that the glacial period corresponding to MIS 14 was milder, on a planetary scale, than those occurring at more recent dates. On the other hand, MD03-2699 records evidence a common general trend of warm and relative stable interglacial periods in contrast to high-frequency variability during the glacial inceptions and glacials.

The MD03-2699 records cover the interglacial periods of MIS 9.3, MIS 11.3 and MIS 13.3 and 13.1. SST during interglacial MIS 9.3 was warmer than during the present interglacial (Fig. 2). This is in agreement with other records from the Iberian margin [*Desprat et al.*, 2007a; *Martrat et al.*, 2007] and with the temperatures in the EPICA ice core record [*Jouzel et al.*, 2007]. Our SST profile, however, highlights that the interglacials prior to MIS 9.3 lasted longer and had more stable mean annual surface temperatures.

The warmest phase of MIS 11, MIS 11.3, lasted 30 ka and is synchronous with the major forest expansion episodes documented for the northestern Iberian Peninsula [*Desprat et al.*, 2005; 2007b]. During this interval maximum SST of 18ºC is recorded. The uniform profile interrupted by a short cooling event (1ºC) around 412 ka (Fig. 2). A similar pattern was registered in core MD01-2443, south of MD03-2699, and at the mid-latitude North Atlantic IODP site U1313 (Fig. 2) where the minimum between the two plateaus within MIS 11.3 occurred at 413 ka and was more pronounced which is probably linked to more variable condition in the western North Atlantic and admixture of subpolar surface waters at that time [*Stein et al.*, 2009; *Voelker et al.*, 2009]. On the other hand, IODP site U1313 shows a temperature maximum of 19ºC during MIS11.3 which is related to a stronger influence of the Gulf Stream /North Atlantic Drift at the site.

The composed Iberian SST records for the last 6th climate cycles (Fig. 5) show that the warmer interglacials were MIS 5.5 (Eemian) with 21ºC, followed by MIS 9.3 (20ºC) and MIS 7.5 (19ºC). The maximum temperatures during MIS 11.3 (18ºC) were similar to those reconstructed for the Holocene.

6.2. Climate cyclicity

Orbital parameters, atmospheric greenhouse gas concentrations and ice-sheet dynamics changed along the studied time period [*Berger*, 1978; *Delmotte et al.*, 2004; *Luthi et al.*, 2008; *Siegenthaler et al.*, 2005]. Comparison with the SST profile in MD03-2699 shows influence of all three orbital cycles, e.g. obliquity, eccentricity and precession (Table 1). Virtual comparison of the SST curve and these orbital cycles does not allow to identifying a specific time period of change from dominance of obliquity to eccentricity/precession (Fig. 5). Calculation of the cross-correlation curves between SST and these orbital cyclicities for several time intervals is useful for this purpose. They have been performed for the time periods encompassing MIS 15-9, MIS 14-9, MIS 13-9, MIS 12-9 and MIS 11-9. As shown in Table 1, the latter is the one in which the significance of eccentricity is higher than obliquity. The boundary between MIS 12 and 11 is approximately located at 430 ka. That is, the estimated Mid-Brunhes time.

The record of SST in MIS 11 shows warmer temperatures than those of the previous interglacial (MIS 13; Fig. 2). In contrast, the interglacials that followed MIS 11, MIS 9, MIS 7 and MIS 5 exhibit higher SST than MIS 11. A similar pattern is observed in EPICA temperatures in which the interglacial periods equivalent to MIS 11, MIS 9, MIS 7 and MIS 5 are warmer than those equivalent to MIS 13 and 15 (EPICA, 2004). In this case, the temperatures of the glacial periods are also warmer before 430 ka than after this event. There seems to be an amplitude increase after the mid-Brunhes that, in the context of MD03-2699 core, is reflected in warmer SST in the interglacial MIS.

However, the transition between dominance of obliquity and eccentricity has not always been observed to occur at 430 ka. In a SST study in the southeastern subtropical Pacific [*Calvo et al.*, 2001] the change from obliquity to eccentricity dominance was observed at 320 ka. Moreover, despite dominance of the eccentricity period in SST from MD03-2699 after 430 ka the warming of Termination IV closely matches obliquity (Fig. 5). Both this study and the Pacific Ocean results reported in *Calvo et al.* [2001] show that deglaciation in Termination I was following the obliquity change. These results are consistent with the recent studies of *Drysdale et al.*, [2009] on speleothems from Antro del

Corchia cave (Italy) in which a dependence of Termination I and II from obliquity was observed.

Table 1. Cross-correlation of the main records determined in MD03-2699 and orbital cyclicities.

	period	**significance**	**phase**
SST	100	0.72	-15
MIS 9-15	41	0.85	-36
	20	0.58	148
SST	100	0.74	25
MIS 9-14	41	0.81	-36
	19	0.74	150
SST	100	0.71	23
MIS 9-13	41	0.82	-29
	19	0.53	151
SST	100	0.66	9.7
MIS 9-12	41	0.71	-31
	21	0.51	111
SST	100	0.75	-9.0
MIS 9-11	42	0.55	-57
	22	0.45	101
Hexacosanol index	100	0.76	-141
MIS 9-15	41	0.59	102
	18	0.69	0
Alkenones	100	0.60	125
MIS 9-15	39	0.43	37
	18	0.49	38
Alkan-1-ols	100	0.64	139
MIS 9-15	42	0.50	53
	18	0.57	-8.9
Alkanes	100	0.67	115
MIS 9-15	42	0.48	28
	17	0.54	-60

Other proxies studied in MD03-2699 also reflect contributions from all three orbital cycles although at a lower degree of significance (Table 1). The n-hexacosan-1-ol index show a higher dominance of eccentricity in all time sections selected for study (Table 1). This feature is somewhat in contrast with the above described change of predominant orbital cyclicities in the studied SST record of the core.

In any case, MIS 13 is characterized by relatively low $\delta^{18}O$ values indicating a lower sea level than during the subsequent interglacials [*Hodel, et al.*, 2003; *Lisiecki and Raymo*, 2005] and a maximum in surface and deep ocean $\delta^{13}C$ levels. This low sea level is consistent with cool Antarctic temperatures [*Jouzel et al.*, 2007], low CO_2 and CH_4 concentrations [*Luethi, et al.* 2008; *Siegenthaler et al.*, 2005], and low summer SST in the South Atlantic [*McClymont et al.*, 2005]. They coincided with extremely strong Asian, Indian and African summer monsoons, weakest Asian winter monsoon and lowest Asian dust and iron fluxes [*Guo et al.*, 2009]. Pervasive warm conditions were evidenced by the records from the Asian monsoon zone [*Yin and Guo*, 2007] and northern high-latitude regions [de *Vernal and Hillaire-Marcel*, 2008]. Accordingly, *Guo et al.* [2009] proposed a strong asymmetry of hemispheric climates during MIS 13 with a warmer northern hemisphere and a cooler southern hemisphere. Nevertheless, our record in the Iberian margin shows a MIS 13 cooler than the subsequent interglacials which is against this recent consideration (Fig. 2 and Fig.5).

6.3. Abrupt variability

Several short-lived abrupt climatic changes have been identified in the SST record of MD03-2699. These oscillations were superimposed to the glacial-interglacial changes between MIS 15.1 and MIS 14, MIS 13.1 and MIS 12 and MIS 11.3 and MIS 10 (Fig. 5). Some of these oscillations involved extreme coolings and occurred concurrently with increases of $C_{37:4}$ indicating the arrival of subpolar waters to the site [*Bard, et al.*, 2000; *Cacho, et al.*, 2001; *Rosell-Melé, et al.*, 1998; *Villanueva, et al.*, 1998]. As shown in studies encompassing the last climatic cycle in the Portuguese Margin, [*Abreu, et al.*, 2003; *Bard,*

et al., 2000; *Eynaud, et al.*, 2009; *Martrat, et al.*, 2007; *Naughton, et al.*, 2009; *Pailler and Bard*, 2002; *Voelker, et al.*, 2006] the presence of low-salinity surface waters is linked in particular to the Heinrich events (H). These events are marked by very cold conditions over the eastern side of the Atlantic and adjacent landmasses. Before the onset of Heinrich events the thermal front, which represents the zone of strongest temperature gradient between relatively warm temperatures to the south and cold temperatures to the north, was probably situated in the northern limit of the IRD belt near 50ºN [*Cortijo, et al.*, 2000]. After being released by the Northern Hemisphere ice sheets, icebergs migrated southward during the Heirinch event and maxima of IRD deposition occurred between 40 and 50°N in the central North Atlantic. Melting icebergs generated a substantial drop of sea-surface temperatures in the North Atlantic region [*Cortijo, et al.*, 1997; *Hemming*, 2004] favoring the southward displacement of the polar front down to the mid-latitudes of the North Atlantic. SST cooling affected the North Atlantic as far south as the southern Azores and the Iberian margin [*Eynaud, et al.*, 2009; *Lopez-Martínez, et al.*, 2006; *Naughton, et al.*, 2009; *Voelker, et al.*, 2006].

These cold events are in phase with increases in % $C_{37:4}$ and often concurrent with the presence of IRD grains. For this reason, they are identified as Heinrich-type (Ht) episodes (Ht 1 to 8 in Fig. 2). Ht4, one of the most pronounced events in our record, occurred along with termination V, Ht5 during MIS 12.2 and Ht1 during MIS 10.2, i.e. glacial maxima. Other abrupt coolings were observed during the glacial inceptions of MIS 15.1 (Ht8), MIS 13 (Ht6, Ht7) and MIS 11 (Ht2, Ht3 during MIS 11.24). Similar events were identified in the record of IODP site U1313 based on the dolomite contents [*Stein, et al.*, 2009]. Two of the Ht episodes, Ht2 and Ht3, were coincident with two IRD peaks in ODP site 980 (IRD <150 μm) but were not recorded in the middle north Atlantic site IODP U1313 indicating that subpolar water excursions were not uniformly spread in this ocean during glacial periods. On the other hand, the Heinrich-type event during MIS 10.4 that is prominently recorded in the dolomite record of IODP site U1313 [*Stein, et al.*, 2009] had no major impact on SST at the Estremadura site.

The most prominent SST minima of 8ºC and 12ºC and % $C_{37:4}$ maxima are observed during Ht4 and Ht1 at 427 and 341 ka, respectively and during Ht7 at 473.5 ka (10ºC). The close-up of Ht4 (Fig. 3) shows that this episode was composed of three phases: two

coolings and an intermediate small warming. During these cooling phases the polar front migrated south so that arctic surface waters reached the Estremadura site, but maximum IRD deposition only occurred in the second cooling phase which indicates that these latitudinal displacements could occur or not together with significant ice melting. This type of complexity has also been observed in several other sites in the Iberian Margin in the last deglaciation [*Martrat, et al.*, 2007; *Naughton, et al.*, 2009; *Rodrigues, et al.*, in press; *Rodrigues, et al.*, submitted; *Voelker, et al.*, 2006]. Thus, during this episode a first cold phase coincided with H1, the second with the Younger Dryas and there was the Boelling-Allerød in between. Accordingly, abrupt shifts in the position of the polar front during deglaciations were common and they can be traced back at least to termination V.

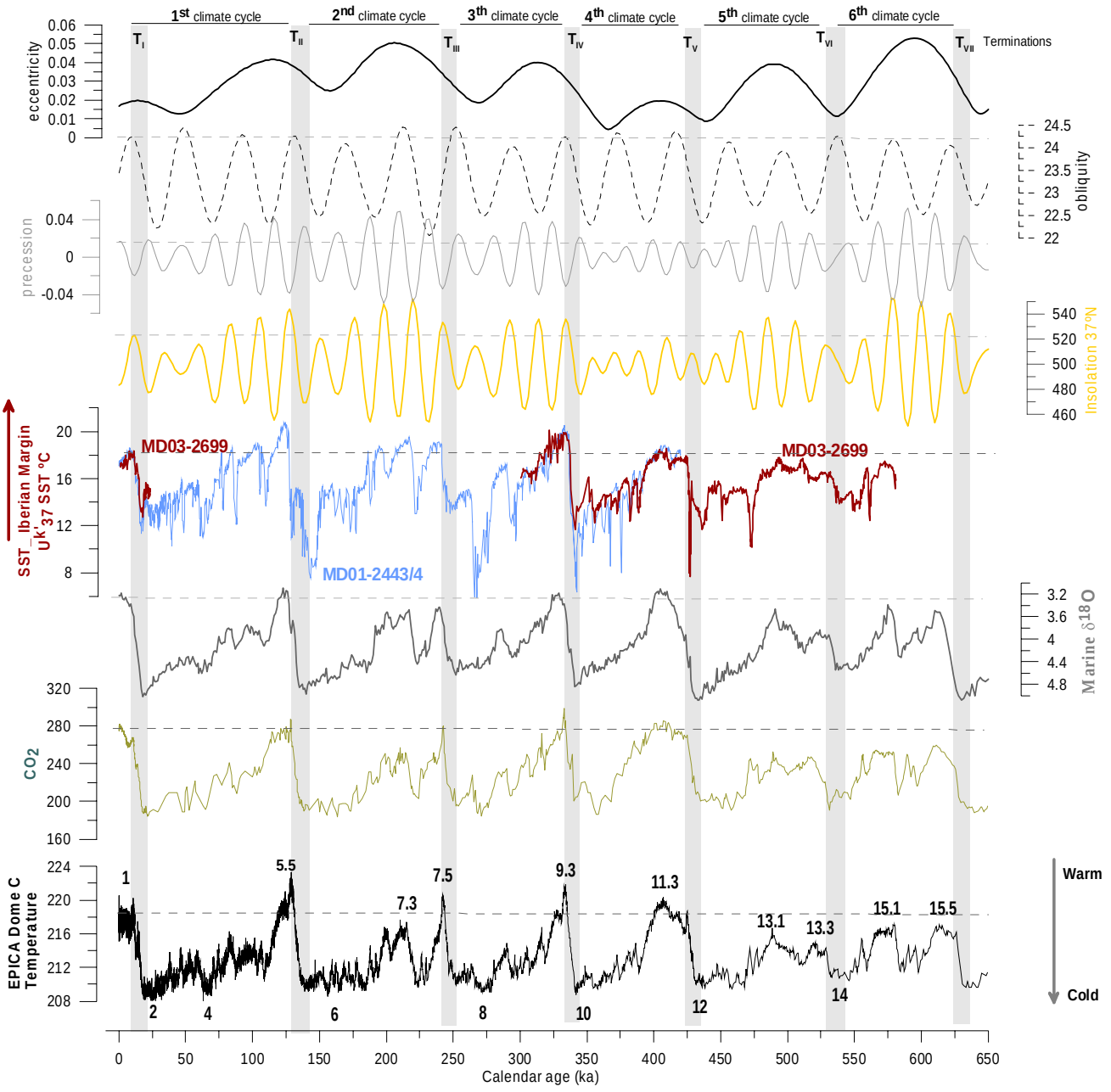

Figure 5: Comparison of the Iberian Margin Sea Surface record of the last 570 ky with other paleoarchives over the last six climate cycles. From bottom to top: Temperature (ºK) from the ice core EPICA dome C [*Jouzel, et al.*, 2007]. CO_2 concentration in EPICA dome C ice[*Luthi, et al*, 2008]. Benthic $\delta^{18}O$ LR04 stack [*Lisiecki and Raymo*, 2005]. Composite of the alkenone-based SST values in cores MD01-2443 and MD01-2444 (420-0 ka) [*Martrat, et al.*, 2007] and core MD03-2699 (21-0 ka and 570-300 ka), this study. Daily insolation at 37ºN during the summer solstice, precession, obliquity and the eccentricity of the Earth's orbit [*Berger*, 1978]. The grey band marks the terminations and the dash horizontal lines show the mean values of the Holocene.

Ht8 occurred at 559 ka right at the beginning of MIS 14, which is somewhat similar to Ht6 at the beginning of MIS 12 (Fig. 2). During Ht8 SST decreased abruptly by 5ºC reaching values colder than during glacial MIS 14. This abrupt cooling occurred together with high percentages of $C_{37:4}$ indicating again a southern displacement of polar waters during this episode.

Within their chronological constraints, Ht events 1, 2, 3, 6, 7 and 8 in MD03-2699 seem to have their counterparts in the EPICA δD record (Fig. 2, 5). The significance of the temporal concurrence of these events remains to be investigated. Better age models and identification of abrupt SST episodes in other ocean sites will help to assess the climate relevance of these concurrent episodes.

6.4. Eolian inputs and productivity

Imprints of the cooling events are also observed in the records of total alkenone concentrations and the continental biomarkers (Fig. 4). Alkenone concentrations and, to some extent, TOC currently reflect changes in productivity [*Villanueva et al.*, 1998b; 2001] whereas changes in n-alkan-1-ols and n-alkanes reflect variations in wind inputs [*Lopez-Martinez et al.*, 2006]. Overall, alkenone, n-alkan-1-ol and n-alkane profiles show similar trends indicating that strong winds also increased biogenic productivity at the site. In general, both continental and productivity biomarkers increased at the deglaciations and reached high values at the beginning of the warm periods showing a strong drop after these increments.

Strong drops in productivity are also observed during the Ht which likely correspond to decreases due to the arrival of cold subpolar waters. This reduction in productivity also agrees with reconstructions in the open North Atlantic and the Norwegian sea during these episodes [*Nave, et al.*, 2007]. During these events the concentrations of terrigenous biomarkers were also lower which in this case may likely reflect a reduction of temperate and humid forests [*Desprat, et al.*, 2007b; *Abreu, et al.*, 2005; *Tzedakis, et al.*, 2004].

The pattern of the terrigenous biomarkers during MIS 11 with maxima during the early phase is similar to the dust record off north-western Africa, ODP site 958 [*Helmke, et al.*, 2008]. Thus the strengthening of the trade winds over northwestern Africa occurred synchronously with the increase in terrestrial input on the western Iberian margin suggesting also a strenghtening of easterly winds in that region. Strong easterly winds induce upwelling leading to increased productivity as reflected by the higher concentration of total alkenones during the early phase of MIS 11.3 when the sea level was still rising. The total biomarker concentration started to decline with the onset of the humid period in Africa, that is before ending of the first SST plateau which indicates that the shift in atmospheric circulation over Africa also impacted Iberia.

In general terms MIS 11.3 and MIS 9.3 show similar conditions, but the major difference concerns the ventilation of the surface to subsurface water masses and their impact on the meridional overturning circulation [*Voelker, et al.*, 2009]. This difference is corroborated by MD03-2699's SST and the biomarker signals during MIS 9.3 when productivity decreased earlier than in the previous interglacials. In this episode the hexacosanol index is accompanied by a heavier values of $\delta^{13}C$ (Fig. 4), an index reflecting oxygenation associated to bottom current intensity, shows lower values indicating the presence of less ventilated bottom waters. In detail, the MIS 9.3 SST record reveals a warmer interval at the beginning of the interglacial (335 to 332.5 ka) with temperatures close to 20ºC, i.e. 2ºC warmer than during MIS 11.3, followed by a decreasing trend associated with millennial-scale variability of 2ºC in amplitude during the second half until 320.4 ka, prior to onset of the next glacial inception starting with stadial MIS 9.2 (around 322 ka). The productivity increase is contemporary with maxima in the terrigenous markers suggesting, like during early MIS 11.3, stronger winds (Fig. 4). The productivity patterns observed in core MD03-2699 differ from those recorded at IODP site U1313 where productivity during the interglacials was minimal and high during the glacial periods [*Stein, et al.*, 2009]. This difference highlights the different responses of open ocean productivity (U1313) and upwelling-related productivity (MD03-2699) to the respective climate forcing.

6.5. Holocene versus MIS 11.3

The orbital parameters of MIS 11.3 and the present interglacial, the Holocene, are rather similar (Fig. 5). Eccentricity was at a minimum during MIS 11 and the Holocene. The insolation at 65ºN and precession were similar as well. Sea level reconstructions based on benthic $\delta^{18}O$ values suggest that sea level 410 ka ago was at a level similar to the last 10 ka including the present days. The alkenone-based SST also show that climate conditions during MIS 11.3 were not significantly different from those measured during the elapsed portion of the Holocene.

Holocene maximum SST values close to 19ºC occurred between 10.5 and 9.7 ka [*Rodrigues et al.*, 2009] while the MIS 11.3 record reveals two warmer phases, the first with maximum SST close to 18ºC (427 to 412 ka) and a second with temperatures close to 19ºC (407 to 395 ka). Both periods display a SST decrease following the maximum values that, however, in the case of MIS11, are interrupted by the second SST increase. In both cases, the long-term SST decrease during interglacial conditions is of 1.5ºC at Estremadura site MD03-2699. The results obtained confirm the expected parallelism between the first part of MIS 11 (427 to 412 ka) and the last 10.5 ka. This observed parallelism was a pre-condition for further comparison of these two periods in the assessment of MIS 11 as a possible model for the future Holocene evolution. However, the forthcoming climate conditions of the Holocene remain an open question.

7. CONCLUSIONS

The use of alkenone-based SST, tetra-unsaturated alkenones, IRD, total alkenones, TOC, terrigenous biomarkers and hexacosanol index has allowed the reconstruction of hydrological and climate variability, including productivity and wind conditions, in the western Iberian margin.

The present results extend the existing biomarker record from core MD01-2443 back in time to the 6th climatic cycle (580 ka). The new results for the period from 580 to

300 ka show a general trend of warm and relative stable interglacial periods and high-frequency variability during the glacial inceptions and glacials. Average interglacial SST increases from MIS 13 to MIS 11.3 and MIS 9.3 by 2ºC, respectively. However, periods of interglacial warmth were longer prior to MIS 9 with MIS 13 showing relative stable conditions for about 54 ka, the longest period during the last 580 ka. The interglacial MIS 11.3 (425 to 395.5 ka) was recorded as a long warm period with SST close to 18ºC, but is subdivided into three intervals: a first SST plateau (425 – 414 ka) with mean SST of 17.5ºC, a second one from 410 to 395 ka with average SST of 18°C and an intermediate colder period around 412 ka when SST was around 17ºC.

The warmest interglacial, MIS 9.3, shows a 15.8 ka interval with SST around 19ºC, but the second half of this interglacial, after 329 ka, was marked by a 2ºC amplitude millennial-scale variability.

Cross-correlation of SST and the orbital cycles shows a change of predominant periodicity from obliquity to eccentricity around 430 ka, the time of the mid-Brunhes event. This change is consistent with the observed differences in Antarctica ice temperature (EPICA, 2004). After 430 ka there seems to be an amplitude increase in both cases. However, despite this eccentricity dominance, the warming of Termination IV closely matches obliquity.

Sub-orbital scale SST variability marks the colder periods (glacial inceptions and glacials). The cold episodes during those stadial/interstadial oscillations, in particular during MIS 12 and MIS 10, were associated with increases in $C_{37:4}$ and the presence of IRD grains indicating that these periods are linked to meltwater pulses reaching the Iberian margin. The most pronounced of these events are related to Heinrich-type events. In our record we have identified 8 Heinrich-type events: Ht1 in MIS10.2; Ht2, Ht3 (MIS 11.24) during the glacial inception of MIS 11; Ht4 at the onset of termination V; Ht5 (MIS 12.2); Ht6 and Ht7 at the glacial inception of MIS 12; and Ht8 (MIS 15.1).

The general pattern recorded during the deglaciations are similar to the younger climatic cycles, i.e. two cooling events separated by a warming related to the south- and northward migration of the polar front and the associated expansion and retreat of arctic water masses.

Glacial conditions are marked by low SST, in particular during the glacial maxima as defined by the heavier benthic $\delta^{18}O$ values. Glacial MIS14 shows higher SST values than during the other glacial maxima suggesting a strong influence of the subtropical Azores Current during this period.

Productivity increases were contemporary with maxima in the terrigenous biomarkers implying, in particular during early MIS 11.3, stronger easterly winds which enhanced upwelling. The low values of C_{37} alkenone concentrations recorded during the Heinrich-type events indicate reduced productivity during these periods.

The composed Iberian SST records over the last 6th climate cycles show that SST of the MIS 11.3 is analogous to the present interglacial, the Holocene.

ACKNOWLEDGEMENTS

The Fundação para a Ciência e a Tecnologia (FCT) through the PORTO (PDCT/MAR/58282/2004) and SEDPORT projects (PDCTM/40017/2003), and postdoctoral (SFRH/ BPD/ 21691/2005) and PhD (SFRH/ BP/13749/ 2003) fellowships funded A.V. and T.R.. The Spanish Ministry of Science and Technology (REN2003-08642-C02-01), the Consolider-Ingenio 2100 Project CE-CSD2007-0067 are acknowledged Coring of MD03-2699 was made possible through an European Access to Research Infrastructure grant. The staff of the DGM lab, namely C. Trindade and Dr. C.N. Prabhu to helped with the picking AMS dating samples. Furthermore we thank Filipa Naughton for her valuable suggestions which greatly improved this manuscript.

8. REFERENCES

Abreu, L. d., et al. (2005), Ocean Climate variability in the Eastern North Atlantic during interglacial MIS 11: A partial analogue to the Holocene, *Palaeogeography*, *20*.

Abreu, L. d., et al. (2003), Millennial-scale oceanic climate variability off the Western Iberian margin during the last two glacial periods, *Marine Geology*, *3297*, 1-20.

Ambar, I. (1994), Alguns aspectos da Física do Oceano, 21-34 pp, Fundação Calouste Gulbenkian, Lisbon.

Amore, F. O., et al. (in prep.), Coccolithophore record during the Middle Pleistocene in the North and South Atlantic: Productivity and Dissolution patterns, *Marine Micropalentology in. prep*.

Bard, E., et al. (2000), Hydrological Impact of Heinrich Events in the Subtropical Northeast Atlantic, *Science*, *289*, 1321-1324.

Bauman, K.-H., and T. Freitag (2004), Pleistocene fluctuations in the northern Benguela Current system as revealed by coccolith assemblages, *Marine Micropaleontology*, *52*, 195-215.

Berger, A. L. (1978), Long-Term Variations of Daily Insolation and Quaternary Climatic Changes *Journal of the Atmospheric Sciences*, *35*, 2362-2367.

Billups, K., et al. (2004), Millenial-scale flutuations in subtropical northwestern Atlantic surface ocean hydrography during the mid-Pleistocene, *Palaeogeography*, *19*.

Billups, K., et al. (2006), Mid Pleistocene climate instability in the subtropical nortwertern Atlantic, *Global and planetary change*.

Bond, G. C., and R. Lotti (1995), Iceberg Discharges into the North Atlantic on Millennial Time Scales During the Last Glaciation, *Science*, *267*, 1005-1010.

Bowen, D. Q. (2009), Sea level 400 000 years ago (MIS 11): analogue for present and future sea-level, *Clim. Past Discuss.*, *5*, 1853-1882.

Cacho, I., et al. (2001), Variability of the Western Mediterranean Sea Surface Temperature during the last 25,000 years and its connection with the Northern hemisphere climatic changes, *Paleoceanography*, *16*, 40-52.

Chen, M.-T., et al. (2002), Late Quaternary sea-surface temperature variations in the southeast Atlantic: a planktic foraminifer faunal record of the past 600 000 yr (IMAGES II MD962085), *Marine Geology*, *180*, 163-181.

Cortijo, E., et al. (2000), Rapid climatic variability of the North Atlantic Ocean and global climate: a focus of the IMAGES program., *Quaternary Science Reviews*, *19*, 227-241.

Cortijo, E., et al. (1997), Changes in sea surface hydrology associated with Heinrich event 4 in the North Atlantic Ocean between 40°N and 60°N, *Earth and Planetary Science Letters*, *146*, 29-45.

Delmotte, M., et al. (2004), Atmospheric methane during the last four glacial-interglacial cycles: Rapid changes and their link with Antarctic temperature, *Journal of Geophysical Research*, *109*.

Desprat, S., et al. (2005), Is vegetation responsible for glacial inception during periods of muted insolation changes?, *Quaternary Science Reviews*.

Desprat, S., et al. (2007a), Climate variability of the last five isotopic interglacials: direct land-sea.ice correlation from the multiproxy analysis of north western Iberian margin deep-sea cores., in *The climate of the past interglacials*, edited by F. Sirocko, et al., Elsevier.

Desprat, S., et al. (2007b), Climate variability of the last five isotopic interglacials: direct land-sea.ice correlation from the multiproxy analysis of north western Iberian margin deep-sea cores., in *The climate of the past interglacials*, edited by F. Sirocko, et al., Elsevier.

Droxler, A. W., and J. W. Farrell (2000), Marine Isotope Stage 11 (MIS 11): new insights for a warm future, *Global and Planetary Change*, *24*, 1-5.

Eglinton, G., et al. (1992), Molecular record of secular sea surface temperature changes on 100-year timescales for glacial terminations I, II and IV *Nature*, *356*.

EPICA, c. m. (2004), Eight glacial cycles from an Antartic ice core, *Nature*, *429*.

Eynaud, F., et al. (2009), Position of the Polar Front along the western Iberian margin during key cold episodes of the last 45 ka, *G-cubed*, *10*.

Fiúza, A., et al. (1982), Climatological space and time variation of the Portuguese coastal upwelling, *Oceanol. Acta*, *5*, 31-40.

Fiúza, A. F. G. (1983), Upwelling patterns off Portugal, edited, pp. 85-98.

Flores, J. A., et al. (2003), Calcareous planton dissolution pattern and coccolithophore assemblages during the last 600 kyr at ODP Site 1089 (cape Basin, South Atlantic): paleoceanographic implications., *Palaeogeography Palaeoclimatology Palaeoecology*, *196*, 409-426.

Flower, B. P., et al. (2000), North Atlantic intermediate to deep water circulation and chemical stratification durinhg the past 1 Myr, *Palaeogeography*, *15*, 388-403.

Grimalt, J. O., et al. (2001), Sea Surface pleotemperature errors in Uk'37 estimation due to alkenone measurements near the limit of detection, *Paleoceanography*, *16*, 226-232.

Guo, Z. T., et al. (2009), Strong asymmetry of hemispheric climates during MIS-13 inferred from correlating China Loess and Antarctica ice records, *Climate of The Past*, *5*, 21-31.

Helmke, J. P., et al. (2008), Uniform climate development between the subtropical and subpolar Northeast Atlantic across marine isotope stage 11, *Climate of The Past*, *4*.

Hemming, S. (2004), Heinrich events: massive late Pleistocene detritus layers of the North Atlantic and their global climate imprint., *Rev. Geophys*, *42*, 1-43.

Hodell, D. A., et al. (2008), Onset of "Hudson Strait" Heinrich events in the eastern North Atlantic at the end of the middle Pleistocene transition (~640 ka)?, *Palaeogeography*, *23*, PA4218.

Hodell, D. A., et al. (2003), Pleistocene vertical carbon isotope and carbonate gradients in the South Atlantic sector of the Southern Ocean, *Geochemistry Geophysics Geosystems*, *4*.

Imbrie, J., et al. (1993), On the Struture and origin of Major Glaciation Cycles 2- The 100,000 Year Cycle, *Paleoceanography*, *8*, 699-735.

Jouzel, J., et al. (2007), Orbital and Millennial Antarctic Climate Variability over the Past 800,000 Years, *Sciencexpress*.

Lisiecki, L. E., and M. E. Raymo (2005), A Pliocene-Pleistocene stack of 57 globally distributed benthic d18O records, *Palaeogeography*, *20*.

Lopez-Martínez, C., et al. (2006), Abrupt wind regime changes in the North Atlantic Ocean during the past 30,000-60,000 years, *Palaeogeography*, *21,* PA4215, doi:10.1029/2006PA001275.

Loulergue, L., et al. (2008), Orbital and Millennial-scale features of atmosferic CH4 over the past 800,000 years, *Nature*, *453*, 383.

Loutre, M. F. (2003), Clues from MIS 11 to predict the future climate a modelling point of view, *Earth and Planetary Science Letters*, *212*, 213-224.

Loutre, M. F., and A. Berger (2003), Marine Isotope Stage 11 as an analogue for the present interglacial, *Global and planetary change*, *762*, 1-9.

Luethi, D., et al. (2008), High-resolution carbon dioxide concentration record 650,000-800,000 years before present, *Nature*, *453*, 379.

Luthi, D., et al. (2008), High-resolution carbon dioxide concentration record 650,000-800,000 years before present, *Nature*, *453*, 379.

Martrat, B., et al. (2007), Four Climate Cycls of Recurring Deep and Surface Water Destabilizations on the Iberian Margin, *Science 317*, 502-507.

Masson-Delmotte, V., et al. (2006), Past temperature reconstructions from deep ice cores: relevance for future climate change, *Climate of The Past*, *2*, 145-165.

McClymont, E. L., et al. (2005), Alkenone and coccolith records of the mid-Pleistocene in the south-east Atlantic: Implications for the Uk'37 Index and South African climate, *Quaternary Science Reviews*, *24*, 1559-1572.

McManus, J., et al. (2003), Marine Isotope Stage 11 (MIS 11): Analog for Holocene and Future Climate?

McManus, J. F., et al. (1999), A 0.5- Million-Year Record of Millennial-Scale Climate Variability in the North Atlantic, *Science*, *283*, 971-975.

Mix, A. C., et al. (1995), Benthic foraminifer stable isotope record from site 849, 0-5Ma: local and global climate changes. , *Proceedings of the Ocean Drilling Program. Scientific Results*, *138*, 371-412.

Moita, M. T. (2001), Estrutura variabilidade e dinâmica do fitoplânton na Costa de Portugal Continental, 272 pp, Facudade de Ciências de Lisboa, Lisboa.

Müller, P., et al. (1998), Calibration of the alkenone index Uk'37 based on core-tops the eastern South Atlantic and global ocean (60ºN-60ºS), *Geochimica et Cosmochimica Acta*, *62*, 1757-1772.

Naughton, F., et al. (2009), Wet to dry climatic trend in north-western Iberia within Heinrich events, *Earth and Planetary Science Letters*.

Nave, S., et al. (2007), Primary productivity response to Heinrich events in the North Atlantic Ocean and Norwegian Sea, *Palaeogeography*, *22*.

Oppo, D. W., et al. (1998), Abrupt Climate Events 500,000 to 340,000 years agoÇ: Evidence from Subpolar North Atlantic Sediments, *Science*, *279*.

Pailler, D., and E. Bard (2002), High frequency paleoceanographic changes during the past 140 000 yr recorded by the organic matter insedimentaf the Iberin Margin, *Paleoceanigrphy, paleoclimatology, Palaeoecology*, *2799*, 1-22.

Peliz, Á., et al. (2005), Winter upper ocean circulation in the Western Iberian basin-Fronts, Eddies and Poleward Flows: an overview, *Deep-Sea Research I*, *52*, 621-646.

Raffi, I., et al. (2006), A review of calcareous nannofossil astrobiochronology encompassing the past 25 million years, *Quaternary Science Reviews*, *25*, 3113-3137.

Rodrigues, T., et al. (in press), Interdependences of changes in sea surface temperature, productivity and fluvial inputs in the continental shelf of the Iberian margin (Tagus mud patch) during the Holocene,*G3*.

Rodrigues, T., et al. (submitted), The last glacial-interglacial transition (LGIT) in the western mid-latitudes of the North Atlantic: abrupt sea surface temperature change and sea level implications.

Rosell-Melé, A., et al. (1998), Variability of the Arctic front during the last climatic cycle: application of a novel molecular proxy, *Terra Nova*, *10*.

Roucoux, K. H., et al. (2006), Climate and vegetation changes 180000 to 345000 years ago recorded in a deep-sea core off Portugal, *Earth and Planetary Science Letters*, *249*, 307-325.

Salgueiro, E., et al. (submitted), Temperature and Productivity Changes off the Western Iberian Margin during 2 the last 150 ky, *Quaternary Science Reviews*, *under revision*.

Shackleton, N. J., et al. (1990), An alternative astronomical calibration of the lower Pleistocene time scale based on ODP Site 677, *Trans. R. Soc. Edinb. Earth Sci*, *81*, 251-261.

Shackleton, N. J., et al. (2000), Phase relationships between millennial-scale eventes 64,000-24.000 years ago, *Palaeogeography*, *15*, 565-569.

Siegenthaler, U., et al. (2005), Stable Carbon Cycle-Climate Relationship During the late Pleistocene, *Science*, *310*.

Stein, R., et al. (2009), Variability of surface water characteristics and Henrich-like events in the Pleistocene midlatitude North Atlantic Ocean: Biomarker and XRF records from IODP Site U1313 (MIS16-9), *Palaeogeography 24* PA2203.

Tzedakis, P. C. (2009), The MIS 11 - MIS 1 analogy, southern European vegetation, atmospheric methane and the "early anthropogenic hypothesis", *Climate of The Past Discussions*, *5*, 1337-1365.

Tzedakis, P. C., et al. (2004), The Duration of Forest Stages in Southern Europe and Interglacial Climate Variability, *Science*, *306*, 2231-2235.

Tzedakis, P. C., et al. (2003), Comparison of changes in vegetation in northeast Greeece with records of climate variability over the last 450 000 years, *Earth and Planetary Science Letters*, *212*, 197-212.

van Kreveld, S., et al. (2000), Potential links between surging ice sheets, circulation changes, and the Dansgaard-Oeschger cycles in the Irminger Sea, 60-18 kyr, *Paleoceanography*, *15*, 425-442.

Vernal, A. d., and C. Hillaire-Marcel (2008), Natural Variability of Greenland Climate, Vegetation, and Ice Volume During the Past Million Years, *Science*, *320*, 1622-1625.

Villanueva, J., et al. (1997), Clean-up procedures for the unbiased estimation of C_{37} alkenone sea surface temperatures and terrigenous *n*-alkane in paleoceanography, *Journal of Chromatography 757*, 145-151.

Villanueva, J., et al. (1998a), A biomarker approch to the organic matter deposied in the North Atlantic during the last climatic cycle, *Geochimica et Cosmochimica Acta*, *61*, 4633-4646.

Villanueva, J., et al. (1998b) Precessional forcing of productivity in the North Atlantic Ocean, *Paleoceanography, 13,* 561-571.

Villanueva, J., et al. (2001) A latitudinal productivity band in the central North Atlantic over the last 270 kyr: An alkenone perspective, *Paleoceanography, 16,* 617-626.

Voelker, A. H. L., et al. (2006), Mediterranean outflow strengthening during northern hemisphere coolings: A salt source for the glacial Atlantic?, *Earth and Planetary Science Letters*, *245*, 39-55.

Voelker, A. H. L., et al. (2009), Variations in mid-latitude North Atlantic surface water properties during the mid-Brunhes: Does Marine Isotope Stage 11 stand out?, *Climate of The Past Discuss*, *5*, 1553-1607.

Weirauch, D., et al. (2008), Evolution of Millennial-Scale Climate Variability During the Mid Pleistocene, *Paleoceanography*, *23*.

Wright, A. K., and B. P. Flower (2002), Surface and deep ocean circulation in the subpolar North Atlantic during the mid-Pleistocene revolution, *Palaeogeography*, *17*.

Yin, Q. Z., and Z. T. Guo (2007), Strong summer monsoon during the cool MIS-13, *Climate of the Past Discussions*, *3*, 119-1132.

Zahn, R., et al. (1997), Thermoaline instability in the North Atlantic during meltwater events: Stable isotope and ice-rafted detritus records from core SO75-26KL, Portuguese Margin, *Paleoceanography*, *12*, 696-710.

Chapter 6

CONCLUSIONS

GENERAL REMARKS AND PRESPECTIVES

1. CONCLUSIONS

The high resolution study performed within this thesis' framework allowed the reconstruction of the climate variability on the western Iberian Margin during particular key periods such as the Holocene and the late Pleistocene. This provides new insights into understanding present-day climate and will aid in the forecasting climate evolution in the future.

In order to characterize and understand the main climate changes over the last 13,5 ka, we performed a high resolution multi-proxy study on a sedimentary sequence (composed of several sedimentary cores) retrieved in the Tagus mud patch, an area highly sensitivite to the Tagus river regime and global sea level changes. The same approach was applied to a deep-sea core retrieved from the Estremadura spur, to better understand the climate variability during the late Pleistocene (570-300 ka). The proxies used for our reconstruction include: i) alkenone-based sea surface temperature estimations ($U^{k'}_{37}$-SST); ii) quantification of terrigenous biomarkes: *n*-alkanes and *n*-alcohols to determine the evolution of continental plants; iii) quantification of the total concentration of alkenones and organic carbon to understand marine productivity; and finally iv) quantification of tetra-unsaturated alkenone percentages to reconstructed extreme cold events associated with the major input of freshwater masses.

The high resolution reconstruction of SST, marine productivity and terrigenous input into the Tagus mud patch off Lisbon (Portugal) done within the framework of HOLSMEER EU project "Late Holocene shallow marine environments of Europe" resulted in 3 scientific papers. The first publication, presented in Chapter 2, deals with a high resolution record of Sea Surface Temperatures (SST), riverine discharges and biological productivity for the last 2,000 years obtained in a sedimentary sequence recovered from the Tagus deposition centre off Lisbon (Portugal).

This work evidences the high sensitivity of the Tagus river regime to the climatic variability of the last two millennia and reveals a record of a major earthquake felt in the region in 1755, as recorded by a large peak in MS centred at 90 cm. The SST - $U^{k'}_{37}$ for the latest Holocene (2,000 years) off Lisbon, can be correlated to the GRIP borehole temperature, allowing the identification of a warm period (MWP) that spans from 550 to 1300 AD, as well as the Little Ice Age (LIA). The marine geological data presented here point to drier continental conditions and increased coastal upwelling

conditions during the MWP, and indicate increased river influx and river induced marine productivity during the LIA. Because negative NAO is correlated with precipitation anomaly fields in the Tagus basin, during the LIA, increased influx of terrigenous material into the studied site is hypothesized to reflect NAO-like variability with a more persistent negative state. During the milder few centuries of the MWP coastal upwelling, favorable conditions are attributed to a more persistent NAO positive state.

The two other papers have been published in the HOLSMEER special issue of the journal "The Holocene" and are attached as appendices. The first paper, presented in appendix 1, compares the results obtained from the Tagus Prodelta (W Portugal) record with the one from the Muros Ría (NW Spain) over the last two millennia, showing that the most abrupt changes detected in both areas occurred during the transition between the MWP and the LIA, although with opposing hydrographic signals. In the Tagus Prodelta, the MWP is characterized by high productivity and increasing coastal upwelling whereas the LIA is marked by high precipitation values as demonstrated by the increase of riverine input into the shelf. In the Muros Ria, a major transition from a fluvial regime to an open marine regime occurred at AD 1200. The climatic changes recorded both in the northern and southern site can be explained by long-term NAO trends. The reversal in both areas is attributed to a latitudinal migration of the Azores/Lisbon and Iceland pressure poles.

The second paper, presented in appendix 2, is a compilation of the climate variability of all the records produced within the project and confirms that the major climate oscillations occurring over the last 2000 years, MWP (550 to 1300 AD) and LIA (1300 to 1900 AD) are well correlated with the GRIP borehole temperature and point to conditions that could be explained by more negative North Atlantic Oscillation (NAO) during the LIA, while the MWP climate is likely to have been dominated by the positive mode of NAO. This high-resolution proxy data, from a key area characterized by specific phenomena and where instrumental record data is available was extremely important to estimate the relative magnitude of past changes and allow the scaling of proxy data against 100 years of instrumental record. However, the instrumental observations are short and the longer climate reconstructions depend on proxy data needing calibration. Thus, appendix 3 presents a first attempt to calibrate sediment proxy data for both

continental climate and oceanic productivity to the existing 100 years instrumental time-series of data for SST, precipitation, river runoff and upwelling strength.

The main conclusion reveal that reconstructions obtained through the application of the encountered equations to a previously published 2,000 yr composite record of cores D13902 and PO287-26G confirm conditions estimated from proxy data. The two equations for spring river flow retrieve quite close values after 1200 AD, however, they diverge for older periods and give negative values, indicating an analog problem, that is lack of instrumental data for low river flow conditions. On the contrary, the upwelling index reconstructions give positive values at all times, again indicating a lack of instrumental data for stronger upwelling conditions.

The extension of this high resolution study to the Holocene period (last 11.5 ka) using the Tagus mud patch core D13882 is presented in Chapter 3. SST and other marine and continental proxies' reconstructions reveal that this period was punctuated by several climatic oscillations which have also been previously documented from both open sea and inland sites. Furthermore, this record also allowed a better understanding of the mechanisms involved in the sea-land interaction during that period. In particular, the SST profile shows a general Holocene SST decreasing trend (from 19ºC to 15ºC) that perfectly matches summer insolation at 37ºN, with maximum SST values, reflecting the Holocene thermal maximum, occurring between 11 and 7 ka. Rapid cooling episodes of about 1-2ºC, appear superimposed on the general SST cooling trend, similar to those observed in other NE Atlantic and Mediterranean records. The longest and most extreme cooling episode, lasted about 700 years, and occurred between 8.6 and 7.9 ka and is associated with the so-called 8.2 ka event recorded elsewhere in the North Atlantic region. On a decadal to sub-decadal time scale, high SST variability is materialized by instrumentaly measured cooling events and increasing river discharge synchronous with prevailing NAO negative phases. This suggests that the inner-shelf area near the Tagus River mouth has been particularly sensitive to NAO index changes not only during the last 100 yr, but this relationship apperars to have been consistent during the whole Holocene. The increase in deforestation from agricultural practices, around 3 to 1.5 ka, has favored the input of continental suspended load rich in nutrients into the shelf triggering an increase of marine productivity in that area.

To get a better insight into the effect of the last deglaciation, and in particular of the last glacial-interglacial transition (LGIT) over Western Iberia, a high resolution study of the shallow core D13882, also retrieved from the inner-shelf of the Tagus mud patch was combined and extended through deep-sea core MD03-2699. This study presented in Chapter 4, allowed us to obtain the highest resolution record for the LGIT on this region. The comparison between MD03-2699 deep-sea core sea surface temperatures profile to other Iberian margin SST records allowed the demonstration that Heinrich event 1 (H1) was the most extreme cold event (11º to 13º C) detected over the last 21 ka in that region. Moreover, a latitudinal SST gradient emerges along the Iberian margin, with colder conditions in the northern region. The sharp increase in SST around 15 ka marks the beginning of the warm Bølling-Allerød interstadial (B-A) in the western Iberian margin during which maximum SSTs values of 17°C. This suggests that this warming episode started about 1000 yr prior to Meltwater Pulse 1A (MWP -1A) and reached its maximum values during or just slightly after this sea-level rise episode. In contrast, the shallow SST record (core D13882) shows that the final stages of the B-A period are marked by SST values around 11ºC, that is, 3 to 5°C lower than those recorded in other western Iberian margin sites. In addition, the presence of high continental biomarkers' and tetra-unsaturated alkenone concentrations during this period indicate the increase of freshwater input triggering a decrease in the SST values for that shallow area. This freshwater input although possibly associated with the melting of ice sheets is most certainly reflecting the strong input of freshwater by the Tagus River. The high-resolution alkenone based SST estimates of core D13882 further show that the YD event is composed by two cold phases surrounding a relatively warm one. That is, a 3ºC cooling episode detected at around 12.9 ka is followed by a continuous temperature increase up to 11ºC at 12.0 ka and followed by a second cooling phase (about 2°C) after 11.8 ka. The glacial-interglacial transition is marked by a sharp SST increase from 10ºC to 17ºC in the shallow core, contemporaneous with a strong sea level rise and consequent retreat of the coastline in the Tagus mud patch which probably precluded the input of terrigenous material to the inner-shelf. The abrupt SST increase of 7ºC in 40 yr together with the decrease of continental input to the Tagus mud patch occurs contemporaneously with the well-known mwp-1B. The synchronous timing between the drastic melting episode 1B and the abrupt marine and terrestrial warming at the mid-latitude of western Iberia, together with warm temperatures over Greenland,

suggest that this melting water episode and consequent sea level rise were initiated in the Northern Hemisphere.

To evaluate the natural climate evolution and the anthropogenic contribution to the present-day interglacial, we compare our previously described Holocene records with those reflecting previous interglacial periods. Although the forcing mechanisms liable for climate conditions in each interglacial need to be evaluated as an integrated period of each climate cycle, numerous researchers have attempted to simulate these glacial-interglacial cycles, in order to understand what drives these oscillations and which feedbacks alter their original properties. Presently, it is believed that the orbital forcing is the main driver mechanism responsible for both the onset and the termination of glaciations, however, glacial inceptions and terminations are also dominated by other forcing and feedback mechanisms within the climate system.

In order to look for a better understanding of those mechanisms, we performed the first multi-proxy study covering the period between 580 and 300 ka in the western Iberian margin in deep-sea core MD03-2699, which is presented in Chapter 5. The results show a general trend of warm and relatively stable interglacial periods separated by high-frequency climate variability during the glacial inceptions and glacial periods. SST-$U^{k'}_{37}$ records reveal that the warmest conditions, with temperatures close to 20ºC, occurred during the MIS 9.3 and the coldest ones reaching SST of 8ºC during termination V. The previous interglacials periods (MIS 13 and MIS 11) are cooler but lasted longer than the youngest interglacial period (MIS 9). Cross-correlation of SST and the orbital cycles shows a change of predominant periodicity from obliquity to eccentricity around 430 ka, the time of the mid-Brunhes event. Within this time interval sub-orbital SST variability punctuated both glacial inceptions and glacial periods. The most extreme cold episodes detected in particular during MIS 12 and MIS 10, are associated with the increase of tetra-unsaturated ($C_{37:4}$) alkenones and the presence of Ice Rafted Detritus (IRD). This evidence indicates that these extreme cold episodes are linked to massive meltwater pulses into the North Atlantic region that affected surface waters as far south as the Iberian margin. These extreme events can be considered Heinrich-type events (Ht). In detail, we identify 8 Heinrich-type events: Ht1 (coincident with MIS 10.2), Ht2, Ht3, Ht4 (coincident with the onset of termination V), Ht5 (coincident with MIS 12.2); Ht6, Ht7 (during the glacial inception of MIS 12), and finally Ht8 (coincident with the glacial inception of MIS 14). The general SST pattern

recorded during the transition from MIS 12 to MIS 11 (termination V) is similar to those detected during more recent deglaciations (i.e. terminations III, II and I). This pattern is composed of two cooling events separated by a warming phase which is associated with changes in the position of the polar front. Glacial conditions are marked by lower SST in particular during the glacial maxima as defined by the heavier benthic $\delta^{18}O$ values. Glacial MIS 14 shows higher SST values than all other glacial maxima suggesting a stronger influence of a subtropical like Azores Current during this period. During glacial periods and glacial inceptions, including Heinrich-type events, the productivity and terrigenous input into the Iberian margin was low.

The Iberian SST records over the last 6th climate cycles show that SST of MIS 11c is analogous with the present interglacial, the Holocene.

Appendix 4 presents new planktonic stable isotope and ice-rafted debris records from three core sites in the mid-latitude North Atlantic (IODP Site U1313, MD01-2446, MD03-2699) and its comparison to the records of ODP Sites 1056/1058 and 980. The idea behind this work is to reconstruct the hydrographic conditions during the middle Pleistocene spanning Marine Isotope Stages (MIS) 9–14 (300–540 ka). The new records fill the gap between ODP Sites 1056 and 980 and reveal, that experienced hydrographic conditions North Atlantic mid-latitude, which encompasses the southern edge of the North Atlantic ice-rafted debris (IRD) belt recorded by large SST gradients during glacials and stadials, while more similar to those in the subtropical or the subpolar gyre during interglacials, especially during MIS 11. The two new records off Portugal, MD01-2446 and MD03-2699 furthermore, allow for the first time to reconstruct and evaluate the full transition from glacial MIS 12 to MIS 11 in this eastern boundary upwelling system. The study sites reflect western and eastern basin boundary currents as well as north to south transect sampling of subpolar and transitional water masses. Planktonic 18O records indicate that during peak interglacial MIS 9 and 11 hydrographic conditions were similar among all the sites with relative stable conditions and confirm prolonged warmth during MIS 11c also for the mid-latitudes. Sea surface temperature (SST) reconstructions further reveal that in the mid-latitude North Atlantic MIS 11c is associated with two plateaus, the younger one of which is slightly warmer. Enhanced subsurface northward heat flux in the eastern boundary current system, especially during early MIS 11c, is denoted by the presence of tropical planktonic foraminifer species. MIS 13 was generally colder and more variable than the younger

interglacials. The greatest differences between the sites occurred during the glacial inceptions and glacials. Then, a north-south trending hydrographic front is likely to have separated the nearshore and offshore waters off Portugal. While offshore waters originated from the North Atlantic Drift as indicated by the similarities between the records of IODP Site U1313, ODP Site 980 and MD01-2446, nearshore waters as recorded in core MD03-2699 derived from the Azores Current and thus the subtropical gyre. A strong Azores Current influence is seen especially during MIS 12, when SST dropped significantly only during the Heinrich-type ice-rafting event at the onset of termination V. Given the subtropical overprint on Portuguese nearshore sites such as MD03-2699 and MD01-2443 caution needs to be taken to interpret their records as basin-wide climate signals.

2. GENERAL REMARKS AND PRESPECTIVES

The Holocene climate variability is still poorly understood and enhanced knowledge of its possible problems requires an integrated approach through the study of several paleoclimatic archives, and above all the comparison with previous interglacials. Determining the climatic evolution of past interglacials, similar to the Holocene, is crucial to evaluate the future climate. Our results agree with the indication that MIS 11 is the best candidate to be the analogue for MIS 1, the Holocene, due to similar Earth's astronomical configuration. However, the timing and duration of both interglacials is still controversial. Other previous interglacial periods, such as MIS 7, MIS 13 and MIS 19 are characterized by different climate state baselines in terms of insolation, atmospheric greenhouse gas concentrations and ice volume, as shown by ice and marine records. These intervals provide the opportunity to study the Earth's system sensitivity and climate changes under a wide range of forcings. Previous isotopic interglacial records, covering the last 570 ka, have shown similarities between their climatic dynamic patterns, despite different astronomical forcing and dissimilarities concerning duration, warmth magnitude and forest succession. It is therefore of extreme importance to compare the Holocene to a large set of interglacial periods to better understand the natural climatic interglacial variability and associated driving processes.

Besides, detecting the natural climate variability during overall warm periods, would also be of extreme importance to follow key issues such as: a) the detailed

relationships between the high-frequency variability observed in temperate and high latitudes during interglacial periods and b) the role of global ice-volume/sea-level variations in both abrupt and longer-term climate changes.

Evidence of a pervasive millennial-scale climatic variability in the North Atlantic region and borderlands has been recorded throughout past climatic cycles of the Late Pleistocene. The abrupt climatic changes appear to occur regardless of the glacial state but recent works suggest that ice volume might have an indirect influence on the amplitude and frequency of the millennial climatic changes.

To further develop the knowledge on the past environmental conditions, the application of new paleoenvironmental proxies is crucial. Proxies based on the fractioning of light stable isotopes in natural systems including δD of individual organic compounds in deep-sea sediments will be off great importance. A combination of δD of individual organic compounds with marine carbonate $\delta^{18}O$ records are expected to allow for a more precise description of past environmental changes, including the reconstruction of paleohydrologic conditions. Following this path, I believe that the compound-specific δD of *n*-alkane and alkenone biomarkers preserved in sediments may also be used to characterize and quantify the magnitude of the continental hydrologic conditions (δD of *n*-alkane) as of the marine surface water changes (δD of alkenones).

Appendices

Appendix 1

CLIMATE CHANGE AND COASTAL HYDROGRAPHIC RESPONSE ALONG THE ATLANTIC IBERIAN MARGIN (TAGUS PRODELTA AND MUROS RIA) DURING THE LAST TWO MILLENNIA

S.M. Lebreiro,[1]* G. France´s,[2] F.F.G. Abrantes,[1] P. Diz,[2] H.B. Bartels-Jónsdóttir, [1] Z.N. Stroynowski, [1] I.M. Gil, [1] L.D. Pena,[3] **T. Rodrigues, [1]** P.D. Jones,[4] M.A. Nombela[2], I. Alejo[2], K.R. Briffa,[4] I. Harris,[4] and J.O. Grimalt, [5]

1 INETI, Department of Marine Geology, Estrada da Portela, Zambujal, 2721-866 Alfragide, Portugal;

2 University of Vigo, Facultad de Ciencias, Department of Marine Geosciences, 36200 Vigo, Spain;

3 University of Barcelona, Department of Stratigraphy, Paleontology and Marine Sciences, Calle Martý´ Franques, 08028 Barcelona, Spain;

4 University of East Anglia, Climatic Research Unit, Norwich NR4

7TJ, UK;

5 Institute of Chemical and Environment Research (CSIC), Department of Environmental Chemistry, Jordi Girona, 18, 08034 Barcelona, Spain)

The Holocene **16**, 1003-1015 (2006)

The Holocene 16,7 (2006) pp. 1003–1015

Climate change and coastal hydrographic response along the Atlantic Iberian margin (Tagus Prodelta and Muros Ría) during the last two millennia

S.M. Lebreiro,[1]* G. Francés,[2] F.F.G. Abrantes,[1] P. Diz,[2] H.B. Bartels-Jónsdóttir,[1] Z.N. Stroynowski,[1] I.M. Gil,[1] L.D. Pena,[3] T. Rodrigues,[1] P.D. Jones,[4] M.A. Nombela,[2] I. Alejo,[2] K.R. Briffa,[4] I. Harris[4] and J.O. Grimalt[5]

([1]INETI, Department of Marine Geology, Estrada da Portela, Zambujal, 2721-866 Alfragide, Portugal; [2]University of Vigo, Facultad de Ciencias, Department of Marine Geosciences, 36200 Vigo, Spain; [3]University of Barcelona, Department of Stratigraphy, Paleontology and Marine Sciences, Calle Martí Franques, 08028 Barcelona, Spain; [4]University of East Anglia, Climatic Research Unit, Norwich NR4 7TJ, UK; [5]Institute of Chemical and Environment Research (CSIC), Department of Environmental Chemistry, Jordi Girona, 18, 08034 Barcelona, Spain)

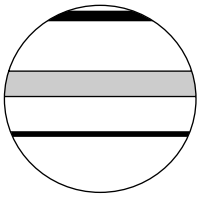

Abstract: The Tagus Prodelta (W Portugal) and the Muros Ría (NW Spain) are areas of high deposition rates registering high-resolution palaeoclimatic records for western Iberia. We compare the climatic conditions of the two areas over the last two millennia based on proxies of temperature (sea surface temperatures and oxygen isotopes), continental input (grain size, iron and magnetic susceptibility) and productivity (inorganic and organic carbon, carbon isotopes, benthic foraminifera and diatoms). Biogeochemical changes in the Tagus Prodelta reflect widely recognized North Atlantic climatic periods encompassing the Roman Period (AD 0–350), the Dark Ages (AD 400–700), the 'Mediaeval Warm Period' (MWP; AD 800–1200) and the 'Little Ice Age' (LIA; AD 1300–1750). The atmospheric North Atlantic Oscillation (NAO) drives the Tagus Prodelta multidecadal, long-term variability in precipitation-river input during cold periods (negative NAO) and marine upwelling during warmer periods (positive NAO), a scheme that is reversed in the Galician region. The Muros Ría shows only local hydrodynamics until AD 1150, including a 'suboxic' event in the inner Ría around AD 500–700. Since AD 1150 Atlantic warm upwelled waters have ventilated the outer Ría but only reach the inner Ría at AD 1750. The twentieth-century records are also interpreted as a reflex of the inverse NAO mode in both areas, resulting in amplification of the LIA biogeochemical water conditions. Centennial-scale solar activity appears to be another important forcing mechanism (or the only one, if solar activity drives the NAO and 'Bond-cycles') behind changes in the hydrography of the Tagus Prodelta, and primary production, bottom ventilation and organic carbon degradation in the Muros Ría.

Key words: Iberia, Tagus River, Muros Ría, NAO, 'Mediaeval Warm Period', 'Little Ice Age', hydrographic change, climatic change, HOLSMEER project.

*Author for correspondence (e-mail: susana.lebreiro@ineti.pt)

 10.1177/0959683606hl990rp

Introduction

The Tagus Prodelta and the Muros Ría are representative areas of shallow marine-continental processes in which hydrography is profoundly affected by climatic changes. Only the analysis of high sedimentation rate sequences can provide insights into decadal and (multi-)decadal climate variability characterized by the North Atlantic Oscillation (NAO) or solar activity; we do not yet know how widely these affect the Earth's biogeochemical cycles. Furthermore, regional-scale histories of different proxy variables are needed to expand our knowledge on climate variability beyond the instrumental record (Jones *et al.*, 2001). Only in this way can we estimate the natural and human contribution to climate variability and provide more accurate predictions for the future.

Today, the western Iberian climate is mainly determined by the atmospheric NAO, the eastern North Atlantic surface circulation, particularly the Portuguese–Canary boundary current, and the intermediate Eastern North Atlantic Central Water (ENACW). The Portuguese–Canary boundary brings cool water from the northernmost latitudes along the Iberian margin. The ENACW, which Fiúza (1983) defined with two origins, subtropical (st) and subpolar (sp), converge at Cape Finisterre. Upwelling of ENACWst (salty and warm) or ENACWsp (fresh and cold) into the Muros Ría depends on favourable northerly winds from late spring to early autumn and the interannual hydrographic position of the front between these two watermasses (Álvarez-Salgado *et al.*, 1993; Varela *et al.*, 2005). In the south, ENACWst upwells along the Tagus Prodelta. The NAO determines the direction and speed of the westerlies and precipitation over Europe and the Atlantic. The NAO Index measures the difference in atmospheric pressure at sea level between the Icelandic and Lisbon poles, mainly in winter (Hurrell, 1995). Close to the Lisbon pole, significant climate anomalies are evidenced by NAO impact on the precipitation anomaly fields (mm/month) determined for a 40 yr time series from southern to northern Iberia (Trigo *et al.*, 2002a,b).

The Tagus Prodelta is an organic-rich, fine-sediment prism located off the Tagus River on the Portuguese continental shelf (Monteiro and Moita, 1971; Cabeçadas and Brogueira, 1997) (Figure 1). The Tagus mouth is preceded by a 340 km^2 (at high tide) tidal lagoon estuary-type (Vale and Sundby, 1987). The output of freshwater to the estuary is 80–720 m^3/s, occasionally reaching 2200 m^3/s (Loureiro, 1979). The suspended sediment load entering the estuary is 4×10^5 t (c. Vale, unpublished data, 1987), as estimated from catastrophic floods such as that of 1979, amounting to a volume of sediment sufficient to deposit a 7-mm thick sheet over its entire surface (Vale and Sundby, 1987). Estuary sediments are mud and sand facies responding to changes in current and river flow regimes. The stronger river flood events are registered in the shelf sediments, alternating with productive episodes resulting from coastal upwelling enhancement (Abrantes *et al.*, 2005a).

The Muros Ría (97 km^2) is a drowned river system deeply incised into the coastline that traps fluvial material rather than discharging it onto the Spanish continental shelf (Oliveira *et al.*, 2002). The most significant freshwater input comes from the River Tambre (54 m^3/s mean discharge), which mostly influences the estuarine characteristics of the inner Ría. The outer Ría is under strong oceanic control, exhibiting a residual circulation in two layers (Fraga and Margalef, 1979; Prego, 1990). Muros is the only Galician Ría without a group of islands at its mouth, which favours oceanic intrusion.

Off Iberia, primary production patterns are mainly conditioned by (1) summer persistent upwelling of cool and nutrient-rich ENACW from 100–300 m depth; (2) water column stratification; (3) nutrient availability; and (4) the composition and distribution of phytoplankton (Fraga, 1981; Estrada, 1984; Varela *et al.*, 1987; Abrantes, 1988; Ríos *et al.*, 1992; Abrantes and Moita, 1999). During upwelling conditions (summer), water column chorophyll *a* concentrations increase to 6 mg/m^3 in the Tagus (Moita, 2001) and >7 mg/m^3 in Muros (Nogueira *et al.*, 1997). Diatoms are the main contributors at both sites, while coccolitophorids dominate the phytoplankton during non-upwelling, non-productive conditions (winter) (Bode *et al.*, 1994; Abrantes and Moita, 1999). On the Tagus shelf, solar irradiation and river discharge

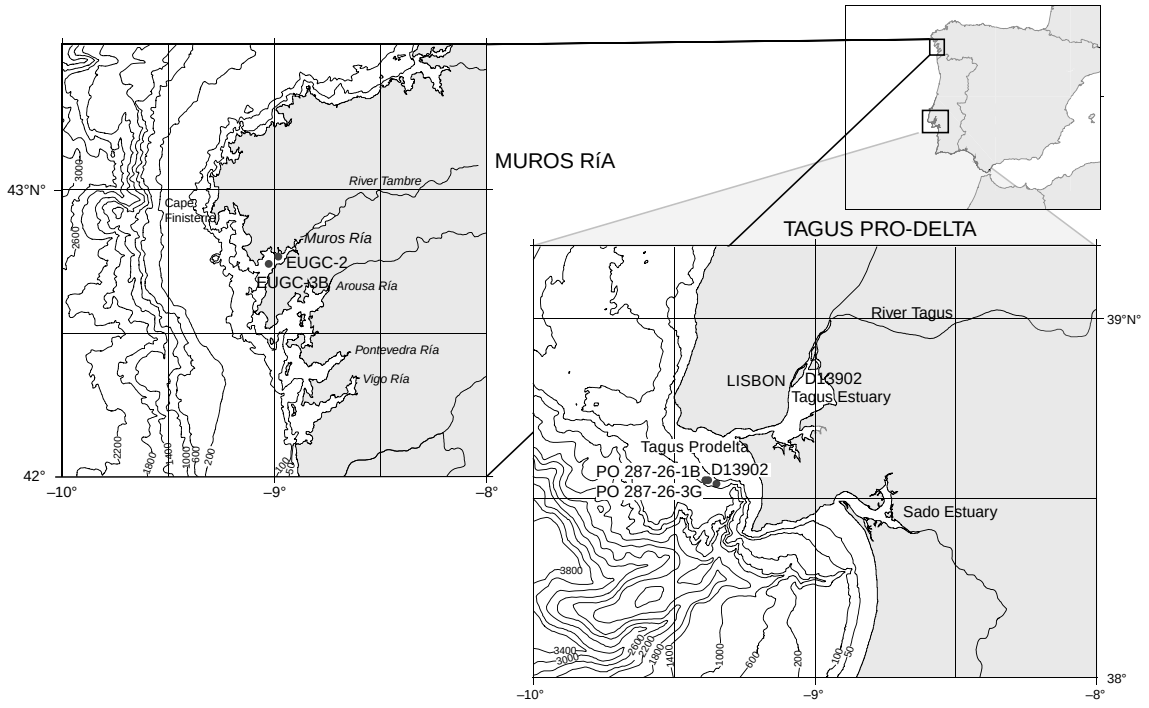

Figure 1 Geographic location of targeted areas in the Iberian Margin. Position of cores studied in the Tagus Prodelta and Muros Ría

results in maximum water stratification in summer, redistributing nutrients in the water column (Moita, 2001). In the two-layer stratified estuary of Muros, with a surface freshwater outflow and a bottom oceanic inflow circulation, the export of nutrients and phytoplankton to the ocean reinforce the upwelling effect (Estrada, 1984). Furthermore, remineralization of organic matter enriches the subsurface water inflow which brings nutrients back into the Ría (Estrada, 1984). The range of primary production rates off Lisbon (0.6–1.6 g C/m^2 per day; Antoine and Morel, 1996; Behrenfeld *et al.*, 2001) and NW Spain (0.7–3.7 g C/m^2 per day; Nunes *et al.*, 1984; Prego, 1993) are similar to those recorded in the Benguela (0.5 g C/m^2 per day; Brown and Field, 1986; Brown *et al.*, 1991) and Peru upwelling regions (1.9 g C/m^2 per day; Barber and Smith, 1981) or the California coastal upwelling system (0.5–2.6 g C/m^2 per day; Pilskaln *et al.*, 1996). Thus, in the Galician rías, productivity is primarily influenced by shelf winds as well as coastal and estuarine processes (Varela *et al.*, 2001; Varela *et al.*, 2005). On the Tagus Prodelta, primary productivity can be triggered either by an intensification of coastal upwelling along the Atlantic Iberian margin (Abrantes, 1988; Abrantes and Moita, 1999) or increased input of nutrients by the river into the area.

This paper presents high-resolution palaeodata, including O and C stable isotopes, benthic foraminifera, diatoms, grain size and land-derived major chemical elements, from two Iberian sedimentary systems: the Tagus Prodelta (Portugal) and the Muros Ría (NW Spain). Our objective is to analyse the regional response to 'high-frequency' climate forcing mechanisms, such as the NAO and solar activity.

Material and methods

Core description

From the Tagus Prodelta, a spliced sediment sequence composed of box core PO287-26-1B, gravity core PO287-26-3G and giant piston core D13902, collected during the Portuguese PALEO1 campaign onboard the R/V *Poseidon*, in 2002, and the British *Discovery* 249 cruise, in 2000, were used for this study. From the Muros Ría, two gravity cores EUGC-2 (inner Ría) and EUGC-3B (outer Ría), were collected during the B/O *Mytilus* cruise, in 2001. The records of both areas cover the last 2000 years (Table 1, Figure 1).

Although the recovered length of core D13902 is 600 cm, the sediment above 189 cm was disturbed, as demonstrated by ^{14}C datings (Abrantes *et al.*, 2005a; see samples AAR-7823, OS-37286, AAR-7824, table 4 in Bartels-Jónsdóttir *et al.*, 2006), and discarded, and 0 cm assigned to depth 189 cm. In this study only the interval between 189 and 400 cm, which covers the last 2000 years, is considered. From core PO287-26-3G, located about 2 km from D13902 (Figure 1), only the section 0–150 cm was considered, in an effort to partially substitute the 350-yr hiatus in core D13902 arising from the AD 1755 Lisbon earthquake and tsunami (Abrantes *et al.*, 2005a). Core EUGC-2 contains modern sediments at its top, but in core EUGC-3B the top has been dated to AD 1470. The upper part of the sequence was lost during recovery.

Chronology

For the Tagus Prodelta, accelerator mass spectrometry (AMS) ^{14}C dating of either molluscs or planktonic foraminifera was performed on 18 samples from the three cores. ^{14}C ages were 400 year reservoir-age corrected after a test on three regional live-colleted pre-bomb mollusc shells (Abrantes *et al.*, 2005a) and calibrated using CALIB 4.4 (Stuiver *et al.*, 1998a) (Table 2). ^{210}Pb analyses were performed on 18 samples (16 in PO287-26-1B and 2 in D13902). For the Tagus Prodelta spliced sequence we follow the age model proposed in Abrantes *et al.* (2005a). In this sequence a 1-cm sampling interval gives a mean time resolution of 1.5 years between AD 2001 and 1759 and 8.4 years between AD 1600 and 0 (Figure 2). For the Muros Ría cores, a total of eight samples were dated by AMS ^{14}C (four for each core) on benthic foraminifera and entire articulated bivalve shells (Table 2). Sedimentation rates have been calculated by interpolation between dated points (Figure 2).

Table 1 Location, water depth and core length for the five cores in the Tagus Prodelta and Muros Ría

Core number	Core type	Water depth (m)	Core length[a] (m)	Latitude (N)	Longitude (W)
PO287-26-1B	box	96	0.51	38°33.49′	9°21.84′
PO287-26-3G	gravity	96	3.05 (1.50)	38°33.49′	9°21.84′
D13902	piston	90	6.00 (2.10)	38°33.24′	9°20.13′
EUGC-2	gravity	33.3	3.50 (2.00)	42°45.5′	8°59.9′
EUGC-3B	gravity	37.9	4.10 (1.60)	42°45.1′	9°00.2′

[a]Numbers in parentheses indicate metres of core corresponding to the last 2000 years.

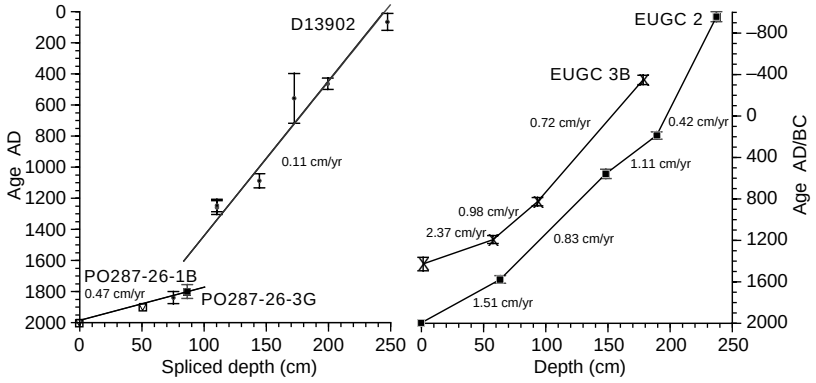

Figure 2 Age models and sedimentation rates for the Tagus Prodelta (left: triangles, PO287-26-1B; squares, PO287-26-3G; circles, D13902) and Muros Ría (right) cores

Table 2 Results of ^{14}C AMS datings of the Tagus Prodelta box-core PO287-26B, gravity-core PO287-26G and piston-core D13902 (levels in italic correspond to ages not considered for the age model) (above); and Muros Ría cores EUGC-3B and EUGC-2 (below)

Core/(depth) (cm)	Laboratory code	Spliced depth (cm)	Species	^{14}C age BP	Reservoir corr. ^{14}C yr age	Calendar years BP	SD (±1 s)	Age AD	$\delta^{13}C$	Sed rate (cm/yr)
PO287-26B (32–33)	AAR-8368.2-K[a]	51	mollusk shell	440	40	51	25	1899	−1.09	0.45
D13902 (27–28)	OS-37286[b]	75.4	mollusk shell	492	92	111	39	1839	0	0.11
D13902 (31–32)	*AAR-8338*[a]	*79.4*	*mollusk shell*	*2150*	*1700*	*1700*	*80*	–	*0*	
D13902 (37–38)	*AAR-7826*[a]	*85.4*	*mollusk shell*	*8955*	*8555*	*8555*	*70*	–	*+0.01*	
D13902 (46–47)	*AAR-8301*[a]	*94.4*	*mollusk shell*	*7075*	*6675*	*6675*	*50*	–	*+0.79*	
D13902 (62–63)	AAR-7207[a]	110.4	mollusk shell	1160	760	691	45	1259	+1.44	0.11
D13902 (62–63)	AAR-7208[a]	110.4	*turritella*	1185	785	704	40	1246	+2.15	0.12
D13902 (96–97)	AAR-7209[a]	144.4	mollusk shell	1370	970	863	45	1087	+2.19	0.13
D13902 (124–125)	OS-37307[b]	172.4	foraminifera[c]	1880	1480	1394	160	556	0	0.14
D13902 (151–152)	AAR-7828[a]	199.4	mollusk shell	2007	1607	1487	37	463	+2.68	0.15
D13902 (199–200)	AAR-7826[a]	247.4	mollusk shell	2340	1940	1885	55	65	+0.71	0.16
PO287-26-3G (86–87)	OS-42381[b]		mollusk shell	545	145	147	45	1801	+0.86	0.17
EUGC-3B (1–2)	AAR-8453[a]		*Nonion commune*	920	520	522	65	1429	−2.53	
EUGC-3B (57–58)	AAR-7966[a]		*Venus nux*	1229	829	799	39	1193	−1.97	2.37
EUGC-3B (93–94)	AAR-7502[a]		*Myrtea spinifera*	1575	1183	1172	40	826	−0.84	0.98
EUGC-3B (178–179)	AAR-7967[a]		*Myrtea spinifera*	2623	2223	2347	45	−349	−0.14	0.72
EUGC-2 (63–65)	AAR-7969[a]		*Lucinoma borealis*	730	330	370	37	1581	+1.00	1.51
EUGC-2 (148–149)	AAR-8508[a]		*Nonion commune*	1855	1455	1390	45	561	−5.33	0.83
EUGC-2 (189–190)	AAR-8662[a]		*Nonion commune*	2170	1770	1761	35	190	−4.08	1.11
EUGC-2 (237–238)	AAR-7970[a]		*Myrtea spinifera*	3136	2736	2904	47	−955	+0.31	0.42

[a]AMS ^{14}C Laboratory of the University of Aarhus (Denmark).
[b]National Ocean Sciences AMS Facility of the Woods Hole Oceanographic Institution (USA).
[c]*Globigerina bulloides*, *Globigerinoides ruber* white and *Globigerinella calida*.

Non-destructive physical properties

Low-field magnetic susceptibility of core D13902 was carried out in U-channels at a 4 cm interval resolution at the LSCE/CNRS, Gif-sur-Yvette, France; for the other four cores, magnetic susceptibility was measured using a Multi Sensor Core Logger system at 1 cm interval at the University of Bremen, Germany (ARI-Paleostudies Program). Fe, Ti, K, Ca, Sr abundance in counts per second was measured by means of non-destructive scanning X-ray fluorescence (Jansen *et al.*, 1998) at 1 cm resolution for four cores, and 2 cm interval for core D13902, at the University of Bremen, Germany (ARI-Paleostudies Program). Only Fe is shown here.

Textural data

Grain size was determined for the size fraction less than 2 mm using a Coulter LS230 laser particle analyser. Sample treatment consisted of organic matter removal with hydrogen peroxide (H_2O_2) and dispersion with sodium hexametaphosphate (0.033M). Prior to analysis, samples were homogenized and stirred. Resolution is 1 cm for the three Tagus Prodelta cores and 2 cm for Muros core EUGC-3B.

$CaCO_3$ and C_{org}

From an initial volume of 2 mg of dried, ground and homogenized sample, calcium carbonate was calculated by the difference between total carbon and organic carbon (C_{org}) measurements using a CHNS-932 Leco element analyser. The C_{org} is combusted at 400°C. Data are presented in weight percentage. The relative precision of two repeated measurements of both samples and standards was 0.03wt%. Sample resolution is 1 cm for cores PO287-26-1B and D13902, 5 cm for core PO287-26-3G and 2 cm for core EUGC-3.

Foraminifera

Samples for foraminiferal counts were wet-sieved at 63 μm and dry-sieved at 125 and 2000 μm. Benthic foraminifera were analysed in the >125 μm fraction. Resulting from the observation that biogenic carbon from high C_{org} sediments suffers dissolution when the samples are stored in a sodium hexametaphosphate 0.033M solution (unpublished INETI-DGM data, 2006), samples were washed only with distilled water. Total benthic foraminiferal assemblages were identified counting at least 300 individuals. Agglutinated foraminifera are excluded in the calculations for the Tagus Prodelta because of their poor preservation potential (Bartels-Jónsdóttir *et al.*, 2006), but considered an important part of the assemblage in Muros because no significant taphonomic loss was observed. Sample resolution in the Tagus Prodelta is 1 cm in PO287-26-1B, 2–5 cm in PO287-26-3G and approximately 3–4 cm in D13902; in Muros, sample resolution is 2 cm for both EUGC-2 and EUGC-3B.

Oxygen and carbon isotopes

Oxygen and carbon stable isotopes were analysed using a Finnigan MAT 251 mass spectrometer at the Department of Geosciences of the University of Bremen (Germany). All samples were measured relative to the VPDB standard with reproducibility of 0.07‰ for $\delta^{18}O$ and 0.06‰ for $\delta^{13}C$. Measurements were performed on the benthic species *Uvigerina* sp. 221 and planktic *G. bulloides* and *G. inflata* (PO287-26-1B, PO287-26-3G and D13902) at every centimetre, and on *Nonion commune* (EUGC-2 and EUGC-3B) at 2 cm interval resolution. On average, six specimens from the ≥ 250 μm fraction were used for the Tagus Prodelta and about 20 specimens from the ≥ 125 μm fraction for the Muros Ría.

Diatoms

For diatom slide preparation, a fixed amount of 1–2 g of fresh sediment from each sample was cleaned following Abrantes *et al.* (2005b) and placed to dry on plates (Battarbee, 1973). To calculate diatom fluxes (number of valves per square centimetre per year), diatom frustules were counted following the counting protocol of Schrader and Gersonde (1978) and Abrantes (1988). Cores PO287-26-1B and EUGC-3B were sampled at 1 cm resolution, PO287-26-3G at 5 cm and D13902 unevenly between 5 and 12 cm.

Results and discussion

Major North Atlantic climatic periods

The last two millennia circumscribe five relatively well time-constrained climatic periods, Roman Period (RP; ~AD 0–400; eg, Lamb, 1985), Dark Ages (DA; ~AD 400–700; eg, Keigwin and Pickart, 1999; Mikkelsen and Kuijpers, 2001), 'Mediaeval Warm Period' (MWP; AD 800–1300; eg, Hughes and Diaz, 1994; Hass, 1996), 'Little Ice Age' (LIA; AD 1350–1900; eg, Bradley and Jones, 1993) and a warming twentieth century, indicated by instrumental temperature measurements of the last two centuries, extended using proxy records back in time.

Oxygen isotopes have been widely used to infer water temperatures (eg, Shackleton, 1974; Keigwin, 1996) in marine records. As no significant ice volume changes have occured during the last 2000 years, $\delta^{18}O$ should reflect bottom water temperature at our sites, and deviations from other independently derived temperatures indicate salinity effects.

In the Tagus Prodelta, $\delta^{18}O$ oscillates between 1.9 and 1.15‰, clearly defining four distinct intervals. Two periods with 1.55‰ average values, AD 0–350 (encompassing the Roman Period) and 1.6‰ AD 1250–1850 (the so-called 'Little Ice Age'); the latter is punctuated by a relatively lighter event centred at AD 1400. Lighter $\delta^{18}O$ values are found between AD 400 and 650 (corresponding to the Dark Ages) and AD 800–1250 ('Mediaeval Warm Period'), reaching mean values around 1.4–1.5‰, and during the twentieth century, with the lighest oxygen isotope values (1.3‰) (Figure 3A). At this location, major fluctuation in the $\delta^{18}O$ is probably related to strong temperature changes at interannual time scale rather than to salinity changes. In the Muros Ría, although the data have a smaller amplitude (1.9-1.6‰), values remain around 1.7–1.8‰ until AD 1750, with the exception of the interval AD 1200–1300 in the outer Ría, becoming gradually lighter towards the present in the inner Ría (Figure 3A). In general, the lighter oxygen isotopes at the Tagus Prodelta point to water temperatures reflecting warmer/less saline waters than the Muros Ría (Figure 3A, Figure 4).

To support the hypothesis that lighter $\delta^{18}O$ reflects higher water temperature, we compared the $\delta^{18}O$ results from the Tagus Prodelta with SST based on the alkenone $U^{k'}_{37}$ index. High values (17.5°C) are observed during AD 0–900, with a gradual decrease of 2°C up to AD 1400. Low temperatures (15°C) remain until AD 1900, when SST starts to oscillate with high amplitude between 14 and 17°C (Rodrigues, 2004; Abrantes *et al.*, 2005a) (Figure 3B). Clearly, temperature explains the difference in $\delta^{18}O$ in the intervals AD 400–1250 (DA–MWP) and AD 1250–1850 (LIA). The warmings in the RP and the last century, however, are not fully supported by our data. In the Vigo Ría, south of Muros, a similar SST record exists (Diz *et al.*, 2002); this is probably representative for all the Galician region (Figure 3B). Here, since AD 1150, relatively warmer/less saline waters came into the Ría (outer

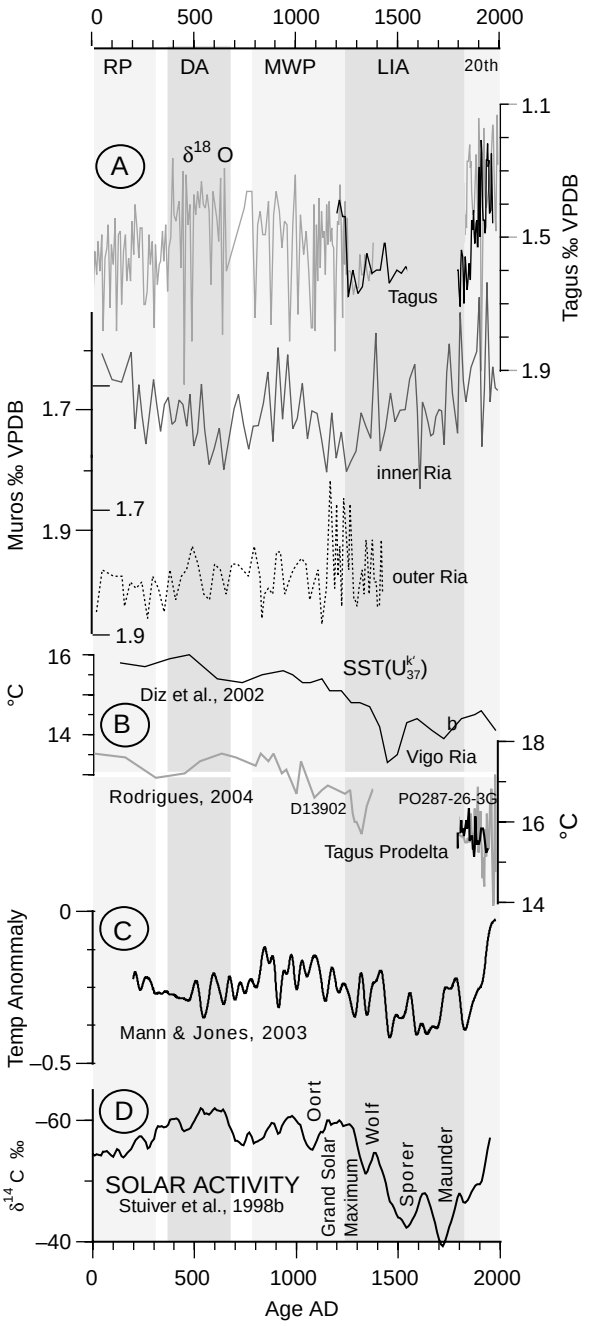

Figure 3 Comparison of temperature indicators between the Tagus Prodelta and the Muros Ría. A, stable oxygen isotopes; B, $U^{k'}_{37}$ sea surface temperatures for the Tagus and the Vigo Ría; C, temperature anommaly; D, ^{14}C solar activity. Note different scales in $\delta^{18}O$. RP, Roman Period; DA, Dark Ages; MWP, 'Mediaeval Warm Period'; LIA, 'Little Ice Age', 20th, twentieth century. See text for details

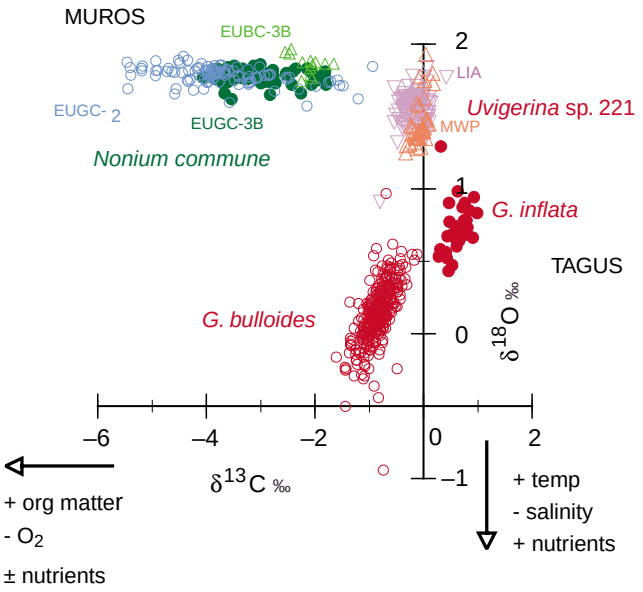

Figure 4 Water masses characterization on the basis of oxygen and carbon stable isotopes for the Tagus Prodelta (*G. bulloides*, *G. inflata* and *Uvigerina* sp. 221) and Muros Ría (*Nonium commune*). EUBC-3B is a box-core from the Muros Ría at the same position as gravity core EUGC-3B. 0.24‰ in $\delta^{18}O \equiv \Delta 1°C$ (Shackleton, 1974)

site EUGC3B), only to reach and affect the inner Ría much later, around AD 1700.

Additionally, our $\delta^{18}O$ records can be compared with the North Atlantic temperature variability registered by instrumental data, showing that the two major established global temperature climatic periods MWP and LIA (see discussion in Jones and Mann, 2004) are well marked in the Iberian margin (Figure 3C). Moreover, the DA is demarcated from the MWP in our records. The Tagus SST do not mirror the rapidly warming twentieth-century curve of Mann and Jones (2003), hence the very light oxygen isotopes values must indicate lower salinity rather than higher temperature.

Climatic conditions and the productivity record

C_{org}, $CaCO_3$, $\delta^{13}C$ and micro-organisms provide good indications of past changes in productivity (eg, Broecker and Peng, 1982; Zahn *et al.*, 1987; Fisher and Wefer, 1999) (Figure 5).

Organic carbon in the Tagus core shows very low values (0.5–1.5 wt%) for the period AD 500–1250, and relatively higher values between AD 0–400 and AD 1250–1850 (1–1.7 wt%). For the last century values increase to near 2.3 wt%, exceeding all previous maxima levels (Figure 5B). An inverse correlation exists between organic and inorganic carbon (Figure 5A,B). The Muros Ría contains higher than average organic carbon, although within a similar range of variation (2.5–3.5 wt%). Nevertheless, organic and inorganic carbon curves follow each other quite closely. The higher content of organic carbon in the Muros Ría relative to the Tagus Prodelta highlights different environments and either stronger productivity or better *in situ* organic carbon preservation in the Ría (Figure 5B). Comparing both areas, organic carbon in the outer site of the Muros Ría diverges from the Tagus Prodelta between AD 400 and 1300 (DA and MWP), suggesting different water conditions in the two areas. However, the Tagus and Muros inorganic carbon mimic each other (data available only for outer site and AD 0–1400).

$\delta^{13}C$ of benthic foraminifera in the Tagus Prodelta fluctuates between 0.4 and −0.9‰. It shows relatively low values between AD 100 and 500, increases until around AD 1300 with a minimum centred at AD 650 (Figure 5C). The lowest values are documented during the last century (Suess effect). The Muros Ría presents a higher range variation in $\delta^{13}C$ (−1 to −5.4‰), with the largest fluctuations for the inner Ría, more negative values between AD 100 and 1500, and rapid increase for the last 500 years. Lighter values (−5‰) are evident for the interval AD 550–700, indicating stagnant water conditions. $\delta^{13}C$ is less negative and more constant for the outer Ría, until around AD 1200 when a sharp increase occurs. More positive $\delta^{13}C$ are indicative of more ventilated, mixed waters, influenced by marine upwelling. In the Tagus Prodelta, $\delta^{13}C$ data validate our previous interpretation of light $\delta^{18}O$,

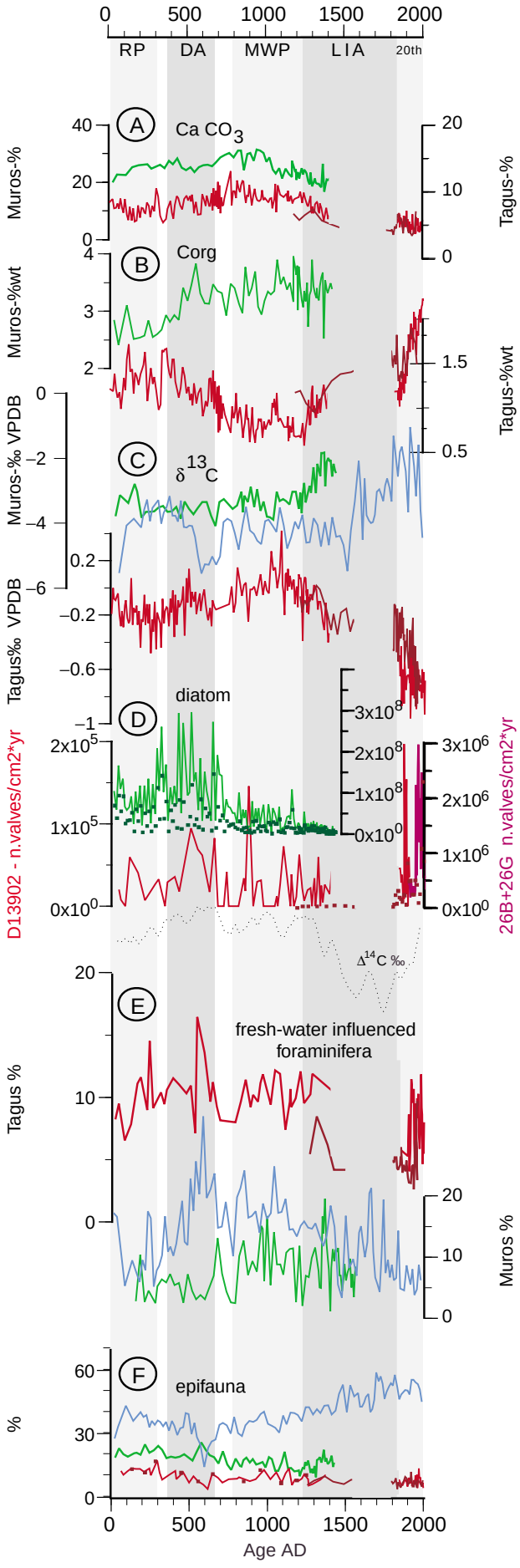

reflecting temperature and not salinity during the DA, MWP, and hence suggests intense upwelling during these times. In contrast, river runoff is dominant during the RP, the LIA and the twentieth century. However, in the Muros Ría and in light of the carbon isotope results, the same water mass influenced the Ría until AD 1150, although slightly better ventilation and/or less organic matter accumulation characterized the outer Ría (Figure 5C). Since AD 1150 the inflow of warmer, oceanic waters caused more intense bottom ventilation in the outer Ría, very likely due to reinforced upwelling. The enhancement of bottom ventilation is delayed in the inner Ría by 400 years. A similar pattern is found in the neighbouring Vigo Ría (Diz *et al.*, 2002). Therefore, as opposed to the Tagus Prodelta area, in the Muros Ría the LIA is marked by marine influence. The fact that the Muros Ría records much higher values and variability in the $\delta^{13}C$ data than in the Tagus Prodelta reflects the importance of organic matter preservation-related processes in the more protected environment of the Ría (Figure 4).

Diatom accumulation rate in the Tagus Prodelta indicates periods of productivity with pulses centred at AD 550, AD 900 and weakly at AD 100 and AD 1100. These four pulses of diatoms, composed by the mixing and upwelling-related species (mainly *Paralia sulcata* (Ehrenberg) Cleve and *Chaetoceros* spp.), are tied with the RP, the DA and the MWP. The four pulses also coincide with heavier $\delta^{13}C$ manifesting ventilation and turbulence. With the onset of the LIA, since AD 1300, diatom concentrations seem to diminish, coeval with a steady decrease in $\delta^{13}C$. This weakening of upwelling conditions is coherent with an increase in phytoliths (Gil *et al.*, 2006), ie, a shift to continental river inputs. Much higher fluxes ($\times 10$) characterize the last 100 years (Figure 5D), partially owing to better preservation. It is known that in general, one order of magnitude in the abundance of diatoms is lost by dissolution in the surface sediments, as well as diversity in the fossil assemblage (Bao *et al.*, 1997; Abrantes and Moita, 1999). During the last century, and in particular around AD 1900, brackish diatoms are more frequent, together with less negative $\delta^{13}C$, reaching the lightest values at present. This reinforces the climatic tendency to more continental influence since the onset of the LIA (Figure 5C). Spread of brackish diatoms and phytoliths for the last 150 years further confirm the very light $\delta^{18}O$ signal for this period, not only because of lower SST (Figure 3A) but also less saline waters.

In the Muros Ría, a single diatom record exists (EUGC-3B), but diatoms show higher abundances in the Muros Ría (two orders of magnitude) than in the Tagus Prodelta, with accumulation rate peaks over 1.5×10^8 valves/cm^2 per yr. This core, in the outer Ría, reveals a stronger diatom concentration between AD 270 and 670, marking three peak episodes, and a much weaker pulse around AD 50. There is some overlap with the earlier Tagus pulses (Figure 5D), encompassing the RP and partially the DA. Contrary to the

Figure 5 Comparison of productivity indicators between the Tagus Prodelta (red, darker red for PO287-26-3G) and the Muros outer (green) and inner (blue) Ría. A, Calcium carbonate; B, organic carbon; C, carbon stable isotopes; D, diatom accumulation rates (*Chaetoceros* in bold squares); E, benthic foraminifera species influenced by freshwater; and F, benthic foraminifera epifauna. We considered 'freshwater influence' the species driving in estuarine and shelf environments influenced by freshwater flux from rivers producing brackish water conditions. See text for details. Note change of scales between Tagus and Muros in C_{org}, $CaCO_3$, $\delta^{13}C$ and diatom AR. Also in the Tagus Prodelta records, change of scale in diatom AR for box PO287-26-1B and gravity core PO287-26-3G. The curve of ^{14}C solar activity from Figure 3D is given for reference. RP, Roman Period; DA, Dark Ages; MWP, 'Mediaeval Warm Period'; LIA, 'Little Ice Age'; 20th, twentieth century

Tagus Prodelta, light and quite constant $\delta^{18}O$ until AD 1100, poor water ventilation and an increment in 1 wt% of organic carbon (Figure 5B) point to diatom productivity as a result of nutrient input by the Tambre River, in a system that remained isolated from Atlantic influence. Varela *et al.* (2001) stated that although the Tambre fluvial output into the Ría is low, it can still be a significant source of nutrients for phytoplankton blooms. From AD 670 to 1470 (mid-MWP), diatom concentrations decay in the Muros. The assemblage itself changes too, from local benthic species, to open-ocean centrics (*Thalassiosira* spp., *Rhizosolenia* spp., Z.N. Stroynowski, personal communication, 2005) and, most notably, the assemblage shows an increase in *Chaetoceros* spp. Lower species diversity and the change in the species assemblage suggests an increase in frequency of upwelling events but the drop in productivity is interpreted as a decrease in preservation (Stroynowski, personal communication, 2006). This poor preservation could be due to a decrease in bottom waters or surface sediment porewater silica saturation (Bernárdez *et al.*, 2006). Unfortunately, we do not have the upper record of EUGC-3B and cannot verify the evolution of diatom concentrations in the Ría after AD 1470.

Benthic foraminifera are grouped, in the two areas, by (1) specific assemblages according to the different environments; (2) species tolerant to salinity changes that are good markers of periods of river discharge (referred to as a 'brackish' assemblage in the Tagus and an 'inner assemblage' in Muros, and integrated as 'fresh-water influence' in Figure 5E) or coastal upwelling (shelf assemblage for the Tagus and outer assemblage for Muros); and (3) indicators of labile (epifauna) or refractory organic matter availability at the bottom and, therefore, degree of ventilation of the water masses.

In the Tagus Prodelta, benthic foraminifera assemblages are dominated by typical continental shelf *Cassidulina laevigata*, *Hyalinea balthica*, *Bolivina* spp. and opportunistic species (Bartels-Jónsdóttir *et al.*, 2006). *C. laevigata* and *H. balthica*, show an inverse abundance until AD 900 and convergence since then (Bartels-Jónsdóttir *et al.*, 2006). Together they denote persistent upwelling for the period AD 400–1300. *H. balthica* and *Nonion commune* (*N. arterizans* according to Bartels-Jónsdóttir *et al.*, 2006) have also been related to upwelling by Levy *et al.* (1993) and Diz *et al.* (2002, 2006). Both are abundant for AD 0–400, and reflect high flux of fresh labile organic matter related to upwelling and primary productivity (Bartels-Jónsdóttir *et al.*, 2006). Around AD 1800 *H. balthica* becomes very rare, being almost absent in the last 100 years. At AD 1330, the onset of the LIA is marked by a significant faunal change to low foraminiferal fluxes and diversity because of reduced quality and quantity of food. *Bolivina* spp., together with *Stainforthia fusiformis*, show rather low values from AD 0 to 1300, after which they increase to the highest values during the last century (Bartels-Jónsdóttir *et al.*, 2006). These species show high correlation with the increasing organic carbon content, which is, at this location, mainly of terrigenous origin. Species tolerant to salinity changes or brackish environments, such as *Ammonia beccarii*, *Haynesina* spp. and *Elphidium* spp., compose an important group of the total assemblage (Bartels-Jónsdóttir *et al.*, 2006) (Figure 5E), showing two times higher average values from AD 0 to 1300 (includes the RP, DA and MWP) than during AD 1300–1850 (LIA). During the last century average abundance increases to similar values as in the MWP (10%). In the Tagus Prodelta, epibenthic foraminifera (species such as *Valvulineria bradyana*, *Cibicides* spp., *Cancris auriculus* and *Planorbulina mediterraniensis* that live at the surface of the sediment) decrease from 13% during AD 0–500, to 10% until AD 1300 and 8% to AD 1800 (Figure 5F). In soft sediments the epibenthic species also live in the top centimetre of the sediment (shallow infaunal) and are known to respond to good quality food levels at the sediment–water interface (Diz *et al.*, 2004). On the basis of benthic foraminiferal assemblages changes, Bartels-Jónsdóttir *et al.* (2006) distinguished four well-defined consecutive phases in the Tagus Prodelta waters for the last 2000 years, which fit the four climatic periods. In the RP (AD 0–400) upwelling conditions bring nutrients from deep waters, leading to flux of fresh labile organic matter; in the DA and MWP (AD 400–1400) even more persistent upwelling occurs; at AD 1300–1400 a significant climatic change happens with a decrease in the quality of food available in bottom waters presumably caused by river runoff that remains over the LIA (AD 1400–1800); and the last two centuries that are warm and reveal the effect of anthropogenic activities.

In the Muros Ría, the external site (EUGC-3B) is dominated by *Bulimina gibbalelongata*, *Nonion commune*, *Rectuvigerina phlegeri* and *Uvigerina* sp. (referred to as the outer Ría assemblage), while in the inner site (EUGC-2) *Eggerelloides scaber* and *Elphidium gerthi* (inner Ría assemblage), as well as epifaunal taxa (*C. refulgens*, *P. mediterranensis*, *Rosalina* spp., *G. praegeri*, *L. lobatula* and *E. pulchella*) are the most abundant. Similar assemblages are found in the neighbouring Vigo Ría (Diz *et al.*, 2004, 2006). In the Galician rías, *A. beccarii* is considered as a separated marker because its presence could indicate transport processes from shallower areas. EUGC-3B is dominated by high values (40–50%) of the outer Ría assemblage from AD 0 to 600 and between AD 1000 and 1200, low values occur between AD 850 and 1000, and there is a sharp decrease around AD 1200 (Figure 5E). The inner Ría assemblage in core EUGC-3B shows low-amplitude variability around 5% from AD 0 to 500, and higher amplitude centred at 8% between 500 and 1250 AD, followed by a gradual decrease. *A. beccarii* follows a similar pattern, with very low values after the abrupt change at AD 1250. In core EUGC-2, the inner assemblage exhibits increasing values (up to 30%) from AD 0 to 600 (Figure 5E), and then a progressive decrease is recorded to present times, on which important fluctuations are superimposed. *A. beccarii* oscillates around 5% up to AD 1250, when its percentage abundance declines as at the outer site. In the outer Muros Ría, the epifaunal species are rather stable until around AD 1100 when they increase and the $\delta^{13}C$ becomes heavier (Figure 5B). In the inner Ría, the epifauna falls slightly during the first 1000 years of the record collapsing at AD 500–700. This minimum coincides with a well-marked event of lighter carbon isotopes assumed to represent stagnant water. These species increase again during the last millennium reflecting steadily enhanced marine upwelling conditions (Figure 5F). The evolution of the assemblages during the last 2000 years emphasizes the different conditions between the outer and the inner sites, with core EUGC-3B and EUGC-2 dominated by the inner assemblage and the epifauna until AD 1100. Thus a widespread inner Ría benthic assemblage, associated with light and quite constant $\delta^{13}C$, and high organic carbon of terrestrial provenance, reveals local conditions until AD 1100 (Figure 5E). Progressively, after AD 1250 the outer assemblage becomes more abundant, indicating improved water ventilation, also supported by heavier $\delta^{13}C$ isotopes, suggesting a more active circulation caused by intrusion of upwelling waters that reach the inner part with a delay of 300 years. The Muros Ría behaviour resembles that of the Vigo Ría to the south (Diz *et al.*, 2002).

In summary, benthic foraminiferal assemblages are mainly controlled by water mass properties (temperature/salinity), and primary productivity and oxygen concentration in the bottom

(Figure 4). Even in shallow water environments it is difficult to discriminate the effect of these factors in benthic foraminiferal assemblages (van der Zwaan *et al.*, 1999). In the Tagus Prodelta, the assemblages show prevailing upwelling conditions until around AD 1300, when they are overtaken by river-induced productivity. Even in the Muros Ría assemblage, which shows only strictly local dynamics until AD 1150, the later period is influenced by the open marine regional Atlantic signal with invasion of upwelled waters. The strong 'suboxic' event detected between AD 550 and 700 in the inner Ría, is barely recognized either in the outer Ría or the Tagus Prodelta.

Evolution of Tagus Prodelta and Muros Ría sedimentary regimes during major climatic changes

The two sedimentary systems compared in this study are affected by different dominant marine and continental processes at different times. The Tagus Prodelta is situated in a marine domain affected by river discharge (from the Tagus River). The Muros Ría is a semi-enclosed environment dominated by continental input (Tambre River) and processes involving organic matter production and preservation, and is only temporarily influenced by more open coastal processes.

The Tagus Prodelta, between AD 400 and 1300, shows percentages of sand above 45%, corresponding with mean grain size greater than 70 μm. This sand fraction contains mainly biogenic particles such as marine foraminifera (Figures 6A, 4E). Before AD 400 sand values do not exceed 45% and from AD 1100 to present values decrease dramatically to about 10% around AD 1900, pointing to abrupt changes in the regime from dominant marine to fluvial inputs at ~AD 1300. Magnetic susceptibility variations represent magnetic minerals concentrated in the fine fraction (< 63 μm) (Figure 6B). Major elements, such as Fe, Ti, and K, widely considered as continental-derived markers (eg, Adegbie *et al.*, 2003) (Figure 6C) mimic magnetic susceptibility and finer grain-size fractions, supporting evidence for fine continental sediment input from river discharge. Instead, $CaCO_3$ content reflects abundant marine foraminiferal sands (Figure 5A). In general terms, low organic carbon coincides with low values of terrigenous markers (Fe, Ti, K) and greater grain size.

We have mean grain size data only for the outer Muros Ría core (EUGC-3B). Between AD 400 and 1100, sand rises to 27%, with a relative minimum around AD 600 (Figure 6A), consisting of biogenic grains, mainly fragmented mollusc shells and agglutinated foraminifera. In this interval Fe concentration is low (Figure 6C). A slow increase in the mud content occurs from AD 1100 to 1470 (top sequence is missing) in core EUGC-3B, suggesting the contribution of very fine biogenic components, probably calcareous nannoplankton (Figure 5A). Fe and Ti concentrations from AD 0 to 400 and AD 1100 to 1900 in cores EUGC-3B (outer Ría) and EUGC-2 (inner Ría) are high, corresponding to fine grain sizes. Over the last century, land markers (Fe, Ti, K) mimic the Tagus Prodelta record. Low TOC corrrelates with high terrigenous markers in the outer Ría, the inverse of the Tagus.

Comparing the two areas, there is double the amount of sand in the Tagus record than in the Muros Ría. At first glance, based on grain size and major land markers, the two sedimentary environments appear apparently similar: finer sediments and high Fe-Ti during the coldest periods and coarse biogenic sands and low Fe-Ti during warm periods. However, assumed correlation between Ca–Sr, and Fe–Ti, with provenance of marine and terrigenous components, respectively (eg, Arz *et al.*, 1999) is correct in the Tagus, but shows an inverse trend in Muros.

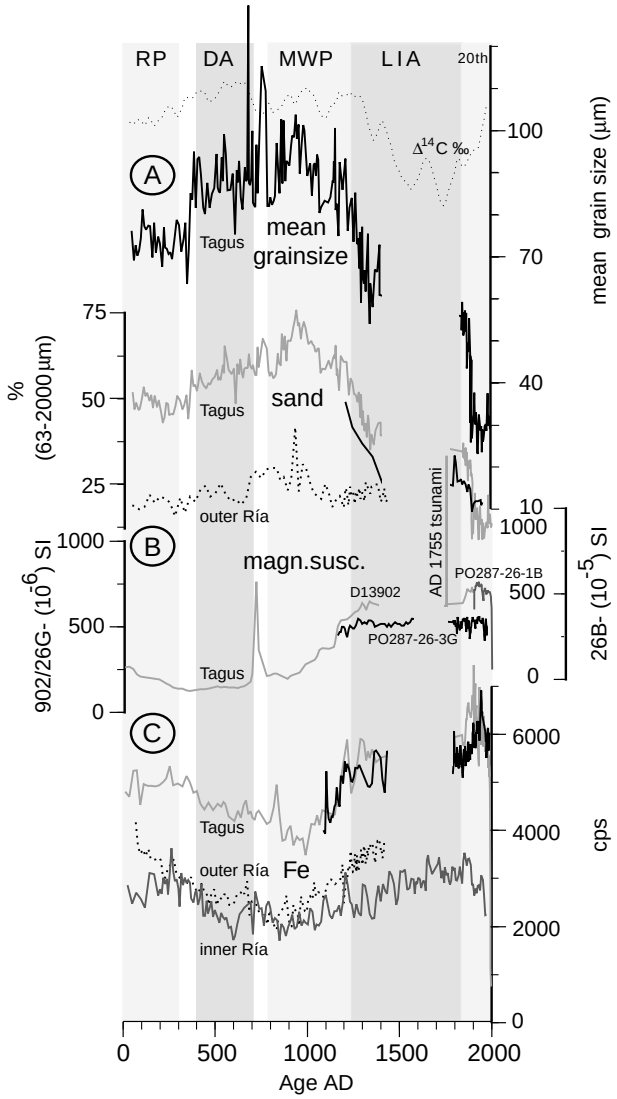

Figure 6 Comparison of land input indicators between the Tagus Prodelta and the Muros Ría. A, mean grain size and % sand; B, magnetic susceptibility; C, Fe in counts per second, similar to Ti and K. Note change of scale in magnetic susceptibility for the Tagus core PO287-26-1B. The curve of ^{14}C solar activity from Figure 3D is given for reference. RP, Roman Period; DA, Dark Ages; MWP, 'Mediaeval Warm Period'; LIA, 'Little Ice Age'; and 20^{th}, twentieth century. See text for details

Regarding the faunal species as independent indicators, the two sedimentation regimes diverge in their character. During the DA and MWP (AD 400 to 1300) in the Tagus Prodelta, coarse biogenic sand is of marine origin, concurrent with shelf foraminiferal species such as *C. laevigata* and upwelling-related diatom species, while in the Muros, coarse biogenic sand coincides with brackish foraminifera, the dominant inner assemblage, and more benthic diatoms, likely indicating freshwater discharge of the Tambre River. During the colder LIA (AD 1300–1850), high mud accumulation and Fe-land markers, but absence of diatoms in both areas, point to stratified waters. Although productivity is related to increased river-runoff in the Tagus Prodelta (Abrantes *et al.*, 2005a) intensification of upwelling conditions with better water ventilation occurs in Muros. In the neighbouring Vigo Ría, upwelling-related nannoplankton species dominate during the LIA (Álvarez *et al.*, 2005). Since AD 1900, the Tagus Prodelta has been under the influence of a strong continental regime, as proved by a 90% mud grain size and higher terrestrial Fe content, as well as high abundance of species dependent on refractory organic

matter (*Bulimina marginata*), presence of phytoliths, and lighter C and O isotope values. In Muros, a reinforcement of the upwelling conditions are indicated by heavier C isotopes and a higher proportion of marine foraminiferal species. Although we do not have a SST for the Muros Ría, Diz *et al.* (2002) show both $\delta^{18}O$ and SST curves for the Vigo Ría and, taking into account the close similarity between the Tagus and Muros isotope curves, we can assume a comparable SST (western Galicia). The twentieth-century SST show, for both south and north Iberia, temperatures similar to those characterizing the LIA.

Climate forcing mechanisms

The Holocene spectrum of the carbon isotope benthic foraminifera of core EUGC-3B was analysed by Pena *et al.* (L.D. Pena, G. Francés, P. Diz, M.A. Nombela and I. Alejo, unpublished data, 2006) who found a mean periodicity of 1500 ± 500 years (the so-called 'Bond events'). The DA and LIA would be the two most recent 'cold' isotopic events (Bond *et al.*, 2001). At the millennial-scale, Pena and co-authors attributed changes in hydrographic conditions to the N–S migration of the ENACWsp/ ENACWst front, and linked the cold episodes (warmer, eg, MWP) with enhancement of ENACWsp (ENACWst) upwelling, and hence heavier $\delta^{13}C$ (lighter), indicating ventilation at the sea floor, and retention of the organic matter produced in the Ría. Bond *et al.* (2001) demonstrated statistically significant coherence among records in millennial (hematite stained grains) and centennial (^{14}C, ^{10}Be) bands. It seems then that a solar forcing mechanism underlies the North Atlantic millennial-scale surface hydrographic changes (Stuiver *et al.*, 1997; Chapman and Shackleton, 2000; Bond *et al.*, 2001; Mayewski *et al.*, 2004). In fact, solar activity, reflected in atmospheric $\Delta^{14}C$ concentrations, forces changes in the oceanic circulation with centennial-scale (the 80 yr Gleissberg cycle) cyclicity (Keller, 2004). Several other authors have specifically coupled the MWP/LIA to changes in solar activity (Crowley, 2000; Bard *et al.*, 2000; Keller, 2004), including workers foccusing on Iberia (Diz *et al.*, 2002; Desprat *et al.*, 2003). Higher production rates of cosmogenic nuclides are related to reduced solar irradiance (Masarik and Beer, 1999).

If one looks into the higher frequency of curves from our Tagus and Muros sites, both millennial (DA, MWP, LIA) and centennial-scale variability is observed. Our proxies for temperature, salinity, primary productivity and water ventilation (oxygen and carbon isotopes, organic carbon, foraminifera and diatom records) match strikingly the atmospheric $\Delta^{14}C$ swings. This cannot be a coincidence. In the DA and MWP period, the Tagus foraminiferal oxygen isotopes follow closely each maximum/minimum of the solar activity curve (Figure 3A,D). In addition, the main concentration of diatoms match the three solar maxima (Figure 5D). High C_{org} (Figure 5B) and lower mean grain size values (Figure 6A) are, however, tied to reduced solar output. Therefore, indicators of oceanic circulation and dominant upwelling during the DA and MWP seem to have a more direct relationship with maximum solar centennial-scale irradiance. Conversely, indicators of terrestrial inputs coincide with minimum solar activity during the LIA. This is in agreement with our previous hypothesis of an oceanic (terrestrial) influenced MWP (LIA). According to Keller (2004) the magnitude of solar forcing does not necessarily respond to the amount of solar activity, as indirect solar forcings, like biogeochemical intermediate processes, could account significantly for climate variability. In fact, if we analyse the Muros Ría, for the same DA and MWP period, the primary productivity-related proxies are the ones connected with solar maxima. For example, what we called the 'suboxic' light $\delta^{13}C$ DA-event, localized in the inner Ría, is contemporaneous with diatom blooms, high C_{org}, reduced epifauna and flux of freshwater (Figure 5B–F) and links with the DA highest solar irradiance over the last 2000 years. Thus, in the Ría, solar forcing at a millennial scale seems to influence hydrographic changes, while primary production and organic carbon degradation processes appear to reflect the centennial scale of solar activity.

Most of our records reveal an enhancement of biogeochemical processes during the twentieth century not seen during the previous 1900 years. This might be due to less oxidation of sediment given the shorter passage of time since deposition. On the other hand, Mayewski *et al.* (2004) might be correct in stating that indirect natural feedbacks amplify the weak forcing related to fluctuations in solar output. Furthermore, Lean and Rind (2001) and Keller (2004) conclude that less than half of the twentieth-century warming was caused by an increase in solar irradiance.

However, hydrography is not only affected by millennial and/ or solar activity. At a multidecadal scale, the atmospheric NAO system with persistent positive (stronger pressure differences) and negative (weaker North–South gradient) modes during the MWP and LIA, respectively, seem to cause biogeochemical changes in the subtropical eastern North Atlantic (Abrantes *et al.*, 2005a), and also in the western North Atlantic (Sargasso Sea; Keigwin, 1996). In the Tagus Prodelta, long-term negative NAO characterizes the LIA, with storminess, excess precipitation and river discharge, while the MWP presents more frequent extreme positive NAO, producing enhanced upwelling (Abrantes *et al.*, 2005a). Álvarez *et al.* (2005) present the opposite scenario for DA-MWP and LIA at the Vigo Ría, in agreement with the climatic changes we propose here for the Muros Ría. After reconstructing precipitations for the last five centuries, Pauling *et al.* (2006) assert that winter precipitation over southern Iberia is mainly maintained by the negative NAO mode, whereas European winter precipitation is rather insensitive to NAO. The northwest of Iberia, Galician Rías Baixas, is positioned between the two NAO poles, explaining the contrary sedimentary conditions when compared with the Tagus during the MWP/LIA. The results of Pauling *et al.* (2006) also suggest that the connection of precipitation to large-scale atmospheric circulation over decadal timescales is not stable on its own, requiring complementary patterns, other than the NAO, to explain precipitation variability. Kirov and Georgieva (2002) go further, suggesting the influence of long-term solar activity on the NAO, forcing the position and strength of its poles. With respect to the DA, the Tagus light oxygen isotopes, SST and solar irradiance correlate with the North Atlantic low temperatures of Mann and Jones (2003), supposely regulated by the atmospheric NAO (Figure 3A,C,D). In detail, however, there are significant discrepancies, and biological feedbacks cannot be ignored.

Overall, in the Iberian peninsula, high-resolution sedimentary sequences reveal solar irradiance plus the NAO (or maybe the latter is also forced by solar irradiance), as the two (or one) main climatic driving mechanism(s) inducing changes in atmospheric and water circulation, and climate as a whole.

Conclusions

Solar activity and the NAO are the two forcing mechanisms behind the changes of temperature/salinity and primary production in the water and the sediment regimes in the Tagus

Prodelta and Muros Ría. Our biogeochemical proxies respond to climatic variability at millennial and centennial to the (multi-)decadal scales.

The most distinct change occurs at the transition between the MWP and the LIA in both areas, although with opposing hydrographic signals. In the Tagus, ocean circulation (productivity and coastal upwelling) dominates the MWP whereas precipitation (river flux and continental inputs into the shelf) takes over during the LIA. In the Muros, at AD 1200 a fluvial regime switches to an open marine regime. Before AD 1200, local processes related to productivity and organic carbon preservation characterize the Ría. We attribute these climatic changes to long NAO trends, either dominant river runoff mode (NAO^-) or dominant upwelling mode (NAO^+) in the northern and southern sites. The reversal in both areas depends on the latitudinal migration of the persistent position of the Azores/Lisbon and Iceland pressure poles. In the Tagus area it is also possible to distinguish the RP and DA on the basis of hydrographic changes. The DA could have been as warm as the MWP. In the inner Muros Ría, a 'suboxic' event is detected in the DA (AD 500–700). Solar irradiance maxima and minima are closely connected to biogeochemical changes in both areas over the last 2000 years.

Acknowledgements

We are grateful to participants and crews of *Discovery* 249, *Poseidon* PALEO I, and B/O *Mytilus* cruises, and for laboratory technical assistance in grain size, LECO, isotopes, foraminifera and diatoms at the INETI-Laboratory of Marine Geology. Thanks to C. Kissel for the magnetic susceptibility measurements in Gif-sur-Yvette, to M. Siegl for isotope measurements and the ARI-Program at the University of Bremen, to E. Salgueiro and S. Vaqueiro for XRF measurements at the Bremen Core Repository, to J. Heinemeier for helpful discussions during the construction of age models, to A. Ferreira for critical data discussion and A. Voelker for comments on the manuscript. The comments of an anonymous reviewer helped to improve the final version of this paper. Financial support was provided by EU project HOLSMEER (EVK2-CT-2000-00060). T. Rodrigues was supported by the Fundação para a Ciência e Tecnologia, INGMAR project.

References

Abrantes, F. 1988: Diatom assemblages as upwelling indicators in surface sediments off Portugal. *Marine Geology* 85, 15–39.

Abrantes, F. and **Moita, T.** 1999: Water column and recent sediment data on diatoms and coccolithophorids, off Portugal, confirm sediment record as a memory of upwelling events. *Oceanologica Acta* 22, 319–36.

Abrantes, F., Lebreiro, S., Rodrigues, T., Gil, I., Bartels-Jónsdóttir, H., Oliveira, P., Kissel, C. and **Grimalt, J.O.** 2005a: Shallow marine sediment cores record climate variability and earthquake activity off Lisbon (Portugal) for the last 2,000 years. *Quaternary Science Reviews* 24, 2477–94.

Abrantes, F., Gil, I., Lopes, C. and **Castro, M.** 2005b: Quantitative diatom analyses – a faster cleaning procedure. *Deep-Sea Research I* 52, 189–98.

Adgebie, A.T., Schneider, R.R., Röhl, U. and **Wefer, G.** 2003: Glacial millennial-scale fluctuations in central African precipitation recorded in terrigenous sediment supply and freshwater signals offshore Cameroon. *Palaeogeography, Palaeoclimatology, Palaeoecology* 197, 323–33.

Álvarez, M.C., Flores, J.A., Sierro, F.J., Diz, P., Francés, G., Pelejero, C. and **Grimalt, J.** 2005: Millennial surface water dynamics in the Ría de Vigo during the last 3000 years as revealed by coccoliths and molecular biomarkers. *Palaeogeography, Palaeoclimatology, Palaeoecology* 218, 1–13.

Álvarez-Salgado, X.A., Rosón, G., Pérez, F.F. and **Pazos, Y.** 1993: Hydrographic variability off the Rías Baixas (NW Spain) during the upwelling season. *Journal of Geophysical Research* 98, 14 447–55.

Antoine, D. and **Morel, A.** 1996: Oceanic primary production 1. Adaptation of a spectral light-photosynthesis model in view of application to satellite chrorophyll observations. *Global Biogeochemical Cycles* 10, 43–55.

Arz, H.W., Patzold, J. and **Wefer, G.** 1999: Climatic changes during the last deglaciation recorded in the sediment cores from the northeastern Brazilian Continental Margin. *Geo-Marine Letters* 19, 209–18.

Bao, R., Varela, M. and **Prego, R.** 1997: Mesoscale distribution patterns of diatoms in surface sediments as tracers of coastal upwelling on the Galician Shelf (NW Iberian Peninsula). *Marine Geology* 144, 117–30.

Barber, R.T. and **Smith, R.L.** 1981: Coastal upwelling ecosystems. In Longhurst, A.R., editor, *Analysis of marine systems*. Academic Press, 33–68.

Bard, E., Raisbeck, G., Yiou, F. and **Jouzel, J.** 2000: Solar irradiance during the last 1200 years based on cosmogenic nuclides. *Tellus B* 52, 985–91.

Bartels-Jónsdóttir, H.B., Knudsen, K.L., Abrantes, F., Lebreiro, S. and **Eiríksson, J.** 2006: Climate variability during the last 2000 years in the Tagus Prodelta, western Iberian Margin: benthic foraminifera and stable isotopes. *Marine Micropaleontology* 59, 83–103.

Battarbee, R.W. 1973: A new method for estimation of absolute microfossil numbers with reference especially to diatoms. *Limnology Oceanography* 18, 647–52.

Behrenfeld, M.J., Randerson, J.T., McClain, C.R., Feldman, G.C., Los, S.O., Tucker, C.J., Falkowski, P.G., Field, C.B., Frouin, R., Esaias, W.E., Kolber, D.D. and **Ollack, N.H.** 2001: Biosphere primary production during an ENSO transition. *Science* 291, 2594–97.

Bernárdez, P., Francés, G. and **Prego, R.** 2006: Benthic–pelagic coupling and postdepositional processes as revealed by the distribution of opal in sediments: the case of the Ría de Vigo (NW Iberian Peninsula). *Estuarine, Coastal and Shelf Science*, in press.

Bond, G., Kromer, B., Beer, J., Musceler, R., Evans, M.N., Showers, W., Hoffmann, S., Lotti-Bond, R., Hajdas, I. and **Bonani, G.** 2001: Persistent solar influence on North Atlantic climate during the Holocene. *Science* 294, 2130–36.

Bode, A., Casas, B. and **Varela, M.** 1994: Size-fractioned primary productivity and biomass in the Galizian shelf (NW Spain): net plankton versus nanoplankton dominance. *Sciencia Marina* 58, 131–41.

Bradley, R.S. and **Jones, P.D.** 1993: 'Little Ice Age' summer temperature variations: their nature and relevance to recent global warming trends. *The Holocene* 3, 367.

Broecker, W.S. and **Peng, T.H.** 1982: *Tracers in the sea*. Eldigio Press.

Brown, P. and **Field, J.** 1986: Factors limiting phytoplankton production in a nearshore upwelling area. *Journal of Plankton Research* 8, 55–68.

Brown, P., Painting, S. and **Cochraine, K.** 1991: Estimates of phytoplankton and bacterial biomass and production in the northern and southern Benguela ecosystems. *South African Journal of Marine Science* 11, 537–64.

Cabeçadas, G. and **Brogueira, M.J.** 1997: Sediments in a Portuguese coastal area – pool sizes of mobile and immobile forms of nitrogen and phosphorus. *Marine Freshwater Research* 48, 559–63.

Chapman, M.R. and **Shackleton, I.N.** 2000: Evidence of 550-year and 1000-year cyclicities in North Atlantic circulation patterns during the Holocene. *The Holocene* 10, 287–91.

Crowley, T. 2000: Causes of climate change over the past 1000 years. *Science* 289, 270–77.

Desprat, S., Sánchez-Goñi, M.F. and **Loutre, M.-F.** 2003: Revealing climatic variability of the last three millennia in northwestern Iberia using pollen influx data. *Earth and Planetary Science Letters* 213, 63–78.
Diz, P., Francés, G., Pelejero, C., Grimalt, J.O. and **Vilas, F.** 2002: The last 3000 years in the Ría de Vigo (NW Iberian Margin): climatic and hydrographic signals. *The Holocene* 12, 459–68.
Diz, P., Francés, G., Costas, S., Souto, C. and **Alejo, I.** 2004: Distribution of benthic foraminifera in coarse sediments, Ría de Vigo, NW Iberian Margin. *Journal of Foraminiferal Research* 34, 258–75.
Diz, P., Francés, G. and **Rosón, G.** 2006: Effects of contrasting upwelling–downwelling on benthic foraminiferal distribution in the Ría de Vigo (NW Spain). *Journal of Marine Systems* 60, 1–18.
Estrada, M. 1984: Phytoplankton distribution and composition off the coast of Galizia (NW Spain). *Journal of Plankton Research* 6, 417–34.
Fisher, G. and **Wefer, G.,** editors 1999: *Use of proxies in paleoceanography: examples from the south Atlantic*. Springer, 1–68.
Fiúza, A.F.G. 1983: Upwelling pattern off Portugal. In Suess, E. and Thiede, J., editors, *Coastal upwelling: its sediment record.* Plenum, 85–98.
Fraga, F. 1981: Upwelling off the Galician coast, NW Spain. In Richards, F.A., editor, *Coastal upwelling*. American Geophysical Union, 176–82.
Fraga, F. and **Margalef, R.** 1979: Las Rías Gallegas. In Universidad de Santiago de Compostera, editor, *Estudio y explotación del mar en Galicia*, *La Coruña*. University of Santiago, 101–21.
Gil, I.M., Abrantes, F. and **Hebbeln, D.** 2006: The North Atlantic Oscillation forcing through the last 2000 years: spatial variability as revealed by high-resolution marine diatom records from N and SW Europe. *Marine Micropaleontology* 60, 113–29.
Hass, H.C. 1996: Northern Europe climate variations during the late Holocene: evidence from marine Skagerrak. *Palaeogeography, Palaeoclimatology, Palaeoecology* 123, 121–45.
Hughes, M.K. and **Diaz, H.F.** 1994: Was there a 'Medieval Warm Period' and if so, where and when? *Climate Change* 26, 109.
Hurrell, J.W. 1995: Decadal trends in the North Atlantic Oscillation: regional temperatures and precipitation. *Science* 269, 676–79.
Jansen, J.H.F., van der Gaast, S.J., Koster, B. and **Vaars, A.J.** 1998: CORTEX, a shipboard XRF-scanner for element analysis in split sediment cores. *Marine Geology* 151, 143–53.
Jones, P.D. and **Mann, M.** 2004: Climate over the past millennia. *Reviews of Geophysics* 42, 1–42.
Jones, P.D., Osborn, T.J. and **Briffa, K.R.** 2001: The evolution of climate over the last millennium. *Science* 292, 662–67.
Keigwin, L.D. 1996: The Little Ice Age and Medieval Warm Period in the Sargasso Sea. *Science* 274, 1504–508.
Keigwin, L.D. and **Pickart, R.S.** 1999: Slope water current over the Laurentian Fan on interannual to millenial time scales. *Science* 286, 520–23.
Keller, C.F. 2004: 1000 years of climate change. *Advances in Space Research* 34, 315–22.
Kirov, B. and **Georgieva, K.** 2002: Long-term variations of ENSO, NAO and solar activity. *Physics and Chemistry of the Earth* 27, 441–48.
Lamb, H.H. 1985: *Climate history and the future*. Princeton University Press, 835 pp.
Lean, J. and **Rind, D.** 2001: Earth's response to a variable sun. *Science* 292, 234–36.
Levy, A., Mathieu, R., Poignant, A., Rosset-Moulinier, M., Ubaldo, M.L. and **Ambroise, D.** 1993: Recent foraminifera from the continental margin of Portugal. *Micropaleontology* 39, 75–87.
Loureiro, J.M. 1979: *Curvas de duração dos caudais médios diários no rio Tejo*. Technical Report, Serviço Hidráulico (DGRAH), Lisbon.
Mann, M.E. and **Jones, P.D.** 2003: Global surface temperatures over the past two millennia. *Geophysical Research Letters* 30, 5.1–5.4.
Masarik, J. and **Beer, J.** 1999: Simulation of particle fixes and cosmogenic nuclide production in the Earth's atmosphere. *Journal of Geophysics Research* 104, D10, 12099.
Mayewski, P.A., Rohling E.E., Stager, J.C., Karlén, W., Maasch, K.A., Meeker, L.D., Meyerson, E.A., Gasse, F., van Kreveld, S., Holmgren, K., Lee-Thorp, J., Rosqvist, G., Rack, F., Staubwasser, M., Schneider, R.R. and **Steig, E.J.** 2004: Holocene climate variability. *Quaternary Research* 62, 243–55.
Mikkelsen, N. and **Kuijpers, A.** 2001: *Natural climate variations in a geological perspective*. Gads Forlag.
Moita, M.T. 2001: Estructura, variabilidade e dinâmica do fitoplâncton na costa de Portugal continental. Ph.D. Thesis, Universidade de Lisboa, 272 pp.
Monteiro, H. and **Moita, I.** 1971: Morfologia e sedimentos da plataforma continental e vertente continental superior ao largo da Penísula de Setúbal. *Congresso de Geologia*, 301–30.
Nogueira, E., Pérez, F. and **Ros, A.** 1997: Seasonal patterns and long-term trends in an estuarine upwelling ecosystem (Ría de Vigo, Spain). *Estuarine, Coastal and Shelf Science* 44, 285–300.
Nunes, T., Mariño, J., Iglesias, M., González, N., Campos, M.J. and **Cabanas, J.M.** 1984: Condiciones ambientales, producción primaria y sucesión de especies fitoplanctónicas en la Ría de Arousa (NW de España). *Cuadernos Area Ciencias Mariñas, Sem. Estudios Galegos* 1, 163–72.
Oliveira, A., Rocha, F., Jouanneau, J., Dias, A., Weber, O. and **Gomes, C.** 2002: Clay minerals from the sedimentary cover from the Northwest Iberian shelf. *Progress in Oceanography* 52, 233–47.
Pauling, A., Luterbacher, J., Casty, C. and **Wanner, H.** 2006: Five hundred years of gridded high-resolution precipitation reconstructions over Europe and the connection to large-scale circulation. *Climate Dynamics* 26, 387–405.
Pilskaln, C., Paduan, J., Chavez, F., Anderson, R. and **Berelson, W.** 1996: Carbon export and regeneration in the coastal upwelling system of Monterey Bay, central California. *Journal of Marine Research* 54, 1149–78.
Prego, R. 1990: Las sales nutrientes en las rías gallegas. *Informe Técnico Scientia Mariña* 157, 31.
——. 1993: General aspects of carbon biogeochemistry in the Ría of Vigo, northwestern Spain. *Geochimica Cosmochimica Acta* 57, 2041–52.
Ríos, A.F., Pérez, F.F. and **Fraga, F.** 1992: Water masses in the upper and middle North Atlantic Ocean east of the Azores. *Deep-Sea Research* 39, 645–58.
Rodrigues, T. 2004: Climatic variation and terrigenous input in the Tagus Prodelta during the last 13.5 kyr. Masters Thesis, University of Aveiro, 117 pp.
Schrader, H-J. and **Gersonde, S.** 1978: Diatoms and silicoflagellates. *Utrecht Micropaleontological Bulletin* 17, 12–17.
Shackleton, N.J. 1974: Attainment of isotopic equilibrium between ocean water and the benthonic foraminifera genus *Uvigerina*: isotopic changes in the ocean during the last Glacial. *Colloques Internationaux du C.N.R.S.* 219, 203–209.
Stuiver, M., Braziunas, T.F., Grootes, P.M. and **Zielinski, G.A.** 1997: Is there evidence for solar forcing of climate in the GISP2 oxygen isotope record? *Quaternary Research* 48, 259–66.
Stuiver, M., Reimer, P.J. and **Braziunas, T.F.** 1998a: High precision radiocarbon age calibration for terrestrial and marine samples. *Radiocarbon* 40, 1127–51.
Stuiver, M., Reimer, P.J., Bard, E., Beck, J.W., Burr, G.S., Hughen, K.A., Kromer, B., McCormac, F.G., van der Plicht, J. and **Spurk, M.** 1998b: INTCAL 98 radiocarbon age calibration, 24,000–0 cal BP. *Radiocarbon* 40, 1041–83.
Trigo, R.M., Osborn, T.J. and **Corte-Real, J.** 2002a: The North Atlantic Oscillation influence on Europe: climate impacts and associated physical mechanisms. *Climate Research* 20, 9–17.
—— 2002b: Influência da Oscilação do Atlântico Norte no clima do continente Europeu e o caudal dos rios ibéricos Atlânticos. *Finisterra* 37, 5–31.
Vale, C. and **Sundby, B.** 1987: Suspended sediment fluctuations in the Tagus estuary on semi-diurnal and fortnightly time scales. *Estuarine, Coastal and Shelf Science* 25, 495–508.
Van der Zwaan, G.J., Duijnstee, L.A.P., den Dulk, M., Ernest, S.R., Jannink, N.T. and **Kouwenhoven, T.J.** 1999: Benthic foraminifers,

proxies or problems? A review of paleoecological concepts. *Earth Science Reviews* 46, 213–36.

Varela, M., Campos, M.J., Penas, E., Sánchez, J., Larrañaga, A., de Castillejo, F.F., del Río, G.D. and **Cabanas, J.M.** 1987: Composición y distribución del fitoplacton en la plataforma de Galicia durante la campaña Breogán-684 (junio 1984). *Boletín del Instituto Español de Oceanografía* 4, 75–94.

Varela, M., Prego, R., Belzunce, M.J. and **Salas, F.M.** 2001: Inshore–offshore differences in seasonal variations of phytoplankton assemblages: the case of a Galician Ría Alta (Ría de A Coruña) and its adjacent shelf (NW Spain). *Continental Shelf Research* 21, 1815–38.

Varela, R.A., Rosón, G., Herrera, J., Torres-López, S. and **Fernández-Romero, A.** 2005: A general view of the hydrographic and dynamical patterns of the Rias Baixas adjacent shelf area. *Journal of Marine Systems* 54, 97–114.

Zahn, R. and **Sarnthein, M.** 1987: Benthic isotope evidence for changes of the Mediterranean Outflow during the late Quaternary. *Paleoceanography* 2, 543–59.

Appendix 2

VARIABILITY OF THE NORTH ATLANTIC CURRENT DURING THE LAST 2000 YEARS BASED ON SHELF BOTTOM WATER AND SEA SURFACE TEMPERATURES ALONG AN OPEN OCEAN/SHALLOW MARINE TRANSECT IN WESTERN EUROPE

Jón Eirýksson[1*], Helga Bára Bartels-Jónsdóttir,[2] Alix G. Cage,[3] Esther Ruth Gudmundsdóttir[1], Dorthe Klitgaard-Kristensen[4], Fabienne Marret[5], **Teresa Rodrigues[6],** Fatima Abrantes[6], William E.N. Austin[3], Hui Jiang[7], Karen-Luise Knudsen[2] and Hans-Petter Sejrup[8]

1Earth Science Institute, Askja, University of Iceland, IS-101 Reykjavý´k, Iceland;
2Department of Earth Sciences, University of Aarhus, DK-8000 Aarhus C, Denmark;
3School of Geography and Geosciences, University of St Andrews, StAndrews KY16 9AL, UK;
4Norwegian Polar Institute, Polar Environmental Centre, 9296 Tromsø, Norway;
5Department of Geography, University of Liverpool, Roxby Building, Liverpool L69 7ZT, UK;
6Instituto Nacional de Engenharia, Tecnologia e Inovac¸a˜o, Departamento de Geologia Marinha (INETI-DGM), PT-2720 Alfragide, Portugal;
7State Key Laboratory of Estuarine and Coastal Research, East ChinaNormal University, 200062 Shanghai, P.R. China;
8Department of Earth Sciences, University of Bergen, Allegaten 41, N-5007 Bergen, Norway)

The Holocene **16**, 1003-1015 (2006)

The Holocene 16,7 (2006) pp. 1017–1029

Variability of the North Atlantic Current during the last 2000 years based on shelf bottom water and sea surface temperatures along an open ocean/shallow marine transect in western Europe

Jón Eiríksson,[1]* Helga Bára Bartels-Jónsdóttir,[2] Alix G. Cage,[3] Esther Ruth Gudmundsdóttir,[1] Dorthe Klitgaard-Kristensen,[4] Fabienne Marret,[5] Teresa Rodrigues,[6] Fatima Abrantes,[6] William E.N. Austin,[3] Hui Jiang,[7] Karen-Luise Knudsen[2] and Hans-Petter Sejrup[8]

([1]Earth Science Institute, Askja, University of Iceland, IS-101 Reykjavík, Iceland; [2]Department of Earth Sciences, University of Aarhus, DK-8000 Aarhus C, Denmark; [3]School of Geography and Geosciences, University of St Andrews, St Andrews KY16 9AL, UK; [4]Norwegian Polar Institute, Polar Environmental Centre, 9296 Tromsø, Norway; [5]Department of Geography, University of Liverpool, Roxby Building, Liverpool L69 7ZT, UK; [6]Instituto Nacional de Engenharia, Tecnologia e Inovação, Departamento de Geologia Marinha (INETI-DGM), PT-2720 Alfragide, Portugal; [7]State Key Laboratory of Estuarine and Coastal Research, East China Normal University, 200062 Shanghai, P.R. China; [8]Department of Earth Sciences, University of Bergen, Allegaten 41, N-5007 Bergen, Norway)

A HOLOCENE SPECIAL ISSUE

Abstract: Marine localities on the west European shelf have been studied to reconstruct the nearshore palaeoceanography of the last two millennia. The sites form a transect from the Iberian margin northeastward via Scotland to western Norway and Iceland. Proxies used for palaeoclimatic reconstructions include stable isotopes, benthic and planktonic foraminfera, diatoms, dinoflagellates, as well as geochemical and sedimentological parameters. Major changes as well as long-term trends in oceanographic conditions are observed in the records, including a general cooling trend through much of the last millennium. There is a clear linkage between the atmospheric processes and the oceanic circulation, and the ocean temperature variability in the records can be correlated with the so-called 'Mediaeval Warm Period' and 'Little Ice Age'. These oscillations are, however, by no means unique within the last two millennia. As an example, sea surface temperatures to the north of Iceland and on the Iberian margin were higher in the Roman Warm Period than at any time during the 'Mediaeval Warm Period'. However, the palaeoceanographic record generally supports a distinct cooling at the transition between the 'Mediaeval Warm Period' and the 'Little Ice Age'. While a number of records indicate a warming of coastal and shelf waters during the last 200 years, the twentieth century does not appear to be unusual when the proxy records spanning the last two millennia are examined.

Key words: North Atlantic Ocean, sea surface temperature, climate variability, palaeoceanography, North Atlantic Current, Holocene, HOLSMEER project.

*Author for correspondence (e-mail: jeir@hi.is)

 10.1177/0959683606hl991rp

Introduction

This study aims to add information to, and improve understanding of, temporal and spatial palaeoceanographic varibility along the eastern part of the northern North Atlantic on a common timescale. The sites range from being proximal to the path of the North Atlantic Current to the southern boundary of the Arctic, providing an extensive overview of the coastal realms in northwestern and western Europe. The target of the project is an acquisition of reliably dated continuous climate records from the coastal realm covering the last two millennia.

One of the objectives of the HOLSMEER project (Late Holocene Shallow Marine Environments of Europe) (Scourse *et al.*, 2006, this issue) was to obtain data on the natural variability of the regional ocean circulation in order to understand processes governing the climate system of western Europe. For the documentation of temporal changes in water masses affecting European shelf environments during the last two millennia, marine sediment cores from shelf settings off North Iceland, Western Norway and Iberia, as well as Scotland have been studied (Figure 1).

Natural variability of the ocean circulation on millennial timescales has played a major role in the past global climate system. The termination of the last glacial cycle in the northern North Atlantic and the transition involving climate–ocean reorganization from the glacial ocean into the Holocene one is a well-documented example (Ruddiman, 1977; Ruddiman and McIntyre, 1981; Duplessy *et al.*, 1981; Bond *et al.*, 1992, 1993; Kroon *et al.*, 1997; Boessenkool *et al.*, 2001). Most studies indicate that this transition was associated with variability in the position and shape of the oceanographic Polar Front separating Atlantic and Arctic surface water masses.

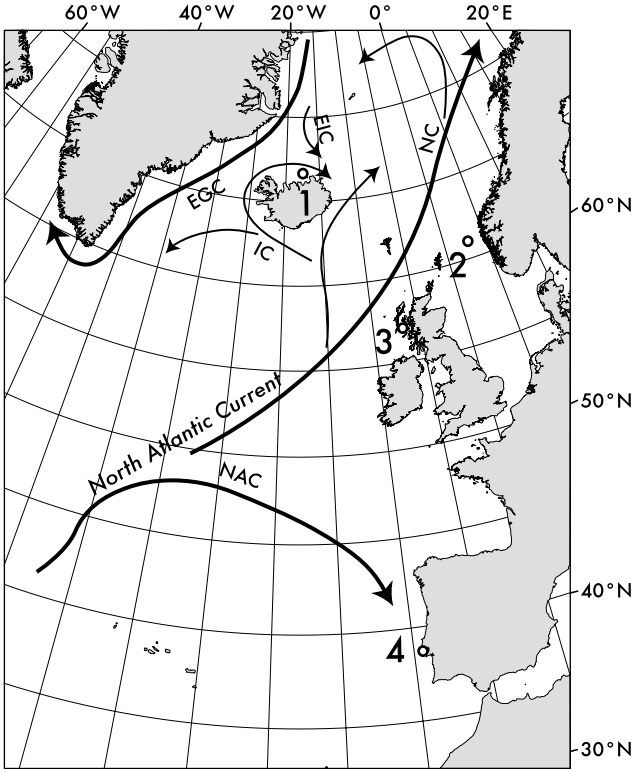

Figure 1 Location map and modern surface ocean circulation in the northern North Atlantic. 1, North Iceland shelf; 2, Norwegian margin (Norwegian Channel); 3, Scottish Sea Loch (Loch Sunart); 4, Iberian margin off Portugal (Tagus Prodelta). NAC, North Atlantic Current; NC, Norwegian Current; EGC, East Greenland Current; IC, Irminger Current; EIC, East Icelandic Current

For the Holocene, it has been suggested that climatic conditions related to the strength of the Atlantic's conveyor circulation have been modulated over a period of around 1500 years (Bond *et al.*, 1999). Major components of the ocean circulation in the region include the North Atlantic Current carrying warm, saline surface waters from low latitudes towards Europe, and the East Greenland Current outflow from the Arctic Ocean through the Fram Strait, carrying sea ice and cold, fresh surface waters into the Nordic Seas and the northern North Atlantic Ocean (Hansen and Østerhus, 2000). The role of the inflow of Arctic Water into the northern North Atlantic and the Nordic Seas was exemplified by so-called salinity anomalies that occurred during the latter half of the twentieth century (Malmberg, 1984; Dickson *et al.*, 1988; Belkin *et al.*, 1998). These events were characterized by lowered sea surface salinity and temperature, and increased sea ice in the Iceland Sea (Dickson *et al.*, 1988).

The strength of the North Atlantic Current is generally related to deep water formation in the Nordic Seas, which is again associated with southward overflow across the Greenland-Iceland-Faeroe-Scotland Ridge (Swift, 1986; Dickson *et al.*, 1996). The North Atlantic Current is expected to be strong during active deep water formation and weak during periods of freshening of the surface waters north and northeast of Iceland, ie, during periods with strong input of Polar Water from the East Greenland Current and the East Icelandic Current (Dickson *et al.*, 1996; Malmberg and Jónsson, 1997).

During the present interglacial, the Holocene (11 500 cal. yr BP to the present), relatively stable atmospheric conditions are indicated by one of the most important Northern Hemisphere climate data archives available, the Greenland ice core stable isotope record (Dansgaard *et al.*, 1971; Johnsen *et al.*, 1972, 1992; O'Brien *et al.*, 1995). Holocene variability, however, is recorded in the Greenland ice cores by several other geochemical parameters (Mayewski *et al.*, 1994). In a recent review of Holocene climate data archives, Mayewski *et al.* (2004) concluded that the Holocene climate has been highly variable on a millennial timescale, incorporating several rapid climate change events, with the early Holocene events being related to or influenced by the glacial world scenario because the Northern Hemisphere ice caps were still melting away.

The HOLSMEER project addresses important questions related to the background levels of natural climate variability versus modern industrialization-induced global warming, and the combination of many sites, multiple proxies and high temporal resolution adds to the value of the project for understanding the ocean–atmosphere interaction in the region.

The North Iceland HOLSMEER sites were chosen because they are located at the Polar Front boundary between warm and cold surface water masses, recording changes in temperature, salinity and sea ice, whereas the Norwegian, Scottish and Iberian sites reflect variability in the surface temperature related to the physical properties of the North Atlantic Current, the strength of the global thermohaline circulation and atmospheric and oceanic circulation variability.

A number of micropalaeontological, chemical and sedimentological proxies were studied along an open ocean transect extending from the Iberian margin to Scotland, western Norway and Iceland. Comparing the various proxies within a site and between sites is, however, not always straightforward because, although the sites are located at shallow-water localities, some of the proxies reflect surface parameters while others are related to bottom conditions. This depth variability adds to seasonal variability, which also has to be taken into account. Seasonality is quite pronounced at the North Iceland

shelf with Atlantic Water dominating the water column during summer and autumn, while Arctic waters, cooling and vertical mixing dominate the water column during the winter months, to create a new water mass (Stefánsson, 1962; Hurdle, 1986; Johannesen *et al.*, 1994). On the Scottish west coast, the development of seasonal stratification of the water column is initiated in April/May and normally breaks down in October.

Seasonality is also quite marked at the Iberian margin, with southward flow of surface currents and more enhanced upwelling during summer months while the winter months are characterized by a northward flow of surface currents (Fiúza, 1983). The Portuguese HOLSMEER site is furthermore influenced by fluvial runoff during winter months (Trigo *et al.*, 2002; Abrantes *et al.*, 2005).

Sites and research methods

Site information and core material

Iberian margin

The surface water masses found along the Portuguese margin mainly originate from the North Atlantic Current, being affected by narrow, warm, northward-flowing currents during the autumn and winter and by the southward-flowing cool Portugal Current during summers (Fiúza, 1983). The surface waters of the Portuguese margin are also affected by freshwater runoff and seasonal upwelling. These water masses constitute the surface mixed layer down to the thermocline at about 70–110 m (Schönfeld, 1997). The water depth at the coring sites is close to the thermocline depth. Below the thermocline, the interval down to 600 m is occupied by the North Atlantic Central Water (NACW). This water mass plays an important role in the summer upwelling, which is an important feature of the present-day oceanography along the Iberian margin. During periods of persistent northerly winds, the surface mixed layer along the coast is displaced westward by the Coriolis force, being compensated by upwelling of cool, nutrient-rich NACW water. The present-day oceanographic conditions along the Iberian margin are thus sensitive to the wind regime and to precipitation and runoff from the Tagus. According to Abrantes *et al.* (2005), the modern sea surface temperature values range from 15.5°C (winter) to 19.5°C (summer).

Samples from the Iberian margin were obtained on two oceanographic cruises, RV *Discovery* 249, and the PALEO1 on the RV *Poseidon* (Lebreiro *et al.,* 2006, this issue). A composite sequence is used from intervals of piston core D13902 (600 cm long), gravity core PO287-26-3G (305.5 cm) and box core PO287-26-1B (33 cm) retrieved from the southern part of the Tagus Prodelta at 90 and 96 m water depth (Figure 1). Data from the intervals 18–150 cm of core PO287-26-3G and 240–400 cm of core D13902 were included, together with the entire box core. The chronology for the composite sequence is based on calibrated radiocarbon dates and using data from the age model presented by Abrantes *et al.* (2005), modified by Bartels-Jónsdóttir *et al.* (2006). Results presented here include stable isotope analyses as well as alkenone biomarker analyses for the calculation of sea surface temperatures on the basis of the UK' 37 index.

West Scotland margin

Samples from the northwest British margin were obtained from Loch Sunart, a sea loch (fjord) on the west coast of Scotland (GC023, 56°40.324′N, 5°50.328′W). Stable isotope data have been obtained from the benthic environment of the main sedimentary basin of the sea loch, which maintains a connection with the open shelf through frequent deep-water renewal events across a deep (> 30 m) rock sill (Gillibrand *et al.*, 2002, 2005). The age model for the core is based on radiocarbon dating of marine bivalved molluscs (eg, Cage, 2005), but the record post AD 1100 is either missing or disturbed by coring processes. Summer bottom water temperatures in the loch have been estimated using a benthic foraminiferal transfer function approach modified after Sejrup *et al.* (2004; Cage, 2005). The Loch Sunart basin, despite its restricted coastal location, is strongly influenced by exchange with coastal water. It therefore provides a site of exceptionally high sediment accumulation (up to 0.5 cm/yr) and provides proxy records that reflect both variability in the physical properties (primarily temperature) of the North Atlantic and the strength of westerlies in the region. The latter, which is an important forcing mechanism in fjordic hydrography, is very closely coupled to the predominant mode of atmospheric forcing at this latitude, namely the North Atlantic Oscillation (eg, Ruprecht *et al.*, 2002; Trigo *et al.*, 2002).

Norwegian margin

The main water masses in the Norwegian Channel are the Atlantic Water and Norwegian Coastal Current waters. The continuation of the North Atlantic Current, the Norwegian Current transports warm, saline water into the southeastern Nordic Seas along the Norwegian continental margin. A branch of the Norwegian Current flows into the Norwegian Channel, following the western slope of the channel towards the south (Furnes *et al.*, 1986), and is the main route for the import of Atlantic Water (7.5–9.0°C, salinity > 35 psu) into the North Sea. The other major current in the Norwegian Channel is the Norwegian Coastal Current (NCC; temperature 3–18°C, salinity < 34.7 psu) that flows along the Norwegian coast (data retrieved 28 June 2006 from http://www.imr.no). During wintertime, the NCC is expressed in a well-defined wedge-shaped water mass that reaches down to 150 m water depth at the Norwegian coast, whereas during summertime large sea surface lateral extensions westwards onto the North Sea plateau are observed as result of the wind stress forcing (Furnes *et al.,* 1986).

From the Norwegian Channel two cores (Figure 1), the box core HM115-16TBC (60°51.991′N, 03°43.955′E, water depth 338 m, length 38 cm) and the gravity core HM115-16GC (60°52′N, 03°44′E, water depth 345, length 475 cm) have been investigated for content of organic walled dinoflagellates, benthic and planktonic foraminiferal faunas and stable isotopes (D. Klitgaard-Kristensen, H.P. Sejrup, M. Smelror, H.J.B. Birks and H. Haflidason, unpublished data, 2004). The two cores have been combined into one record by using dating (AMS ^{14}C and ^{210}Pb) and foraminiferal fauna.

The majority of the faunal and floral species in the stratigraphic record are found to be associated with Atlantic Water based on previous investigations of the content of these in surface sediment samples (Sejrup *et al.*, 1981; Quale and van Weering, 1985; Rochon *et al.*, 1998; Klitgaard-Kristensen *et al.*, 2001), hence interpreted to reflect past variability of the Atlantic Water. In order to capture temperature changes in the Atlantic Water, the results from the benthic stable isotope record are also included. This approach has recently been used on records from western Norwegian fjord basin (Mikalsen *et al.*, 2001; Sejrup *et al.*, 2001; Klitgaard-Kristensen *et al.,* 2004).

North Icelandic shelf

The North Icelandic shelf is within the boundary between Atlantic Water, which is brought to the area by the relatively warm, high-salinity Irminger Current on the one hand, and

cold, low-salinity surface water of the East Icelandic Current (Polar Water) on the other (Figure 1). The East Icelandic Current is partly derived from the East Greenland Current (Polar Water) and partly from the Norwegian Atlantic Current (Atlantic Water) (Stefánsson, 1962; Swift, 1986; Johannesen *et al.*, 1994; Malmberg and Jónsson, 1997; Hansen and Østerhus, 2000). At present the Norwegian Sea Deep Water (NSDW) replaces the mixed surface-water masses at about 3–400 m depth off North Iceland. During periods of strong overflow in the Denmark Strait and across the Iceland-Faeroe Ridge, the cold deep water masses (NSDW) may be expected to influence the deepest topographic basins north of Iceland (Eiríksson *et al.*, 2000). The modern summer sea surface temperature in the study area is relatively constant, generally around 6–7°C, while the winter sea surface temperature is around 1–3°C (Jiang *et al.*, 2002).

On the North Icelandic shelf, dinoflagellate cyst data were obtained from core MD992271 (66°30.07′N; 19°30.33′W, water depth 345 m) and stable isotope, diatom and sedimentological data from core MD992275 (66°33.10′N, 17°41.98′W, water depth 410 m, Figure 1), both obtained on the 1999 IMAGES cruise. Age models for both cores are based on tephrochronology (Larsen *et al*., 2002; Eiríksson *et al*., 2004).

Proxies and methods

Iberian margin

Oxygen isotope analyses were carried out at 1 cm intervals in all three Iberian margin cores. An average number of six specimens from the >250 μm fraction of the benthic species *Uvigerina* sp. 221 was used for each measurement. For the planktonic record, specimens of the planktonic foraminifera *Globigerina bulloides* were used. The laboratory procedures are described in Bartels-Jónsdóttir *et al*. (2006). The alkenone-based SST reconstruction from the Iberian margin is based on procedures described by Abrantes *et al*. (2005).

West Scotland margin

The age–depth model of core GC023 is primarily based upon ^{14}C-dated marine molluscs applying a regional marine reservoir age correction ($\triangle R = -26 \pm 14$ yr), which has been derived from a pre-bomb dating programme of museum collection material (Cage *et al.,* 2006). Despite some uncertainties regarding the dating of the second millennium AD in the GC023 record, we calculate an average sample resolution equivalent to 7 years. The epibenthic foraminifera *Cibicides lobatulus* was picked from the size-range 125–250 μm, and samples were analysed on a MAT251 with Kiel Device at the University of Bremen, Germany. Stable isotope measurements are reported on the VPDB scale, relative to the NBS-19 standard, with the following precision: $\delta^{18}O = 0.035 \pm 0.015‰$; $\delta^{13}C = 0.025 \pm 0.011‰$.

Norwegian margin

In the Norwegian margin record, the stable oxygen isotopes in benthic foraminifera have been measured on the benthic species *Uvigerina mediterranea*. Specimens (one to two individuals) were picked from the 0.125–1000 μm fraction. Stable isotope analyses were conducted at the mass spectrometry laboratory at Department of Earth Science, University of Bergen. Prior to analyses, drops of methanol were added to all samples, followed by ultrasound treatment for 1 min in methanol to remove the fine-grained particles. The methanol was removed using a syringe and the samples allowed to evaporate to dryness in a drying cabinet. The foraminifer shells were then loaded into individual reaction glasses, and each sample was reacted with three drops of H_3PO_4 using a MAT Carbo Kiel III automated preparation line. Isotope ratios were measured on a Finnigan MAT 251 mass spectrometer. The data are reported as $\delta^{18}O$ versus the Vee Pee Dee Belemnite (VPDB) standard after calibration with NBS-19 standard (Coplen, 1995). Analytical precision of the system as defined by replicate measurements of carbonate standards is $\pm 0.07‰$ for $\delta^{18}O$. The age model is based on ^{210}Pb and ^{137}Cs measurements and six radiocarbon AMS dates and yields a time resolution of 4–22 years for the last 2000 years (D. Klitgaard-Kristensen, H.P. Sejrup, M. Smelror, H.J.B. Birks and H. Haflidason, unpublished data, 2004).

North Icelandic shelf

Oxygen isotopes were measuered on the planktonic sinistrally coiled *Neogloboquadrina pachyderma* as well as on the benthic species *Islandiella norcrossi* (Cushman) from the 125–1000 μm fraction of each foraminiferal sample, when possible. The $\delta^{18}O$ values were measured on a Finnigan MAT 251 mass spectrometer at the Stable Isotope Laboratory, University of Bergen, following standard procedures (cf. Knudsen *et al.,* 2004a,b).

Foraminiferal content in the North Iceland shelf record was analysed in the 125–1000 μm sand fraction, and this grain size interval was also used for ice-rafted debris (IRD) analyses (for discussion of the origin of IRD, see Eiríksson *et al.*, 2004; Knudsen *et al.*, 2004b). The planktonic assemblages are dominated by sinistrally coiled *Neogloboquadrina pachyderma*. The percentages of this species are calculated relative to the total planktonic content. Carbonate content was determined by titration on a UIC coulometer, and the sortable silt grain size parameter was calculated from results from a Malvern Mastersizer.

A modern diatom–environmental variable data set from around Iceland (Jiang *et al.*, 2001, 2002) covers areas with sufficient environmental gradients for the deduction of quantitative relationships between diatom species and environmental variables. A Monte Carlo permutation test with forward selection shows that diatom distribution in the area is primarily controlled by summer and winter sea surface temperatures (SSTs, SSTw). These variables are therefore suitable climatic parameters for quantitative reconstruction of palaeorecords based on diatoms in the region.

Diatom samples were extracted from 1 cm thick slices taken at 5 cm intervals from the uppermost 5.3 m of core MD992275. The mean sample resolution is less than 20 years. The CALIBRATE program was used to quantitatively reconstruct the SSTs and SSTw (Juggins and ter Braak, 1992; Jiang *et al.*, 2002). WA-PLS using six components was employed for quantitative reconstruction of the SSTs and WA-PLS using five components for the SSTw. Root mean squared errors of prediction based on the leave-one-out jackknifing ($RMSEP_{(Jack)}$) test are 0.98°C for the SSTs and 0.92°C for the SSTw (Juggins and ter Braak, 1992; Jiang *et al.*, 2002). For dinoflagellate cyst-based SST reconstructions on the North Icelandic shelf, the upper 300 cm of core MD992271 were subsampled at 5 cm intervals. Laboratory procedure for dinocyst analyses consists of repeated acidic treatments (cold HCl (10%) and HF (32–40%)) and sieving at 10 and 118 μm (cf. Marret *et al.*, 2004). Oxidation was avoided as it has been demonstrated that sensitive dinocyst taxa may disappear during the treatment (cf. Marret, 1993). A tablet of exotic marker spores (*Lycopodium clavatum*) was added at the beginning of the procedure for calculating the concentration of dinocysts. The remaining material was mounted in glycerine gel coloured with safranin for light microscopic observation.

Reconstructions of sea surface parameters were obtained from the modern analogue technique, adapted from Guiot and Goeury (1996) with the current $N = 940$ dinocyst data base (see de Vernal *et al.*, 2005). Validation of the modern data set with the WOA01 (Conkright *et al.,* 2002) hydrographical data gives a degree of accuracy as follows: ± 1.31°C and ± 1.93°C for winter and summer sea surface temperatures (SSTs) respectively, and ± 2.94 psu and ± 3.00 psu for winter and summer salinity, respectively. On the whole, the degree of accuracy of estimates is of the same magnitude as the standard deviations around the average for modern SSTs, salinity or sea-ice cover (see also Rochon *et al.*, 1998; de Vernal and Hillaire-Marcel, 2000).

Results

Iberian margin

Alkenones

On the Iberian Atlantic margin, the alkenone record of the Tagus Prodelta (Figure 2A) shows a relatively stable sea surface temperature from AD 0 to around AD 900, with a slight cooling of 0.5°C in the second and third centuries AD, recovering at AD 500–600. A distinct cooling trend begins after about AD 900, and the sea surface temperature apparently becomes more unstable at the same time. However, the time resolution of the record is considerably lower before AD 900 than after, possibly obscuring early fluctuations. The temperature of the last 500 years of the record fluctuates around 16°C, which corresponds to a temperature drop of 1.5°C compared with the first millennium of the record. A sharp cooling is observed during the fourteenth century, with the temperature rising moderately again towards AD 1450.

Sustained periods of sea surface temperatures over 17°C are not observed on the Iberian margin after AD 1000. This is most probably related to advection of colder subpolar surface waters from the north and possibly increased upwelling. As other sedimentary parameters reveal increased sedimentation of terrigenous material during the same period, this shift towards colder sea surface temperatures (SST) and increased precipitation on the western Iberian peninsula points to a change in the dominant features of the atmospheric circulation above the North Atlantic.

Planktonic stable isotopes

The planktonic oxygen isotope record of the Iberian margin (Figure 2B) shows a considerable variability through the last 2000 years. Instrumental data show that interannual variability in salinity (0.1 psu) is much smaller than variability in temperature (*c.* 4°C) in the Tagus Prodelta (Abrantes *et al.*, 2005; Terese Moita, personal communication, 2006). Thus, most of the fluctuations in the oxygen isotopes are probably related to variability in the temperature and only partly to variations in the salinity of the surface waters. However, persistent periods of increased precipitation over the Iberian peninsula resulting from strengthened westerlies across the Atlantic presumably also contribute to a decrease in the planktonic isotopic values.

Relatively light isotope values are found in the beginning of the record and between around AD 400 and 1400. Heavier isotope values parallel the alkenone SST cooling trend from the fourteenth century into the eighteenth century. This would be consistent with strengthening of the cool southward-flowing Portugal Coastal Current and/or enhanced upwelling during this time interval (Bartels-Jónsdóttir *et al.*, 2006). A clear trend towards lighter values is seen in the planktonic oxygen isotope record from the eighteenth century to the present day. Light value peaks are observed at around 100 BC, AD 150, AD 800, AD 1400 and in the latter half of the twentieth century.

Benthic stable isotopes

The bottom water conditions of the Tagus Prodelta are expected to be strongly influenced by the surface oceanography because of the shallow water depth of only 90 m, and the record is suggested to be influenced mainly by temperature, but to some extent also by salinity changes. The benthic $\delta^{18}O$ values show considerably less variability than the planktonic ones (Figure 2C). At the beginning of the record, benthic isotope values are relatively high, corresponding to temperatures fluctuating around 13.2°C, assuming a constant salinity (Bartels-Jónsdóttir *et al.*, 2006), with a distinct but short, particularly heavy interval centred around AD 200. This is followed by a slight decrease around AD 400. The benthic isotopic values then remained relatively light until around AD 1300 (650 cal. BP, Figure 2C). Shortly before AD 1300, a trend towards heavier values sets in, and the values remain high until the eighteenth century. Since AD 1800, the benthic oxygen isotope values have been relatively light.

A possible explanation for the heavy benthic isotopic values during the period AD 1450 to 1750 in the Tagus Prodelta may be the enhancement and maintenance of the cool Portuguese Coastal Current transporting cold subpolar waters to the Iberian margin. This is in agreement with a study by deMenocal *et al.* (2000), who recorded lower temperatures during the so-called 'Little Ice Age' (LIA) off NW Africa and proposed both a stronger Eastern Boundary Current and/or an enhancment of upwelling during the LIA. The benthic stable isotope record shows clearly that during the last 100 years the bottom temperature was higher, by almost 2°C, than at any time during the last *c.* 2000 years.

West Scotland margin

Benthic stable isotopes

Using a benthic foraminiferal summer bottom water temperature transfer function (modified after Sejrup *et al.*, 2004), we have confirmed that long-term changes in benthic foraminiferal $\delta^{18}O$ trace the temperature history of bottom water in Loch Sunart (Cage, 2005). Benthic foraminiferal $\delta^{18}O$ records summer bottom water temperature in the range 10–13°C throughout the first millennium AD. During this time, temperatures were typically 2°C warmer than the present day, and there is a cooling trend in bottom water temperature since around AD 900 (Figure 2D). Benthic foraminiferal $\delta^{13}C$ data suggest that the exchange between basin water and coastal waters has changed over this same time interval, a mechanism that could have been driven by enhanced westerlies.

Numerical modelling experiments of Loch Sunart circulation (Gillibrand *et al.*, 2005) investigated the forcing mechanisms at play during two recent extremes of the NAO. The results suggest that main basin salinity remains extremely stable in response to both the strength of westerlies and freshwater forcing driven by changing pattern of precipitation. We are therefore confident that the benthic $\delta^{18}O$ records reflect changing coastal temperature, but these may be complicated in shelf environments by the timing of seasonally triggered reproduction and growth in foraminifera (eg, Scourse *et al.*, 2004). Our data suggest that coastal temperatures over the last 2000 years are repeatedly influenced by a high frequency (multidecadal) 1–2°C variability that overprints a longer-term (centennial) climate signal, the most pronounced expression of which is a cooling trend at around AD 900.

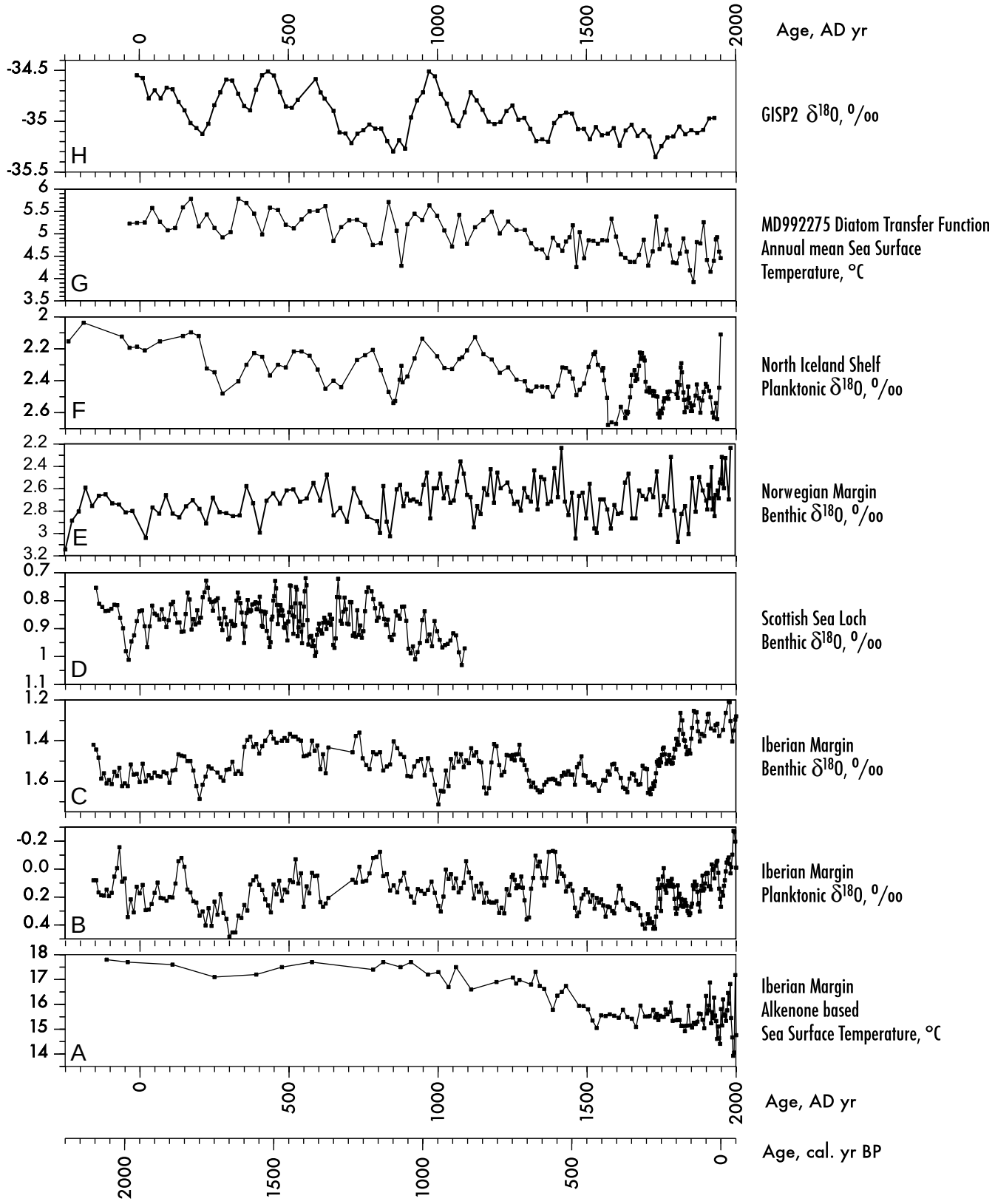

Figure 2 Palaeoceanographic parameters from open ocean shallow marine sites in western Europe. (A) Sea surface temperature record from the Iberian margin based on alkenones. (B) $\delta^{18}O$ record from the Iberian margin based on the planktonic foraminifera *Globigerina bulloides*. (C) $\delta^{18}O$ record from the Iberian margin based on the benthic foraminifera *Uvigerina* sp. 221. (D) Benthic foraminiferal $\delta^{18}O$ record from Loch Sunart based on *Cibicides lobatulus* (3 pt. running mean). (E) Norwegian margin $\delta^{18}O$ record based on the benthic foraminiferal species *Uvigerina mediterranea*. (F) North Iceland shelf record of $\delta^{18}O$ based on the planktonic foraminiferal species *Neogloboquadrina pachyderma* sinistral (3 pt. running mean). (G) Mean annual sea surface temperature record from the North Iceland shelf based on diatom transfer function. (H) Greenland ice core GISP2 oxygen isotope record (50 yr smoothing filter). Age scales in calibrated years BP for marine records, GISP2 ice years in the Greenland ice core. Age scales are given in years BC and AD as well as in years PB (before 1950)

Norwegian margin

Benthic stable isotopes

The benthic isotope record is interpreted to primarily reflect (annual) temperature changes in the inflowing Atlantic Water into the Northern North Sea. This follows from previous studies of oxygen isotope records of benthic foraminifera in cores presently underlying inflowing Atlantic Water in this region. These investigations inferred, based on the similarity between the proxy records and instrumental time series (annual temperature and salinity variations), that the isotope records mainly reflected temperature (Mikalsen *et al.,* 2001; Klitgaard-Kristensen *et al.,* 2004). If interpreted as temperature only, this means that a maximum amplitude of about 2°C is recorded (0.6‰) for the last two millennia. The long-term temperature development shows relatively low temperatures from AD 100 to 400, 600–900 and 1400–1900, whereas higher temperatures than average are seen from AD 400 to 600, 900–1400 and for the last 80 years (Figure 2E). These periods are, however, not only prolonged periods of high or low temperatures but also interrupted by shorter periods exhibiting warmer or colder conditions.

North Icelandic shelf

Planktonic stable isotopes

The planktonic oxygen isotope record from the North Icelandic shelf (Figure 2F) shows a variability of close to 2°C through the last 2000 years. There is an overall cooling trend through the entire period. The isotopic values are relatively low (around 2.1–2.2‰) until about AD 200, indicating a sustained warm surface ocean north of Iceland during the Roman Warm Period (RWP). A subsequent cooling in the time interval from AD 200 to 900 is indicated by generally heavier $\delta^{18}O$ values. The values are fluctuating, and distinct coolings are suggested by peak values around AD 300, 700 and 850. The isotopic values indicate a slight increase in temperature between AD 900 and 1100. Apparently, however, the surface waters during the interval corresponding to the 'Mediaeval Warm Period' (MWP) were not as warm as during the RWP. After AD 1100 there is clear evidence of a cooling trend, which continues through the remainder of the record. The isotopic values are particularly high after AD 1500. Short intervals of light isotopic values in this latter interval probably reflect periodic influx of low-salinity surface waters to the area. This indicates strengthening of the cold, fresh East Icelandic Current during the last few hundred years (Knudsen *et al.*, 2004b).

Diatoms

An annual mean sea surface temperature record based on diatom transfer function reconstructions is presented in Figure 2G. Temperature values range between 4 and 6°C. A long-term cooling trend characterizes the record as a whole. A cooling trend from AD 300 to 800 is followed by a relatively warm period from AD 800 to 1300. After a sharp temperature drop between AD 1250 and 1350, the last part of the record, from AD 1300 to 1950, is characterized by reconstructed temperature values that generally lie below 5°C. Within the period AD 1300 to 1950 the temperature trend is opposite to the one observed at the Norwegian margin site, with a general cooling.

Planktonic proxies and sedimentological parameters

The results of a multiproxy study of HOLSMEER site MD992275 on the North Iceland shelf are presented in Figure 3. The parameters all relate to the oceanography of the region, where the oceanographic Polar Front is located today. In the temperature reconstructions based on diatoms, consistently low sea surface temperatures, both summer and winter, appear to have prevailed since AD 1300 on the North Iceland shelf (Figure 3F, 3G). A sharp drop in sea surface temperature, observed between AD 1200 and 1400, coincides with an increase of the percentage of *Neogloboquadrina pachyderma* sinistral. This is probably an indication of a weakened Irminger Current and a concurrent southward shift of the Polar Front.

The decrease in planktonic isotope values after AD 1100 leads to generally heavy values after AD 1300 (Figure 2F). Intervals of light values within these last few hundred years coincide with cold periods reflected by the diatom record. This presumably reflects short-term incursions of relatively fresh surface waters with an Arctic component brought by the East Icelandic Current. Parts of the sixteenth century enjoyed relatively mild surface waters north of Iceland, terminated by sharp cooling at close to AD 1600 (Figure 2F, 3C, F, G). There is clearly a very close relationship between the carbonate content (Figure 3E) and the sea surface temperature record, with consistently low values after AD 1200. An increase is observed after AD 1900.

All these changes are interpreted to reflect variable strength of the Irminger Current, an interpretation that is supported by the sortable silt content. Sluggish bottom circulation is indicated by the sortable silt parameter at the base of the record, but the values between around AD 0 and AD 900 indicate the liveliest currents of the 2000 year record. A decreasing trend is then observed from AD 900 to 1900, with a slight increase towards the top after AD 1900. Percentages of the sinistrally coiled *Neogloboquadrina pachyderma* (Figure 3C) show that for sustained periods, arctic conditions have prevailed on the North Iceland shelf, with values exceeding 95%. The lowest percentages are observed after AD 1900 towards the top of the record, and between AD 300 and 450. The latter interval is also characterized by high reconstructed sea surface temperatures (diatom based), light planktonic $\delta^{18}O$ values, a slightly increased sortable silt mean, and a carbonate peak.

Generally, arctic conditions are indicated by the planktonic fauna at around AD 700 (Figure 3C), supported by low sea surface temperature and heavy planktonic $\delta^{18}O$ values (Figure 2F). This cold interval precedes the beginning of the MWP at AD 750 (Figure 4), the onset of which can be identified by increasing sea surface temperatures, rising carbonate content and sortable silt mean, as well as decreasing percentages of *Neogloboquadrina pachyderma* sinistral. The planktonic $\delta^{18}O$ record of the MWP starts with relatively light values around AD 750, but an interval with heavy values is observed around AD 900, followed by light values until AD 1250.

High percentages of *Neogloboquadrina pachyderma* sinistral characterize the interval AD 1350 to 1700 and the values fluctuate strongly between AD 1700 and 1900, with minima close to AD 1800 and 1900. A period of ice-rafting was also observed from just after AD 1300 until 1400, coinciding with the onset of the LIA (Eiríksson *et al.*, 2004; Knudsen *et al.*, 2004a). After a short-lived period of higher than average IRD flux in the early twentieth century, the values fall to background values at the top of the record.

Dinoflagellate record

A total of 26 taxa were identified, with three dominant taxa, ie, cysts of *Pentapharsodinium dalei*, *Operculodinium centrocarpum* and *Spiniferites ramosus*. The downcore variation of dinocyst spectra is suggested to indicate the relative influence of the Irminger Current and East Icelandic Current. Transfer function reconstructions, based on a modern data set from the Northern Hemisphere (de Vernal *et al.*, 2005), show an increasing trend in

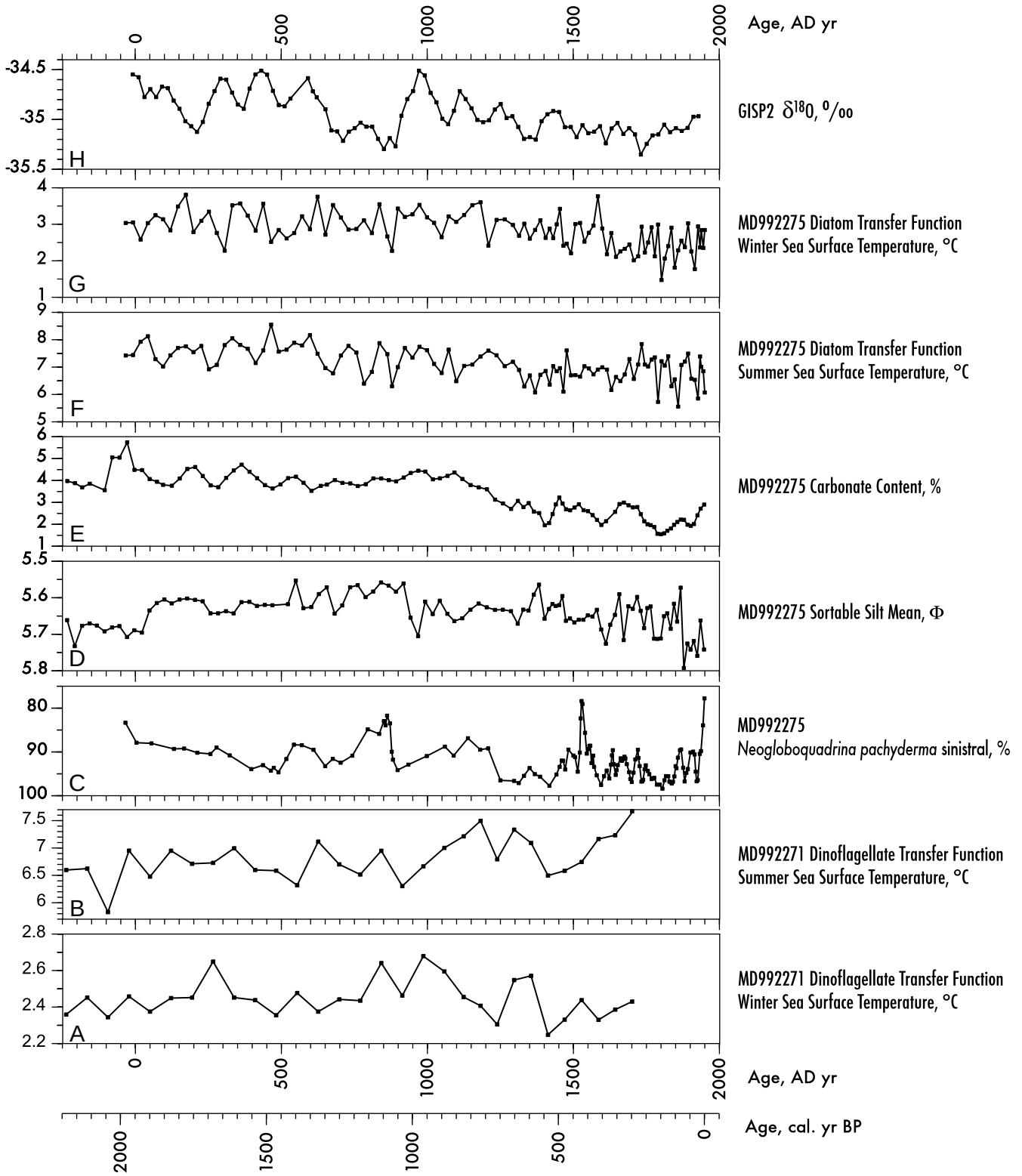

Figure 3 A record of palaeoceanographic proxies from the oceanographic Polar Front, North Iceland shelf. The Greenland ice core GISP oxygen isotope record is shown at the top. (A) Dinoflagellate cyst transfer function derived winter sea surface temperature record from core MD992271 on the North Iceland shelf. (B) Dinoflagellate cyst transfer function derived summer sea surface temperature record from core MD992271. (C) Percentages of the benthic foraminiferal species *Neogloboquadrina pachyderma* sinistral (3 pt. running mean). (D) Sortable silt (10–63 μm fraction) mean size in core MD992275 (3 pt. running mean). (E) Total carbonate content, weight percent, in core MD992275 (3 pt. running mean). (F) Summer sea surface temperature record from the North Iceland shelf based on diatom transfer function. (G) Winter sea surface temperature record from the North Iceland shelf based on diatom transfer function. (H) Greenland ice core GISP2 oxygen isotope record (50 yr smoothing). Age scales in calibrated years BP for marine records, GISP2 ice years in the Greenland ice core. Age scales are given in years BC and AD as well as in years PB (before 1950)

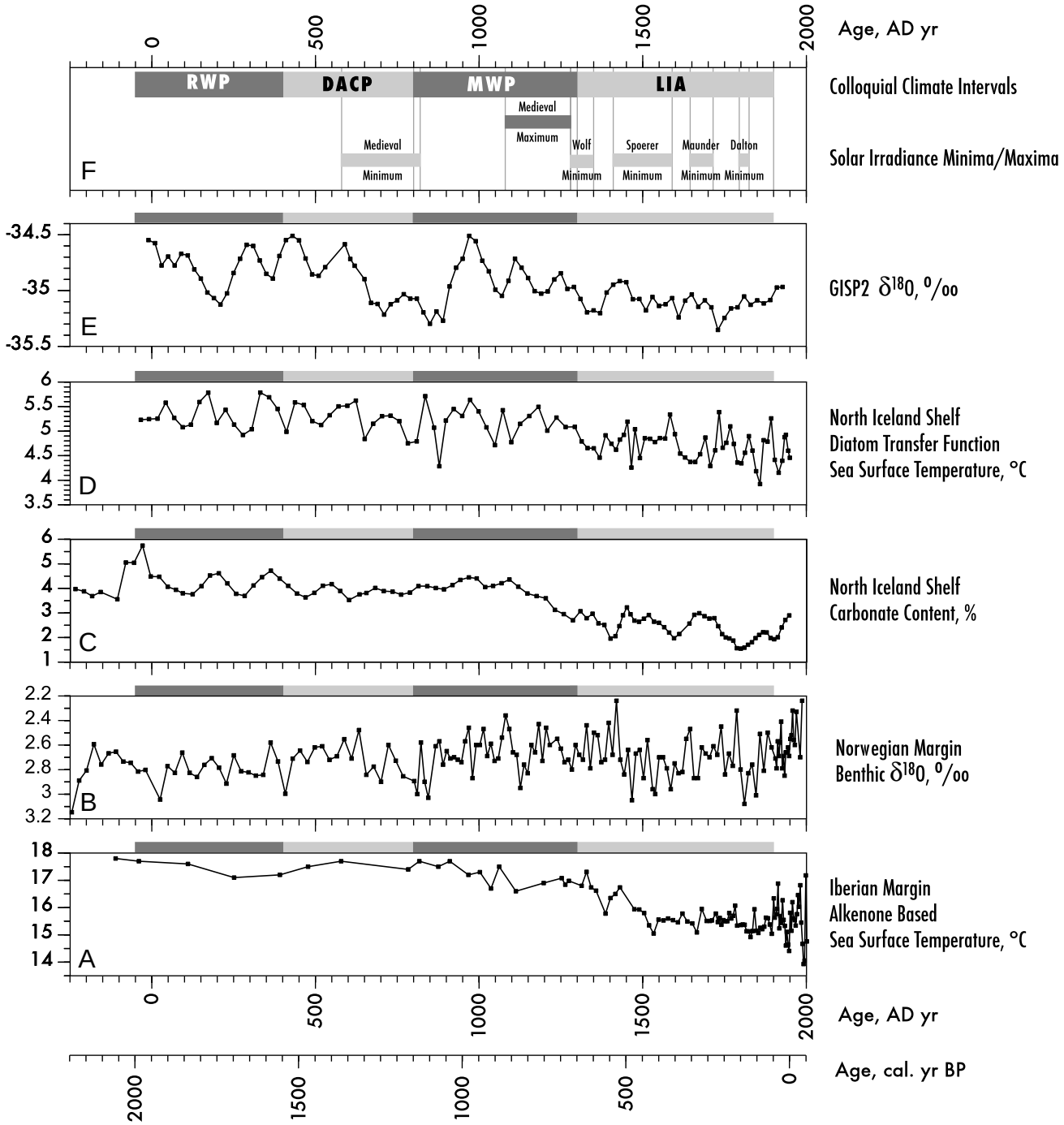

Figure 4 Selected oceanographic parameters for the last two millennia from shallow water open ocean sites in western Europe compared with a Greenland ice core record. (A) Sea surface temperature record from the Iberian margin based on alkenones. (B) Norwegian margin $\delta^{18}O$ measurements of the benthic foraminiferal species *Uvigerina mediterranea*. (C) Total carbonate content, weight percent, in core MD992275 (3 pt. running mean). (D) Mean annual sea surface temperature record from the North Iceland shelf based on diatom transfer function. (E) Greenland ice core GISP2 oxygen isotope record (50 yr smoothing filter). (F) Informal Holocene climate history terms are shown as shaded bars along the top of the panel (duplicated on the lower panels of each diagram; warm, dark; cool, light) including the Roman Warm Period (RWP, 50–400 BC), the Dark Ages Cold Period (DACP, AD 400–800), the 'Mediaeval Warm Period' (MWP, AD 800–1300) and the 'Little Ice Age' (LIA, AD 1300–1900). Solar irradiance minima and maxima are also shown on panel (F). Age scales in calibrated years BP for marine records, GISP2 ice years in the Greenland ice core. Age scales are given in years BC and AD as well as in years PB (before 1950)

summer SST whereas winter SST varies little, though with a general decrease since AD 1000 (Figure 3A, B).

Discussion

Atmospheric conditions in the northern North Atlantic region are commonly described with the North Atlantic Oscillation (NAO) winter index (Hurrell *et al.*, 2003), which is a measure of the pressure difference between the Iceland Low and the Azores High. A linkage between oceanic circulation and atmospheric processes is constituted by convective renewal of intermediate and deep waters in the Labrador Sea and the Nordic Seas, which leads to the formation and export of North Atlantic Deep Water; this plays a role in driving the global thermohaline circulation (Hurrell *et al.,* 2003). The winter

convection at these sites is apparently linked to the NAO winter index on a decadal timescale (Dickson *et al.*, 1996). A linkage was clearly exemplified during salinity anomaly events during the latter half of the twentieth century. Instrumental temperature and salinity data through that time interval have been presented by Knudsen *et al.* (2004a) for a specific site off North Iceland.

These salinity anomalies propagated along the subpolar gyre of the North Atlantic during negative phases of the NAO. Strong southward air flow east of Greenland resulting from the high-pressure field strengthens the East Greenland Current and its offshoot, the East Icelandic Current, transporting freshwater from the Arctic Ocean through the Fram Strait and into the Labrador Sea and the Nordic Seas. The Arctic Water, being channelled into the southern limb of the North Atlantic subpolar gyre, cools and reduces the salinity of the North Atlantic Current. Some of this influence may then be reflected by a southward shift of the divergence of the North Atlantic Current and carried towards the Iberian margin. During intervals of preferred negative state of the NAO, cooling and freshening of the surface waters may thus be expected to influence the region as a whole.

Selected environmental parameters that are considered to be climate related for each of the four study areas (Figure 1) are shown in Figure 4. In general, the parameters reflect annual mean temperature at the sea surface. Given the latitudinal variability from site to site, the range of proxies used and the age model uncertainties, it is not expected that detailed fluctuations should be replicated in these records. However, some common longer-term trends are observed. Informal terms traditionally used in discussing the upper Holocene atmospheric part of climate history include the Roman Warm Period (RWP, 50–400 BC), the Dark Ages Cold Period (DACP, AD 400–800), the 'Mediaeval Warm Period' (MWP, AD 800–1300) and the 'Little Ice Age' (LIA, AD 1300–1900). There is a continuing debate on the global significance of these climate intervals, which are clearly not well constrained in many records, and the boundaries between them are not strictly defined anywhere (for recent reviews see eg, Soon and Baliunas, 2003; Mayewski *et al.*, 2004; Goosse *et al.*, 2005).

In many environmental settings, coastal and shallow marine records are more prone to fluctuations in climate and are therefore more likely to exhibit greater variability in climatic reconstructions than observed in purely oceanic or terrestrial reconstructions This is due to the complex interaction of marine and terrestrial processes. To the advantage of such records, minor environmental changes are more likely to be preserved in the sedimentary record given high enough sedimentation rates.

The GISP2 $\delta^{18}O$ record, reflecting atmospheric conditions in the northern North Atlantic realm, shows a relatively clear cooling trend starting during the latter half of the RWP and extending to about AD 900, covering the DACP (Figure 4). A parallel trend is evident in the marine environment, reflected by the diatom-based SST reconstruction for the North Icelandic shelf, and the trend is also present in the total carbonate content, which reflects coccolith productivity (Andrews and Giraudeau, 2003). A very similar cooling trend is seen in the planktonic $\delta^{18}O$ record from the Norwegian margin (Berstad *et al.*, 2003). A cooling trend appears to be present in the Scottish sea loch benthic $\delta^{18}O$ record from *c.* AD 250 to 600 (Figure 2D). At the same time, the Iberian margin alkenone-based SST record is relatively warm but with slight cooling towards the end of the RWP.

The MWP is observed in the GISP2 $\delta^{18}O$ record with a clear atmospheric warming beginning at about AD 900. In the ocean, the alkenone-based Iberian margin record (Figure 4) does not show any change at the start of the MWP, nor do the benthic isotope data (Figure 2A, C). However, the alkenone-based SST values begin to fluctuate at AD 1000, and a slight cooling trend is seen after about AD 900. It is important to note that the alkenone-based SST record indicates higher temperatures during the RWP than in the MWP on the Iberian margin. On the other hand, planktonic isotopes at the Iberian margin site show a period of warm conditions at the start of the MWP, at AD 800, but the values remain at about the same level as during the RWP. In the Scottish sea loch record, the cooling trend extending well into the DACP is reversed and the MWP starts relatively warm, but this is followed by a distinct cooling trend for the remainder of the available record (Figure 2D). In the Norwegian margin and North Iceland shelf records there is a clear reversal of the cooling trend of the DACP towards the start of the MWP (Figure 2E, F, G).

Common to all the marine records shown in Figure 4 is a cooling trend setting in towards or at the end of the MWP, and an interval from AD 1300 to 1900 fluctuating around a lower temperature level than before. Generally, twentieth-century sea surface temperatures are not higher than those reconstructed for the MWP nor the RWP. However, a distinct temperature rise is evident towards modern values since the end of the LIA.

The configuration of the modern oceanic circulation in the northern North Atlantic suggests that the shallow marine realm from the Iberian margin to North Iceland (Figure 1) should respond coherently to variability of the heat transport of the North Atlantic Current. However, the surface currents may also be strongly affected by atmospheric processes, which in turn are most probably coupled to solar irradiance variability or maybe to volcanic forcing (cf. Crowley, 2000; Lean, 2002, Church *et al.,* 2005). Although it has been suggested that the North Iceland shelf SST record variability covaries with solar insolation (Jiang *et al.*, 2005), no simple relationship is evident between the solar minima/maxima and the marine HOLSMEER records seen in Figure 4. However, the Wolf Minimum coincides with the cooling trend at the transition towards the LIA, being preceded by the MWP maximum.

Summary and conclusions

Oceanic variability, spanning the last 2000 years, is recorded in HOLSMEER sites from the northern North Atlantic and has been correlated with atmospheric data from the Greenland ice cores. The atmospheric and marine records exhibit some common features, especially in the second millennium AD. With the available chronologies it is not possible to correlate short-term variations on a decadal timescale, but some parallel trends appear to be present. In summarizing the results, we use the atmospheric climate interval terms such as the Roman Warm Period (RWP), The Dark Age Cold Period (DACP), the 'Mediaeval Warm Period' (MWP) and the 'Little Ice Age' (LIA) in a chronological sense (cf. Figure 4). As a reference record, the GISP2 $\delta^{18}O$ record, shows a relatively cold latter part of the RWP with warming towards the end, and then a clear cooling trend throughout the DACP extending to about AD 900 (Figure 4). The onset of the MWP is fairly clear in the GISP2 $\delta^{18}O$ record, with a clear warming beginning at AD 900 followed by a cooling trend through the LIA extending into the eighteenth century. This is followed by warming continuing into the twentieth century.

A cooling trend towards the end of the RWP (about AD 200–300) followed by a warming trend close to the transition

to the DACP (at about AD 400) is apparently a common feature of both the oceanic and the atmospheric records. The DACP is a period of generally decreasing temperatures. The Iberian margin temperature record (Figure 4) does not show any change at the start of the MWP, nor do the benthic isotope data (Figure 2). However, the alkenone-based SST values begin to fluctuate at AD 1000, and reduced upwelling and warm conditions are indicated by stable isotopes at the start of the MWP at AD 800. On the west coast of Scotland, the cooling trend is reversed and the MWP starts relatively warm, but this is followed by a distinct cooling trend for the remainder of the record. In the Norwegian margin and North Iceland shelf records, there is a clear reversal of the cooling trend of the DACP towards the start of the MWP.

All the records show an interval from AD 1300 to 1900 (coiniciding with the reported climatic event, the LIA) in which the climate fluctuates around the lowest temperature level seen within the past two millenia. A reversal of the cooling within the LIA is quite clear but not synchronous in many of the records, and it appears to be more distinct and to set in earlier in the southern sites. The twentieth century does not appear to be exceptional in terms of palaeoceanographic proxies for the last 2000 years. However, most of the records do indicate warming coastal and shelf waters during the last 200 years.

Acknowledgements

The present paper is a contribution to the European Union 5th framework project HOLSMEER (Contract No. EVK2-CT-2000-00060). Core material was obtained from the MD9922 IMAGES Cruise in 1999. We are grateful to the Institut Français pour la Recherche et la Technologie Polaires (IFRTP) for the IMAGES coring operations onboard the *Marion Dufresne*. In addition to the European Union 5th framework grant, scientific work was supported by grants from the Icelandic Research Council and the Danish Natural Science Research Council. We are grateful to Niels Norgaard-Pedersen for supplying the stable isotope data presented from GC023, Loch Sunart.

References

Andrews, J.T. and **Giraudeau, J.** 2003: Multi-proxy records showing significant Holocene environmental variability: the inner N. Icelandic shelf (Húnaflói). *Quaternary Science Reviews* 22, 175–93.

Abrantes, F., Lebreiro, S., Rodrigues, T., Gil, I., Bartels-Jónsdóttir, H., Oliveira, P., Kissel, C. and **Grimalt, J.O.** 2005: Shallow-marine sediment cores record climate variability and earthquake activity off Lisbon (Portugal) for the last 2,000 years. *Quaternary Science Reviews* 24, 2477–94.

Bartels-Jónsdóttir, H.B., Knudsen, K.L., Abrantes, F., Lebreiro, S. and **Eiríksson, J.** 2006: Climate variability during the last 2000 years in the Tagus Prodelta, western Iberian Margin: benthic foraminiferal and stable isotopes. *Marine Micropalaeontology* 59, 83–103.

Belkin, I.M., Levitus, S., Antonov, J. and **Malmberg, S.-A.** 1998: 'Great salinity anomalies' in the North Atlantic. *Progress in Oceanography* 41, 1–68.

Berstad, I.M., Sejrup, H.P., Klitgaard-Kristensen, D. and **Haflidason, H.** 2003b: Variability in temperature and geometry of the Norwegian Current over the past 600 yr; stable isotope and grain size evidence from the Norwegian margin. *Journal of Quaternary Science* 18, 591–602.

Boessenkool, K.P., Brinkhuis, H., Schönfeld, J. and **Targarona, J.** 2001: North Atlantic sea-surface temperature changes and the climate of western Iberia during the last deglaciation; a marine palynological approach. *Global and Planetary Change* 30, 33–39.

Bond, G., Heinrich, H., Broecker, W.S., Labeyrie, L., McManus, L., Andrews, J.T., Huon, S., Jantschik, R., Clasen, S., Simet, C., Tedesco, K., Klas, M., Bonani, G. and **Ivy, S.** 1992: Evidence for massive discharges of icebergs into the glacial Northern Atlantic. *Nature* 360, 245–249.

Bond, G., Broecker, W., Johnsen, S., McManus, J., Labeyrie, L., Jouzel, J. and **Bonani, G.** 1993: Correlations between climate records from North Atlantic sediments and Greenland ice. *Nature* 365, 143–147.

Bond, G.C., Showers, W., Elliot, M., Evans, M., Lotti, R., Hajdas, I., Bonani, G. and **Johnsen, S.** 1999: The North Atlantic's 1–2 kyr climate rhythm: relation to Heinrich Events, Dansgaard/Oeschger Cycles and the Little Ice Age. *Geophysical Monograph Series* 112, 35–58.

Cage, A.G. 2005. The modern and late Holocene marine environments of Loch Sunart, NW Scotland. Ph.D. Thesis, University of St Andrews, 399 pp.

Cage, A.G., Heinemeier, J. and **Austin, W.E.N.** 2006: Marine radiocarbon reservoir ages in Scottish coastal and fjordic waters. *Radiocarbon* 48, 31–43.

Church, J.A., White, N.J. and **Arblaster, J.M.** 2005: Significant decadal-scale impact of volcanic eruption on sea level and ocean heat content. *Nature* 438, 74–77.

Conkright, M.E., Locarnini, R.A., Garcia, R.A., O'Brien, T.D., Boyer, T.P., Stephens, C. and **Antonov, J.I.** 2002: *World Ocean atlas 2001: objective analyses, data statistics, and figures, CD-ROM documentation*. National Oceanographic Data Center, 17pp.

Coplen, T.B. 1995: New IUPAC guidelines for the reporting of stable hydrogen, carbon, and oxygen isotope-ratio data. *Journal of Research of the National Institute of Standards and Technology* 100, 285.

Crowley, J.T. 2000: Causes of climate change over the past 1000 years. *Science* 289, 270–77.

Dansgaard, W., Johnsen, S.J., Clausen, H.B. and **Langway, C.C.** 1971: Climatic record revealed by the Camp Century ice core. In Turekian, K., editor, *The late Cenozoic glacial ages*. Yale University Press, 37–56.

de Menocal, P., Ortiz, J., Guilderson, T. and **Sarnthein, M.** 2000: Cohesent high- and low-latitude climate variability during the Holocene warm period. *Science* 288, 2198–202.

de Vernal, A. and **Hillaire-Marcel, C.** 2000: Sea-ice cover, sea-surface salinity and halo-thermocline structure of the northwest North Atlantic: modern versus full glacial conditions. *Quaternary Science Reviews* 19, 65–85.

de Vernal, A., Eynaud, F., Henry, M., Hillaire-Marcel, C., Londeix, L., Mangin, S., Matthiessen, J., Marret, F., Radi, T., Rochon, A., Solignac, S. and **Turon, J.-L.** 2005: Reconstruction of sea-surface conditions at middle to high latitudes of the Northern Hemisphere during the Last Glacial Maximum (LGM) based on dinoflagellate cyst assemblages. *Quaternary Science Reviews* 24, 897–924.

Dickson, R.R., Meincke, J., Malmberg, S.A. and **Lee, A.J.** 1988: The 'Great salinity anomaly' in the northern North Atlantic 1968–1982. *Progress in Oceanography* 20, 103–51.

Dickson, R.R., Lazier, J., Meincke, J., Rhines, P. and **Swift, J.** 1996: Long-term coordinated changes in the convective activity of the North Atlantic. *Progress in Oceanography* 38, 241–95.

Duplessy, J.C., Delibrias, G., Turon, J.-L., Pujol, C. and **Duprat, J.** 1981: Deglacial warming of the northeastern Atlantic Ocean: correlation with the paleoclimatic evolution of the European continent. *Palaeogeography, Palaeoclimatology, Palaeoecology* 35, 121–44.

Eiríksson, J., Knudsen, K.L., Haflidason, H. and **Henriksen, P.** 2000: Late-glacial and Holocene palaeoceanography of the North Icelandic shelf. *Journal of Quaternary Science* 15, 23–42.

Eiríksson, J., Larsen, G., Knudsen, K.L., Heinemeier, J. and **Símonarson, L.A.** 2004: Marine reservoir age variability and water mass distribution in the Iceland Sea. *Quaternary Science Reviews* 23, 2247–68.

Fiúza, A.F.d.G. 1983: Upwelling patterns off Portugal. In Thiede, J. and Suess, E., editors, *Coastal upwelling: its sediment record, part A*. Plenum Press, 85–98.

Furnes, G.K., Hackett, B. and **Sætre, R.** 1986: Retroflection of Atlantic water in the Norwegian Trench. *Deep Sea Research* 33, 247–65.

Gillibrand, P., Cage, A. and **Austin, W.E.N.** 2005. A preliminary investigation of bottom water response to climate forcing in a Scottish fjord: evaluating the influence of the NAO. *Continental Shelf Research* 25, 571–87.

Gillibrand, P.A., Turrell, W.R. and **Elliott, A.J.** 2002: Deep-water renewal in the upper basin of Loch Sunart, a Scottish fjord. *Journal of Physical Oceanography* 25, 1488–503.

Goosse, H., Renssen, H., Timmermann, A. and **Bradley, R.S.** 2005: Internal and forced climate variability during the last millennium: a model-data comparison using ensemble simulations. *Quaternary Science Reviews* 24, 1345–60.

Guiot, J. and **Goeury, C.** 1996: PPPbase, a software for statistical analysis of paleoecological data. *Dendrochronologia* 14, 295–300.

Hansen, B. and **Østerhus, S.** 2000: North Atlantic–Nordic Seas exchanges. *Progress in Oceanography* 45, 109–208.

Hurdle, B.G. 1986: *The Nordic Seas*. Springer Verlag, 777 pp.

Hurrell, J.W., Kushnir, Y., Ottersen, G. and **Visbeck, M.** 2003: An overview of the North Atlantic Oscillation. In Hurrell, J.W., Kushnir, Y., Ottersen, G. and Visbeck, M., editors, *The North Atlantic Oscillation: climatic significance and environmental impact*. American Geophysical Union, Geophysical Monograph 134, 1–35.

Jiang, H., Seidenkrantz, M.-S., Knudsen, K.L. and **Eiríksson, J.** 2001: Diatom surface sediment assemblages around Iceland and their relationships to oceanic environmental variables. *Marine Micropaleontology* 41, 73–96.

Jiang, H., Seidenkrantz, M.-S., Knudsen, K.L. and **Eiríksson, J.** 2002: Late Holocene summer sea-surface temperatures based on a diatom record from the north Icelandic shelf. *The Holocene* 12, 137–47.

Jiang, H., Eiríksson, J., Schulz, M., Knudsen, K.L. and **Seidenkrantz, M.-S.** 2005: Evidence for solar forcing of sea-surface temperature on the North Icelandic Shelf during the late Holocene. *Geology* 33, 73–76.

Johannesen, T., Jansen, E., Flatøy, A. and **Ravelo, A.C.** 1994: The relationship between surface water masses, oceanographic fronts and paleoclimatic proxies in surface sediments of the Greenland, Iceland, Norwegian Seas. In Zahn, R., Pedersen, T.F., Kaninski, M.A. and Labeytic, L., editors, *Carbon cycling in the glacial ocean: constraints on the ocean's role in global change*. Quantitative Approaches in Paleoceanography. NATO ASI Series, I. 17, Springer-Verlag, 61–85.

Johnsen, S.J., Dansgaard, W. and **Clausen, H.B.** 1972: Oxygen isotope profiles through the Antarctic and Greenland Ice Sheets. *Nature* 235, 429–30.

Johnsen, S.J., Clausen, H.B., Dansgaard, W., Fuhrer, K., Gundestrup, N., Hammer, C.U., Iversen, P., Jouzel, J., Stauffer, B. and **Steffensen, J.P.** 1992: Irregular glacial interstadials recorded in a new Greenland ice core. *Nature* 359, 311–13.

Juggins, S. and **ter Braak, C.J.E.** 1992: *CALIBRATE – a program for species–environment calibration by (weighted-averaging) partial least squares regression*. Environmental Change Research Centre, University College London.

Klitgaard-Kristensen, D., Sejrup, H.P. and **Haflidason, H.** 2001: The last 18 kyr fluctuations in Norwegian Sea surface conditions and implications for the magnitude of climatic change: evidence from the North Sea. *Paleoceanography* 16, 455–67.

Klitgaard-Kristensen, D., Sejrup, H.P., Haflidason, H., Berstad, I.M. and **Mikalsen, G.** 2004: Eight-hundred-year temperature variability from the Norwegian continental margin and the North Atlantic thermohaline circulation. *Paleoceanography* 19, PA2007, 10.1029/2003PA000960.

Knudsen, K.L., Eiríksson, J., Jansen, E., Jiang, H., Rytter, F. and **Gudmundsdottir, R.E.** 2004a: Palaeoceanographic changes off North Iceland through the last 1200 years: foraminifera, stable isotopes, diatoms and ice rafted debris. *Quaternary Science Reviews* 23, 2231–46.

Knudsen, K.L., Jiang, J., Jansen, E., Eiríksson, J., Heinemeier, J. and **Seidenkrantz, M.-S.** 2004b: Environmental changes off North Iceland during the deglaciation and the Holocene: foraminifera, diatoms and stable isotopes. *Marine Micropaleontology* 50, 273–305.

Kroon, D., Austin, W.E.N., Chapman, M.R. and **Ganssen, G.M.** 1997: Deglacial surface circulation changes in the northeastern Atlantic: temperature and salinity records off NW Scotland on a century scale. *Paleoceanography* 12, 755–63.

Larsen, G., Eiríksson, J., Knudsen, K.L. and **Heinemeier, J.** 2002: Correlation of Late Holocene terrestrial and marine tephra markers, North Iceland: implication for reservoir age changes. *Polar Research* 21, 283–90.

Lean, J. 2002: Solar forcing of climate change in recent millennia. In Wefer, G., Berger, W.H., Begre, K.E. and Jansen, E., editors, *Climate developement and history of the North Atlantic realm*. Springer-Verlag, 75–88.

Lebreiro, S.M., Francés, G., Abrantes, F.F.G., Diz, P., Bartels-Jónsdóttir, H.B., Stroynowski, Z., Gil, I.M., Pena, L.D., Rodrigues, T., Jones, P.D., Nombela, M.A., Alejo, I., Briffa, K.R., Harris, I. and **Grimalt, J.O.** 2006: Climate change and coastal hydrographic response along the Atlantic Iberian margin (Tagus Prodelta and Muros Ría) during the last two millenia. *The Holocene* 16, 1003–15 (this issue).

Malmberg, S.A. 1984: Hydrographic conditions in the East Icelandic Current and sea ice in North Icelandic waters, 1970–1980. In Meincke, J., Otto, L., Lee, A.J. and Dickson, R.R., editors, *Hydrobiological variability in the North Atlantic and adjacent seas. Rapports et procès-verbaux des Réunions 185*. Conseil international pour l'exploration de la mer, 170–78.

Malmberg, S.A. and **Jónsson, S.** 1997: Timing of deep convection in the Greenland and Iceland Seas. *ICES Journal of Marine Science* 54, 300–309.

Marret, F. 1993: Les effets de l'acétolyse sur les assemblages de kystes de dinoflagellés. *Palynosciences* 2, 267–72.

Marret, F., Eiríksson, J., Knudsen, K.-L., Turon, J.-L. and **Scourse, J.** 2004: Distribution of dinoflagellate cyst assemblages in surface sediments from the northern and western shelf of Iceland. *Review of Palaeobotany and Palynology* 128, 35–53.

Mayewski, P.A., Meeker, L.D., Whitlow, S., Twickler, M.S., Morrison, M.C., Bloomfield, P., Bond, G.C., Alley, R.B., Gow, A.J., Grootes, P.M., Meese, D.A., Ram, M., Taylor, K.C. and **Wumkes, W.** 1994: Changes in atmospheric circulation and ocean ice cover over the North Atlantic during the last 41,000 years. *Science* 263, 1747–51.

Mayewski, P.A., Rohling, E.E., Stager, C.J., Karlen, W., Maasch, K.A., Meeker, D.L., Meyerson, E.A., Gasse, F., van Kreveld, S. and **Holmgren, K.** 2004: Holocene climate variability. *Quaternary Research* 62, 243–55.

Mikalsen, G., Sejrup, H.P. and **Aarseth, I.** 2001: Late Holocene changes in ocean circulation and climate: foraminiferal and isotopic evidence from Sulafjorden, western Norway. *The Holocene* 11, 437–46.

O'Brien, S.R., Mayewski, P.A., Meeker, L.D., Meese, D.A., Twickler, M.S. and **Whitlow, S.I.** 1995: Complexity of Holocene climate as reconstructed from a Greenland ice core. *Science* 270, 1962–64.

Quale, G. and **van Weering, T.J.E.** 1985: Relationship of surface sediments and benthic foraminiferal distribution patterns in the Norwegian Cannel (northern North sea). *Marine Micropalaeontology* 9, 469–88.

Rochon, A., de Vernal, A., Sejrup, H.-P. and **Haflidason, H.** 1998: Palynological evidence of climate and oceanographic changes in the North Sea during the last deglaciation. *Quaternary Research* 49, 197–207.

Ruddiman, W.F. 1977: Late Quaternary deposition of ice-rafted sand in the subpolar North Atlantic (lat 40° to 60°N). *Geological Society of America Bulletin* 88, 1813–27.

Ruddiman, W.F. and **McIntyre, A.** 1981: The north Atlantic Ocean during the last deglaciation. *Palaeogeography, Palaeoclimatology, Palaeoecology* 35, 145–214.

Ruprecht, T.P., Schröder, S.S. and **Ubl, S.** 2002: On the relation between NAO and water vapour transport towards Europe. *Meteorologische Zeitschrift* 11, 395–401.

Schönfeld, J. 1997: The impact of the Mediterranean Outflow Water (MOW) on benthic foraminiferal assemblages and surface sediments at the southern Portuguese continental margin. *Marine Micropaleontology* 29, 211–36.

Scourse, J.D., Kennedy, H., Scott, G.A. and **Austin, W.E.N.** 2004: Stable isotopic analyses of modern benthic foraminifera from seasonally stratified shelf seas: disequilibria and the 'seasonal effect'. *The Holocene* 14, 747–58.

Scourse, J., Sejrup, H.-P., Jones, P.D. and **HOLSMEER project participants** 2006: Late Holocene oceanographic and climate change from the western European margin: the results of the HOLSMEER project. *The Holocene* 16, 931–35 (this issue).

Sejrup, H.P., Fjæran, T., Hald, M., Beck, L., Hagen, J., Miljeteig, I., Morvik, I. and **Norvik, O.** 1981: Benthonic foraminifera in surface samples from the Norwegian continental margin between 62N and 65N. *Journal of Foraminiferal Research* 11, 277–95.

Sejrup, H.P., Haflidason, H., Flatebø, T., Klitgaard Kristensen, D., Grøsfjeld, K. and **Larsen, E.** 2001: Late glacial–Holocene environmental changes and climate variability: evidence from Voldafjorden, western Norway. *Journal of Quaternary Science* 16, 181–98.

Sejrup, H.P., Birks, H.J.B., Klitgaard Kristensen, D. and **Madsen, H.** 2004: Benthonic foraminiferal distributions and quantitative transfer functions for the northwest European continental margin. *Marine Micropaleontology* 53, 197–226.

Soon, W. and **Baliunas, S.** 2003: Proxy climatic and environmental changes of the past 1000 years. *Climate Research* 23, 89–110.

Stefánsson, U. 1962: North Icelandic waters. *Rit fiskideildar* 3, 1–269.

Swift, J.H. 1986: The Arctic waters. In Hurdle, B.G., editor, *The Nordic Seas*. Springer-Verlag, 129–53.

Trigo, R.M., Osborn, M.R.P. and **Corte-Real, J.** 2002: The North Atlantic Oscillation influence on Europe: climate impacts and associated physical mechanisms. *Climate Research* 20, 9–17.

Appendix 3

PROXY CALIBRATION TO INSTRUMENTAL DATASET: IMPLICATIONS FOR PALEOCEANOGRAPHIC RECONSTRUCTIONS

Abrantes F[*1]., Lopes C[1,2], **Rodrigues T.[1,3],** Gil I[1,2], Witt L[4]., Grimalt J.O.[3] and Harris I.[5]

1 -National Laboratory for Energy and Geology (LNEG), Unidade de Geologia Marinha, Aptdo 7586, 2721-866 Amadora, Portugal, Tel. (351) 21 0924636, Fax (351) 21 471 9018, *fatima.abrantes@ineti.pt
2 - CIMAR, Porto - Portugal
3 - Department of Environmental Chemistry, Institute of Environmental Assessment and Water Research (IDÆA. CSIC), Barcelona – Spain
4 - Pacific Fisheries Environmental Lab, Pacific Grove, CA - USA
5 - Climatic Research Unit, University of East Anglia -United Kingdom

Geochemistry, Geophysics, Geosystems, (2009)

Geochemistry Geophysics Geosystems G3
AN ELECTRONIC JOURNAL OF THE EARTH SCIENCES
Published by AGU and the Geochemical Society

Article
Volume 10, Number 9
22 September 2009
Q09U07, doi:10.1029/2009GC002604
ISSN: 1525-2027

Proxy calibration to instrumental data set: Implications for paleoceanographic reconstructions

F. Abrantes
Unidade de Geologia Marinha, Laboratório Nacional de Energia e Geologia, Apartado 7586, P-2721-866 Amadora, Portugal (fatima.abrantes@ineti.pt)

C. Lopes
Unidade de Geologia Marinha, Laboratório Nacional de Energia e Geologia, Apartado 7586, P-2721-866 Amadora, Portugal

CIMAR, Porto, Portugal

T. Rodrigues
Unidade de Geologia Marinha, Laboratório Nacional de Energia e Geologia, Apartado 7586, P-2721-866 Amadora, Portugal

Department of Environmental Chemistry, Institute of Environmental Assessment and Water Research, CSIC, Jordi Girona, 18, E-08034Barcelona, Catalonia, Spain

I. Gil
Unidade de Geologia Marinha, Laboratório Nacional de Energia e Geologia, Apartado 7586, P-2721-866 Amadora, Portugal

CIMAR, Porto, Portugal

L. Witt
Environmental Research Division, SWFSC, NMFS, NOAA, 1352 Lighthouse Avenue, Pacific Grove, California 93950-2097, USA

J. Grimalt
Department of Environmental Chemistry, Institute of Environmental Assessment and Water Research, CSIC, Jordi Girona, 18, E-08034Barcelona, Catalonia, Spain

I. Harris
Climatic Research Unit, University of East Anglia, Norwich NR2 4HG, UK

[1] High-resolution proxy data analyzed on two high-sedimentation shallow water sedimentary sequences (PO287-26B and PO287-28B) recovered off Lisbon (Portugal) provide the means for comparison to long-term instrumental time series of marine and atmospheric parameters (sea surface temperature (SST), precipitation, total river flow, and upwelling intensity computed from sea level pressure) and the possibility to do the necessary calibration for the quantification of past climate conditions. XRF Fe is used as proxy for river flow, and the upwelling-related diatom genus *Chaetoceros* is our upwelling proxy. SST is estimated from the coccolithophore-synthesized alkenones and $U^{k'}_{37}$ index. Comparison of the Fe record to the instrumental data reveals its similarity to a mean average run of the instrumentally measured winter (JFMA) river flow on both sites. The upwelling diatom record concurs with the upwelling indices at both

sites; however, high opal dissolution, below 20–25 cm, prevents its use for quantitative reconstructions. Alkenone-derived SST at site 28B does not show interannual variation; it has a mean value around 16°C and compares quite well with the instrumental winter/spring temperature. At site 26B the mean SST is the same, but a high degree of interannual variability (up to 4°C) appears to be determined by summer upwelling conditions. Stepwise regression analyses of the instrumental and proxy data sets provided regressions that explain from 65 to 94% of the variability contained in the original data, and reflect spring and summer river flow, as well as summer and winter upwelling indices, substantiating the relevance of seasons to the interpretation of the different proxy signals. The lack of analogs and the small data set available do not allow quantitative reconstructions at this time, but this might be a powerful tool for reconstructing past North Atlantic Oscillation conditions, should we be able to find continuous high-resolution records and overcome the analog problem.

Components: 6986 words, 9 figures, 2 tables.

Keywords: proxy; calibration; paleoceanography; latest Holocene; Portugal; inner shelf.

Index Terms: 4999 Paleoceanography: General or miscellaneous; 1616 Global Change: Climate variability (1635, 3305, 3309, 4215, 4513); 0424 Biogeosciences: Biosignatures and proxies.

Received 1 May 2009; **Revised** 20 July 2009; **Accepted** 31 July 2009; **Published** 22 September 2009.

Abrantes, F., C. Lopes, T. Rodrigues, I. Gil, L. Witt, J. Grimalt, and I. Harris (2009), Proxy calibration to instrumental data set: Implications for paleoceanographic reconstructions, *Geochem. Geophys. Geosyst.*, *10*, Q09U07, doi:10.1029/2009GC002604.

Theme: Circum-Iberia Paleoceanography and Paleoclimate: What Do We Know?
Guest Editors: A. Voelker, F. Abrantes, M. F. Sánchez Goñi, and C. Ruehlmann

1. Introduction

[2] Forecasts of future climatic trends depend on widespread accurate and quantitative records of past climate. *Briffa and Osborn* [2002], on a revision of a new tree ring–derived temperature record for the past millennium, state "We need more independent reconstructions, based on improved proxy records, and we need to know why it was once so warm and then so cool, before we can say whether 21st-century warming is likely to be nearer the top or the bottom of the latest IPCC range of 1.4°C to 5.8°C" [*Watson et al.*, 2001]. Furthermore, in 2002, recommendation 3 of the U.S. National Research Council report on "Abrupt Climate Change" [*Committee on Abrupt Climate Change*, 2002] reinforces the need for (1) coordinated projects to produce especially robust, multiparameter, high-resolution histories of climate change and ecological response; (2) better geographic coverage and higher temporal resolution; and (3) additional proxies, including those that focus on water (e.g., droughts, floods, etc). Additional emphasis is put on the need for records of the last 2,000 years, so that warming and associated changes of the last 100 years can be assessed in context.

[3] Given that the instrumental record is short, only about 100 years at most, longer climate reconstructions depend on proxy data that needs calibration. Up to now, much of the sediment proxy data calibration has been of two types: (1) definition of empirical correlations based on the comparison of spatial distribution of a certain proxy and a certain property and (2) the establishment of direct relationships through sediment trap studies. Nevertheless these studies are recent and the available time series are yet too short to allow totally reliable calibrations. The existence of high-resolution proxy data from key areas characterized by specific phenomena and from areas where instrumental record data is available is of great importance to estimate the relative magnitude of past changes. In addition it will also allow the scaling of proxy data against 100 years of instrumental observations.

[4] In this article, we use paleoenvironmental high-resolution records recovered from the inner-shelf deposition center of the suspended matter transported by the Tagus river flow to assess the climate events of this century. To do so, we present what we believe to be a first attempt to calibrate sediment proxy data for both continental climate

and oceanic productivity to the existing 100 years instrumental time series of data for sea surface temperature (SST), precipitation, river runoff and upwelling strength.

2. Regional Setting

[5] The North Atlantic Ocean is one of the key areas in the workings of global climate [*Broecker*, 1997], and on multidecadal, decadal and subdecadal time scales, the North Atlantic Oscillation (NAO) has been identified to have the most recurrent atmospheric teleconnection determining Atlantic climatic conditions. The first instrumental index of the NAO [*Hurrell*, 1995] is based on pressure measurements from Lisbon (Portugal) and Stykkisholmur (Iceland) and the Iberian precipitation and the Tagus (Iberia's longest river) flow has been shown to be highly determined by this single atmospheric circulation mode [*Trigo et al.*, 2002, 2003].

[6] From late fall to early spring rain falls in the Tagus drainage basin contributing to the Tagus flow. The subsequent runoffs transport terrigenous materials to the coast and offshore, where they accumulate in the shelf area off Lisbon. The presence in those sediments of continental materials can be used as a proxy for the Tagus River flow and winter-spring precipitation allowing the reconstruction through time of the determining winter atmospheric circulation mode, that is, the NAO phases.

[7] From late spring to late summer, the occurrence of strong northerly winds generates coastal upwelling along the western Portuguese coast. During this upwelling season, a front between the cold recently upwelled waters and the offshore waters becomes visible in satellite images that also show the existence of upwelling filaments mainly associated to the capes [*Sousa and Bricaud*, 1992; *Relvas et al.*, 2007].

[8] The upwelling jet rooted at Cape of Roca, has an approximate N-S orientation, it is a persistent feature and influences mainly the NW half of the Tagus mud patch. As such, primary production at site 28B is upwelling derived, while at the location of site 26B, primary productivity is mainly associated with the Tagus River discharge of nutrients as demonstrated by *Cabeçadas et al.* [1999]. Although both winter-spring river input of nutrients and summer upwelling feed primary productivity in the area and result in the export of organic carbon, calcareous and siliceous microfossils to the sediments, the combination of a river flow proxy with proxy(ies) for upwelling conditions should allow the reconstruction of the processes that result from these two seasons' main atmospheric conditions.

3. Material and Methods

3.1. Core Characterization

[9] PO287 cores were retrieved in May 2002, during the PALEO1 campaign aboard the German RV Poseidon (Figure 1). Box and gravity cores PO287-26B (52 cm) and 26G (327 cm) were recovered from 38°33.49′N, 9°21.84′W and 96 m water depth, while box core PO287-28B (52 cm) was collected at 38°37.47′N, 9°30.87′W and 105 m water depth. Piston core D13902 (600 cm) was recovered from 38°33.24′N, 9°20.13′W from 90 m water depth during the research cruise D249 on board RV Discovery.

3.2. Methodology Used in the Analyses of the Various Parameters

[10] Magnetic susceptibility (MS in $K10^{-6}$ SI) was continually measured on a multiparameter logging system and bulk sedimentary iron (Fe) was measured, as counts per second (cps), with a profiling X-ray fluorescence scanner at 1 cm spacing [*Jansen et al.*, 1998]. Both measurements were done at the University of Bremen.

[11] All other analyses, including grain size, alkenones with 37 carbon atoms [37alq] and other terrigenous biomakers such as *n*-alkanes and *n*-alcohols ([n-OH]) and diatoms, were done continuously on 1 cm sediment slices. The methods used for each determination were the ones described by *Abrantes et al.* [2005].

[12] Diatom assemblages were defined on the basis of the identification and counting of a minimum of 300 specimens. For samples with very low diatom abundances, which increase the counting time to more than 2 days per sample, the number of identified specimens was reduced to 100 on the basis of the work of *Fatela and Taborda* [2002].

3.3. Instrumental Sea Surface Temperature

[13] Instrumental data for SST and Precipitation are the ones compiled at the CRU Web site (http://www.cru.uea.ac.uk/cru/data/). The SST data corresponds to mean mensal sea surface temperature for an area of 5° × 5° and cover the years 1870 to 1999.

3.4. Tagus River Flow

[14] River flow data has been obtained from the Portuguese National Service for Hidric Resources

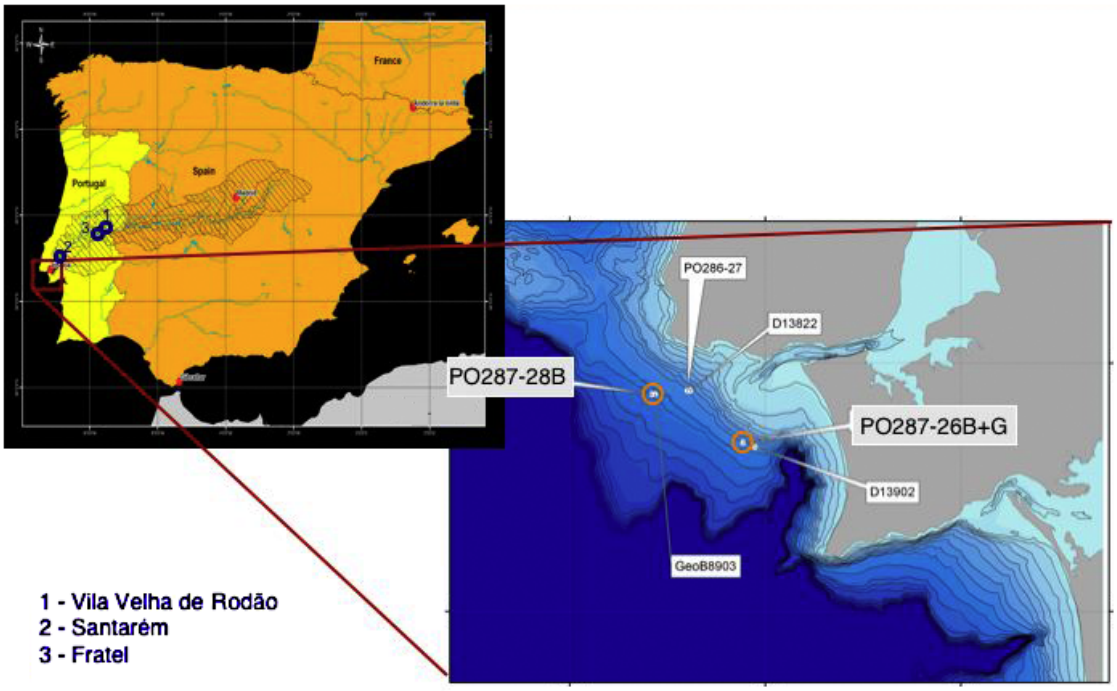

Figure 1. Geographic location of the studied area in relation to the Iberian Peninsula and sites where the instrumental river flow is available. The blowup map shows also the location of box cores PO287-26B and 28B, as well as of gravity core PO287-26G and piston core D13902. Reconstructions of the Tagus River flow and upwelling index are done through the application of the equations encountered by the proxy-instrumental data correlation to the D13902 data used by *Abrantes et al.* [2005].

(SNIRH) (http://snirh.inag.pt). In this paper we use a 103 years data set that results from the combination of the data from different stations, Vila Velha de Rodão (VVR) which covers 1901 to 1974, and Santarém for which there is data between 1944 and 2004. The fact that both stations cover the years 1944 to 1974 allowed for us to verify the agreeability of these two stations' measurements through the calculation of the correlation between the two variables for the winter months (December to March (DJFM) and January to April (JFMA); Figure 2 (left)). Besides, we have verified how this longer data set (103 years) compares with the 82 year record of the Fratel hydrologic station, a data set considered of higher quality and used by *Trigo et al.*

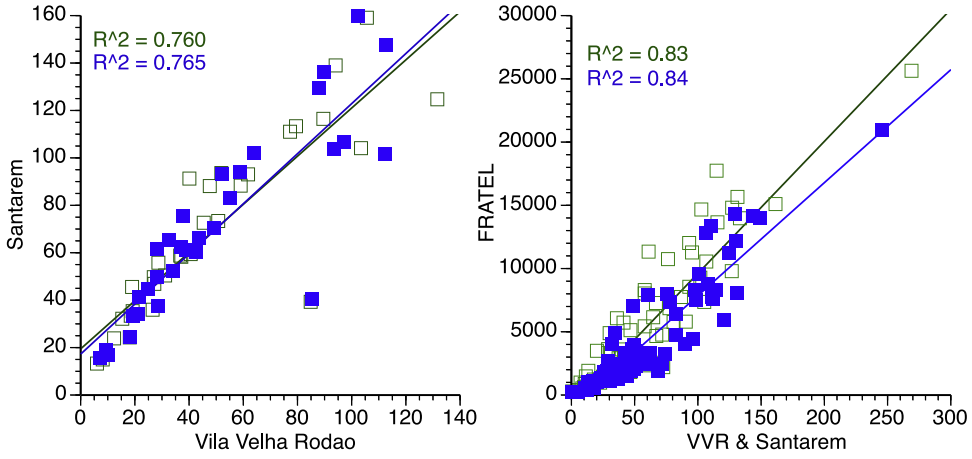

Figure 2. Correlation between the Tagus River total flow in 10^5 dam^3 as instrumentally measured at Vila Velha de Rodão (VVR) and Santarém, and between those and the Fratel station. The values compared are the mean values calculated for the NAO Winter months, December to March (DJFM, solid squares) as well as the mean values for the same number of months but with a 1-month delay, that is, January to April (JFMA, open squares).

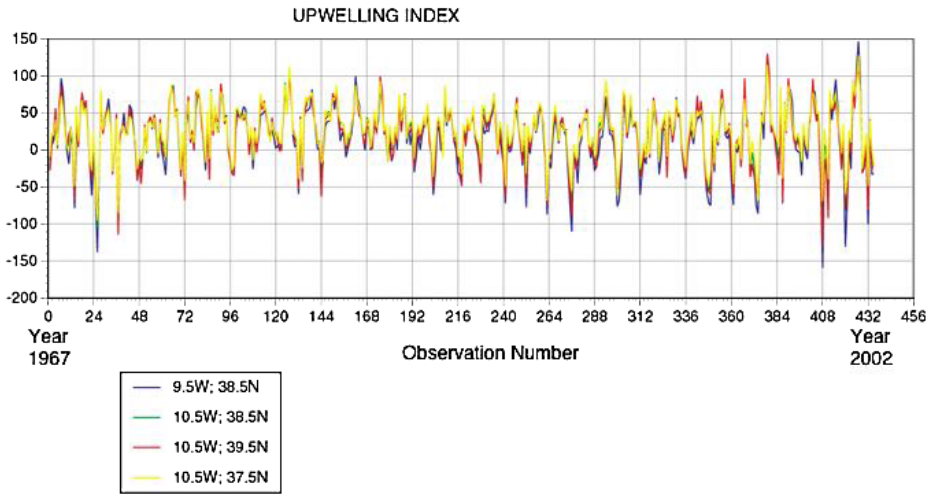

Figure 3. Upwelling indices' (m^3/s/100 m of coastline) variability through time (1967 to 2002) as estimated for four different locations on the Portuguese coast following *Bakun* [1973].

[2002]. Figure 2 (right) shows the regression line and high correlation of those data sets.

3.5. Upwelling Index

[15] Upwelling indices were determined at the National Oceanic and Atmospheric Administration (NOAA) as follows: first, geostrophic winds were calculated from the FNMOC 6-hourly pressure analysis, which is on a 1-degree grid spacing after 1969, a 3-degree grid spacing after 1947, and a 5-degree grid spacing after 1898. Wind stress and Ekman transport were then calculated from these geostrophic winds. Finally, the Ekman transport is rotated to get the offshore component, provided that the orientation of the coast is known, and following *Bakun* [1973] (http://las.pfeg.noaa.gov/las/doc/global_upwell.html).

[16] The 1-degree index was calculated for four different geographic locations in the vicinity of our sites (38.5°N 9.5°W; 38.5°N 10.5°W; 37.5°N 10.5°W and 39°N 9.5°W), but their comparison showed very good agreement for the overall region (Figure 3). As so, we have chosen the data for 38°N, 9°30′W, the closest to the study sites, for comparison to the proxies for upwelling-derived primary productivity.

3.6. Multiple Stepwise Regressions

[17] One of the first steps in proxy calibration is the study of the existence of possible "links" between instrumental data and the properties that we can measure in the sediments [*Lopes et al.*, 2006]. These "links" are measured and expressed as statistical values of significant correlations, strong regressions and robust calibrations and/or validations [*Crosta and Koç*, 2007]. The ultimate goal of these statistical analyses is to develop transfer functions (statistical models that allow us to reconstruct the instrumental measurements back in the past).

[18] As previously mentioned, the temporal length of the instrumental data and the resolution of the sediment records are not suitable enough, at this point, to develop transfer functions (as they are defined [e.g., *Crosta and Koç*, 2007]). However, regression coefficients can be found and point us on the right direction in order to achieve this goal.

[19] The multiple stepwise regressions were done using the instrumental data as the independent variables and the several sediment measured properties as the dependent variables. The stepwise regression is a process in which at each step the addition or not of a variable is evaluated by an F test at the 95% confidence level [*Pisias et al.*, 1997]. The final equations are thus evaluated by the final regression coefficient and the RMSE (root mean squared error).

4. Chronology

[20] An age-depth model for both cores has been constructed by integrating the ^{210}Pb determinations done at the Nederlands Instituut voor Onderzoek der Zee (NIOZ) for 9 levels in each box core and three deeper samples from core D13902 for base activity determinations.

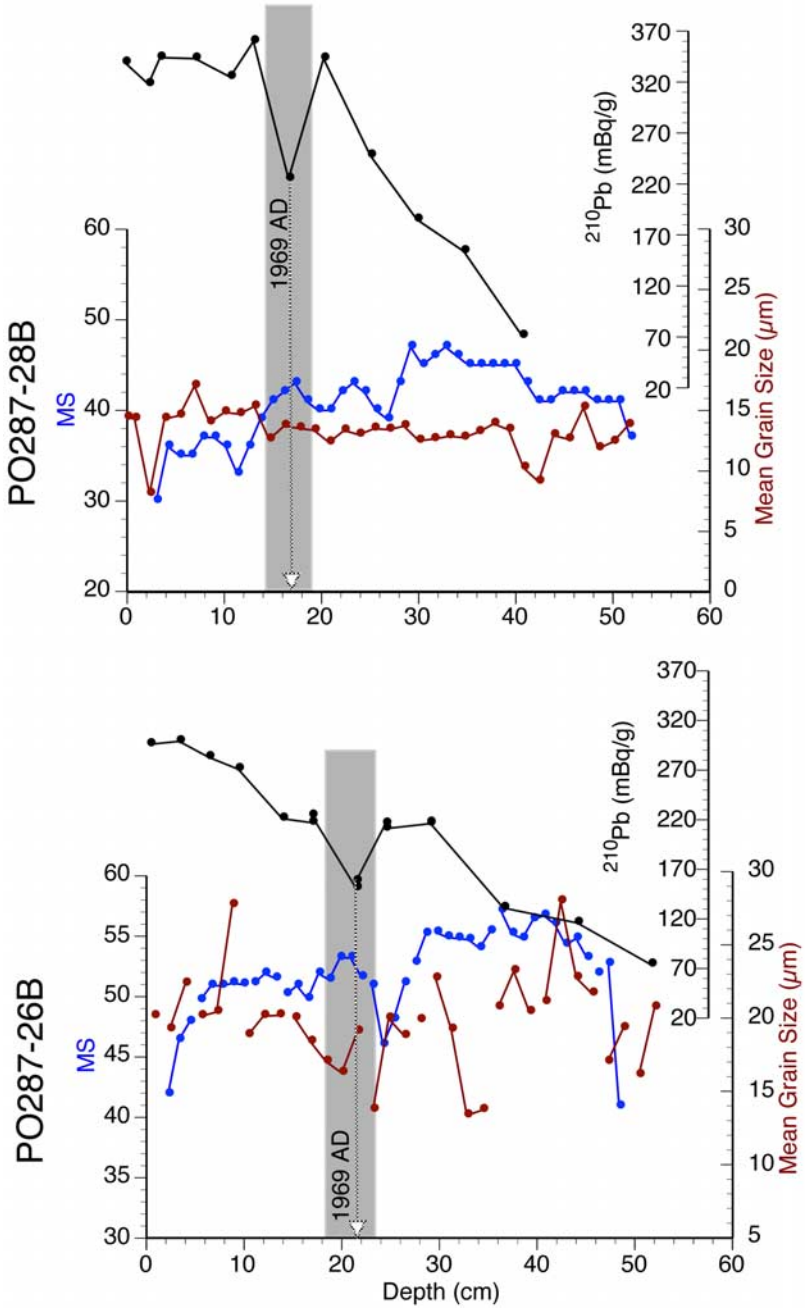

Figure 4. The ^{210}Pb (mBq/g), magnetic susceptibility (MS − K × 10^{-6} SI), and mean grain size (μm) distribution along box cores (top) PO287-28B and (bottom) PO287-26B. Gray band marks the levels disturbed by the 1969 earthquake and tsunami [*Abrantes et al.*, 2008].

[21] AMS ^{14}C analysis was preformed on a sample from a 36–37 cm depth in box core 26B, reservoir corrected by 400 years [*Abrantes et al.*, 2005] converted to calendar ages with the INTCAL04 data set [*Reimer et al.*, 2004]. Calibrated ages are presented in years anno Domini (A.D.).

[22] Correlation between the two cores 28B to 26B was further done on the basis of the MS record (Figure 4). Furthermore, as discussed by *Abrantes et al.* [2008], the minimum in total ^{210}Pb found in both box cores represents a 5 to 8 cm "tsunamite" emplaced at an estimated age of 1970 ± 4, and is attributed to the 1969 A.D. earthquake-related tsunami felt in the Lisbon area.

[23] The definition of the 2,000 year long spliced sequence age model (D13902 and PO287 26B, G) followed the line of reasoning presented by *Abrantes et al.* [2005] although the conversion of

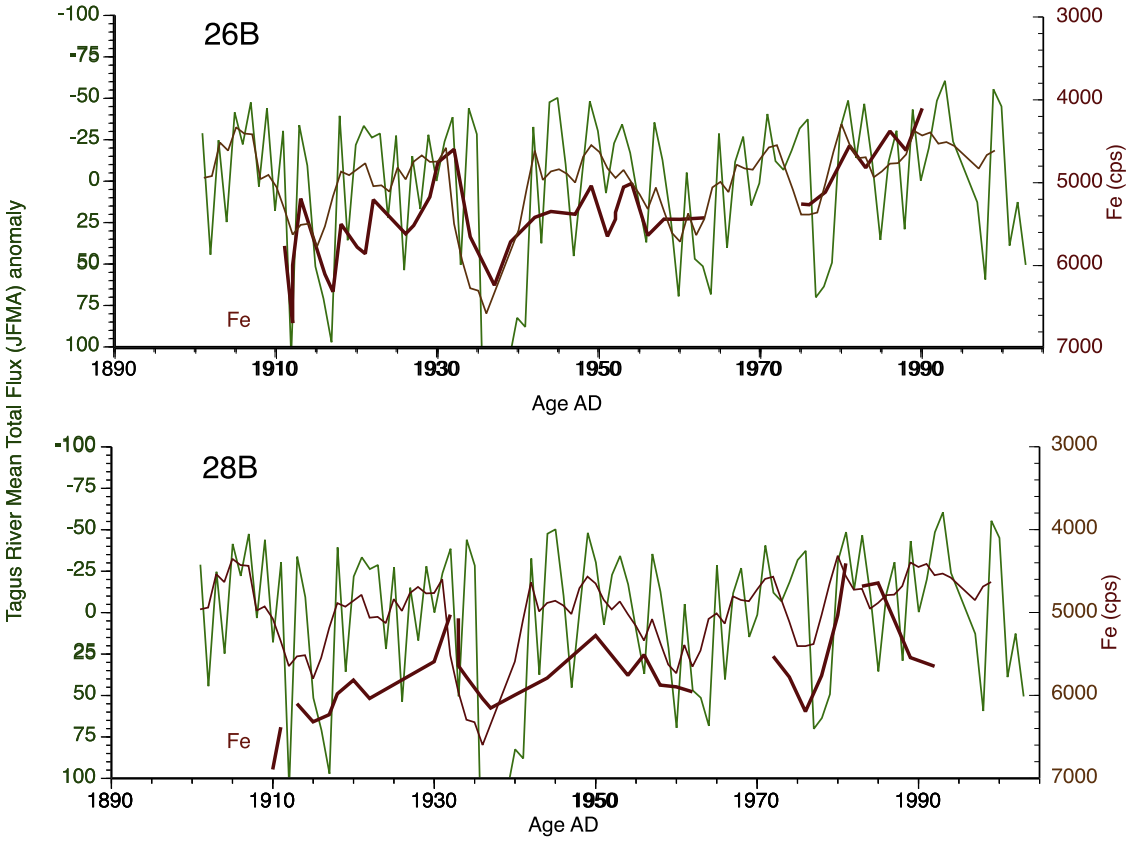

Figure 5. Distribution of the Fe content (cps, brown thick line), the winter (JFMA) Tagus River Mean Total Flux anomaly (green thin line), and a five-point mean average run of the (JFMA) Tagus River Mean Total Flux anomaly (brown thin line) along cores (top) PO287-26B and (bottom) PO287-28B. Data relative to the tsunami-disturbed layer are not included.

the conventional AMS ^{14}C ages into calendar ages is based on the new INTCAL04 data set [*Abrantes et al.*, 2008].

[24] The final estimated sedimentation rates vary between 0.14 and 1.45 cm/a with a mean value of 0.73 cm/a in core 26B, while in 28B they oscillate between 0.24 and 1.41 cm/a with a mean value of 0.63 cm/a.

5. Results and Discussion

5.1. Precipitation and River Input

[25] The precipitation regime in the Iberian Peninsula is characterized by large interannual variability as well as high variability in the amount and distribution of rainfall [*Fiuza*, 1984; *Trigo and DaCamara*, 2000], but most precipitation occurs mainly between November and April. The Tagus is the longest river of the Iberian Peninsula and satellite-derived estimations of its plume suspended load, between May 1992 and January 1993 [*Williams*, 1994], indicate that the Tagus suspended load is high throughout the year, as actually revealed also by a September space shuttle image [*Abrantes et al.*, 2005, Figure 8]. However, short but strong rainfall can lead to flood events that can cause a river flux up to 12000 m^3/s, 10^6 times higher than the month average (0.9 m^3/s), and, 30 times higher than the mean annual flux (400 m^3/s). During the February 1979 flood event, the suspended load reached 300 mg/l and a stationary value of 20 mg/l was found for the following month [*Vale*, 1981].

[26] As part of the essentially fine-grained particles transported by the river, one can include Fe particles (resultant from the weathering of continental rocks and soils), and continental derived organic matter. The Fe content of the sediments has been used as a simple chemical proxy for the input of land-derived materials and Fe variations are considered to be a direct measure of rainfall and river input by several authors such as *Haug et al.* [2001] and *Itambi et al.* [2009]. On this basis, the Fe content of this sedimentary sequence has been assumed to be mainly determined by continental

precipitation and thus able to portray winter precipitation conditions on the continent. Therefore it can be calibrated to winter mean river flow (mean value of the considered month's total flow measured in Santarem and/or VVR) and precipitation. A comparison of the Fe (cps) content on both cores, to the Tagus winter (JFMA) mean flow anomaly and a 5 point mean average run of this anomaly for the winter mean flow is presented in Figure 5. Although not comparable point by point, a good general agreement is observed in terms of trend and the correlation coefficients between Fe and the mean river flow at all seasons for each site as well as both sites is significantly related to the river flow (Table 1) and consequently to the magnitude of winter precipitation. On this basis, quantitative estimations of the river paleoflow at this location should be possible through the application of regression equations that are obtained from the comparison of the instrumental data set to the proxy data of 26B and 28B, and its application to the data covering the last 2,000 years in the D13902 and PO287-26G cores [*Abrantes et al.*, 2005].

5.2. Upwelling and Productivity

[27] A qualitative and quantitative study of the water column phytoplankton along the Portuguese coast at the four seasons by *Moita* [2001], confirms the findings of *Sousa and Bricaud* [1992] and *Abrantes and Moita* [1999] in identifying coastal upwelling as the determinant process for the primary production patterns observed off Portugal. On the basis of the same work, the phytoplankton assemblage associated with that hydrographic process, dominant during both spring and summer, was mainly composed of chain forming diatoms, of small and medium size like *Chaetoceros*. A compilation of the observations for the Tagus prodelta region in particular, is presented in Table 2 and reveal that here, as along the entire coast, diatoms only dominate the phytoplankton community during upwelling periods [*Moita*, 2001].

[28] *Abrantes and Moita* [1999] compared the distribution pattern of total phytoplankton biomass, diatoms and coccolithophores abundance (# cells/l and % abundance) as well as diatom assemblages in the water column, during a nonupwelling and an upwelling situation, and the same groups distribution in the sediments. Their results indicate that the total diatom distribution pattern in the sediments is a clear record of the diatom dominance of the phytoplankton during the upwelling season. Furthermore, also the coccolithophores, even though clearly more important in winter phytoplankton, show a distribution in the sediments that is connected to the distribution of the same group during upwelling periods. On the basis of these results the authors conclude that, on the Portuguese margin diatoms produced during blooms are preserved with greater efficiency than those produced during nonbloom periods as defended also by *Nelson et al.* [1995].

[29] Upwelling conditions through time should then give a reasonable indication of the related productivity at the study sites. As a measure of the upwelling conditions, we have used the upwelling index calculated by NOAA following *Bakun* [1973]. In the sediments, total diatoms and *Chaetoceros* resting spores can be the proxies for productivity generated by upwelling. Figure 6 shows the comparison of the upwelling-related genus *Chaetoceros* abundance along the two box cores and the various upwelling indices. The first observation that can be noticed is the higher diatom abundance in core 28B, an expected result considering the continuous influence of upwelling conditions at this site. A second very important observation is the fact that diatoms disappear in both sites below 1950, that is, 20–25 cm downcore, certainly due to important dissolution. When we compare the diatom data to the upwelling indices, a good agreement is visible for the 1-degree index, but it becomes less and less good when the lower-resolution indices are used, an evaluation confirmed by the correlations to the upwelling indices (Figure 6 and Table 1).

[30] These results call our attention for the need to use high-resolution instrumental data if a comparison to high sedimentation rate sequences is the aim.

5.3. Sea Surface Temperature

[31] Instrumentally recorded sea surface temperature (SST) variability over the last century shows that, on a regional scale, interannual to decadal climate variability is the norm [*Rodrigues et al.*, 2009]. Estimates from the sediment record are based on the $U^{k'}_{37}$ index, an index derived from the alkenones, a biomarker produced by coccolithophores. The index calculation followed the equation proposed by *Müller et al.* [1998], for which the error of estimate is of 1.5°C. Visual observation of its variability during the last century (Figure 7) shows little oscillation around 16°C at site 28B. At site 26B on the contrary, and even though the average value is also 16°C, the amplitude of variability is up to 4°C. When these

Table 1. Correlation Coefficients Found Between Proxies and Instrumental Data for a 99.9 Confidence Level[a]

	River Flux VVR and Santarem		River Flux Fratel							Upwelling 1 × 1				Upwelling 3 × 3	Upwelling 5 × 5	Instrumental SST				
	Winter (D-M)	Winter (J-A)	Annual	Winter (D-M)	Winter (J-A)	Spring	Summer	Fall	Upseason	Annual	Summer	Winter (D-M)	Winter + Spring	Summer	Summer	Annual	Upseason	Summer	Winter (D-M)	Spring
26B	N = 70		N = 53							N = 24				N = 70	N = 70	N = 70				
SST (°C)	0.08	0.14	0.09	0.05	0.07	0.07	0.19	0.01	0.13	*0.35*	0.35	0.03	0.17	0.08	−0.21	−0.14	−0.18	−0.25	***−0.31***	0.03
[n-alk] ng/g	−0.06>	−0.01	−0.10	−0.10	−0.08	0.06	0.10	−0.12	0.09	−0.48	−0.17	**−0.53**	**−0.58**	0.13	−0.18	−0.15	−0.09	−0.09	−0.04	−0.08
[n-OH] ng/g	0.00>	0.03	−0.02	−0.09	−0.07	0.04	0.07	−0.12	0.10	*−0.54*	−0.37	*−0.51*	**−0.74**	0.21	0.00	0.23	0.18	0.08	0.07	0.26
[37alq] ng/g	0.06>	0.02	0.01	0.06	0.09	−0.09	−0.27	0.03	−0.26	−0.47	−0.15	*−0.55*	**−0.57**	*0.34*	*0.31*	0.19	0.11	0.10	0.24	0.10
28B	N = 79		N = 79							N = 36				N = 79	N = 79	N = 79				
SST (°C)	−0.12	−0.06	−0.06	−0.05	−0.04	0.08	0.20	−0.15	0.14	0.37	0.21	**0.45**	**0.47**	0.01	−0.10	−0.24	−0.14	−0.12	−0.11	−0.19
[n-alk] ng/g	0.09	0.09	0.11	0.15	0.12	0.14	0.08	0.02	0.11	0.28	0.06	−0.03	0.19	0.19	−0.18	**−0.43**	−0.28	−0.27	−0.20	**−0.37**
[n-OH] ng/g	0.03	0.03	0.09	0.13	0.12	0.07	−0.14	0.00	−0.07	0.15	−0.11	−0.17	0.01	*0.28*	0.21	−0.09	−0.05	0.01	0.00	−0.03
[37alq] ng/g	0.00	−0.03	−0.03	0.04	0.03	−0.10	***−0.36***	0.01	*−0.30*	0.11	−0.13	−0.11	−0.03	0.17	0.21	0.07	0.03	0.01	0.06	0.11
[38alq] ng/g	0.02	0.01	0.09	0.17	0.14	−0.07	−0.22	0.06	−0.22	0.27	0.00	−0.19	0.01	0.23	0.16	−0.03	−0.04	−0.06	0.03	0.02
26B+28B	N = 149		N = 132							N = 60				N = 149	N = 149	N = 149				
SST (°C)	0.03	0.08	0.05	0.02	0.04	0.06	0.17	−0.02	0.11	**0.35**	0.27	0.22	0.27	0.06	−0.16	−0.17	−0.17	−0.20	−0.12	−0.04
[n-alk] ng/g	0.00	0.02	−0.02	−0.02	−0.04	−0.03	0.09	0.00	0.03	−0.05	−0.08	−0.18	−0.13	0.04	−0.15	−0.09	−0.03	−0.03	−0.09	−0.02
[n-OH] ng/g	0.01	0.02	−0.01	−0.03	−0.04	−0.04	0.04	0.04	0.01	−0.15	−0.18	−0.26	−0.28	0.11	−0.02	0.12	0.13	0.07	0.08	0.16
[37alq] ng/g	0.01	−0.01	0.01	0.04	0.06	0.05	−0.16	−0.02	−0.09	−0.02	0.17	−0.04	−0.03	0.12	0.15	−0.01	−0.04	−0.04	0.03	−0.03
26B	N = 35		N = 24							N = 16				N = 19	N = 36					
FWDiatom Ab	−0.18	−0.13	−0.08	0.08	−0.11	−0.04	−0.05	−0.08	−0.02	−0.40	***−0.76***	*−0.65*	*−0.69*	−0.36	0.12					
Total Diatom Ab	−0.10	−0.03	0.07	0.20	0.25	0.26	−0.16	−0.13	−0.11	**0.65**	0.53	0.45	0.50	0.04	0.34					
Upwelling Forms Ab	−0.09	−0.04	0.03	0.13	0.27	0.33	−0.14	−0.09	−0.13	**0.78**	*0.65*	*0.68*	0.64	0.04	0.33					
28B	N = 37		N = 31							N = 12				N = 19	N = 38					
FWDiatom Ab	−0.10	−0.05	0.01	−0.04	0.01	0.03	−0.11	0.03	−0.04	**−0.55**	*−0.40*	−0.17	−0.15	−0.03	0.37					
Total Diatom Ab	−0.03	−0.04	0.09	0.05	0.15	−0.06	*−0.44*	0.20	**−0.42**	**−0.64**	−0.27	−0.59	−0.52	0.01	0.33					
Upwelling Forms Ab	0.07	0.05	0.18	0.15	0.22	0.01	−0.34	0.25	−0.34	−0.44	0.05	**−0.53**	−0.44	0.00	0.20					
26B + 28B	N = 72		N = 55							N = 28				N = 38	N = 74					
FWDiatom Ab	−0.13	−0.07	−0.02	−0.02	−0.02	−0.01	−0.09	0.03	−0.03	**−0.51**	*−0.47*	−0.30	−0.31	−0.13	0.16					
Total Diatom Ab	−0.05	−0.04	0.08	0.05	0.13	−0.02	*−0.35*	0.13	−0.30	−0.01	0.04	−0.16	0.01	0.03	0.28					
Upwelling Forms Ab	0.02	0.02	0.13	0.10	0.17	0.02	−0.28	0.16	−0.27	0.15	0.27	−0.01	0.12	0.01	0.16					
Fe 26B (N = 39)	0.58	**0.60**	*0.58*	*0.49*	*0.46*	**0.63**	*0.45*	0.29	*0.52*											
Fe 28B (N = 36)	0.35	0.31	*0.51*	*0.45*	**0.53**	*0.44*	−0.01	0.23	0.16											
Fe 26B + 28B (N = 75)	*0.43*	*0.40*	**0.47**	*0.41*	*0.45*	**0.47**	0.14	0.21	0.26											

[a] N represents the number of observations. Numbers in italic represent significant correlation coefficients at $p > 0.01$, and numbers in bold refer to the most significant correlation coefficient, either positive or negative.

Geochemistry Geophysics Geosystems G3
ABRANTES ET AL.: PROXY CALIBRATION TO INSTRUMENTAL DATA SET
10.1029/2009GC002604

Table 2. Contribution of Coccolithophores and Diatoms to the Water Column Total Phytoplankton Biomass at the Two Site Locations[a]

	Chl *a* (mg/m^3)	Total Phytoplankton (#cells/L)	Diatoms (#cells/L)	Coccolithophores (#cells/L)	Dinoflagellates (#cells/L)
26B					
Summer 1985	3.8	6.4E+04	3.6E+03	1.4E+04	7.7E+03
Winter 1986	0.4	2.4E+04	3.2E+03	1.5E+04	1.5E+03
Spring 1986	5.8	2.0E+04	1.0E+03	1.6E+04	5.8E+02
28B					
Summer 1985	2.5	8.3E+04	4.4E+03	2.8E+04	2.4E+04
Winter 1986	0.2	8.0E+03	8.8E+02	6.4E+03	4.8E+02
Spring 1986	5.0	2.1E+04	1.1E+03	1.2E+04	3.6E+02

[a] Data from *Moita* [2001].

estimated SST records are compared with the longer available series of instrumental SST from the SW coast of Portugal, the 28B alkenone-derived SST mainly represents winter temperature values, while the high variability observed for 26B closely follows the summer upwelling variability. Nevertheless, no significant correlations exist between the alkenone-derived SST and the instrumental SST. However, if correlations to all instrumental data sets are calculated, the PO287-26B alkenone-derived SSTs do show a positive significant correlation to the summer 1-degree resolution upwelling index (Table 1), indicating both the interplay between upwelling and the lower temperature of river waters as also visible in satellite images [*Rodrigues et al.*, 2009, Figure 6]. That is, in years in which the strong upwelling conditions affect the normal river flow, warmer waters dominate site 26B. As for core 28B, the only significant correlation found is a positive correlation

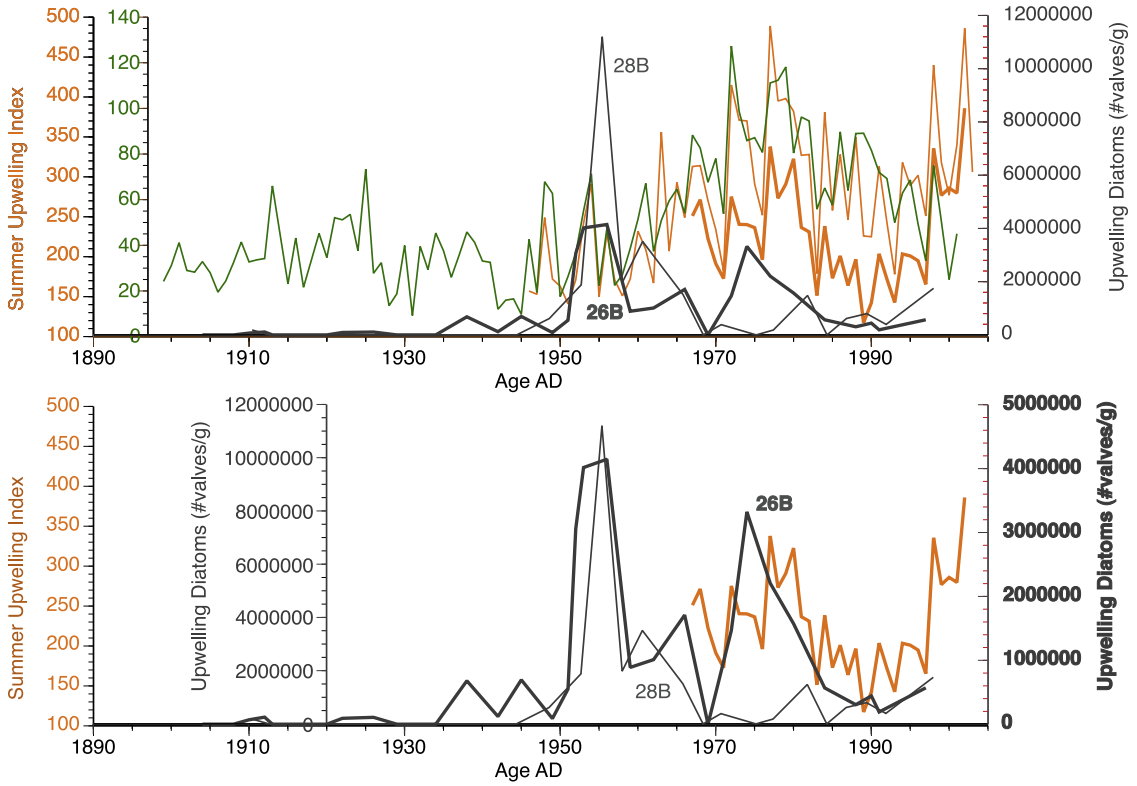

Figure 6. (top) Distribution of upwelling-related diatoms' abundance (#valves/g) in box cores PO287-26B (thin gray) and PO287-28B (thick gay) and the estimated upwelling indices, 1967–2001, 1 × 1° (thick orange); 1947–2003, 3 × 3° (thin orange); 1900–2005, 5 × 5° (thin green and different scale). (bottom) Distribution of the abundance (#valves/g) of upwelling-related diatoms in box cores PO287-26B (thin gray) and PO287-28B (thick gray), now on different scales, and the higher-resolution estimated summer upwelling index (1967–2001, 1 × 1°, thick orange).

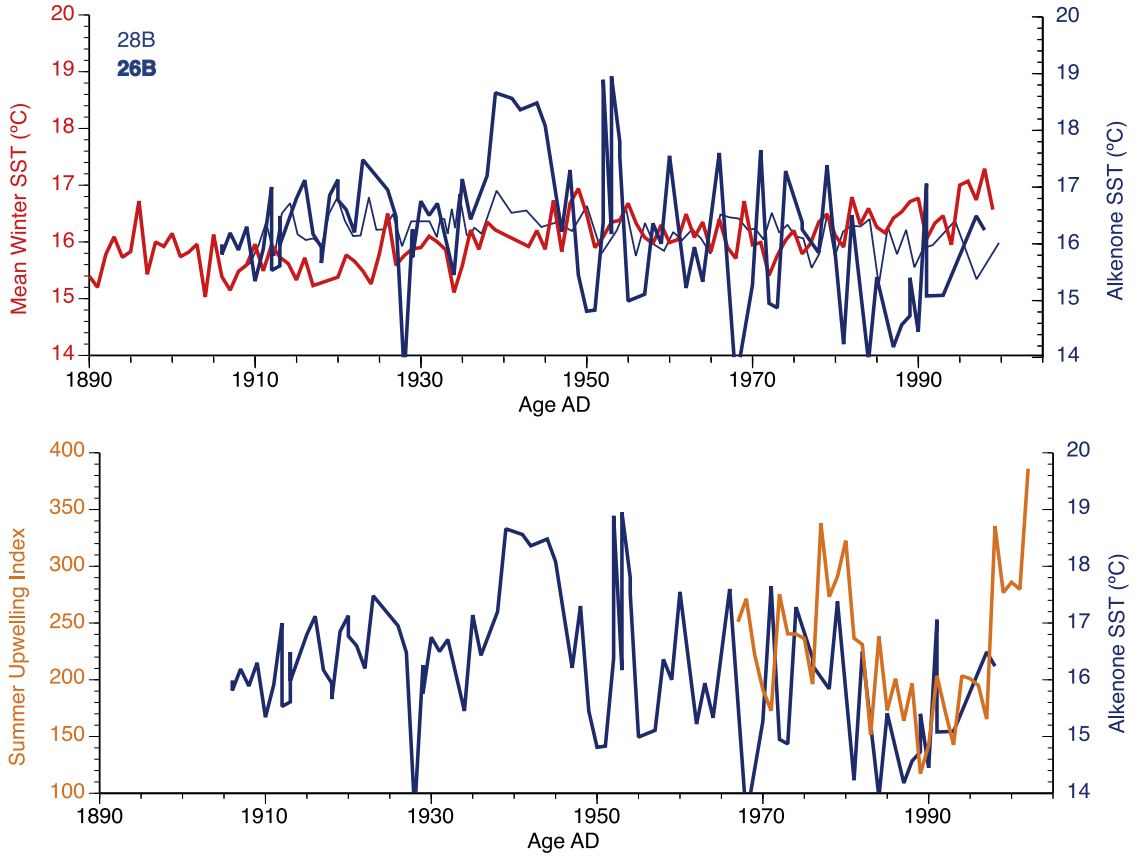

Figure 7. A. Comparison of the alkenone-derived SST along PO287-26B (thick blue) and 28B (thin blue) with the instrumentally measured winter SST (thick red). B. Comparison of the alkenone-derived SST along PO287-26B (thick blue) and the higher resolution estimated summer upwelling index (1967–2001, 1 × 1° - thick orange).

for the 1-degree resolution upwelling index calculated for the winter and spring months (Table 1). Thus, at core 28B location, the alkenone producers dominate the phytoplankton (as it can also be seen in Table 2) mainly during the winter-spring seasons and appear to be generated during winter upwelling pulses, therefore recording winter upwelling waters temperature.

[32] According to *Moita* [2001] at site 26B location coccolithophores abundance (as number of cells/L) in the summer plankton is equal to the values found in winter and spring [*Moita*, 2001, Table 2]. During upwelling conditions the increase in new nutrients and the uncoupling observed between phytoplankton and zooplankton blooms work together toward the occurrence of exceptional export conditions. In addition, the data of *Abrantes and Moita* [1999] shows that there is better preservation capacity of organisms produced during bloom conditions. Therefore, at site 26B, where the influence of upwelling is intermittent, occurring only in years of strong upwelling and/or low river flow, it is to be expected that the $U^{k'}_{37}$ temperature (alkenone-derived SST) signal found in the sediments be weighted toward the upwelling-season months.

5.4. Reconstructions

[33] Although the good agreement found between the various independent traditional semiquantitative methods allowed us to reconstruct the history of river flow and primary productivity during the last 2,000 years [*Abrantes et al.*, 2005], for those findings to be useful for climate modeling we need quantitative reconstructions. One way to quantify the existing relationship between each one of the acting processes that we want to reconstruct and the various sediment proxies that reflect them is through the calculation of existing regressions. In the regression equations analysis we allowed all the measured variables from the sediments to interact. The reasoning for this approach is that there is more than one physical process interacting in our study area. That is, strong upwelling conditions

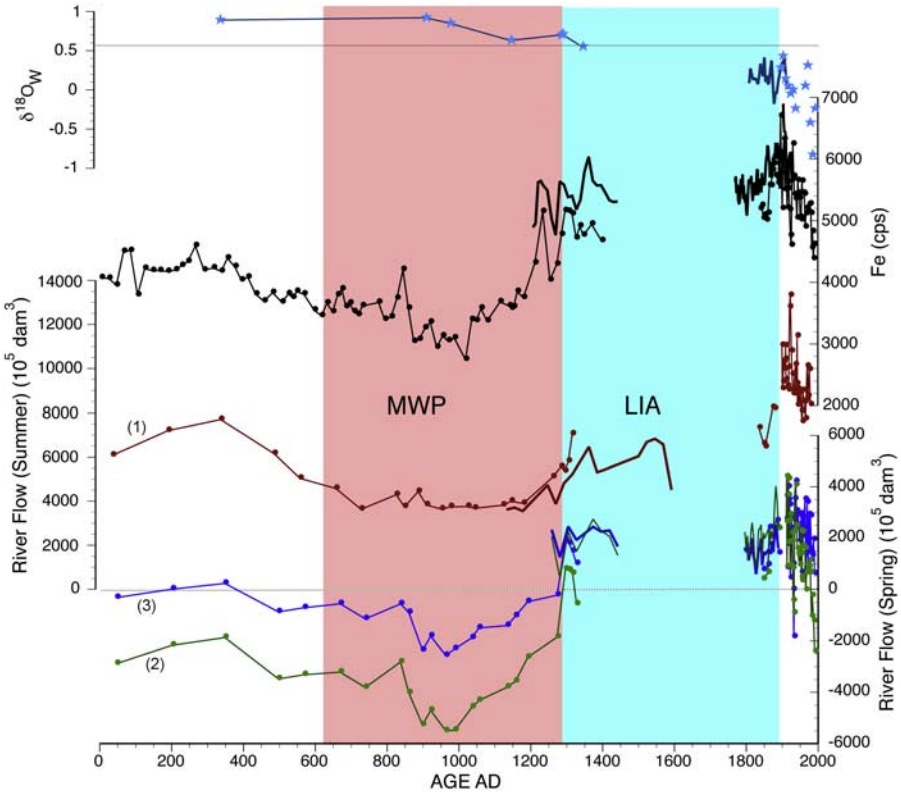

Figure 8. Spring and summer river total flow reconstructed from the application of functions (1), (2), and (3) to the data of piston core D13902 (lines with dots) and gravity core PO287-26G (lines) [*Abrantes et al.*, 2005]. Fe content as well as the δ^{18}OW variation downcore are also plotted for comparison. (1) $RF_{summer} = 2172.58 - 5.66$[37alq] + 3.37[n-alk] (28B) − 91%, (2) $RF_{spring} = -14873.83 + 3.0352$[Fe] (28B) − 55%, and (3) $RF_{spring} = -8673.46 + 2.0790$[Fe] + 0.6680[n-OH] − 2.1293[n-alk] (26B) − 94%.

during some months and strong river influence during others. Since each sediment sample represents in average two years, the processes mentioned before will be represented by all the measured properties, in different proportions.

5.4.1. River Flow

[34] Figure 8 presents the spring and summer river flow (RF) reconstructed values using the multiple regression equations found. For the river flow, we obtained the following regressions, considering the full time series or a 3 year averaged time series:

$$\text{Fratel } RF_{summer} = 2172.58 - 5.66[37alq] + 3.37[n-alk] \quad \text{for core 28B, r2} = 0.9;\ \text{RMSE} = 276.18 \tag{1}$$

$$\text{Fratel 3 year average } RF_{spring} = -14873.83 + 3.0352[Fe] \quad \text{for core 28B; r2} = 0.6;\ \text{RMSE} = 1136.5 \tag{2}$$

$$\text{Fratel 3 year average } RF_{spring} = -8673.46 + 2.0790[Fe] + 0.6680[n-OH] - 2.1293[n-alk] \text{for core 26B; r2} = 0.9 \text{ and RMSE} = 261.60 \tag{3}$$

[35] Surprisingly [Fe] does not enter in equation (1). In this case, the summer river flow signal is given by a combination of C_{37} total alkenones concentration ([37alq]) and total *n*-alkane concentration ([*n*-alk]). This is most probably a reflection of a combination of a lower transport capacity by the river but also of low sediment availability.

[36] Downcore (Figure 8), the highest Fe contents (as cps units) are observed above 1200 A.D., while a broad minimum occurs between 500 and 1200 A.D. When the two equations for spring river flow are applied quite close values are retrieved after 1200 A.D., but diverge for older periods and give negative values. Considering the co-occurrence of these negative values with low Fe contents, those negative values are interpreted as a reflection of a lack of instrumental data for low river flow conditions, that is, a no-analog problem. Although, the occurrence of negative values does not instill much confidence on the estimated values, at least the regression equations using independent proxies yield similar predictions that are also comparable with the water oxygen isotopical signal ($\delta^{18}O_W$),

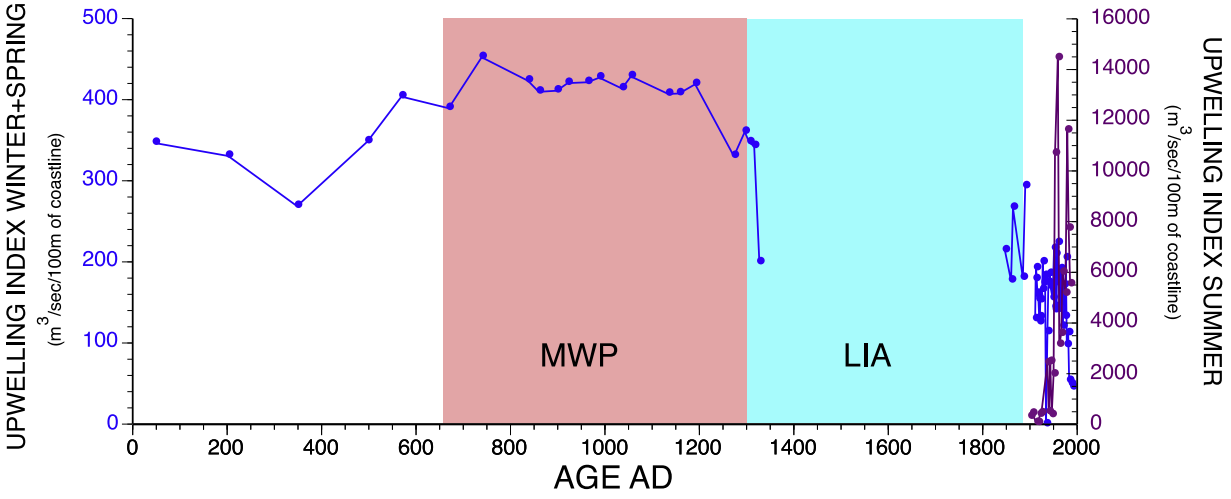

Figure 9. Summer and winter spring upwelling index reconstructed from the application of functions (4) and (5) to the data of core D13902 [*Abrantes et al.*, 2005]. (4) $UI_{summer} = 140.02 + 3.47 \times 10^{-5}$ (*Chaetoceros* abundance) − 0.0171[Fe] (28B) − 64% and (5) $UI_{winter+spring} = 573.19 - 0.0346$[n-OH] − 0.266[37alq] (26B) − 64%.

another independent proxy for river flow presented by *Abrantes et al.* [2005] (Figure 8).

5.4.2. Upwelling Conditions

[37] The main proxy for upwelling are the diatoms, in particular the upwelling-related genus *Chaetoceros*; however, the disappearance of diatoms in both cores below ±20 cm is indicative of the strong opal dissolution observed in this region.

[38] For the upwelling indexes (UI) the following regressions were found:

$$5-\text{degree 3 year average } UI_{summer} = 140.02 + 3.47 \times 10^{-5}(\textit{Chaetoceros}\text{ abundance}) - 0.0171[\text{Fe}] \text{ for core 28B, } r^2 = 0.64;$$
$$\text{RMSE} = 13.33\left(\text{m}^3/\text{s}/100\text{ m of coastline}\right) \quad (4)$$

$$1-\text{degree 3 year average } UI_{winter+spring} = 573.19 - 0.0346[\text{n}-\text{OH}] - 0.266[37\text{alq}]\text{for core 26B;}$$
$$r2 = 0.66;\ \text{RMSE} = 53.51\left(\text{m}^3/\text{s}/100\text{ m of coastline}\right) \quad (5)$$

[39] Equation (4) relates the upwelling diatom genus *Chaetoceros* and Fe to the 5-degree resolution summer upwelling index; however, as it includes diatoms, its utilization is limited to the top levels, that is, where diatoms are present (Figures 6 and 9).

[40] A second function (5) relates the 1-degree Winter+Spring upwelling to [37alq] and total concentration of *n*-alcohols ([n-OH]). Its application downcore to data measured by *Abrantes et al.* [2005] along the PO287-26G and D31902 composite sequence results in the curve presented in Figure 9 and although the small number of data points in the Little Ice Age (LIA) interval, the existing values indicate lower upwelling conditions as compared to the Medieval Warm Period (MWP).

[41] The trends found downcore when equations based on independent proxies for both river flow and upwelling confirm the indications given by the direct proxies, that is, Fe for river flow and diatoms for upwelling. However, the objective of quantification is not achieved, since different regressions lead to totally different values, demonstrating that we cannot trust the reconstructed flow in quantitative terms.

[42] Given the high correlation between the atmospheric conditions along the Iberian margin and the NAO index [*Hurrell*, 1995], the inferred low river flow and relatively higher upwelling during the MWP but higher river flow and lower upwelling during the LIA have been interpreted as a sign of dominant NAO minima during the LIA, and a more long-term positive NAO state in the MWP [*Abrantes et al.*, 2005]. In this study, one of our final goals was to extend the reconstruction of the NAO index through the use of marine sediments proxy data. However, the disturbing effect of the sedimentary sequence by historical earthquakes and tsunamis prevents this otherwise high sedimentation rate site to be a good continuous site. Furthermore, the lack of instrumental data for

extreme conditions generates a no-analog problem and prevents a trustable reconstruction.

6. Conclusions

[43] We describe an attempt to reconstruct the Tagus winter river flow (JFMA) using a series of proxies analyzed along two high resolution sediment box cores recovered from the Tagus mud patch, off Lisbon (Portugal). These cores cover the last 100 years, and the comparison of the Fe (cps), alkenone-derived SST and upwelling-related diatoms to the Tagus River flow, SST and upwelling index prove correct the use of those sediment components as proxies to the listed climate-related variables.

[44] Alkenone-derived SST values are essentially similar to winter temperatures and pretty much constant at site 28B but highly variable at site 26B, which is a reflex of the mutual exclusive interplay of the river flow and upwelling and the different temperatures of the waters associated to each process. Furthermore, it proves that the occasional influence of a strong process, such as summer upwelling conditions at site 26B, is more important for the definition of the sediment record than the continuous influence of the river flow.

[45] Stepwise regression analyses of the instrumental and proxy data sets provided regressions that can be indicative of possible later transfer function development. The equations reflect spring and summer river flow, as well as summer and winter upwelling indices.

[46] Reconstructions obtained through the application of the encountered equations to a previously published 2,000 year composite record of cores D13902 and PO287-26G, confirm conditions estimated from proxy data. The two equations for spring river flow retrieve quite close values after 1200 A.D.; however, they diverge for older periods and give negative values, indicating an analog problem, that is, lack of instrumental data for low river flow conditions. On the contrary, the upwelling index reconstructions give positive values at all times, again indicating a lack of instrumental data for stronger upwelling conditions.

Acknowledgments

[47] This work was conducted as a follow-up of the Holsmeer project (EVK2-CT-2000-00060), with further financial support from LNEG (former INETI) and Fundação para a Ciência e Tecnologia through the INGMAR project. The authors acknowledge the captain and crew of the PO287 and D134 campaigns, C. Monteiro and A. Inês for laboratory support, and three anonymous reviewers for their constructive comments.

References

Abrantes, F., and T. Moita (1999), Water column and recent sediment data on diatoms and coccolithophorids, off Portugal, confirm sediment record as a memory of upwelling events, *Oceanol. Acta*, *22*, 319–336, doi:10.1016/S0399-1784(99)80055-3.

Abrantes, F., et al. (2005), Shallow-marine sediment cores record climate variability and earthquake activity off Lisbon (Portugal) for the last 2000 years, *Quat. Sci. Rev.*, *24*, 2477–2494, doi:10.1016/j.quascirev.2004.1004.1009.

Abrantes, F., et al. (2008), Sedimentological record of tsunamis on shallow-shelf areas: The case of the 1969 AD and 1755 AD tsunamis on the Portuguese Shelf off Lisbon, *Mar. Geol.*, *249*, 283–293, doi:10.1016/j.margeo.2007.12.004.

Bakun, A. (1973), Coastal upwelling indices, west coast of North America, 1946–1971, *NOAA Tech. Rep.*, *NMFS SSRF-671*, 103 pp., U.S. Dep. of Commer., Washington, D. C.

Briffa, K. R., and T. J. Osborn (2002), Blowing hot and cold, *Science*, *295*, 2227–2228, doi:10.1126/science.1069486.

Broecker, W. S. (1997), Thermohaline circulation, the Achilles heel of our climate system, *Science*, *278*, 1582–1588, doi:10.1126/science.278.5343.1582.

Cabeçadas, L., et al. (1999), Phytoplankton spring bloom in the Tagus coastal waters: Hydrological and chemical conditions, *Aquat. Ecol.*, *33*, 243–250, doi:10.1023/A:1009941313169.

Committee on Abrupt Climate Change (2002), *Abrupt Climate Change: Inevitable Surprises*, 230 pp., Natl. Acad. Press, Washington, D. C.

Crosta, X., and N. Koç (2007), Diatoms: From micropaleontology to isotope geochemistry, in *Proxies in Late Cenozoic Paleoceanography*, pp. 327–369, Elsevier, New York.

Fatela, F., and R. Taborda (2002), Confidence limits of species proportions in microfossil assemblages, *Mar. Micropaleontol.*, *45*, 169–174.

Fiuza, A. (1984), *Hidrologia e Dinâmica das Águas Costeiras de Portugal*, 294 pp., Univ. de Lisboa, Lisbon.

Haug, G. H., et al. (2001), Southward migration of the Intertropical Convergence Zone through the Holocene, *Science*, *293*, 1304–1308, doi:10.1126/science.1059725.

Hurrell, J. (1995), Decadal trends in the North Atlantic Oscillation: Regional temperatures and precipitation, *Science*, *269*, 676–679, doi:10.1126/science.269.5224.676.

Itambi, A. C., et al. (2009), Millennial-scale northwest African droughts related to Heinrich events and Dansgaard-Oeschger cycles: Evidence in marine sediments from offshore Senegal, *Paleoceanography*, *24*, PA1205, doi:10.1029/2007PA001570.

Jansen, J. H. F., et al. (1998), CORTEX, a shipboard XRF-scanner for element analyses in split sediment cores, *Mar. Geol.*, *151*, 143–153, doi:10.1016/S0025-3227(98)00074-7.

Lopes, C., et al. (2006), Diatoms in northeast Pacific surface sediments as paleoceanographic proxies, *Mar. Micropaleontol.*, *60*, 45–65, doi:10.1016/j.marmicro.2006.02.010.

Moita, T. (2001), Estrutura, variabilidade e einamica do fitoplancton na Costa de Portugal continental, thesis, 272 pp., Univ. of Lisbon, Lisbon.

Müller, P. J., et al. (1998), Calibration of the alkenone paleotemperature index UK′37 based on core-tops from the eastern South Atlantic and the global ocean (60°N–60°S), *Geochim. Cosmochim. Acta*, *62*, 1757–1772, doi:10.1016/S0016-7037(98)00097-0.

Nelson, D., et al. (1995), Production and dissolution of biogenic silica in the ocean: Revised global estimates, comparison with regional data and relationship to biogenic sedimentation, *Global Biogeochem. Cycles*, *9*, 359–372, doi:10.1029/95GB01070.

Pisias, N. G., et al. (1997), Radiolarian-based transfer functions for estimating mean surface ocean temperatures and seasonal range, *Paleoceanography*, *12*, 365–379, doi:10.1029/97PA00582.

Reimer, P., et al. (2004), Marine04 marine radiocarbon age calibration, 26 - 0 ka BP, *Radiocarbon*, *46*, 1029–1058.

Relvas, P., et al. (2007), Physical oceanography of the western Iberia ecosystem: Latest views and challenges, *Prog. Oceanogr.*, *74*, 149–173, doi:10.1016/j.pocean.2007.1004.1021.

Rodrigues, T., J. O. Grimalt, F. G. Abrantes, J. A. Flores, and S. M. Lebreiro (2009), Holocene interdependences of changes in sea surface temperature, productivity, and fluvial inputs in the Iberian continental shelf (Tagus mud patch), *Geochem. Geophys. Geosyst.*, *10*, Q07U06, doi:10.1029/2008GC002367.

Sousa, F., and A. Bricaud (1992), Satellite-derived phytoplankton pigment structures in the Portuguese upwelling area, *J. Geophys. Res.*, *97*, 11,343–11,356, doi:10.1029/92JC00786.

Trigo, R. M., and C. C. DaCamara (2000), Circulation weather types and their influence on the precipitation regime in Portugal, *Int. J. Climatol.*, *20*, 1559–1581, doi:10.1002/1097-0088(20001115)20:13<1559::AID-JOC555>3.0.CO;2-5.

Trigo, R. M., et al. (2002), The North Atlantic Oscillation influence on Europe: Climate impacts and associated physical mechanisms, *Clim. Res.*, *20*, 9–17, doi:10.3354/cr020009.

Trigo, R. M., et al. (2003), The impact of the North Atlantic Oscillation on hydroelectric power generation in the Iberian Peninsula, abstract P1.9 presented at 14th Symposium on Global Change and Climate Variations, Am. Meteorol. Soc., Long Beach, Calif.

Vale, C. (1981), Entrada de matéria em suspensão no estuário do Tejo durante as chuvas de Fevereiro de 1979, *Recursos Hídricos*, *2*, 37–45.

Watson, R., et al. (2001), *Climate Change 2001: Synthesis Report*, Intergov. Panel on Clim. Change, Geneva, Switzerland.

Williams, D. (1994), Satellite study of the Tagus sediment plume, technical report, Mar. Geol. Dep., Inst. of Geol. and Min., Lisbon.

Appendix 4

VARIATIONS IN MID-LATITUDE NORTH ATLANTIC SURFACE WATER PROPERTIES DURING THE MID-BRUNHES: DOES MARINE ISOTOPE STAGE 11 STAND OUT?

A. H. L. Voelker[1,2], **T. Rodrigues**[1], R. Stein[3], J. Hefter[3], K. Billups[4], D. Oppo[5], J. McManus[5],*, and J. O. Grimalt[6]

1Dept. Geologia Marinha, Laboratorio Nacional de Energia e Geologia (LNEG; ex-INETI), Estrada da Portela, Zambujal, 2721-866 Alfragide, Portugal
2CIMAR Associate Laboratory, Rua dos Bragas 289, 4050–123 Porto, Portugal
3Alfred-Wegener-Institute for Polar and Marine Research, Columbusstrasse, 27568 Bremerhaven, Germany
4College of Marine and Earth Studies, University of Delaware, 700 Pilottown Road, Lewes, DE 19958, USA

Climate of the Past Discussions, **5,** 1-55 (2009)

Clim. Past Discuss., 5, 1–55, 2009
www.clim-past-discuss.net/5/1/2009/

Climate of the Past Discussions

Climate of the Past Discussions is the access reviewed discussion forum of *Climate of the Past*

Variations in mid-latitude North Atlantic surface water properties during the mid-Brunhes: Does Marine Isotope Stage 11 stand out?

A. H. L. Voelker[1,2], T. Rodrigues[1], R. Stein[3], J. Hefter[3], K. Billups[4], D. Oppo[5], J. McManus[5,*], and J. O. Grimalt[6]

[1]Dept. Geologia Marinha, Laboratorio Nacional de Energia e Geologia (LNEG; ex-INETI), Estrada da Portela, Zambujal, 2721-866 Alfragide, Portugal
[2]CIMAR Associate Laboratory, Rua dos Bragas 289, 4050–123 Porto, Portugal
[3]Alfred-Wegener-Institute for Polar and Marine Research, Columbusstrasse, 27568 Bremerhaven, Germany
[4]College of Marine and Earth Studies, University of Delaware, 700 Pilottown Road, Lewes, DE 19958, USA

[5]Geology and Geophysics, Woods Hole Oceanographic Inst., Woods Hole, MA 02543, USA
[6]Department of Environmental Chemistry, Institute of Chemical and Environmental Research (CSIC), Jordi Girona 18, 08034-Barcelona, Spain
*now at: Department of Earth and Environmental Science, Columbia University, Lamont-Doherty Earth Observatory, 61 Route 9W, Palisades, NY 10964–8000, USA

Received: 16 May 2009 – Accepted: 20 May 2009 – Published: [redacted]

Correspondence to: A. Voelker (avoelker@softhome.net)

Published by Copernicus Publications on behalf of the European Geosciences Union.

Abstract

New planktonic stable isotope and ice-rafted debris records from three core sites in the mid-latitude North Atlantic (IODP Site U1313, MD01-2446, MD03-2699) are combined with records of ODP Sites 1056/1058 and 980 to reconstruct hydrographic conditions during the middle Pleistocene spanning Marine Isotope Stages (MIS) 9–14 (300–540 ka). Together the study sites reflect western and eastern basin boundary currents as well as north to south transect sampling of subpolar and transitional water masses. Planktonic $\delta^{18}O$ records indicate that during peak interglacial MIS 9 and 11 hydrographic conditions were similar among all the sites with relative stable conditions and confirm prolonged warmth during MIS 11c also for the mid-latitudes. Sea surface temperature (SST) reconstructions further reveal that in the mid-latitude North Atlantic MIS 11c is associated with two plateaus, the younger one of which is slightly warmer. Enhanced subsurface northward heat flux in the eastern boundary current system, especially during early MIS 11c, is denoted by the presence of tropical planktonic foraminifer species. MIS 13 was generally colder and more variable than the younger interglacials. The greatest differences between the sites existed during the glacial inceptions and glacials. Then a north-south trending hydrographic front separated the nearshore and offshore waters off Portugal. While offshore waters originated from the North Atlantic Drift as indicated by the similarities between the records of IODP Site U1313, ODP Site 980 and MD01-2446, nearshore waters as recorded in core MD03-2699 derived from the Azores Current and thus the subtropical gyre. A strong Azores Current influence is seen especially during MIS 12, when SST dropped significantly only during the Heinrich-type ice-rafting event at the onset of Termination V. Given the subtropical overprint on Portuguese nearshore sites such as MD03-2699 and MD01-2443 caution needs to be taken to interpret their records as basin-wide climate signals.

CPD

5, 1–55, 2009

1 Introduction

The Brunhes polarity chron encompasses the last 780 ka (kiloannum = thousand year) and its middle section is often considered as a particularly warm period during the last 1000 ka, when warm surface waters penetrated polewards and sea levels were generally higher than at Present (Droxler et al., 2003). MIS 11 and 9 are part of this warm interval. Interglacial MIS 11c was the first interglacial period after the mid-Pleistocene transition with atmospheric greenhouse gas concentrations and temperatures over Antarctica (Petit et al., 1999; Siegenthaler et al., 2005; Spahni et al., 2005; Jouzel et al., 2007) at levels similar to those during subsequent interglacials including the current one, the Holocene. Based on temperature related proxy records from the oceans (Hodell et al., 2000; Lea et al., 2003; McManus et al., 2003; de Abreu et al., 2005; Helmke et al., 2008) and from Antarctica (Petit et al., 1999; Jouzel et al., 2007) it was an unusually long lasting interglacial and northern heat piracy, i.e. the enhanced advection of warm waters from the South into the North Atlantic, was at its maximum (Berger and Wefer, 2003). The early temperature rise during the high amplitude transition from glacial MIS 12 to MIS 11c leads to two possible definitions for the duration of the interglacial period within MIS 11. Based on the interval of maximum warmth in marine records, the interglacial period lasted at minimum from to 420 to 396 ka (McManus et al., 2003; Helmke et al., 2008). The definition of an interglacial as the period of ice volume minimum/sea-level highstand (Shackleton, 1969), however, shortens this interval to 409 to 396 ka (based on the LR04 chronology; Lisiecki and Raymo, 2005). This shorter period is also the interval, when full interglacial conditions, including minimal ice-rafting, occurred in the Nordic Seas (Bauch et al., 2000). Because of the similarity in the eccentricity signal (Loutre and Berger, 2003), MIS 11c is the interglacial often used as equivalent to the Holocene. In the subpolar North Atlantic at ODP Site 980 the peak interglacial period, MIS 11c, is recorded as a long, stable interval with relatively small SST variations (Oppo et al., 1998; McManus et al., 2003), while the later phase of MIS 11, contemporary with the built-up of continental ice sheets during the

inception of glacial MIS 10, is marked by millennial-scale variability linked to ice-rafting events and southward incursions of arctic surface waters (Oppo et al., 1998; McManus et al., 1999). On the western boundary of the subtropical gyre at ODP Site 1056, on the other hand, peak interglacial conditions were more variable in the surface water as evidenced by short-term incursions of colder surface waters, while thermocline conditions were relative stable and comparable to the Holocene (Chaisson et al., 2002; Billups et al., 2004). During the transition to MIS 10 the Gulf Stream waters at ODP Site 1056 experienced higher temperature variability linked to cooling episodes in the surface and thermocline waters (Chaisson et al., 2002; Billups et al., 2004), episodes that are contemporary with those recorded at ODP Site 980.

The interglacial after MIS 11c was MIS 9e – following (Tzedakis et al., 1997) we are dividing MIS 9 into five substages instead of three (Bassinot et al., 1994). MIS 9e is a better analog for the Holocene than MIS 11c if tilt and insolation are emphasized for the comparison (Ruddiman, 2006). During MIS 9e ice volume minimum and temperature maximum coincided e.g. (McManus et al., 1999; Martrat et al., 2007) with the sea-level highstand being dated approximately to 334 to 306 ka (Stirling et al., 2001). In the Antarctic ice core records, MIS 9e is marked by an early maximum in temperature (Petit et al., 1999; Watanabe et al., 2003; Jouzel et al., 2007) and greenhouse gas concentrations (Petit et al., 1999; Loulergue et al., 2008), when values even exceeded pre-industrial Holocene levels. Such an overshooting is, however, not seen in high-resolution marine or terrestrial records from the northern hemisphere (McManus et al., 1999; Prokopenko et al., 2002; Tzedakis et al., 2004; Martrat et al., 2007; Desprat et al., 2009; Tzedakis et al., 2009).

As mentioned above, MIS 11c marked a transition in interglacial conditions, the so called mid-Brunhes event (Jansen et al., 1986). Mid-Pleistocene interglacials prior to MIS 11c were colder in Antarctica (EPICA Members, 2004) and had lower carbon dioxide concentrations (Siegenthaler et al., 2005; Lüthi et al., 2008). The LR04 benthic stack (Lisiecki and Raymo, 2005) clearly reveals that ice volume was larger during MIS 13 than during MIS 11 or 9. In terrestrial records from Tenaghi Philippon (Tzedakis

et al., 2006), Lake Baikal (Prokopenko et al., 2002) or the Chinese Loess Plateau (Guo et al., 2000), on the other hand, MIS 13 does not differ greatly from some of the subsequent interglacials, especially MIS 11. Besides these differences in climatic responses on land and in the ocean, MIS 13 is unique in the timing of full interglacial conditions. Maximum warmth and ice volume minimum of all the other interglacials during the last 700 ka occurred during the first substage after the Termination, i.e. after the transition from a glacial maximum to the interglacial sea-level highstand. During MIS 13, however, the interval of ice volume minimum (Lisiecki and Raymo, 2005) and maximum warmth in the EDC ice core record (Jouzel et al., 2007) coincided not with the first, but with the third substage, MIS 13a. Thus we regard MIS 13a as the full interglacial interval within MIS 13, even if atmospheric carbon dioxide concentrations were at a similar level during both warm substages, MIS 13c and 13a (Siegenthaler et al., 2005), and nitrous dioxide peaked during MIS 13c (Spahni et al., 2005).

One of the reasons why MIS 13 is so different, might be that its preceding glacial, MIS 14, was so weak with sea level lowering only about as half as during MIS 16, 12 or 10. Consequently, also the amplitude of Termination VI was much lower than during Terminations V or IV. MIS 12, on the other hand, was one of the most extreme glacials during the last 1000 ka, when sea level was probably lower than during the last glacial maximum (MIS 2) (Lisiecki and Raymo, 2005). Sea level during MIS 10 was similar to MIS 2, even though MIS 10 lasted only half as long as MIS 12. In regard to dust flux in Antarctica MIS 14 is also the weakest and MIS 12 the strongest glacial (Lambert et al., 2008). This pronounced difference between the mid-Brunhes glacials is, however, not evident in the EDC temperature and greenhouse gas records (Jouzel et al., 2007; Loulergue et al., 2008; Lüthi et al., 2008). Greenhouse gas concentrations during the MIS 10 glacial maximum were actually lower than during MIS 12 and 14.

One of the most prominent features of the last glacial inception is the periodic occurrence of major ice-rafting events, the so called Heinrich events (e.g. Hemming, 2004). During the Brunhes chron Heinrich-type ice-rafting events were first observed at the end of MIS 16 (Hodell et al., 2008) and then more regularly within MIS 12 and 10 (Mc-

Manus et al., 1999; Hodell et al., 2008; Ji et al., 2009). McManus et al. (1999) showed that the onset of millennial-scale climate variability, including ice-rafting events, is linked to a threshold value of 3.5‰ in benthic $\delta^{18}O$. As soon as this ice volume threshold was passed the Atlantic meridional overturning circulation (AMOC) became less stable resulting in oscillations between weaker and stronger AMOC modes. Most of the existing evidence for millennial-scale AMOC variability during the mid-Brunhes and its impacts on surface and deep waters is linked to the inception of MIS 10 (Poli et al., 2000; Billups et al., 2004; de Abreu et al., 2005; Hall and Becker, 2007; Martrat et al., 2007; Dickson et al., 2008; Stein et al., 2009). Only records from ODP Sites 980 and 1058 cover the older glacials with sufficient resolution (McManus et al., 1999; Flower et al., 2000; Billups et al., 2006; Weirauch et al., 2008) and here we present the previously unpublished planktonic $\delta^{13}C$ records for these sites.

The new records fill the gap between ODP Sites 1056 and 980 and reveal, if hydrographic conditions in the mid-latitude North Atlantic, which encompasses the southern edge of the North Atlantic ice-rafted debris (IRD) belt (Ruddiman, 1977; Hemming, 2004) and experienced large SST gradients during glacials (Calvo et al., 2001; Pflaumann et al., 2003) and stadials (Chapman and Maslin, 1999; Oppo et al., 2001), were more similar to those in the subtropical or the subpolar gyre during interglacials, especially during MIS 11. The two new records off Portugal, MD01-2446 and MD03-2699, furthermore, allow for the first time to reconstruct and evaluate the full transition from glacial MIS 12 to MIS 11 in this eastern boundary upwelling system. By combining the planktonic foraminifer stable isotope records from three new sites in the mid-latitude North Atlantic Ocean with those from ODP Sites 980 and 1056/1058 we aim (1) to map hydrographic conditions within the major surface currents (Fig. 1) and thus to identify potential latitudinal or longitudinal gradients in the North Atlantic during the interval spanning from MIS 9c to 14 (300–540 ka); (2) to trace the potential sources of the subsurface waters and their changes on glacial and interglacial timescales; and (3) to address the question, how stable or variable hydrographic conditions were in the mid-latitude North Atlantic during MIS 11 and how they differed from those during its

neighboring interglacials, MIS 13 and 9. Our interpretation is supported by IRD records for the three new sites and for alkenone-based SST data for MIS 11 from two of those sites.

2 Core sites and modern hydrographic setting

The three new core sites are IODP Site U1313, MD01-2446 and MD03-2699 (Table 1; Fig. 1). IODP Site U1313, which re-occupies the position of DSDP Site 607, was drilled in 2005 with R/V Joides Resolution during International Ocean Drilling Program (IODP) Expedition 306 (Channell et al., 2006). Calypso piston cores MD01-2446 and MD03-2699 were retrieved with R/V Marion Dufresne during the Geosciences cruise in 2001 and the PICABIA cruise in 2003, respectively. For tracing central/mode water masses within in the North Atlantic we combine the new records with those of ODP Site 980 in the subpolar North Atlantic and of ODP Sites 1056 and 1058 from the western subtropical gyre (Table 1; Fig. 1a).

Surface waters at all sites are derived in one form or another from the Gulf Stream and the North Atlantic Current (NAC). ODP Sites 1056 and 1058 are located directly below the Gulf Stream, while ODP Site 980 is influenced by the Rockall Trough branch of the NAC (Fratantoni, 2001; Brambilla and Talley, 2008). Even though IODP Site U1313 is located south of the core NAC pathway, drifter data shows that surface waters in this area are derived from the NAC, partly through recirculation off the Grand Banks (Fratantoni, 2001; Reverdin et al., 2003).

Gulf Stream/NAC derived surface waters off the western Iberian Peninsula are transported by two currents, the Portugal Current and the Azores Current. The Portugal Current (PC) is the NAC recirculation branch within the northeastern North Atlantic (Fig. 2a) and is centered west of 10° W off Portugal (Peliz et al., 2005). Thus it is the current influencing site MD01-2446 (Fig. 1b). The PC advects freshly ventilated surface and subsurface waters slowly southward. The subsurface component of the PC is subpolar Eastern North Atlantic Central Water (ENACW) that is formed by winter

cooling in the eastern North Atlantic (McCartney and Talley, 1982), including along the NAC's Rockall Trough branch (Brambilla and Talley, 2008). The Azores Current (AzC) diverges from the Gulf Stream and moves in large meanders between 35 and 37° N across the North Atlantic. Its northern boundary forms the subtropical Azores front. In the eastern basin the AzC splits into several branches, one of which is the Canary Current, its major recirculation, and another, the eastern branch, enters into the Gulf of Cadiz (Fig. 1). During winter, waters from this eastern branch recirculate northward as the Iberian Poleward Current (IPC) (Peliz et al., 2005), thereby bending the subtropical front northward along the western Iberian margin (Fig. 1b). Similar to the PC, the IPC includes a subsurface component: ENACW of subtropical origin. Subtropical ENACW is formed by strong evaporation and winter cooling along the Azores front (Rios et al., 1992) and is less ventilated, warmer and saltier than its subpolar counterpart (van Aken, 2001). IPC waters influence site MD03-2699, especially during fall and winter. During spring and summer (mainly May to September), on the other hand, the upwelling filaments that form off Peniche and Cape Roca can reach as far offshore as site MD03-2699, so that either upwelled waters or the seasonal, nearshore branch of the PC (Fiúza, 1984; Alvarez-Salgado et al., 2003) affect the site. Subtropical ENACW is generally upwelled south of 40° N and subpolar one north of 45° N. In between either water mass can be upwelled depending on the strength of the wind forcing. Strong winds can cause subpolar ENACW to be upwelled also south of 40° N.

Outside of the western Iberian upwelling zone plankton blooms drive surface water productivity (Table 1). Site MD01-2446 falls within the mid-latitude regime of (Levy et al., 2005) that is associated with a bloom that starts in fall and peaks in spring. The northern boundary of this regime is at 40±2° N, so that IODP Site U1313 either follows this regime or experiences a major late spring bloom and a smaller fall bloom like it is typical for the subpolar regime and for ODP Site 980. ODP Sites 1056 and 1058, on the other hand, follow the subtropical regime with a weak fall bloom.

3 Methods

Sediment samples for stable isotope and lithics analyses of IODP Site U1313 and cores MD03-2699 and MD01-2446 were prepared in LNEG's Laboratorio de Geologia Marinha following the established procedure. After freeze drying samples were washed with deionized water through a 63 μm-mesh and the coarse fraction residue was dried in filter paper at 40°C and weighted. Sample intervals are 1–3 cm for core MD03-2699 and 2–3 cm for core MD01-2446. IODP Site U1313 was sampled continuously with 2 cm-wide scoops. Site U1313 stable isotope samples were taken from the secondary splice (Voelker et al., 2009) and biomarker samples from the primary splice (Stein et al., 2009).

For planktonic stable isotope measurements in cores MD03-2699 and MD01-2446 and IODP Site U1313, 8–10 clean specimens of *Globorotalia inflata* were picked from the fraction >315 μm. *G. inflata* is one of the dominant species in the planktonic foraminifer fauna associated with the NAC (Ottens, 1991). Its stable isotope values reflect hydrographic conditions at the base of the seasonal thermocline (Cléroux et al., 2007); conditions that are close to those in the winter mixed layer. Details on stable isotope measurements for ODP Site 980 are given by Oppo et al. (1998) and McManus et al. (1999), for ODP Site 1056 by Chaisson et al. (2002) and Billups et al. (2004) and for ODP Site 1058 by Billups et al. (2006). Because of laboratory offsets ODP Site 1056 *N. dutertrei* δ^{18}O values needed to be adjusted by +0.2‰ in order to match absolute values of ODP Site 1058.

Benthic isotope records of cores MD03-2699 and MD01-2446 and IODP Site U1313, here just used to establish chronostratigraphies, are based on 2–4 lean specimens of *Cibicidoides wuellerstorfi*, *Cibicidoides mundulus* or *Cibicidoides pachyderma* (the last only in MD03-2699). At few levels where *C. wuellerstorfi* was absent *Uvigerina* sp. was picked instead. All *Cibicidoides* sp. δ^{18}O data is corrected by +0.64‰ to the *Uvigerina* sp. level (Shackleton, 1974). Benthic and planktonic stable isotope samples were measured in a Finnigan MAT 252 mass spectrometer at Marum (University Bremen,

Germany). The mass spectrometer is coupled to an automated Kiel carbonate preparation system and the long-term precision is ±0.07‰ for $\delta^{18}O$ and ±0.05‰ for $\delta^{13}C$ based on repeated analyses of internal and external (NBS-19) carbonate standards.

The number of lithic fragments was determined in the fraction >315 μm and is presented as "#/g" (normalized by the respective sample's dry weight). Lithics are primarily interpreted as IRD. The coarser size fraction was chosen 1) to minimize modification of the IRD signal by wind deposition and lateral advection at slope site MD03-2699 and 2) to avoid scientific overlap for Site U1313 within the science party of IODP Exp. 306. Using a coarser size fraction allows to identify all the ice-rafting events (e.g. Voelker, 1999) and only this is relevant for the current study, but might underestimate the absolute intensity of an ice-rafting event.

Biomarker samples of IODP Site U1313 and core MD03-2699 were prepared following established procedures (Villanueva et al., 1997; Calvo et al., 2003). Core MD03-2699 samples were analysed in a Varian gas chromatograph either at the Dept. of Environmental Chemistry of CSIC (Barcelona) or at the Dept. de Geologia Marinha of LNEG (Rodrigues et al., 2009). Site U1313 samples were measured in a gas chromatograph/time-of-flight mass spectrometer at the Alfred-Wegner Institute, Bremerhaven (Hefter, 2008; Stein et al., 2009). Alkenone-based sea surface temperatures (SST) for both sites were calculated using the unsaturation index $U_k^{37'}$ of Müller et al. (1998) and thus should reflect annual mean SST.

IODP Site U1313, MD01-2446 and MD03-2699 data will be stored at the World Data Centre Mare (http://www.wdc-mare.org/; http://www.pangaea.de).

4 Chronostratigraphy

Ages for most of the cores shown in this paper are derived from the LR04 stack (Lisiecki and Raymo, 2005). The benthic record of IODP Site U1313, the re-occupation of DSDP Site 607, was directly correlated with the stack with most correlation points being isotopic maxima (Voelker et al., 2009). The record of MD01-2446 was correlated

with the Site U1313 curve in the interval where the two overlap and to the LR04 stack for the interval from late MIS 10 to MIS 9. The resulting records are shown in Fig. 2a and their age/depth relations in Fig. 2c.

Establishing the age model for intermediate depth site MD03-2699 was more difficult as the deep water δ^{18}O signal here is modified by the Mediterranean Outflow (MOW) during glacials and glacial inceptions (Voelker et al., 2007). The age model for this core is based on the correlation of its benthic δ^{18}O records to the one of ODP Site 980 (on LR04 time) and two nannofossil events. ODP Site 980 was chosen as reference curve over the LR04 stack as it is from intermediate water depths (Table 1) too. Consequently, water mass signals during times of lower MOW influence at site MD03-2699 were similar at both sites (Fig. 2b). The two nannofossil events (Amore et al., unpubl. data) corroborating the age model are the acme of *Gephyrocapsa caribbeanica* (Flores et al., 2003; Baumann and Freitag, 2004) and the last/highest observed occurrence (LO or HO) of *Pseudoemiliania lacunosa.* The *G. caribbeanica* acme begins in late MIS 14 and therefore helps to constrain the core's basal age. The LO of *P. lacunosa* is placed at the depth of 1895 cm which has an age of 453.6 ka with the current age model, in agreement with (Raffi et al., 2006).

Due to stronger winnowing by the MOW as evidenced by foraminifer sands, sedimentation rates in core MD03-2699 subsided during glacial maxima, especially during MIS 12 (Fig. 2c). Overall, sedimentation rates of core MD03-2699 and IODP Site U1313 are similar, while they are lower in core MD01-2446 (Fig. 2c). Temporal resolution of the planktonic stable isotope records are 100–600 years for IODP Site U1313, 90–1210 years for core MD03-2699 and 280–1820 years for core MD01-2446.

ODP Site 980 records are shown on the LR04 age model of Lisiecki and Raymo (2005) in this paper and the *N. pachyderma* (r) stable isotope records have a temporal resolution of 40 to 3230 years. The age scale of ODP Site 1056 was transferred to LR04 time using the Billups et al. (2004) correlation points between ODP Sites 1056 and 980 (here placed on LR04 time). For ODP Site 1058 we are using the alternative age model of Weirauch et al. (2008) that correlates ODP Site 1058 with ODP

Site 677, as this age model results in a better agreement between hydrographic conditions at (I)ODP Sites 1058 and U1313 during MIS 14. Temporal resolution of the *N. dutertrei* stable isotope records varies between 110 to 1830 years for ODP Site 1056 and 40 to 2260 years in ODP Site 1058.

5 Results

5.1 IODP Site U1313

The record of IODP Site U1313 (Fig. 3) spans the interval from 560 to 355 ka fully capturing interglacial MIS 13 and MIS 11 as well as the MIS 14 to 13 deglaciation (Termination VI). MIS 13 and 11 both contain pronounced cooling events that separate intervals of peak warmth (δ^{18}O<1.75‰). *G. inflata* δ^{18}O values show the familiar glacial to interglacial variations with lowest values during the early part of MIS 11 between 417 and 396 ka (MIS 11c). Similarly, MIS 13 contains two warm stages, MIS 13c and 13a, with lowest δ^{18}O values recorded during the early stages. Other than during the distinct cooling events, the range of individual δ^{18}O fluctuations is relatively small in comparison to the pronounced δ^{18}O variability during glacial MIS 12. Termination V is the one of the largest glacial to interglacial transition of the middle Pleistocene while Termination VI is probably one of the smallest (Lisiecki and Raymo, 2005). The *G. inflata* δ^{18}O values of IODP Site U1313 decreased ~1.5‰ and 1‰, respectively. Both events, however, reveal a reversal toward higher δ^{18}O values midway through the transition, similar to the Younger Dryas during the last Termination.

Although MIS 11 may have been the warmest interval of the past 1000 ka, the G. inflata δ^{13}C record contains a maximum in the later stage of MIS 13 (MIS 13a; Fig. 3). High δ^{13}C values are a typical signal for mid-Brunhes planktonic and benthic δ^{13}C records (e.g. Hodell et al., 2003). During MIS 13c and 11c, δ^{13}C values were at a similar level, but on average 0.5‰ lower than during MIS 13a. Terminations VI and V were associated with pronounced δ^{13}C minima.

Melting icebergs reached IODP Site U1313, located within the area of high IRD sedimentation during Heinrich events (Hemming, 2004), during all the mid-Brunhes glacials, but IRD deposition was more pronounced and frequent during MIS 12 (Fig. 3). The first IRD event recorded at site U1313 during the transition from MIS 13 to 12 occurred at 490 ka followed by a 23 ka long period with continuous, but not intense IRD sedimentation. After 467 ka, the record reveals four intervals of increased IRD deposition with the last interval exhibiting three short-term maxima. All of the IRD maxima as well as the IRD peak during MIS 10c (isotopic event 10.4) contain dolomite grains (Stein et al., 2009) and are thus interpreted as Heinrich-type ice-rafting events. During MIS 13a IRD deposition ceased for 12 ka (506.4–494.3 ka). During Termination V continuous IRD deposition ended already at 415.9 ka and during MIS 11c melting icebergs did not reach Site U1313 between 410.7 and 399.6 ka (Fig. 6).

5.2 Core MD01-2446

The G. inflata δ^{18}O record of core MD01-2446, the offshore site off Portugal, shows the same features as the Site U1313 record with relative stable conditions during the interglacials and millennial-scale variability during glacial inceptions and glacials (Fig. 4). In contrast to Site U1313 conditions in the thermocline waters were more variable during MIS 13 and cooling during MIS 13b was less. The interval with values <1.75‰ during MIS 11c lasted from 419.4 until 395.6 ka or even 394.3 ka, if one excludes the short excursion down to 1.8‰ at 395.3 ka. During MIS 9e, such light isotope values are observed continuously between 335 and 317 ka. MIS 11c and 9e δ^{18}O values were in the same range and even some values during MIS 13a reached this level (Fig. 4). The MD01-2446 record shows several δ^{18}O oscillations during Terminations VI and IV, while the Termination V sequence looks similar to the Site U1313 record but with less pronounced cooling during the Heinrich-type ice-rafting event.

Also analogous to the Site U1313 record, *G. inflata* δ^{13}C was heaviest during MIS 13a and values during MIS 13c and 11c were in a similar range. In contrast, δ^{13}C values during interglacial MIS 9e were much lower and kept on rising during the

interglacial to reach maximum values only during MIS 9d (Fig. 4). δ^{13}C minima during glacials were lower than at Site U1313. In contrast to Site U1313, *G. inflata* recorded a pronounced δ^{13}C minimum between 452 and 443 ka offshore Portugal. During MIS 10, lower δ^{13}C values occurred especially between 351 and 342 ka.

Although Site U1313 received continuous but in comparison to the other glacials small amounts of IRD during MIS 14 (Fig. 3), (coarse) IRD deposition offshore Portugal was nearly negligible and no IRD was deposited during MIS 13 after 523 ka (Fig. 4). During MIS 12, melting icebergs started to reach the Portuguese margin after 472 ka, i.e. significantly later than at IODP Site U1313. The last two IRD peaks in core MD01-2446 during MIS 12 coincided with the last interval of increased IRD deposition at Site U1313 and its Heinrich-type IRD events. At site MD01-2446, however, IRD deposition greatly diminished between the Heinrich-type events. During MIS 10, phases of intensive ice rafting coincided with stadial MIS 10c and with Termination IV. Minor amounts of lithic grains, generally clear quartz grains, were deposited throughout MIS 9e (Fig. 4), especially until 322 ka. However, as the tropical planktonic foraminifera species *G. menardii* is found in the same samples as the quartz grains and mean annual SST further south on the margin exceeded 19°C (Martrat et al., 2007) these grains were more likely deposited by strong westerly winds during the upwelling season than by melting ice. During MIS 11c, coarse lithics were not deposited between 410.8 and 393.6 ka with the exception of one quartz grain found at 404.2 ka that was probably also wind-transported. After 393.6 ka minor amounts of lithics were encountered throughout the glacial inception.

5.3 Core MD03-2699

At nearshore site MD03-2699 the glacial to interglacial pattern that is so clearly evident at the other two sites is more difficult to detect (Fig. 5). While glacial maxima of MIS 12 and 10 are recorded as distinct δ^{18}O maxima and interglacials as distinct minima, glacial inceptions are characterized by relatively large δ^{18}O variability masking a clear

designation into substages. Furthermore, large fluctuations (>0.5‰) in δ^{18}O values are evident during the early stages of MIS 13 (MIS 13c). In fact, Termination VI is entirely masked by high amplitude δ^{18}O variations, and the MIS 13 cool event (isotopic event 13.2) sees a return to glacial-like δ^{18}O values. Warmer thermocline temperatures (δ^{18}O<1.75‰) dominated during interglacial MIS 11c between 417 and 393.6 ka and during MIS 9e from 336.2 to 316.6 ka.

All three glacial inceptions covered by the record reveal millennial-scale oscillations and δ^{18}O values remained relatively low until the subsequent glacial maximum was reached (Fig. 5). Values during the warm phases of these oscillations were in the range of the MIS 13a levels, especially during MIS 12. Also values during interstadial MIS 14b (isotopic event 14.3) reached such levels. During interstadial MIS 9c (311.5–315 ka) thermocline δ^{18}O values (temperatures) were as low (warm) as during MIS 13a or the warm oscillations recorded during MIS 12b and 10b.

Overall, the shape of the δ^{13}C record mimics the pattern described for IODP Site U1313 and site MD01-2446 with heaviest δ^{13}C values recorded during MIS 13 and 11. Contrary to those records heavy δ^{13}C values persisted throughout MIS 12b (Fig. 6). The same is seen during the inception of MIS 10 and in particular during MIS 10c and 10b. Like at site MD01-2446 interglacial MIS 9e is associated with increasing δ^{13}C values that reached higher levels only during MIS 9d and 9c. During MIS 11c the δ^{13}C record shows a stepwise recovery from the minimum during Termination V. The first "plateau" with values generally between 0.75 and 0.9‰ lasted from 416.5 to 401.4 ka, followed by a second maximum with values mainly between 1 and 1.25‰ from 401.1 to 394.4 ka. Also the MIS 13 record of MD03-2699 shows more structure than in the previous records. Although highly variable, early MIS 13c is associated with a maximum in δ^{13}C values, followed by a broad minimum lasting from late MIS 13c to MIS 13b and a subsequent maximum with the highest values (up to 1.47‰) recorded at site MD03-2699 during MIS 13a. The lowest δ^{13}C values of the record were recorded during the colder phases of MIS 14.

Trace amounts of lithics >315 μm were found during MIS 14, early MIS 13c and

MIS 13b (Fig. 5). During MIS 12 the first, but minor IRD peak occurred at 470 ka. Continuous IRD deposition started after 442 ka and lasted until 422.8 ka. IRD peaks during this interval coincided with the Heinrich-type events recorded at IODP Site U1313. After this interval with intensive IRD deposition, minor amounts of lithics (mainly quartz grains) were detected until 410 ka. In three levels during MIS 11c (Fig. 6e) 1 or 2 quartz grains were observed, but these grains are most likely wind-transported from the Portuguese coast. A significant IRD peak occurred around 388 ka within MIS 11b (isotopic event 11.24; Figs. 5, 6e). After this first MIS 11 stadial, minor amounts of lithics were deposited on and off throughout MIS 11a (Fig. 6e). As all those periods of lithic grain deposition coincided with the presence of tetra-unsaturated alkenones (Rodrigues et al., 2009), which are linked to fresher surface waters (Bard et al., 2000), the lithics are interpreted as IRD. MIS 10 is associated with another extended period (362.2–333.4 ka) of ice rafting. Maximum IRD concentrations, however, occurred during MIS 10b. A small IRD peak is also associated with stadial MIS 9d.

5.4 Sea surface temperature reconstructions for MIS 10 to 12

Annual mean SST at IODP Site U1313 varied between 7.7 and 20.2°C (Fig. 6b). The coldest SST was recorded during the Heinrich-type ice-rafting events during MIS 12 and 10c (isotopic event 10.4). SST rose quickly after the onset of Termination V increasing by nearly 8.5°C between 427 and 423 ka. During MIS 11c two SST plateaus with values around 18°C are observed with the second plateau, which also experienced minimally warmer SST, coinciding with the interglacial sea level highstand (408–396 ka). During the subsequent glacial inception, the more pronounced cooling occurred during the MIS 11b stadial (isotopic event 11.24; ~390 ka).

At core site MD03-2699 mean annual SST were relatively warm during MIS 12 with 11.7 to 15.8°C (Fig. 6e). SST then dropped to values below 8°C during the Heinrich-type event at the beginning of Termination V. Similar to the *G. inflata* δ^{13}C records the SST data also shows two plateaus for MIS 11c. The first plateau with SST around 17.6°C lasted from 425 to 413.7 ka, followed until 410 ka by an interval with more vari-

able SST and some values as low as 16.8°C. The second SST plateau with values exceeding 18°C lasted from 410 to 402.5 ka, but SST dropped permanently below 17.5°C only after 396.6 ka with the transition into stadial MIS 11b. During the glacial inception of MIS 10, the SST record reveals four cold/warm cycles whose amplitude weakened towards MIS 10d (Fig. 6e). MIS 10b was associated with warmer SST that were as warm as the warm oscillations within MIS 11a.

5.5 Comparison to published records

North Atlantic ODP Site 980's δ^{18}O data was discussed in previous publications (Oppo et al., 1998; McManus et al., 1999) and is shown in Fig. 7. This site's δ^{13}C record of *N. pachyderma* (r) reveals the lowest δ^{13}C values during the earliest phase of MIS 12 and during the colder intervals of MIS 10 (Fig. 7). δ^{13}C levels recorded during interglacials MIS 13a and 11c were similar and about 0.5‰ heavier than those during interglacial MIS 9e. With the onset of the inception of glacial MIS 12 (480 ka), δ^{13}C values declined continuously towards the MIS 12b minimum (isotopic event 12.2). During the inception of glacial MIS 10, on the other hand, δ^{13}C values remained relatively high between 390 and 360 ka; levels that frequently exceeded the MIS 9e values. The inception of MIS 10 is nevertheless modified by higher frequency variability.

For western subtropical Atlantic ODP Sites 1056/1058 the *N. dutertrei* stable isotope records are also shown in Fig. 7. *N. dutertrei* records conditions towards the bottom of the seasonal thermocline (Billups et al., 2004) with the highest flux in winter (Deuser and Ross, 1989). Thus its living conditions are comparable to those of *G. inflata* (Fairbanks et al., 1980; Deuser and Ross, 1989; Cléroux et al., 2007). Contrary to the other sites in this study, heaviest δ^{13}C values were not concurrent with the sea level highstands of MIS 13a and 11c, both of which exhibit relatively low values (Fig. 7). Times with highest δ^{13}C values coincided with late MIS 14 to 13c and with stadial MIS 11b. For most of the record covered by Site 1056 (MIS 12–10; darker green line in Fig. 7), δ^{13}C values varied between 0.75 and 1.5‰ and dropped to a longer lasting minimum only during the glacial maximum of MIS 10 (isotopic event 10.2). Thus there was no

major difference between glacial MIS 12 and warm MIS 11. A similar pattern is seen at ODP Site 1058 where interglacial MIS 13a and higher values during glacial MIS 12 reached comparable levels (lighter green line in Fig. 7). However, δ^{13}C values declined from MIS 13a to the MIS 12 glacial maximum (isotopic event 12.2), despite of millennial-scale variability overprinting the record.

6 Discussion

6.1 Hydrographic conditions off Portugal

Although core sites MD03-2699 and MD01-2446 are located only about 170 km apart, their *G. inflata* δ^{18}O records are very different in that the nearshore site displays large and rapid fluctuations suggesting very different hydrographic conditions, especially during the glacial inceptions and glacials. The two sites are more similar during interglacial MIS 9e, 11c and 13a, but with core MD03-2699 revealing slightly lower values, thus indicating warmer waters (Figs. 7, 8). We suggest that the higher variability in the δ^{18}O record of core MD03-2699 reflects variations in upwelling of deeper waters into the thermocline.

Regarding the single or double point δ^{18}O maxima recorded during the peak warmth of MIS 11 in core MD03-2699, duplicate analyses confirmed the heavier δ^{18}O values and the accompanying δ^{13}C values are not analytical outliers. Furthermore, parallel measurements in *Orbulina universa* (Voelker et al., unpubl.data) as well as any of the other proxy records (e.g. XRF data, carbonate; Voelker et al., unpubl.data) existing for this core do not contain any sign of reworking or core disturbances at or around those levels. Thus the *G. inflata* values are seen as to be correct and appear to reflect the presence of very cold wintertime thermocline waters. Since the cold spell at 412.65 ka is associated with seven coarse lithic (IRD) grains (Fig. 6e) the source for the cooling seems to be advection of ice-transporting subpolar waters. At the beginning of the younger cooling event that lasted from 401.7 to 401.4 ka, one quartz grain was found.

As this cooling of about 4°C occurred during the MIS 11c sea-level highstand, upwelling of the deeper subpolar ENACW induced by strong winds – thus making the lithic grain a dust grain – is more likely the cause for the cooling. The short cooling at 326.3 ka during MIS 9e and the high variability in both δ^{18}O and δ^{13}C during MIS 13c and b are probably also related to the influence of upwelled waters. Increased productivity during MIS 13c, most probably related to upwelling, is indicated by higher organic carbon concentrations (Voelker et al., unpubl. data). While the interglacial δ^{18}O levels are similar at the two sites and for MIS 11c also in agreement with those recorded for core MD01-2443 (Fig. 6f; de Abreu et al., 2005), *G. inflata* δ^{13}C values at site MD01-2446 are generally higher than at site MD03-2699 indicating that more nutrients were available in the offshore waters either because of lower nutrient consumption (open ocean vs. upwelling regime) or because the waters offshore had already higher preformed nutrient concentrations.

The alkenone-derived SST (Fig. 6e) indicates extremely stable mean annual surface water temperatures during MIS 11c in the nearshore waters off Portugal. The new record from core MD03-2699 agrees well with the one of core MD01-2443 (Fig. 6g; Martrat et al., 2007). Both records show two plateaus within MIS 11c and a short minimum prior to the second, warmer plateau coinciding with the MIS 11c sea-level highstand (note that the minimum in MD01-2443 is shifted towards older ages with the Tzedakis et al. (2009) age model (Fig. 6g), while with the de Abreu et al. (2005) age model (not shown) the minima are aligned). Such a strong SST stability over thousands of years is not seen in the NAC waters at IODP Site U1313 (Fig. 6b) where temperatures, however, reached values similar to those off Portugal. While not as clearly marked as at the Portuguese sites, Site U1313 also recorded two intervals with warmer SST during MIS 11c separated by a minimum, which at 41° N was more pronounced. More variable conditions in the NAC waters are probably linked to admixing of subpolar surface waters, especially during the first MIS11c temperature plateau when hydrographic conditions in the Nordic Seas (Helmke and Bauch, 2003) and the Arctic Ocean (Knies et al., 2007), thus in the subpolar and polar regions, were still unstable

due to freshwater release. The stability in annual mean temperatures off Portugal, on the other hand, must be related to a dominant influence of the subtropical AzC and IPC waters and thus confirm that the hydrographic (winter-time) situation off Portugal during MIS 11c was similar to the Present (Fig. 1b). Since the temperature trends were similar along the different North Atlantic surface currents it appears that the signal originated in the tropical/subtropical regions of the Atlantic Ocean and was advected northwards. This agrees with the observation of Kandiano and Bauch (2007) that northward advection of subtropical waters is causing the SST optimum at Rockall Plateau site M23414. Tropical planktonic foraminiferal species also contributed significantly to the MIS 11c fauna of core MD01-2443 (de Abreu et al., 2005). In cores MD03-2699 and MD01-2446, the deeper dwelling tropical species *Globorotalia menardii* and *Sphaeroidinella dehiscens*, both of which do not occur in the modern fauna off western Iberia (Salgueiro et al., 2008), were found in MIS 11c (Fig. 6d) and 9e samples. Thus it appears that within the North Atlantic's eastern boundary system heat was transported northward not only by the IPC, but also at subsurface level through an enhanced contribution of the eastern boundary undercurrent to the IPC's subsurface component. This enhanced flux of tropical subsurface waters, which are nutrient poor, could also contribute to the lower *G. inflata* δ^{13}C values at site MD03-2699. It, furthermore, confirms that heat flux into the North Atlantic was at its maximum during the mid-Brunhes (Berger and Wefer, 2003).

MIS 11c interglacial conditions off Portugal ended around 395 ka with the onset of the 11b stadial (isotopic event 11.24). Cooling during this stadial was gradual and coldest conditions were reached only towards the end of the stadial coincident with IRD maxima around 388 ka (Figs. 4, 6). Even though site MD03-2699 received more IRD, δ^{18}O-inferrred surface water-cooling seems to have been similar between the two sites (Fig. 8d). Since SST at MD01-2443, located just about 1 degree further south than MD03-2699, reveal less cold temperatures, subtropical IPC waters probably still influenced the southern margin and their presence might have enhanced iceberg melting near site MD03-2699. The pollen record of core MD01-2447 at 42° N (Desprat et

al., 2005) confirms maximum cooling towards the end of the stadial also for northern Iberia, but more importantly it shows that cooling along with the IRD peaks recorded at site MD03-2699 and MD01-2446 was restricted to the winters. Since melting icebergs and colder surface waters reached the western Iberian margin much later than IODP Site U1313 (Figs. 3, 6a, b) or ODP Site 980 (Fig. 6c), where IRD deposition peaked 1000 years prior but persisted until the end of the stadial (Oppo et al., 1998), a latitudinal front must have existed north of the Iberian Peninsula. In addition, it appears that it took ≥1000 years of meltwater flux into the subpolar and northern transitional regions to weaken AMOC enough to push this front as far south as 39° N.

MIS 11a and thus the glacial inception of MIS 10 is marked by four stadial/interstadial cycles, the first interstadial of which is associated with isotopic event 11.23 (Figs. 3–6). The cycles are best depicted in the alkenone SST records (Fig. 6b, e). Cooling during the second stadial is much stronger on the northern (Desprat et al., 2005) and middle Iberian margin (MD03-2699) than in the NAC waters (IODP Site U1313). Therefore a European or Scandinavian source for the cooling is more likely than advection with the NAC from the western subpolar gyre, the typical source region for ice-rafting events during MIS 3. Such an eastern source region is supported by the stronger IRD signal at ODP Site 980 (Fig. 6c; Oppo et al., 1998) than at IODP Site U1313, even given the differences in the IRD size fraction. The subsequent stadials had only small impacts on the SST at site MD03-2699, but were associated with short, but strong coolings in the *G. inflata* δ^{18}O record indicating the presence of colder surface waters during some of the winters (a more detailed discussion of the δ^{18}O data follows below). The cold temperatures recorded by *G. inflata* might be linked to the ones recorded in the MD01-2443 alkenone record (Fig. 6g; assuming an offset due to age models for stadial III). However, since alkenones represent annual mean temperatures and thus smooth a more seasonal signal like the *G. inflata* δ^{18}O data and since MD01-2443's cold alkenone SST are not reflected in the faunal based SST (de Abreu et al., 2005), these for this latitude unusually cold SST outside of a Heinrich event or glacial maximum need to be confirmed by other records from the northern Iberian margin or the Bay of Bis-

caye, i.e. regions closer to potential sources for such cold waters. Such confirmation is especially important because stadials II and III did not coincide with Heinrich-type events (Hodell et al., 2008; Stein et al., 2009) and such strong coolings are (so far) not detected in other records either along the NAC path – IODP Site U1313 (Fig. 6a, b) and core M23414 (Kandiano and Bauch, 2003) – or more locally in the planktonic δ^{18}O records of cores MD01-2446 (Fig. 4) and MD01-2447 (Desprat et al., 2005). In addition, at ODP Site 980 ice-rafting and cooling as indicated by the presence of *N. pachyderma* (s) was much lower during stadial III than stadial II (Fig. 6c). The pollen based terrestrial temperature records for core MD01-2447 also reveal only minor cooling during the younger stadials (Desprat et al., 2005), conform with the MD03-2699 SST record. Thus for the moment the SSTs recorded in core MD03-2699 appear to be more realistic for the western Iberian margin during MIS 11a than the MD01-2443 signal.

With the onset of MIS 11a the *G. inflata* δ^{18}O and δ^{13}C records of core MD03-2699 start to diverge from the offshore signal at site MD01-2446 (Fig. 8d). For most of the glacial inception, δ^{18}O values in core MD03-2699 stayed low, while values in core MD01-2446 increased as is to be expected with gradual cooling and increasing ice volume. The difference between these two relative closely located core sites can only be caused by a strong hydrographic front. Because *G. inflata* is reflecting winter mixed-layer conditions this front must have been the northward trending subtropical front, in a manner similar to the present when the front allows warmer subtropical water to flow across the location of core MD03-2699 (Fig. 1b). The strong IPC influence on the southwestern margin is confirmed by the *G. inflata* δ^{18}O values and warm SST of core MD01-2443 (Fig. 6f, g; de Abreu et al., 2005), which, with the exception of the unusually high values between 375 and 381 ka, have levels similar to those of core MD03-2699. The signal at offshore site MD01-2446, on the other hand, agrees well with the NAC record of IODP Site U1313 (Fig. 8c) and therefore in the PC's source waters. The northward extending subtropical front and thus the dominant IPC influence on nearshore waters off Portugal persisted into the glacial. Only during those

times when *G. inflata* δ^{18}O values in core MD03-2699 became temporarily higher and reached MD01-2446 levels (Fig. 8d), like during stadials II and III, did the front not exist and colder waters also penetrated into the nearshore regions. During early MIS 10 the subsurface component of the IPC was strengthened again with deep dwelling tropical foraminifer species (Fig. 6d) being advected to the mid-latitude nearshore Portuguese margin. The increased (temporary) subsurface northward heat flux could explain why mean annual SST and the winter mixed layer at site MD03-2699 were hardly impacted by the Heinrich-type event during stadial MIS 10c (isotopic event 10.4), even though melting icebergs reached this site (Figs. 5, 6e). Since the signals for warmer surface to subsurface waters and IRD deposition occur in the same levels, seasonality at site MD03-2699 must have been very high during MIS 10.

The pattern with a strong subtropical front separating sites MD03-2699 and MD01-2446 and with subtropical IPC waters dominating the nearshore waters of the Portuguese margin is not only seen for the glacial inception of MIS 10, but also during MIS 12 and with lesser intensity during MIS 14b (isotopic event 14.3) and the glacial inception starting with stadial MIS 9d (Fig. 8d). Therefore the presence of a northward extending subtropical front off Portugal is a typical feature for the glacial inceptions and glacials of the mid-Brunhes period. For the transition from MIS 13a to 12a four short-term colder episodes are detected in the *G. inflata* δ^{18}O record of core MD03-2699. Values during those times did not, however, reach the colder MD01-2446 levels (Fig. 8d), except for the short IRD event at 470 ka (Fig. 5) that like stadial MIS 11b also had more likely an eastern source because a pronounced IRD peak is recorded at site M23414 (Kandiano and Bauch, 2003) and ODP Site 980 (Oppo et al., 1998) but not at IODP Site U1313 (Fig. 3). Overall, wintertime hydrographic conditions in the nearshore waters off Portugal appear to have been warmer and more stable during MIS 12 than during the subsequent glacial inception. Such temperature "stability" points to a strong influence of the subtropical Azores Current in this region and is conform to evidence from the western Mediterranean Sea. There planktonic δ^{18}O records of ODP Sites 976, 977 and 975 (Pierre et al., 1999; von Grafenstein et al., 1999) reveal

significantly warmer surface waters during glacial MIS 12 and 14 than during MIS 10. Some of the waters advected polewards with the IPC might actually be responsible for the continuously warm SST at ODP Site 980 during the early MIS 12 (McManus et al., 1999), a signal quite different from the NAC and PC records of IODP Site U1313 and core MD01-2446 that depict several smaller scale warm/cold oscillations throughout MIS 12b (Figs. 3, 4).

During late MIS 12, minimum alkenone SST of core MD03-2699 are similar to minimum temperatures recorded during early MIS 10 (Fig. 6e). SST in nearshore waters off Portugal, however, rose continuously towards the deglaciation. During the MIS 12 glacial maximum at 430 ka a SST gradient of $\geq$6°C existed between IODP Site U1313 and MD03-2699 (Fig. 6b and e, respectively) indicating that a front – either just the subtropical front off Portugal or even the polar front – separated the surface waters in this mid-latitudinal band. The trend of rising SST off Portugal was abruptly interrupted by the significant cooling associated with the Heinrich-type ice-rafting event around 427 ka at the onset of the deglaciation (Hodell et al., 2008; Stein et al., 2009). Without this event, SST off Portugal would probably have increased gradually towards MIS 11. This Heinrich-type event had a major impact on the hydrography in the North Atlantic, even leaving a fresher water signal in the *G. inflata* records of core MD01-2446 (low δ^{18}O values contemporary with light δ^{13}C values; Fig. 4), and led to a temporary AMOC shut down (Voelker et al., 2009), just like its younger counterparts. A Heinrich-type event is also associated with Termination IV as evident by core MD01-2446's records (Fig. 5), where the presence of melting icebergs led to strong oscillations in the planktonic δ^{18}O values.

6.2 Basinwide surface water circulation and linkages to thermocline water sources

Both the PC and the IPC also have a subsurface component of subpolar or subtropical waters, respectively, whose properties contribute to those in the deep winter mixed layer in which deeper dwelling foraminifer like *G. inflata* calcify their tests. By tapping

into subsurface waters deep winter mixing replenishes the nutrients available in the upper water column. Since δ^{13}C values measured in planktonic foraminifer tests are related to nutrient concentrations (Broecker and Peng, 1982; Ortiz et al., 1996) we are using them to trace the subsurface/mode waters in the North Atlantic. Such an approach is facilitated by the fact that the subpolar mode water is formed during winter along the NAC branches around the Rockall Plateau (Brambilla and Talley, 2008) and thus in close vicinity to ODP Site 980. Because the mode water is directly advected southward with the Portugal current the transport way is relatively short minimizing the time during which the δ^{13}C signal could be modified. Furthermore, the selected planktonic foraminifer species represent conditions in winter and thus prior to the spring blooms and upwelling season during which the δ^{13}C would be altered due to nutrient consumption. The comparison between sites focuses on trends and not on absolute values because the δ^{13}C values of the different species were not corrected to dissolved inorganic carbon (DIC) levels (except for the ODP Site 980 *N. pachyderma* (r) values in Fig. 8a and b where the correction was added to minimize the plot's δ^{13}C range). Thus only the δ^{13}C values of the *G. inflata* based records of IODP Site U1313, MD01-2446 and MD03-2699 are directly comparable.

In the direct comparison it becomes clear that the offshore core MD01-2446 is very similar to North Atlantic IODP Site U1313 (Figs. 7, 8c) indicating that for most of the studied interval hydrographic conditions, i.e. temperature and salinity properties, were not much different in the NAC and the PC. For most of the time the *G. inflata* δ^{13}C values at both sites were comparable and generally heavier than at site MD03-2699. However, there were also intervals when the two open ocean records diverged. One such example is the interstadial associated with isotopic event 11.23 when warm conditions in the NAC at IODP Site U1313 lasted longer than in the PC record of core MD01-2446 that is more comparable with the NAC record at ODP Site 980 (Figs. 7, 8a–c). Thus it might be that the NAC's main flow path was shifted more southward than its current position (Fig. 1) and that the NAC waters reaching the Rockall Plateau and feeding the PC were already modified by entrainment of subpolar waters. A strong

linkage in water mass conditions between the Rockall Plateau NAC branch and the PC is confirmed by the δ^{13}C records (Figs. 7, 8b). This relationship is especially evident during MIS 12 when the MD01-2446 δ^{13}C data follows the ODP Site 980 record, especially the pronounced δ^{13}C minimum during early MIS 12 that is only recorded at these two sites (Fig. 7). Thus it appear that the poorly ventilated surface to subsurface waters advected southward with the PC during MIS 12 were formed near or above the Rockall Plateau, probably in regions similar to those of modern subpolar mode water formation (Brambilla and Talley, 2008). Enhanced influence of eastern basin waters is also consistent with a stronger imprint of the 470 ka IRD event in these records. MIS 12 δ^{13}C values at IODP Site U1313, on the other hand, stayed fairly constant despite the strong temperature and salinity oscillations indicated by the δ^{18}O data and the presence of melting icebergs (Fig. 3). Thermocline waters in this region were better ventilated than in the eastern basin indicating that Gulf Stream waters (ODP Site 1056 and 1058; Fig. 7) still reached this latitude, in agreement with the relative warm SST during most of MIS 12 (Stein et al., 2009) that also imply northward heat advection. The persistent nutrient supply by the thermocline waters supported increased phytoplankton production near Site U1313 (Stein et al., 2009). Even though supported only by isotope data for early MIS 10, the same pattern with well ventilated thermocline waters supporting high productivity (Stein et al., 2009) is also seen then, while the MD01-2446 and ODP Site 980 records indicate that the Rockall Plateau was – similar to MIS 12 – the source region for the PC waters (Fig. 8b). Thus while during mid-Brunhes glacial intervals Gulf Stream derived NAC waters penetrated at least until 41° N in the western basin, their influence was diminished in the eastern basin. Especially during early MIS 12, the position of the polar front appears to have been tilted in the North Atlantic reaching further to the south in the eastern than western basin. The glacial differences are also well seen in the scatter plots (Fig. 9a) with divergences towards higher/lower δ^{13}C values in IODP Site U1313 and core MD01-2446, respectively. However, these plots also reveal that during most of the time, in particular during the interglacial intervals (lower δ^{18}O values), conditions at the three sites influenced by the NAC and PC were not much

different (Fig. 9b); thus making the NAC like today the dominant hydrographic feature in the mid-latitude North Atlantic.

Although the NAC and PC records at IODP Site U1313, ODP Site 980 and site MD01-2446 agree well, there is one interval when the MD01-2446 record diverges from the others and this is the δ^{13}C minimum associated with Termination V (Fig. 8a–c). During the onset of the deglaciation δ^{13}C levels are similar at the three sites. However, while the δ^{13}C minimum at Site U1313 lasted for 10 ka, which is similar to ODP Site 980 (Fig. 8a), at site MD01-2446 it ended after only 5 ka, which is also sooner than at site MD03-2699 (Fig. 8d). The late glacial and deglacial δ^{13}C minima are generally linked to poorly ventilated and thus nutrient-rich water masses such as Subarctic Intermediate Water (Venz et al., 1999) or Antarctic Intermediate Water, the later of which penetrated as far north as 61.5° N during the last deglaciation (Rickaby and Elderfield, 2005). The presence of better ventilated waters at site MD01-2446 therefore implies the formation of well ventilated mode water, may be similar to the formation of subtropical NACW along the Azores front during modern winters, somewhere south of 41° N and offshore of western Iberia. A different length of the deglacial δ^{13}C minimum is not seen for Termination VI, when it lasted about 8 ka at both IODP Site U1313 and site MD01-2446, or for Termination IV, when lesser ventilated surface to subsurface waters were present in the eastern North Atlantic basin (ODP Site 980, MD01-2446, MD03-2699; Fig. 8b, d) also throughout the subsequent interglacial and thus for almost 20 ka. Hydrographic conditions during MIS 9e were different than during the other interglacial intervals. This is not only evidenced by the prolonged δ^{13}C minimum but also by the persistent, if low presence of the polar species *N. pachyderma* (s) in the planktonic foraminifer fauna off Iberia during the first half of the interglacial (de Abreu et al., 2005; Desprat et al., 2009). Based on the deciduous quercus pollen record of core MD03-2697 at 42° N (Desprat et al., 2009) the climatic optimum occurred during the second half of the interglacial – comparable, but not equal to the 2nd warmer phase of MIS 11c. Warmer surface waters in the PC and NAC during the 2nd half of the interglacial are supported by the δ^{18}O record of core MD01-2446 and the alkenone SST

record of IODP Site U1313 (Stein et al., 2009). The prolonged δ^{13}C minimum implies advection of poorly ventilated waters into the mid-latitude North Atlantic. These waters were most likely Subarctic Intermediate Water since the records of ODP Site 982 on the northern Reykjanes ridge (57.5° N) reveal the same δ^{13}C minimum accompanied by persistent, but low input of IRD (Venz et al., 1999). Thus ice-bearing arctic waters must have penetrated from the Nordic Seas southward across the Iceland-Faeroe ridge into the subpolar gyre where they mixed with the NAC waters since this is one of the region were subpolar mode water is formed at Present (Brambilla and Talley, 2008). Besides the poor ventilation the advection of subpolar waters to the Iberian margin had no impact because mean annual and summer SST in the nearshore band stretching from site MD01-2443 (Martrat et al., 2007) over MD03-2699 (Rodrigues et al., 2009) to MD03-2697 (Desprat et al., 2009) exceeded 18°C. Thus the contributions of *N. pachyderma* (s) to the planktonic foraminifer fauna are more likely an indicator for increased upwelling of the colder subpolar ENACW off Iberia and thus stronger winds because only those would cause subpolar ENACW to be upwelled south of 40° N. With windier conditions during early MIS 9e, the lithic grains found at site MD01-2446 (Fig. 4) could be wind transported.

As already mentioned above the δ^{13}C values in records for NAC and PC waters were mostly heavier than at site MD03-2699 in agreement with subpolar source waters being better ventilated than subtropical ones. Given that the δ^{18}O and SST data implies a strong IPC influence on the latter record, the δ^{13}C values of core MD03-2699 should show some resemblance to those values recorded in the subtropical Gulf Stream waters at ODP Sites 1056 and 1058 (Figs. 7, 8e). Based on the scatter plots (Fig. 9c, d) there is only minor overlap between the records from the western and eastern side of the North Atlantic basin and that seems mainly to be restricted to MIS 11 as implied by the MD01-2443 data (Fig. 9d). The *N. dutertrei* δ^{13}C record of ODP Site 1056 shows a similar pattern to core MD03-2699 during MIS 11c with lighter values indicating relatively more nutrients during the early phase and heavier values during the later phase of the interglacial (Fig. 8e). Consequently, this two-step feature in nutri-

ent concentrations is a subtropical gyre signal. Trends and even absolute $\delta^{13}C$ values were also similar at ODP Sites 1056 and 1058 and site MD03-2699 between 495 and 440 ka and after 350 ka (Fig. 8e); thus during those glacial times, when SSTs and $\delta^{18}O$ data of core MD03-2699 indicate a strong subtropical water influence. The good correspondence during MIS 12 might indicate that cross-Atlantic transport with the AzC was strong with little admixing of transitional waters. This enhanced AzC (heat) flux towards the southern Iberian margin would also explain why MIS 12 is much warmer in western Mediterranean Sea records than MIS 10 (Pierre et al., 1999; von Grafenstein et al., 1999). During the inception of MIS 10, nutrient concentrations at site MD03-2699 were higher than at ODP Site 1056 indicating that the Gulf Stream waters were greatly modified before reaching the western Iberian margin, if they contributed to the subsurface waters there at all. The $\delta^{13}C$ records between the two sites also diverged during MIS 13c and b, when upwelling from either subtropical or subpolar ENACW influenced site MD03-2699. The records were also decoupled during the glacial maximum of MIS 12, when the subtropical front did not separate waters at site MD03-2699 from those recorded in core MD01-2446 and subpolar waters influenced the western Iberian margin.

6.3 Comparison of the interglacials

The new records from the mid-latitude North Atlantic confirm MIS 11c to be a long and relative stable interglacial in comparison to either MIS 13 or MIS 9. Especially the NAC and PC waters experienced only minor changes in the hydrographic conditions and nutrient levels. Thus conditions in the mid-latitude North Atlantic were comparable to those of ODP Site 980 (Oppo et al., 1998; McManus et al., 2003). Based on the $\delta^{18}O$ records hydrographic conditions in those waters were also stable during MIS 9e, while MIS 13c and 13a experienced some small-scale oscillations and consequently less stable conditions (Fig. 7). MIS 13c and 13a are also confirmed to have been colder in than the subsequent interglacials with only short intervals during MIS 13a

reaching δ^{18}O values comparable to MIS 11c or 9e levels (Figs. 4–6). In the sites affected by subtropical waters (ODP Sites 1056 and 1058; MD03-2699) variability in the surface water properties was slightly higher during MIS 11c and 9e than in the NAC and PC records, while MIS 13 appears more stable in the Gulf Stream waters (Figs. 7, 8e). At site MD03-2699, on the other hand, MIS 13c and 13a were quite different. Hydrographic conditions during MIS 13c were highly variable due to intense upwelling (see Sect. 6.1), but were more stable and comparable to ODP Site 1058 during MIS 13a (Fig. 8e).

Overall, MIS 11c and 9e appear to have experienced comparable temperature and salinity conditions in the mid-latitude North Atlantic. However, there is one major difference and that is the ventilation of the surface to subsurface waters and their impact on the AMOC. While no impact of the poorly ventilated and potentially fresher waters during MIS 9e is seen in the planktonic δ^{18}O records presented here, they affected the ventilation of the deeper North Atlantic Deep Water (NADW) as evidenced by the benthic isotope record of IODP Site U1308 (Hodell et al., 2008), where well ventilated NADW at 3870 m water depth was only recorded after 323.5 ka, and of core MD01-2446 (Voelker, unpublished data), where until 325 ka NADW ventilation was highly variable. Because the upper NADW as recorded at ODP Site 980 (McManus et al., 1999) was well ventilated, only the deeper branch was affected – either because the Iceland-Scotland Overflow Waters (ISOW) exiting from the Nordic Seas were poorly ventilated or AMOC was shallower during early MIS 9e. Anyhow, a shallower AMOC or poorly ventilated ISOW sets MIS 9e apart from MIS 11c, when AMOC was so strong already early within the deglaciation that after 426 ka well ventilated NADW penetrated as deep as 3870 m (Hodell et al., 2008; Voelker et al., 2009).

The new records extend the region with stable temperature conditions during MIS 11c down to 39° N and confirm that overall hydrographic conditions in the North Atlantic basin were similar to today. Some new insights into hydrographic conditions in the subtropical gyre could be gained from the records of core MD03-2699. They are:

1. the existence of two SST plateaus with the second period experiencing slightly warmer temperatures and coinciding with the sea level highstand
2. within the respective plateaus very stable SST in the nearshore waters off Portugal lasting several thousands of years
3. increased northward heat flux of subsurface tropical waters with the eastern boundary undercurrent, especially during the early phase of the interglacial
4. a two step evolution in planktonic $\delta^{13}C$ indicating poorer ventilated subtropical waters during the early phase and better ventilated ones during the second phase; the transition in $\delta^{13}C$ occurred during the sea level highstand and thus later than the transition to warmer SST
5. the formation of well ventilated mode waters in the vicinity of core MD01-2446 during transition from glacial MIS 12 to interglacial MIS 11c.

7 Conclusions

By combining the records of six core sites spanning the latitudes from 32 to 55.5° N and the major surface water currents linked to the subtropical and transitional waters in the North Atlantic Ocean we are able to trace hydrographic conditions from MIS 9 to 14. Overall, planktic foraminiferal $\delta^{18}O$ values and alkenone derived SSTs indicate that surface water temperature and salinity conditions during the interglacials MIS 11c and MIS 9e were not much different and very stable along the NAC and PC. Surface water ventilation, on the other hand, differed with MIS 9e being associated with poorly ventilated surface waters that impacted the deeper branch of the AMOC. In the eastern boundary system off Portugal northward heat flux of tropical waters with the subsurface undercurrent is observed during MIS 11c and MIS 10 as indicated by the presence of tropical species. During early MIS 11c these northward advected (sub)tropical waters even reached the Rockall Plateau (Kandiano and Bauch, 2007). Along with

the enhanced northward heat flux hydrographic conditions in the offshore waters off Portugal were such that well ventilated mode waters were formed during the glacial to interglacial transition. So far these mode waters have only been recorded at site MD01-2446 and it remains to be seen in the future if their impact was locally restricted. MIS 13 is confirmed as colder than the subsequent interglacials and except for site MD03-2699 conditions during MIS 13c and 13a were not much different along the major currents. Due to apparently strong upwelling during MIS 13c the planktonic isotope records of core MD03-2699 experienced pronounced variability, while conditions during MIS 13a were relative stable and comparable to those in the Gulf Stream. Overall, it appears that conditions in the mid-latitude North Atlantic were not much different during MIS 11c than during MIS 9e and, if one neglects the generally lower temperatures, also during MIS 13a. Current pathways and associated fronts were similar to today during all the interglacials. The difference between the interglacials lies in the ventilation of the subsurface waters. Here MIS 9e stands apart because the continuous admixing of arctic waters into the transitional waters of the mid-latitude North Atlantic.

Based on the closely spaced core sites MD03-2699 and MD01-2446 it is evident that a strong hydrographic front existed off Portugal, especially during the glacial inceptions and glacials. This front appears to have been equal to the northward extending subtropical front that exists during modern winters (Fig. 1b). East of the front, i.e. in the nearshore waters off Portugal, a strong influence of subtropical waters is recorded at sites MD03-2699 and MD01-2443. Given this overprint of subtropical waters caution should be taken to interpret surface water records from nearshore sites off Portugal as basin-wide signals, at least for the mid-Brunhes interval studied here. Accordingly, the pronounced SST stability recorded in these waters during MIS 11c might be more typical for the subtropical gyre than a Gulf Stream/NAC signal (Fig. 6). Future records off NW Iberia and off NW Africa, i.e. up- and downstream, might help to shed some light onto this question. The hydrographic front disappeared sporadically during stadials of the glacial inception of MIS 10, but cooling episodes in the nearshore waters were much shorter than those recorded offshore (Figs. 7, 8d).

Increased heat transport with the AzC across the Atlantic is also seen during MIS 12 when $\delta^{13}C$ records of ODP Sites 1056 and 1058, representing Gulf Stream waters, and of core MD03-2699 were most similar (Fig. 8e). The alkenone SST record of core MD03-2699 confirms relative warm waters at this site and warming from the glacial maximum to the interglacial would probably have been continuously if it had not been interrupted by a Heinrich-type ice-rafting event at the onset of the deglaciation that left a freshwater signal in the offshore waters at site MD01-2446. Cooling during this event is comparable to the cooling observed during younger Heinrich events (e.g. de Abreu et al., 2003). While the nearshore waters off Portugal had a subtropical source during MIS 12, the offshore waters were derived from the Rockall Plateau region as the close correspondence between the records of ODP Site 980 and core MD01-2446 reveal (Fig. 8b). The surface waters in the eastern basin were poorer ventilated than those in the western basin (IODP Site U1313), even though the western basin experienced stronger salinity oscillations linked to more frequent ice-rafting events. Thus during most of MIS 12 NAC waters still reached IODP Site U1313, confirmed by the SST record (Stein et al., 2009), but did not enter into the eastern basin. Consequently, during MIS 12 the position of the polar front was tilted reaching further south in the eastern basin and coming in close contact with the subtropical front off Portugal.

Acknowledgements. This study used samples provided by the Integrated Ocean Drilling Program (IODP) and by the British Ocean Sediment Core Research Facility (BOSCOR). The Fundação para a Ciência e a Tecnologia (FCT) through the PORTO (PDCT/MAR/58282/2004) and SEDPORT projects (PDCTM/40017/2003), and postdoctoral (SFRH/BPD/21691/2005) and PhD (SFRH/BP/13749/2003) fellowships funded A. V. and T. R. Coring of MD03-2699 was made possible through a European Access to Research Infrastructure grant. We thank IPEV, Yvon Balut and the captain and crews of R/V Marion Dufresne for their support in retrieving the two Calypso cores. Special thanks go to Monika Segl (Marum, University Bremen) for the measuring of the isotope samples, to Lucia de Abreu for sampling core MD01-2446, and to Miguel Reis of the ITN in Lisbon for access to the freeze dryer in his lab. The staff of the DGM lab and J. P. Ferreira and B. Montanari are greatly appreciated for their support in sampling and sample preparation. U. Paczek, M. Ferreira, B. Montanari and C. Trindade helped with the

picking of some of the stable isotope samples.

References

Alvarez-Salgado, X. A., Figueiras, F. G., Perez, F. F., Groom, S., Nogueira, E., Borges, A. V., Chou, L., Castro, C. G., Moncoiffe, G., and Rios, A. F.: The Portugal coastal counter current off NW Spain: new insights on its biogeochemical variability, Prog. Oceanogr., 56, 281–321, 2003.

Amore, F. O., Flores, J. A., Filippelli, G. M., Sierro, F. J., Voelker, A. H. L., and Rodrigues, T.: Coccolithophore record during the Middle Pleistocene in the North and South Atlantic: Productivity and Dissolution patterns, Mar. Micropalentology, in preperation.

Bard, E., Rostek, F., Turon, J. L., and Gendreau, S.: Hydrological Impact of Heinrich Events in the Subtropical Northeast Atlantic, Science, 289, 1321–1324, 2000.

Bassinot, F. C., Labeyrie, L. D., Vincent, E., Quidelleur, X., Shackleton, N. J., and Lancelot, Y.: The astronomical theory of climate and the age of the Brunhes-Matuyama magnetic reversal, Earth Planet. Sc. Lett., 126, 91–108, 1994.

Bauch, H. A., Erlenkeuser, H., Helmke, J. P., and Struck, U.: A paleoclimatic evaluation of marine oxygen isotope stage 11 in the high-northern Atlantic (Nordic seas), Global Planet. Change, 24, 27–39, doi:10.1016/S0921-8181(99)00067-3, 2000.

Baumann, K. H. and Freitag, T.: Pleistocene fluctuations in the northern Benguela Current system as revealed by coccolith assemblages, Mar. Micropaleontol., 52, 195–215, doi:10.1016/j.marmicro.2004.04.011, 2004.

Berger, W. H. and Wefer, G.: On the Dynamics of the Ice Ages: Stage-11 Paradox, Mid-Brunhes Climate Shift, and 100-ky Cycle, in: Earth's Climate and Orbital Eccentricity: the Marine Isotope Stage 11 Question, edited by: Droxler, A. W., Poore, R. Z., and Burckle, L. H., Geophysical Monograph, American Geophysical Union, Washington, D.C., 41–59, 2003.

Billups, K., Chaisson, W., Worsnopp, M., and Thunell, R.: Millennial-scale fluctuations in subtropical northwestern Atlantic surface ocean hydrography during the mid-Pleistocene, Paleoceanography, 19, no.2, PA2017, doi:10.1029/2003PA000990, 2004.

Billups, K., Lindley, C., Fisler, J., and Martin, P.: Mid Pleistocene climate instability in the subtropical northwestern Atlantic, Global Planet. Change, 54, 251–262, 2006.

Brambilla, E. and Talley, L. D.: Subpolar Mode Water in the northeastern Atlantic: 1. Averaged

properties and mean circulation, J. Geophys. Res., 113, C0425, doi:10.1029/2006JC004062, 2008.
Broecker, W. S. and Peng, T.-H.: Tracers in the Sea, Tracers in the Sea, ELDIGIO Press, Lamont-Doherty Geological Observatory, Columbia University, Palisades, New York, 690 pp., 1982.
Calvo, E., Villanueva, J., Grimalt, J. O., Boelaert, A., and Labeyrie, L.: New insights into the glacial latitudinal temperature gradients in the North Atlantic. Results from Uk37' sea surface temperatures and terrigenous inputs, Earth Planet. Sc. Lett., 188, 509–519, 2001.
Calvo, E., Pelejero, C., and Logan, G. A.: Pressurized liquid extraction of selected molecular biomarkers in deep sea sediments used as proxies in paleoceanography, J. Chromatogr. A, 989, 197–205, 2003.
Chaisson, W. P., Poli, M. S., and Thunell, R. C.: Gulf Stream and Western Boundary Undercurrent variations during MIS 10–12 at Site 1056, Blake-Bahama Outer Ridge, Mar. Geol., 189, 79–105, 2002.
Channell, J. E. T., Kanamatsu, T., Sato, T., Stein, R., Alvarez Zarikian, C. A., Malone, M. J., and the.Expedition.303/306.Scientists: Proceedings IODP, 303/306, Integrated Ocean Drilling Program Management International, Inc., College Station TX, 2006.
Chapman, M. R. and Maslin, M. A.: Low-latitude forcing of meridional temperature and salinity gradients in the subpolar North Atlantic and the growth of glacial ice sheets, Geology, 27, 875–878, 1999.
Cléroux, C., Cortijo, E., Duplessy, J.-C., and Zahn, R.: Deep-dwelling foraminifera as thermocline temperature recorders, Geochem. Geophy. Geosy., 8, Q04N11, doi:10.1029/2006GC001474, 2007.
de Abreu, L., Shackleton, N. J., Schoenfeld, J., Hall, M., and Chapman, M.: Millennial-scale oceanic climate variability off the Western Iberian margin during the last two glacial periods, Mar. Geol., 196, 1–20, 2003.
de Abreu, L., Abrantes, F. F., Shackleton, N. J., Tzedakis, P. C., McManus, J. F., Oppo, D. W., and Hall, M. A.: Ocean climate variability in the eastern North Atlantic during interglacial marine isotope stage 11: A partial analogue to the Holocene?, Paleoceanography, 20, PA3009, doi:10.1029/2004PA001091, 2005.
Desprat, S., Sanchez Goni, M. F., Turon, J. L., McManus, J. F., Loutre, M. F., Duprat, J., Malaize, B., Peyron, O., and Peypouquet, J. P.: Is vegetation responsible for glacial inception during periods of muted insolation changes?, Quaternary Sci. Rev., 24, 1361–1374, 2005.

Desprat, S., Sánchez Goñi, M. F., McManus, J. F., Duprat, J., and Cortijo, E.: Millennial-scale climatic variability between 340 000 and 270 000 years ago in SW Europe: evidence from a NW Iberian margin pollen sequence, Clim. Past, 5, 53–72, 2009.
Deuser, W. G. and Ross, E. H.: Seasonally Abundant Planktonic-Foraminifera of the Sargasso Sea – Succession, Deep-Water Fluxes, Isotopic Compositions, and Paleoceanographic Implications, J. Foramin. Res., 19, 268–293, 1989.
Dickson, A. J., Leng, M. J., and Maslin, M. A.: Mid-depth South Atlantic Ocean circulation and chemical stratification during MIS 10 to 12: implications for atmospheric CO_2, Clim. Past, 4, 333–344, 2008.
Droxler, A. W., Alley, R. B., Howard, W. R., Poore, R. Z., and Burckle, L. H.: Introduction: Unique and Exceptionally Long Interglacial Marine Isotope Stage 11: Window into Earth Warm Future Climate, in: Earth's Climate and Orbital Eccentricity: The Marine Isotope Stage 11 Question, edited by: Droxler, A. W., Poore, R. Z., and Burckle, L. H., Geophysical Monograph, American Geophysical Union, Washington, D.C., 1–14, 2003.
EPICA Members: Eight glacial cycles from an Antarctic ice core, Nature, 429, 623–628, 2004.
Fairbanks, R. G., Wiebe, P. H., and Be, A. W. H.: Vertical-Distribution and Isotopic Composition of Living Planktonic-Foraminifera in the Western North-Atlantic, Science, 207, 61–63, 1980.
Fiúza, A. F. G.: Hidrologia e Dinamica das Aguas Costeiras de Portugal, Faculdade de Ciências da Universidade de Lisboa, Universidade de Lisboa, Lisbon, 294 pp., 1984.
Flores, J. A., Marino, M., Sierro, F. J., Hodell, D. A., and Charles, C. D.: Calcareous plankton dissolution pattern and coccolithophore assemblages during the last 600 kyr at ODP Site 1089 (Cape Basin, South Atlantic): paleoceanographic implications, Palaeogeography, Palaeoclimatology, Palaeoecology, 196, 409–426, 2003.
Flower, B. P., Oppo, D. W., McManus, J. F., Venz, K. A., Hodell, D. A., and Cullen, J. L.: North Atlantic intermediate to deep water circulation and chemical stratification during the past 1 Myr, Paleoceanography, 15, 388–403, 2000.
Fratantoni, D. M.: North Atlantic surface circulation during the 1990's observed with satellite-tracked drifters, J. Geophys. Res., 106, 22067–22093, 2001.
Guo, Z. T., Biscaye, P., Wei, L. Y., Chen, X. F., Peng, S. Z., and Liu, T. S.: Summer monsoon variations over the last 1.2 Ma from the weathering of loess-soil sequences in China, Geophys. Res. Lett., 27, 1751–1754, 2000.
Hall, I. R. and Becker, J.: Deep Western Boundary Current variability in the subtropical northwest Atlantic Ocean during marine isotope stages 12–10, Geochem. Geophy. Geosy., 8,

Q06013, doi:10.1029/2006GC001518, 2007.
Hefter, J.: Analysis of Alkenone Unsaturation Indices with Fast Gas Chromatography/Time-of-Flight Mass Spectrometry, Anal. Chem., 80, 2161–2170, 2008.
Helmke, J. P. and Bauch, H. A.: Comparison of glacial and interglacial conditions between the polar and subpolar North Atlantic region over the last five climatic cycles, Paleoceanography, 18, no. 2, 1036, doi:10.1029/2002PA000794, 2003.
Helmke, J. P., Bauch, H. A., Röhl, U., and Kandiano, E. S.: Uniform climate development between the subtropical and subpolar Northeast Atlantic across marine isotope stage 11, Clim. Past, 4, 181–190, 2008.
Hemming, S. R.: Heinrich events: Massive late Pleistocene detritus layers of the North Atlantic and their global climate imprint, Rev. Geophys., 42, 1–43, doi:10.1029/2003RG000128, 2004.
Hodell, D. A., Charles, C. D., and Ninnemann, U. S.: Comparison of interglacial stages in the South Atlantic sector of the southern ocean for the past 450 kyr: implifications for Marine Isotope Stage (MIS) 11, Global Planet. Change, 24, 7–26, doi:10.1016/S0921-8181(99)00069-7, 2000.
Hodell, D. A., Kanfoush, S. L., Venz, K. A., Charles, C. D., and Sierro, F. J.: The Mid-Brunhes Transition in ODP Sites 1089 and 1090 (Subantarctic South Atlantic), in: Earth's Climate and orbital eccentricity: The Marine Isotope Stage 11 Question, edited by: Droxler, A. W., Poore, R. Z., and Burckle, L. H., Geophysical Monograph, American Geophysical Union, Washington, D.C., 113–130, 2003.
Hodell, D. A., Channell, J. E. T., Curtis, J. H., Romero, O. E., and Röhl, U.: Onset of 'Hudson Strait' Heinrich Events in the Eastern North Atlantic at the end of the Middle Pleistocene Transition (~640 ka)?, Paleoceanography, 23, PA4218, doi:10.1029/2008PA001591, 2008.
Jansen, J. H. F., Kuijpers, A., and Troelstra, S. R.: A Mid-Brunhes Climatic Event: Long-Term Changes in Global Atmosphere and Ocean Circulation, Science, 232, 619–622, doi:10.1126/science.232.4750.619, 1986.
Ji, J., Ge, Y., Balsam, W., Damuth, J. E., and Chen, J.: Rapid identification of dolomite using a Fourier Transform Infrared Spectrophotometer (FTIR): A fast method for identifying Heinrich events in IODP Site U1308, Mar. Geol., 258, 60–68, 2009.
Jouzel, J., Masson-Delmotte, V., Cattani, O., Dreyfus, G., Falourd, S., Hoffmann, G., Minster, B., Nouet, J., Barnola, J. M., Chappellaz, J., Fischer, H., Gallet, J. C., Johnsen, S., Leuenberger, M., Loulergue, L., Luethi, D., Oerter, H., Parrenin, F., Raisbeck, G., Raynaud, D.,

Schilt, A., Schwander, J., Selmo, E., Souchez, R., Spahni, R., Stauffer, B., Steffensen, J. P., Stenni, B., Stocker, T. F., Tison, J. L., Werner, M., and Wolff, E. W.: Orbital and Millennial Antarctic Climate Variability over the Past 800,000 Years, Science, 317, 793–796, doi:10.1126/science.1141038, 2007.

Kandiano, E. S. and Bauch, H. A.: Surface ocean temperatures in the north-east Atlantic during the last 500,000 years: evidence from foraminiferal census data, Terra Nova, 15, 265–271, 2003.

Kandiano, E. S. and Bauch, H. A.: Phase relationship and surface water mass change in the Northeast Atlantic during Marine Isotope Stage 11 (MIS 11), Quaternary Res., 68, 445–455, 2007.

Knies, J., Matthiessen, J., Mackensen, A., Stein, R., Vogt, C., Frederichs, T., and Nam II, S.: Effects of Arctic freshwater forcing on thermohaline circulation during the Pleistocene, Geology, 35, 1075–1078, 2007.

Labeyrie, L. D. and Duplessy, J. C.: Changes in the oceanic $^{13}C/^{12}C$ ratio during the last 140,000 years: High-latitude surface water records, Palaeogeogr. Palaeocl., 50, 217–240, 1985.

Lambert, F., Delmonte, B., Petit, J. R., Bigler, M., Kaufmann, P. R., Hutterli, M. A., Stocker, T. F., Ruth, U., Steffensen, J. P., and Maggi, V.: Dust-climate couplings over the past 800,000 years from the EPICA Dome C ice core, Nature, 452, 616–619, 2008.

Laskar, J., Robutel, P., Joutel, F., Gastineau, M., Correia, A. C. M., and Levrard, B.: A long-term numerical solution for the insolation quantities of the Earth, Astron. Astrophys., 428, 261–285, doi:210.1051/0004-6361:20041335, 2004.

Lea, D. W., Pak, D. K., and Spero, H. J.: Sea Surface Temperatures in the Western Equatorial Pacific During Marine Isotope Stage 11, in: Earth's Climate and orbital eccentricity: The Marine Isotope Stage 11 Question, edited by: Droxler, A. W., Poore, R. Z., and Burckle, L. H., Geophysical Monograph, American Geophysical Union, Washington, D.C., 147–156, 2003.

Levy, M., Lehahn, Y., André , J. M., Mémery, L., Loisel, H., and Heifetz, E.: Production regimes in the northeast Atlantic: A study based on Sea-viewing Wide Field-of-view Sensor (SeaWiFS) chlorophyll and ocean general circulation model mixed layer depth, J. Geophys. Res., 110, C07S10, doi:10.1029/2004JC002771, 2005.

Lisiecki, L. E. and Raymo, M.: A Pliocene-Pleistocene stack of 57 globally distributed benthic $\delta^{18}O$ records, Paleoceanography, 20, PA1003, doi:10.1029/2004PA001071, 2005.

Loulergue, L., Schilt, A., Spahni, R., Masson-Delmotte, V., Blunier, T., Lemieux, B., Barnola, J. M., Raynaud, D., Stocker, T. F., and Chappellaz, J.: Orbital and millennial-scale features of atmospheric CH_4 over the past 800,000[thinsp]years, Nature, 453, 383–386, 2008.

Loutre, M. F. and Berger, A.: Marine Isotope Stage 11 as an analogue for the present interglacial, Global Planet. Change, 36, 209–217, 2003.

Lüthi, D., Le Floch, M., Bereiter, B., Blunier, T., Barnola, J. M., Siegenthaler, U., Raynaud, D., Jouzel, J., Fischer, H., Kawamura, K., and Stocker, T. F.: High-resolution carbon dioxide concentration record 650,000–800,000 years before present, Nature, 453, 379–382, 2008.

Martrat, B., Grimalt, J. O., Shackleton, N. J., de Abreu, L., Hutterli, M. A., and Stocker, T. F.: Four Climate Cycles of Recurring Deep and Surface Water Destabilizations on the Iberian Margin, Science, 317, 502–507, doi:10.1126/science.1139994, 2007.

McCartney, M. S. and Talley, L. D.: The Subpolar Mode Water of the North Atlantic Ocean, J. Phys. Oceanogr., 12, 1169–1188, 1982.

McManus, J., Oppo, D. W., and Cullen, J. L.: A 0.5-million-year record of millennial-scale climate variability in the North Atlantic, Science, 283, 971–975, 1999.

McManus, J., Oppo, D., Cullen, J., and Healey, S.: Marine Isotope Stage 11 (MIS 11): Analog for Holocene and Future Climate?, in: Earth's Climate and orbital eccentricity: The Marine Isotope Stage 11 Question, edited by: Droxler, A. W., Poore, R. Z., and Burckle, L. H., Geophysical Monograph, American Geophysical Union, Washington, D.C., 69–86, 2003.

Müller, P. J., Kirst, G., Ruhland, G., von Storch, I., and Rosell-Melé, A.: Calibration of the alkenone paleotemperature index Uk37' based on core-tops from the eastern South Atlantic and the global ocean (60° N-60° S), Geochim. Cosmochim. Acta, 62, 1757–1772, 1998.

Oppo, D. W., McManus, J., and Cullen, J. C.: Abrupt climate change events 500,000 to 340,000 years ago: Evidence from subpolar North Atlantic sediments, Science, 279, 1335–1338, 1998.

Oppo, D. W., Keigwin, L. D., McManus, J. F., and Cullen, J. L.: Persistent suborbital climate variability in marine isotope stage 5 and Termination II, Paleoceanography, 16, 280–292, 2001.

Ortiz, J. D., Mix, A. C., Rugh, W., Watkins, J. M., and Collier, R. W.: Deep-dwelling planktonic foraminifera of the northeastern Pacific Ocean reveal environmental control of oxygen and carbon isotopic disequilibria, Geochim. Cosmochim. Acta, 60, 4509–4523, 1996.

Ottens, J. J.: Planktic foraminifera as North Atlantic water mass indicators, Oceanologica Acta, 14, 123–140, 1991.

Peliz, A., Dubert, J., Santos, A. M. P., Oliveira, P. B., and Le Cann, B.: Winter upper ocean circulation in the Western Iberian Basin – Fronts, Eddies and Poleward Flows: an overview, Deep Sea Research Part I: Oceanographic Research Papers, 52, 621–646, 2005.

Petit, J. R., Jouzel, J., Raynaud, D., Barkov, N. I., Barnola, J. M., Basile, I., Bender, M., Chappellaz, J., Davis, M., Delaygue, G., Delmotte, M., Kotlyakov, V. M., Legrand, M., Lipenkov, V. Y., Lorius, C., Pépin, L., Ritz, C., Saltzman, E., and Stievenard, M.: Climate and atmospheric history of the past 420,000 years from the Vostok ice core, Antarctica, Nature, 399, 429–436, 1999.

Pflaumann, U., Sarnthein, M., Chapman, M., d'Abreu, L., Funnell, B., Huels, M., Kiefer, T., Maslin, M., Schulz, H., Swallow, J., Kreveld, S. V., Vautravers, M., Vogelsang, E., and Weinelt, M.: Glacial North Atlantic: Sea-surface conditions reconstructed by GLAMAP 2000, Paleoceanography, 18, 10-11–10-28, doi:10.1029/2002PA000774, 2003.

Pierre, C., Belanger, P., Saliège, J. F., Urrutiaguer, M. J., and Murat, A.: Paleoceanography of the western Mediterranean during the Pleistocene: oxygen and carbon isotope records at Site 975, in: Proceedings ODP, Scientific Results, edited by: Zahn, R., Comas, M. C., and Klaus, A., Ocean Drilling Program, College Station, TX, 481–488, 1999.

Poli, M. S., Thunell, R. C., and Rio, D.: Millennial-scale changes in North Atlantic Deep Water circulation during marine isotope stages 11 and 12: Linkage to Antarctic climate, Geology, 28, 807–810, 2000.

Prokopenko, A. A., Williams, D. F., Kuzmin, M. I., Karabanov, E. B., Khursevich, G. K., and Peck, J. A.: Muted climate variations in continental Siberia during the mid-Pleistocene epoch, Nature, 418, 65–68, 2002.

Raffi, I., Backman, J., Fornaciari, E., Palike, H., Rio, D., Lourens, L., and Hilgen, F.: A review of calcareous nannofossil astrobiochronology encompassing the past 25 million years, Quaternary Sci. Rev., 25, 3113–3137, 2006.

Reverdin, G., Niiler, P. P., and Valdimarsson, H.: North Atlantic Ocean surface currents, J. Geophy. Res., 108(C1), 3002, doi:10.1029/2001JC001020, 2003.

Rickaby, R. E. M., and Elderfield, H.: Evidence from the high-latitude North Atlantic for variations in Antarctic Intermediate water flow during the last deglaciation, Geochem. Geophy. Geosy., 6, 1–12, 2005.

Rios, A. F., Perez, F. F., and Fraga, F.: Water Masses in the Upper and Middle North-Atlantic Ocean East of the Azores, Deep-Sea Res. I, 39, 645–658, 1992.

Rodrigues, T., Voelker, A. H. L., Grimalt, J., and Abrantes, F.: Millennial-scale variability in

marine and terrestrial climate records off Portugal during MIS 9–15, in preperation.
Ruddiman, W. F.: Late Quaternary deposition of ice-rafted sand in the subpolar North Atlantic (lat 40° to 65°N), Geol. Soc. Am. Bull., 88, 1813–1827, 1977.
Ruddiman, W. F.: Orbital changes and climate, Quaternary Sci. Rev., 25, 3092–3112, 2006.
Salgueiro, E., Voelker, A., Abrantes, F., Meggers, H., Pflaumann, U., Loncaric, N., Gonzalez-Alvarez, R., Oliveira, P., Bartels-Jonsdottir, H. B., Moreno, J., and Wefer, G.: Planktonic foraminifera from modern sediments reflect upwelling patterns off Iberia: Insights from a regional transfer function, Mar. Micropaleontol., 66, 135–164, doi:10.1016/j.marmicro.2007.09.003, 2008.
Shackleton, N. J.: The last interglacial in the marine and terrestrial records, Proceedings of the Royal Society of London, 6, 183–190, 1969.
Shackleton, N. J.: Attainment of isotopic equilibrium between ocean water and the benthonic foraminifera genus Uvigerina: Isotopic changes in the ocean during the last Glacial, Colloques Internationaux du C. N. R. S., 219, 203–209, 1974.
Shackleton, N. J., Hall, M. A., and Vincent, E.: Phase relationships between millennial-scale events 64,000–24,000 years ago, Paleoceanography, 15, 565–569, 2000.
Siegenthaler, U., Stocker, T. F., Monnin, E., Luthi, D., Schwander, J., Stauffer, B., Raynaud, D., Barnola, J. M., Fischer, H., Masson-Delmotte, V., and Jouzel, J.: Stable Carbon Cycle-Climate Relationship During the Late Pleistocene, Science, 310, 1313–1317, 2005.
Spahni, R., Chappellaz, J., Stocker, T. F., Loulergue, L., Hausammann, G., Kawamura, K., Flückiger, J., Schwander, J., Raynaud, D., Masson-Delmotte, V., and Jouzel, J.: Atmospheric Methane and Nitrous Oxide of the Late Pleistocene from Antarctic Ice Cores, Science, 310, 1317–1321, 2005.
Stein, R., Hefter, J., Grützner, J., Voelker, A., and Naafs, B. D. A.: Variability of surface-water characteristics and Heinrich-like Events in the Pleistocene mid-latitude North Atlantic Ocean: Biomarker and XRD records from IODP Site U1313 (MIS 16–9), Paleoceanography, 24, PA2203, doi:10.1029/2008PA001639, 2009.
Stirling, C. H., Esat, T. M., Lambeck, K., McCulloch, M. T., Blake, S. G., Lee, D. C., and Halliday, A. N.: Orbital Forcing of the Marine Isotope Stage 9 Interglacial, Science, 291, 290–293, 2001.
Tzedakis, P. C., Andrieu, V., de Beaulieu, J. L., Crowhurst, S., Follieri, M., Hooghiemstra, H., Magri, D., Reille, M., Sadori, L., Shackleton, N. J., and Wijmstra, T. A.: Comparison of terrestrial and marine records of changing climate of the last 500,000 years, Earth Planet.

Sci. Lett., 150, 171–176, 1997.
Tzedakis, P. C., Roucoux, K. H., de Abreu, L., and Shackleton, N. J.: The Duration of Forest Stages in Southern Europe and Interglacial Climate Variability, Science, 306, 2231–2235, 2004.
Tzedakis, P. C., Hooghiemstra, H., and Palike, H.: The last 1.35 million years at Tenaghi Philippon: revised chronostratigraphy and long-term vegetation trends, Quaternary Sci. Rev., 25, 3416–3430, 2006.
Tzedakis, P. C., Pälike, H., Roucoux, K. H., and de Abreu, L.: Atmospheric methane, southern European vegetation and low-mid latitude links on orbital and millennial timescales, Earth Planet. Sci. Lett., 277, 307–317, 2009.
van Aken, H. M.: The hydrography of the mid-latitude Northeast Atlantic Ocean – Part III: the subducted thermocline water mass, Deep-Sea Res. I, 48, 237–267, 2001.
Venz, K. A., Hodell, D. A., Stanton, C., and Warnke, D. A.: A 1.0 Myr record of Glacial North Atlantic Intermediate Water variability from ODP site 982 in the northeast Atlantic, Paleoceanography, 14, 42–52, 1999.
Villanueva, J., Grimalt, J. O., Cortijo, E., Vidal, L., and Labeyrie, L.: A biomarker approach to the organic matter deposited in the North Atlantic during the last climatic cycle, Geochim. Cosmochim. Acta, 61, 4633–4646, 1997.
Voelker, A., Martin, P., Lebreiro, S., and Abrantes, F.: Millennial-scale Deep/Intermediate Water Changes at the Mid-depth Portuguese Margin During Marine Isotope Stage (MIS) 11, Quaternary International, 167–168, 436, 2007.
Voelker, A. H. L.: Zur Deutung der Dansgaard-Oeschger Ereignisse in ultra-hochauflösenden Sedimentprofilen aus dem Europäischen Nordmeer, DSc dissertation, Berichte-Reports, Institut für Geowissenschaften, Universität Kiel, no. 9, University of Kiel, Kiel, Germany, 278 pp., 1999.
Voelker, A. H. L., Grützner, J., and Hodell, D. A.: High-frequency Changes in Surface and Deep Water Hydrography in the Mid-latitude North Atlantic during Marine Isotope Stages 11–15: New Insights from IODP Sites U1313 and U1308, Geochem. Geophy. Geosy., in revision, 2009.
von Grafenstein, R., Zahn, R., Tiedemann, R., and Murat, A.: Planktonic δ^{18}O records at Sites 976 and 977, Alboran Sea: Stratigraphy, forcing, and paleoceanographic implications, in: Proceedings ODP, Scientific Results, edited by: Zahn, R., Comas, M. C., and Klaus, A., Ocean Drilling Program, College Station, TX, 469–479, 1999.

Watanabe, O., Jouzel, J., Johnsen, S., Parrenin, F., Shoji, H., and Yoshida, N.: Homogeneous climate variability across East Antarctica over the past three glacial cycles, Nature, 422, 509–512, 2003.

Weirauch, D., Billups, K., and Martin P.: Evolution of Millennial-Scale Climate Variability During the Mid Pleistocene, Paleoceanography, 23, PA 3216, doi:10.1029/2007PA001584, 2008.

Table 1. Locations of core sites and their respective hydrographic and productivity regimes.

Site	Latitude	Longitude	Water depth	Surface water sources	Productivity regime
ODP site 980	55°29.09′ N	14°42.13′ W	2168 m	Rockall Trough branch of North Atlantic Current	Subpolar regime
IODP site U1313	41°00.07′ N	32°57.40′ W	3412 m	North Atlantic Current derived waters	Transitional zone between subpolar and mid-latitude regimes
MD01-2446	39°03.35′ N	12°37.44′ W	3570 m	Portugal Current	Mid-latitude regime
MD03-2669	39°02.20′ N	10°39.63′ W	1895 m	Upwelling and Iberian Poleward Current	Seasonal upwelling
MD01-2443	37°52.89′ N	10°10.57′ W	2941 m	Upwelling and Iberian Poleward Current	Seasonal upwelling
ODP site 1056	32°29.10′ N	76°19.80′ W	2167 m	Gulf Stream	Subtropical regime
ODP site 1058	31°41.40′ N	75°25.80′ W	2985 m		

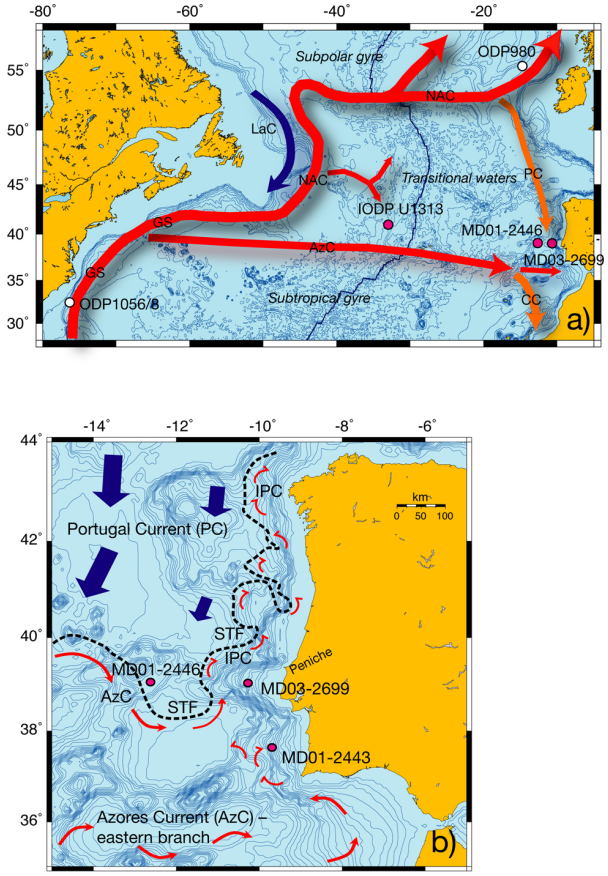

Fig. 1. **(a)** Core locations and major surface water currents in the North Atlantic (Fratantoni, 2001): GS = Gulf Stream; NAC = North Atlantic Current; AzC = Azores Current; CC = Canary Current; PC = Portugal Current; LaC = Labrador Current. **(b)** Winter circulation scheme off Portugal after (Peliz et al., 2005) with IPC = Iberian Poleward Current and STF = Subtropical front.

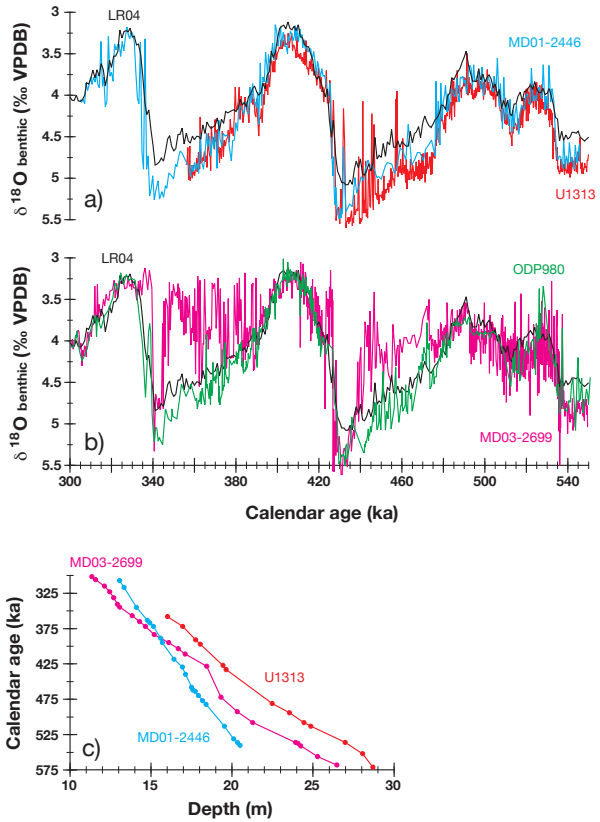

Fig. 2. **(a)** Benthic δ^{18}O records of IODP site U1313 (red) and MD01-2446 (cyan) in comparison to the LR04 stack (black) (Lisiecki and Raymo, 2005); **(b)** Benthic δ^{18}O record of MD03-2699 (magenta) in comparison to ODP site 980 (green; on LR04 timescale) and the LR04 stack (black). **(c)** Age-depth relationships for IODP site U1313, MD01-2446 and MD03-2699.

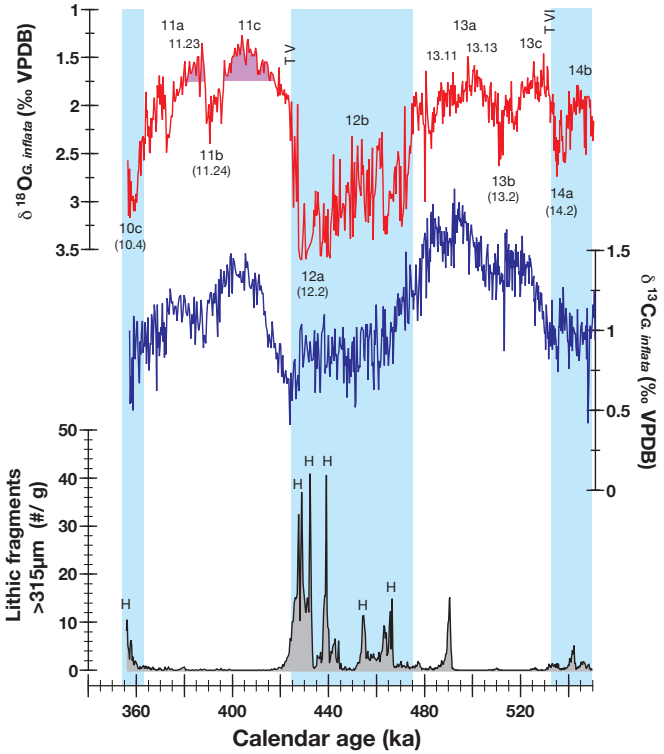

Fig. 3. Surface water records for IODP site U1313 in the mid-latitude North Atlantic. From top to bottom: *G. inflata* δ^{18}O (‰VPDB), *G. inflata* δ^{13}C (‰VPDB), and lithics concentration (#/g). Blue bars mark glacial MIS 10, 12 and 14. Substages (e.g. 11c) are indicated above and below the δ^{18}O record as well as some isotopic events (e.g. 10.4). T IV, V and VI refer to Terminations VI, V and VI. H indicates IRD peaks with Heinrich-type signatures (Stein et al., 2009).

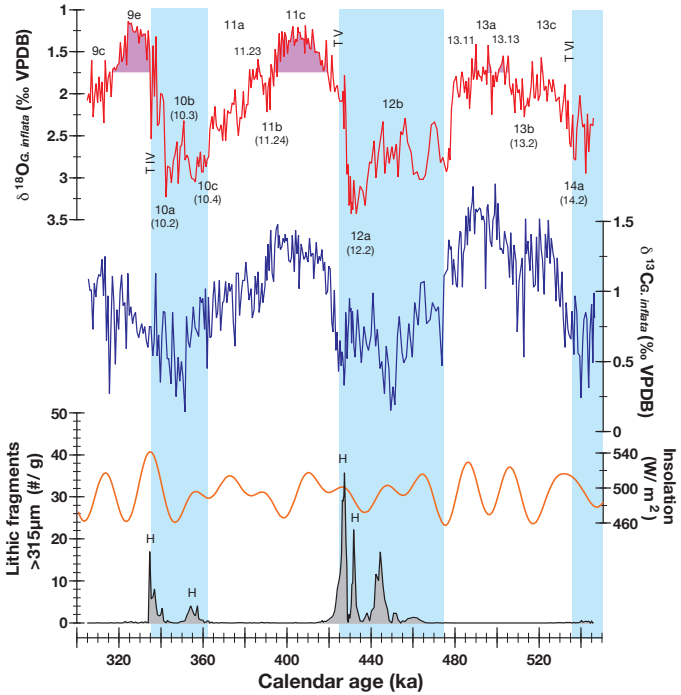

Fig. 4. Surface water records for core MD01-2446, the offshore site off Portugal. From top to bottom: *G. inflata* δ^{18}O (‰VPDB), *G. inflata* δ^{13}C (‰VPDB), June 21st insolation at 65° N (Laskar et al., 2004), and lithics concentration (#/g). Blue bars mark glacial MIS 10, 12 and 14. Substages (e.g. 11c) are indicated above and below the δ^{18}O record as well as some isotopic events (e.g. 10.4). T IV, V and VI refer to Terminations VI, V and VI. H indicates Heinrich-type ice-rafting events.

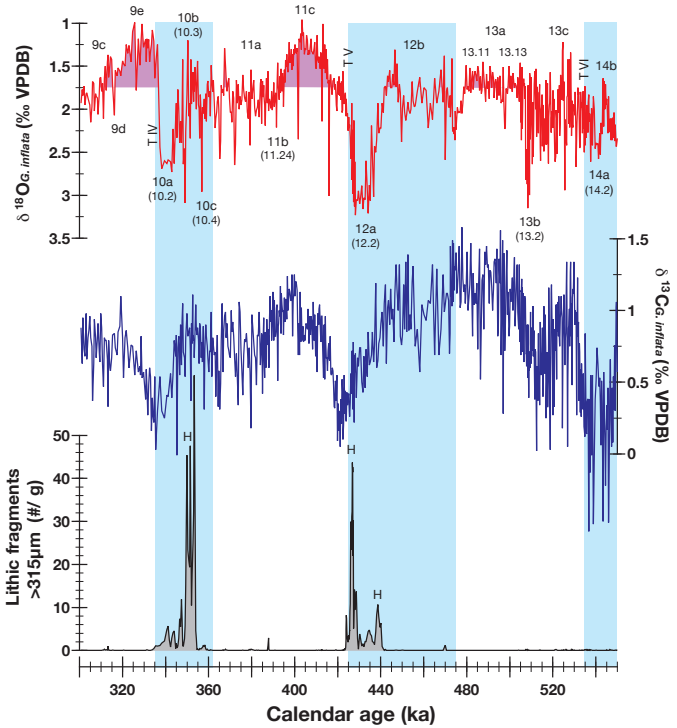

Fig. 5. Surface water records for core MD03-2699, the nearshore site off Portugal. From top to bottom: *G. inflata* δ^{18}O (‰VPDB), *G. inflata* δ^{13}C (‰VPDB), and lithics concentration (#/g). Blue bars mark glacial MIS 10, 12 and 14. Substages (e.g. 11c) are indicated above and below the δ^{18}O record as well as some isotopic events (e.g. 10.4). T IV, V and VI refer to Terminations VI, V and VI. H indicates Heinrich-type ice-rafting events.

CPD
5, 1–55, 2009

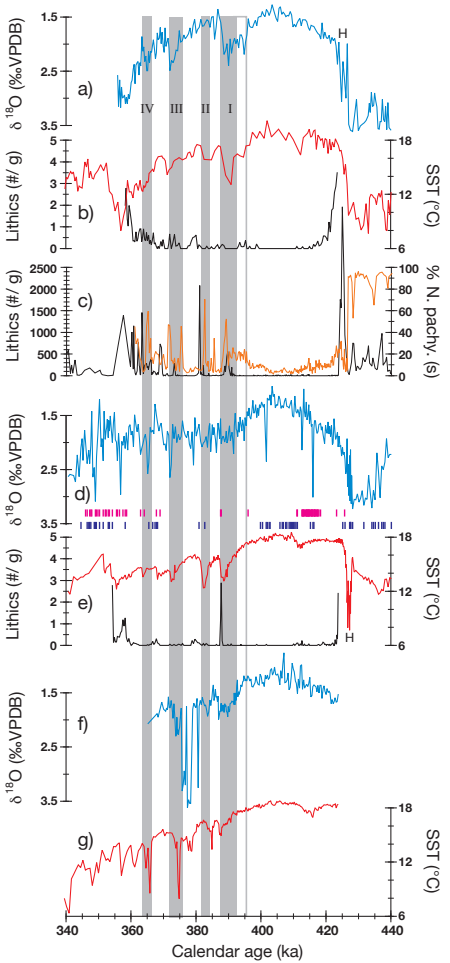
a)
b)
c)
d)
e)
f)
g)
IV
III
II
I
H
δ18O (‰VPDB)
Lithics (#/ g)
SST (°C)
% N. pachy. (s)
Calendar age (ka)
340
360
380
400
420
440

Fig. 6.

Fig. 6. Close-ups of MIS 11 in the records of IODP Site U1313 **(a, b)**, ODP Site 980 **(c)**, MD03-2699 **(d, e)** and southern Portuguese site MD01-2443 **(f, g)**; (de Abreu et al., 2005; Martrat et al., 2007).*G. inflata* δ^{18}O records are shown in blue (a, d, f), alkenone-based mean annual sea surface temperature (SST) records in red (b, e, g). The abundance of Lithics >315 μm (black; only sections with <4 grains/g) are shown for IODP Site U1313 (b) and core MD03-2699 (e) and >150 μm for ODP Site 980 (c; Oppo et al., 1998). Panel (c) also includes the % *N. pachyderma* (s) record of ODP Site 980 (orange; Oppo et al. 1998). In panel (d) magenta bars indicate presence of *Globorotalia menardii* and dark blue ones of Sphaeroidinella dehiscens in the respective levels. MD01-2443 data is shown using the age model of (Tzedakis et al., 2009) that links the MD01-2443 benthic δ^{18}O data to the EDC δD record on the EDC 3 timescale (Jouzel et al., 2007) following the approach of (Shackleton et al., 2000). Grey bars indicate stadials (numbered I to IV) within MIS 11a. The bar outlined in grey during the oldest stadial marks the interval when cold conditions already prevailed at (I)ODP Sites U1313 and 980. H denotes the Heinrich-type ice-rafting event associated with Termination V.

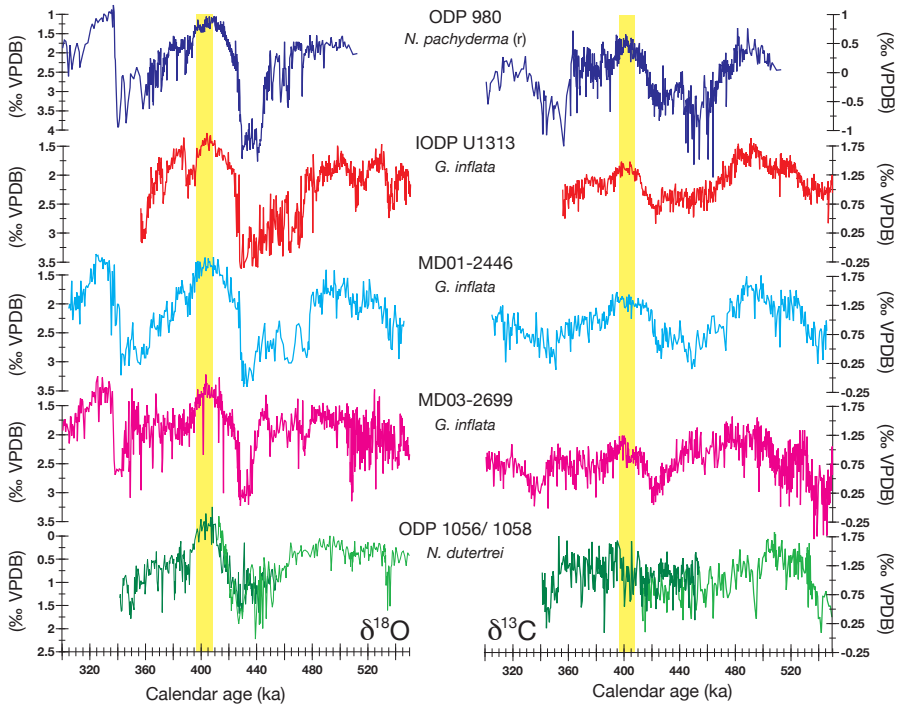

Fig. 7. North Atlantic planktonic foraminifer stable isotope records with $\delta^{18}O$ records on the left and $\delta^{13}C$ records on the right. Sites are arranged from North to South: ODP Site 980 (dark blue), IODP Site U1313 (red), MD01-2446 (light blue), MD03-2699 (magenta), and ODP Sites 1056 (dark green) and 1058 (light green) combined. Yellow bars highlight the period of the MIS 11c sea level highstand.

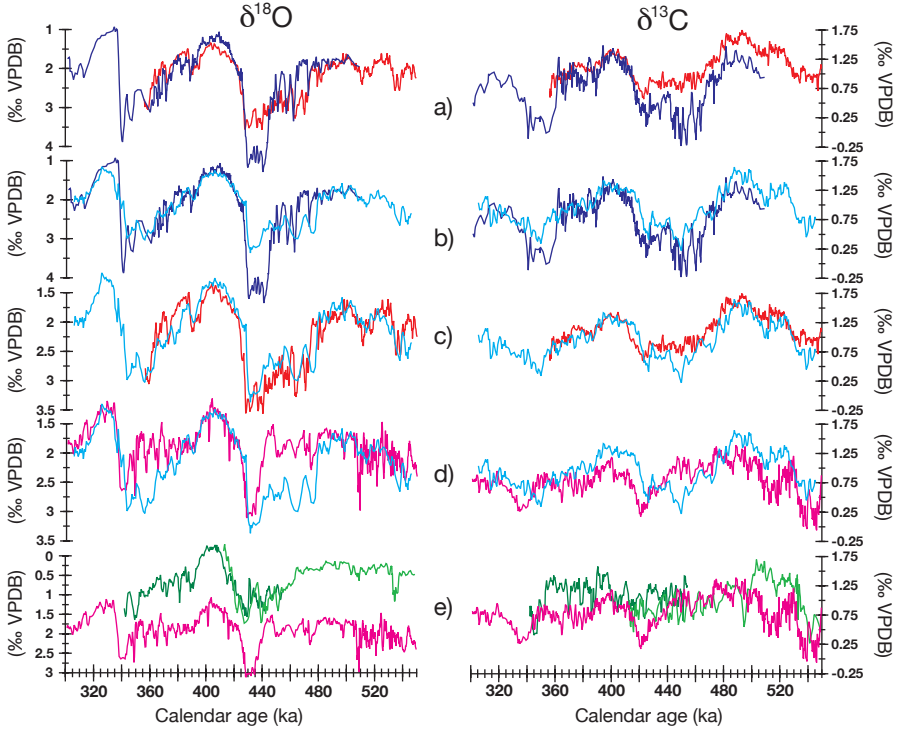

Fig. 8. Direct comparison between sites based on 3 point average records (δ^{18}O left, δ^{13}C right side). Colors for sites as in Fig. 7. **(a)** IODP Site U1313 vs. ODP Site 980. For better comparison ODP Site 980 *N. pachyderma* (r) δ^{13}C data was adjusted to dissolved inorganic carbon (DIC) by adding 0.85‰(Labeyrie and Duplessy, 1985). **(b)** MD01-2446 vs. ODP Site 980 (with δ^{13}C adjusted); **(c)** MD01-2446 vs. IODP Site U1313; **(d)** MD01-2446 vs. MD03-2699; **(e)** ODP Sites 1056 and 1058 vs. MD03-2699.

CPD
5, 1–55, 2009

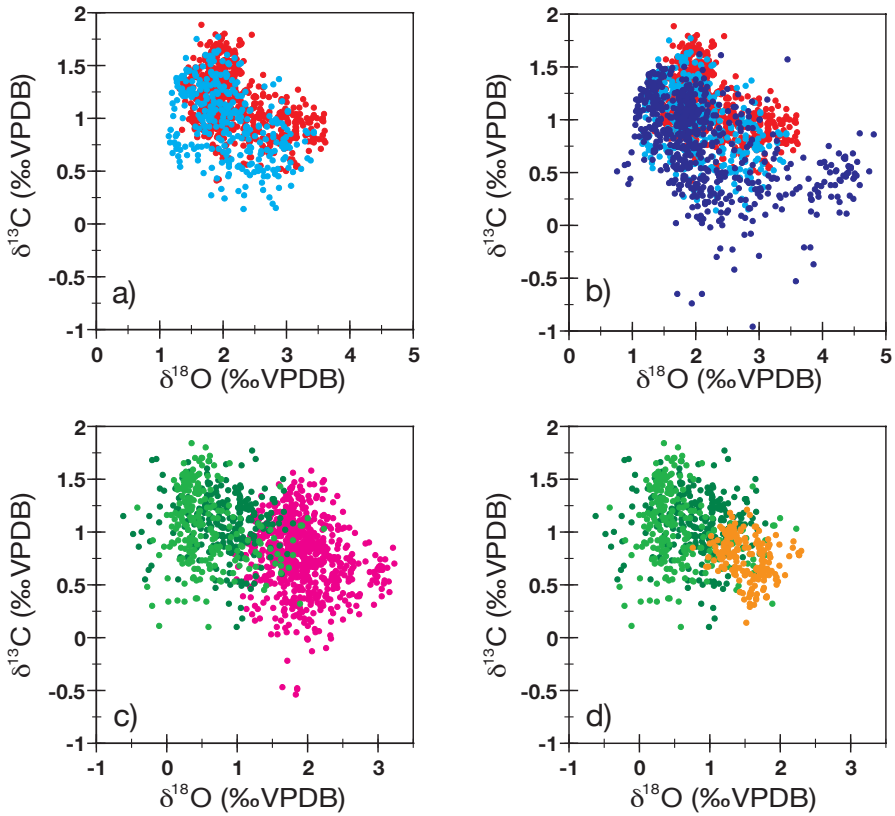

Fig. 9. $\delta^{18}O$ versus $\delta^{13}C$ scatter plots of the records shown in Fig. 7. **(a)** IODP Site U1313 (red) and MD01-2446 (light blue); **(b)** IODP Site U1313 (red), MD01-2446 (light blue), and ODP Site 980 (dark blue); **(c)** MD03-2699 (magenta) and ODP Sites 1056 (dark green) and 1058 (light green); **(d)** ODP Sites 1056 (dark green) and 1058 (light green) and MD01-2443 (orange; de Abreu et al., 2005; with extreme values between 375 and 381 ka excluded).